UNIVERSITÉ DE STRASBOURG

Ecole Doctorale des Sciences de la Vie et de la Sante (ED 414)

Inserm U1113 - Voies de signalisation du développement et du stress cellulaire dans les cancers digestifs et urologiques

THÈSE présentée par :

Cynthia LICONA

soutenue le : **24 avril 2015**

pour obtenir le grade de : **Docteur de l'université de Strasbourg**

Discipline/ Spécialité : Aspects Moléculaires et Cellulaires de la Biologie

Identification et caractérisation de l'activité biologique des composés organométalliques anticancéreux

THÈSE dirigée par:

M. GAIDDON Christian	Directeur de Recherche, Université de Strasbourg.
M. MELLITZER Georg	Chargé de Recherche, Université de Strasbourg.

RAPPORTEURS:

M. CHEVET Eric	Directeur de Recherche, Université de Rennes.
Mme. CASINI Angela	Assistante du Professeur, Université de Groningen.

AUTRES MEMBRES DU JURY:

Mme. DONTENWILL Monique	Directeur de Recherche, Université de Strasbourg.
M. SADLER Peter	Professeur, Université de Warwick

A mis padres Evangelina y Arturo,
por siempre creer en mi.

Acknowledgements

Fist of all, I want to thank the members of my jury, Dr. Angela Casini, Dr. Monique Dontenwill, Dr. Peter Sadler and Dr. Eric Chevet for accepting this invitation to critically examine my manuscript. I sincerely want to thank you for the time you giving me by reading my thesis, and specially to Dr. Casini and Dr. Sadler for coming from far.

≈ ≈ ≈ ≈

Dad, I did it!....Dad? Do you remember when I was six, we were eating an ice cream together in Coyoacan (a tiny village in Mexico), we were talking about nothing and everything, and suddenly I ask you why people died? You answer me “because of diseases”, and then you explain me that there were some diseases that doctors can not heal, like cancer….since then, that thought never got out of my mind. Over the years this idea matured, and I knew that I wanted to do something to help people, help doctors and at the same time leave a little rock in this mountain of knowledge. I know, too ambitious….but at that age I thought that everything was possible, you taught me that, so I met science and I fell in love, I did my highschool, my college, university, master’s degree in the same line, science, and came to France…. then…

Christian Gaiddon gave me the chance to continue with my dream. Thank you for giving me the chance to become a member of your team, for teaching me, help me when I need it, share with me your passion for science. Georg, thanks for always encourage me, for cheer me up, for advice me. Thanks to all the member of my team, Veronique, Christophe, Shawn, Paula, Marie-Elodie and, even if they are not in the lab anymore Orphee and Yannick, for all those crazy moment we shared together, for comfort me when my experiments turn wrong, an for sharing your techniques with me. Thanks to the team “upstairs”: Jean-Noël, Isabelle G, Isabelle D, Claire, Mathilde, and special thanks to Elisabeth for seeding so many cells for me, and Leonor for your work, you always had a smile for me. Thanks for making this four years so perfect. Each member of the group, contributed to make this happen.

Furthermore, I want to thank my mom, dad and my brother for always believe in me, to be sure that I could accomplish what I wanted, for your support, your help and advice. And for understand that I needed to go far, far away to accomplish this dream.

Dr. Conchita and Dr. Luis you are my mentors, you were the first persons that taught me the field of science, the rigor that science needs, and the respect for mice that give their life to science. Still thank you for that, and for always staying in touch. Thanks to my Mexican friends, Odile, Deyanira, Eugenia, Mitzi and Ivan, you are my best friends, even the distance cannot break our friendship. I love you from all my heart.

This dream cannot be accomplished with out my prince charming, my husband Stéphan, thanks for rendering my dream just perfect, for your lovely attentions and for your unconditional love.

So, here I am, writing this words, I ended my Ph.D. program, and you know what? In a very humble way, I think I did it, I think after all these years working in science, I left a little rock in the mountain of science.

Make your life a dream, and your dream a reality.

Fais de ta vie un rêve, et d'un rêve, une réalité.

Haz de tu vida un sueño, y de tu sueño una realidad.

Antoine de Saint-Exupéry

Table of Contents

I INTRODUCTION.....1

I. CANCER AND THERAPIES 1

I.A. Statistics in cancer 1

I.B. Most common cancer treatments. 2

II. ORGANOMETALLICS IN CANCER 9

II.A. Platinium compounds 10

II.B. Mode of action of Platinum compounds. 12

II.B.1. Recognition of platinum–DNA adducts 13

II.B.2. DNA repair mechanism 14

II.B.3. Cisplatin and p53 19

II.B.4. Cisplatin and oxidative stress 20

II.C. Conclusion Schema of Cisplatin Mechanism of Action 21

II.D. Cisplatin Drug Resistance 22

II.D.1. Transporters and Reduced platinum accumulation 22

II.D.2. Novel Mechanisms of Cisplatin Resistance 23

II.E. Strategies for overcoming cisplatin resistance 24

II.F. Cisplatin side effects 24

III. RUTHENIUM COMPOUNDS 26

III.A. Interesting Ruthenium Features. 26

III.B. Different Ru based molecules. 27

III.B.1. NAMI-A 27

III.B.2. KP1019, ... 31

III.B.3. Rapta T 34

III.B.4. RM175 35

III.B.5. DW1/2 37

III.B.6. RUTENIUM DERIVED COMPOUNDS (RDC) 38

III.C. Recapitulative Schema mode of action of Ru compounds. 43

III.D. Other groups that developed Ruthenium based compounds. 44

III.E. Other metals used in the development of anticancer compounds 45

IV. THESIS OBJECTIVES 47

IV.A. Objective 1 47
IV.B. Objective 2 48
IV.C. Objective 3 48
V. RESULTS (OBJECTIVE 1) 49
V.A. Differential mode of action between ruthenium-based and cisplatin revealed by transcriptomic analyses: the example of histone-deacetylases. 49
V.B. Differential regulation of the HIF-1 pathways by platinum and ruthenium anticancer organometallic drugs. 77
VI. RESULTS (OBJECTIVE 2) 103
VI.A. Induction of caspase 8 and reactive oxygen species by ruthenium-derived anticancer compounds with improved water solubility and cytotoxicity. 103
VI.B. Subcellular localization and transport kinetics of ruthenium organometallic anticancer compounds in living cell: a dose dependent role for amino acid and iron transporters. 113
VI.C. Discovery and investigation of anticancer ruthenium-aerene Schiff-base complexes via water-promoted combinatorial three component assembley 123
VI.D. Exchange of ruthenium to osmium in organometallic compound tunes redox potential and cancer cell selectivity via ROS and oxydo-reductase enzymes regulation. 141
VII. RESULTS (OBJECTIVE 3) 160
VII.A. Design of porphyrin-dota-like scaffolds as all in one multimodal heterometallic complex for medical imaging. 160
VII.B. Gold-phosphine-phorphyrin as potential metal-based theranostics. 176
VIII. DISCUSSION 189
IX. PERSPECTIVES 195
X. Conclusion 197
XI. Bibliography 198

INTRODUCTION

I. CANCER AND THERAPIES

I.A. Statistics in cancer

According to the WHO cancer is a leading cause of death worldwide. 14.1 million adults in the world were diagnosed with cancer and there were 8.2 million deaths from cancer in the world in 2012, and in this respect cancer has reached epidemic proportions worldwide (1-3).

The most common causes of worldwide cancer death are:

- Lung (1.59 million deaths)
- Liver (745 000 deaths)
- Stomach (723 000 deaths)
- Colorectal (694 000 deaths)
- Breast (521 000 deaths)
- Oesophageal cancer (400 000 deaths).

Here in France where I did my Ph.D. lung and colorectal are the most frequent cancers in men and in women (4) (Figure 1).

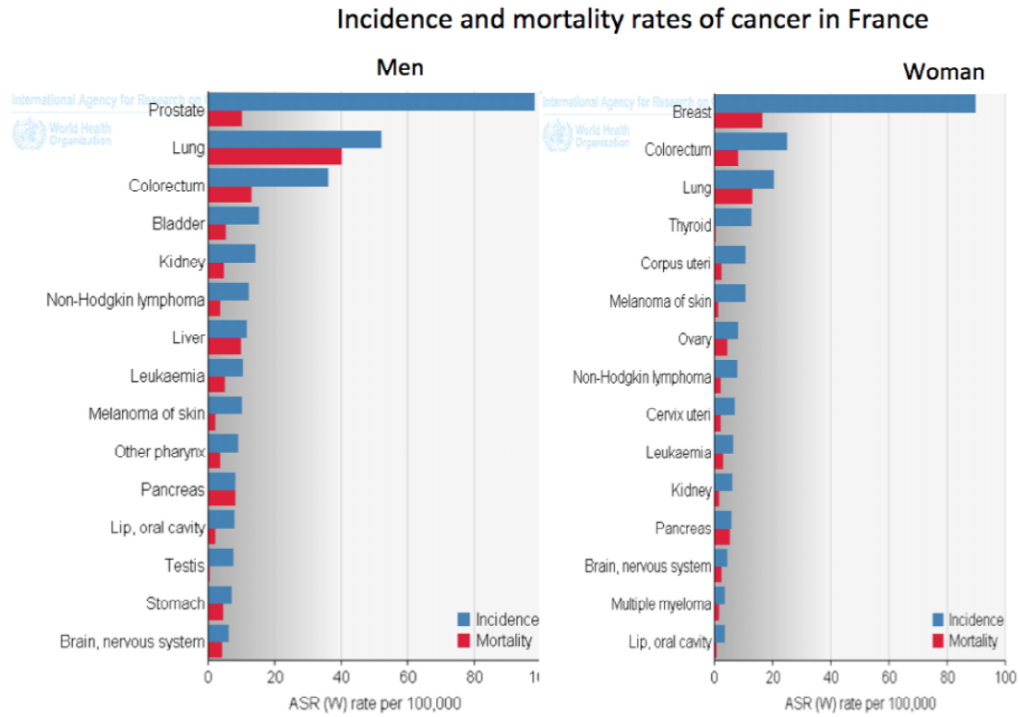


Figure 1. Estimated age-standardized incidence and mortality rates in France

I.B. Most common cancer treatments.

Cancer is an important health problem that is why scientists and doctors continuously developed different treatments with the aim to cure cancer. Its important to understand that each type of cancer is treated with a different approach and every patient will react differently; hence each patient has a specific treatment plan. In order to improve the success of the therapy two main approaches can be combined, neoadjuvant therapy when a treatment is given before the main treatment, and adjuvant therapy when it is given in addition to the main therapy.
Below I will shortly describe the most common treatments (5):

Surgical resection

Surgery, in which cancer is physically removed from the body, is the oldest type of cancer treatment and still the most effective. Frequently surgery is combined with chemo- or radiation-therapy or, which can be given before of after the operation.

There are many types of surgery that may include:

Curative surgery: Performed when a tumor appears to be confined to one area and it is likely that all of the tumor can be removed.

Debulking surgery: Debulking surgery, removal of only part of the tumor, is done when removing all of a tumor would cause too much damage to nearby organs or tissues.

Diagnostic surgery: Such as a biopsy.

Palliative surgery: Used to treat symptoms of advanced cancer, like when the tumor is causing pain or disability.

Preventative surgery: Removes body tissue that is non-cancerous, but is likely to become it. An example is the removal of pre-cancerous polyps in the colon.

Staging surgery: Performed to find out how much cancer there is and how far it has spread.

Radiotherapy

It is estimated that 45% to 60% of cancer cases are treated with radiotherapy. Radiation therapy uses high-energy radiation like X-rays, gamma rays or charged particles in order to damage DNA of cancer cells leading to cell death, in this manner tumor size can be reduced (6).

Radiotherapy is mostly applied in four different ways:

External-beam radiation: This is the most common type of radiation treatment. Radiation is given from a machine called linear accelerator or Linac, which can treat large areas if necessary.

Internal radiation: This type of radiation treatment, also known as brachytherapy, involves placing the radiation source inside the treatment area or into the tissue surrounding it. These radioactive implants may be permanent or temporary.

Systemic radiation: In this therapy a radioactive material, such as radioactive iodine, is injected into the blood in order to reach the cancer cells.

Palliative radiation: This therapy intends to maintain the good patient's quality of life were long-term cancer control is not possible. It is used to control the symptoms associated with many localized tumors that cannot be treated by other methods (such as surgical removal), like pain or bleeding.

Targeted therapies

The ultimate goal of these therapies is to target molecular mechanisms that are "only" present in the cancer cells or at least more represented in the cancer cells due to over-expression for example. In addition, targeted therapies act by blocking essential signaling pathways or mutant proteins that are required for tumor cell growth and survival. These pathways can be inhibited at multiple levels: by binding and neutralizing ligands (for example molecules that bind to specific receptor sites on cells), by blocking receptor signaling within the cancer cell or by interfering with downstream intracellular molecules.

In the following I will briefly describe now three well know examples of molecules frequently used for targeted therapy.

Epidermal Growth Factor Receptor (EGRF): EGFR, also known as HER1, is a tyrosine kinase that, when activated by binding of specific ligands, triggers intracellular signaling that leads to cell proliferation, migration and invasion.
As EGFR is present also on normal cells, its inhibition can lead to significant dermatologic and gastrointestinal toxicities. One example of an EGFR inhibitor used for targeted therapy Cetuximab (Erbitux), which is used for the treatment of metastatic colorectal cancer and, is an antibody, which blocks the binding of EGF to its receptor due to its 5-10 higher affinity for it (7).

HER2/neu: HER2 is a tyrosine kinase receptor related to epidermal growth factor receptor. This molecule has a principal role in breast cancer, and it is estimated that its overexpressed in 25% of patients with breast cancer HER2/neu is overexpressed. Its overexpression is associated with disease recurrence and bad prognosis. One example of a targeted therapy for HER2/neu is Trastuzumab (Herceptin), which is used in metastatic breast cancer and which, like Cetuximab is an antibody blocking the binding of the ligand to its receptor (8).

Vascular Endothelial Growth Factor (VEGF): One example is Bevacizumab (Avastin) which is a monoclonal antibody blocking the activation of VEGF. VEGF induces angiogenesis. During tumor development, angiogenesis is required to provide oxygen and metabolites to cancer cells and eliminate waster product. Indeed, cancer cell proliferation favors hypoxia, low pH and radical oxidized species (ROS) production (9). Hence, the inhibition of VEGF limits cancer growth by preventing *angiogenesis*, a key process in cancer development and progression.
Angiogenesis refers to the process of the development of new blood vessel. In normal cells, these vessels rapidly mature and become stable blood vessels. However, tumor angiogenesis and physiological angiogenesis have many differences that include aberrant vascular structure, altered endothelial-cell–pericyte interactions, abnormal blood flow, increased permeability and delayed maturation. These characteristics are partly due to the overexpression of VEGF. In this way, inhibition of VEGF may normalize the vasculature within a tumor, thereby improving delivery of other chemotherapeutic agents. Unfortunately, as VEGF is also needed in normal blood vessels side effects can occur, like bleeding, thrombosis and hypertension (10,11). The expression of VEGF in cancer cells is induced by hypoxia through

hypoxia-inducible transcription factor 1 (HIF-1), which overexpression has been associated with increased patient mortality in several cancer types (12).

HIF-1 is a heterodimer consisting of the hypoxic response factor HIF-1α and the constitutively expressed aryl hydrocarbon receptor nuclear translocator (ARNT) (also known as HIF-1β) (13). In presence of oxygen, HIF-1α is hydroxylated by the redox enzymes proline hydroxylases PHD1, 2 and 3. Hydroxylated HIF-1α (OH) is recognized by pVHL (the product of the von Hippel–Lindau tumor suppressor gene), which together with a multisubunit ubiquitin ligase complex, tags HIF-1α with polyubiquitin allowing the recognition by the proteasome and subsequent degradation. However, in response to hypoxia, PHD hydroxylation is inhibited leading to HIF-1α accumulation and translocation to the nucleus. There, HIF-1α dimerises with HIF-1β, binds to hypoxia-response elements (HREs) within the promoters of target genes, such as VEGF. In addition, the synthesis of HIF-1α in hypoxic conditions is regulated, by the hyperactivity of the RAS/MAPK and PI3K-AKT-mTOR pathway following the activation of growth factor protein tyrosine kinase (PTK) (14,15).

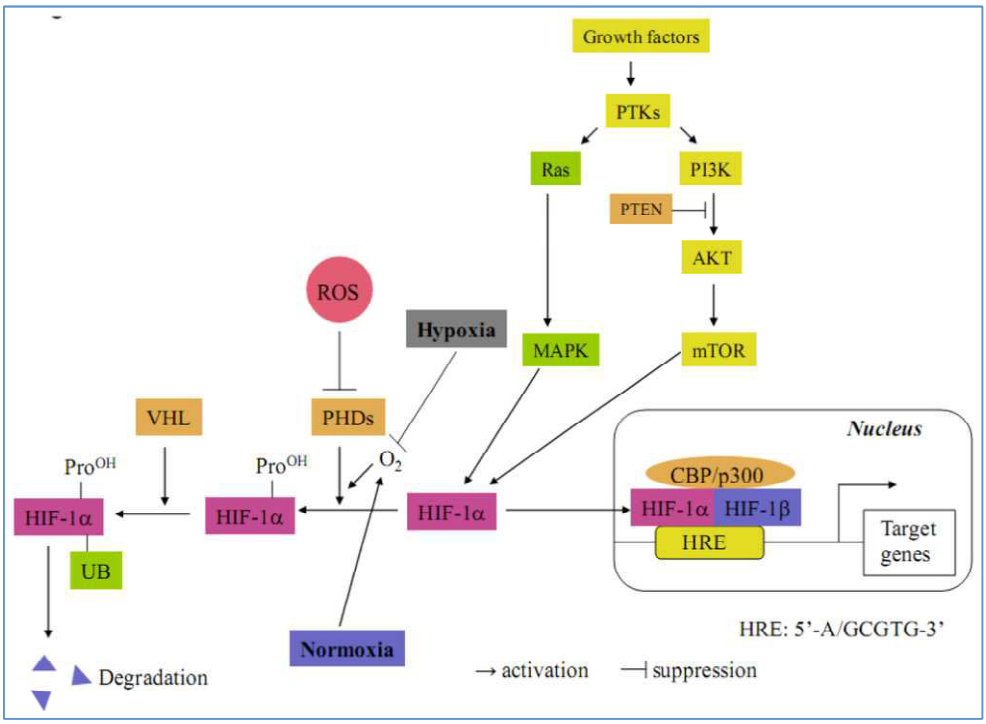


Figure2. HIF-1 α regulation

*Image from: Cancers **2013**, 5(1), 15-26.*

In addition to the three described examples above, many other different targeted therapies have been approved for the use in cancer treatment. These therapies include hormone therapies, gene expression modulator, apoptosis inducer, immunotherapies, and toxin delivery molecules. The later, are of great interest, because it is a dynamic approach in which one can specifically deliver a toxin or a poison to or into the cancer cells.

Toxin delivery molecules: To this purpose antibodies, liposomes, micelles carriers, or others strategies can be used to give specificity to the delivery molecule thereby targeting the toxin specifically to the cancer cell and not to normal "non-cancerous" cells. For example, there are several groups that are trying to combine nanorods, different biological carriers and radiation prodrugs, (16,17) with cisplatin to target it specifically to cancer cells.

Scientists had expected that targeted cancer therapies would be less toxic than traditional chemotherapy drugs because cancer cells are more dependent on the targets than are normal cells. However, targeted cancer therapies can have substantial side effects (18,19). One is that cancer cells can become resistant to them. Resistance can occur in two ways: the target itself changes through mutation so that the targeted therapy no longer interacts well with it, and/or the tumor finds a new pathway to achieve tumor growth that does not depend on the target.

Photodynamic therapy (PDT)

PDT involves two individually non-toxic components that are combined to induce cellular and tissue effects in an oxygen-dependent manner. The first component of PDT is a photosensitizer, a photosensitive molecule that localizes to a target cell and/or tissue and the second component involves the administration of light of a specific wavelength that activates the sensitizer. The photosensitizer transfers energy from light to molecular oxygen, to generate reactive oxygen species (ROS). These reactions occur in the immediate locale of the light-absorbing photosensitizer. As example, compounds containing porphyrin provide properties required for PDT (20).

The principal drawback of this therapy is that the light needed to activate most photosensitizers cannot pass through more than about one-third of an inch of tissue

(25mm). For this reason, PDT is usually used to treat tumors on or just under the skin or on the lining of internal organs or cavities. PDT is a local treatment and generally cannot be used to treat cancer that has spread (metastasized).

There is currently one photosensitizing agent on the market, Photofrin® which is a photosensitizing agent, it is used for the ablation of high-grade dysplatia in Barrett's esophagus patients who do not undergo esophagectomy. However, like other cancer treatments, it has some side effects, which are photosensitivity reaction, nausea and chest pain (21).

Chemotherapy

Besides radiotherapy, chemotherapy is the second most widely used therapy for cancer treatment. The word chemotherapy means the use of any drug (such as aspirin or penicillin) to treat any disease, but to most people chemotherapy refers to drugs used for cancer treatment. Cancer chemotherapy was born in the late 1940s and early 1950 when mustine hydrochloride (mustard gas) was found to have anti-tumor and anti-leukaemic properties. While treatments like radiation and surgery are considered as local treatments chemotherapy is a systemic treatment.

There are three possible goals of the chemotherapy:

Cure: If possible, chemotherapy is used to cure the cancer, meaning that the cancer disappears and does not return. When giving a treatment that has a chance of curing a person's cancer, the doctor may describe it as treatment with curative intent.

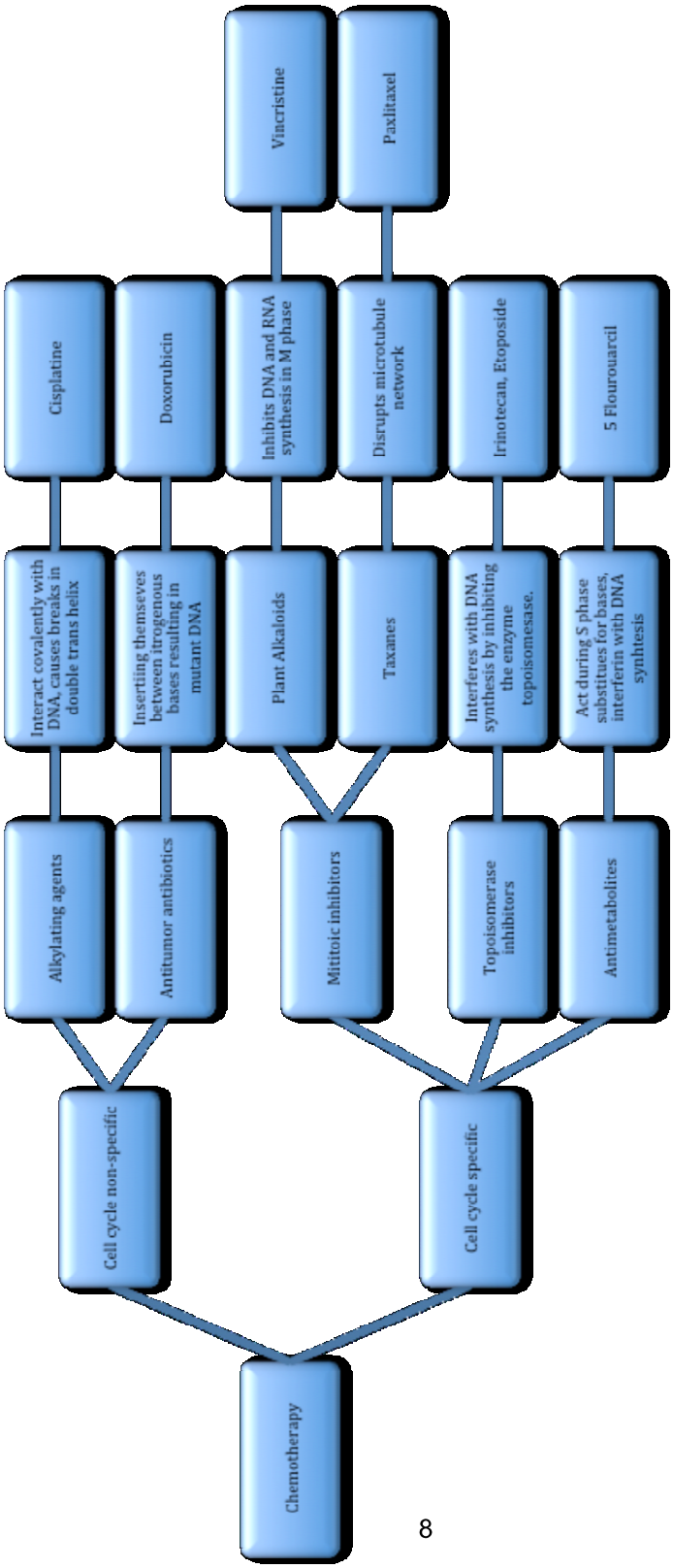
Control: If cure is not possible, the goal may be to control the disease by decreasing the size of tumors and/or stop the cancer from growing and spreading.

Palliation: When the cancer is at an advanced stage, chemotherapy drugs may be used to relieve symptoms caused by the cancer.

Like radiotherapy and targeted therapy, chemotherapy is often combined with surgery. It is estimated that 22% of patients with cancer are treated with chemotherapy. However, this treatment has two main drawbacks; the frequent strong side effects and the development of resistance that make the treatment ineffective (22-27).

Depending on the mechanism of action (cell cycle specific or non specific), chemotherapies are further classified into different families. In order to have a quick overview of this classification, I present this classification in the next schema.

Chemotherapy classification



Schema 1. Chemotherapy classification by mechanism of action

II. ORGANOMETALLICS IN CANCER

During my Ph.D. I could participate in the development of new organometallic anticancer drugs and the elucidation of their mechanism of action. Here I want to present why organometallics compounds are of great interest for the development of new anticancer therapies.

Since ancient times, metal compounds have been successfully used for the treatment of a variety of diseases. Egyptians knew about the therapeutic potential of gold salts. In chemotherapy, organometallic compounds have great interest and they play a key role in cancer treatment among today's society. For example, cisplatin is used in approximately 70% of all cancer patients (28).
Organometallic compounds are a type of coordination complexes containing at least one direct, covalent metal-carbon bond. They have a great structural variety (from linear to octahedral), which allows in comparison to organic compounds the synthesis of huge a variety of molecules with different stereochemistry in comparison to organic compounds. Furthermore, they are kinetically stable, usually uncharged, relative lipophilic and their metal atom is in a low oxidation state (29,30). Its precisely of these characteristics that organometallics offers ample opportunities in the design of novel classes of medicinal compounds, potentially with new metal-specific modes of action (31-33).

According to Pedro Martins et al. (34), the mechanism of action of an organometallic compound can be described at least in one of seven cases:

1. Direct binding of the metal fragment to the target.
2. The metal has a structural role and binding to the biological target occurs through non-covalent interactions.
3. The activity and assimilation is due to the organic ligands and the metal is a carrier for delivering them *in vivo*.
4. The metal center causes cell damage by inducing the production of reactive oxygen species (ROS).
5. The organometallic compound is photoactive and behaves as photosentitizer.
6. The metal is a radiation enhancer.
7. The metal is radioactive.

Among the organometallic ant-cancer drugs, it is estimated that 50-70% of cancer patients are treated with a platinum compound (35), among which cisplatin is the most famous and used one. However, and unfortunately, like other anti-cancer therapies, platinum base drugs can have strong side effect and the resistance issue can in some cases force the doctor to stop the treatment and in sever cases these drawbacks can lead to death (36).

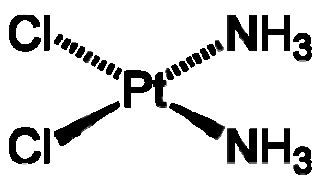
II.A. Platinium compounds

The modern era of metal-based anticancer drugs began with the discovery of the platinum(II) complex cisplatin, cis-diamminedichloroplatinum(II) (cis-DDP). Cisplatin was first synthesized by M. Peyrone in 1844 and its chemical structure was elucidated by Alfred Werner in 1893. In 1960 Barnett Rosenberg observed that bacteria and cells were killed in the electric field between platinum electrodes, making the molecule famous.

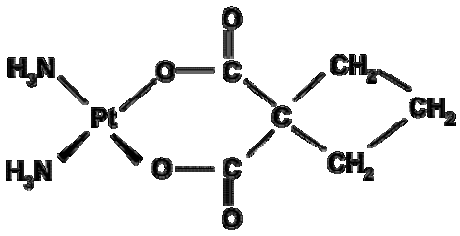
Nowadays, cisplatin and its successors carboplatin and oxaliplatin are among the most important chemotherapeutics used against a wide variety of different cancers (37). Cisplatin (1978), carboplatin (1989) and oxaliplatin (2002) are FDA approved platinum anticancer drugs that are used in clinic world wide for the treatment of sarcomas, ovarian, head and neck, bladder, cervical and lymphomas cancers, while nedaplatin, lobaplatin, and heptaplatin are only approved for clinical use in Japan, China and Korea (38), respectively.

Cisplatin (Platinol)

Cisplatin has been used for more than three decades in standard chemotherapy, either as a single therapeutic modality or in combination with other cytotoxic gents. The compound produces intrastrand and interstrand DNA cross-links and forms DNA adducts, thereby inhibiting the synthesis of DNA, RNA, and proteins. It is used as a first line treatment in testicular-, ovarian-, lung-, head-and-neck-, stomach-, colon-, bladder- and cervix-cancers (39).

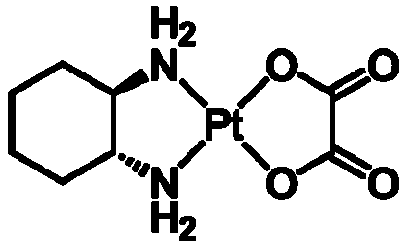


Carboplatin (Paraplatin)



Carboplatin or Cis diammine (1,1-cyclobutanecarboxylato) platinum (II) has the same active diamine platinum moiety like cisplatin, but it is bonded to an organic carboxylate group that allows increased water solubility and slower hydrolysis, resulting in a less reactive compound with diminished side effects, in particular the nephrotoxicity (40). Carboplatin induce the same types of DNA adducts like cisplatin, but a higher concentration (20 to 40 fold) of carboplatin is required to be efficient and the rate of adduct formation is about 10-fold slower. Carboplatin is currently part of the first-line combination therapy of ovarian and lung cancer. Unfortunately, its cross-resistance with cisplatin limits its application in cisplatin-resistant malignancies (41). Furthermore, the main drawback of carboplatin is its myelosuppressive effect, which refers to the decrease in the production of the blood cells and platelets, sometimes dropping as low as 10% of its usual production levels (42).

Oxaliplatin (Eloxatin)



Oxaliplatin is distinguished from the other platinum compounds by a di-amino-cyclohexane (DACH) ring, which is bound to the platinum molecule, and which interferes with resistance mechanisms to the drug. Oxaliplatin and cisplatin are structurally distinct, but form the same types of adducts. However, oxaliplatin adducts (DACH-Pt-DNA) are bulkier and more hydrophobic than cisplatin adducts. This DACH ring also confers a more effective inhibition of DNA synthesis and superior cytotoxicity. The differences in the structure between adducts produced by cisplatin and oxaliplatin are consistent with the observation that oxaliplatin adducts apparently are not recognized or processed by the miss match repair system (MMR) in the same way (cisplatin adducts are more easily recognized) (43). Furthermore, loss of MMR produces low levels of resistance to cisplatin, which is not the case for oxaliplatin (44).

II.B. Mode of action of Platinum compounds.

Cisplatin, carboplatin and oxaliplatin are composed of doubly charged platinum ion surrounded by four ligands. They have amine ligands on one side forming stronger interactions with the platinum ion, and chloride ligands or carboxylate compounds on the other side. This allows the formation of leaving groups, thus the platinum ion is capable to form covalent bonds with DNA (41).

Platinum compounds belong to the family of alkylanting agents making them highly reactive (45). Cisplatin becomes activated once it enters the cell. In the cytoplasm the chloride ions of cisplatin are displaced by water molecules, this hydrolyzed product is highly electrophic and can react with any nucleophile, including the sulfhydryl groups on proteins and nitrogen donor atoms on nucleic acids. Cisplatin binds to the N7 reactive center on purine residues triggering DNA damage, which leads to cell cycle arrest and subsequent apoptotic cell death (16,17,46-49).

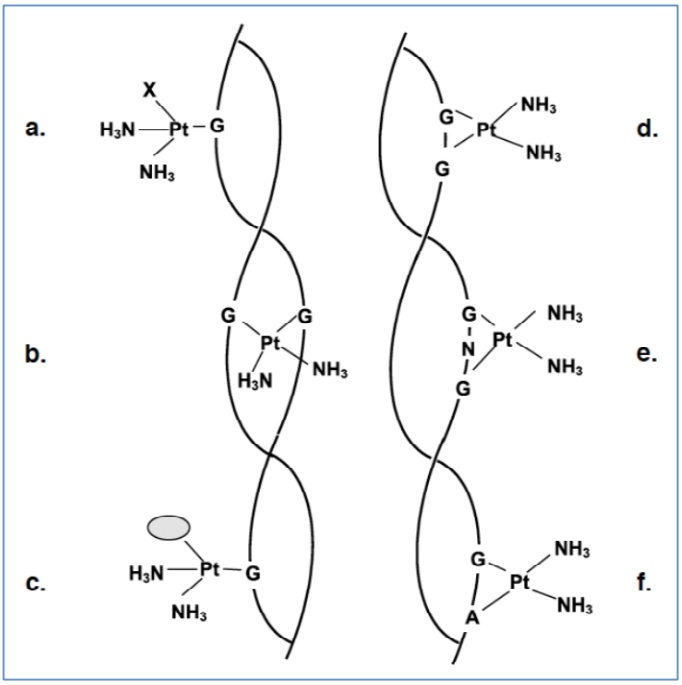


Figure 3. Different types of cisplatin adducts.

Image from Cancer Treatment Reviews ***28****:6, 291-303*

As mentioned above, platinum compounds form DNA adducts. The most abundant one are intrastrand crosslinks between two adjacent bases 1,2-d(GpG) (Figure 3d), and 1,2-d(ApG) (Figure 3f), with 65% and 25% of all DNA adduct cases, respectively. Minor adducts are, monofunctionally bound cisplatin to a guanine base (Figure 3a,c),

interstrand crosslinks (ICLs) between two guanines (Figure 3b) and intrastrand crosslinks between two guanines separated by one or more other bases (Figure 3e). However, which type of adduct is most responsible for the cytotoxic effect of cisplatin has never been fully elucidated (50).

II.B.1. Recognition of platinum–DNA adducts

The role of high-mobility group box proteins.

More than a dozen proteins have been identified that bind to cisplatin-modified DNA, recognizing specifically the 1,2-intrastrand crosslinks (47). Of these, the most important belong to the high-mobility group (HMG) box proteins. HMG-domain proteins are divided into two groups, sequence-specific and sequence-neutral. The biological functions of HMG-domain proteins are diverse and include chromatin remodeling, transcription initiation, and RNA polymerase nucleosome bypass. Several types of HMG proteins, including HMG1, HMG2 and UBF bind to DNA–cisplatin adducts with high affinity and specificity. The multifaceted nature of this protein family suggests that many different critical cellular functions may be interrupted as a result of these interactions (51). In this respect, the HMGB1 protein has been connected to several DNA-dependent pathways. For example it can interact with the DNA mismatch repair pathway, directly interact with the tumor-suppressor protein p53 and enhances p53 DNA-binding activity and the nuclear excision repair (51,52).

However, HMG-domain proteins are not the only ones that can bind to cisplatin-damaged DNA, other proteins involved in DNA damage recognition can also bind with it, particularly those involved in transcription-coupled nucleotide excision repair (NER) (47,53).

Cisplatin stimulates H2AX phosphorylation

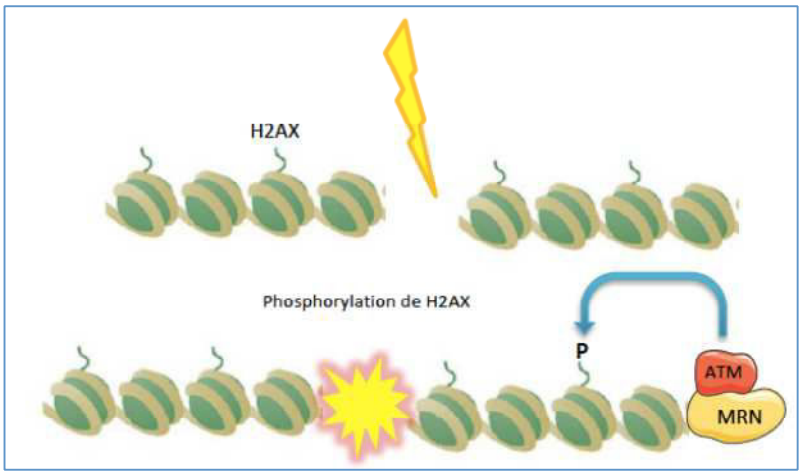


Figure 4. Phosphorylation of H2AX

Another mechanism by which double stranded breaks (DSB) are detected is due to the phosphorylation of histone the H2A histone family, member X (H2AX). DNA is normally wrapped around a core histone molecule forming the nucleosome complex. Histone cores are made up of individual histone proteins. One of those proteins is H2, and H2AX is a variant of the H2A protein family. H2AX is phosphorylated by kinases such as ataxia talagiectasia mutated (ATM) and ATM-Rad3-related (ATR), that in turn can induce other proteins like for example p53, Chk2, BRCA1, and others, leading to multiple cellular responses (apoptosis, cell cycle arrest, DNA repair). Phosphorylated γ-H2AX is the first step in recruiting and localizing DNA repair proteins. It has been shown that ionizing radiation or cytotoxic agents quickly lead to the formation of phosphorylated γ-H2AX containing foci, which showed to represent a robust biomarker for DSB (54,55)

II.B.2. DNA repair mechanism

The cellular response to platinum-DNA damage is complex and involves recognition and repair steps. Depending on the nature of the platinum-DNA lesion, one of two primary repair pathways that have been defined will be involved: mismatch repair and nucleotide excision (56).

Nucleotide excision repair (NER)

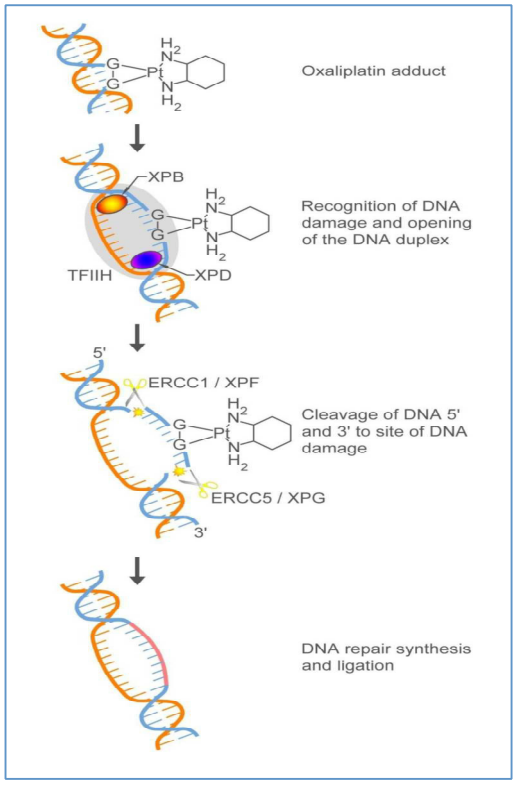


Figure 5. Nucleotide excision repair mechanism, interaction with oxaliplatin *Image from: Pharmaceuticals 2013, 6(8), 988-1038.*

Platinum-induced lesions cause distortions in DNA structure that are recognized by multiple DNA repair pathways. These DNA distortions are mainly repaired by the nucleotide excision repair (NER) system. The NER pathway consists of several steps: damage recognition, dual incision/excision, repair synthesis, and ligation. Approximately 30 proteins participate in this repair process (51,57).

NER can be divided into two subpathways: global genomic NER (GG-NER) and transcription coupled NER (TC-NER). In human cells, the lesions are recognized by different sets of proteins of these sub-pathways. After damage recognition, the general transcription factor complex TFIIH, containing the XPB and XPD helicases, mediates DNA strand separation at the site of the lesion. XPA verifies the damage and opens the DNA and replication protein A (RPA) stabilizes the opened DNA complex and is also involved in positioning the XPG and ERCC1–XPF endonucleases responsible for the DNA incisions around the lesion. After removal of the damage-containing oligonucleotides, typically 24–32 nucleotides in length, general replication factors fill in the remaining gap and close it (17,58-61).

It has been suggested, that the favorable clinical response of testicular cancer to cisplatin correlates with its low capacity for removal cisplatin–DNA adducts and low levels of the nucleotide-repair proteins XPA and ERCC1-XPF. These observations are consistent with the idea that the modification of DNA by cisplatin is the major mechanism of its cytotoxicity and that the NER pathway primarily corrects the dominant cisplatin lesions (52).

Homologous recombination pathway (HR)

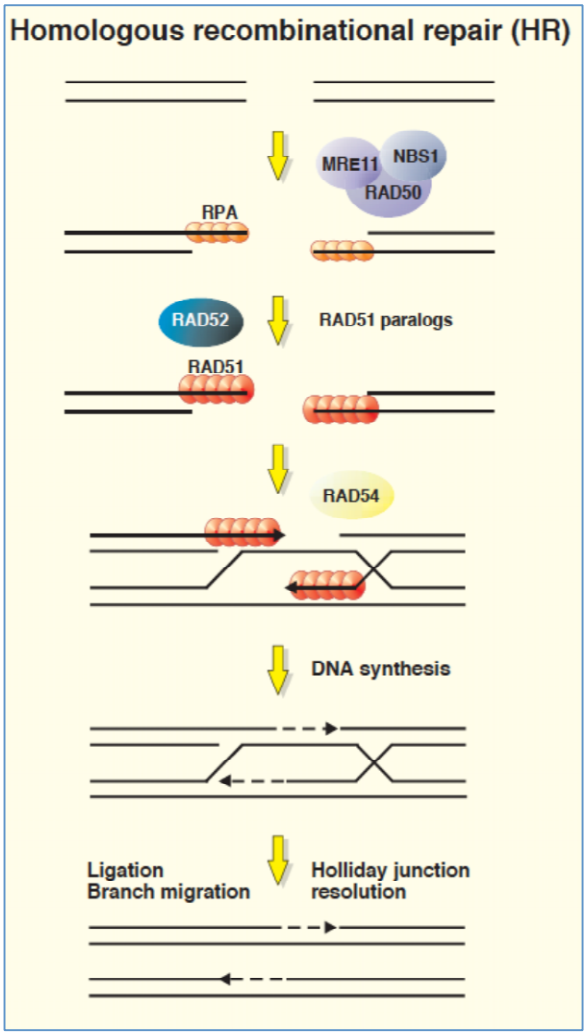


Figure 6. Homologous recombination repair. *Image from: Journal of Cell Science 117, 515-517,2004*

Although to a lesser extent, platinum compounds can also cause platinum-DNA interstrand adducts, which are repaired by the homologous recombination pathway (HR) (50).

This pathway is associated with BRCA1/2 and plays an important role in platinum sensitivity (56). HR uses a homologous DNA template and is highly accurate, whereas NHEJ rejoins the broken ends without using a template and is often accompanied by loss of some nucleotides. During HR, double strand breaks (DSBs) are converted to 3' single-stranded DNA (ssDNA) tails, which are bound by RPA. Processing of DSBs probably then requires the MRE11-RAD50-NBS1 complex. RAD52 interacts with RPA and promotes binding of RAD51 to the ssDNA. Subsequently, the RAD51 bound ssDNA invades a homologous molecule in a reaction stimulated by RAD54. After DNA synthesis and ligation, two Holliday junctions are formed and branch migration occurs (62).

Accumulating evidence suggests that BRCA1 functions not only in association with the DNA repair machinery, but also in DNA damage induced cell cycle checkpoint control. Additionally, BRCA1 may regulate the expression of genes involved in DNA damage repair and, significantly, it directly participates in the repair process itself (56,63). In this respect, BRCA1/2-deficient cancers often have a better response to DNA cross-linking agents such as platinum analogs, and to poly (ADP-ribose) polymerase (PARP) inhibitors.

Non- Homologous End Joining (NHEJ)

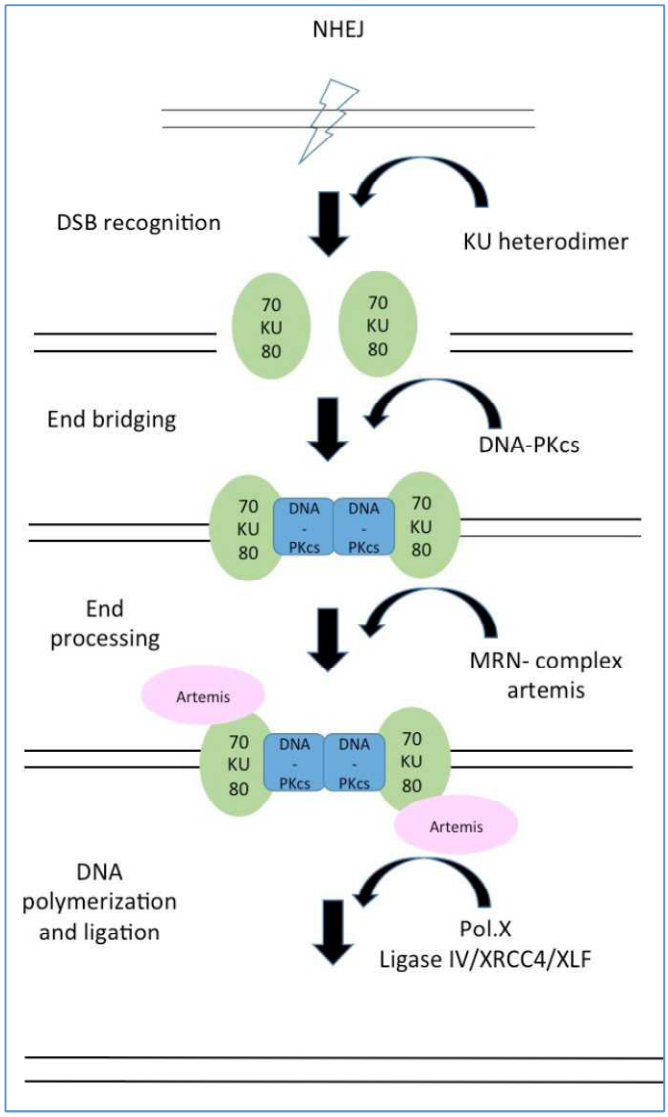


Figure 7. NHEJ pathway
Nature 447, 951-958 (21 June 2007)

NHEJ pathway promotes double strand repair in all phases of the cell, whereas HR only in S phase. NHEJ uses a simple splice mechanism to rejoin the two free ends of DNA. The process is initiated by binding of the KU70–KU80 heterodimer to the free dsDNA ends and involves the activation of downstream steps by the binding of DNA-dependent protein kinase catalytic subunit (DNA-PKcs). Damaged DNA is processed to remove any 5′- or 3′-ssDNA tails, and the resulting ends are directly rejoined by the DNA ligase IV-XRCC4 complex (64).

Human cells that are defective for KU70, KU80, DNA-PKcs, DNA ligase IV or XRCC4, are insensitive to platinum or other interstrand crosslinks-inducing (ICL) drugs, confirming the studies made in yeast and mice showing that the NHEJ pathway is not required for ICL repair (65).

Mismatch repair (MMR)

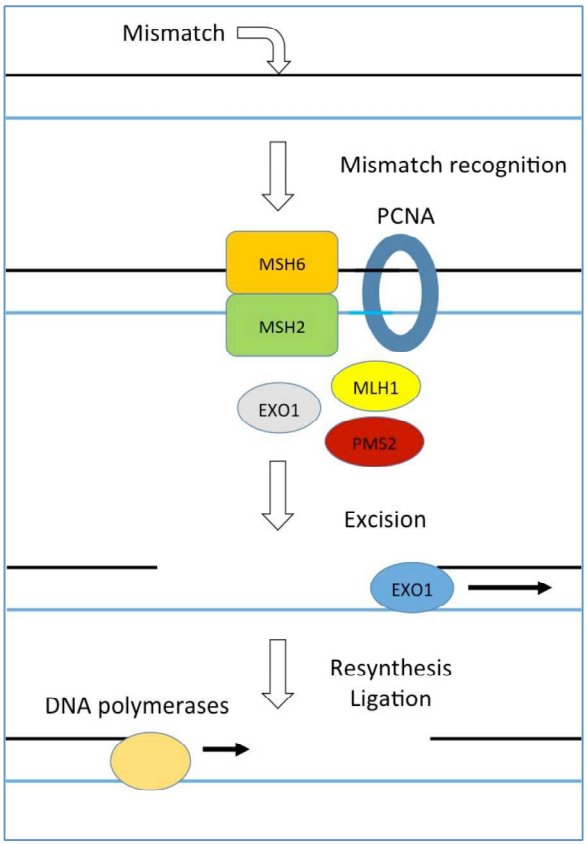


Figure 8. Mismatch repair process.
Figure modified from "DNA Repair - On the Pathways to Fixing DNA Damage and Errors" book edited by Francesca Storici in 2011

Another mechanism used to repair DNA damages induced by platinum drugs is the mismatch repair (MMR). The function of the MMR is to scan newly synthesized DNA and remove mismatches that result from nucleotide incorporation errors made by DNA polymerases. The initial step of MMR is the binding of MSH2–MSH6 heterodimers to single base-pair mismatches. MLH1–MLH3, post-meiotic segregation 2 (PMS2), as well as the EXO1 exonuclease, are then recruited to this complex, and Proliferating cell nuclear antigen (PCNA) links then the DNA polymerase to the DNA template and the complex. The lesion is then digested by exonucleases, such as EXO1, and filled-in by translational and/or replicative DNA polymerases.

Normal function of MMR seams to be important for the efficacy of platinum compounds because its dysfunction it may result in cisplatin resistance or tolerance (66). For example, in human ovarian tumor cell lines selected for cisplatin resistance, the resistance phenotype is often correlated with a reduction or loss of expression of MSH2 or MLH1. However there is a lot of discrepancy about this subject and until now there are no strong data to proof a relation between MMR and cytotoxicity of cisplatin (52).

II.B.3. Cisplatin and p53

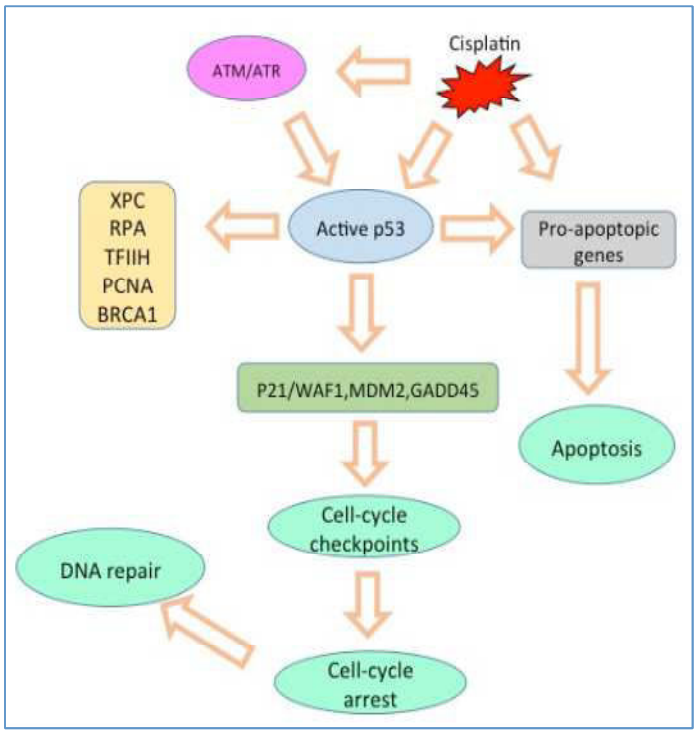


Figure 9. Activation of p53 by cisplatin
Modified from Nature Reviews Vol.4, 2005

p53 is an important tumor-suppressor protein that is mutated in more than 50% of all human tumors. The p53 protein has a crucial role in many cellular processes; in particular it inhibits cell proliferation by inducing either cell-cycle arrest or apoptosis in response to cellular stress.

Upon DNA damage, ATM phosphorylates and thereby activates p53 leading to the up-regulation of its target p21/Waf1, the 45kd-growth arrest and DNA damage (GADD45), and mouse double minute 2 homolog (Mdm2). In this way p53 participates in the mechanisms regulating cell cycle progression and DNA repair. For example, p53 can interact with crucial components of the nucleotide excision repair (NER) machinery, such as XPC, TFIIH and RPA, indicating a role in DNA repair (49).

Moreover, p53 also activates the apoptotic process, which depends on the ratio between Bax and its opposing but closely related antiapoptotic counterpart Bcl-2. For instance, exposure of cells to cisplatin leads to the activation of p53 and the Bax : Bcl-2 ratio increases and apoptosis proceeds (49).

Although p53 plays an important role in cisplatin induced DNA damage response, it does not always depend on it, suggesting the existence of alternate pathways. The relationship between p53 status and cisplatin cytotoxicity depends on several factors, including tumor cell type, activation of specific signaling pathways and the presence of other genetic alterations (40,52).

II.B.4. Cisplatin and oxidative stress

Generation of Reactive oxygen species (ROS) is a normal physiological process that has an important role in cell metabolism, proliferation, differentiation, cell death, angiogenesis, metastasis and tumor invasion other processes. It is therefore not surprising that the cell has developed sophisticated mechanisms and specific redox-enzymes maintaining the redox balance within the cell (28).

Some of these specific redox-enzymes are:

Superoxide dismutase: which catalyze the dismutation of O_2•- in to oxygen or into H_2O_2 In humans, there are three kinds of SOD: the cytosolic Cu/Zn-SOD, the mitochondrial Mn-SOD, and the extracellular SOD (again containing a Cu/Zn core).

Catalase: a heme-based enzyme, which catalyzes the transformation of H_2O_2 in to water and oxygen, it can scavenge ~6 million molecules of H_2O_2 per minute.

Thioredoxin reductases (trxR) : catalyzes the reduction of the small redox protein thioredoxin by NADPH dependent mechanism. It is playing an important role in the mechanisms controlling the intracellular redox environment, cellular growth, and apoptosis. For example this enzymes are capable to inhibit HIF-1 and VEGF.

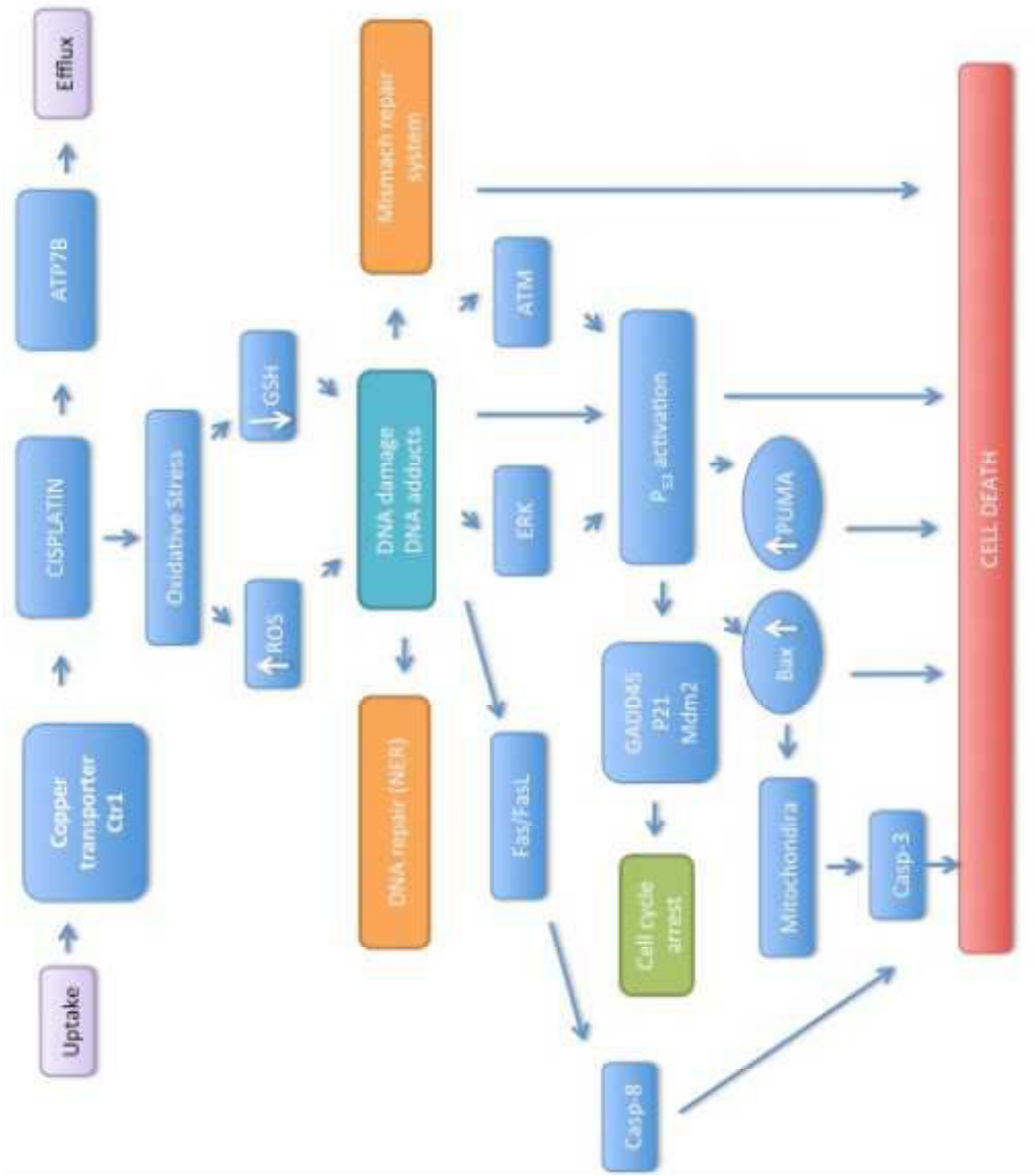
Glutathione peroxidases (GPx) : is the general name for a family of multiple isozymes. So far five GPx have been identified in humans (all containing selenium) that catalyze the reduction of H_2O_2 or organic hydroperoxides to water (or corresponding alcohols) using reduced GSH as an electron donor.

In general, disturbance of the oxidant-antioxidant balance is called *oxidative stress*. Cancer cells exhibit greater reactive oxygen species stress than normal cells do, partly due to oncogenic stimulation, increased metabolic activity and mitochondrial malfunction (67,68). The main ROS having physiological relevance are superoxide (O_2•-), hydrogen peroxide (H_2O_2), as well as the hydroxy radical (OH•).

Cisplatin, besides inducing DNA damage, also induces reactive oxygen species that can trigger cell death. In this respect it has been shown, that oxidative stress is one of the most important mechanisms involved in cisplatin-induced nephrotoxicity. The mitochondrion is the primary target for cisplatin induced oxidative stress, resulting in loss of mitochondrial protein sulfhydryl groups, calcium uptake inhibition and

reduction of mitochondrial membrane potential. However, the formation of reactive oxygen species strongly depends on the concentration of the drug and the duration of the exposure (40,69).

II.C. Conclusion Schema of Cisplatin Mechanism of Action



Schema 2. Conclusion of Cisplatin Mechanism of Action.

II.D. Cisplatin Drug Resistance

A major clinical limitation of the use of cisplatin is the intrinsic or acquired resistance to the drug. Cisplatin resistance is a multifactorial process and can arise from reduced platinum uptake, increased efflux, intracellular detoxification by glutathione, metallothioneins and other antioxidants, increased DNA repair (nucleotide excision repair and mismatch repair), changes in DNA methylation status, defective apoptosis, modulation of signaling pathways, or presence of quiescent non-cycling cells (39,40,49,56).

II.D.1. Transporters and Reduced platinum accumulation

One of the most prominent characteristics of cellular resistance to cisplatin is the decreased uptake or increased efflux of cisplatin leading to lower intracellular concentrations of the drug.

Copper transporter 1 in Cisplatin uptake

In addition to passive diffusion, copper transporter CTR1 is a major influx transporter that plays an important role in mediating uptake of platinum compounds (70). Genetic knockout of CTR1 results in cellular resistance to cisplatin. Cells with increased CTR1 expression exhibit increased platinum accumulation and, in most instances, increased sensitivity to cisplatin (40,56,71).

ATP7A/B efflux

ATP7A and ATP7B (Copper-transporting ATPase 1) proteins have been proposed to be involved in cellular import and export of cisplatin, carboplatin, and oxaliplatin (72). They are located in the trans-Golgi and are known to mediate the copper homeostasis (73). Overexpression of these transporters is associated with increased resistance of cells to cisplatin, carboplatin, and in some cases oxaliplatin (74). However, it is not known whether either ATP7A or ATP7B function directly as transporters of cisplatin (52).

Inactivation of cisplatin by Glutathione

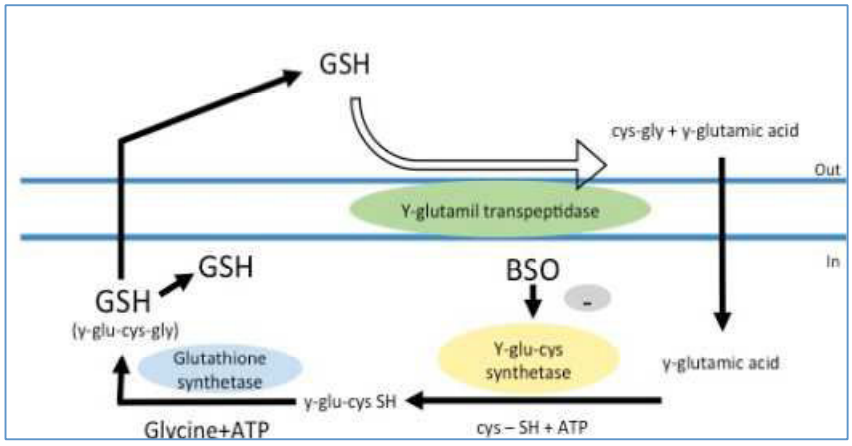


Figure 10. Glutathione synthesis.

Glutathione can participate directly or indirectly in many important cellular functions including detoxification of xenobiotics, amino acid transport, synthesis of DNA precursors, and protection from free radical damage. Cisplatin is able to react directly with sulfur groups (such as glutathione) and intracellular levels of glutathione have been linked to cisplatin detoxification and inactivation (75). Elevated GSH levels have been found in some cisplatin resistant cell lines and depletion of GSH by BSO increased cisplatin sensitivity of some cell lines but not of others (76). This feature is of great interest because doctors could pretreat cancer patient with BSO, which could potentiate the toxicity of cisplatin (77).

II.D.2. Novel Mechanisms of Cisplatin Resistance

Transmembrane Protein 205 and Cisplatin Resistance.

Shen's group in 2010 report what may be a novel mechanism of cisplatin resistance (78). They identified a membrane protein named TMEM205, which expression showed to be increase in the cispaltin resistant cell line CP-r and which when over expressed confers approximately 2.5-fold resistance to cisplatin. Analysis of TMEM205 expression profiles in normal human tissues indicates a differential expression pattern with higher expression levels in the liver, pancreas, and adrenal glands. The authors concluded that overexpression of TMEM205 may play a role in cellular resistance to platinum and could also be a valuable biomarker or target in cancer chemotherapy. However, the exactly mechanism of action is not well established, but TMEM205 has been shown to be co-located with RAB8 a known GTPase involved in vesicular traffic (40,56,78).

II.E. Strategies for overcoming cisplatin resistance

Based on the above described mechanisms of cisplatin resistance, several strategies have been proposed to circumvent the resistance phenotype. Specifically targeting the resistance mechanism can be achieved by increasing cisplatin accumulation in tumors, interfering with cisplatin detoxification pathways, and modulating DNA repair. There exist preclinical studies that use the proteasome inhibitor bortezomib that prevents the degradation of the influx transport hCTR1 in ovarian cancer cells. This study showed the increase in cisplatin accumulation in tumor cells and tumor efficacy. Other compounds like the anticancer agent 6-(7- nitro-2,1,3-benzoxadiazol-4-ylthio)hexanol (NBDHEX), an inhibitor of GST, and molecules that inhibit specifics DNA repairs pathways (Chk1 inhibitors) are in clinical trials showing encouraging results (46).

II.F. Cisplatin side effects

Cisplatin treatment has been associated with several toxic side effects and below is a short description of the most frequent and most severe side effects.

Cardiotoxicity: Different cardiac events have been reported in many case reports where cancer patients have been treated with cisplatin including electro-cardiographic-changes, arrhythmias, myocarditis, cardiomyopathy and congestive heart failure.

Hepatotoxicity: Cisplatin hepatotoxicity has been shown to be exacerbated by increased expression of cytochrome P450-2E1 enzyme. Recent studies have shown that selenium agents could protect from cisplatin-induced Hepatotoxicity (79).

Nephrotoxicity: Nephrotoxicity has been classified to be the most severe drug-related adverse effect, renal lesions are primarily observed in the proximal tubules characterized by hydropic degeneration, necrosis and occasional tubular atrophy. The kidney accumulates cisplatin to a greater degree than other organs and is the major route for its excretion (46,80). Studies made in rats showed that the inhibition of L-carnitine by cisplatine is the main reason of kidney toxicity (81,82).

Myelotoxicity: Compared to cisplatin and oxaliplatin, carboplatin exerts the highest myelosuppressive effect, this causes thrombocytopenia (decrease of

thrombocytes, commonly known as platelets, present in the blood) and neutropenia (low number of neutrophils – a white blood cell).

Gastrointestinal toxicity: Among the clinical approved platinum-compounds cisplatin exerts the greatest emeotogenic effect (induce vomit). More than 90% of patients who received cisplatin have around ten vomiting episodes within the first day of administration in the absence of affective antiemetic therapy (drug that is effective against vomiting and nausea). Nausea, vomiting and diarrhea are common adverse effects of oxaliplatin and carboplatin but hey are generally mild or moderate and less emeotogenic than cisplatin.

Neurotoxicity: The mechanism of cisplatin-induced neurotoxicity has not yet been fully elucidated. Cisplatin appears to affect neurons in the dorsal root ganglia. In addition it may act as a calcium channel blocker, altering intracellular calcium homeostasis resulting in apoptosis of exposed neurons (83). Cisplatin-induced sensory neuropathy, which is predominantly characterized by symptoms such as numbness and tingling, parenthesia of upper and lower extremities, reduced deep-tendon reflexes and leg weakness with gait disturbance (80,84).

Other less frequent occurring side effects are: ototoxicity (hearing loss), skin toxicity and visual disturbance are reported (26,80,85).

Regardless of the achievements of current platinum drugs, there are some major drawbacks: they are efficient only on a limited range of cancers; some tumors can have acquired or intrinsic resistance; and they often cause severe side-effects. In this respect, to over come the problems associated with the use of platinum drugs researchers have over the past years intensively investigated the use of other metals for the development of new organometallic compounds.

During my Ph.D., I worked on the development of new Ruthenium based anti-cancer compounds.

III. RUTHENIUM COMPOUNDS

III.A. Interesting Ruthenium Features.

From all the metals investigated so far to replace Cisplatin, like gold, rhenium, rhodium, titanium, manganese, iron, etc. ruthenium turned out to show the most promising results. Indeed, ruthenium compounds exhibit high cytotoxicity against cancer cells, they are no cross-resistances with cisplatin, and they display reduced toxicity on healthy tissues (86). Therefore ruthenium-based compounds may represent new and efficient therapeutic agents to be used as an alternative to platinum drugs.

In 1950's, the Australian chemist Francis Dwyer started to investigate the biological activities of simple coordination complexes such as ruthenium complexes with 2,20 -bipyridine and 1,10-phenanthroline (phen) ligands. He discovered that some very hydrophobic complexes displayed bacteriostatic and bacteriocidal activities and were capable of inhibiting tumor growth in a mouse xenograph model (87).

In the 1970's Clarke et al. reported pentaammine- (purine)-ruthenium(III) complexes capable of inhibiting DNA and protein synthesis in human nasopharyngeal carcinoma cells *in vitro*, which triggered the interest in ruthenium complexes as potential anticancer pharmaceuticals (88). Today, there are two Ru-based anticancer drugs in clinical trials: NAMI-A, developed in Trieste by Mestroni, Alessio, and coworkers, and KP1019, developed by Keppler and coworkers in Vienna.

According to the literature ruthenium compounds have four main features (89-93):

- The possibility, to occupy a high number of spatial positions with up to 30 stereo isomers due to their expanded set of octahedral coordination geometry, and to carry a high number of potential accessory molecules.
- The access to the oxidations states II, III and perhaps IV in the biological fluids. The possibility to get low reactive prodrugs with the ruthenium ion at +3 oxidation state that can be reduced and, then activated selectively in solid tumor masses where the low oxygen content can create a reducing environment. This hypothesis is referred to by Michael Clarke as: the selective mechanism of "activation by reduction".

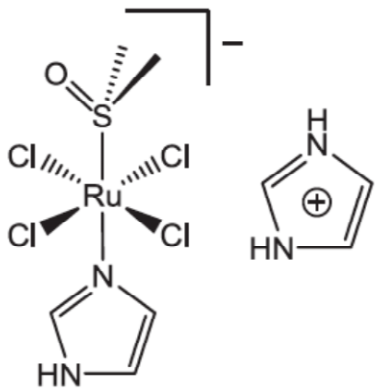
- They have a slow ligand exchange kinetics and the facility to exchange with O- and N-donor molecules in a way very similar to that of platinum drugs.
- The ability of ruthenium to mimic iron in binding to biomolecules such as human serum transferrin and other proteins, which makes ruthenium-based agents markedly less toxic than platinum drugs. It is presumed that they have the capacity to be transported into tumor cells by transferrin, given the presumed higher need of iron of these rapidly dividing cells.
- They can bind to DNA in a different manner than that of platinum drugs.

III.B. Different Ru based molecules.

One of the first ruthenium compounds described to have anticancer activity was ruthenium red, and further work showed the anticancer potential of ruthenium-containing drugs. Since then, several teams have synthesized and characterized new compounds containing ruthenium(II) or ruthenium(III). Here I will show the main compounds studied and characterized so far, but there are many other compounds which so far are less developed and less characterized.

III.B.1. NAMI-A

-



[ImH][trans-RuCl4(DMSO)(Im)] (Im = imidazole, DMSO = dimethylsulfoxide) (NAMI-A), is a Ru(III) complex molecule with DMSO and imidazole coordinated to the ruthenium. This class of compounds are studied by Giovanni Mestroni and Gianni Sava.

NAMI-A was the first ruthenium drug to reach human clinical development. A phase I, and pharmacokinetic study using this agent, began in 1999 and was reported in 2004 (94). In this study the dose finding and PK determination were done, as well as the toxicity evaluation in 24 patients with a wide variety of metastatic solid tumors (including colorectal, lung, melanoma, ovarian, and pancreatic cancers) refractory to conventional therapies were treated according to a dose escalation protocol.

Nami-A and antimetastatic effects.

Metastasis refers to the capability of a cancer cell to leave the primary tumor, travel via the circulation to a distant tissue site, and form there a secondary tumor. Metastasis process consists of five main steps that are collectively termed the metastatic cascade (95).

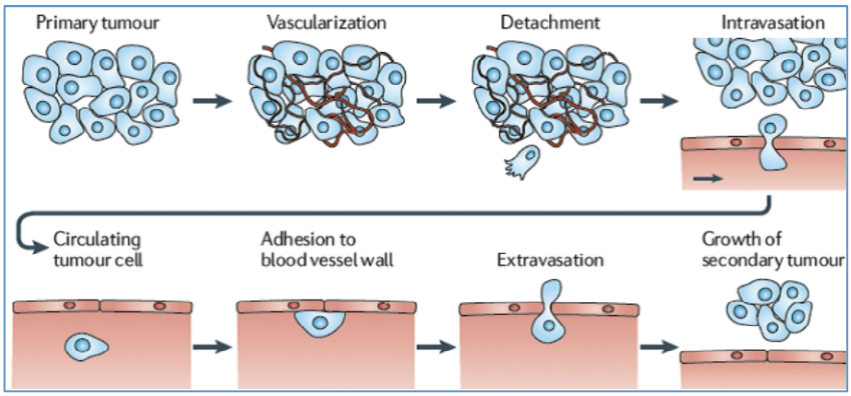


Figure 11. Cancer metastasis.
Image from the website http://wirtzlab.johnshopkins.edu

1) Detachment and migration: Individual cells detach from the primary tumor and invade adjacent, healthy tissue. During this process, several lytic enzymes are secreted which degrade the ECM (extracellular matrix) such as fibronectin and collagen, therefore, facilitate migration cell. In addition molecules like integrins and the transforming growth factor (TGF) have also an important role in this step.

2) Intravasation: The intrusion of cancer cells into the blood and lymphatic vessels. After the attachment on the endothelial cells via adhesion molecules, the neoplastic cells secrete proteolytic enzymes enabling them to infiltrate the blood vessel.

3) Circulation: The aberrant cell travels via the blood stream and has to withstand the conditions present in the blood. These are toxic for cancer cells due to the high concentration of oxygen and cytotoxic lymphocytes. A selection for particularly resistant and aggressive tumor cells takes place.

4) Extravasation: The cells often get stuck in the capillaries of an organ and leave the blood stream by penetrating the endothelium through proliferation and/or proteolytic enzymes. Metalloproteins have a key role in this step because they can enhance tumor survival and invasion.

5) Colonization, proliferation and angiogenesis: The neoplastic cell settles at a distant tissue site and starts a secondary tumor. The latter proliferates and induces neo-angiogenesis in order to ensure sufficient vascularization.

In this respect, it has been shown that NAMI-A is capable of effectively inhibiting the development and growth of pulmonary metastases in all solid tumors tested so far, including human tumors (non small cell lung cancer) engrafted into nude mice. NAMI-A is capable not only of preventing the formation of metastases but also of inhibiting their growth once established. In the panorama of Ruthenium drugs existing today, NAMI-A is the only one capable of such selective and unique property to stop lung metastases with high efficiency (96). However and unfortunately, NAMIA-A appears to lack direct cytotoxic effects (97,98).

Mechanisms of action of NAMI-A

The proposed mechanisms of action conferring its antimetastatic effect can be attributed to its interact with integrins, in particular the beta-1 integrins (96). In addition, it is also capable to trigger fibrotic reactions to tumor growth mediated by a balanced regulation of TGFβ1 in fibroblasts and tumor cells, inhibits matrix metalloproteinases like MMP-2 and MMP9 (99) and can increase extracellular matrix around the tumor vasculature, preventing neoplastic cells form invading nearby tissues and blood vessels (91,100).

Another important characteristic of NAMI-A is that it alters tumor angiogenesis. It was shown that NAMI-A almost entirely inhibits neo-angiogenesis induced by vascular endothelial growth factor (VEGF) resulting from apoptosis of endothelial cells via the modulation of protein kinase C, dephosphorylation of extracellular signal-regulated kinase (ERK) and inhibition of c-myc transcription (101).

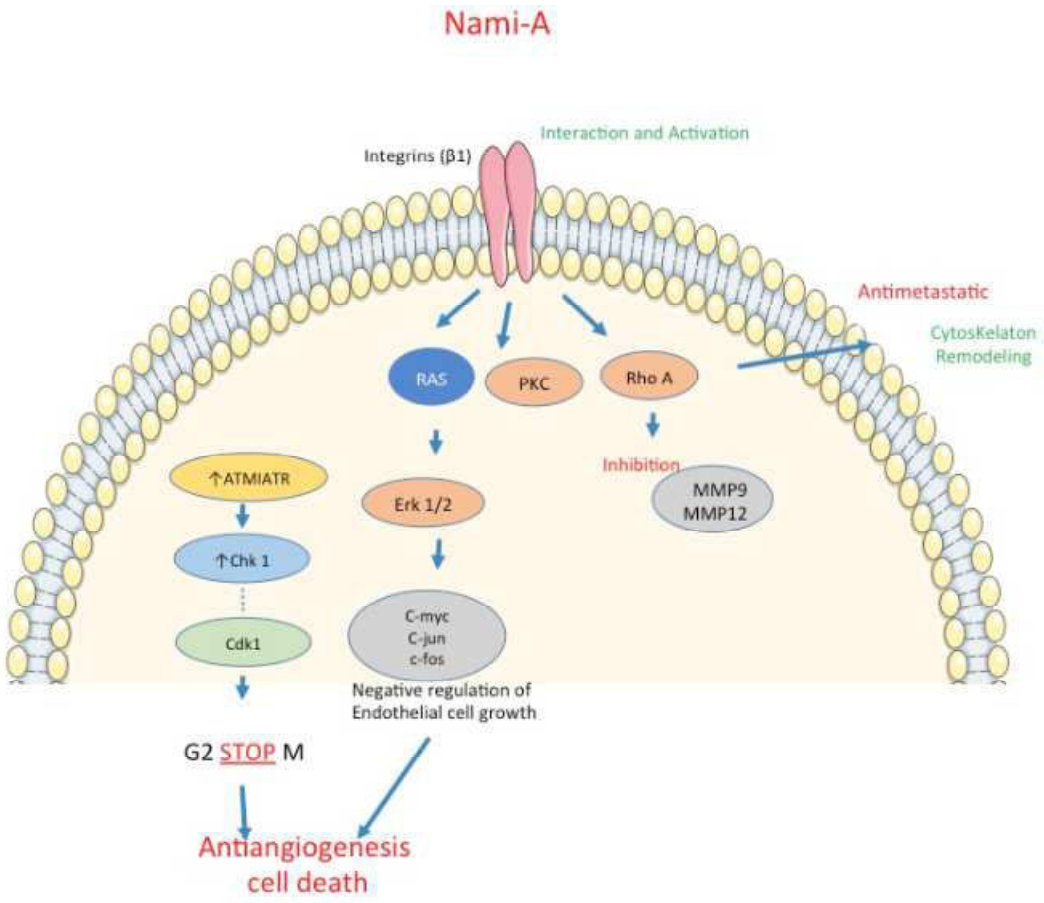


Figure 12. General mechanism of action of Nami-A (89,91,94).

Tissue Distribution

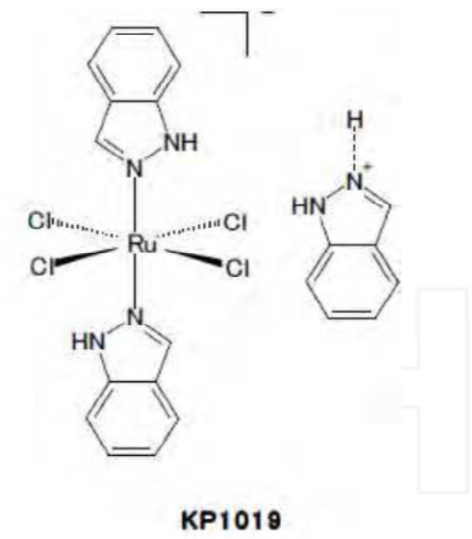
When given intravenous (i.v) or intraperitoneal to mice and rats, NAMI-A distributes to the whole body concentrating in collagen rich tissues (both fibrillar or basement membrane collagens), the kidney and the liver. In mice, blood half time presence following i.v. administration is about 20 h; t the half time presence in the lungs (organ rich of collagen) is about 180 h while the half time presence in the kidney (principal eliminating organ) is about 90 h. (91,100).

Clinical Protocol and Side effects

Patients received NAMI-A as a 3 h intravenous infusion daily for 5 days every 3 weeks. Twelve dose levels were administered in two-patient cohorts, ranging from 2.4 mg/m2 /day (12 mg/m2 /cycle) to 500 mg/m2 /day (2500 mg/m2 /cycle). At a dose of 400 mg/m2 /day, patients developed transient painful blisters on the hands and feet. At 500 mg/m2 /day, blisters developed again and persisted for weeks to

months. Formation of blisters was considered a dose-limiting toxicity, which was used to define the maximum tolerated dose recommended for phase II studies.
Other side effects of NAMI-A included anemia, lymphopenia, fatigue, anorexia, stomatitis, peripheral edema, alopecia, nausea (controlled with granisetron), diarrhea, tinnitus, and infusion-site phlebitis. Biochemical abnormalities included mild creatinine elevations (all reversible in less than 3 weeks) and hyperbilirubinemia. Two patients experienced hypersensitivity reactions that resolved with dexamethasone.

III.B.2. KP1019



KP1019

Indazolium trans-[(tetrachloride)bis(1H-indazole)ruthenate(III)] (KP1019). Four equatorial chlorides and two symmetrical axial N-donor heterocycles characterize the molecule. This molecule has been developed by Keppler and co-worker. KP1019 is the second ruthenium-based molecule to enter clinical trials (102). KP1019 is generally considered a prodrug, with a reduction potential accessible to biological reductants. Indeed, it has been suggested that KP1019 undergoes activation *in vivo* through reduction from Ru (III) to Ru (II), which then promotes interactions with biomolecules after labilization of the Ru (II)–Cl bonds (88). KP1019 showed limited cytotoxic effects, and studies reported that the cytotoxic effect is mediated by oxidative stress, inducing the formation of H_2O_2 in the cells. Moreover, the induction of apoptosis was characterized by the down-regulation of bcl2, causing the depolarization of the mitochondria and activation of caspace 3 (103). KP1019 undergoes DNA interactions similar to cisplatin but with a 15 fold lower intensity in terms of DNA-DNA and DNA-protein crosslinks. Also KP1019 induces DNA strand-breaks they are not sufficiently severe to induce cell death (91).

KP1019 and iron metabolism

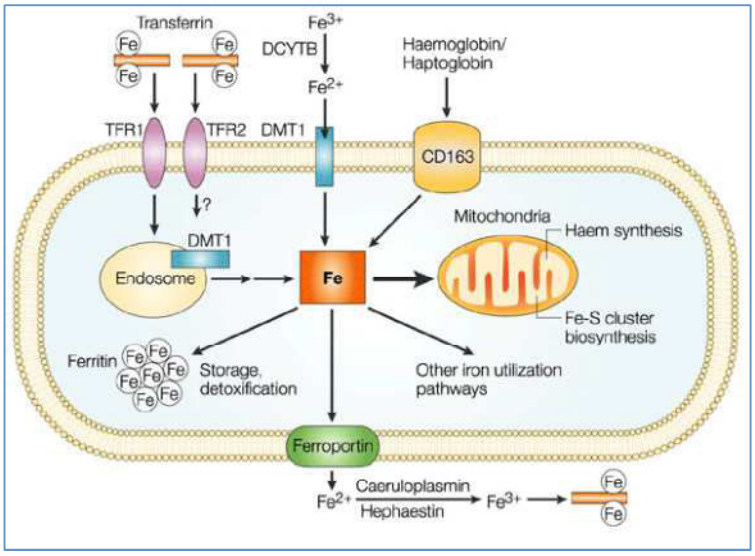


Figure 13. Iron metabolism.

Image from Nature Reviews Microbiology 2, 946-953 (December 2004)

In general, Iron is delivered to tissues by circulating transferrin, the binding of the transferrin to the cell-surface transferrin receptor 1 (TFR1), which is expressed on the surface of the cell, allows the iron transfer to the early endosome. Fe^{3+} is reduced to Fe^{2+} by the cytochrome b-like ferrireductase (Dcytb). Divalent metal transporter 1 (DMT-1) further functions to transfer Fe^{2+} across the endosomal membrane into the cytoplasm. Iron is then transported to mitochondria for the synthesis of haem or iron–sulfur clusters. Furthermore, ferritin is localized in the cytosol and is in charge of the storage of the excess iron and the detoxification. Finally, ferroportin function is to export iron outside the cell (104). From the chemical point of view, ruthenium is closely related to iron for two reasons: i) a good affinity to transferrin and ii) and the necessity of being activated by reduction into the more active Ru (II) state. KP1019 is administered intravenously and known to interact with serum proteins, which is of great relevance. In fact, studies have shown strong affinities for both compounds to proteins in the bloodstream, particularly transferring and serum albumin (105). Accordingly, it has been suggested that these proteins act not only as ruthenium carriers and delivery systems, but are also essential for tumor targeting (102).

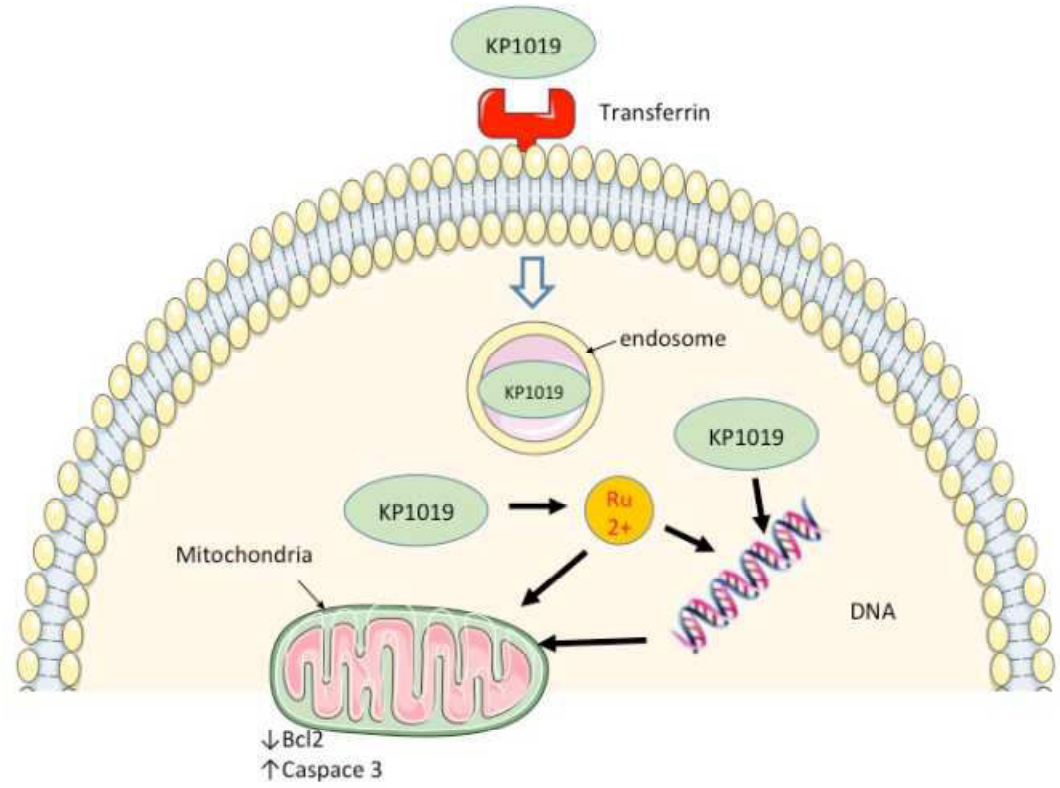
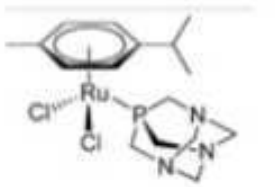


Figure 14. KP1019 mechanism of action (92,106).

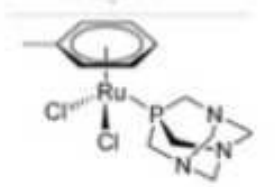
Clinical Protocol

KP1019 has already completed a phase I clinical trial with eight patients with various types of solid tumors refractory to standard therapy. These patients were treated with escalating doses of KP1019 starting at 25mg/ patient and stopping at 600mg/patient, because of solubility problems of the drug, twice weekly for 3 weeks (102). No dose-limiting toxicity occurred and only mild toxicities related to the treatment have been observed. The pharmacokinetic disposition was characterized by a small volume of distribution, low clearance and long half-life. Furthermore, Only a small fraction of ruthenium was excreted by the kidneys (102,107,108).

III.B.3. Rapta T



RAPTA-C



RAPTA-T

Rapta compounds (Ruthenium Aeren PTA, where PTA= (1,3,5-triaza-7-phosphoadamantane), were developed by Dyson and co-workers, and are characterized by the presence of the PTA. This ligand confers biological characteristics that make these complexes to be selectively activated in the hypoxic milieu of solid tumors.

RAPTA was inspired by the Sadler molecule RM175, in where the chelating ligand ethylendiamine was replaced with the PTA group, in order to achieve a selective activation at low pH levels, which is a characteristic of hypoxic solid tumors. *In vitro*, RAPTA-T inhibited some steps of the metastatic process such as detachment from the primary tumor cell mass, migration/invasion, and re-adhesion to a new growth substrate in MDA-MB-231 cells line. *In vivo* RAPTA-C and RAPTA-T showed to inhibit lung metastasis with however only mildly effect the primary tumor. This antimetastatic effect appears to be related with the proteins of the extracellular matrix such as fibronectin and collagen. Because of this results the authors suggested that RAPTA-T can modulate the cytoskeleton (109,110).

Mechanism of Action of Rapta T

RAPTA-C is capable to inhibit cell growth by triggering G2/M phase arrest and apoptosis in Ehrlich ascites carcinoma cells lines by increasing the p21 expression in a p53-dependent manner and by decreasing the expression of cyclin E. RAPTA-C treatment triggered the mitochondrial apoptotic pathway, this was confirmed by the change in Bax to bcl-2 ratios, resulting in cytochrome c release and caspase-9 activation. In addition c-Jun NH2 - terminal kinase (JNK) was proven to be a critical mediator in RAPTA-C-induced cell growth inhibition (111).

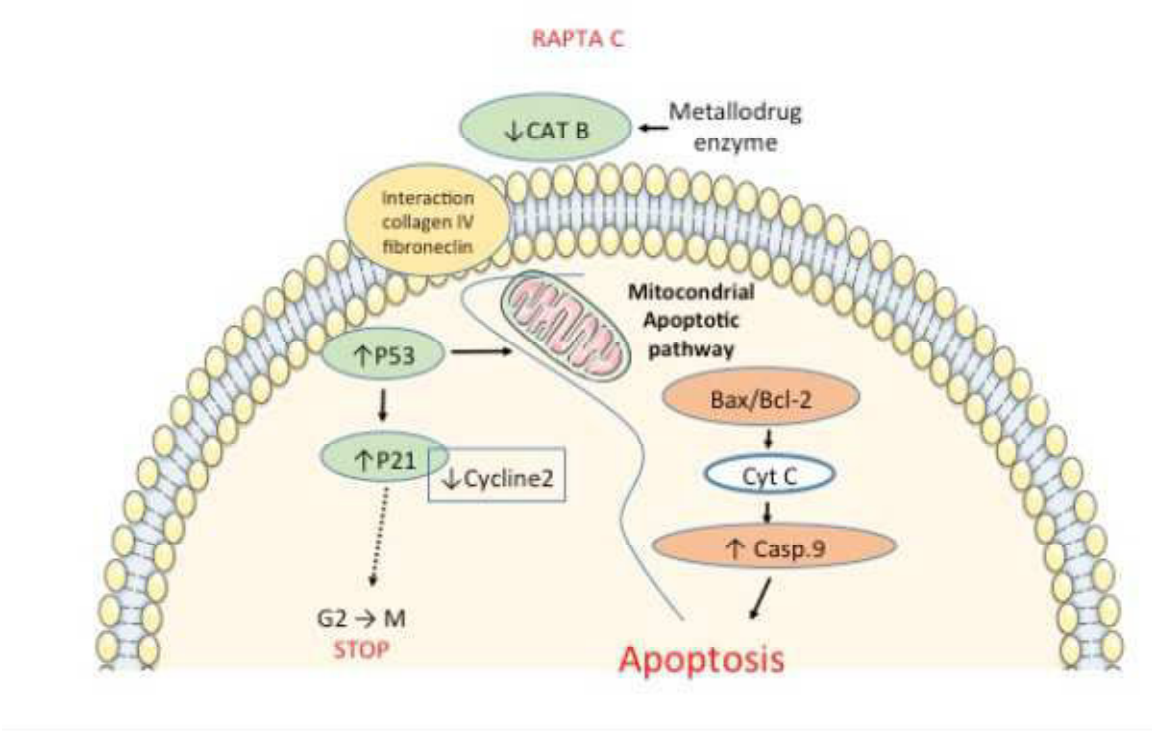
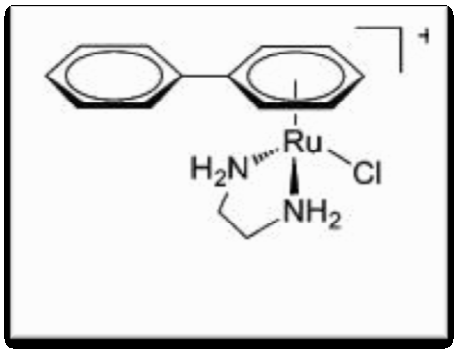


Figure15. Rapta C mechanism of action (89,112-114).

III.B.4. RM175



The [(η6- aerene)Ru (II-Cl) (ethylene-diamine)][PF_6] RM175 is developed by Peter Sadler and co-workers, These compounds showed *in vitro* promising cytotoixic effect in ovarian cancer cells. Special attention was attracted by the interaction of this compound with nucleobases after equation of the chloride (115). Furthermore, other studies by Chen and co-workers showed than, that DNA is a potential target of RM175, due to its strong selective binding to N7 of guanine (G) bases on DNA oligomers (116,117).

Mechanism of Action

RM175 binds to DNA either by covalent and non-covalent (intercalation) bonds, and it seems to induce cell death via the increase of p53, the cell cycle inhibitor p21/WAF-1 and the proapoptotic gene Bax (118) expression, respectively.

Fluorescence-trapping experiments in A549 cells suggested that this potency arose from an increase in reactive oxygen species (ROS). Surprisingly, this Ru complex acts as a catalyst for the oxidation of the tripeptide glutathione (GSH), which is a strong reducing agent present in millimolar concentrations in cells (119).

Interestingly, *in vivo* treatment with RM175 of both ovarian A2780 carcinoma and its cisplatin-resistant variant engrafted in nude mice showed a significant delay in cancer growth (120).

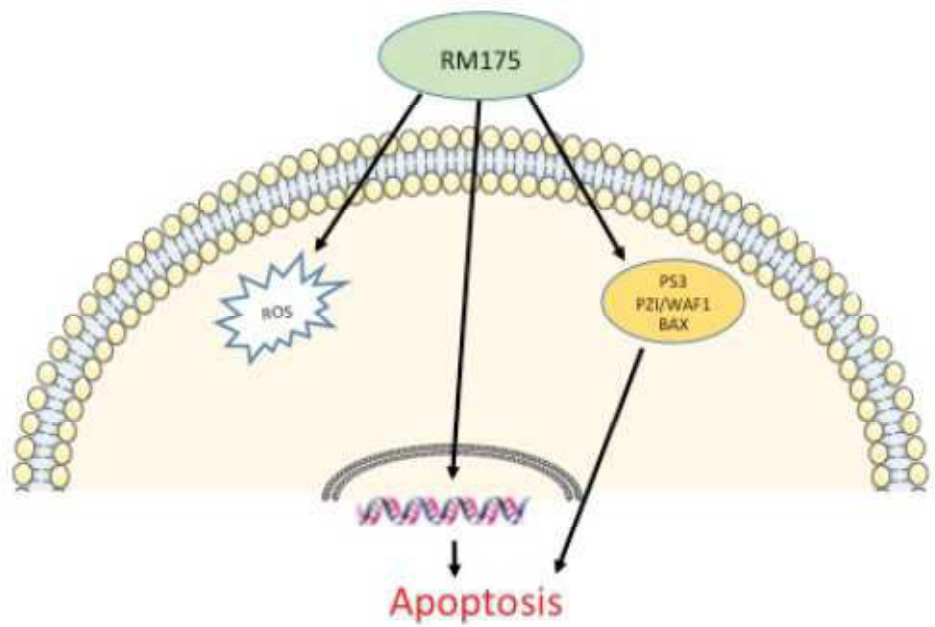
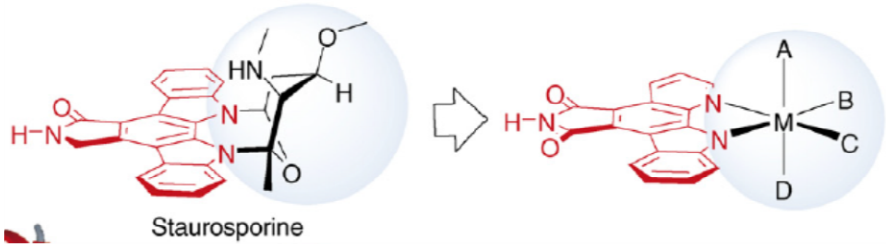


Figure 16. RM175 mechanism of action (115,119,120)

III.B.5. DW1/2



This molecule is characterized by the inhibition of glycogen synthase kinase GSK3β, with a high selectivity. This molecule has been synthesized by E. Meggers at the University of Pennsylvania. E. Meggers had the idea to use metal complexes as a structurally inert scaffolds for enzyme inhibitors. The ATP-competitive indolocarbazole alkaloid staurosporine, potent inhibitor of various kinases, was used as a lead structure to further develop the compound by replacing the carbohydrate unit of staurosponine with ruthenium fragments. In these molecules, the metal is not playing any direct role in the inhibition, but it allows the spatial organization of the substituents around the metal center.

Protein kinases are a large family of homologous proteins with 518 members in the human genome. Up to 30% of all human proteins may be modified by kinase activity, and kinases are known to regulate the majority of cellular pathways, especially those involved in signal transduction. Staurosporine, an alkaloid produced in *Streptomyces staurospores* originally as an antifungal agent, is an inhibitor of a broad spectrum of protein kinases, as Staurosporine exhibits a strong anticancer properties, many staurosporine derivatives have been developed as anticancer drugs.

Mechanism of Action

These molecules seem to be highly toxic toward human melanoma cells. The ruthenium staurosporine complex induces apoptosis with an important role of p53 but the idea of also p53-independent apoptosis is not discarded. Other results also indicate an apoptotic mechanism involving depolarization of mitochondrial membrane potential, caspase cleavage, and elevated NOXA expression. Treatment of melanoma cells with DW1/2 was instead found to decrease levels of Mdm2 and Mdm4, two known inhibitor of p53 protein levels (121).

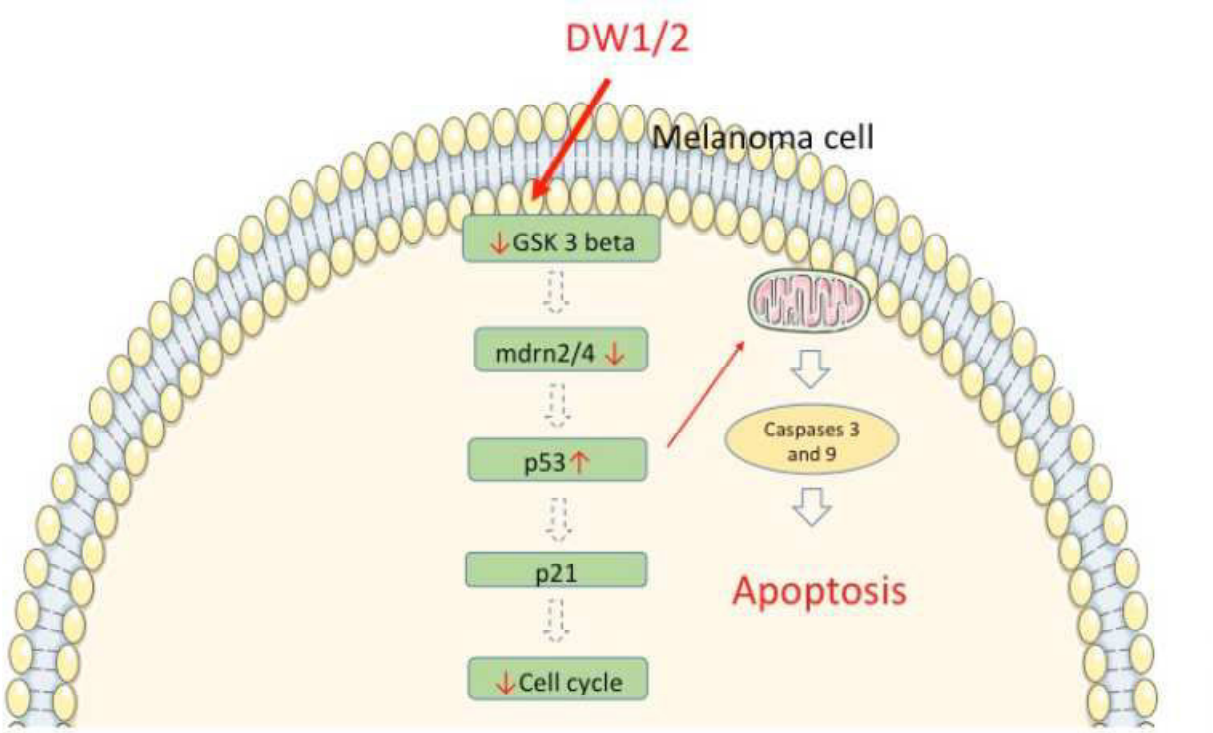
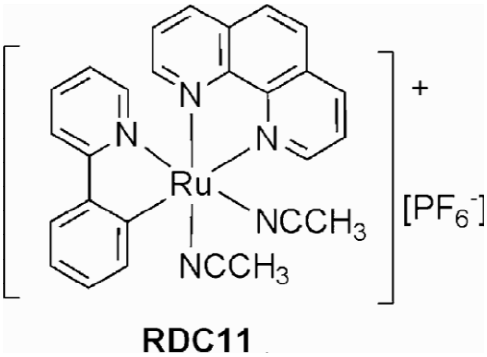


Figure 17. DW1/2 Mechanism of action

III.B.6. RUTENIUM DERIVED COMPOUNDS (RDC)



RDC11

[ruthenium(phenanthroline)(κ-C,N-(2-phenyl-pyridine) (NCMe)2]PF6 (RDC11)

These molecules are called RDCs *(Ruthenium-Derived Compounds)* and are developed by M. Pfeffer and C. Gaiddon at the University of Strasbourg.

Chemical Structure

Most of the ruthenium-containing compounds described so far have ligands that are bound to the metal via a heteroatom (N, O, S). In order to improve the stability of ruthenium complexes, the groups of Dr. Pfeffer and of Dr. Gaiddon have in an interdisciplinary effort generated and tested the biological of over 100 new ruthenium-

based complexes in which the ligand is bound to the metal via strong covalent bonds C-M. This C-M bond is thought to improve clearly improved the stability of the molecule, conferred a specific range of redox potential and allowed them to be efficient mediators of electron transfer to or from oxidized or reduced active sites of redox enzymes, affecting thereby their activity (122,123). Moreover, these ligands may additionally confer useful physical properties to the organometallic moiety (such as fluorescence), thus enabling the metal and ligand to be traced in the cell *in vivo*.

Cytotoxicity and in vivo properties

RDCs showed to be highly cytotoxic (IC_{50} in around 1µM for the most active molecules) for several cancer cell lines that are sensitive or resistant to cisplatin compared to others ruthenium compounds developed at this time. One of the compounds, RDC11 was particularly investigated based on its biological properties (IC_{50} 1-5µM in most cell lines) and physico-chemical properties (simplicity to synthesized, purified and stability). *In vivo* studies performed with several models of tumor growth showed that, for example, RDC11 is able to reduce tumor growth. Furthermore, in contrast to cisplatin, RDC11 did not cause severe side effects on the liver, kidneys, or the neuronal sensory system as the biomedical analysis of blood markers showed (86,124).

RDC and resistance mechanism

One of the mechanisms of resistance of cisplatin involves the transporter ATP7B. This transporter is charged of expulse cisplatin from the cell, Gaiddon's group overexpressed this protein and showed that cells became resistant to cisplatin but not to RDC. Moreover, it was published that RDCs and cisplatin are capable to induced p53 and p73 protein levels but with different intensities and kinetics. However, in contrast to cisplatin-induced apoptosis, overexpression of ΔNp73, a p53 and p73 dominant-negative isoform, only partly reduced RDC-induced apoptosis, suggesting p53-dependent and p53-independent modes of action (124).

The fact that cancer cells which developed any of the two resistance mechanisms against chemotherapies (p53 inactivation or ATP7B overexpression) were still sensitive toward RDCs suggested that RDCs induce apoptosis by other pathways than those induced by cisplatin.

RDC11 and the Reticulum Endoplasmic Stress Pathway

The group of C. Gaiddon demonstrated that an alternative signaling pathway, called the Reticulum Stress pathway (ER stress) was involved in the cytotoxicity effect of RDC11.

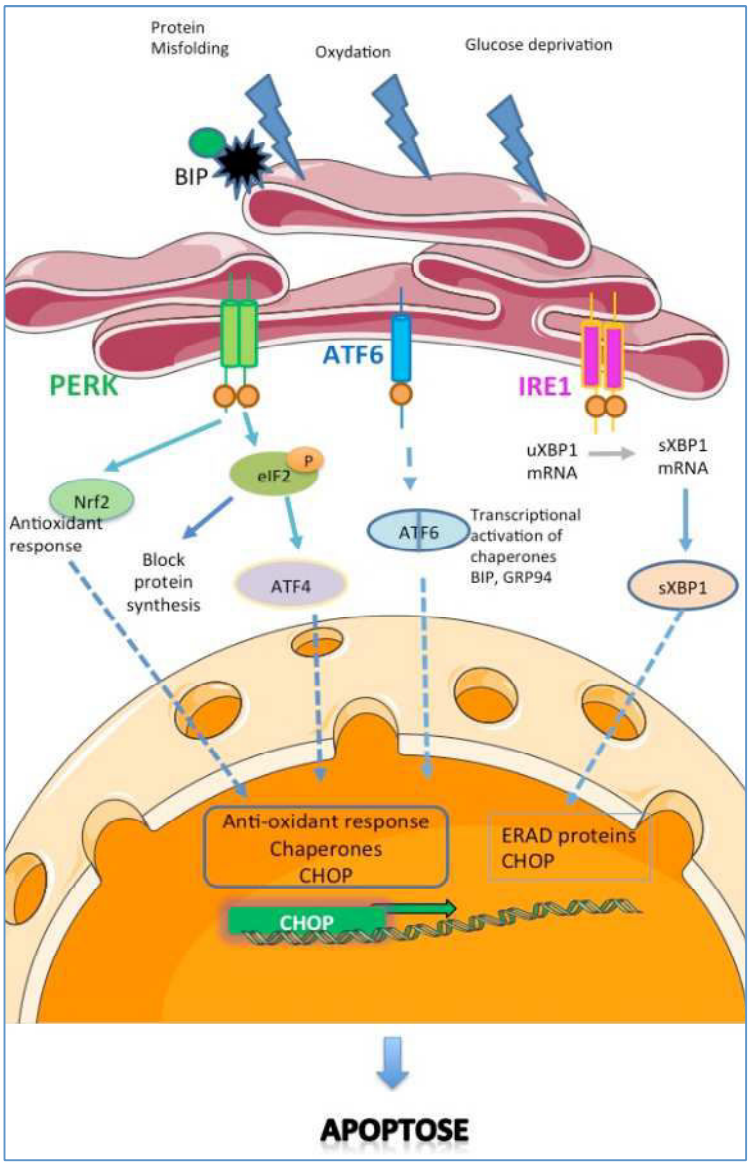


Figure 18. Endoplasmic Reticulum Stress Pathway (125).

The endoplasmic reticulum (ER) is the principal organelle responsible for the folding and maturation of proteins and the maintenance participating in their cellular homeostasis. ER stress is activated by a variety of factors like protein misfolding, oxidation or glucose deprivation, which triggers the unfolded protein response (UPR), which then either leads ER homeostasis or cell death.

In order to restore the ER homeostasis three major stress sensor control pathways are used, the inositol-requiring enzyme 1α (IRE1α), protein kinase RNA-like ER kinase (PERK) and activating transcription factor 6 (ATF6). IRE1α processes the mRNA encoding the transcription factor X-box binding protein 1 (XBP1). This leads to the expression of an active transcription factor (XBP1s) that up-regulates a subset of UPR target genes related to protein folding, ER-associated protein degradation (ERAD), protein quality control, and organelle biogenesis. Moreover, activation of PERK attenuates general protein synthesis through phosphorylation of the eukaryotic translation initiator factor 2α (eIF2α). EIF2α

phosphorylation allows the selective translation of the *ATF4* mRNA, which encodes a transcription factor that induces the expression of genes involved in antioxidant responses (like NRF2), amino acid metabolism, autophagy and apoptosis. Likewise, ATF4 controls the expression of the pro-apoptotic components GADD34 (growth arrest and DNA damage-inducible 34) and C/EBP-homologous protein (CHOP). In addition, ATF6 controls the up regulation of selected UPR target genes. Many components of the UPR trigger apoptosis under chronic ER stress conditions the C/EBP homologous protein (CHOP) is one of the main regulators and is often used as a maker of this pathway (126-129).

The group of C. Gaiddon has shown that RDC11 is capable to activate target genes of the ER stress pathway, such as Bip, XBP1, PDI, and CHOP. The activation of CHOP led to the expression of two pro-apototic target genes, (TRB3 and CHAC1). In addition, it they showed that the cytotoxicity of RDC11 is dependent on the activity of the transcription factor CHOP. This finding represents the first report of a regulation of this pathway by a ruthenium-containing compound (86). The ability of RDC11 to induce multiple and independent stress response pathways represents an interesting property for anticancer drugs that might allow a broader spectrum of action and maybe explain why RDCs are less sensitive toward cisplatin resistance mechanisms.

RDC and DNA interaction

Using Förster resonance energy transfer (FRET) and force extension measurements by optical tweezer, it was shown that RDC11 intercalates into double helix DNA molecule. However, RDC11 and cisplatin induce different structural changes of the DNA double strand, and the affinity of cisplatin for DNA is 2 orders of magnitude higher than that of RDC11 (130). They also showed that RDC was capable to induce DNA damage using as a marker the phosphorylation of histone H2AX at serine 147. Nevertheless, results showed that RDC11 induced less DNA damages than cisplatin, which correlated with its lower affinity to DNA (86).

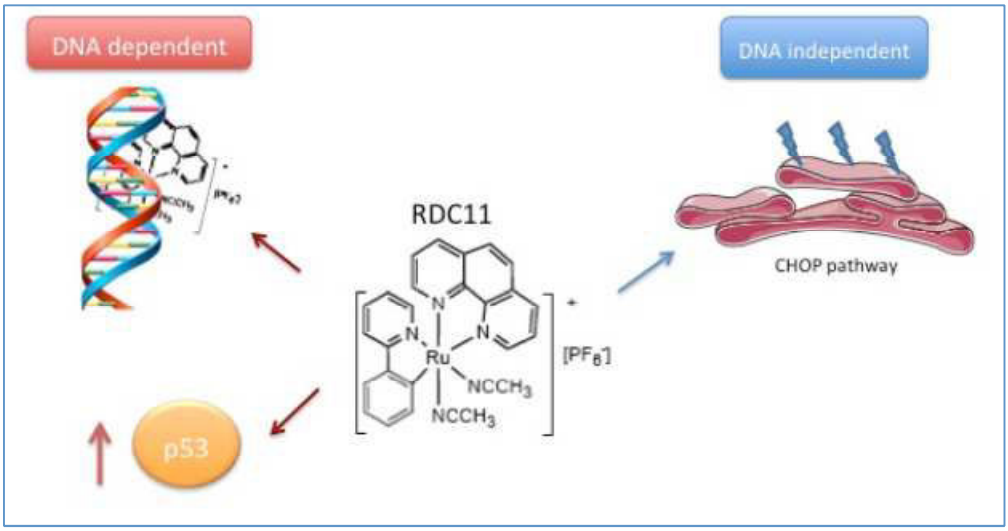
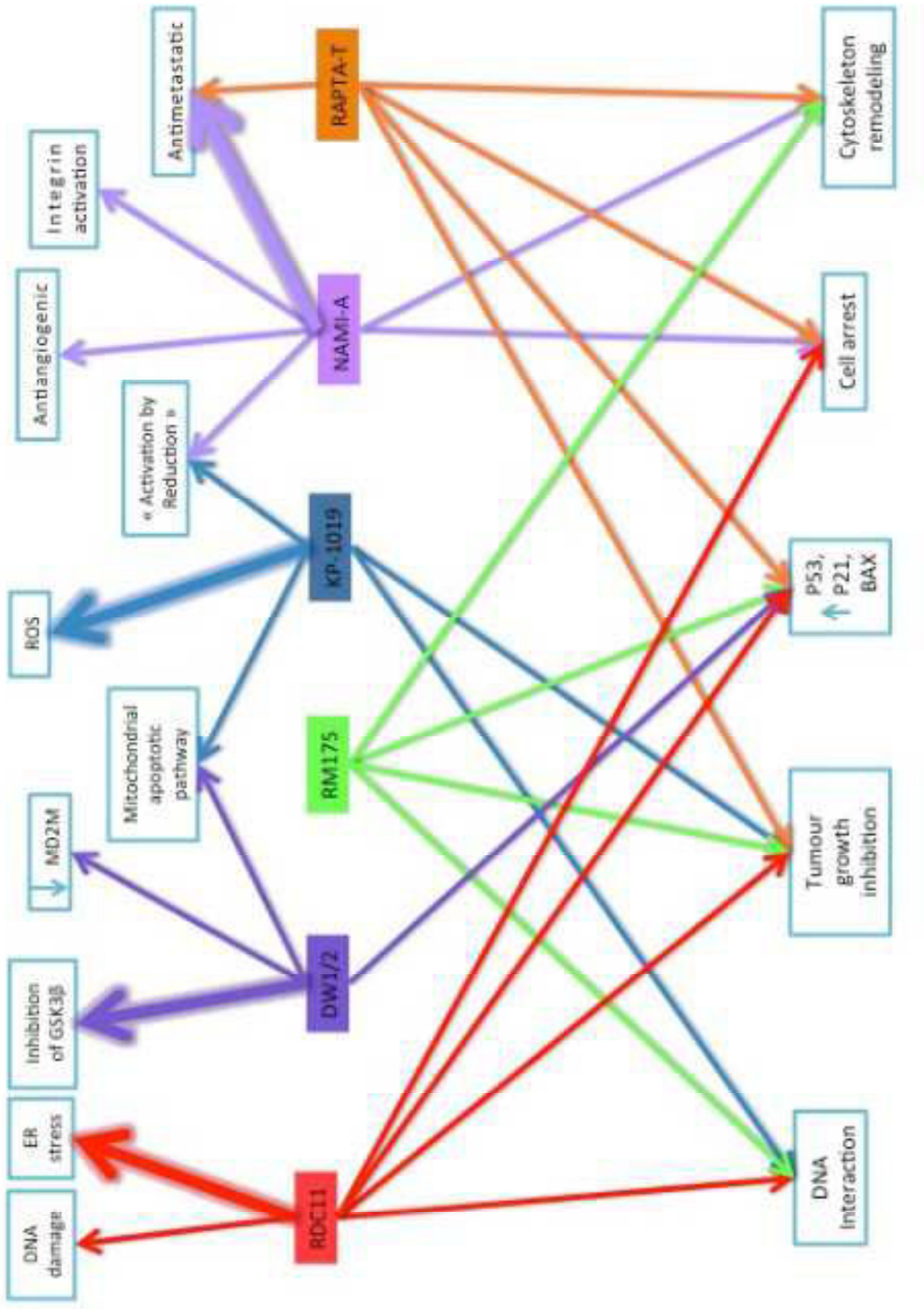


Figure 17. RDC working model.

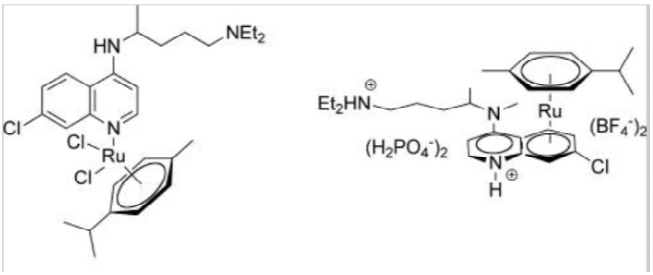
III.C. Recapitulative Schema mode of action of Ru compounds.



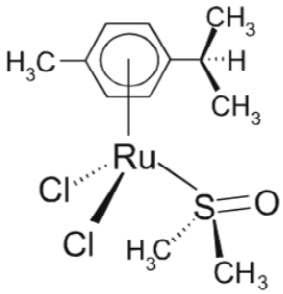
Schema 2. Principal Mode of Action of Ru compound

III.D. Other groups that developed Ruthenium based compounds.

The field focusing on the design and development of anticancer ruthenium drugs is very active and there are many other groups that work with Ruthenium based compounds. However, their research is less far developed, but still showing encouraging results. In the following, I choose to cite just two groups that present for me particular interests.



The group of Sánchez-Delgado coupled different Ru arene complexes to chloroquine (CQ), which is known to be an effective antimalarial compound as well as having anticancer properties. It is interesting to observe that developed compounds had a consistently higher potency against CQ-resistant parasites than the standard drug chloroquine diphosphate (CQDP). In addition, two of their compounds inhibited the growth of two HCT-116 colon cancer cell lines with IC values between 20 and 35 μM (131).



Sheldrick's groupe an interesting approach, an automated multidimensional protein identification technology (MudPIT) combined with a biphasic liquid chromatography with electrospray ionization tandem mass spectrometry (MS/MS), to analyze tryptic peptides from *Escherichia coli* cells treated with [(η -p-cymene)RuCl (DMSO)]. They showed that five proteins, namely, the cold-shock protein CspC, the three stress-response proteins ppiD, osmY, and SucC, and the DNA damage-inducible helicase dinG were the target of their Ru arene compounds (132).

III.E. Other metals used in the development of anticancer compounds

Of course Ru is not the only metal that has innovative properties; a lot of other metals like iron, cobalt, gold, gallium, nickel, mangenese, rhodium, rhenium, paladium, titanium, osmium have also shown excellent anticancer properties. However, with the exception of Rhenium and Iridium, which present an interest in imaging, the rational behind the use of other metals is not always evident. Nevertheless, compounds with titanium and gallium central atoms have already been evaluated in phase I and phase II clinical trials (133). In a briefly way here are some of them:

Rhodium and Iridium

Rhodium and iridum compounds have shown interesting antitumor properties, however their exact mode of cytotoxic action is still unknown. Sheldrick and co-workers showed that Ir(III) and Rh(III) complexes bind DNA through intercalation of their polypyridyl ligands, and this interaction with the DNA might significantly contribute to the cytotoxic activity of the agents (29,134).

Gold

Gold compounds are used for treating arthritis and cancer, and have potential for the treatment of AIDS, malaria and Chagas disease. Principally three drugs are already in the market effecting and slowing down the progression of rheumatoid arthritis (133). A large variety of gold(I) and gold(III) compounds are reported to possess relevant anti-proliferative properties *in vitro* against selected human tumor cell lines, and several studies have proved that they can be used to develop highly efficient metal-based drugs with possible applications in the treatment of cancer (135).

Titanium

Some titanium compounds have already enter in clinical trials phase I and II, under which Titanocene is the most successful one. Titanocene dichloride, $TiCl_2Cp_2$ or MTK4, had been recognized as active anticancer drug against breast and gastrointestinal carcinomas. Titanium may also replace iron in transferrin facilitating its uptake into tumor cells (136,137).

Gallium

Gallium appears to operate through the displacement of metal ions in iron metabolism or bone. In large part, action of gallium complexes seems to be a consequence of the similarity of gallium(III) to iron(III): Gallium interferes with the cellular transport of iron by binding to transferrin, and also interferes with the action of ribonucleotide reductase, which then results in inhibition of DNA synthesis (137). Among the developed gallium compounds, tris (8-quinolinolato)gallium(III) (KP46/FFC11) has finished phase I clinical trial. The side effects observed included neutropenia and anemia, stomatitis and conjunctivitis, dizziness, headache and acne, fatigue and diarrhea (133,138).

Osmium

The group of Keppler has shown that osmium compounds can be potent cyclin-dependent kinases inhibitors showing anti-proliferative activity but with no significant differences to similar Ru compounds (139). Colangelo and co-worker showed that osmium seems to have telomerase-inhibitor activity (140). Dyson and coworkers working on osmium analogues of RAPATA-C (141) with the aim to improve its activity. There are also the equivalent of NAMI-A with osmium as metal (142). Our group has also developed several compounds showing that some of them can be more cytotoxic than Ru compounds (143). Once again this properties are cell line, structure and ligand dependent. In a general way osmium compounds seem to have different redox properties and a high cytotoxic activity than ruthenium. Furthermore, it seems that their mechanism of action is different form platinum based compounds (144-146).

IV. Thesis objectives

The general objective of the research of our group is to develop innovative and efficient anticancer therapies. To do so, we believe that the characteristic of metal-based compounds described above represent an advantage. However, the data available show also that, so far, the biological activities of the compounds designed and tested are not sufficient, illustrated by a lack of high cytotoxicity *in vitro* or enough anticancer activity *in vivo*. In addition, the marketing value of such cytotoxic compounds has drastically been reduced by the more fashion like "targeted therapy" molecules developed by the pharmaceutical industry, and despite the general and everyday use of platinum-based cytotoxic drugs to treat patients.

Therefore, to change this situation, my PhD had two main objectives thought to gain novel information to ultimately improve the activity of the metal-based compounds. These studies were developed in close collaboration with Dr. Pfeffer who is a long-term collaborator of the laboratory and bring precious expertise in the chemistry side of our projects.

IV.A. Objective 1

The first objective is to investigate in detail the mode of action of a RDC11. As indicated above, RDC11 is a ruthenium-based compound in which ruthenium is bound to the carbon atom of one of the ligand. RDC11 has shown high cytotoxic activity in several cell lines and *in vivo* anticancer activity. The identification of RDC11 precise mode of action might provide critical information to optimize the structure of the compounds and eventually make it selective for a specific target. Using several experimental approaches I was able to analyze the contribution of two molecular mechanisms in the biological activity of RDC11. In particular I identified a direct target for RDC11, PHD2. These studies led to two manuscripts:

- Differential mode of action between ruthenium-based and cisplatin revealed by transcriptomic analyses: the example of histone-deacetylases.
- Differential regulation of the HIF-1 pathways by platinum and ruthenium anticancer organometallic drugs.

IV.B. Objective 2

The second objective was to test novel metal-based compounds that have been modified in a way to that would help us to understand the physico-chemical determinants important for their biological activity. We have used two strategies: i) change the ligands surrounding the metal (collaborations with Dr. Pfeffer and with Dr. Han; ii) change the metal (osmium instead of ruthenium, collaboration with Dr. Pfeffer). In each case we compared the cytotoxicity and also whether the modifications affected the signaling pathways triggered by the compounds. Interestingly, some of the new compounds generated presented fluorescent properties that allowed us to investigate their subcellular location and their mode of import. These structure/function studies led to 4 manuscripts.

- Induction of caspase 8 and reactive oxygen species by ruthenium-derived anticancer compounds with improved water solubility and cytotoxicity
- Subcellular localization and transport kinetics of ruthenium organometallic anticancer compounds in living cell: a dose dependent role for amino acid and iron transporters.
- Discovery and investigation of anticancer ruthenium-aerene Schiff-base complexes via water-promoted combinatorial three component assembly
- Exchange of ruthenium to osmium in organometallic compound tunes redox potential and cancer cell selectivity via ROS and oxydo-reductase enzymes regulation.

IV.C. Objective 3

Beside the two main objectives of my PhD described above, I participated in interesting collaborative projects related to the use of metal-based compounds into medical imaging and theranostics. In these cases, the ligands, and sometimes the metal, were significantly different from the one used by Dr. Pfeffer. This collaboration with the group of Pr. Gros and Dr. Bodio from Dijon led to two publications.

- Design of porphyrin-dota-like scaffolds as all in one multimodal heterometallic complex for medical imaging.
- Gold-phosphine-phorphyrin as potential metal-based theranostics

V. Results (Objective 1)

V.A. Differential mode of action between ruthenium-based and cisplatin revealed by transcriptomic analyses: the example of histone-deacetylases.

Differential mode of action between a ruthenium-based compound and cisplatin revealed by transcriptomic analyses: the example of histone-deacetylases

Licona Cynthia[1,2#], Spaety Marie-Elodie[1,2#], LeQuellenec Elea[1,2], Armant Olivier[3], Meng Xianjun[1,2], Spencer John[4], Pfeffer Michel[2,5], Mellitzer Georg[1,2], Gaiddon Christian[1,2]

[1]INSERM 1113, Molecular Signaling of the Cell Stress Response and Pathology, 3 av. Molière, 67200, Strasbourg, France

[2]Université de Strasbourg, 4 rue Blaise Pascal, 67000, France

[3]Karlsruhe Institute of Technology (KIT), Institute of Toxicology and Genetics (ITG), Hermann-von-Helmholtz-Platz 1, 76344 Eggenstein-Leopoldshafen, Germany

[4]Department of Chemistry, School of Life Sciences, University of Sussex, Falmer, Brighton, East Sussex, BN1 9QJ, UK

[5]Institut de Chimie, UMR7177, Laboratoire de Synthèses Métallo-Induites, 4 rue Blaise Pascal, 67000, France

Corresponding author: Christian Gaiddon, gaiddon@unistra.fr

[#] Indicates that both authors contributed equally to this work.

Short title: Ruthenium drug transcriptome points to epigenetic

Summary

Ruthenium-based compounds have been developed as potential replacements for platinum-based compounds in cancer therapy. Their clinical development is handicapped by the lack of consensus on their mode of action. In this study, we performed an unbiased study on gene expression triggered by cisplatin and an organoruthenium compound (RDC11) with anticancer activity. Clustering analyses showed gene expression signatures specific for cisplatin (42%) and for RDC11 (30%). Signaling pathway analyses pointed to specificities distinguishing RDC11 from cisplatin. As an example, cisplatin triggers preferentially p53 and folate biosynthesis while RDC11 induces preferentially reticulum endoplasmic stress and trans-sulfuration pathways. We confirmed these signatures by additional methods and we further focused on one involving epigenetic enzymes. We showed that RDC11 and cisplatin regulated differently histone deacetylases (HDACs). In addition, a HDAC inhibitor antagonized RDC11 activity while it synergized with cisplatin. This study provides critical information for the characterization of signaling pathways important for ruthenium-based compounds and differentiates them from cisplatin.

Introduction

Transition metals complexes, including those of ruthenium, have been under investigation for several years as scaffolds for generating novel molecules harboring anticancer properties. These metals present interesting properties that are likely to provide advantages for designing cytotoxic compounds such as: a octahedral geometry, a wide variety of redox potentials, accessibility of numerous oxidation states (I to IV) and interesting exchange ligand rate allowing covalent interactions with biological macromolecules (1, 2). In addition, ruthenium is hypothesized to be less toxic than platinum as it might be eliminated by iron metabolism mechanisms. A multitude of ligands have been used to produce different ruthenium complexes in the redox state (II) or (III). Most of the compounds were generated through complexation with a nitrogen containing the ligand. Alternatively, organo-ruthenium compounds were generated through a covalent bond with a carbon (C) of the ligands. *In vitro* and *in vivo* biological studies established that several of these ruthenium-based compounds show high cytotoxicity towards a wide range of cancer cells, anticancer properties, and reduced side effects (1-12). In addition, ruthenium-based complexes are not affected by platinum-induced resistance mechanisms. Based on these characteristics, two ruthenium-based complexes, NAMI-A and KP1019, have been tested in phase I and II clinical trials (13, 14). However, the lack of success in ruthenium compounds late stage clinical trial may reside in part in the relative lack of understanding of their exact mode of action and the important chemical determinants involved.

In this respect, the mechanism of action of ruthenium-based complexes remains a matter of debate. Several modes of action have been proposed, which include interaction with DNA and activation of DNA damage pathways (15-19), inhibition of kinases (20) or other enzymatic activities (21, 22), including extracellular metallo-proteases (23). This variability may be due to differences in the structure of the ruthenium complexes. The differences reside in the variation of the nature of the ligands but also the type of bond linking the ligand to the ruthenium atom. In addition, no global approaches have been described so far that would give a more exhaustive and comprehensive understanding of the signaling pathways that are triggered in response to ruthenium-based compounds.

In this study, we have analyzed changes in gene expression induced by RDC11. RDC11 is an organo-ruthenium compound that contains two acetonitriles, one phenantroline, and one phenylpyridine ligands bound to the metal. The phenylpyridine is attached to the ruthenium by a sigma bond between the ruthenium and the carbon of the ligand. We previously demonstrated that RDC11 has a high cytotoxicity (IC_{50} between 1-5µM) on multiple cell lines including cisplatin resistant cells (18, 24). Importantly, RDC11 reduces tumor growth in different models, including mouse syngeneic models (melanoma, lung cancer) and human xenografted models (glioma and ovarian cancer), with a reduced toxicity towards healthy tissues compared to cisplatin (24, 25).

We have also previously shown that RDC11 and related compounds such as RDC34 induce p53-dependent and Endoplasmic Reticulum (ER) stress pathways. However, we also showed that both pathways could not account for all the biological effect of RDC11-related compounds (18, 25, 26).

To identify novel signaling pathways that could elucidate for the biological activity of RDC11, we have used an unbiased approached that allowed us to establish the status of the cellular transcriptome. In addition, we have performed this analysis comparatively to cisplatin in order to characterize specific signatures or similarities between cisplatin and our organoruthenium compound.

Results:

The organoruthenium complex RDC11 presents a distinct transcriptomic signature

To identify similarities and specificities in the gene regulations caused by a ruthenium-based complexes and platinum-based complexes, we treated cancer cells (U87) at the IC_{50} values for RDC11 (2µM) and cisplatin (3µM) (Fig. 1A, B). U87 cells were chosen as we have previously shown them to respond to RDC11 and cisplatin when xenografted in nude mice (25). We also chose to treat the cells at the IC_{50} of the compounds and not to use an identical concentration because we wanted to identify gene regulations associated with a similar cytotoxicity. We also tested two time points, 6h and 24h, in order to identify early and later events in the gene regulations (Fig. 1C). These two time points may also allow us to find temporal and functional relationships between specific early and late events. For the identification of regulated genes we used Affymetrix hugene10stv1 arrays and each condition (Control: Ct; RDC11 6h: R6; RDC11 24h: R24; cisplatin 6h: C6; cisplatin 24h, C24) was performed in triplicate.

Principal component analysis of the normalized data using RMA and probe-level linear models validated that the data are reproducible (Fig. 1D and Supplementary Fig. S1-S2A). To detect differentially expressed genes, we performed the comparative analysis between control and treated groups 6 hours and 24 hours after exposure. 4540 probe sets with fold change $\geq \pm 1.5$ and adjusted p-value ≤ 0.05 were considered as significantly regulated in at least one comparative analysis (Supplementary Fig. S3B). 922 probe-sets are mis-regulated by cisplatin and 748 probe-sets by RDC11 6 hours after exposure. After 24 hours, 2910 and 2314 probe-sets are regulated by cisplatin and RDC11 respectively (Figure 1E and 1F). 22% to 28% (n=207) of the probe-sets are regulated both by RDC11 and cisplatin 6 hours after treatment. These numbers increase to 38% to 48% (n=1107) by 24 hours (Fig. 1E).

To find groups of genes with similar expression pattern across the different conditions and thus potentially involved in the same regulatory pathways, we performed hierarchical clustering analysis on the set of 4540 mis-regulated probe-set (Fig. 2A, B). Differences in gene regulation are already detectable 6 hours after exposure. For instance the cluster 10, 4 and 15 are made of

genes downregulated at 6 hours of cisplatin treatment compared to control. Overall, the effect on gene regulation is higher after 24 hours both in term of genes regulated and differences in gene expression levels (Fig. 2A).

One group of genes (cluster **6**, n=776) is characterized by low/moderate gene expression levels 6 hours after treatment with RDC11 or cisplatin, and high expression levels 24 hours after RDC11 or cisplatin treatment (Fig. 2A). Gene set enrichment analysis revealed that this cluster is highly enriched for genes with functions in apoptosis (FDR < 10^{-5}) such as p21, IRF1, NFKBIB, I-kB, ATF-3, PP2A regulatory, Caspase-7, C/EBP zeta, NF-kB, PPP2R5A, suggesting that apoptosis is induced by both chemicals at 24 hours. In addition to this common set of genes, clustering revealed a specific group of genes induced either by RDC11 or cisplatin. For instance the cluster **8** (n=753), which is characterized by high expression levels 24 hours after cisplatin treatment but moderate expression in other conditions, is enriched for genes in "apoptosis and survival Apoptotic Activin A" signaling (FDR < 10^{-3}) such Activin A, ActRIIA, Bcl-XL, p53, H-Ras, SHIP, c-Fos, while this pathway is not significant regulated in R24. Cluster **7** (n=409) is another example highlighting intrinsic differences in the transcriptional changes induced by RDC11 and cisplatin with a group of genes highly expressed in R24 and with moderate or low expression levels in other conditions. Some effect of the cisplatin is mediated by specific down regulation of a set of 710 genes (cluster **10**) enriched for function in cell adhesion via ephrin signaling (FDR < 10^{-5}) such Ephrin-A, Tiam1, FAP-1, Ephrin-A5, Fyn, GRB10, Intersectin, VAV-2, NCK2 (Grb4), FAK1 (Supplementary table T1). Clustering into the different groups was confirmed by soft clustering (Fig. 2B). Identifying again a group of genes, soft cluster A, showing a moderate decrease in their expression at 6 hour, which is further downregulated at 24 hours of treatment with cisplatin or RDC11, respectively. Another example for the different effect of cisplatin and RDC11 on a group of genes is soft-cluster B, where cisplatin shows only a very low/moderate effect on their expression, whereas this group of genes is strongly upregulated by RDC11 at 24 hours of treatment (Fig. 2B). Together, these data suggest that cisplatin and RDC11 share some mechanism activating apoptosis, but overall the mechanism of actions of these drugs is distinct. Indeed, although the absolute number of genes regulated in common by both chemicals reached a maximum of 48% 24 hours after the treatment (Fig. 1E), the levels of regulation as well as the early and late responses are different, making the transcriptional imprint unique for each chemical in the condition tested here.

In order to assess a possible relative generalization of the findings to other cancer cell types and to validate some of the regulations observed using the arrays, we performed RT-qPCR analyses on U87 cells, HCT116 colon cancer cells and AGS gastric cancer cells. For this, several genes were chosen randomly and a representative set is shown in supplementary figures 3A and B. Results were compared to the data obtained by the microarray analyses. In each cell line, drugs were applied at their IC_{50} value for 6 or 24 hours. RT-qPCR experiments showed a good correlation with the results of the arrays when RNAs from U87 or HCT116 cells were used.

However, the correlation was weaker with RNAs from treated AGS cells, indicating that some of the mechanisms might be cell line-specific.

The organoruthenium complex RDC11 modulates pathways distinct from cisplatin

As indicated above, gene set enrichment analyses of different databases identified pathways commonly or differently affected by RDC11 and cisplatin. Figure 3A shows the number of genes identified by gene set enrichment analyses that are upregulated in RDC11 treated cells for the indicated pathway between 6 hours and 24 hours when compared to control conditions (Fig. 3A). As already seen in the clustering analyses (Fig. 2A), the overall regulations intensified with time, such as genes involved in apoptosis (i.e. APAF1, Caspase 3). In correlation with apoptosis-related genes, several genes involved in selected pro-apoptotic pathways, such as p53 target genes, ER stress-related and oxidative stress-related genes are induced over time. Importantly, the expression of several genes of these pathways are already induced at 6 hours. In addition, genes involved in other cellular processes, such as several DNA damage-related genes, a few miRNAs, and multiple genes encoding enzymes involved in epigenetic control are upregulated over time by RDC11 (Fig. 3A).

Interestingly, when we compared the number of genes involved in these pathways and present at 24 hours in RDC11 or cisplatin treated cells, several differences can be identified (Fig. 3B). For example, p53-, DNA damage- and apoptosis-related genes are more present in cisplatin-treated cells. Inversely, ER stress- and oxidative stress-related genes are more present in RDC11-treated cells. Note that the number of miRNAs and epigenetic-related genes present in RDC11- and cisplatin-treated cells is similar. More strikingly, gene set enrichment analyses revealed that several cellular metabolic processes were very selectively regulated by either RDC11 or cisplatin (Fig. 3C). For example, trans-sulfuration and aminoacyl tRNA synthetase are selectively induced by RDC11. In contrast, in cisplatin-treated cells, genes involved in sterol biosynthesis and sucrose metabolism are preferentially regulated.

All together the gene set enrichment analyses indicated that RDC11 and cisplatin present each a preference in signaling pathways they regulate. These results clearly demonstrate that cisplatin and the ruthenium-based complex RDC11 have a different mode of action and pinpoint to some potential mechanisms that may account for the cytotoxicity of RDC11.

Cisplatin is a more potent inducer of the p53 pathway than the organoruthenium complex RDC11

To further validate some of the compound specific signatures identified by the gene set enrichment analyses, we performed RT-qPCR to measure the expression of p53 target genes in HCT116. Cells were treated for 6 hours and 24 hours with cisplatin or RDC11 at their IC50. *Gdf15*, *fas*, *bak1* and *plk3* were all induced by cisplatin and RDC11 at 24 hours (Fig. 4A, B, C, D). However, the induction by cisplatin was stronger and occurred often already at 6 hours of

treatment. We then followed the protein level for p53 under the same experimental conditions. P53 proteins were more abundant in cisplatin-treated cells compared to RDC11-treated cells (Fig. 4E). In addition, increased p53 protein expression was also seen at 6 hours in cisplatin-treated cells. To assess the importance of p53 in RDC11 biological activity, we used pifithrin, which is considered to be a p53 inhibitor. Survival of cancer cells was assessed using MTT assays. Pifithrin did not block the biological activity of RDC11 except at doses of RDC11 above the IC_{75} values (75 % of the maximal effect of RDC11, Fig. 4F). The results indicated that RDC11 is less capable of inducing p53 signaling than cisplatin, but p53 may still play a role in the biological activity of RDC11.

RDC11 is a more potent inducer of the ER pathway than cisplatin

We also focused on the ER stress pathway that produced a more selective signature for RDC11. RT-qPCR showed that several genes, *ditt3*, *atf4*, *chac1*, *dnajb2*, involved in the ER stress pathway were preferentially induced by RDC11 (Fig. 5A, B, C, D). Some of these genes were also induced by cisplatin, but in a significantly lesser extent. To further document the induction of the ER stress pathway we analyzed the production of the spliced form of XBP1 (XBPs). XBP1s is generated from IRE1 that is itself activated by the ER stress pathway. Figure 6E shows that RDC11 strongly induced the production of XBP1s while cisplatin had no or little effect. To assess whether eif-2α, a component of the ER stress pathway, is essential in the biological activity of RDC11 we used salubrinal, a known inhibitor of eif-2α. Cell survival was assessed by a MTT assay and revealed that salubrinal did not significantly alter the cytotoxicity of RDC11 (Fig. 5F). These results showed that although RDC11 stimulates preferentially the expression of components of the ER stress pathway, the activity of eif-2α is not required for RDC11 cytotoxicity.

RDC11 and cisplatin regulate different genes encoding epigenetic enzymes

Gene set enrichment analyses revealed that genes encoding histones and enzymes involved in epigenetic regulations were modulated significantly by both RDC11 and cisplatin (Fig. 3A, B, Table 1 supplementary data). Epigenetic regulations are involved in multiple biological processes, including cell death, differentiation, and metastasis (27). To have a better understanding of the role of epigenetic enzymes in RDC11 cytotoxicity, we first followed the expression of some of them that were regulated in our microarrays analyses. Figure 6A and B show the expression of HDAC and histone methyltransferases that were significantly regulated by cisplatin and/or RDC11 according to our microarray analyses. Interestingly, HDAC4 is selectively repressed by cisplatin while HDAC9 is selectively increased by RDC11. To validate these regulations, RT-qPCR experiment were performed using RNA prepared from AGS gastric cancer cells treated with cisplatin or RDC11. We chose HDAC4 that was selectively repressed by cisplatin, and EZH2 that was induced by both RDC11 and cisplatin. As observed in the

microarrays, RT-qPCR showed that EZH2 is induced by RDC11 and cisplatin (Fig. 6C), whereas HDAC4 is specifically repressed by only cisplatin (Fig. 6D). To assess whether these regulations impact also on the protein levels of HDAC4 and EZH2, we performed Western-blot analyses. Like for the RNA levels, RDC11 and cisplatin induced the protein levels of EZH2 at 24 hours (Fig. 6E), whereas only cisplatin repressed the protein level of HDAC4 (Fig. 6F).

To investigate the importance of these regulations on RDC11 biological activity, we followed the acetylation of histone H3 using a specific antibody for K7 acetylation. We observed that the acetylation of histone H3 was induced by cisplatin and RDC11 6 hours after the treatments (Fig. 6E). Interestingly, the acetylation of histone H3 was reduced 24 hours after RDC11 treatment, while staying elevated for cisplatin.

An HDAC inhibitor antagonizes RDC11 activity but synergizes with cisplatin in gastric cancer cells

To further assess the importance of HDAC regulation in cisplatin and RDC11 biological activity in gastric cancer cells, we used the HDAC inhibitor SAHA. MTT assays were first performed to establish the dose response curve of RDC11, cisplatin and SAHA in AGS cells (Fig. 7A, B and supplementary data). In a second step, combination treatments were performed by combining treatment with the two drugs at specific concentrations (i.e. IC_{25}, IC_{50}) accordingly to the isobologram protocol (28). The results were then analyzed using isobologram statistical analyses. This analysis performed with different combinations of HDAC inhibitor and RDC11 showed an antagonistic effect of the HDAC inhibitor on the cytotoxicity of RDC11 (Fig. 7D). In contrast, the HDAC inhibitor synergized with cisplatin cytotoxicity (Fig. 7C). This result showed again a significant difference between the mode of action of RDC11 and cisplatin. In particular, it suggests that HDAC activity might be required for RDC11 cytotoxicity but not for cisplatin.

Discussion

Nowadays, the precise identification of the mode of action of a drug destined for therapeutic purpose is crucial. In oncology, it allows the selection of the group of patients that have the best chance of responding to the treatment in an “a la carte” (personalized) therapeutic approach in which the mode of action of the drug matches the genetic profile of specific tumors. It also provides markers to follow the activity of the drugs during the therapy and point to the direction of a possible combination therapy by combining the compound with other therapeutic molecules. In addition, the identification of the direct target(s) is a clear advantage in developing a rational optimization process aiming at an improvement of the therapeutic activity. The general development of ruthenium-based anticancer compounds toward clinical use has been clearly handicapped by the lack of consensus about their mode of action and the long-lasting misconception that ruthenium-based compounds represent a succedaneum of platinum-based

compounds by acting like them. The unbiased and global transcriptomic approach presented in this study provides an unique perspective on the respective characteristics of the organoruthenium compound RDC11 and cisplatin by providing information at two levels: i) a statistical evaluation of the difference and the similarities between the genes regulated by both drugs, ii) a list of novel genes, signaling pathways and metabolic processes regulated by RDC11 that represents a source of information for pathways potentially regulated by other ruthenium-based compounds. Finally, this study illustrates also how such information may provide hints for developing novel combination treatments. In this present case, we focused on histone deacetylase (HDAC) regulation.

Specificities in RDC11 and cisplatin transcriptomic profiles

Bio-statistical analyses of the microarray data showed significant differences in the number and quality of the genes regulated by RDC11 or cisplatin. Among the 4540 genes that we identified to be regulated, less than a third were common to RDC11 and cisplatin (Fig. 1). About 40% were specifically regulated by cisplatin and a third by RDC11. This difference is even more marked at 6 hours post-treatment as only 1.5% of the regulated genes are common between cisplatin and RDC11-treated cells. The clustering analyses further highlighted the existence of 17 gene clusters that show significant variation of the expression profile over time between RDC11 and cisplatin after treatment (Fig. 2). The significant differences in the transcriptomes controlled by RDC11 and cisplatin indicate that both compounds should trigger different signaling pathways, likely reflecting distinctive mode of actions.

A more detailed analysis of the signaling pathways or cellular mechanisms that are controlled by the regulated genes confirmed the existence of common and distinctive effects between RDC11 and cisplatin. Apoptosis, DNA damage, p53, epigenetic, miRNA, ER stress and oxidative stress were amongst the mechanisms that were regulated by both drugs (Fig. 3). However, the number and the intensity of activation of the genes included in those pathways were often significantly different between RDC11 and cisplatin. For example, cisplatin induces a higher number of genes involved in DNA damage, p53, and apoptosis, while RDC11 favors oxidative- and ER stress-related genes. The differences between both drugs are even more accentuated on specific metabolic pathways (Fig. 3C). For example, RDC11 specifically regulates ribosome biogenesis, while cisplatin favors sucrose metabolism.

Respective contribution of the p53 and ER stress pathway in RDC11 activity

Some of these specificities were previously documented by our group, such as the preferential activation of the p53 pathway by cisplatin or the ER stress pathway by RDC11 in glioblastoma cells (24, 25, 29). Here, we further extended these observations by showing that these specificities are common to cancer cells of different origin, such as colon cancer cells (HCT116) or gastric cancer cells (AGS). In addition, we extended the observation to an additional pool of

genes and to the protein level for a marker of the ER stress pathway (Fig. 4, 5). Altogether, these novel observations validate the preferential activation of the ER stress pathway by RDC11 in different cancer cell lines. With the endoplasmic reticulum being also the place of protein translation, is also interesting to note that RDC11 triggered a ribosomal biogenesis response along with the ER stress pathway (Fig. 3C).

Interestingly, the preferential activation of the p53 pathway by cisplatin correlates with a preferential activation of DNA damage response by cisplatin. Hence, compared to RDC11, cisplatin appears to induce a coherent DNA-damage/p53 pathway response, which is also consistent with the preferential binding of cisplatin to DNA as compared to RDC11 (24, 25, 29).

The exact contribution of the p53 pathway and the ER stress pathways in RDC11 activity have already been investigated previously in glioblastoma cells. Using a dominant inhibitor and p53-/- cell lines, we previously showed that p53 is not absolutely necessary for RDC11 cytotoxicity (24, 25). We confirmed here these results by showing that a known inhibitor of p53 (pifithrin) does not drastically alter the activity of RDC11. We also inhibited eIE2α, a component of the ER stress pathway, with salubrinal. RDC11 cytotoxicity was not significantly affected by the inhibition of eIE2α. This result apparently contradicts previous data showing that the ER stress transcription factor CHOP is partly necessary for RDC11 full cytotoxicity (25). This apparent contradiction highlights the complexity of the ER stress pathway and might be explained by the fact that the activation of eIE2α by PERK represents only a part of the mechanisms triggered by the ER stress pathway (30). For example, CHOP can be induced by other mechanisms related to the ER stress pathway, such as ATF6.

Respective role of epigenetic regulators in RDC11 and cisplatin cytotoxicity

Amongst the mechanisms that were regulated differently by RDC11 and cisplatin, several genes encoding for histones and histone-modifying enzymes were identified. These genes and in particular HDACs, are playing a critical role in various biological process and represent interesting therapeutic targets (27). Our study showed that whereas EZH2 was induced by both RDC11 and cisplatin, HDAC4 was preferentially repressed by cisplatin. This repression of HDAC4 by cisplatin was also observed *in vivo* in fragments of human colon cancer xenografted in nude mice (Fig. 6F). In addition, we observed that these gene regulations impact on the acetylation of histone H3 at lysine 9 in a time- and drug-dependent pattern. In particular, 6 hours after treatment, RDC11 represses H3 acetylation while cisplatin already induced it. Such differential drug response correlates with a profound difference in the impact of HDAC inhibitors on RDC11 and cisplatin biological activity. Indeed, a known HDAC inhibitor, SAHA, had a synergistic anticancer activity with cisplatin in the AGS human gastric cancer cells as previously observed by other with cancer cell lines of a different origin (31). In contrast, we demonstrate here that an HDAC inhibitor inhibits RDC11 biological activity as revealed by the antagonistic effect observed in the isobologram analysis. This result suggests that, in contrast to cisplatin,

RDC11 biological activity might require the full activity of some HDACs by modifying either the histones or some of their other targets. From a more therapeutic point of view, this study indicates that RDC11 is not a good candidate to be used in combinatory therapy with HDAC inhibitors for it might depend on the expression and/or activity of HDACs in the tumor. It also confirms the potential advantage of combining HDAC inhibitors with platinum-based therapies in gastric cancers.

Overall this study demonstrates that RDC11 and cisplatin have different modes of action and trigger the regulation of different signaling pathways. If both lead to regulation of pro-apoptotic effectors and cell cycle inhibitors, the intermediate mechanisms are quite different. These differences have profound consequences as it will define how we might use RDC11 on tumors with specific signatures (i.e. p53 mutated or not) or with specific other therapeutic molecules. It remains to establish how these findings can be generalized to other ruthenium-based compounds or even other metal-based compounds. Our previous studies, as well as those of others showing that ruthenium- or osmium-based compounds with different ligands trigger similar regulation of p53 and ER-stress pathways suggest that the findings of this study might serve for inspiration in other metal-based related compounds by pointing out potential targeted signaling pathways (24) (19, 20, 32, 33).

Significance

Ruthenium-based compounds have been developed for several years as a possible replacement for platinum-based compounds, but only few of them have so far reached early phase (I and II) clinical trial. Their further clinical development and optimization are handicapped by the lack of consensus on their mode of action that is yet often considered being similar to cisplatin. In this study, we performed an unbiased comparative study on gene expression triggered by cisplatin and an organoruthenium compound (RDC11) that previously showed anticancer activity *in vivo*. Clustering analyses showed gene expression signatures specific for cisplatin (1920 genes, 42%) and for RDC11 (1357 genes, 30%). Gene ontology and signaling pathway analyses further pointed to specificities distinguishing RDC11 from cisplatin. As an example, cisplatin triggers preferentially p53, DNA damage and folate biosynthesis mechanisms while RDC11 induces preferentially reticulum endoplasmic stress, oxidative stress and trans-sulfuration signaling pathways. Using RNA and protein expression analyses, we confirmed these preferential gene signatures and we further focused on one involving epigenetic enzymes. We showed that RDC11 and cisplatin regulated differently histone deacetylases and methyltransferases. At the functional level, we showed that HDAC inhibitors antagonized RDC11 activity while it synergized with cisplatin in gastric cancer cells. This study represents the first approach that summarizes the significant differences in the mode of action of organoruthenium compounds compared to

cisplatin. In addition, it provides critical information for the further characterization of signaling pathways important for ruthenium-based compounds.

Experimental procedures

Chemicals

Cisplatin, pifithrin, SAHA and salubrinal were purchased from Sigma. RDC11 was synthesized and purified as previously described (18).

Cell cultures

U87, AGS and HCT116 cells were obtained from ATCC. Cells were manipulated and cultured in DMEM with 10% FCS (Dominique Dutcher™) and 1% Penicillin + Streptomycin (Sigma) at 37°C with 5% CO_2 atmosphere as previously described (34).

Cell survival assay

2000 cells were seeded per well in 96-well microplates (Falcon Multiwell), 48 h prior to any treatment. Cisplatin and RDC11 were applied for 48 h in fresh medium. MTT assay was performed as previously described by replacing the medium with fresh medium supplemented with 5 mg/L MTT (Sigma) for 1h (35). Cells were lysed in isopropanol with 0.04 N HCl. Measurements were performed at 550 nm.

Quantitative PCR.

Cultured cells were lysed with 1ml of TRIzol (Invitrogen) per $10x10^6$ cells and RNA extracted according to manufacturer's instructions. RNA samples were ethanol-precipitated twice and 1 µg was used for reverse transcription (High-Capacity cDNA Reverse Transcription Kit, Applied Biosystems). qPCR was performed using 2 ng/µl cDNA (RNA equivalent) according to manufacturers' instructions (SYBR Green PCR Master Mix, Applied Biosystems) and with 400 µM of each primer (Supplemental data, table 1). Expression levels were normalized using average of 18S.

Statistical analysis

Statistical analyses were performed using a one-way ANOVA test followed by a Tukey post-test allowing a comparison between all the conditions. * Indicate statistical differences in graphs. Statistical Analyses were performed using Prism (GraphPad software).

Western blotting.

Cells or tissue were lysed with LB (125mM Tris-HCl pH 6.7, NaCl 150mM, NP40 0.5%, 10% Glycerol). Proteins (20µg) were denatured and deposited directly (75mg of proteins) onto a SDS-PAGE gel. Western blotting was performed using antibodies raised against p53 (rabbit anti-p53,

FL-393, Santa Cruz, CA), XBP1s (Santa Cruz, CA), EZH2 (Cell Signaling), H3 (Cell Signaling), H3K9 (Abcam) and HDAC4 (Biolegend). Secondary antibodies (anti-rabbit, anti-mouse: Sigma, MA) were incubated at 1:1000. Loading was controlled with actin (rabbit anti- β-actin, Sigma, 1:4000) (36).

Statistical analysis of Microarray data

Data obtained from Affymetrix hugene10stv1 arrays (http://www.ncbi.nlm.nih.gov / geo / query / acc.cgi?acc=GSE66493) were analyzed in R version 3.0.1. Raw data were first extracted from the CEL files and visualized using the package *affyPLM* to detect potential hybridization artifacts. Probeset annotations were retrieved from Ensembl (GRCh37.p10 release 69) with Biomart (BMC Genomics 2009, 10:22 doi: 10.1186 / 1471-2164-10-22) for 32325 probe-set corresponding to 25489 mapped genes. Normalization was performed either with RMA model from the *affy* package (Bioinformatics. 2004 Feb 12;20(3):307-15.) or with probe-level linear models (*affyPLM*) (Bioinformatics. 2004;20:307–315). The normalization methods were compared by plotting ROC curves using the respective adjusted p-values values as predictor. Differential expression analysis was performed with the *limma* package (BMC Genomics. 2006 Oct 9;7:252. Clustering was performed on a selection of 4540 probsets showing at least one condition with $|FC| \geq 1.5$ and adjusted p-value ≤ 0.05. Hierarchical clustering was carried out with Pearson's correlation and the complete-linkage method. Clusters were defined by 1.5 times the height of the longest branch. Soft clustering was performed with the package *Mfuzz* using the parameters c=8 and m=1.6 (37). Gene Set enrichment analysis was carried out with MetaCore (Thomson Reuters) using human annotations, p-values ≤ 0.05 were considered as significant.

Author Contributions

LC & SME: performed and analyzed experiments. LE performed experiments. AO analyzed microarray data. MX performed experiments. PS analyzed data. SJ synthesized chemicals, red and commented manuscript. PM synthesized chemicals, red and commented manuscript. MG designed, analyzed experiments, red and commented manuscript. GC designed, analyzed and wrote the article.

Acknowledgment

This project is supported by the Centre National pour la Recherche Scientifique (CNRS, France) (CG), ARC, Ligue contre le Cancer, AFM, European action COST CM1105 and SMSdrug.net. We are also thankful for the technical support of E. Martin.

References

1. Bruijnincx, P. C., and Sadler, P. J. (2008) New trends for metal complexes with anticancer activity. Curr Opin Chem Biol 12, 197-206
2. Jakupec, M. A., Galanski, M., Arion, V. B., Hartinger, C. G., and Keppler, B. K. (2008) Antitumour metal compounds: more than theme and variations. Dalton Trans, 183-194
3. Markman, M. (2003) Toxicities of the platinum antineoplastic agents. Expert Opin Drug Saf 2, 597-607
4. Kelland, L. (2007) The resurgence of platinum-based cancer chemotherapy. Nat Rev Cancer 7, 573-584
5. Allardyce, C. S., and Dyson, P. J. (2001) Ruthenium in medicine: current clinical uses and future prospects. Platinum Metals Rev. 45, 62
6. Dyson, P. J., and Sava, G. (2006) Metal-based antitumour drugs in the post genomic era. Dalton Trans, 1929-1933
7. Giraldi, T., Sava, G., Bertoli, G., Mestroni, G., and Zassinovich, G. (1977) Antitumor action of two rhodium and ruthenium complexes in comparison with cis-diamminedichloroplatinum(II). Cancer Res 37, 2662-2666
8. Keppler, B. K., Balzer, W., and Seifried, V. (1987) Synthesis and antitumor activity of triazolium-bis(triazole)-tetrachlororuthenate (III) and bistriazolium-triazolepentachlororuthenate (III). Two representatives of a new class of inorganic antitumor agents. Arzneimittelforschung 37, 770-771
9. Sava, G., Pacor, S., Zorzet, S., Alessio, E., and Mestroni, G. (1989) Antitumour properties of dimethylsulphoxide ruthenium (II) complexes in the Lewis lung carcinoma system. Pharmacol Res 21, 617-628
10. Fruhauf, S., and Zeller, W. J. (1991) New platinum, titanium, and ruthenium complexes with different patterns of DNA damage in rat ovarian tumor cells. Cancer Res 51, 2943-2948
11. Morris, R. E., Aird, R. E., Murdoch Pdel, S., Chen, H., Cummings, J., Hughes, N. D., Parsons, S., Parkin, A., Boyd, G., Jodrell, D. I., and Sadler, P. J. (2001) Inhibition of cancer cell growth by ruthenium(II) arene complexes. Journal of medicinal chemistry 44, 3616-3621
12. Scolaro, C., Bergamo, A., Brescacin, L., Delfino, R., Cocchietto, M., Laurenczy, G., Geldbach, T. J., Sava, G., and Dyson, P. J. (2005) In vitro and in vivo evaluation of ruthenium(II)-arene PTA complexes. Journal of medicinal chemistry 48, 4161-4171
13. Hartinger, C. G., Zorbas-Seifried, S., Jakupec, M. A., Kynast, B., Zorbas, H., and Keppler, B. K. (2006) From bench to bedside--preclinical and early clinical development of the anticancer agent indazolium trans-[tetrachlorobis(1H-indazole)ruthenate(III)] (KP1019 or FFC14A). J Inorg Biochem 100, 891-904
14. Rademaker-Lakhai, J. M., van den Bongard, D., Pluim, D., Beijnen, J. H., and Schellens, J. H. (2004) A Phase I and pharmacological study with imidazolium-trans-DMSO-imidazole-tetrachlororuthenate, a novel ruthenium anticancer agent. Clin Cancer Res 10, 3717-3727
15. Mei, H. Y., and Barton, J. K. (1988) Tris(tetramethylphenanthroline)ruthenium(II): a chiral probe that cleaves A-DNA conformations. Proc Natl Acad Sci U S A 85, 1339-1343
16. Brabec, V. (2002) DNA modifications by antitumor platinum and ruthenium compounds: their recognition and repair. Prog Nucleic Acid Res Mol Biol 71, 1-68
17. Zeglis, B. M., Pierre, V. C., and Barton, J. K. (2007) Metallo-intercalators and metallo-insertors. Chem Commun (Camb), 4565-4579
18. Gaiddon, C., Jeannequin, P., Bischoff, P., Pfeffer, M., Sirlin, C., and Loeffler, J. P. (2005) Ruthenium (II)-derived organometallic compounds induce cytostatic and cytotoxic effects on mammalian cancer cell lines through p53-dependent and p53-independent mechanisms. J Pharmacol Exp Ther 315, 1403-1411
19. Hayward, R. L., Schornagel, Q. C., Tente, R., Macpherson, J. S., Aird, R. E., Guichard, S., Habtemariam, A., Sadler, P., and Jodrell, D. I. (2005) Investigation of the role of Bax, p21/Waf1 and p53 as determinants of cellular responses in HCT116 colorectal cancer cells exposed to the novel cytotoxic ruthenium(II) organometallic agent, RM175. Cancer Chemother Pharmacol 55, 577-583

20. Smalley, K. S., Contractor, R., Haass, N. K., Kulp, A. N., Atilla-Gokcumen, G. E., Williams, D. S., Bregman, H., Flaherty, K. T., Soengas, M. S., Meggers, E., and Herlyn, M. (2007) An organometallic protein kinase inhibitor pharmacologically activates p53 and induces apoptosis in human melanoma cells. Cancer Res 67, 209-217
21. Ang, W. H., De Luca, A., Chapuis-Bernasconi, C., Juillerat-Jeanneret, L., Lo Bello, M., and Dyson, P. J. (2007) Organometallic Ruthenium Inhibitors of Glutathione-S-Transferase P1-1 as Anticancer Drugs. ChemMedChem
22. Dougan, S. J., Habtemariam, A., McHale, S. E., Parsons, S., and Sadler, P. J. (2008) Catalytic organometallic anticancer complexes. Proc Natl Acad Sci U S A 105, 11628-11633
23. Gava, B., Zorzet, S., Spessotto, P., Cocchietto, M., and Sava, G. (2006) Inhibition of B16 melanoma metastases with the ruthenium complex imidazolium trans-imidazoledimethylsulfoxide-tetrachlororuthenate and down-regulation of tumor cell invasion. J Pharmacol Exp Ther 317, 284-291
24. Vidimar, V., Meng, X., Klajner, M., Licona, C., Fetzer, L., Harlepp, S., Hebraud, P., Sidhoum, M., Sirlin, C., Loeffler, J. P., Mellitzer, G., Sava, G., Pfeffer, M., and Gaiddon, C. (2012) Induction of caspase 8 and reactive oxygen species by ruthenium-derived anticancer compounds with improved water solubility and cytotoxicity. Biochem Pharmacol 84, 1428-1436
25. Meng, X., Leyva, M. L., Jenny, M., Gross, I., Benosman, S., Fricker, B., Harlepp, S., Hebraud, P., Boos, A., Wlosik, P., Bischoff, P., Sirlin, C., Pfeffer, M., Loeffler, J. P., and Gaiddon, C. (2009) A Ruthenium-Containing Organometallic Compound Reduces Tumor Growth through Induction of the Endoplasmic Reticulum Stress Gene CHOP. Cancer Res
26. Klajner, M., Licona, C., Fetzer, L., Hebraud, P., Mellitzer, G., Pfeffer, M., Harlepp, S., and Gaiddon, C. (2014) Subcellular localization and transport kinetics of ruthenium organometallic anticancer compounds in living cells: a dose-dependent role for amino Acid and iron transporters. Inorganic chemistry 53, 5150-5158
27. Abend, A., and Kehat, I. (2015) Histone deacetylases as therapeutic targets - From cancer to cardiac disease. Pharmacol Ther 147C, 55-62
28. Tallarida, R. J. (2006) An overview of drug combination analysis with isobolograms. J Pharmacol Exp Ther 319, 1-7
29. Klajner, M., Hebraud, P., Sirlin, C., Gaiddon, C., and Harlepp, S. (2010) DNA binding to an anticancer organo-ruthenium complex. J Phys Chem B 114, 14041-14047
30. Nagelkerke, A., Bussink, J., Sweep, F. C., and Span, P. N. (2014) The unfolded protein response as a target for cancer therapy. Biochim Biophys Acta 1846, 277-284
31. Diyabalanage, H. V., Granda, M. L., and Hooker, J. M. (2013) Combination therapy: histone deacetylase inhibitors and platinum-based chemotherapeutics for cancer. Cancer Lett 329, 1-8
32. Chatterjee, S., Kundu, S., Bhattacharyya, A., Hartinger, C. G., and Dyson, P. J. (2008) The ruthenium(II)-arene compound RAPTA-C induces apoptosis in EAC cells through mitochondrial and p53-JNK pathways. J Biol Inorg Chem 13, 1149-1155
33. Suntharalingam, K., Johnstone, T. C., Bruno, P. M., Lin, W., Hemann, M. T., and Lippard, S. J. (2013) Bidentate ligands on osmium(VI) nitrido complexes control intracellular targeting and cell death pathways. J Am Chem Soc 135, 14060-14063
34. Sohm, F., Gaiddon, C., Antoine, M., Boutillier, A. L., and Loeffler, J. P. (1999) The retinoblastoma susceptibility gene product/Sp1 signalling pathway is modulated by Ca2+/calmodulin kinases II and IV activity. Oncogene 18, 2762-2769
35. Gaiddon, C., de Tapia, M., and Loeffler, J. P. (1999) The tissue-specific transcription factor Pit-1/GHF-1 binds to the c-fos serum response element and activates c-fos transcription. Mol Endocrinol 13, 742-751
36. Antoine, M., Gaiddon, C., and Loeffler, J. P. (1996) Ca2+/calmodulin kinase types II and IV regulate c-fos transcription in the AtT20 corticotroph cell line. Mol Cell Endocrinol 120, 1-8
37. Futschik, M. E., and Carlisle, B. (2005) Noise-robust soft clustering of gene expression time-course data. J Bioinform Comput Biol 3, 965-988

Figure legends

Figure 1: A. Schematic representation of cisplatin and RDC11. B. Survival curve of U87 glioblatoma cells treated with cisplatin or RDC11. Cells were treated for 48 hours in 96-well plates and their survival was evaluated by MTT assay (n=8). C. Schematic representation of the experimental protocol used for the microarray analysis. D. Principal Component Analysis. Plotting of two principal components from RMA normalized data using probe probe-level linear models. Biological replicates for the 5 different conditions cluster together and no outliers are detected within the dataset. E. Venn diagram. Significantly mis-regulated probe sets between control and exposed conditions are compared to highlight genes shared or specific to each group. C6: Cisplatin exposure for 6hrs; C24: Cisplatin exposure for 24hrs; R6: Ruthenium exposure for 6hrs; R24: Ruthenium exposure for 24hrs. F. Vulcano plots. Plotting of the log10 of the fold change (x-axis) in function of the -log10 of the adjusted *p* values (y-axis). Unexposed cells are used as reference. Significant differential expression in microarray data are shown in red for the four comparative analysis using the threshold: $|FC| \geq 1.5$ and adjusted p-value ≤ 0.05.

Figure 2: A. Hierarchical clustering. Clustering of expression of 4540 probe-set significantly regulated in at least one treated group compared to control. Rows represent gene expression and columns biological samples. Gene expression levels are represented as scaled expression values (row Z-score from -3 to +3). Blue: low expression, Red: high expression, white: moderate expression. 17 different clusters are detected, indicated by they number and different color next the probe-set tree. B. Soft clustering of the normalized microarray data. The set of 4540 mis-regulated genes was subjected to soft clustering to find gene families sharing similar expression patterns. Genes belonging to the same cluster, ie. with high membership, are colored in red. Normalized and scaled expression levels are indicated on y-axis. Samples names are indicated below each graph.

Figure 3: Signaling pathways and mechanisms regulated by cisplatin or RDC11. Graphs represents number of genes in the indicated pathways that are regulated by RDC11 at 6 hours or 24 hours (A) or by RDC11 and cisplatin at 24 hours (B, C). Microarray data were analyzed using AltAnalysis and R bioinformatics tools to identify in KEGG, Gene Ontology, miRNA, transcription factors databanks, the signaling pathways and mechanisms corresponding to the mis-regulated genes.

Figure 4: mRNA levels of *gdf15* (A), *fas* (B), *plk3* (C) and *bak1* (D) were assayed in HCT116 colon cancer cells by RT-qPCR. Curves are means of fold induction versus the control (Ct) with SD (n=3). *: $p < 0.01$. E. Proteins were extracted from HCT116 treated with RDC11 (R6, R24) or

cisplatin (C6, C24) for the indicated time. Western blot analysis revealed p53 and actin expression. F. Survival curve of HCT116 cells treated with RDC11 and pifithrin-α (10µM). Cells were treated for 48 hours in 96-well plates and their survival was evaluated by MTT assay (n=8).

Figure 5: mRNA levels of *ddit3* (A), *atf4* (B), *chac1* (C) and *dnajb2* (D) were assayed in HCT116 colon cancer cells by RT-qPCR. Curves are means of fold induction versus the control (Ct) with SD (n=3). *: $p < 0.01$. E. Proteins were extracted from HCT116 treated with RDC11 (R6, R24) or cisplatin (C6, C24) for the indicated time. Western blot analysis revealed XBP1s and actin expression. F. Survival curve of HCT116 cells treated with RDC11 and salubrinal (10µM). Cells were treated for 48 hours in 96-well plates and their survival was evaluated by MTT assay (n=8). Bars are means of fold induction versus the control (Ct) with SD (n=3). *: $p < 0.01$.

Figure 6: Curves are fold induction versus the control (Ct) as obtained after analysis of the microarrays data for selected histone-modifying enzymes in RDC11 (A) and cisplatin (B) conditions. mRNA levels of *ezh2* (C), *hdac4* (D), were assayed in AGS gastric cancer cells by RT-qPCR. Curves are means of fold induction versus the control (Ct) with SD (n=3). *: $p < 0.01$. E. Proteins were extracted from AGS treated with RDC11 (R6, R24) or cisplatin (C6, C24) for the indicated time. Western blot analysis revealed EZH2, HDAC4, histone H3 acetyl lysine 7 (H3AK7), histone H3 (H3) and actin expression. Quantifications of H3AK7/H3 are indicated bellow as measured by Pixi imager. F. mRNA levels of *hdac4* were assayed by RT-qPCR in fragments of human colon cancer xenografted in nude mice and after the treatment with cisplatin or RDC11. Graphs are means of fold induction versus the control (Ct) with SD (n=5). *: $p < 0.01$.

Figure 7: Survival curve of AGS cells treated with SAHA (A) and RDC11 (B). Cells were treated for 48 hours in 96-well plates and their survival was evaluated by MTT assay (n=8). Bars are means of fold induction versus the control (Ct) with SD (n=3). *: $p < 0.01$. Isobologram analyses and combinatory index representations of combinatory treatments between cisplatin with SAHA (C) and RDC11 with SAHA (D). Doses at IC_{75}, IC_{60}, IC_{50}, IC_{30}, IC_{25} were combined and the results were analyzed with the algorithm of Chu and al. using the CompuSyn software. E. Schematic representation of the signaling pathways regulated and important respectively for cisplatin and RDC11.

Figure 1

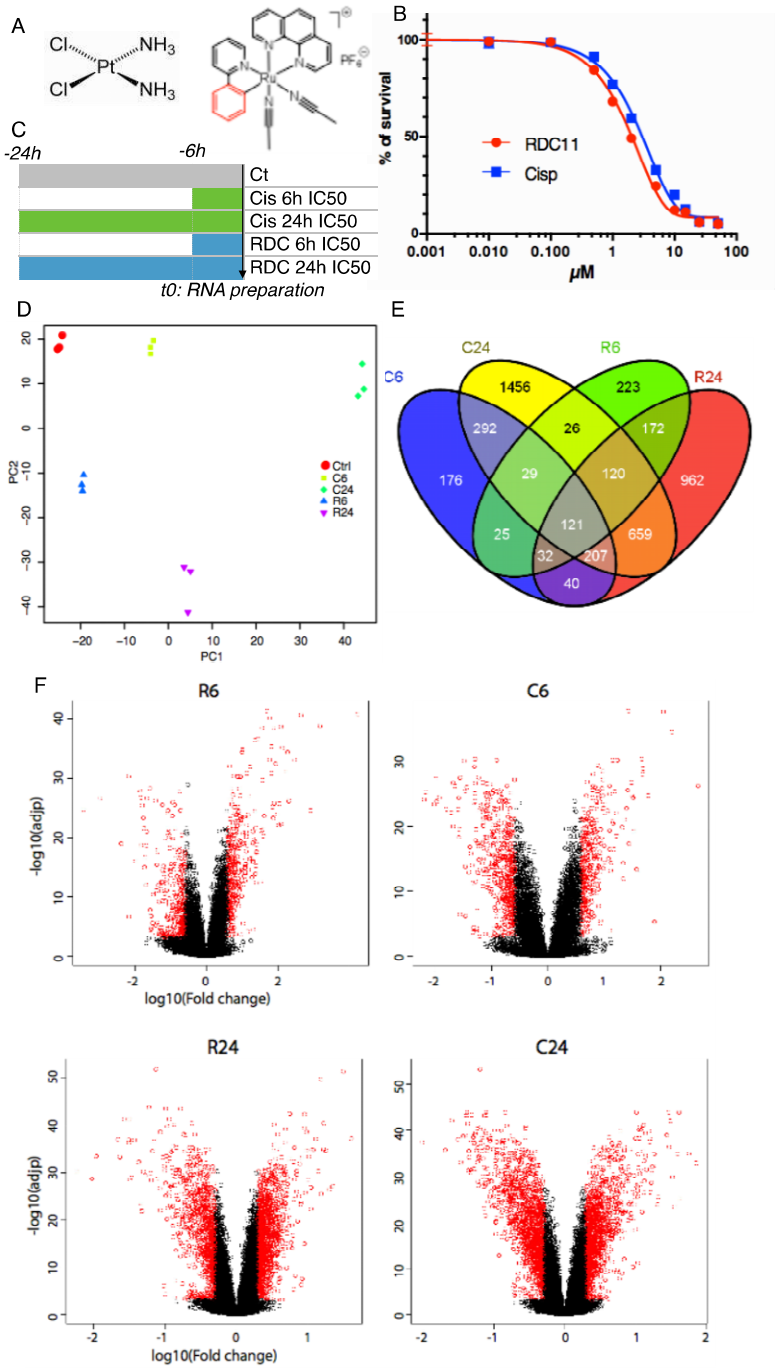

A
Cl
NH3
Pt
Cl
NH3
Ru
PF6
B
100
50
0
% of survival
RDC11
Cisp
0.001
0.010
0.100
1
10
100
µM
C
-24h
-6h
Ct
Cis 6h IC50
Cis 24h IC50
RDC 6h IC50
RDC 24h IC50
t0: RNA preparation
D
PC2
PC1
Ctrl
C6
C24
R6
R24
E
C24
R6
C6
R24
1456
223
292
26
172
176
29
120
962
121
25
659
32
207
40
F
R6
C6
R24
C24
-log10(adjp)
log10(Fold change)

Figure 2

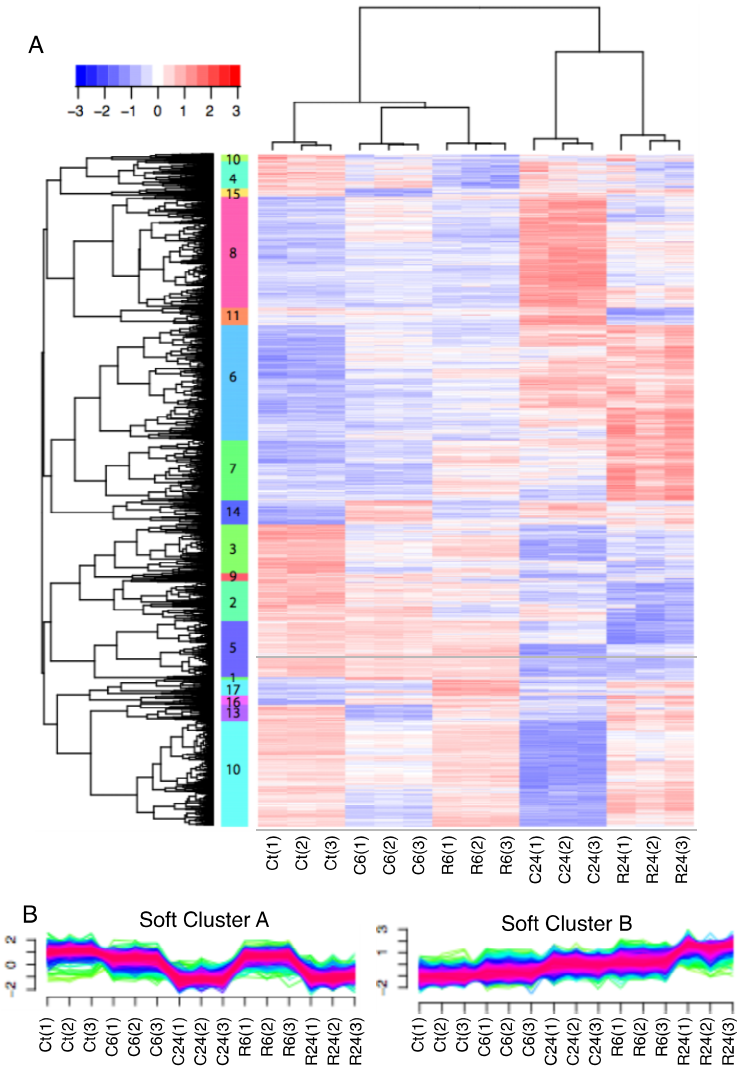

A
−3 −2 −1 0 1 2 3
10
4
15
8
11
6
7
14
3
9
2
5
1
17
16
13
10
Ct(1) Ct(2) Ct(3) C6(1) C6(2) C6(3) R6(1) R6(2) R6(3) C24(1) C24(2) C24(3) R24(1) R24(2) R24(3)
B
Soft Cluster A
Soft Cluster B
Ct(1) Ct(2) Ct(3) C6(1) C6(2) C6(3) C24(1) C24(2) C24(3) R6(1) R6(2) R6(3) R24(1) R24(2) R24(3)

Figure 3

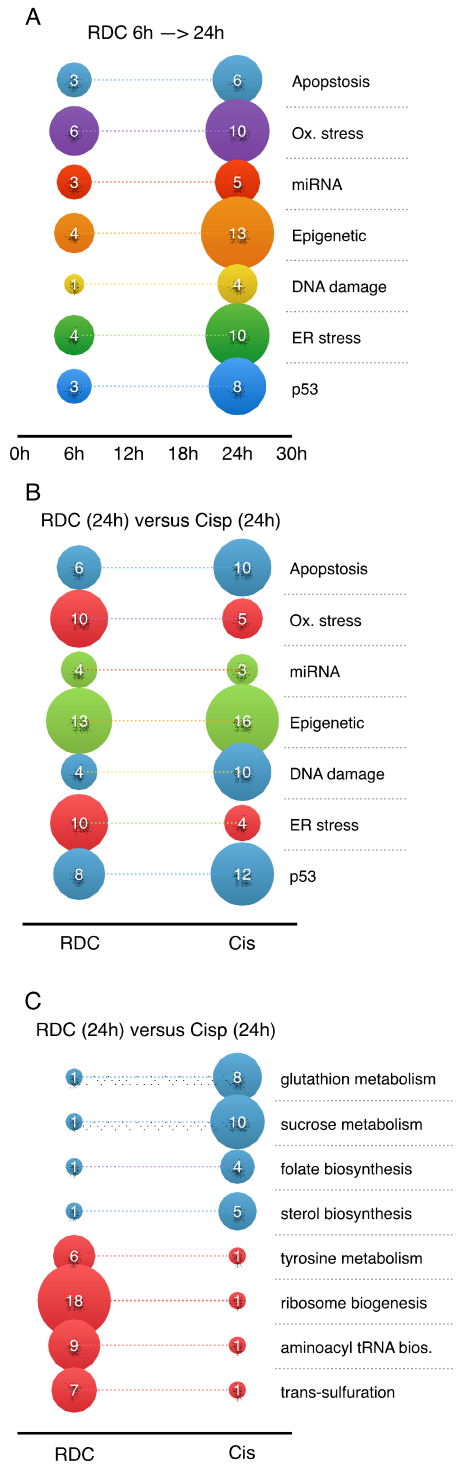

A
RDC 6h —> 24h
3
6
Apopstosis
6
10
Ox. stress
3
5
miRNA
4
13
Epigenetic
1
4
DNA damage
4
10
ER stress
3
8
p53
0h
6h
12h
18h
24h
30h
B
RDC (24h) versus Cisp (24h)
6
10
Apopstosis
10
5
Ox. stress
4
3
miRNA
13
16
Epigenetic
4
10
DNA damage
10
4
ER stress
8
12
p53
RDC
Cis
C
RDC (24h) versus Cisp (24h)
1
8
glutathion metabolism
1
10
sucrose metabolism
1
4
folate biosynthesis
1
5
sterol biosynthesis
6
1
tyrosine metabolism
18
1
ribosome biogenesis
9
1
aminoacyl tRNA bios.
7
1
trans-sulfuration
RDC
Cis

Figure 4

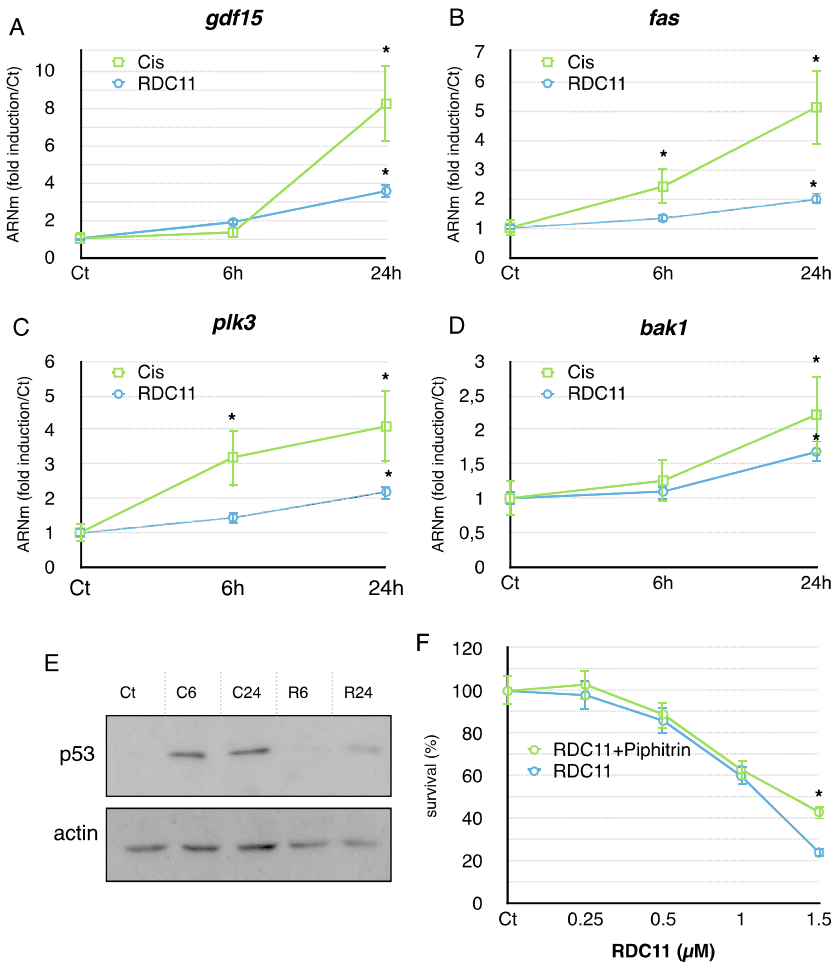

A
gdf15
Cis
RDC11
ARNm (fold induction/Ct)
Ct
6h
24h
B
fas
C
plk3
D
bak1
E
Ct
C6
C24
R6
R24
p53
actin
F
RDC11+Piphitrin
RDC11
survival (%)
RDC11 (μM)

Figure 5

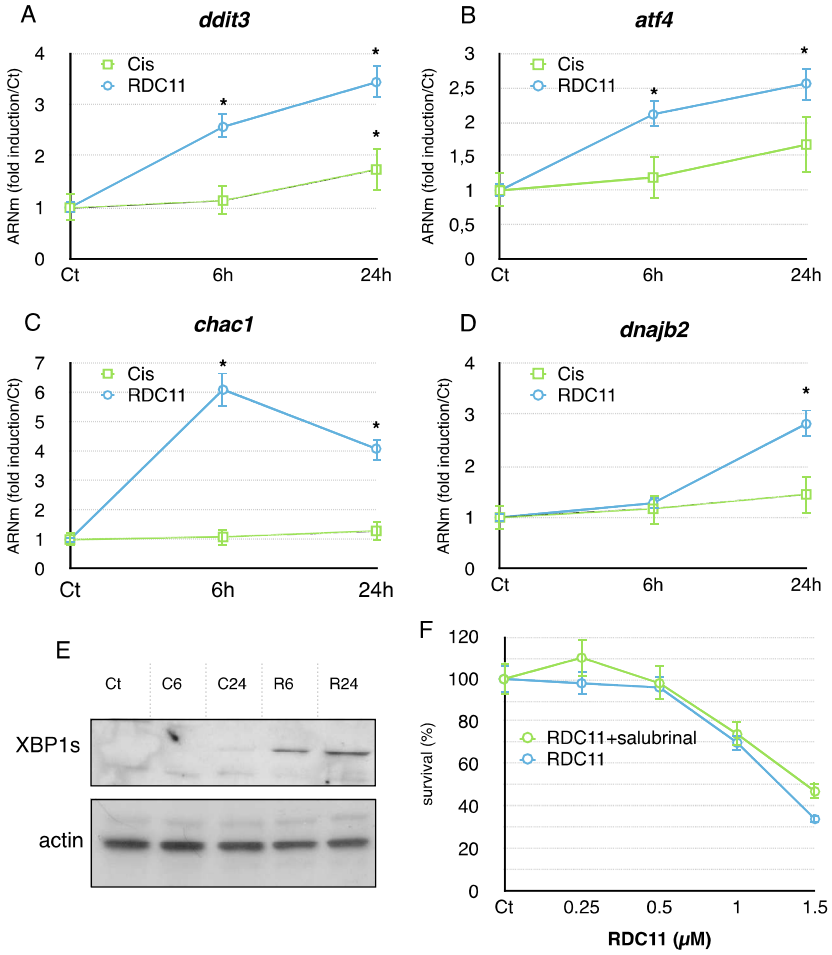

A
ddit3
ARNm (fold induction/Ct)
Cis
RDC11
Ct
6h
24h
B
atf4
C
chac1
D
dnajb2
E
Ct
C6
C24
R6
R24
XBP1s
actin
F
survival (%)
RDC11+salubrinal
RDC11
RDC11 (µM)

Figure 6

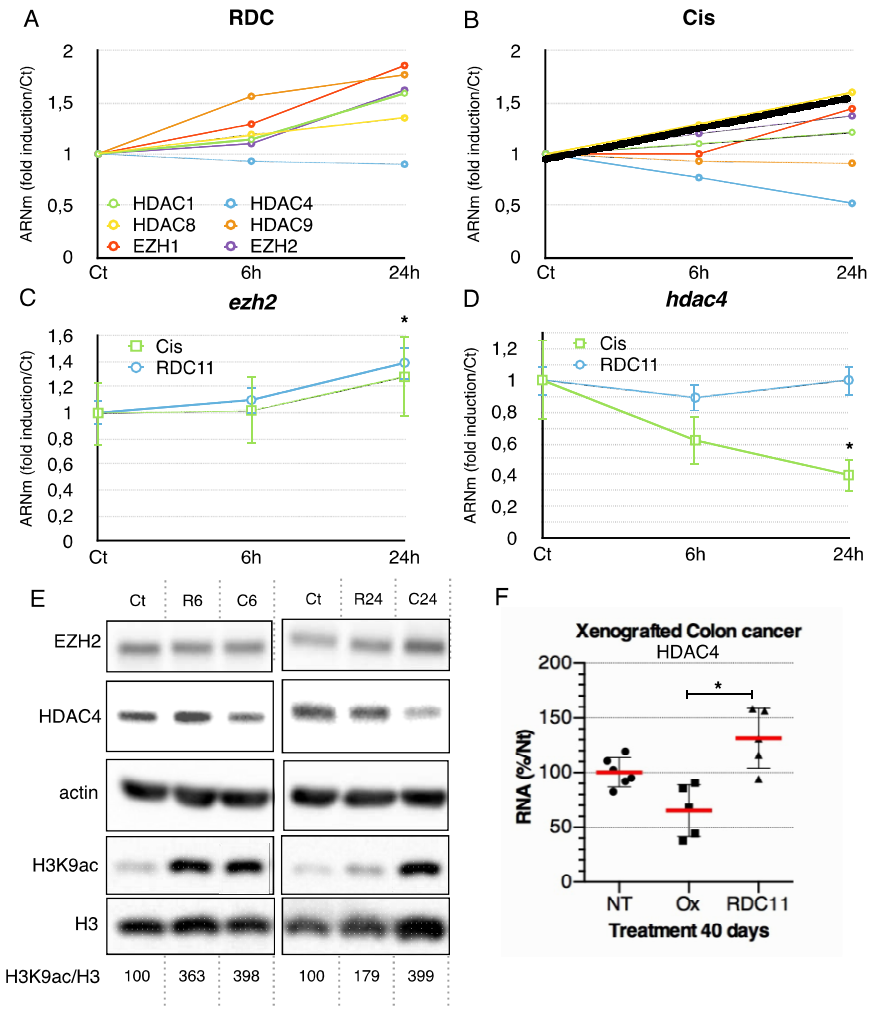
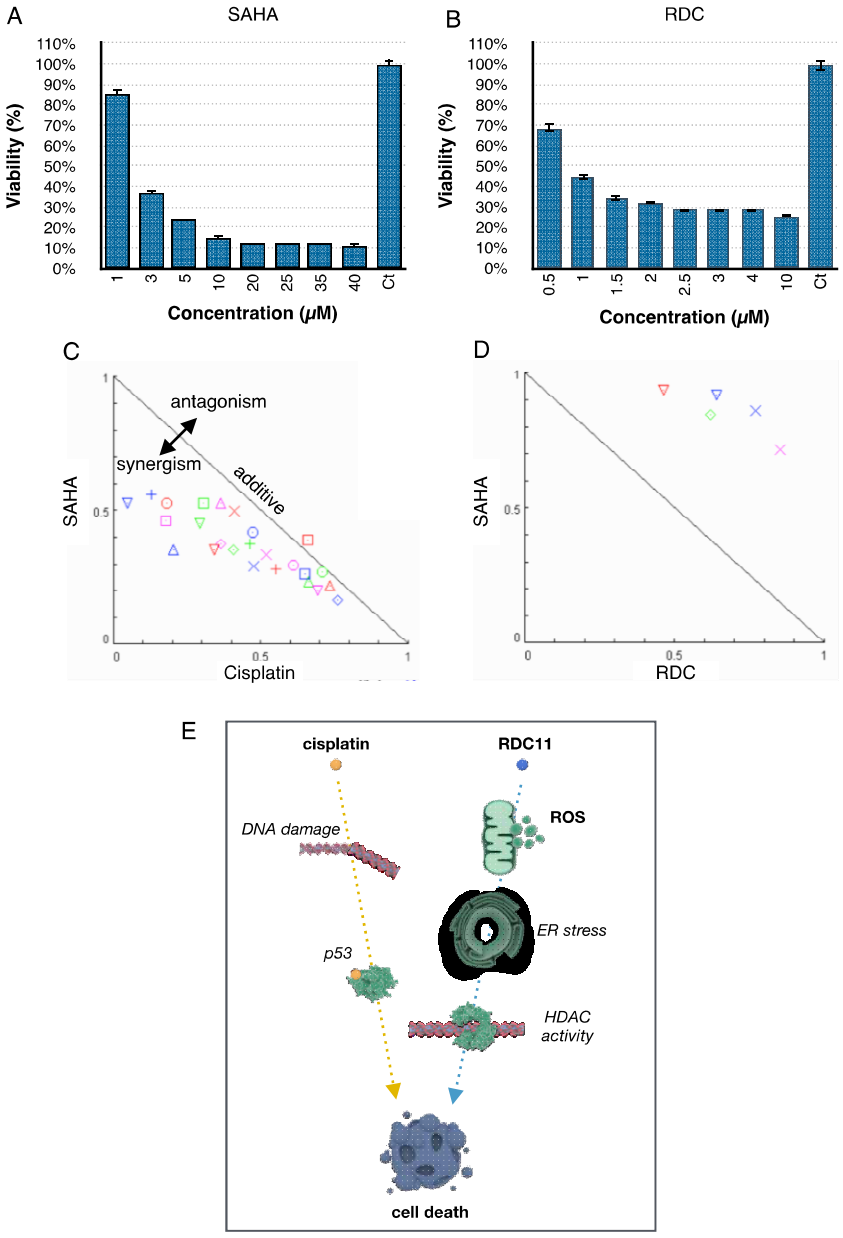

A
RDC
ARNm (fold induction/Ct)
HDAC1
HDAC4
HDAC8
HDAC9
EZH1
EZH2
Ct
6h
24h
B
Cis
C
ezh2
Cis
RDC11
D
hdac4
E
Ct
R6
C6
R24
C24
EZH2
HDAC4
actin
H3K9ac
H3
H3K9ac/H3
100
363
398
179
399
F
Xenografted Colon cancer
HDAC4
RNA (%/Nt)
NT
Ox
RDC11
Treatment 40 days

Figure 7


A
SAHA
Viability (%)
110%
100%
90%
80%
70%
60%
50%
40%
30%
20%
10%
0%
1
3
5
10
20
25
35
40
Ct
Concentration (μM)
B
RDC
Viability (%)
0.5
1
1.5
2
2.5
3
4
10
Ct
Concentration (μM)
C
antagonism
synergism
additive
SAHA
Cisplatin
D
SAHA
RDC
E
cisplatin
RDC11
DNA damage
ROS
ER stress
p53
HDAC
activity
cell death

CGN_C1_HuGene.CEL



CGN_C2_HuGene.CEL



CGN_C3_HuGene.CEL



CGN_C6_1_HuGene.CEL



CGN_C6_2_HuGene.CEL



CGN_C6_3_HuGene.CEL



CGN_C24_1_HuGene.CEL



CGN_C24_2_HuGene.CEL



CGN_C24_3_HuGene.CEL



CGN_R6_1_HuGene.CEL



CGN_R6_2_HuGene.CEL



CGN_R6_3_HuGene.CEL



CGN_R24_1_HuGene.CEL

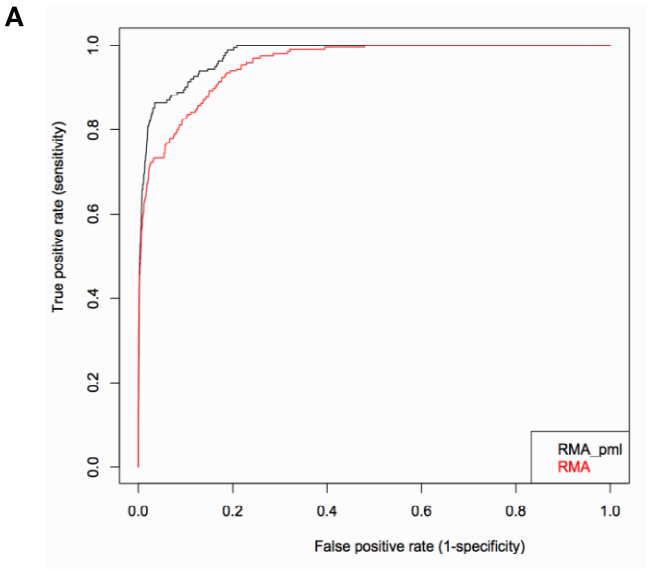


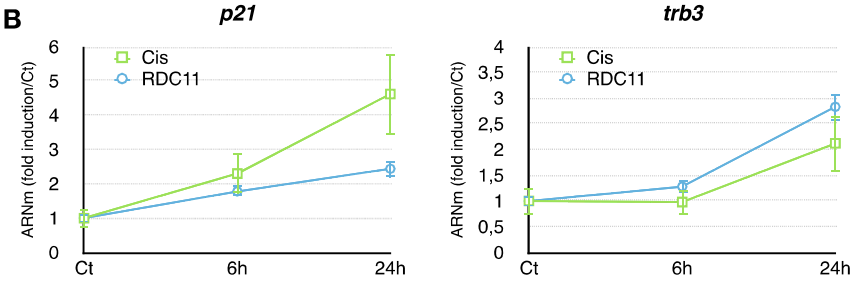
CGN_R24_2_HuGene.CEL



CGN_R24_3_HuGene.CEL

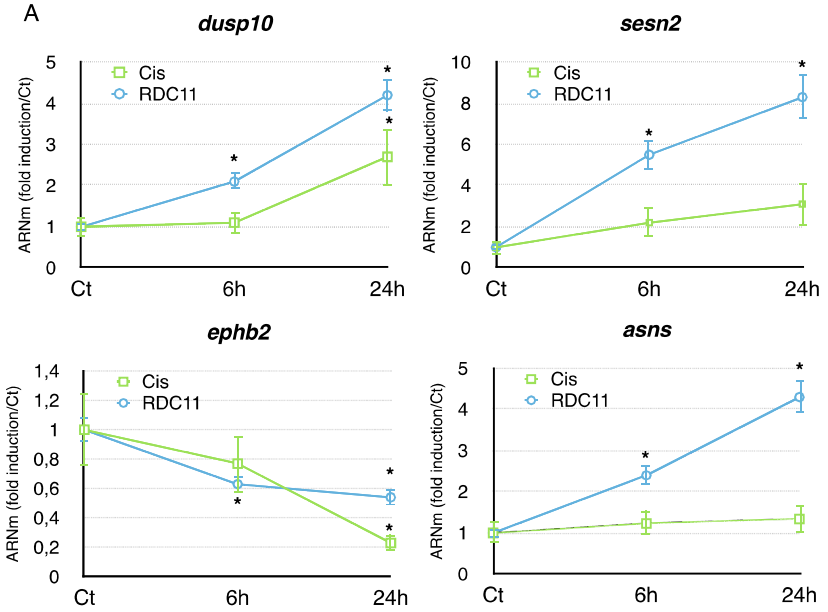






B. mRNA levels of *genes found disregulated in the microarraus: p21* and *trb3* were assayed by RT-qPCR. Curves are means of fold induction versus the control (Ct) with SD (n=3). *: $p < 0.01$.

A



B

		Array		RT-qPCR		RT-qPCR AGS		RT-qPCR HCT116	
		6h	24h	6h	24h	6h	24h	6h	24h
dusp10	*RDC*	+2.5	+4	+2	+4.3	-2.1	-1,2	+4.1	+7.1
	Cis	+1.5	+2.6	+1.1	+2.8	-2.2	-3.1	+1	+1
sesn2	*RDC*	+3.5	+5	+5.8	+8.1	+2	+2.4	+12.2	+7.1
	Cis	+1.7	+2.7	+2.1	+3.3	+1	-1.3	+3.3	+2.1
ephb2	*RDC*	+1	-2.8	–1.6	–1.8	1	1.5	-1.4	-5.2
	Cis	+1	-4.8	–1.3	–3.8	1	-5.6	-1.4	-5.1
asns	*RDC*	+5.2	+5.2	+2.4	+4.3	1	1.5	-1.4	-5.3
	Cis	+3.6	5.7	+1.2	+1.3	-4.9	-2.3	1	-2.1

mRNA levels of *genes found disregulated in the microarraus:* A. *dusp10*, *sesn2*, *eph2*, *asnas* were assayed in U87 (A, B RT-qPCR) colon cancer HCT116 (B) and gastric cancer AGS (B) cells by RT-qPCR. Curves are means of fold induction versus the control (Ct) with SD (n=3). *: $p < 0.01$. In B, number indicate average of fold changes.

Results (Objective 1)

V.B. Differential regulation of the HIF-1 pathways by platinum and ruthenium anticancer organometallic drugs.

Differential regulation of the HIF-1 pathway by platinum and ruthenium anticancer organometallic drugs

Vania Vidimar[1,2,4], Cynthia Licona[1,2], Ali Moussa[2,3], Ricardo Cerón Camacho[6], Ronan Le Lagadec[6], Dominique Guenot[2,5], Jean-Noel Freund[1,2], Georg Mellitzer[1,2], Gianni Sava[4], Michel Pfeffer[2,3], Christian Gaiddon[1, 2*]

[1]UMRS1113 INSERM, Strasbourg, France
[2]Université de Strasbourg, Strasbourg, France
[3]UMR 7177 CNRS, Institut de Chimie, Strasbourg, France
[4]University of Trieste, Department of Life Sciences, and Callerio Foundation Onlus, Trieste, Italy
[5]EA4438, Strasbourg, France
[6]Instituto de Química, UNAM, Circuito Exterior s/n, Ciudad Universitaria, México D. F. 04510, Mexico

[*]Corresponding Author: Christian Gaiddon, U1113 INSERM - Université de Strasbourg, 3 avenue Molière, Strasbourg 67200, France. Phone: +33 03 88 27 77 27, Fax: +33 03 88 26 35 38, Email Address: gaiddon@unistra.fr

Abstract

In recent years, ruthenium-based compounds were developed to overcome the severe side effects and drug-resistance phenomena of current widely used platinum-based anticancer drugs. In contrast to platinum derived drugs, it was suggested that ruthenium compounds exert their cytotoxicity in part independently from DNA and through direct modulation of redox enzymes. Therefore, we have compared the relative activity of platinum (cisplatin) and ruthenium (RDC11) based compounds on the redox metabolic pathway controlled by HIF-1. We showed that, in contrast to cisplatin, RDC11 was able to decrease HIF-1α and HIF-1β protein levels in normoxic and hypoxic conditions, which leads to decreased expression of HIF-1 target genes, such as *VEGF* and *Glut1*. We demonstrated that downregulation of HIF-1α protein levels involved a complex mechanism associating changes in *hif-1α* mRNA synthesis and HIF-1α protein stability. In addition, we provide the first evidence of a direct interaction of RDC11 with a protein target, the redox enzyme PHD2, which stimulates HIF-1α hydroxylation and degradation. Finally, we showed that the inhibitory effect of RDC11 on the HIF-1 pathway is consistent with its ability to reduce angiogenesis *in vivo*. Altogether, our results show that ruthenium derived compounds impact metabolic pathways and might therefore act as anticancer agent via an original mechanism of action involving redox enzymes.

Introduction

Since the discovery of cisplatin, the study of metal-based drugs has turned out to be one of the most promising fields of antitumor chemotherapy research. Cisplatin and its derivatives (oxaliplatin and carboplatin) are widely used as anticancer agents worldwide and are frequently part of combinatory regiments associating targeted therapy. Platinum derivatives exhibit their cytotoxic properties through the interaction with DNA, forming DNA adducts which activate several signaling transduction pathways leading to cell growth arrest or cell death [1] [2] [3]. By affecting the DNA integrity, these platinum-compounds target rapidly dividing cells, including tumor cells as well as healthy tissues. This poor selectivity is the main cause of platinum compounds severe side effects such as neurotoxicity [4, 5]. Furthermore, due to mutation in key signaling pathways causing resistance, only a limited number of tumors can be effectively treated with platinum derivatives [6] [7].

These limitations have prompted the search for less toxic and more effective platinum-free metal-based antitumor drugs. Several metal compounds, as derivatives of iron, gold, titanium, gallium and ruthenium, have been designed on the basis of cisplatin chemical structure in order to ameliorate activity and reduce host toxicity [8] [9] [10] [11] [12] [13]. *In vitro* screening of all these molecules revealed ruthenium-based drugs as the least toxic. It has been proposed that this lower toxicity could be linked to the ability of ruthenium to mimic iron in binding to biomolecules, such as transferrin and albumin, exploiting the mechanisms that the cell is using for the detoxification of iron in healthy tissues [14] [15]. Beside this characteristic, ruthenium compounds present other interesting chemical properties for the development of anticancer compounds: (a) the availability of 6 coordination sites leading to multiple combinations of ligands, (b) a slow rate of ligand exchange, compatible with a reasonable stability in a biological context and (c) several possible oxidation states allowing a potential interference with biological macromolecules.

Therefore, various structures of ruthenium derivatives have been tested *in vivo* and they seem to offer promising anticancer activities, notably against cisplatin-resistant tumors [16], lower general toxicity compared to cisplatin [14] [15] [17] and even antimetastatic activity [18] [19]. To date, two ruthenium complexes have entered clinical trials, namely NAMI-A and KP1019 [20]. NAMI-A is an anti-metastatic compound, currently in phase II clinical trial, able to stabilize the progression of non-small cell lung carcinoma in pre-treated patients [21]. KP1019, which at present undergoes phase I clinical trials under the form of its salt derivate KP1339, is well tolerated and patients with advanced solid tumors experienced disease stabilization for more than two months [16] [22].

Although already tested in clinic and largely studied in pre-clinic, the mode of action of ruthenium derived compounds remains unclear. Since ruthenium derivatives have been often designed to mimic platinum compounds, it was expected that they showed a mechanism of action similar to that of cisplatin, especially for targeting DNA. It has been indeed demonstrated that ruthenium compounds bind DNA, although quite differently from cisplatin [23-25] [26-29]. The later may explain the dissimilar anticancer effects of ruthenium derivatives compared to cisplatin and their ability to exert cytotoxic effects on cisplatin-resistant cancer cells [30] [31] [26]. Since no strict correlation between cytotoxicity and DNA interaction has been found for ruthenium compounds, DNA-independent modes of action have been proposed.

In our lab, we have developed a class of anticancer ruthenium compounds (RDC, ruthenium derived compounds) that present the particularity of having a covalent bond between the ruthenium atom and a carbon atom [26]. The presence of this covalent bond confers a specific range of redox potentials that correlates with the cytotoxicity of the compounds and that allow them to be efficient as mediators of electron transfer to or from oxidized or reduced active sites of redox enzymes, affecting their activity [32] [33]. This ability of ruthenium compounds to affect the activity of cellular redox enzymes is also supported by Sadler and co-workers that have shown that ruthenium derivatives interact with biological nucleophiles such as GSH [34] leading to GSH depletion and increased sensitive to reactive oxygen species (ROS) [35]. In addition, we have shown that the cytotoxicity of one of the RDC, RDC11, is dependent on the activity of the transcription factor CHOP, which is a critical effector of the endoplasmic reticulum stress signaling pathway [17] [36] [29, 37]. This pathway, besides being activated by the accumulation of unfolded proteins, has been proposed to play a role in tumorigenesis via its induction by high glucose, ROS and hypoxia [38]. This observation further supports the idea that ruthenium derived compounds might regulate the activity of redox enzymes affecting the cellular metabolisms.

Therefore, we hypothesized that RDC molecules might regulate other intracellular signaling pathways that control, or are sensitive to the cellular metabolisms. In this study, we analyzed the regulation of one of these pathways, the HIF-1 pathway, that is strongly connected to the adaptive metabolic response of cancer cells to the hypoxia developed in poorly vascularized tumors [39]. HIF-1 (Hypoxia Inducible Factor 1) is a transcription factor that consists of two subunits: a constitutively expressed β subunit (Hif-1β) and a highly regulated α subunit (Hif-1α) [40]. HIF-1 is usually inactive under basal conditions but active in many hypoxic solid tumors, leading to resistance to chemotherapy and aggressive tumor progression [41]. HIF-1 regulates the transcription of genes involved in crucial aspects of cancer biology, such as angiogenesis and glucose metabolism. Angiogenesis is one of the main responses that cancer cells carry out in hypoxic conditions and involves the increase of

VEGF production, while glucose metabolism represents the major source of energy in low-oxygen environments.

HIF-1α is frequently deregulated and overexpressed in cancer and this is often associated with poor prognosis and negative outcome for patients [42]; [43]. Therefore, alterations of the HIF-1 pathway in tumors make them attractive targets for anticancer therapy. Based on these observations and the fact that ruthenium derived compounds might regulate the cellular metabolisms, we compared the regulation of the HIF-1 pathway by both platinum and ruthenium derived compounds.

Materials and Methods

Chemicals. Ruthenium derived compounds were synthesized as previously described [26, 33]. Cisplatin was purchased from Mylan Pharmaceuticals, Deferoxamine Mesylate from Sigma-Aldrich® and MG132 from Calbiochem. Rapamycin was obtained from Tocris Bioscience. Glucose oxidase from *Aspergillus niger* was obtained from Sigma (211 U mg^{-1}), *D*-glucose was obtained from Acros.

Kinetics of enzymatic O_2 uptake

The measurements were made using a homemade Clark electrode with a mylar surface (YSI Yellow springs) equipped with a probe YSI 5331 in a 1.5 mL cell, the temperature of which was controlled at 25 °C. The calibration was performed as follows. The cell was filled with distilled water at 25 °C with stirring and a voltage was recorded. Then the cell was cleaned and filled with the previously deoxygenated water (in vacuum and bubbled with argon) and a lower voltage was recorded. A drop in 0.06 V was referred to 1.21×10^{-3} M of O_2 ($[O_2]$ in water at 25 °C). The buffer was first added into the cell followed by a ruthenium complex solution and GO. The solution was stirred and the recording device was turned on. The reaction was initiated by the addition of a solution of *D*-glucose after 20 s and the cell was immediately sealed. Time intervals between readings were in the range of from 3 to 10 min depending on the concentration of *D*-glucose, which was varied in the range of from 0.0025 M to 0.1 M. The concentrations of ruthenium complexes used are indicated in legends to Figures. Each measurement was made at least in duplicate.

Cell culture and MTT (3-(4,5-Dimethylthiazol-2-yl)-2,5-diphenyltetrazolium bromide) test. Human colorectal adenocarcinoma HCT116 and SW480 cells were maintained at 37°C in normoxic (20% O_2, 5% CO_2) or hypoxic (94% N_2, 5% CO_2, 1% O_2, Tri-Gas Incubator, Sanyo) conditions in DMEM 1 g/L glucose (Dulbecco's modified Eagle's medium; Life Technology) supplemented with 10% heat-inactivated fetal calf serum (Life Technology), penicillin/streptomycin (100UI/ml – 100 µg/ml) and gentamycin (50mg/ml). Cells were

trypsinyzed for maintenance and experimentation plates as previously described [44]. HUVEC (Human Umbilical Vein Endothelial Cells) were grown in Endothelial Cell Basal Media from Cambrex supplemented with L-glutamine and 10% FBS. MTT test was performed using 96-well culture plates (Costar) as previously described [45].

Western Blot. Cells were grown in six-well plates, and for each condition, three wells were treated. Cells were lysed in 120 µl of Laemmli Sample Buffer 1X (125 mM Tris–HCl, pH 6.7, containing 3.3% SDS, 0.7 M 2-mercaptoethanol, 10% glycerol and 0.02% Bromophenol Blue), sonicated for 30 seconds and then boiled for 5 minutes before loading as previously described [46]. Equal amounts of denaturated total-protein extracts were separated on a 12% SDS-polyacrylamide gel and then electro-transferred to nitrocellulose membranes (Bio-Rad Laboratories). Equal loading was ensured by using an antibody directed against actin (1/2000; Sigma). Immunoprobing was controlled with anti-HIF-1α (1/500; BD Transduction Labs), anti-HIF-1β (1/1000; Novus Biologicals), anti-PHD2 (1/1000, Abcam). Nitrocellullose membranes were then probed with a secondary horseradish-peroxidase-conjugated antibody (anti-rabbit or-mouse according to the first antibody, SantaCruz) diluted at 1/5000 and 1/1000 respectively. Antibody reaction was revealed with chemiluminescence detection procedures according to the manufacturer's recommendations (Immun-Star™ HRP Chemiluminescence Kits, Bio-Rad Laboratories) and by using the Molecular Imager® ChemiDoc™ XRS+ System (Bio-Rad Laboratories).

RDC11-matrix affinity precipitation. Cells were grown in 10 cm plates, and for each condition, three plates were used. Precipitations were performed as previously described [47]. Cells were lysed in 1ml of NP40 lysis Buffer 1X (125 mM Tris–HCl, pH 6.7, containing 0.1% NP40, 10% glycerol, 150mM NaCl), sonicated for 30 seconds. Equal amounts of total-protein extracts (3 mg) were incubated 5 hours with 100µl of 50% slurry RDC11-matrix beads. After 4 washes in NP40 lysis buffer, complexes were either boiled or eluted using RDC11 (5µM) or cisplatin (5µM). Proteins were then denaturated in Laemmli sample buffer and separated on a 12% SDS-polyacrylamide gel and then electro-transferred to nitrocellulose membranes (Bio-Rad Laboratories). Immunoprobing was controlled with anti-PHD2 (1/1000, Abcam). Nitrocellullose membranes were then probed with a secondary horseradish-peroxidase-conjugated antibody (anti-rabbit or-mouse according to the first antibody, SantaCruz) diluted at 1/5000 and 1/1000 respectively. Antibody reaction was revealed with chemiluminescence detection procedures according to the manufacturer's recommendations (Immun-Star™ HRP Chemiluminescence Kits, Bio-Rad Laboratories) and by using the Molecular Imager® ChemiDoc™ XRS+ System (Bio-Rad Laboratories). Matrix-RDC11 was synthesized attaching RDC11 onto a Hypogel 400-COOH (Sigma). Successful synthesis was assessed by spectroscopy.

Quantitative reverse transcription-PCR (RT-qPCR). Expression of the different genes was quantitatively assessed by real-time PCR using *18S* as the normalizing gene as previously described [4]. Cells were grown in six-well plates, and for each condition, three wells were treated. After treatment, cells were harvested and total RNA was isolated with TRIzol reagent (Invitrogen) according to the manufacturer's instructions. RNA was quantified using a Nanodrop 2000 Spectrophotometer (Thermo Scientific) and cDNA synthesized from 1µg total RNA using the iScript cDNA synthesis kit (Bio-Rad Laboratories). qPCR was performed in Bio-Rad iCycler thermal cycler using iQ SYBR Green supermix (Bio-Rad Laboratories). Specificity of the amplification was assessed by performing a melting curve analysis.
Nucleotide sequences of the primers were as follows: *VEGF* (forward 5'-ccttgctgctctacctccac-3'; reverse 5'-ccacttcgtgatgattctgc-3'); *GLUT1* (forward 5'-ggttgtgccatactcatgacc-3'; reverse 5'-cagataggacatccagggtagc-3'); *HIF1α* (forward 5'-tttttcaagcagtaggaattgga-3'; reverse 5'-gtgatgtagtagctgcatgatcg-3'); *HIF1β* (forward 5'-aggcttttctgcccaggt-3'; reverse 5'- ctgaaggaggatggagtctga-3'); ENO1 (forward 5'-tcccaacatcctggagaataa-3'; reverse 5'-atgccgatgaccaccttatc-3');.

Determination of the NAD/NADH ratio following RDC11 treatment. Total NAD and NADH levels were quantified according to the protocol provided in the NAD/NADH Assay Kit (Abcam), using $2x10^5$ cells for each condition. Both NAD and NADH were calculated from a standard curve.

***In vitro* angiogenesis.** The anti-angiogenic potential of RDC11 was studied *in vitro* by looking at its ability to inhibit the generation of a capillary-like network by HUVECs. Briefly, 96-well plates were coated with ECMatrix™ (Millipore) which was allowed to polymerize at 37°C for 45 min. 5000 cells were then seeded in 200 µl of medium into each well. 1h later, cells were treated with 200 µl of medium containing cisplatin or RDC11. After 4h, cells were photographed and tube formation or intersections between cells were scored manually and expressed relative to controls.

***In vivo* angiogenesis plug assay.** The *in vivo* anti-angiogenic potential of RDC11, was assessed using the Matrigel plug assay [48]. C57BL/6 female mice (6 weeks old) were injected subcutaneously with 600µl of cold liquid phenol-red free Matrigel (BD Bioscience) supplemented with VEGF (36ng/Matrigel plug; PeproTech), heparin (12U/Matrigel plug; Sigma), TNF-α (0.72ng/Matrigel plug; PeproTech), PBS (for controls) or RDC11 (5µM), near the abdominal midlines and at the base of the neck. The syringes containing Matrigel were kept on ice until the time of injection to prevent gelification. At 37°C (*in vivo*), Matrigel quickly polymerized to form a solid gel. After 4 days, mice were sacrificed and the Matrigel plugs explanted. Matrigel plugs were subsequently washed with PBS, photographed and then

weighed. Their hemoglobin content was evaluated with the Drabkin's reagent kit according to the manufacturer's instructions (Sigma).

In vivo angiogenesis in colon cancer primary xenografted tumors. Fragment of a surgical piece of a human colon tumor was subcutaneously implanted and amplified in nude mice. For the experiment, pre-amplified tumors were extracted and homogenized to be implanted into novel nude mice. Two homogenous tumor samples (100µl) were implanted subcutaneously in mice at each side of their back. Treatments were started once tumors reached 100mm^3 of volume. Tumor volumes and mouse weights were monitored thorough the experiment during 40 days. Vascularization of the tumors was monitored by measuring hemoglobin content by colorimeter and by measuring the expression of Hif-1 target genes by RT-qPCR.

Intracellular reactive oxygen species (ROS) measurement

5-(and-6)-carboxy-2′,7′-dichlorodihydrofluorescein diacetate (carboxy-H2DCFDA) (Molecular Probes) was used to detect intracellular ROS levels according to the manufacturer's instructions and as previously described [49]. For ROS quantification, cells were seeded in 96-well black plates (Greiner Bio-One) and treated with RDCs at the indicated concentrations and times. Afterwards, cells were washed with PBS and incubated with 10µM carboxy-H2DCFDA in DPBS for 1h. Cells were then washed with PBS and fluorescence was measured by a plate reader (Perkin Elmer) with an excitation wavelength of 485 nm and an emission wavelength of 535 nm.

Results

RDC11 induces radical oxidized species and NAD production

We have previously shown that, through their redox potential, ruthenium derived compounds are able to alter the activity of cellular redox enzymes involved in the metabolism, such as the glucose oxidase [32] [33]. We measured the effect of the ruthenium-based compound RDC11 on the activity of glucose oxidase *in vitro* using a Clarke electrode to follow 0_2 consumption in presence of increased concentration of glucose and RDC11 (Fig. 1A-C). Increased quantity of RDC11 reduced the activity of the redox enzyme glucose oxidase. To further explore a potential impact of ruthenium-based compounds on cellular metabolism we examined the effect of RDC11 on several markers of the metabolism in HCT116 human colon cancer cells. In these cells, RDC11 presents, similarly to Cisplatin, an IC50 close to 5 µM (Fig. 1D). We observed that treatment with RDC11 increased over time the amount of reactive oxidized species (ROS) produced by the metabolism, starting already at 1h (Fig. 1E). In addition, we checked the NAD/NADH ratio because of its importance in controlling the activity of cellular enzymes critical for cancer development, such as the PARP and the SIRT [50, 51]. As shown on Figure 1F, RDC11 produced a rapid increase in NAD production over

NADH. Taken together, these data suggest that treatment with RDC11 affects the cellular metabolism.

Platinum and ruthenium compounds differently impact on HIF1 mRNA and protein levels

We then monitored the activity of HIF-1, a key component of the signaling pathways that are sensitive to and control by the cellular metabolism [39], upon RDC11 or cisplatin treatment. For this, we followed the expression levels of its α and β subunits in colon cancer HCT116 and SW480 cells, in normoxic and hypoxic conditions. As expected, HIF-1α was not expressed or only expressed at low levels in the normoxic condition, due to its O_2-dependent prolyl hydroxylation with subsequent ubiquitylation and proteasomal degradation [40] (Fig. 2A, B). RDC11, unlike cisplatin, strongly reduced HIF-1α protein levels in hypoxia in both cell lines and also in normoxia in HCT116 cells after 6 and 24h of treatment. As described HIF-1β was constitutively expressed and RDC11 lowered its expression especially after 24h of treatment in normoxia and hypoxia in both HCT116 and SW480 cells.

As RDC11 reduced HIF-1 protein levels, we investigated its effect on HIF-1 mRNA levels (Fig. 2C, D). RT-qPCR showed that RDC11, was able to strongly reduce *HIF1α* and *HIF-1β* mRNA in both normoxia and hypoxia after 24h of treatment in HCT116 cells, which is consistent with its drastic effect on HIF-1 proteins. However, the lower reduction of *HIF-1α* and *HIF-1β* mRNA observed 6h after RDC11 treatment suggests that other mechanisms also contribute to the rapid and dramatic loss of HIF-1α protein levels.

Ruthenium–based compound RDC11 reduces HIF1 activity

We also analyzed if the drastic decrease of HIF-1 protein levels induced by RDC11 had consequences on the expression of different HIF-1 target genes [40], such as *VEGF* involved in angiogenesis or *Glut1* and Eno1 involved in glucose metabolism. As expected, hypoxia induced the expression of these HIF-1 target genes (Fig. 3). After 24h of treatment, RDC11 drastically reduced the mRNA level of all 3 genes, both in normoxia and hypoxia (Fig. 2). This negative effect was already detected after 6h of treatment. Although Cisplatin was able to reduce VEGF and Glut1 levels in hypoxia, it was overall clearly less effective than RDC11. Altogether, these data indicated that RDC11 was more potent to reduce both HIF-1 protein levels and activity in colon cancer cells than Cisplatin.

RDC11 reduces HIF-1α protein levels through multiple mechanisms

Since RDC11 reduced drastically HIF-1α protein levels already at 6 hours (Fig. 2A), when mRNAs are only moderately affected (Fig. 2C, D), we wondered what mechanisms could be involved. Degradation of HIF-1α protein by the proteasome after hydroxylation by the iron-containing PHD2 enzyme is one of the important mechanisms regulating its cellular levels

[40]. Thus, we assessed if RDC11 was still able to reduce HIF-1α levels in the presence of MG132, a potent and reversible proteasome inhibitor. As expected, in absence of RDC11, the MG132 treatment clearly stabilized HIF-1α proteins (Fig. 4A, B). Strikingly, this accumulation of HIF-1α induced by MG132 was also detected but to a much lower extent in the presence of RDC11, both in normoxia and hypoxia. These results suggest that RDC11 indeed stimulates the degradation of HIF-1α proteins through the proteasome but also uses other mechanisms to drastically reduce its proteins levels. Similar observations were made with another inhibitor of the proteasome pathway (ALLN) and inhibitors of calpaine (ALLM) and caspases (Z-VAD-FMK) were also not able to block the loss of HIF-1α proteins, suggesting that the activity of the ruthenium compound is only partially mediated by protein degradation.

RDC11 interacts with the hydroxylase PHD2

However, we also noted that RDC11 tended to favor the hydroxylated form of HIF-1α (lower band) during hypoxia, in presence and in absence of MG132 (Fig. 2B). To further understand the role of the hydroxylation in the RDC11-induced loss of HIF-1α, we used assessed whether RDC11 could directly interact with PHD2. To do so, we covalently attached RDC11 molecules onto a matrix (Hypogel 400) and we incubated the RDC11-matrix with cellular protein extracts. After several washes, proteins were detached by boiling or by competition with free RDC11 or cisplatin and separated on SDS PAGE before immunoblotting for PHD2 detection (Fig. 5A). A naked matrix (Matrix-Ø) was used to assess the specificity of the interaction. Incubation of cellular extracts with the RDC11-matrice pulled down PHD2. The specificity of the interaction between RDC11 and PHD2 was indicated by the absence of bands when the naked matrix was used or when proteins were eluted with cisplatin.

To further investigate the role of PHD2 in RDC11 regulation of HIF-1α, we use the iron chelator deferoxamine (DFO), which inhibits PHD enzymes (Fig. 5A). As reported, deferoxamin induced HIF-1α stabilization through the accumulation of its non-hydroxylated form (upper band, Fig. 5B). Upon PHD inhibition, RDC11 did not favor the lower and hydroxylated band of HIF1α. In addition, RDC11 had significantly less effect on HIF1α protein level, indicating the partial dependence of RDC11 activity on PHD function. As these data suggested that RDC11 might affect HIF-1α hydroxylation status, we examined the expression of PHD2, the main regulator of HIF-1α, but RDC11 had no effect on PHD2 protein levels (Fig. 5C). Hence, these results indicate that RDC11 interacts directly with PHD2 and that PDH function is important for RDC11-dependent donwregulation of HIF-1 protein level.

RDC11 reduces angiogenesis both *in vitro* and *in vivo*

The ability of RDC11 to reduce HIF-1α and *VEGF* expression led us to hypothesize that it could affect angiogenesis. Therefore, we investigated the effect of RDC11 on angiogenic processes. We first observed that, *in vitro,* RDC11 was able to reduce the formation of intersections between HUVECs 4h after treatment (Fig. 6A) [52]. To assess the effect of RDC11 on angiogenesis *in vivo,* we used an assay in which angiogenesis was induced by different factors embedded in a Matrigel plug implanted subcutaneously in mice. 4 days after the injection, the plugs were extracted and the degree of vascularization was evaluated by assessing the hemoglobin content. The Matrigel plugs containing RDC11 were nearly uncolored, while the control plugs were redder, characteristic of the presence of small blood-filled channels (Fig. 6B). Quantification of the hemoglobin content confirmed this difference. These results showed that RDC11 was able to exert an anti-angiogenic effect both *in vitro* and *in vivo*.

To further analyze the biological activity of RDC11 *in vivo*, we subcutaneously injected in nude mice homogenized colon tumor fragments from a patient. The xenografted mice were then treated with RDC11 (11µmole/Kg) or Oxaliplatin (11µmole/Kg). Tumor volumes were monitored for 40 days. RDC11 reduced significantly tumor size (±45%) compared to Oxaliplatin (Fig. 6D). Tumors were analyzed for hemoglobin content and expression of HIF1α target genes (*vegf* and *glut1*). Treatment of the tumors with RDC11 reduced both the vascularization and the expression of Hif1α target genes (Fig. 6C, E).

Discussion

Platinum-based drugs have greatly contributed to the treatment of cancer despite their severe side effects and drug-resistance phenomena. To overcome these drawbacks, platinum-free metal-based drugs have been thoroughly studied. Others and us have already identified some biological properties of different ruthenium-derived compounds, showing a lack of a strict correlation between DNA damage and their cytotoxicity [17]. In particular, we have previously shown that these compounds are able to alter the activity of redox enzymes that are involved in the cellular metabolism, which seems to correlate with their cytotoxicity [33] [53]. However, the physiological consequences of these alterations are still largely unknown. In this study, we have comparatively investigated the effect of ruthenium and platinum derived compounds on the Hypoxia-Inducible Factor 1 (HIF-1) pathway that is one of the major signaling pathways that are sensitive and that control the cellular metabolism.

We first confirmed that the ruthenium compound RDC11 alters the activity of the redox enzyme glucose oxidase. We also showed that RDC11 impacts on the cellular metabolism, indicated by an increase in the ROS level (Fig. 1), as previously reported [34, 35]. This alteration of the cellular metabolism is further supported by our observation of an increase in the NAD/NADH ratio. This modification of the cellular metabolism might be a direct reflection

of the uncontrolled reduction of cellular redox enzymes that have a redox potential slightly above the one of the ruthenium compounds [53]. As we have previously showed that the optimal redox potential for RDCs is between 0.3V and 0.6V, the redox enzymes or cofactors should have a redox potential above 0.3V to be reduced [33]. In addition, bioinformatic modeling studies indicated that the redox center of the ruthenium compound should be at no more that 3Å from the redox center of the enzyme to be targeted (AD Ryabov, personal communication).

This RDC11-induced perturbation of the cellular metabolism impacted on signaling pathways, namely on the HIF-1 pathway. Indeed, HIF-1α protein levels were dramatically reduced by RDC11 both in normoxia and hypoxia (Fig. 2). Interestingly, cisplatin was less efficient. This points out that platinum- and ruthenium-based molecules can act differently, even so they are sharing similar chemical features. Moreover, RDC11 was able to reduce HIF-1β protein levels. This downregulation of both HIF-1 subunits correlated with a decrease in the expression of several HIF-1 target genes, linked to angiogenesis or glucose metabolism (Fig. 3). On the contrary, cisplatin showed only a minor effect on HIF-1 target genes' expression, suggesting again a different mode of action for the two types of drugs.

We investigated the mechanism of HIF-1α protein decrease by RDC11 and observed that the drug could act at multiple levels. Indeed, we found that the RDC11-induced loss of HIF-1α proteins involved reduction of *HIF-1α* mRNA levels, increase of HIF-1α protein degradation and probably also reduction of HIF-1α protein synthesis. RDC11 drastically decreased *HIF-1α* mRNA levels within 24h (Fig. 2), suggesting repression of the *HIF-1α* promoter or destabilization of the *HIF-1α* mRNA by a yet unknown mechanism. However, the progressive reduction of *HIF-1α* mRNA levels cannot solely account for the dramatic loss of HIF-1α proteins already observed 6h after RDC11 treatment, suggesting the involvement of other mechanisms, such as enhanced degradation by the proteasome pathway. This mechanism is consistent with the fact that HIF-1α is tightly regulated by this mechanism during the shift between normoxia and hypoxia [40]. However, both in normoxia and hypoxia, blocking of the proteasome with inhibitors only slightly impacted on the ability of RDC11 to reduce HIF-1α protein levels (Fig. 4), suggesting that enhanced degradation is not the only mechanism involved.

Nevertheless, RDC11 controls partially the degradation of HIF-1α and its hydroxylation as observed by its change in migration in Western blot (Fig. 4). We showed that RDC11 interact directly with PHD2 and that diminution of HIF-1α protein level caused by RDC11 is partially dependent on the function of PHD enzymes (Fig. 5). Therefore, we might hypothesize that PHD2 is a direct target of RDC11 and that RDC11 might stimulate the activity of PHD2 by a mechanism yet to be discovered. Since this enzyme contains an iron atom [40], it is tempting

to imagine that the redox potential of RDC11 might interfere with this enzyme, maybe somehow stimulating its activity.

The new information gathered on the mode of action of ruthenium compounds through this study is of high interest for anticancer therapy. Indeed, we found that key actors of the tumorigenesis are affected by RDC11. The HIF-1 pathway is playing a prominent role in the nutritional status of cancer cells and by making them able to adapt to oxygen deprivation: consistently, we observed that RDC11 treatment reduced VEGF synthesis and angiogenesis (Fig. 6).

When considering the platinum versus the ruthenium complexes, this study highlights a differential regulation of the HIF-1 pathway. This observation further supports our precedent findings that these two classes of organometallic compounds have different mechanisms of action. Platinum compounds act through DNA, while ruthenium compounds have a more complex mode of action, involving partly DNA, but also an alteration of the activity of redox enzymes involved in the cellular metabolism. In turn, alteration of the cellular metabolism impacts on the regulation of specific signaling pathways, such as the HIF-1 pathway, which normally ensure a cellular homeostasis. The identification of the direct targets of the ruthenium complexes represents an interesting and crucial challenge. Solving this challenge will pave the way for the design of more potent and more selective drugs that might target precise enzymatic activities essential for cancer cells survival, which remains the main obstacles of cancer chemotherapy today.

Acknowledgment

This work is supported by CNRS, ARC (# 3288), La Ligue Contre le Cancer (Comite du Bas-Rhin), ANR, INSERM, INCA, CONECTUS, European COST action CM1105.

References

1. Bernges, F. and E. Holler, *The reaction of platinum(II) complexes with DNA. Kinetics of intrastrand crosslink formation in vitro.* Nucleic Acids Res, 1991. **19**(7): p. 1483-9.
2. Burstyn, J.N., et al., *Formation of cis-diamminedichloroplatinum(II) 1,2-intrastrand cross-links on DNA is flanking-sequence independent.* Nucleic Acids Res, 2000. **28**(21): p. 4237-43.
3. Siddik, Z.H., *Cisplatin: mode of cytotoxic action and molecular basis of resistance.* Oncogene, 2003. **22**(47): p. 7265-79.
4. Benosman, S., et al., *Multiple neurotoxic stresses converge on MDMX proteolysis to cause neuronal apoptosis.* Cell Death Differ, 2007.
5. Benosman, S., et al., *Complex regulation of p73 isoforms after alteration of the amyloid precursor polypeptide (APP) function and DNA damages in neurons.* J Biol Chem, 2011.
6. Wong, E. and C.M. Giandomenico, *Current status of platinum-based antitumor drugs.* Chem Rev, 1999. **99**(9): p. 2451-66.
7. Galanski, M., M.A. Jakupec, and B.K. Keppler, *Update of the preclinical situation of anticancer platinum complexes: novel design strategies and innovative analytical approaches.* Curr Med Chem, 2005. **12**(18): p. 2075-94.
8. Tiekink, E.R., *Gold derivatives for the treatment of cancer.* Crit Rev Oncol Hematol, 2002. **42**(3): p. 225-48.
9. Melendez, E., *Titanium complexes in cancer treatment.* Crit Rev Oncol Hematol, 2002. **42**(3): p. 309-15.
10. Collery, P., et al., *Gallium in cancer treatment.* Crit Rev Oncol Hematol, 2002. **42**(3): p. 283-96.
11. Amin, A. and M.A. Buratovich, *New platinum and ruthenium complexes--the latest class of potential chemotherapeutic drugs--a review of recent developments in the field.* Mini Rev Med Chem, 2009. **9**(13): p. 1489-503.
12. Ott, I. and R. Gust, *Non platinum metal complexes as anti-cancer drugs.* Arch Pharm (Weinheim), 2007. **340**(3): p. 117-26.
13. Vessieres, A., et al., *Metal complex SERMs (selective oestrogen receptor modulators). The influence of different metal units on breast cancer cell antiproliferative effects.* Dalton Trans, 2006(4): p. 529-41.
14. Kratz, F., et al., *The binding properties of two antitumor ruthenium(III) complexes to apotransferrin.* J Biol Chem, 1994. **269**(4): p. 2581-8.
15. Messori, L., et al., *Binding of Antitumor Ruthenium(III) Complexes to Plasma Proteins.* Met Based Drugs, 2000. **7**(6): p. 335-42.
16. Hartinger, C.G., et al., *From bench to bedside--preclinical and early clinical development of the anticancer agent indazolium trans-[tetrachlorobis(1H-indazole)ruthenate(III)] (KP1019 or FFC14A).* J Inorg Biochem, 2006. **100**(5-6): p. 891-904.
17. Meng, X., et al., *A Ruthenium-Containing Organometallic Compound Reduces Tumor Growth through Induction of the Endoplasmic Reticulum Stress Gene CHOP.* Cancer Res, 2009.
18. Sava, G., et al., *Dual Action of NAMI-A in inhibition of solid tumor metastasis: selective targeting of metastatic cells and binding to collagen.* Clin Cancer Res, 2003. **9**(5): p. 1898-905.
19. Sava, G., et al., *Actin-dependent tumour cell adhesion after short-term exposure to the antimetastasis ruthenium complex NAMI-A.* Eur J Cancer, 2004. **40**(9): p. 1383-96.
20. Bergamo, A., et al., *Approaching tumour therapy beyond platinum drugs Status of the art and perspectives of ruthenium drug candidates.* J Inorg Biochem, 2012. **106**(1): p. 90-9.
21. Rademaker-Lakhai, J.M., et al., *A Phase I and pharmacological study with imidazolium-trans-DMSO-imidazole-tetrachlororuthenate, a novel ruthenium anticancer agent.* Clin Cancer Res, 2004. **10**(11): p. 3717-27.

22. Hartinger, C.G., et al., *KP1019, a new redox-active anticancer agent--preclinical development and results of a clinical phase I study in tumor patients.* Chem Biodivers, 2008. **5**(10): p. 2140-55.
23. Mei, H.Y. and J.K. Barton, *Tris(tetramethylphenanthroline)ruthenium(II): a chiral probe that cleaves A-DNA conformations.* Proc Natl Acad Sci U S A, 1988. **85**(5): p. 1339-43.
24. Brabec, V., *DNA modifications by antitumor platinum and ruthenium compounds: their recognition and repair.* Prog Nucleic Acid Res Mol Biol, 2002. **71**: p. 1-68.
25. Zeglis, B.M., V.C. Pierre, and J.K. Barton, *Metallo-intercalators and metallo-insertors.* Chem Commun (Camb), 2007(44): p. 4565-79.
26. Gaiddon, C., et al., *Ruthenium (II)-derived organometallic compounds induce cytostatic and cytotoxic effects on mammalian cancer cell lines through p53-dependent and p53-independent mechanisms.* J Pharmacol Exp Ther, 2005. **315**(3): p. 1403-11.
27. Hayward, R.L., et al., *Investigation of the role of Bax, p21/Waf1 and p53 as determinants of cellular responses in HCT116 colorectal cancer cells exposed to the novel cytotoxic ruthenium(II) organometallic agent, RM175.* Cancer Chemother Pharmacol, 2005. **55**(6): p. 577-83.
28. Chatterjee, S., et al., *The ruthenium(II)-arene compound RAPTA-C induces apoptosis in EAC cells through mitochondrial and p53-JNK pathways.* J Biol Inorg Chem, 2008. **13**(7): p. 1149-55.
29. Klajner, M., et al., *DNA binding to an anticancer organo-ruthenium complex.* J Phys Chem B, 2010. **114**(44): p. 14041-7.
30. Brabec, V. and O. Novakova, *DNA binding mode of ruthenium complexes and relationship to tumor cell toxicity.* Drug Resist Updat, 2006. **9**(3): p. 111-22.
31. Guichard, S.M., et al., *Anti-tumour activity in non-small cell lung cancer models and toxicity profiles for novel ruthenium(II) based organo-metallic compounds.* Biochem Pharmacol, 2006. **71**(4): p. 408-15.
32. Ryabov, A.D., et al., *New synthesis and new bio-application of cyclometalated ruthenium(II) complexes for fast mediated electron transfer with peroxidase and glucose oxidase.* Inorg Chem, 2001. **40**(25): p. 6529-32.
33. Fetzer, L., et al., *Library of second-generation cycloruthenated compounds and evaluation of their biological properties as potential anticancer drugs: Passing the nanomolar barrier.* Dalton Trans, 2011. **40**(35): p. 8869-78.
34. Wang, F., et al., *Competition between glutathione and guanine for a ruthenium(II) arene anticancer complex: detection of a sulfenato intermediate.* J Am Chem Soc, 2005. **127**(50): p. 17734-43.
35. Jakupec, M.A., et al., *Redox-active antineoplastic ruthenium complexes with indazole: correlation of in vitro potency and reduction potential.* J Med Chem, 2005. **48**(8): p. 2831-7.
36. Vidimar, V., et al., *Induction of caspase 8 and reactive oxygen species by ruthenium-derived anticancer compounds with improved water solubility and cytotoxicity.* Biochem Pharmacol, 2012. **84**(11): p. 1428-36.
37. Klajner, M., et al., *Subcellular localization and transport kinetics of ruthenium organometallic anticancer compounds in living cells: a dose-dependent role for amino Acid and iron transporters.* Inorg Chem, 2014. **53**(10): p. 5150-8.
38. Ma, Y. and L.M. Hendershot, *The role of the unfolded protein response in tumour development: friend or foe?* Nat Rev Cancer, 2004. **4**(12): p. 966-77.
39. Wouters, B.G. and M. Koritzinsky, *Hypoxia signalling through mTOR and the unfolded protein response in cancer.* Nat Rev Cancer, 2008. **8**(11): p. 851-64.
40. Ke, Q. and M. Costa, *Hypoxia-inducible factor-1 (HIF-1).* Mol Pharmacol, 2006. **70**(5): p. 1469-80.
41. Semenza, G.L., *Defining the role of hypoxia-inducible factor 1 in cancer biology and therapeutics.* Oncogene, 2010. **29**(5): p. 625-34.
42. Zhong, H., et al., *Overexpression of hypoxia-inducible factor 1alpha in common human cancers and their metastases.* Cancer Res, 1999. **59**(22): p. 5830-5.

43. Dancey, J., *mTOR signaling and drug development in cancer.* Nat Rev Clin Oncol, 2010. **7**(4): p. 209-19.
44. Gaiddon, C., et al., *Constitutively active G(S) alpha-subunits stimulate Pit-1 promoter activity via a protein kinase A-mediated pathway acting through deoxyribonucleic acid binding sites both for Pit-1 and for adenosine 3',5'-monophosphate response element-binding protein.* Endocrinology, 1996. **137**(4): p. 1286-91.
45. Gaiddon, C., M. de Tapia, and J.P. Loeffler, *The tissue-specific transcription factor Pit-1/GHF-1 binds to the c-fos serum response element and activates c-fos transcription.* Mol Endocrinol, 1999. **13**(5): p. 742-51.
46. Sohm, F., et al., *The retinoblastoma susceptibility gene product/Sp1 signalling pathway is modulated by Ca2+/calmodulin kinases II and IV activity.* Oncogene, 1999. **18**(17): p. 2762-9.
47. Benosman, S., et al., *Complex regulation of p73 isoforms after alteration of amyloid precursor polypeptide (APP) function and DNA damage in neurons.* J Biol Chem, 2011. **286**(50): p. 43013-25.
48. Passaniti, A., et al., *A simple, quantitative method for assessing angiogenesis and antiangiogenic agents using reconstituted basement membrane, heparin, and fibroblast growth factor.* Lab Invest, 1992. **67**(4): p. 519-28.
49. Gaiddon, C., Mercken, L, Bancroft, C, and Loeffler, JP, *Transcriptional effects in GH3 cells of Gs alpha mutants associated with human pituitary tumors: stimulation of adenosine 3',5'- monophosphate response element-binding protein-mediated transcription and of prolactin and growth hormone promoter activity via protein kinase A.* Endocrinology, 1995. **136**(10): p. 4331-8.
50. Kim, M.Y., T. Zhang, and W.L. Kraus, *Poly(ADP-ribosyl)ation by PARP-1: 'PAR-laying' NAD+ into a nuclear signal.* Genes Dev, 2005. **19**(17): p. 1951-67.
51. Zhang, T. and W.L. Kraus, *SIRT1-dependent regulation of chromatin and transcription: linking NAD(+) metabolism and signaling to the control of cellular functions.* Biochim Biophys Acta, 2010. **1804**(8): p. 1666-75.
52. Noonan, D.M., R. Benelli, and A. Albini, *Angiogenesis and cancer prevention: a vision.* Recent Results Cancer Res, 2007. **174**: p. 219-24.
53. Ryabov, A.D., *Transition metal chemistry of glucose oxidase, horseradish peroxidase, and related enzymes.* Adv. Inorg. Chem., 2004. **55**: p. 201-270.

Figure legends

Figure 1. RDC11 modulates glucose oxidase, ROS production, and NAD/NADH ratio.

A, Shematic representation of the redox enzymatic reaction involving electron exchanges.

B, Enzymatic reaction of glucose oxidase.

C, Measure of O_2 consumption by glucose oxidase in presence of RDC11. Purified glucose oxidase was incubated with increased concentration of glucose and RDC11. O_2 was measured using a Clarke electrode.

D, HCT116 cells were treated for 48h at the indicated concentrations (µM) of cisplatin and RDC11. Cell viability was determined using the MTT test. Data are representatives of three independent experiments. Bars are means and asterisks indicate statistically significant difference (*=p<0.001) compared to control, as calculated by a One-Way ANOVA test followed by a Tukey post-test over the three independent experiments.

E. HCT116 cells grown on coverslips coated with polyornithine were treated with RDC (5µM) for the indicated time and labeled with carboxy-H2DCFDA. Fluorescence was quantified with a fluorimeter. Bars are mean and asterisks indicate statistically significant difference (p< 0.01) compared to control, as calculated by a one-way ANOVA test followed by a Tuckey post-test over the three independent experiments.

F. RDC11 increases the NAD/NADH ratio. $2x10^5$ HCT116 cells were treated with RDC11 (5µM) for the indicated time. NAD and NADH were subsequently quantified following the manufacturer's protocol. Both NAD and NADH were calculated from a standard curve (***=p<0.001; One-Way ANOVA + Tukey post-test).

Figure 2. RDC11 reduces protein and mRNA levels of HIF-1.

A and **B**, Western blot analysis of HCT116 (A) and SW480 (B) colorectal cancer cells treated with 5µM of cisplatin or 5µM of RDC11 for the indicated time in normoxic (20% O_2) or hypoxic (1% O_2) conditions. Immunoblotting was performed with anti-HIF-1α, anti-HIF-1β and anti-actin antibodies.

C, **D,** expression of *HIF1α* (C) and *HIF1β* (D) mRNA in HCT116 cell treated with 5µM of cisplatin or 5µM of RDC11 at the indicated time in normoxic (20% O_2) or hypoxic (1% O_2) conditions, determined by RT-qPCR. Data represent relative change in the expression of the different genes in comparison with untreated cells (Ct) and were normalized to *18S* expression. Columns, means of triplicates; bars, SD. Asterisks indicate statistically significant difference (***=p<0.001; **=p<0.01; *=p<0.05) compared to control, as calculated by a One-Way ANOVA test followed by a Tukey post-test over the three independent experiments.

Figure 3. RDC11 reduces expression of *HIF1α* target genes.

HCT116 cells were treated with 5 µM of cisplatin or 5 µM of RDC11 for the indicated time in normoxic (20% O_2) or hypoxic (1% O_2) conditions. RT-qPCR was performed using primers for *VEGF*, *GLUT1*, *ENO1*, and *18S* as housekeeping gene. Data represent relative change in the expression of the different genes in comparison with untreated cells (Ct) and were normalized with *18S*. Columns, means of triplicates; bars, SD. Asterisks indicate statistically significant difference (***=p<0.001; **=p<0.01; *=p<0.05) compared to control, as calculated by a One-Way ANOVA test followed by a Tukey post-test over the three independent experiments.

Figure 4. HIF-1α protein reduction involves only partly protease-dependent degradation

A, **B**, Western blot analysis of HCT116 colorectal cancer cells treated with 5 µmol/L of RDC11 for 6h in normoxic (A, 20% O_2) or hypoxic (B, 1% O_2) conditions, in absence or in presence of the indicated protease inhibitors (MG132, 10µM; ALLM, 10µM; ALLN, 10µM; Z-VAD-FMK, 20µM). Immunoblotting was performed with anti-HIF-1α and anti-actin antibodies. Note the presence of two bands for HIF-1α, the upper band that correspond to the non-hydroxylated form and the lower band that is the hydroxylated form.

Figure 5. RDC11 interact with PHD2 and its activity is dependent upon PHD2 function

A, HCT116 cells were lysed and 3mg of protein extract was incubated with RDC11-matrix or empty matrix (Matrix-O) for each indicated condition. After 4 washes, protein complexes were detached by boiling (boiled) or competition with RDC11 (5µM, elu. RDC11) or cisplatin (5µM, elu cis). Proteins were then separated on SDS PAGE and immunoblotted with PHD2 antibodies.

B, HCT116 cells were treated overnight with deferoxamine mesylate (DFO, 150µM) to chemically induce hypoxia and subsequently for six hours with RDC11 5µM. Western blot was done using anti-HIF-1α and anti-actin antibodies.

C, HCT116 cells were treated overnight with 5µM of RDC11 in normoxia (20% O_2) or in chemically-induced hypoxia using deferoxamine mesylate (DFO, 150 µM). Western blot was performed using anti-PHD2 and anti-actin antibodies.

Figure 6. RDC11 inhibits angiogenesis both *in vitro* and *in vivo*.

A. HUVECs were seeded on ECMatrix™ and 1h later treated with cisplatin 5 µM and RDC11 2.5µM and 5µM. After 4 hours, cells were photographed and tube formation or intersections between cells were scored manually and expressed relative to controls. (**=p<0.01; *=p<0.05 vs Control; One-Way ANOVA + Tukey post-test)

B. C57BL/6 mice (6 week old) were injected s.c. three times with 600 µl of cold liquid Matrigel supplemented with VEGF (36ng/Matrigel plug), heparin (12U/Matrigel plug), TNF-α (0.72ng/Matrigel plug), PBS (for controls) or RDC11 (5µM). After 4 days, mice were killed and

the Matrigel plugs explanted. Quantification of the hemoglobin content was performed with the Drabkin's reagent kit.

C, D, E, pre-amplified homogenized fragments of human colon tumors were subcutaneously implanted in nude mice. Mice were treated with oxaliplatin (10µl/Kg) or RDC11 (10µmole/Kg) twice a week once the tumor reached 100mm^3. Tumor size was followed (D). Vascularization was estimated by colorimetric assay detection of hemoglobin (C) and expression of HIF-1 target genes (*vegf* and *glut1*) by RT-qPCR. Bars represented means ± standard deviations (n=8; *=p<0.05 vs Control; One-way ANOVA + Tukey post-test).

Figure 1

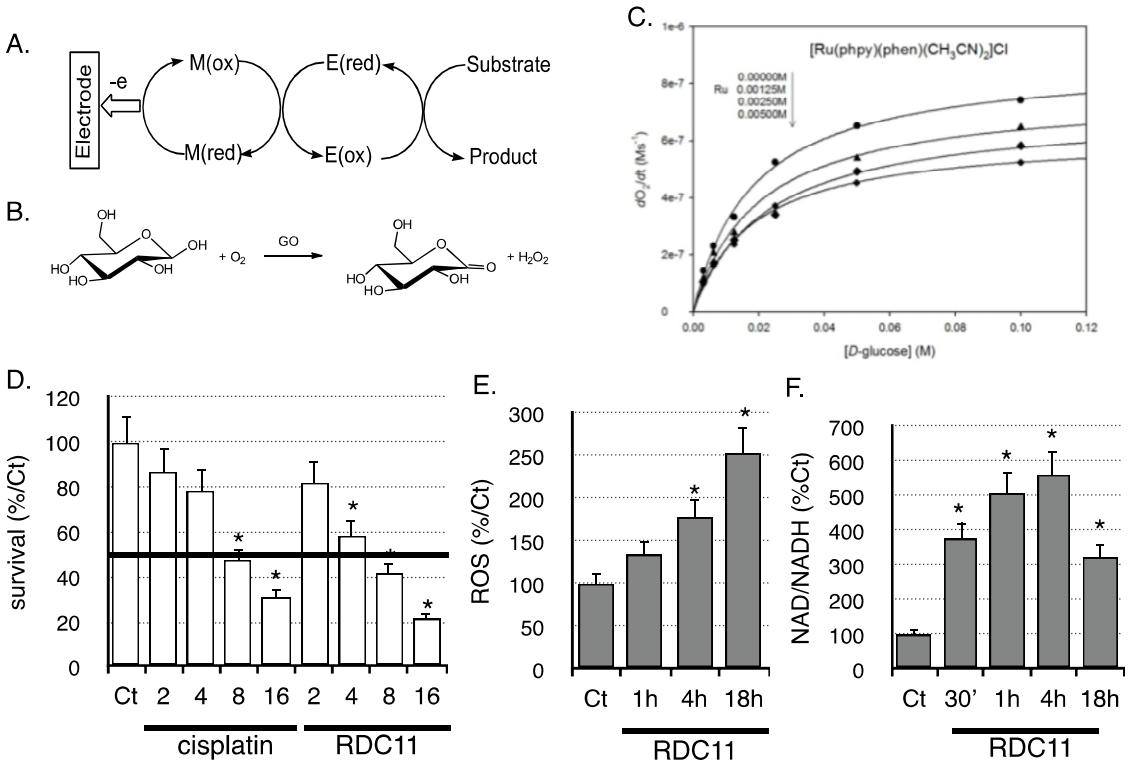
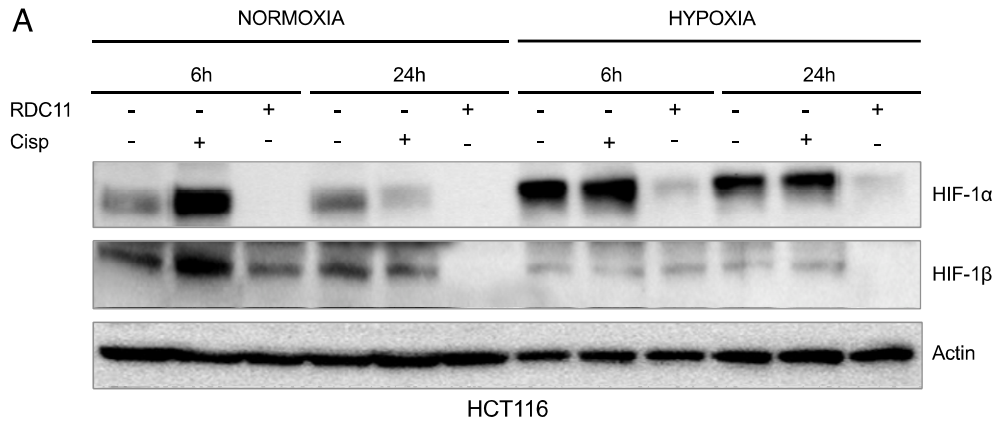
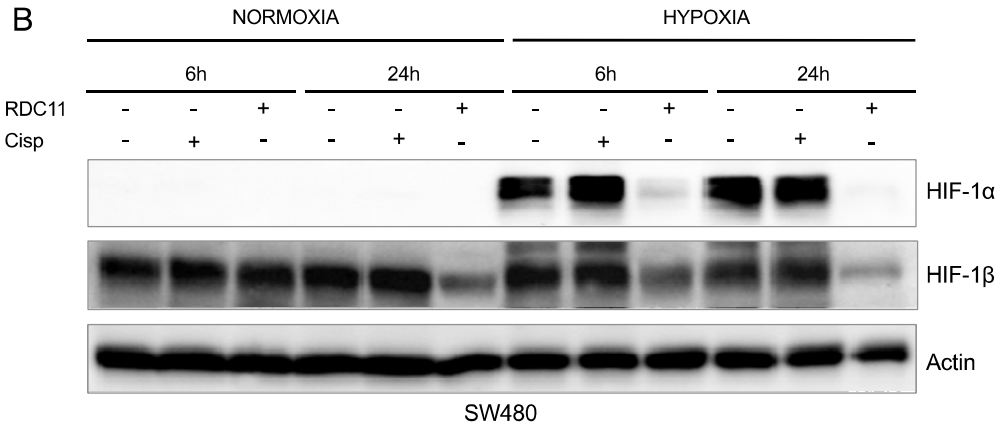

A.
Electrode
-e
M(ox)
M(red)
E(red)
E(ox)
Substrate
Product
B.
GO
+ O2
+ H2O2
C.
[Ru(phpy)(phen)(CH3CN)2]Cl
Ru 0.00000M 0.00125M 0.00250M 0.00500M
dO2/dt (Ms-1)
[D-glucose] (M)
D.
survival (%/Ct)
Ct 2 4 8 16 2 4 8 16
cisplatin
RDC11
E.
ROS (%/Ct)
Ct 1h 4h 18h
RDC11
F.
NAD/NADH (%Ct)
Ct 30' 1h 4h 18h
RDC11

Figure 2


A
NORMOXIA
HYPOXIA
6h
24h
6h
24h
RDC11
Cisp
HIF-1α
HIF-1β
Actin
HCT116


B
NORMOXIA
HYPOXIA
6h
24h
6h
24h
RDC11
Cisp
HIF-1α
HIF-1β
Actin
SW480

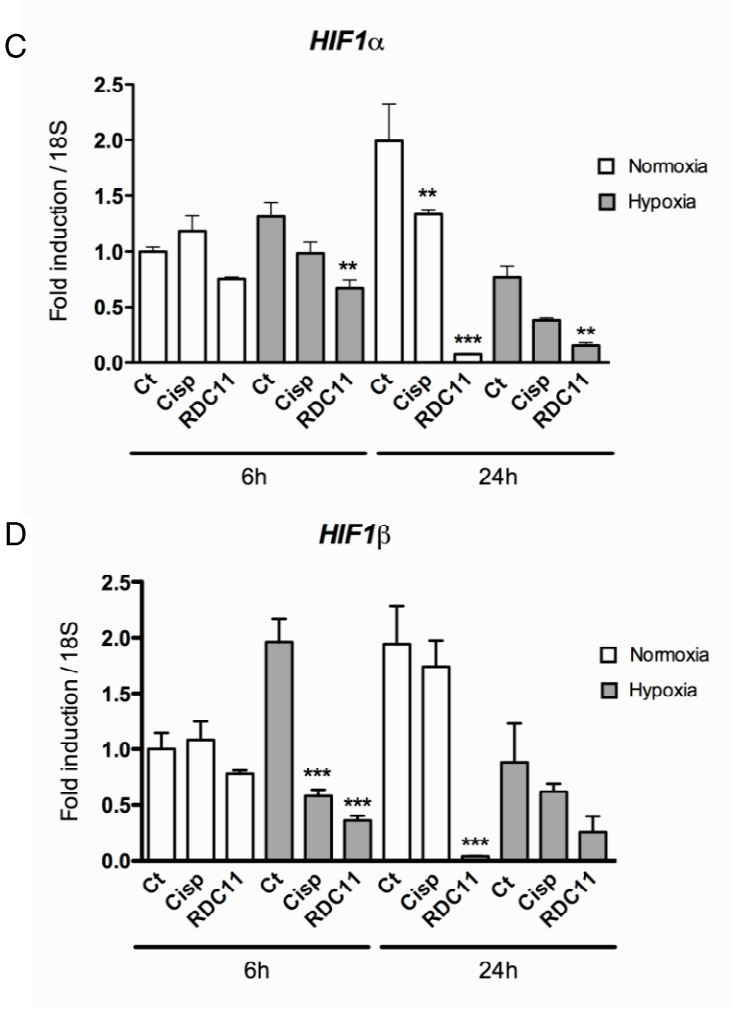

C
HIF1α
Fold induction / 18S
Normoxia
Hypoxia
Ct
Cisp
RDC11
6h
24h
D
HIF1β
Fold induction / 18S
Normoxia
Hypoxia
6h
24h

Figure 3

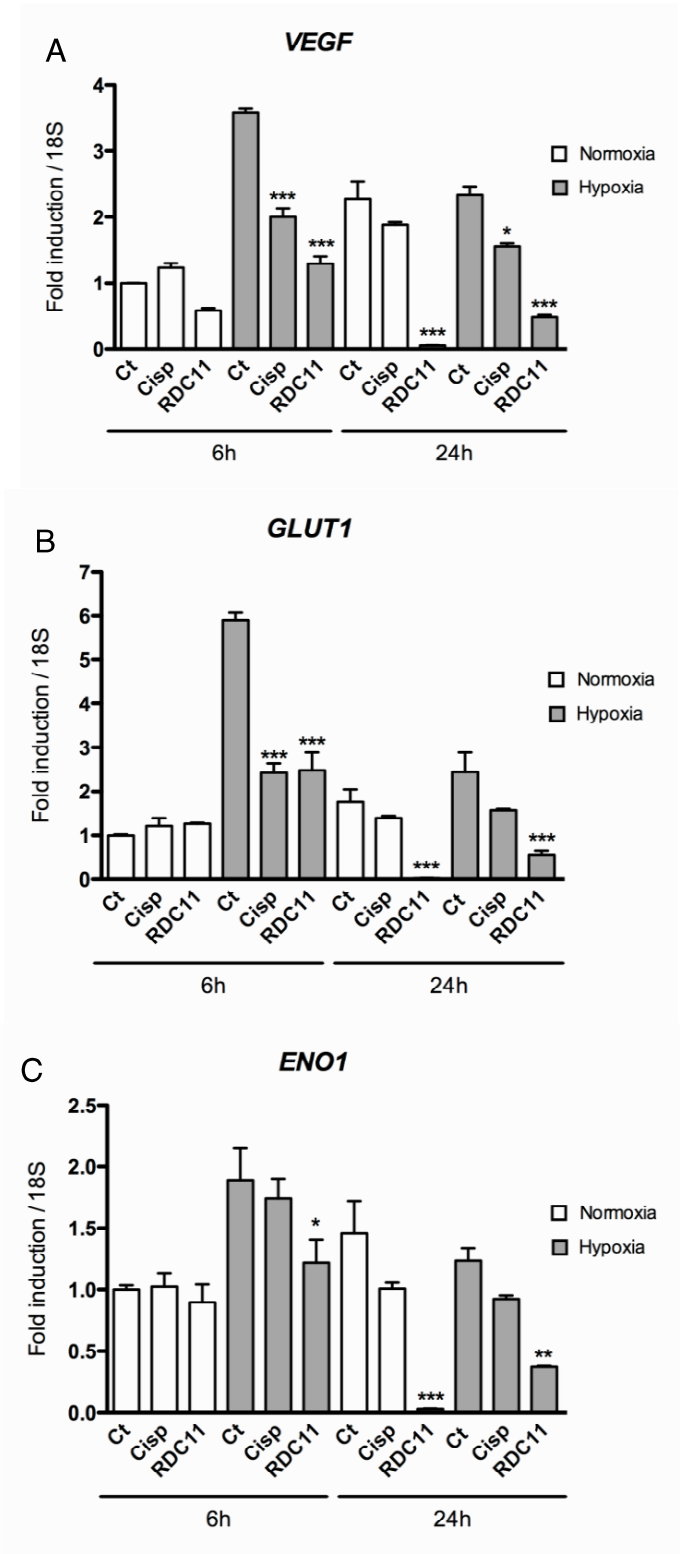

A
VEGF
Fold induction / 18S
Normoxia
Hypoxia
Ct
Cisp
RDC11
6h
24h
B
GLUT1
C
ENO1

Figure 4

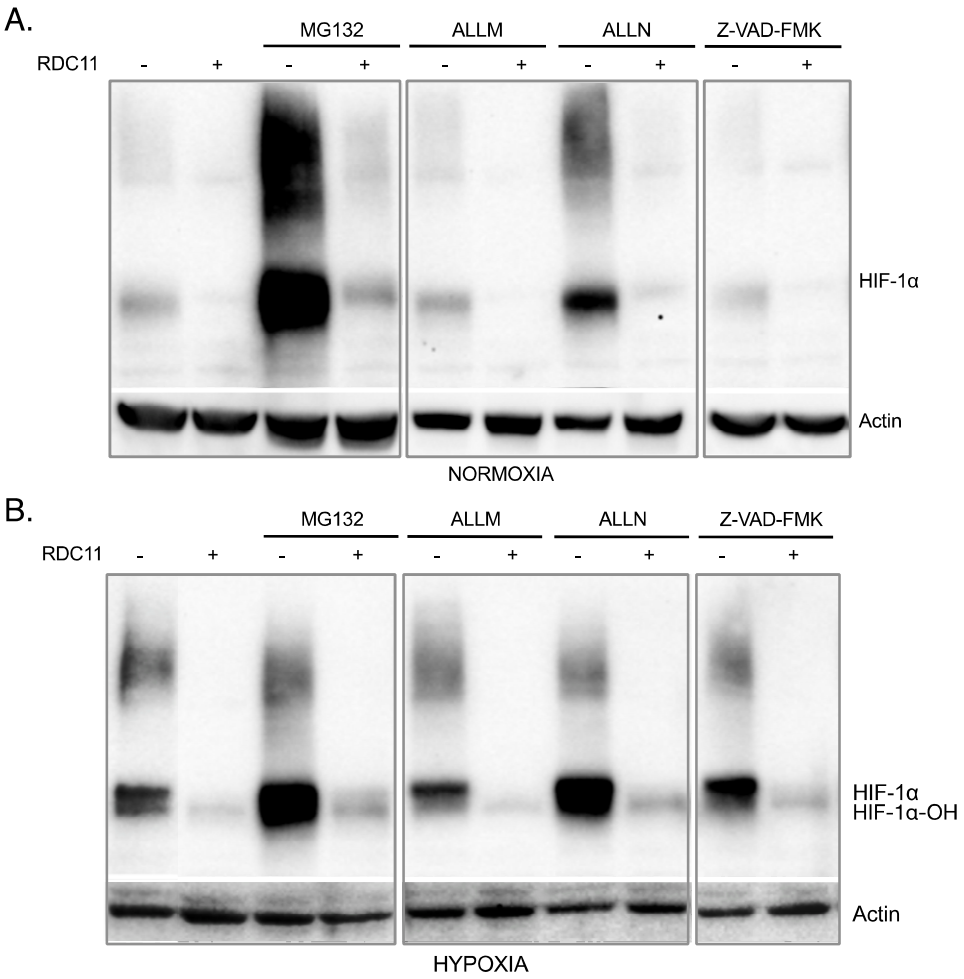

A.
MG132
ALLM
ALLN
Z-VAD-FMK
RDC11
- + - + - + - + - +
HIF-1α
Actin
NORMOXIA
B.
MG132
ALLM
ALLN
Z-VAD-FMK
RDC11
- + - + - + - + - +
HIF-1α
HIF-1α-OH
Actin
HYPOXIA

Figure 5

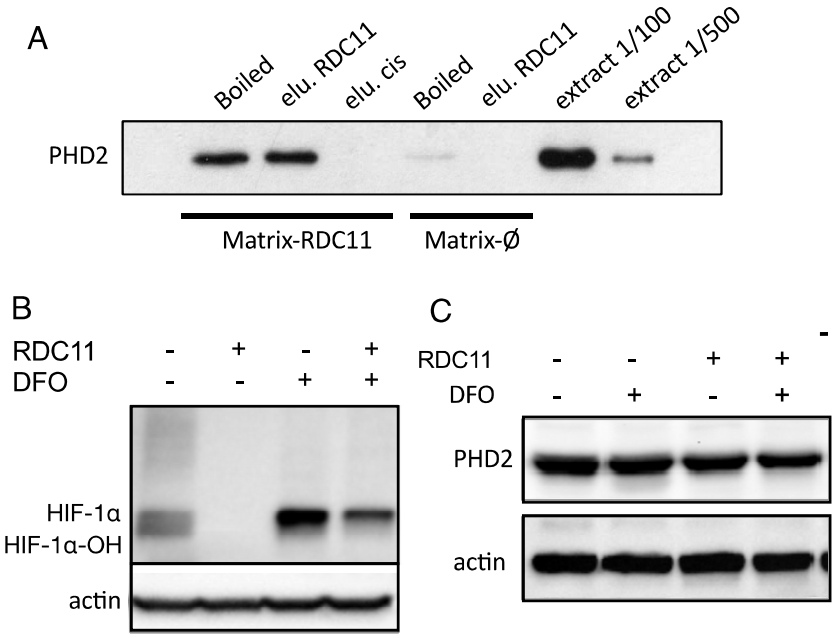
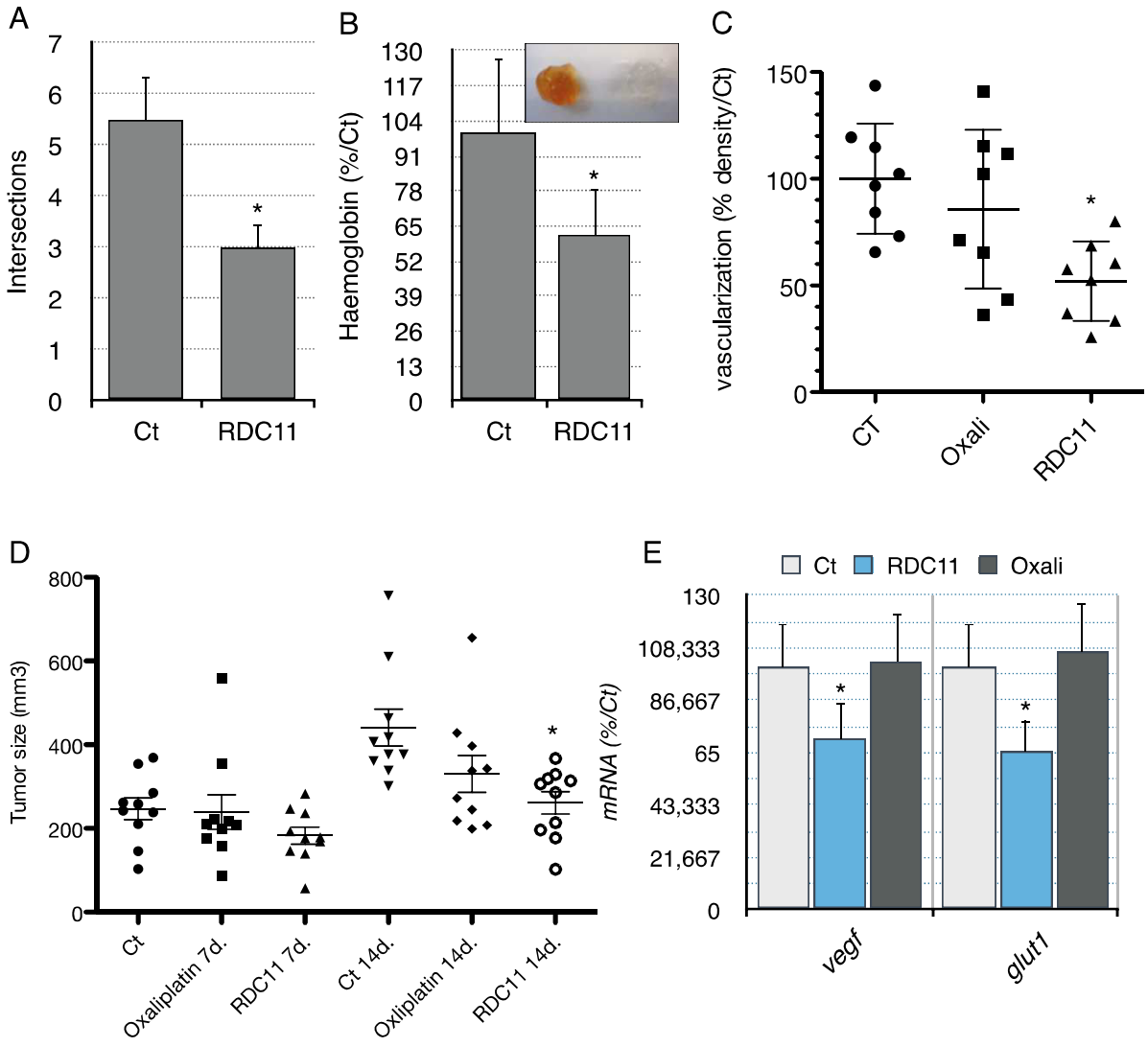

A
Boiled
elu. RDC11
elu. cis
Boiled
elu. RDC11
extract 1/100
extract 1/500
PHD2
Matrix-RDC11
Matrix-Ø
B
RDC11 - + - +
DFO - - + +
HIF-1α
HIF-1α-OH
actin
C
RDC11 - - + +
DFO - + - +
PHD2
actin

Figure 6


A
Intersections
7
6
5
4
3
2
1
0
*
Ct
RDC11
B
Haemoglobin (%/Ct)
130
117
104
91
78
65
52
39
26
13
0
*
Ct
RDC11
C
vascularization (% density/Ct)
150
100
50
0
*
CT
Oxali
RDC11
D
Tumor size (mm3)
800
600
400
200
0
*
Ct
Oxaliplatin 7d.
RDC11 7d.
Ct 14d.
Oxliplatin 14d.
RDC11 14d.
E
Ct
RDC11
Oxali
mRNA (%/Ct)
130
108,333
86,667
65
43,333
21,667
0
*
*
vegf
glut1

VI. Results (Objective 2)

VI.A. Induction of caspase 8 and reactive oxygen species by ruthenium-derived anticancer compounds with improved water solubility and cytotoxicity.

Biochemical Pharmacology 84 (2012) 1428–1436

Contents lists available at SciVerse ScienceDirect

Biochemical Pharmacology

journal homepage: www.elsevier.com/locate/biochempharm

Induction of caspase 8 and reactive oxygen species by ruthenium-derived anticancer compounds with improved water solubility and cytotoxicity

Vania Vidimar [a,d,g,1], Xiangjun Meng [e,g,1], Marcelina Klajner [c,g,1], Cynthia Licona [a,g], Ludivine Fetzer [b,g], Sébastien Harlepp [c,g], Pascal Hébraud [c,g], Marjorie Sidhoum [f,g], Claude Sirlin [b,g], Jean-Philippe Loeffler [f,g], Georg Mellitzer [a,g], Gianni Sava [d], Michel Pfeffer [b,g], Christian Gaiddon [a,g,*]

[a] UMRS682 INSERM, Strasbourg, France
[b] UMR 7177 CNRS, Institut de Chimie, Strasbourg, France
[c] UMR 7504 CNRS, IPCMS, Strasbourg, France
[d] University of Trieste, Department of Life Sciences, and Callerio Foundation Onlus, Trieste, Italy
[e] Department of Gastroenterology, Shanghai First People's Hospital, Shanghai Jiao Tong University, China
[f] UMRS692 INSERM, Strasbourg, France
[g] Université de Strasbourg, Strasbourg, France

ARTICLE INFO

Article history:
Received 5 June 2012
Accepted 27 August 2012
Available online 1 September 2012

Keywords:
Organometallic
Anticancer
Caspase 8
ROS
Ruthenium

ABSTRACT

Organometallic compounds which contain metals, such as ruthenium or gold, have been investigated as a replacement for platinum-derived anticancer drugs. They often show good antitumor effects, but the identification of their precise mode of action or their pharmacological optimization is still challenging. We have previously described a class of ruthenium(II) compounds with interesting anticancer properties. In comparison to cisplatin, these molecules have lower side effects, a reduced ability to interact with DNA, and they induce cell death in absence of p53 through CHOP/DDIT3. We have now optimized these molecules by improving their cytotoxicity and their water solubility. In this article, we demonstrate that by changing the ligands around the ruthenium we modify the ability of the compounds to interact with DNA. We show that these optimized molecules reduce tumor growth in different mouse models and retain their ability to induce CHOP/DDIT3. However, they are more potent inducers of cancer cell death and trigger the production of reactive oxygen species and the activation of caspase 8. More importantly, we show that blocking reactive oxygen species production or caspase 8 activity reduces significantly the activity of the compounds. Altogether our data suggest that water-soluble ruthenium(II)-derived compounds represent an interesting class of molecules that, depending on their structures, can target several pro-apoptotic signaling pathways leading to reactive oxygen species production and caspase 8 activation.

© 2012 Elsevier Inc. All rights reserved.

1. Introduction

Cancer remains one of the first causes of death in industrialized countries. Nevertheless, few examples of successful chemotherapy are still driving the search for more potent, more selective, less prone to resistance and better tolerated drugs. One of these examples is cisplatin, a drug showing a significant role in the management of a number of tumors [1–3]. However, cisplatin likewise platinum-derived drugs display an often-severe toxicity and a relatively frequent inactivity due to natural- or induced-resistance [4–6]. More recently, a significant interest was addressed to ruthenium-based drugs, because of some favorable properties that make them a suitable basis for the development of antitumor drugs, such as their metal oxidation state (Ru(II) or Ru(III)), the fairly facile ligand exchange and the binding to biologically relevant proteins. Compared to many organic compounds, ruthenium-based drugs also offer the advantage of a relatively low cost for their synthesis and purification.

Various ruthenium complexes were shown to present cytotoxicity against cancer cells, ligand-exchange abilities similar to those of platinum complexes, no cross-resistance with cisplatin and a reduced toxicity against healthy tissues at least in part explained by the selective transportation to cancer cells by the iron transport system [1–3,7]. Following the pioneering work with ruthenium red

Abbreviations: CHOP, C/EBP homologous protein; DDIT3, DNA damage inducible transcript 3; FACS, fluorescence activated cell sorter; FRET, Förster resonance energy transfer; NAC, n-acetylcysteine.

* Corresponding author at: U682 INSERM, 3 Avenue Molière, Strasbourg 67200, France. Tel.: +33 03 88 27 77 27; fax: +33 03 88 26 35 38.
E-mail address: gaiddon@unistra.fr (C. Gaiddon).

[1] Authors contributed equally to this work.

0006-2952/$ – see front matter © 2012 Elsevier Inc. All rights reserved.
http://dx.doi.org/10.1016/j.bcp.2012.08.022

[8] a number of ruthenium-based drugs were shown to endow antitumor potential. Indeed, several teams have synthesized and characterized compounds containing ruthenium in oxidative state (II) or (III), showing their anticancer activity [9–16]. Two, namely NAMI-A and KP1019, have successfully passed some initial phases of clinical trials [17,18]. Besides these partial successes, the emergence of new ruthenium-based therapies have been slowed down by limitations, such as a relatively poor level of water solubility, and/or stability in aqueous solutions, a not impressive cytotoxicity (IC50 between 20 and 100 μM), and an uncertainty on the molecular mechanisms of action responsible for the antitumor effect.

The mechanism of action and the direct targets of ruthenium-based drugs are still a matter of debate. Indeed, depending on the drug, several modes of action have been proposed, such as interaction with DNA and activation of DNA damage pathways [19–24], inhibition of kinases [25], or other enzymatic activities [26,27], including extracellular metallo-proteases [28]. The differences observed may be due to variations in their structure. Even if most of the ruthenium-containing compounds have ligands that are relatively weakly bound to the metal via a heteroatom (N, O, S), there are differences in the types of ligands attached.

In order to improve the stability of ruthenium complexes and possibly to enhance their cytotoxicity and their pharmacokinetics, we have previously generated several ruthenium-based complexes in which the ligand is bound to the metal via strong covalent bonds such as a C-M σ bond [22,29]. Beside the stability, these compounds present differences in their Ru(II)/Ru(III) redox potential and a new variety of ligands. We have called these molecules RDCs (Ruthenium-Derived Compounds) and we have previously shown that some RDCs are cytotoxic for several cancer cell lines resistant to cisplatin [22]. One of them, RDC11, showed a good antitumor activity both in vitro and in vivo [30] with an IC50 often between 2 and 5 μM, and anticancer properties on models of ovarian cancer, melanomas and gliomas. Importantly, they showed, compared to cisplatin a reduced neurotoxicity. As we previously showed that cisplatin exerts its neurotoxic effect in part through induction of the p53 pathway [31,32], we analyzed the ability of RDC11 to interact with DNA and induce p53 proteins. We demonstrated that RDC11 exerts its antitumor effect via DNA-dependent and DNA-independent modes of action. We also identified one of the DNA-independent signaling pathways by showing an activation of the endoplasmic reticulum stress pathway, and in particular the transcription factor CHOP/DDIT3. However, the silencing of CHOP/DDIT3 by siRNA was not able to completely abolish RDC11 cytotoxicity, strongly suggesting that other signaling pathways are also involved [30,33,34].

In the present study, we developed RDC11 variants designed for improving cytotoxicity and water solubility. The biological properties of these novel ruthenium-based organometallics are studied in vitro and in vivo.

2. Materials and methods

2.1. Cell culture, MTT test, flow cytometry analysis

B16F10, U87, A172, 3LL, A2780, HCT116, SW480 cells were obtained from ATCC (Manassas, VA). Cells were maintained in DMEM with 10% FBS and incubated in presence of 5% CO_2/95% air at 37 °C. MTT tests were performed with cells cultured in 96-well culture dishes as previously described [35]. Hypodiploid DNA was measured as described [36] using propidium iodide (Sigma, MO). The fluorescence of 10,000 cells was analyzed using a FACScan flow cytometer and CellQuest software (Becton Dickinson, San José, CA).

2.2. Statistical analysis

In MTT ($n = 8$), RT-qPCR ($n = 3$), ROS ($n = 8$), caspase 8 activity ($n = 4$), FACS analysis ($n = 3$), bars are mean ±SD and asterisks indicate a statistically significant difference ($p < 0.01$) compared to control, as calculated by a one-way ANOVA test followed by a Tukey post-test.

2.3. Western blot

Cells were treated in triplicates and Western blots were performed as previously described [37]. Immunoprobing was performed with anti-phospho 137-H2AX antibody (1/3000, Millipore, Molsheim, France), anti-CHOP (1/1000, Santa Cruz Biotechnology, CA), anti-human p53 (421, supernatant 1/3, C. Prives, Columbia University NYC), or actin (Dr. Aunis, Strasbourg) antibodies. Membranes were probed with a secondary horseradish-peroxidase-conjugated antibody (anti-rabbit, -goat or -mouse, 1/2000, Thermo Fisher, IL), and revealed with ECL (Thermo Fisher, IL).

2.4. Quantitative real-time PCR

RNA was extracted using RNAII Nucleospin (Macherey-Nagel, Strasbourg, France). Reverse transcription was performed with 1 μg RNA (iScript kit, Bio-Rad), followed by qPCR in Bio-Rad iCycler thermal cycler using iQ SYBR Green supermix (Bio-Rad Laboratories, Hercules, CA). Starting quantities of genes of interest were reported to those of housekeeping genes (TBP, 18s). Specificity of the amplification was controlled by a melting curve [31]. Probes: for noxa, 5′-ggagatgcctgggaagaag-3′; 5′-cctgagttgagtagcacactcg-3′; for fas, 5′-atggccaattctgccataag-3′, 5′-tgactgtgcagtccctagctt-3′; tbp, 5′-cggctgtttaacttcgcttc-3′, 5′-cacacgccaagaaacagtga-3′.

2.5. Evaluation of mitochondrial membrane potential

The changes in $\Delta\Psi m$ were assessed using the membrane potential sensitive dye JC-1 (5,5′,6,6′-tetrachloro-1,1′,3,3′-tetraethylbenzimidazolylcarbocyanine iodide, Life technology, France). Cells were grown on cover glasses and the staining procedure was the following: DMEM was removed and 10 μg/ml JC-1 solution (in PBS) was added for 15 min [38]. The staining solution was removed and cultures were rinsed with PBS. Subsequently, cells were fixed in 4% PFA for 15 min and then coved with Vectashield mounting medium (Vector labs, CA) on glass slides. Fluorescence was measured at 488 nm excitation/510 nm emission.

2.6. Assay for caspase 8 activity

Caspase 8 activity was assayed by measuring the light intensity using a kit (Caspase-Glo®8 Assay, Promega) and a luminometer (Perkin Elmer HTS 7000, France). Briefly, cells were cultured in 96-well plates in a final volume of 200 μl. Then 50 μl caspase-8 reaction buffer was added and incubated at room temperature for 1 h before measurement.

2.7. FRET

FRET measurements are performed on a home build setup as previously described [34].

2.8. Intracellular reactive oxygen species (ROS) measurement

5-(and-6)-carboxy-2′,7′-dichlorodihydrofluorescein diacetate (carboxy-H2DCFDA) (Life Technology, France) was used to detect intracellular ROS according to the manufacturer's instructions. For

ROS quantification, cells were seeded in 96-well black plates (Greiner Bio-One, France) and treated with RDCs at the indicated concentrations and times. Afterwards, cells were washed with PBS and incubated with 10 μM carboxy-H2DCFDA in DPBS for an hour. Cells were then washed and fluorescence was measured by a plate reader (Perkin Elmer, France) with an excitation wavelength of 485 nm and an emission wavelength of 535 nm.

2.9. Chemical synthesis

RDC11 [39], RDC34,37,40,41,44 [40] were synthesized according to published procedures. All complexes were purified over chromatography columns carried out on Merk aluminum oxide 90 standardized. Complexes were used with a purity >98%, as demonstrated by several protocols [40]. ES-MS spectra and elemental analyses were carried out by the corresponding facilities at the Institut de chimie, Université de Strasbourg and at the Service Central d'Analyse du CNRS, Vernaison.

3. Results

3.1. Generating ruthenium compounds with an IC50 in the nanomolar range

On the basis of previously structure–function studies showing an improved cytotoxicity of RDCs having a phenantroline ligand [22], we substituted the two acetonitrile ligands of RDC11 by a second phenanthroline, naming the new molecule RDC34 (Fig. 1). An equivalent of RDC34 with another counter-ion (PF_{6-}) was also synthesized (RDC37). Previous works have established the ability of RDCs to modulate the activity of cellular enzymes through their redox potential [39]. We therefore modified the redox potential of RDC34 by adding either a NO_2 (electron withdrawing) or a NH_2 unit (electron releasing) on the phenylpyridine ligand, leading to RDC40 and RDC41 respectively. Finally, in order to increase the water solubility of RDC34, we added a spermine unit to the phenylpyridine ligand, leading to RDC44 (water solution of up to 25 mM was obtained) [40].

As colon cancers are one of the indications for platinum-derived treatments, the cytotoxicity of the RDC was first tested on a human colon cancer cells (HCT116). Interestingly, RDC34, RDC37, and RDC40, characterized by the presence of the NO_2 group, showed an increased cytotoxicity (IC50 < 2 μM) (Fig. 1) compared to RDC11 and cisplatin. However, the addition of the NH_2 group decreased the cytotoxic activity (IC50 = 2–4 μM, RDC41) and that of the spermine moiety had an even worse effect with rising the IC50 to over 16 μM. Additional experiments gave IC50s for RDC34, RDC40 and RDC41 of respectively 0.25 μM, 0.75 μM and 2–4 μM (supplementary data 1).

3.2. Effects of the hydrophilic spermine substituent chain on cytotoxicity, cell uptake and DNA binding

The addition of the spermine chain (leading to RDC44) significantly decreased the cytotoxicity (Fig. 1). In order to understand the reason for this behavior, we tested RDCs' cellular uptake. The two phenanthrolines confer to RDC34 and RDC44 luminescent properties allowing us to follow their entry into living cells (Fig. 2A and B). The maximum of accumulation of RDC34 inside the cells was reached 1 h after the compound was added. Cell uptake of RDC44 was lower. In PBS, the emitted intensity of RDC44 is 20% lower than the emission of RDC34, whereas in DMEM, RDC44 cell uptake is strongly diminished (Fig. 2C). However, the increased cell uptake of RDC44 in PBS did not lead to an increased cytotoxicity of this compound as the IC50s were closed to those observed when cells were treated in culture medium (Fig. 2D).

As DNA is one of the direct targets of RDCs, we used the FRET approach based on a double-stranded oligonucleotide labeled at each end by two fluorophores to test RDC/DNA binding. RDC44 showed a higher affinity for DNA compared to RDC34, as demonstrated by the drop in FRET transfer energy that occurred at the lowest concentration of RDC44 (Fig. 2E). The affinity constants are obtained from the analysis of these data according to the McGhee and van Hippel model [41]: $K_a = 2.2 \times 10^3\ M^{-1}$ for RDC34 and $7.8 \times 10^5\ M^{-1}$ for RDC44. The number of base pairs occupied by RDC44 along the DNA chain is equal to 3.9, larger than the occupation site of RDC34 (2.3). It thus seems that the lack of significant cytotoxicity of RDC44 for HCT116 cells can be attributed neither to a default in cell entry and nor to the lack of interaction with DNA.

3.3. Modifications of RDC ligands modulate the selectivity between cancer cell lines

To further characterize the cellular effect of RDC34, we performed FACS analysis on HCT116 cells (Fig. 3A). RDC34, better than cisplatin, induced the accumulation of an elevated subG1

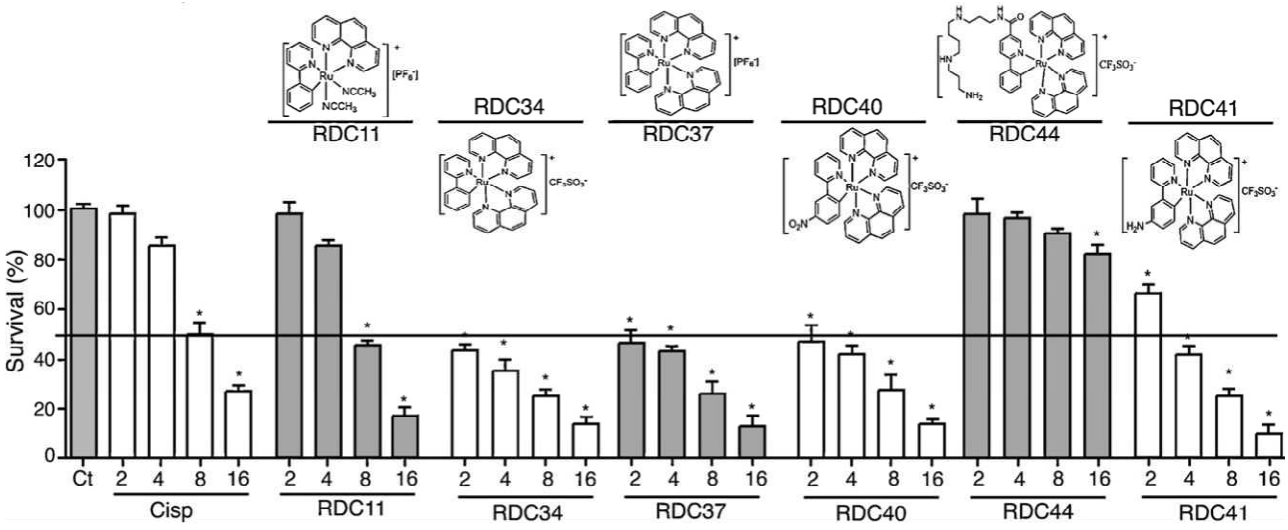


Fig. 1. Optimized RDC for water solubility and cytotoxicity reduce cell growth of HCT116 cells. HCT116 human colon cancer cells were treated for 48 h with cisplatin or RDC (μM). Viability was evaluated using a MTT test (n + 8). Insets: RDC structures. Data are representatives of 3 independent experiments. Statistical analyses are described in Section 2.

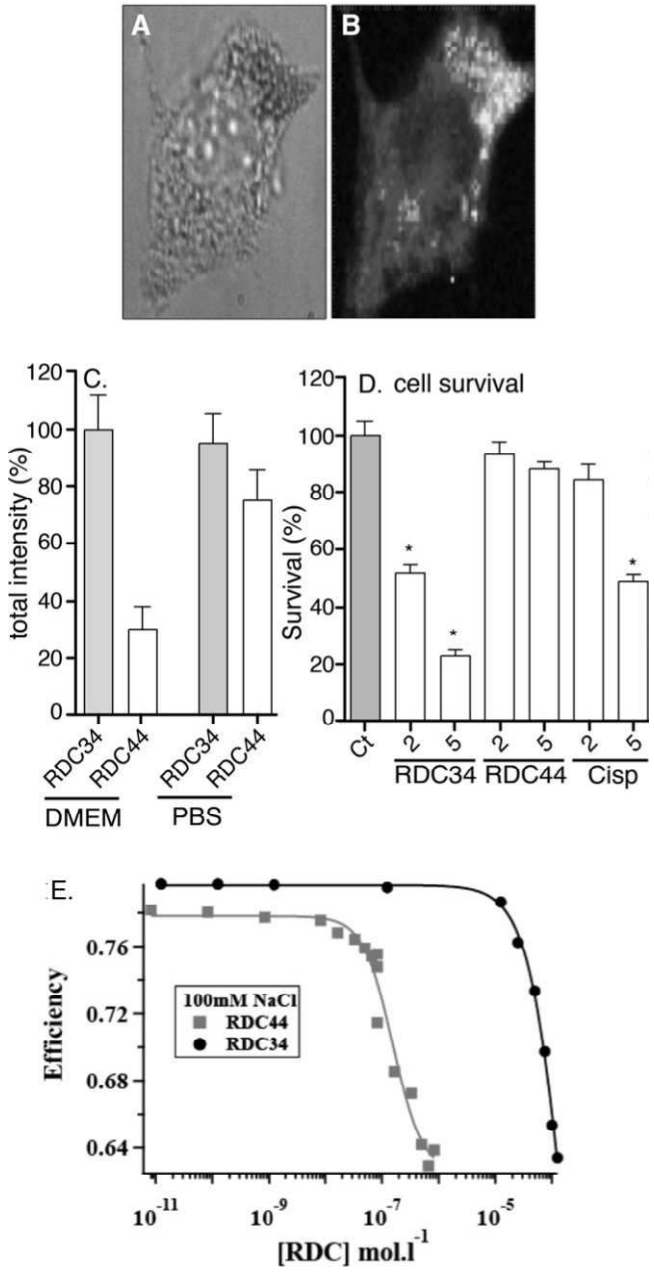


Fig. 2. Cell permeability and DNA interaction of optimized RDC. HCT116 cells incubated with RDC44 and visualized with white light (A) and fluorescence (at 750 nm, B) and quantification (C). Cells were incubated for 1 h with RDCs (5 μM) in either DMEM or PBS. (D) HCT116 cells were treated for 2 h either in DMEM or PBS, medium was replaced by DMEM with serum for 48 h and MTT was performed. Data are representative of three independent experiments. (E) Efficiency of the Förster Resonance Energy Transfer (FRET) between the extremities of a 14 base pairs-long double-stranded DNA labeled with Alexa-488 and Alexa-568. The measurements were performed at the equilibrium of complexation of DNA with the metal complex. Solid line is a guide to the eye.

population at 24 h and 48 h, indicative of cell death. RDC34 induced also a G2/M arrest at 24 h, while cisplatin blocked HCT116 cells in G1.

The cytotoxic potential of RDC11, RDC34 and RDC41 was submitted to the US National Cancer Institute (NCI) test on 60 cancer cell lines (Fig. 3B–D). RDC34 showed a strong cytotoxic effect (indicated by the % of cell survival compared to the initial number) on almost all cell lines (Fig. 3B–D, supplementary data #3). These results were similar to those we obtained on additional cell lines (N2A, U87, F10B16, SW480, supplementary data #2). Kidney-derived cancer cell lines were mostly resistant toward RDC11 and RDC41. Globally, RDC34, unlike RDC11 and RDC41, was endowed with a broader range of sensitive cell isotypes. These tests also showed the negative effect of NH_2 function (RDC41), leading to a significant decrease of cytotoxicity in almost all the cell lines. However, RDC41 showed an activity better than RDC11 on EKVX cells, MDA-MB-435, UACC-257 and HS57BT (supplementary data #3). It is also interesting to stress the significant activity of RDC11 on lung-derived cancer cells, on which RDC41 is only marginally effective.

These data indicate the correlation between the modifications of the ligands around the ruthenium atom and the antitumor activity, and suggest a possibility to modulate the intensity of the cytotoxicity and the specificity for selected tumor types.

3.4. Modifications of RDC ligands change the mode of action: role of caspase 8 and ROS

In order to understand how each modification of the ligands affects RDCs cytotoxicity and specificity, we compared their DNA interactions. RDCs were incubated with double stranded super-coiled DNA and then samples were submitted to migration on an agarose gel (Fig. 4A). RDC34 showed an affinity for DNA slightly greater than that of RDC11, but inferior to RDC40 and RDC41. In particular, RDC40 formed a stable complex with DNA that remained in the loading pocket.

These data stress the lack of correlation between the DNA binding activity and the cytotoxicity. We therefore looked for another possible explanation for the higher cytotoxicity of RDC34. Previous observations indicated that redox potential allowed RDCs to modulate the oxido-reductase enzyme activity. We therefore hypothesized that such regulation might lead to the production of reactive oxygen species (ROS). Incubation of HCT116 cells with RDCs and a fluorescent ROS probe (Fig. 4B–G) showed that RDC34 was the most potent ROS inducer (Fig. 4G and H), suggesting a correlation between the induction of ROS and cytotoxicity, which was confirmed by the reduction of RDC34 cytotoxicity by NAC, a ROS inhibitor (Fig. 5I).

We therefore investigated in more detail the mode of action of RDC34, comparing how this ruthenium compound was regulating the expression of p53 and CHOP, two transcription factors previously shown to be regulated by RDC11 and ROS. We also followed the phosphorylation of H2AX at serine 137, which is a marker for DNA damages [30]. RDC34 was as efficient as RDC11 to induce CHOP, but was more potent to induce p53 protein levels (Fig. 5A, supplementary data 4). In these experimental conditions, cisplatin was unable to regulate CHOP, whereas both RDCs were less able to induce H2AX phosphorylation. Besides the significant induction of p53 protein levels, RDC34 increased the expression of pro-apoptotic p53 target genes involved in either the mitochondrial-dependent apoptotic pathway (noxa, bax, siva) or the mitochondria-independent pathway (fas, trail) (Fig. 5B and C).

A fluorescent probe (JC-1) was used to follow changes in the mitochondrial membrane potential, indicative of the involvement of the mitochondria in the apoptotic processes induced by RDC34 (Fig. 5E and G). The involvement of a mitochondria-independent pathway was conversely tested by following caspase 8 activity. Compared to RDC11, RDC34 was more potent in inducing caspase 8 (Fig. 5H). The concomitant use of ROS and caspase 8 inhibitors reduced the cytotoxicity or RDC34, suggesting their importance for the antitumor activity of this drug (Fig. 5I).

3.5. In vivo antitumor activity of optimized RDCs

To further examine the anticancer potential of the optimized compounds, we tested their activity on tumor growth. A

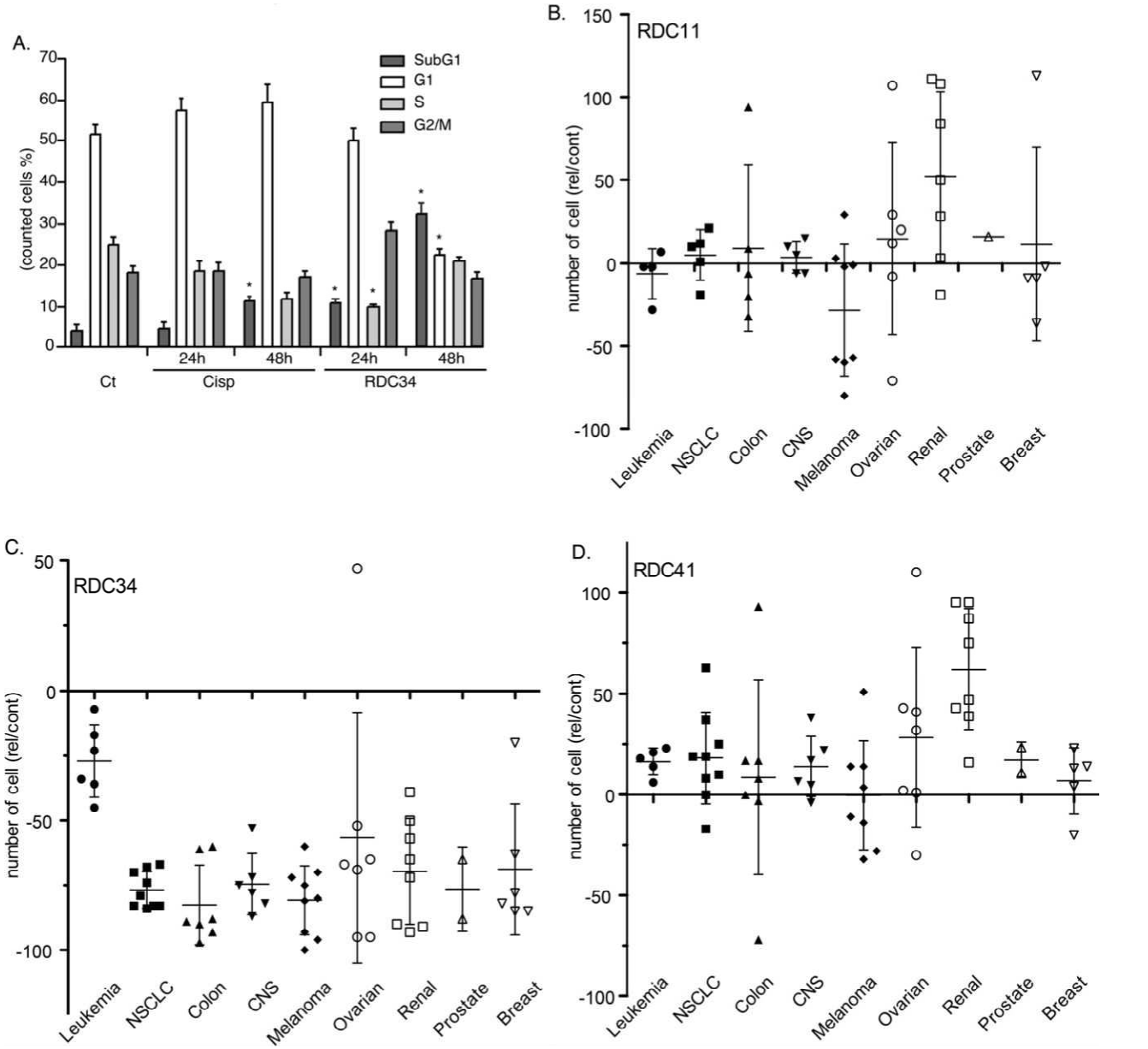


Fig. 3. Optimized RDC induced cytotoxicity on cancer cells of various origins. (A) Cell cycle profile analysis (FACS) of HCT116 cells treated with cisplatin or RDC34 (2.5 μM) for 24 h or 48 h. (B–D) Graph indicating the cytostatic (above 0) and cytotoxic (bellow 0) response of 60 cancer cells lines of the specified origins (detailed in supplementary data #3). The test was performed by the NCI with the indicated RDC at a concentration of 5 μM.

preliminary experiment to evaluate host toxicity after single dose and after chronic treatment (3 weeks, 2 injections a week) showed that repeated doses of RDC34 higher than 4 μmol/kg were lethal (supplementary data #1). Similar results were obtained with RDC44, a compound with significant lower cytotoxicity in vitro (Fig. 1). RDC41 was the most tolerated compound and showed a DL50 of 30 μmol/kg.

We first tested the compounds on a lung cancer as these cancers are commonly treated by cisplatin and we observed a good cytotoxicity of RDC34 on lung cancer cells, such as on 3LL cells (Figs. 3C and 6A). When tested at their maximum tolerated doses on the syngeneic model of 3LL cells implanted subcutaneously in B6 mice, RDC34 (4 μmol/kg, 2×/week), RDC44 (4 μmol/kg, 2×/week) and RDC41 (13 μmol/kg, 2×/week) reduced tumor growth to approximately 40% (Fig. 6A). The anticancer activity of RDC34 on human ovarian cancer cells (A2780) implanted into nude mice (Fig. 6B) showed a significant reduction of tumor growth to approximately 36% of the controls. In both models the activity of RDC34 is slightly higher compared to cisplatin.

4. Discussion

The development of novel anticancer compounds is a constant challenge. In the recent years, metal-based compounds have been the focus of a particular interest based on the proven relative efficiency of platinum-derived compounds and their intrinsic physico-chemical properties of transition metals, such as ruthenium. Especially, the vast possibilities of combination with organic ligands and small ions make ruthenium-based molecules particularly suitable to be modeled and adapted to a specific need. In particular, the wide range of redox states and the hexahedral structure of this metal allow endless metal/ligand combinations with variations in redox state, lipophilic/hydrophilic status, ligand exchange properties, stability, and geometry.

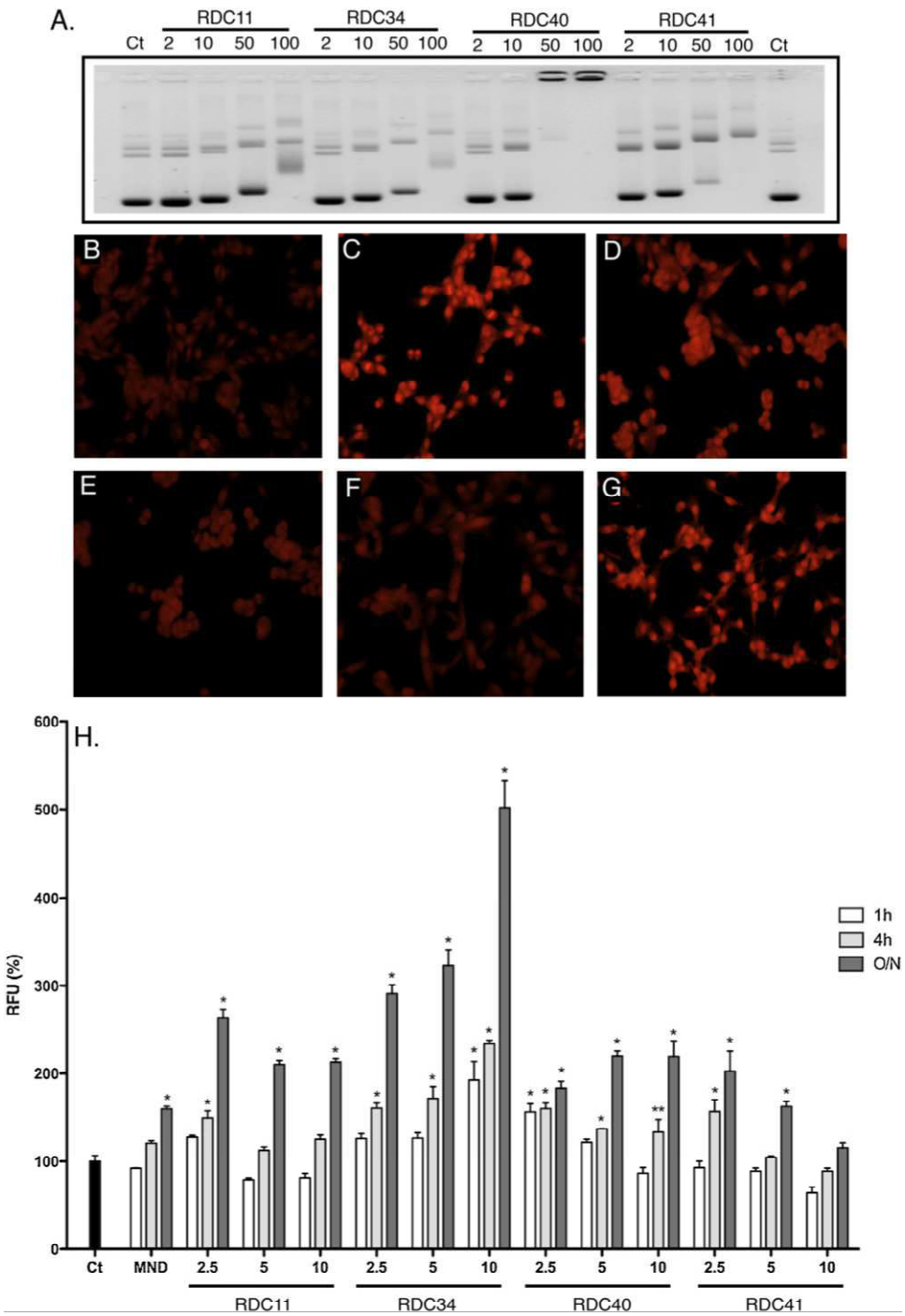


Fig. 4. Interaction of the optimized compounds with DNA and production of reactive oxygen species. (A) Circular double-stranded DNA was incubated with RDCs at the indicated ratio (DNA base pairs/molecule of drugs). Complexes were run on a 1% agarose gel, and then stained with ethidium bromide to observe DNA relaxation. Data are representative of 3 independent experiments. (B–G) HCT116 cells were treated with RDC (2.5 μM) for 16 h and labeled with carboxy-H2DCFDA for 1 h. (B) Control cells, (C) cells treated with the positive control, menadione, (D) cells treated with RDC11, (E) cells treated with RDC40, (F) cells treated with RDC41, (G) cells treated with RDC34. (H) HCT116 cells were treated with RDC as described in B–G, then fluorescence was quantified.

Recently, a ruthenium (II)-based organometallic compound, called RDC11, was shown endowed with anticancer properties. In order to optimize this compound, we have modified the ligands to gain in water solubility and in cytotoxicity.

As we hypothesized, the addition of a second phenanthroline significantly increased the cytotoxicity of the new compound RDC34 in comparison to RDC11, with an IC50 often in the nanomolar range, confirming the important role of the phenanthroline residue in the cytotoxic properties of RDCs. Compared to RDC11, RDC34 is also more toxic when given to mice [30]. However, at the maximum doses free of host toxicity, RDC34 significantly reduces tumor growth in two models. The increased toxicity of RDC34 could be related to its high lipophilicity [40], a property that might favor RDC34 cell uptake and distribution in the body after dosing. Although the addition of a second phenanthroline significantly increased the cytotoxicity, the modification of the phenylpyridine by addition of a NO_2, NH_2 or spermine moiety modify also significantly the cytotoxicity of the RDCs, highlighting

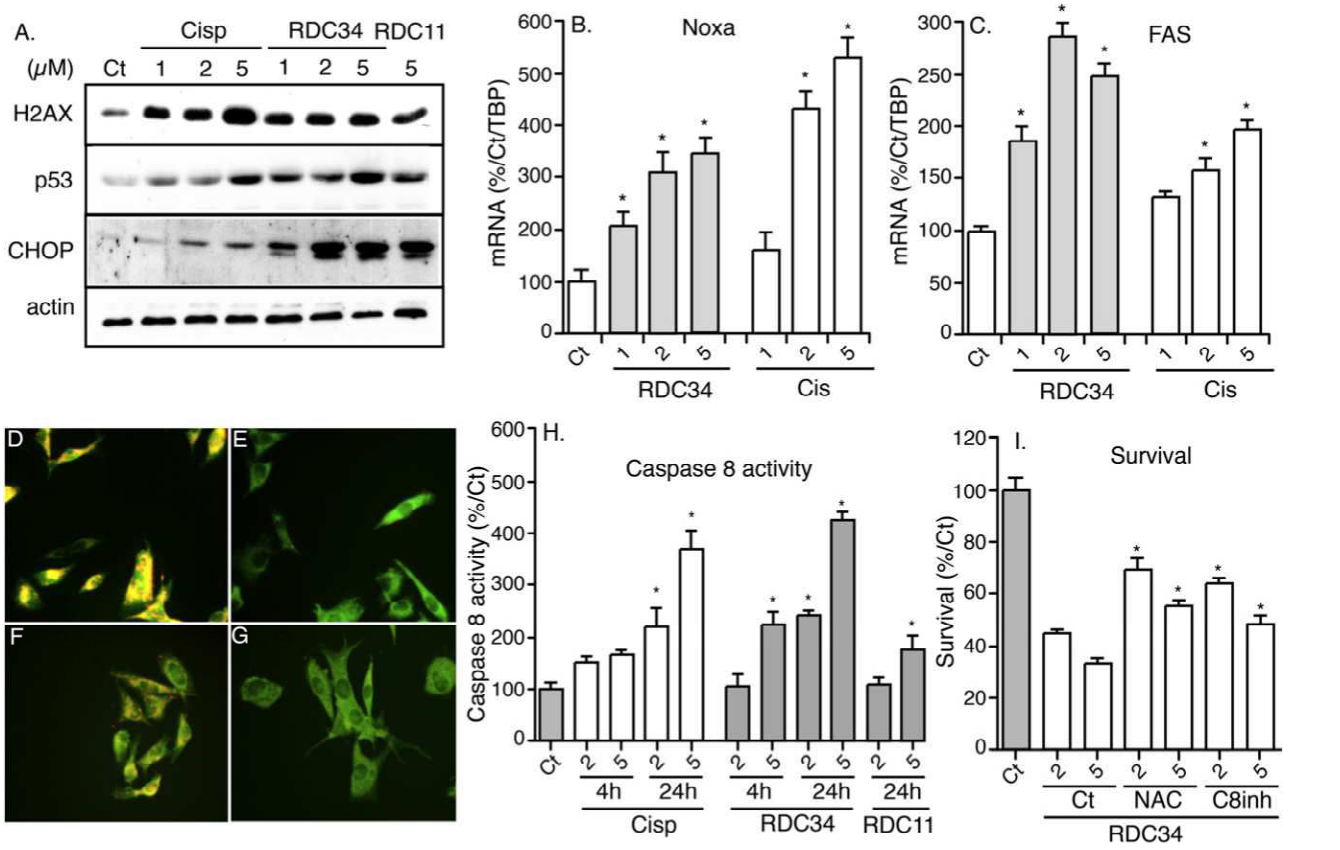


Fig. 5. Optimized RDCs induce multiple signaling pathways, including ROS and caspase 8. (A) Western blot analysis of cells treated for 24 h. Immunoblotting were performed with anti-p53, anti-actin, anti-phospho-H2AX, and anti-CHOP antibodies. Data are representative of 3 independent experiments. (B and C) HCT116 cells were treated with cisplatin, or RDC34 (in μM) for 24 h. RT-qPCR were performed using primers for noxa, and fas. Data are represented as fold inductions relative to untreated cells (Ct) and were normalized with both 18s and TBP levels. (D–G) Cells were incubated with the membrane potential sensitive dye JC-1. We used FCCP as positive control (E). Intracellular distribution of the dye was assessed by confocal microscopy at 488 nm excitation/510 nm emission. (H) Cells were incubated for the indicated time and concentration of drugs (in μM). (I) HCT116 were treated with the combination of drugs (NAC, 10 μM; caspase 8 inhibitor, C8inh 10 μM) added to RDC34 at the indicated concentrations. Survival was tested 48 h after using MTT tests.

the functional interaction occurring between the ligands and their interdependence to produce a specific biological effect.

By adding the spermine chain (RDC44), the NH_2 function (RDC41), and in a lesser extend the NO_2 (RDC40) function, we purposely improve the water solubility of RDC34 as indicated by their LogP, which is 2.35 for RDC34, 2.05 for RDC40, 0.9 for RDC41 and inferior to 0 for RDC44. RDC44 is freely soluble in water up to a concentration of 25 mM, simplifying its in vivo dosing of the experimental animals. However, as observed with RDC44 and in a lesser extent with RDC41 and RDC40, increasing the water solubility decreased the cytotoxicity. Similar observation has been made previously for the ruthenium compound KP1019 and its water-soluble version KP1339 [42]. Although the low cytotoxicity of RDC44 was disappointing, the in vivo studies revealed that RDC44 displayed similar anticancer properties compared to RDC34. A possible explanation could be that the spermine moiety confers a favorable pharmacokinetics of distribution, or alternatively that the spermine is somehow removed after its injection in mice, suggesting that RDC44 is a water-soluble pro-drug of RDC34.

The lower cytotoxicity of RDC44 could be due to a diminished cellular uptake through the lipophilic membrane barrier. Indeed, in standard medium, RDC44 showed a diminished cellular accumulation. However, under PBS conditions both compounds (RDC34, RDC44) can enter the cells and the water-soluble compound RDC44 is still barely able to affect cell survival compared to the lipophilic RDC34. Moreover, RDC44 is still able to interact with DNA with an affinity similar to RDC34. This lack of correlation between the cytotoxicity and the ability to interact with DNA is also supported by the results obtained with RDC40 and RDC41, which display a better affinity to DNA than RDC34, although they show a weaker cytotoxicity. Therefore, our data suggest that the improvement of RDC water solubility does not affect significantly RDC uptake and RDC-DNA interaction. We can therefore hypothesize that besides DNA, RDCs recruit additional direct intracellular targets that can account for a variation in their biological function depending on RDCs lipophilicity.

In favor of this hypothesis is the change of selectivity towards cancer cells of different origins observed in RDCs with variation in their ligands. Indeed, by modifying the ligand around the ruthenium center, we have observed that RDC34 displayed a strong cytotoxicity toward a broad range of cancer cell lines. RDC34 is particularly efficient on cancer cell lines of kidney origin that are poorly affected by RDC11. The introduction of the NH_2 function diminished the cytotoxicity of RDC41 at all levels comparable to that of RDC11. However, few exceptions exist in which RDC41 is more active than RDC11, such as EKVX cells, MDA-MB-435, UACC-257 and HS57BT. It is likely that the ability of the various RDCs to interact with cellular DNA does not explain their selectivity for different cell lines but rather their ability to interact with different intracellular targets and to induce different stress signaling.

As we have published for RDC11, the new generation of improved RDCs triggers at least two mechanisms: an interaction with DNA and an induction of CHOP expression. The interaction

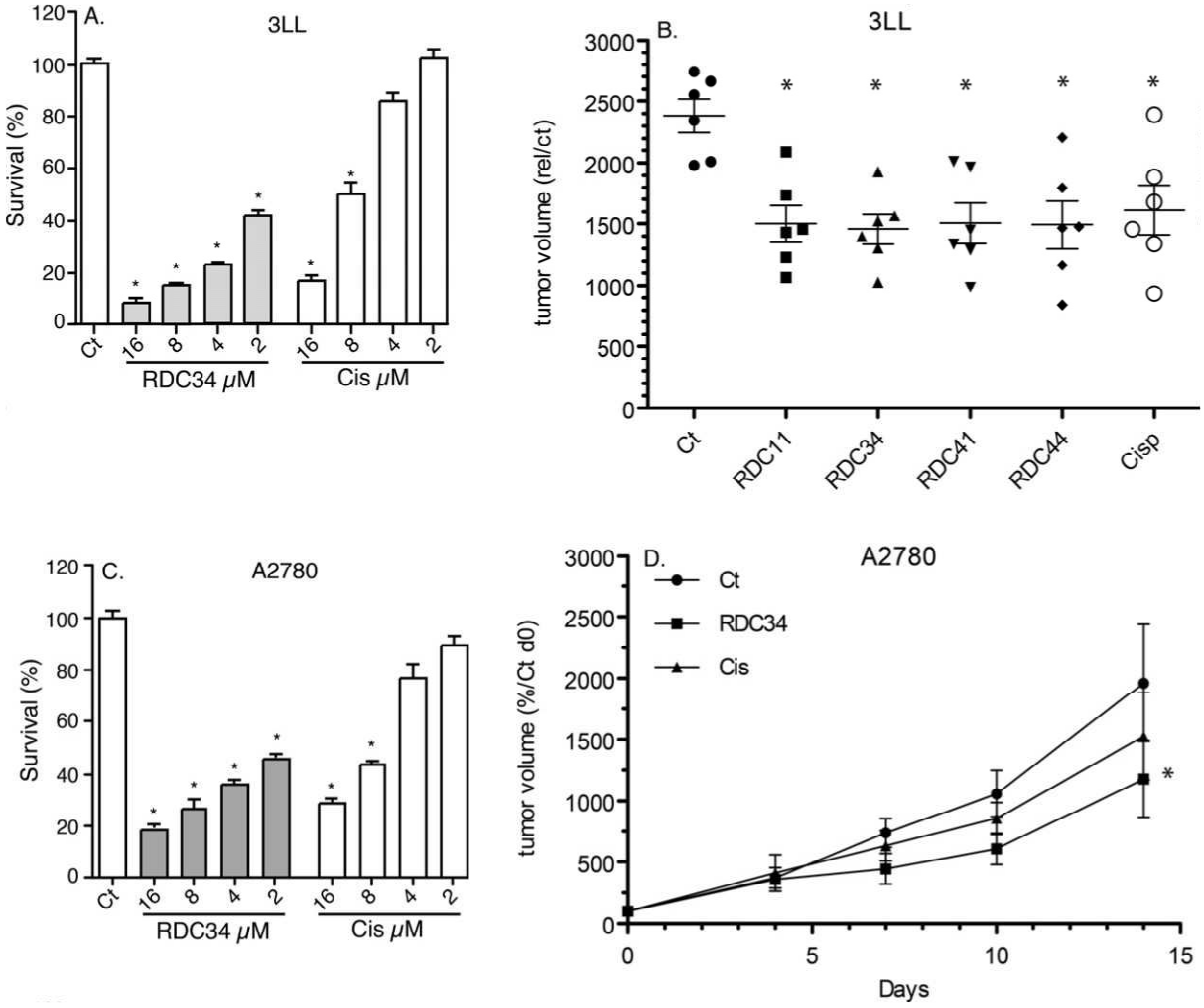


Fig. 6. Anticancer activity of optimized RDC. 3LL cells (A) or A2780 cells (C) were treated for 48 h with cisplatin or RDC (in μM). Viability was evaluated using a MTT test. (B) C57BL/6 mice (8-weeks old) were injected subcutaneously with 5×10^5 3LL cells. Injections of RDC (RDC34 and RDC44 at 4 μmol/kg; RDC41, RDC11 at 13.3 μmol/kg) or cisplatin (13.3 μmol/kg) started when tumors were palpable (±80 mm^3) and were performed twice a week. Solutions were prepared in PBS/5% Cremophore. (D) Nude mice (Swiss nu/nu, 8-weeks old) were injected subcutaneously with 5×10^6 A2780 cells. Injections of RDC34 (4 μmol/kg) or cisplatin (13.3 μmol/kg) were performed twice a week when tumors were palpable. Graph represents tumor volumes. Data are representative of two independent experiments ($n = 7$). Asterisks indicate statistically significant difference ($p < 0.01$) compared to control, as calculated by a one-way ANOVA test followed by a Tukey test.

with DNA does not seem to play a major role in their cytotoxicity, as there is not a good correlation between the cytotoxicity and their ability to interact with DNA. Interestingly RDC34 is a more potent inducer of the p53 protein levels and the p53 target genes compared to RDC11 even though its interaction with DNA is similar to RDC11. This stronger effect might involve the higher ability of RDC34 to induce ROS production, as ROS can induce p53. The role of ROS in the cytotoxicity of ruthenium compounds has been previously suggested [27,43] and is demonstrated by our present study as NAC significantly reduces RDC34 cytotoxicity. However, the correlation between production of ROS and RDC cytotoxicity is only partial, as there is no difference in ROS production between RDC40 and RDC11 even though RDC40 is more cytotoxic than RDC11. Previous studies indicated that RDCs modulate the activity of oxido-reductase enzymes [44], suggesting that the production of ROS might be triggered by alterations of the activity of enzymes committed to produce or remove ROS, although these targeted enzymes remain to be identified yet.

Anyhow, RDC34 is a strong inducer of p53 and p53 target genes connected to the extrinsic pro-apoptotic pathways involving caspase 8. The role of caspase 8 seems crucial to the pathway leading to cell death after treatment with RDC34 since its inhibition reduced these cytotoxic effects.

Overall this study demonstrates the crucial role of modified ligand around the ruthenium center to optimize the molecules in order to improve the cytotoxicity and target cancers subtypes. The variation in cytotoxicity between the compounds tested in the present study might involve several factors: (1) the redox potential, (2) the lipophilic status, and (3) the geometry. These factors might influence the ability of the compound to enter the cells, interact physically with intracellular targets and modify their functions. These factors also certainly affect the pharmacokinetic and the tissues distribution of the compounds in vivo and might explain the differences in toxicity. Moreover, this study shows the possibility of producing a RDC pro-drugs that present fair water solubility without affecting significantly the in vivo anticancer activity of the pharmacophore.

Acknowledgements

This work was supported by CNRS (CG), Association pour la Recherche Contre le Cancer Grant 3288, La Ligue Contre le Cancer,

ANR (PhotoBioMet project, AAPADC project), Institut National du Cancer.

Appendix A. Supplementary data

Supplementary data associated with this article can be found, in the online version, at http://dx.doi.org/10.1016/j.bcp.2012.08.022.

References

[1] Bruijnincx PC, Sadler PJ. New trends for metal complexes with anticancer activity. Curr Opin Chem Biol 2008;12(2):197–206.
[2] Jakupec MA, Galanski M, Arion VB, Hartinger CG, Keppler BK. Antitumour metal compounds: more than theme and variations. Dalton Trans 2008;(2):183–94.
[3] Dyson PJ, Sava G. Metal-based antitumour drugs in the post genomic era. Dalton Trans 2006;(16):1929–33.
[4] Kannarkat G, Lasher EE, Schiff D. Neurologic complications of chemotherapy agents. Curr Opin Neurol 2007;20(6):719–25.
[5] Markman M. Toxicities of the platinum antineoplastic agents. Expert Opin Drug Safe 2003;2(6):597–607.
[6] Kelland L. The resurgence of platinum-based cancer chemotherapy. Nat Rev Cancer 2007;7(8):573–84.
[7] Allardyce CS, Dyson PJ. Ruthenium in medicine: current clinical uses and future prospects. Platinum Metals Rev 2001;45:62.
[8] Anghileri LJ. The in vivo inhibition of tumor growth by ruthenium red: its relationship with the metabolism of calcium in the tumor. Z Krebsforsch Klin Onkol Cancer Res Clin Oncol 1975;83(3):213–7.
[9] Giraldi T, Sava G, Bertoli G, Mestroni G, Zassinovich G. Antitumor action of two rhodium and ruthenium complexes in comparison with cis-diamminedichloroplatinum(II). Cancer Res 1977;37(8 Pt 1):2662–6.
[10] Sava G, Giraldi T, Mestroni G, Zassinovich G. Antitumor effects of rhodium(I): iridium(I) and ruthenium(II) complexes in comparison with cis-dichlorodiammino platinum(II) in mice bearing Lewis lung carcinoma. Chem Biol Interact 1983;45(1):1–6.
[11] Keppler BK, Balzer W, Seifried V, Synthesis. antitumor activity of triazolium-bis(triazole)-tetrachlororuthenate (III) and bistriazolium-triazolepentachlororuthenate (III). Two representatives of a new class of inorganic antitumor agents. Arzneimittelforschung 1987;37(7):770–1.
[12] Sava G, Pacor S, Zorzet S, Alessio E, Mestroni G. Antitumour properties of dimethylsulphoxide ruthenium (II) complexes in the Lewis lung carcinoma system. Pharmacol Res 1989;21(5):617–28.
[13] Fruhauf S, Zeller WJ. New platinum: titanium, and ruthenium complexes with different patterns of DNA damage in rat ovarian tumor cells. Cancer Res 1991;51(11):2943–8.
[14] Novakova O, Kasparkova J, Vrana O, van Vliet PM, Reedijk J, Brabec V. Correlation between cytotoxicity and DNA binding of polypyridyl ruthenium complexes. Biochemistry 1995;34(38):12369–78.
[15] Morris RE, Aird RE, Murdoch Pdel S, Chen H, Cummings J, Hughes ND, et al. Inhibition of cancer cell growth by ruthenium(II) arene complexes. J Med Chem 2001;44(22):3616–21.
[16] Scolaro C, Bergamo A, Brescacin L, Delfino R, Cocchietto M, Laurenczy G, et al. In vitro and in vivo evaluation of ruthenium(II)–arene PTA complexes. J Med Chem 2005;48(12):4161–71.
[17] Hartinger CG, Zorbas-Seifried S, Jakupec MA, Kynast B, Zorbas H, Keppler BK. From bench to bedside—preclinical and early clinical development of the anticancer agent indazolium trans-[tetrachlorobis(1H-indazole)ruthenate(III)] (KP1019 or FFC14A). J Inorg Biochem 2006;100(5–6):891–904.
[18] Rademaker-Lakhai JM, van den Bongard D, Pluim D, Beijnen JH, Schellens JH. A Phase I and pharmacological study with imidazolium-trans-DMSO-imidazole-tetrachlororuthenate: a novel ruthenium anticancer agent. Clin Cancer Res 2004;10(11):3717–27.
[19] Mei HY, Barton JK. Tris(tetramethylphenanthroline)ruthenium(II): a chiral probe that cleaves A-DNA conformations. Proc Natl Acad Sci U S A 1988;85(5):1339–43.
[20] Brabec V. DNA modifications by antitumor platinum and ruthenium compounds: their recognition and repair. Prog Nucleic Acid Res Mol Biol 2002;71:1–68.
[21] Zeglis BM, Pierre VC, Barton JK. Metallo-intercalators and metallo-insertors. Chem Commun (Camb) 2007;(44):4565–79.
[22] Gaiddon C, Jeannequin P, Bischoff P, Pfeffer M, Sirlin C, Loeffler JP. Ruthenium (II)-derived organometallic compounds induce cytostatic and cytotoxic effects on mammalian cancer cell lines through p53-dependent and p53-independent mechanisms. J Pharmacol Exp Ther 2005;315(3):1403–11.
[23] Hayward RL, Schornagel QC, Tente R, Macpherson JS, Aird RE, Guichard S, et al. Investigation of the role of Bax: p21/Waf1 and p53 as determinants of cellular responses in HCT116 colorectal cancer cells exposed to the novel cytotoxic ruthenium(II) organometallic agent, RM175. Cancer Chemother Pharmacol 2005;55(6):577–83.
[24] Chatterjee S, Kundu S, Bhattacharyya A, Hartinger CG, Dyson PJ. The ruthenium(II)-arene compound RAPTA-C induces apoptosis in EAC cells through mitochondrial and p53-JNK pathways. J Biol Inorg Chem 2008;13(7):1149–55.
[25] Smalley KS, Contractor R, Haass NK, Kulp AN, Atilla-Gokcumen GE, Williams DS, et al. An organometallic protein kinase inhibitor pharmacologically activates p53 and induces apoptosis in human melanoma cells. Cancer Res 2007;67(1):209–17.
[26] Ang WHet al. Organometallic ruthenium inhibitors of glutathione-S-transferase P 1-1 as anticancer drugs. ChemMedChem 2007.
[27] Dougan SJ, Habtemariam A, McHale SE, Parsons S, Sadler PJ. Catalytic organometallic anticancer complexes. Proc Natl Acad Sci U S A 2008;105(33):11628–33.
[28] Gava B, Zorzet S, Spessotto P, Cocchietto M, Sava G. Inhibition of B16 melanoma metastases with the ruthenium complex imidazolium trans-imidazoledimethylsulfoxide-tetrachlororuthenate and down-regulation of tumor cell invasion. J Pharmacol Exp Ther 2006;317(1):284–91.
[29] Leyva L, Sirlin C, Rubio L, Franco C, Le Lagadec R, Spencer J, et al. Synthesis of cycloruthenated compounds as potential anticancer agents. Eur J Inorg Chem 2007;(19):3055–66.
[30] Meng Xet al. A ruthenium-containing organometallic compound reduces tumor growth through induction of the endoplasmic reticulum stress gene CHOP. Cancer Res 2009.
[31] Benosman S, Gross I, Clarke N, Jochemsen AG, Okamoto K, Loeffler JP, et al. Multiple neurotoxic stresses converge on MDMX proteolysis to cause neuronal apoptosis. Cell Death Differ 2007.
[32] Benosman S, Meng X, Von Grabowiecki Y, Palamiuc L, Hritcu L, Gross I, et al. Complex regulation of p73 isoforms after alteration of amyloid precursor polypeptide (APP) function and DNA damage in neurons. J Biol Chem 2011;286(50):43013–25.
[33] Bergamo A, Gaiddon C, Schellens JH, Beijnen JH, Sava G. Approaching tumour therapy beyond platinum drugs Status of the art and perspectives of ruthenium drug candidates. J Inorg Biochem 2012;106(1):90–9.
[34] Klajner M, Hebraud P, Sirlin C, Gaiddon C, Harlepp S. DNA binding to an anticancer organo-ruthenium complex. J Phys Chem B 2010;114(44):14041–47.
[35] Gaiddon C, de Tapia M, Loeffler JP. The tissue-specific transcription factor Pit-1/GHF-1 binds to the c-fos serum response element and activates c-fos transcription. Mol Endocrinol 1999;13(5):742–51.
[36] Nicoletti I, Migliorati G, Pagliacci MC, Grignani F, Riccardi C. A rapid and simple method for measuring thymocyte apoptosis by propidium iodide staining and flow cytometry. J Immunol Methods 1991;139(2):271–9.
[37] Sohm F, Gaiddon C, Antoine M, Boutillier AL, Loeffler JP. The retinoblastoma susceptibility gene product/Sp1 signalling pathway is modulated by Ca^{2+}/calmodulin kinases II and IV activity. Oncogene 1999;18(17):2762–9.
[38] Gaiddon C, Tian J, Loeffler JP, Bancroft C. Constitutively active G(S) alpha-subunits stimulate Pit-1 promoter activity via a protein kinase A-mediated pathway acting through deoxyribonucleic acid binding sites both for Pit-1 and for adenosine 3′,5′-monophosphate response element-binding protein. Endocrinology 1996;137(4):1286–91.
[39] Ryabov AD, Kurova VS, Ivanova EV, Le Lagadec R, Alexandrova L. Redox mediation and photomechanical oscillations involving photosensitive cyclometalated Ru(II) complexes: glucose oxidase, and peroxidase. Anal Chem 2005;77(4):1132–9.
[40] Fetzer L, Boff B, Ali M, Xiangjun M, Collin JP, Sirlin C, et al. Library of second-generation cycloruthenated compounds and evaluation of their biological properties as potential anticancer drugs: passing the nanomolar barrier. Dalton Trans 2011;40(35):8869–78.
[41] McGhee JD, von Hippel PH. Theoretical aspects of DNA–protein interactions: co-operative and non-co-operative binding of large ligands to a one-dimensional homogeneous lattice. J Mol Biol 1974;86(2):469–89.
[42] Heffeter P, Bock K, Atil B, Reza Hoda MA, Korner W, Bartel C, et al. Intracellular protein binding patterns of the anticancer ruthenium drugs KP1019 and KP1339. J Biol Inorg Chem 2010;15(5):737–48.
[43] Jakupec MA, Reisner E, Eichinger A, Pongratz M, Arion VB, Galanski M, et al. Redox-active antineoplastic ruthenium complexes with indazole: correlation of in vitro potency and reduction potential. J Med Chem 2005;48(8):2831–7.
[44] Le Lagadec R, Alexandrova L, Estevez H, Pfeffer M, Laurinavius V, Razumiene J, et al. Bis-ruthena(III)cycles [Ru((CN)-N-boolean AND)(2)((NN)-N-boolean AND)]PF6 as low-potential mediators for PQQ alcohol dehydrogenase ((CN)-N-boolean AND = 2-phenylpyridinato or 4-(2-tolyl)pyridinato, (NN)-N-boolean AND = bpy or phen). Eur J Inorg Chem 2006;(14):2735–8.

Results (Objective 2)

VI.B.Subcellular localization and transport kinetics of ruthenium organometallic anticancer compounds in living cell: a dose dependent role for amino acid and iron transporters.

Inorganic Chemistry

Article

pubs.acs.org/IC

Subcellular Localization and Transport Kinetics of Ruthenium Organometallic Anticancer Compounds in Living Cells: A Dose-Dependent Role for Amino Acid and Iron Transporters

M. Klajner,[†,§] C. Licona,[‡,§] L. Fetzer,[§,∥] P. Hebraud,[†,§] G. Mellitzer,[‡,§] M. Pfeffer,[§,∥] S. Harlepp,*[,†,§] and C. Gaiddon*[,‡,§]

[†]UMR7504, I.P.C.M.S., 23 rue du Loess, 67200, Strasbourg, France

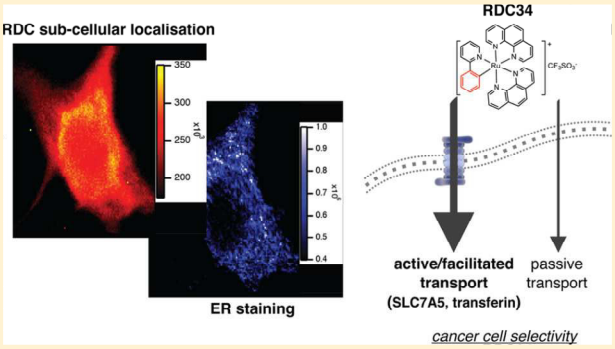
[‡]Molecular Signaling of the Cell Stress Response and Pathology, INSERM 1113, 3 av. Molière, 67200, Strasbourg, France

[§]Université de Strasbourg, Strasbourg, France

[∥]Laboratoire de Synthèses Métallo-Induites, Institut de Chimie, UMR7177, 4 rue Blaise Pascal, Strasbourg, 67000, France

Supporting Information

ABSTRACT: Ruthenium-based compounds are developed for anticancer treatment, but their mode of action including their import mechanism and subcellular localization remains elusive. Here, we used the intrinsic luminescent properties of cytotoxic organoruthenium (Ru(II)) compounds obtained with an anionic cyclometalated 2-phenylpyridine chelate and neutral aromatic chelating ligands (e.g., phenanthrolines) to follow their behavior in living cells. We established that the difference in sensitivity between cancer cells and noncancerous cells toward one of the compounds correlates with its import kinetics and follows a balance between active and passive transport. The active-transport mechanism involves iron and amino-acid transporters, which are transcriptionally regulated by the drug. We also demonstrated a correlation between the accumulation of these compounds in specific compartments (endoplasmic reticulum, nucleus, mitochondria) and the activation of specific cytotoxic mechanisms such as the mitochondrial stress pathway. Our study pinpoints a novel and complex mechanism of accumulation of ruthenium drugs in cancer cells.



INTRODUCTION

In the development and optimization of novel anticancer drugs, several parameters must be taken into account, including the intrinsic cytotoxic activity toward cancer cells and the pharmacokinetics and pharmacodynamics, which altogether are closely linked to the off-target toxicity of the compound toward healthy tissues.[1] These parameters are themselves the consequences of a molecular interaction between the drug and its direct target(s), the drug stability in biological environments, and the water solubility/lipophilicity of the drug. The latter also partly defines the mode of import/export into cells and the accumulation sites of the drug. Fortunate hazard or scientifically-directed adjustments in the balance between these parameters lead to a successful development of a novel anticancer drug.

However, following live import/export mechanisms and the subcellular accumulation sites of a drug often represents a challenge, as the analytical chemistry methods for quantifying the intact drug are not always sensitive enough. Frequently used as an alternative, the modification of the drug with a fluorochrome raises the question about the impact of the additional ligand on the transport mechanisms, localization, or direct-target interaction.

Few examples of successful chemotherapy are still driving the search for more potent, more selective, less prone to resistance, and better-tolerated drugs. In the past years, a significant interest was given to ruthenium-based drugs, because of the favorable properties of these compounds that make them a suitable basis for the development of antitumor drugs, such as the oxidation state, the ligand-exchange rate and the binding to proteins important for cell survival.[2,3] Various ruthenium complexes in oxidative state II or III were shown to present ligand-exchange abilities similar to those of platinum complexes, no cross-resistance with cisplatin, and a selective cytotoxicity for cancer cells with a reduced toxicity for healthy tissues, which at least in part can be explained by the selective transportation to cancer cells by the iron-transport system.[2−13] Two of these compounds, namely NAMI-A and KP1019, have successfully passed initial phase one of clinical trials.[14,15] Besides these initial successes, the emergence of new

Received: January 31, 2014
Published: May 1, 2014

ACS Publications © 2014 American Chemical Society

ruthenium-based therapies has been slowed down by several limitations, such as the relatively poor level of solubility and/or stability these therapies have in aqueous solutions, an unimpressive cytotoxicity (IC_{50} between 10 and 100 μM), and an uncertainty regarding the molecular mechanisms of action responsible for the antitumor effect.

In this respect, the mechanism of action and the direct targets of ruthenium-based drugs are still a matter of debate. Indeed, depending on the drug, several modes of action have been proposed, such as interaction with DNA to activate DNA-damage pathways[16−20] and inhibition of kinases[21] or other enzymatic activities,[22,23] including extracellular metallo-proteases.[24] The differences observed may be due to variations in their structure. Even if the ligands attached to the metal are most of the time only weakly bound to ruthenium via a coordination bond, the different nature of the ligands may be sufficient to induce different behaviors for the various complexes studied so far.

To improve the stability of ruthenium complexes and possibly to enhance their cytotoxicity and their pharmacokinetics, we have previously generated several ruthenium-based complexes in which the ligand is bound to the metal (M) via a strong covalent bond such as a C−M σ bond.[19,25] Besides an increased stability, these compounds present a new variety of ligands, and they differ from each other by their Ru^{II}/Ru^{III} redox factor. We called these molecules ruthenium-derived compounds (RDCs), and we showed previously that several RDCs are cytotoxic for several cisplatin-resistant cancer cell lines.[19] Few of them showed a good antitumor activity both *in vitro* and *in vivo*, with an IC_{50} often between 0.1 and 5 μM, and anticancer property on models of ovarian cancer, melanomas, and gliomas.[26,27] Importantly, they showed a reduced neurotoxicity in comparison to cisplatin.[26] Because we demonstrated previously that cisplatin exerts its neurotoxic effect partly through induction of the p53 pathway,[28,29] we analyzed the ability of RDCs to interact with DNA and induce p53 proteins. These analyses demonstrated that RDC11 exerts its antitumor effect via DNA-dependent and DNA-independent modes of action.[26,30,31]

In the present study, we investigate the mode of import and subcellular localization of organoruthenium compounds to gain additional insights about their mode of action. To achieve this, we took advantage of the luminescence of organoruthenium compounds that present aromatic cycles such as RDC34 and RDC44 that we previously characterized for their anticancer properties.[27] This intrinsic luminescent property of these anticancer ruthenium-based compounds allowed us to perform these studies using living cells and unmodified compounds. This property rules out the possible problems that would have arisen with molecules to which a fluorochrome had to be attached.

EXPERIMENTAL SECTION

Chemical Compounds. RDC34 and RDC44 were synthesized and purified as previously described.[32,33] Briefly, the compounds were characterized by ^{1}H and ^{13}C NMR and high-resolution mass spectrometry (HRMS). Organelle-specific fluorescent dyes ER-Tracker Green, MitoTracker Green, Propidium iodide were prepared and used as indicated by the manufacturer (Invitrogen). 2-Deoxy-D-glucose, Oligomycin A, deferoxamine, and D-phenylalanine were purchased (Sigma). Stock solutions of the RDC were 50 mM in dimethyl sulfoxide (DMSO).

Cell Culture. A172 human glioblastoma cells were obtained from the American Type Culture Collection (ATCC). Cells were manipulated and cultured in Dulbecco's modified Eagle's medium (DMEM) with 10% fetal calf serum (FCS) (Dominique Dutcher) and 1% Penicillin + Streptomycin (Sigma) at 37 °C with 5% CO_2 atmosphere as previously described.[34] For live imaging, cells were cultured on coverslips coated with polyornitine (1 μg/mL) as previously described.[35]

Primary glia cultures were prepared from 7 d old mouse cerebella using enzymatic and mechanical isolation as previously described.[36] Glial cells were separated from neurons by sedimentation and adhesion on uncoated plastic culture plates. After 3 h, unattached neuronal cells were removed by rinsing the plates three times with fresh medium. Attached glial cells were then further cultivated for 5 d before treatment.

Cell Survival. 5000 cells were seeded per well in 96-well microplates (Falcon Multiwell) 48 h prior to any treatment. RDCs were applied for 48 h by diluting the 50 mM DMSO stock solutions in fresh medium (DMEM with 10% serum). 3-(4,5-Dimethylthiazol-2-yl)-2,5-diphenyltetrazolium bromide (MTT) assay was performed as described previously by replacing the medium with fresh medium supplemented with 5 mg/L MTT (Sigma) for 1 h.[37] Cells were lysed in isopropanol with 0.04 N HCl. Measurements were performed at 550 nm.

Confocal Microscopy and RDC Accumulation Measurements. A home-built confocal microscope was used. We first visualized the cells before taking any confocal images, to follow a healthy single layer of cells. The typical scan size was around 60 μm × 60 μm with a step size of 500 nm. The laser was expended through a telescope and feeds the back focal plane of an objective. The sample was moved with piezoelectric devices. The piezoelectric devices had a total range of approximately 100 μm with a capacitive feedback loop. The repeatability of the system was approximately 20 nm, and the precision was ∼1 nm. The integration time was adjusted to obtain a good signal-to-noise ratio. The typical integration time was around 50 ms per pixel. The signal was collected through a 50 μm core multimode fiber coupled to a spectrometer splitting the light in the different wavelengths. A charge-coupled device (CCD) camera collected the signal and returned the emission spectrum. This spectrum was then equally divided in 10 subparts. We summed up the intensities in each part and attributed them to an integrated intensity to each average wavelength.

Correlation Factor and Colocalization. We then obtained 10 different images from the same cell at the different wavelengths. Thus, we could compare the fluorescence from the different organelle-specific dyes used, which mostly emitted around 520 nm, and the ruthenium compounds emitting around 750 nm. The images were aligned by $x-y$ translation whose vector was determined by maximizing the correlation between successive images.

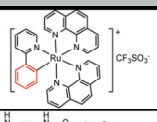
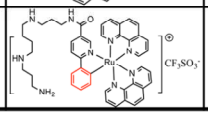
$$r = \left(\frac{1}{n-1}\right)\cdot\sum_{x,y}\frac{(f(x,y)-\overline{f(x,y)})\times(g(x,y)-\overline{g(x,y)})}{\sigma_f\sigma_g}$$

Where r represents the correlation factor, n represents the number of pixels in the image, f was the image obtained from the fluorescent labels, $\overline{f}$ was the average value of that image, g was the image obtained from RDC, $\overline{g}$ the average value of that image, and σ_f, σ_g were the standard deviation of the images.

Import Kinetics. The image acquisition over at least 1 h on the same region and the same cells allowed us to directly compare the fluorescence intensities over time and to link the changes to the intracellular accumulation. We first aligned the images, applying cross-correlation to the stack, and afterward we aligned an X and Y translation to the image to correct the mechanical drift from the time series. This led to a perfect superposition of the images. Then, a region of interest was set such that only the intensity from the cells belonging to the image was taken into account. We summed up the intensity from the region of interest and divided it by the number of pixels involved. The result was an average intensity collected on a cellular area. We obtained from this analysis an intensity versus time array. We used the maximum and minimum intensity values to normalize this

dx.doi.org/10.1021/ic500250e | Inorg. Chem. 2014, 53, 5150−5158

Table 1. Names, Structures, IC_{50} in A172 Human Glioblastomas, Glial, and Neuronal Cells, and Lipophilicity Index for the Ruthenium-Derived Compounds Used

	Compound	Formula	IC_{50} (μM) A172	IC_{50} (μM) Glia	IC_{50} (μM) Neuron	Lipophilicity LogP(o/w)
N-Ru-C structure	RDC34		0.25 ± 0.23	1.2 ± 0.4	1.15 ± 0.6	2.35 ± 0.04
	RDC44		74 ± 2.6	82 ± 5.3	91 ± 3.6	< 0.5

array. The evolution over time therefore represented the average import kinetics.

Western Blot. Cells were lysed as previously described with a lysis buffer (125 mM tris(hydroxymethyl)aminomethane (Tris)-HCl pH 6.7, NaCl 150 mM, NP40 0.5%, 10% glycerol).[38] Proteins were denatured and deposed (75 μg of proteins) on 10% sodium dodecyl sulfate polyacrylamide gel electrophoresis (SDS-PAGE) gel. Western blots were performed using antibodies raised against C/EBP homologous protein (CHOP) (1/1000 dilution, Santa Cruz, CA) or H2AX (S139) (1/2000, Millipore, France) and incubated with the blots overnight. Secondary antibodies (antirabbit, antimouse: Sigma, MA) were incubated at 1:1000 for 2 h. Equal loading of the samples was controlled visualizing actin expression (rabbit anti-β-actin, Sigma, 1:4000).

Quantitative Polymerase Chain Reaction. Cultured cells were lysed with 1 mL of TRIzol per 10 cm^2 (Invitrogen) to extract RNA according to manufacturer's instructions. RNA samples were ethanol-precipitated twice and 1 μg was used for reverse transcription (High-Capacity cDNA Reverse Transcription Kit, Applied Biosystems). Quantitative polymerase chain reaction (qPCR) was performed using 2 ng/μL cDNA (RNA equivalent) according to manufacturer's instructions (SYBR Green PCR Master Mix, Applied Biosystems) and with 400 μM of each primer (Supporting Information, Table 1). Expression levels were normalized using average of 18S and tri-*n*-butyl phosphate (TBP) (TATAA binding protein) RNA expression.

RESULTS

Ruthenium-Derived Anticancer Compounds Present Fluorescent Properties. We have developed several compounds containing ruthenium in redox state II and bound to aromatic ligands.[33] We previously characterized the cytotoxicity and anticancer activity of RDC34 and RDC44 that both present two phenanthrolines (Table 1).[27] RDC44 presents in addition a spermine unit that enforces the water solubility of the compound as indicated by its log p(o/w) using phase-separation experiments[33] (Table 1). RDC34 and RDC44 have an IC_{50} on cancer cells of 0.25 μM and 74 μM, respectively, in A172 glioblastoma cells that express a wild-type p53 gene. Similar results have been observed on p53-mutated cells (Supporting Information, data #1). Here, we are now showing that the toxicity of the compounds on primary cultures of glial and neuronal cells (noncancerous) was decreased as indicated by an increase of the IC_{50} (Table 1). Under similar experimental conditions, we obtained an IC_{50} for cisplatin of 5.4 (±0.8) and 7.9 (±0.6) for A172 and glial cells, respectively. This observation suggested that there is a selectivity of action and/or transport into the cells between cancerous and noncancerous cells for RDC34.

The presence of two phenanthrolines in RDC34 and RDC44 suggested that these compounds could display luminescent properties. Indeed, spectroscopic measurements indicated that RDC34 and RDC44 when excited at 488 nm exhibited light emission with a pick between 730 and 750 nm (Figure 1A). We have previously shown that related RDCs could intercalate between DNA base pairs.[31] Therefore, we measured the change in RDC fluorescence upon interaction with DNA. A 4-fold and 10-fold amplification of fluorescence was observed for RDC34 and RDC44, respectively. An increase in fluorescence for RDC34 and RDC44 was also observed when incubated with RNA or bovine serum albumin (BSA) (Figure 1B,C), indicating that these compounds interact *in vitro* as well with RNA and proteins. It is noteworthy that the overall light-emission intensities of RDC44 alone or in interaction with the biological macromolecules were higher compared to RDC34, in particular with BSA.

Subcellular Localization of Organometallic Ruthenium-Containing Compounds in the Endoplasmic Reticulum. The entry and localization of luminescent RDC34 and RDC44 were followed by confocal microscopy on living cells treated for 2 h with the respective drug. Using the same time and measurement parameters, we observed a strong luminescent emission inside the cells caused by RDC34 (Figure 2A) and a much weaker emission for RDC44 (Figure 2B). Interestingly, the emissions for both compounds were markedly perinuclear, suggesting a possible localization in the endoplasmic reticulum (ER). To verify this, we used ER-Tracker Green dye, which is a specific dye for the ER compartment. This marker revealed a good correlation between the localization of the ER-tracker Green dye and the luminescence of RDC34 or RDC44 (Figure 2C,D). We further confirmed the physical and functional relationship between RDC34 and ER by showing that RDC34 strongly increased in a dose-dependent manner the protein level of the ER stress response transcription factor CHOP (Figure 2E) and the mRNA level of CHAC1, a known target gene (Figure 2F). Interestingly, in the same conditions RDC44 did not affect significantly CHOP protein levels or CHAC1 expression, which could be explained by a poor ability of RDC44 to enter cells (Figure 2B) under these conditions. Indeed, cytotoxic concentration of RDC44 (250 μM) also led to the induction of CHAC1 expression (Supporting Information, data #2).

Taken together, this set of experiments indicated that RDC34, which displays normally a weaker emission intensity *in vitro* than RDC44 (Figure 1), accumulates more efficiently in cells compared to RDC44, this being evidenced by its stronger luminescent emission; moreover, it has a physical and functional relationship with the ER.

Subcellular Localization of RDC in the Nucleus and the Mitochondria. To further investigate the subcellular

dx.doi.org/10.1021/ic500250e | Inorg. Chem. 2014, 53, 5150−5158

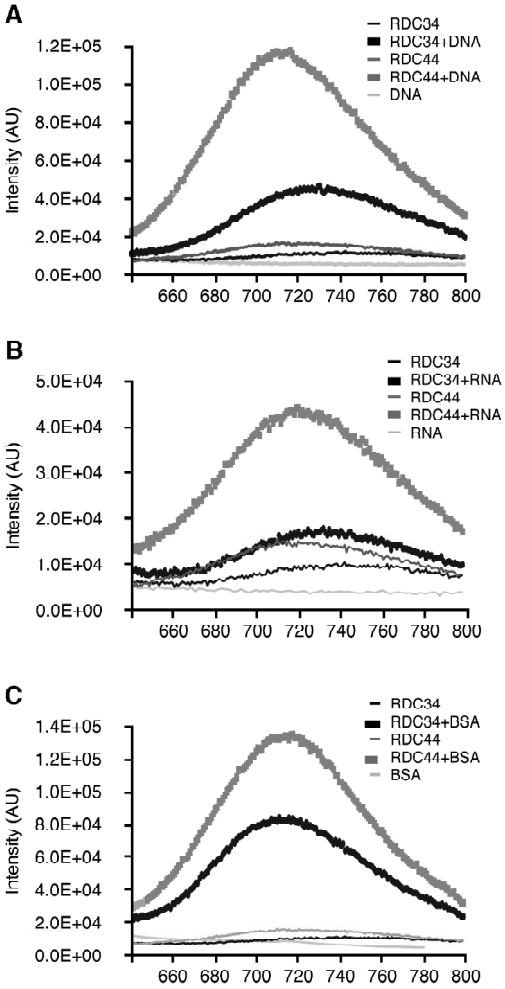


Figure 1. Emission spectra (nm) obtained from RDC34 and RDC44 in interaction with different biopolymers added in large excess compared to RDC molecules. The excitation is set at 488 nm. (A) Lines indicate emission spectra (AU; arbitrary unit) for RDC components (50 μM) alone in aqueous solution, in combination with DNA (sheared salmon sperm DNA, 300 μM), or DNA alone. (B) Lines indicate emission spectra for RDC components (50 μM) alone in aqueous solution, in combination with 16sRNA (60 μM), or 16sRNA alone. (C) Lines indicate emission spectra for RDC components (50 μM) alone in aqueous solution, in combination with BSA (50 μM), or BSA alone.

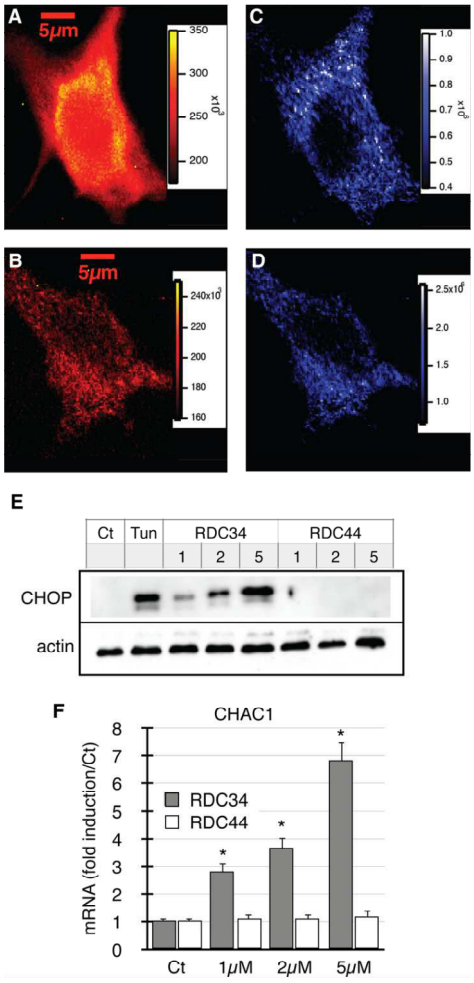


Figure 2. Accumulation of RDC in endoplasmic reticulum and induction of the unfolded protein stress response. A172 cells were incubated for 2 h with RDC34 (A, C) or RDC44 (B, D) at 5 μM, corresponding to the accumulation plateau as indicated by the fluorescence intensity assessed by confocal microscopy. Fluorescence images of RDC34 (A) and RDC44 (B) in A172 cells. Staining of the endoplasmic reticulum was performed using the ER-Tracker Green (C, D). (E) Western blot analysis of cells treated for 24 h at the indicated concentrations (in μM). Tunicamicin (Tun) was used at 5 μg/mL. Immunoblotting was performed with antiactin and anti-CHOP antibodies. Data are representative of three independent experiments. Ct stands for cells treated without the drugs. (F) Cells were treated with RDC34 or RDC44 at the indicated concentration (in μM) for 24 h. Reverse transcription (RT) qPCR was performed using primers for CHAC1. Data are represented as mean (±standard deviation) of fold inductions relative to untreated cells (Ct) and were normalized with both 18s and TBP levels. Asterisks indicate statistically significant difference ($p < 0.01$) compared to control, as calculated by a one-way ANOVA test followed by a Tukey test.

localization of RDC34, we performed colocalization experiments with dyes specific for the nucleus (propidium iodide) and the mitochondria (MitoTracker Green). We observed that part of the RDC34 was localized inside the nucleus as shown in Figure 3A,B. To independently assess the effect of RDC34 and RDC44 on the nucleus, we showed that RDC34 and to a lesser extent RDC44 induced a DNA damage response as indicated by the phosphorylation of histone H2AX (Figure 3E).

The colocalization studies using the MitoTracker Green (Figure 3D) also revealed that some RDC34 molecules may be localized in the mitochondria (Figure 3C,D). Because of the small size and the dispersion of the mitochondria within the cell a precise colocalization was difficult to assess, but calculation indicated a correlation factor of 0.45 suggesting a good colocalization of RDC34 fluorescence with the MitoTracker Green. As mitochondria develop also a stress response upon damages, we analyzed the activation of SATB1/2 proteins and their target gene HSP60, which are markers of this stress response.[39] Interestingly, cells treated with RDC34 showed an induction of both SATB2 and HSP60 expressions (Figure 3F).

Altogether these studies indicated that RDC34 was localized in at least three intracellular compartments, ER, mitochondria, and nucleus. Their localization into these compartments also correlated with the activation of specific stress-response mechanisms, such as CHOP, H2AX, or SATB2.

dx.doi.org/10.1021/ic500250e | Inorg. Chem. 2014, 53, 5150−5158

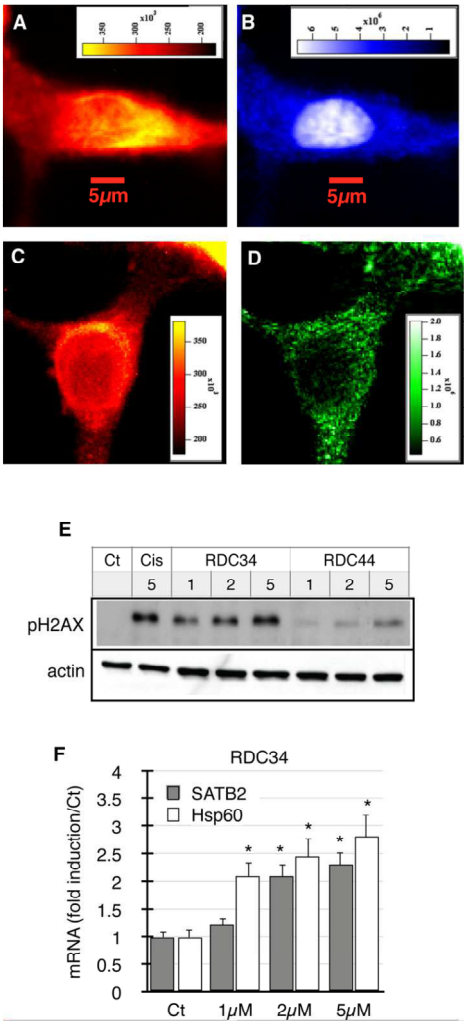


Figure 3. Accumulation of RDC in the nucleus and the mitochondria, and induction of DNA damage and mitochondria stress response. (A, B, C, D) A172 cells were incubated for 2 h with RDC34 (5 μM) to the accumulation plateau as indicated by the fluorescence intensity assessed by confocal microscopy. (B, D) Staining of the nucleus or the mitochondria was performed using the propidium iodide (B) and MitoTracker Green (D), respectively. (E) Western blot analysis of cells treated for 24 h at the indicated concentrations. Immunoblotting was performed with antiactin and anti-H2AX(S139) antibodies. Cisplatin (Cis; 5 μM) was used as positive control. Data are representative of three independent experiments. (F) Cells were treated with RDC34 at the indicated concentrations for 24 h. RT-qPCR was performed using primers for SATB2 and HSP60. Data are represented as mean (±standard deviation) of fold inductions relative to untreated cells (Ct) and were normalized with both 18s and TBP levels. Asterisks indicate statistically significant difference ($p < 0.01$) compared to control, as calculated by a one-way ANOVA test followed by a Tukey test.

Kinetics of Import in Cancerous and Noncancerous Cells. After determination of the intracellular localization, we focused on RDC34 intracellular accumulation over time. For this, we grew cells on polyornitine-treated coverslips, and after replacing culture medium with a RDC34 containing medium we performed time-lapse imaging as shown in Figure 4A. For appropriate comparative evaluation, the same image setup parameters were conserved for all pictures, permitting the direct linking of the intensity evolution to the accumulation. As specified in the Experimental Section, to further analyze the kinetics, we extracted the average intensity from the selected cells and normalized the maximum values obtained at 200 min or at the plateau in the time-lapse analysis with the number of pixels involved to attribute an intensity evolution value between 0 and 1 (Figure 4B,C,D). We observed in all the different tested cells that the curves obtained at 5 μM did not superimpose onto the ones obtained at 10 μM.

If we hypothesize the extracellular solution to be a reservoir of ruthenium compounds and the collected intensity to be the average concentration on the cellular volume, the second Fick's law tells us that the only parameter that influences the kinetics and the maximal intracellular concentration is the initial reservoir concentration. Thus, dividing our time series by the value reached at saturation directly shows whether the kinetics are purely diffusive or not. The fact that the curves do not superimpose therefore means that the kinetics differ from diffusion. Next, we assumed the simplest case where the kinetics are first-order in RDC concentration; in this case an exponential increase of the intensity would be observed, with a characteristic time independent of the initial concentration. Although our observed intensity versus time relationship may be well-described by a single exponential function, the deduced kinetic rate did depend on the initial RDC concentration (Figure 4B). Consequently, a purely passive diffusion mechanism can be excluded, thus suggesting that either facilitated or active transport must take part in the entrance mechanisms of RDC. We then followed the uptake of these drugs in healthy cells as shown in Figure 4C,D. Interestingly, the rate of drug intake at 5 μM was reduced in glial and neuronal cells compared to A172. In addition, we observed no superposition when the only changing parameter was the concentration, as observed in A172 cells. The adjustment was an exponential as described in A172 cells. Surprisingly, when the extracellular concentration was raised to 10 μM the rate of import was higher in healthy cells compared to A172 cells.

Altogether, the kinetic analysis suggested that the import might involve multiple kinds of mechanisms including facilitated and active processes. In addition, the rate of import is dependent on the extracellular concentration of the drug and the cell type.

RDC34 Multiple Intracellular Import Mechanisms Including Amino Acid Transporters. To better understand the mechanisms of RDC34 cellular import, we tested inhibitors of adenosine 5′-triphosphate (ATP) production to discriminate between passive and active mechanisms. We treated cells with oligomycin and 2-deoxy-D-glucose, classically used to inhibit ATP production, to block active import mechanisms.[40] As shown in Figure 5A the percentage of active-import mechanism involved in RDC34 accumulation increased when the concentration of RDC34 applied to the cells was lower than 5 μM. At 1 μM, 50% of the import is mediated by a mechanism dependent upon ATP production.

To further characterize the import mechanisms for RDC34 we focused on the ferritin/transferrin receptor system.[41] Several publications have documented an interaction between ruthenium compounds and transferrin.[42] The interaction is supposed to be based on the fact that ruthenium belongs to the family of iron. Interestingly, we observed that RDC34 increased the expression of ferritin, which is an iron intracellular packaging component, and decreased the expression of the transferrin receptor (TFRC), indicating that RDC34 regulates

dx.doi.org/10.1021/ic500250e | Inorg. Chem. 2014, 53, 5150−5158

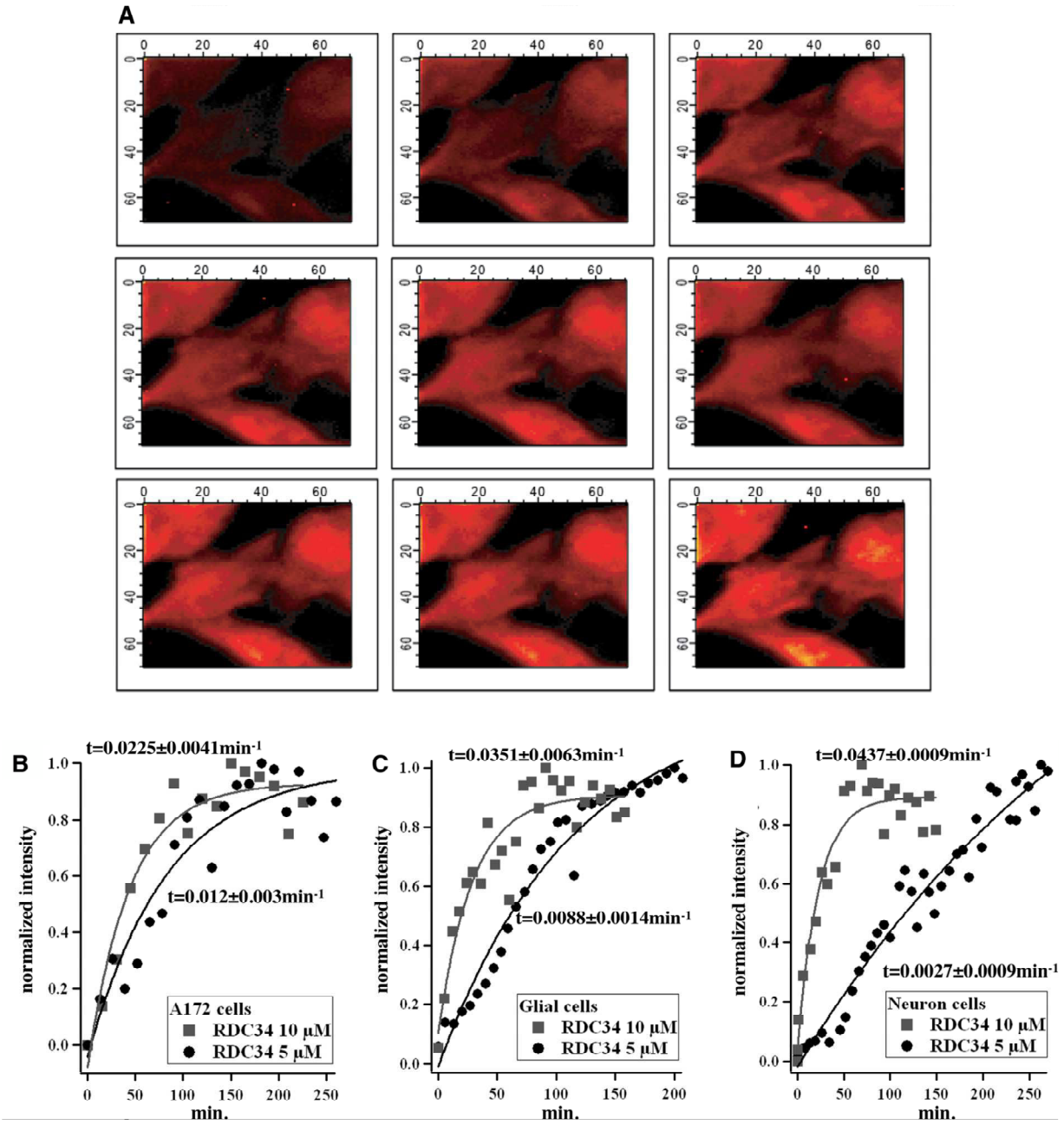


Figure 4. RDC intracellular accumulation observed with confocal microscopy over time. (A) Raw-image time series (left to bottom right) from A172 cells treated with 5 μM RDC34. The delay time between two consecutive images is around 8 min. The intensity range is fixed for all images to highlight the evolution. (B, C, D) The normalized accumulative intensity (1 being the maximal intensity measured) over time for RDC34 at 5 μM and 10 μM and the exponential adjustments in A172 (B), glial (C), and neuronal (D) cells.

like iron the expression of ferritin and TFRC, thus suggesting that the cells might consider RDC34 as iron (Figure 5B). Therefore, we tested how deferoxamine, which is known to chelate iron, might affect RDC import (Figure 5C). We observed that deferoxamine increased by approximately 25% the accumulation of RDC34 inside the cells. This result indicated that chelation of iron from the medium, and therefore leaving more iron transporter available, favored the import of RDC34. It also suggested that deferoxamine did not chelate RDC34.

Additional RT-qPCR analyses of various cellular transporters showed that RDC34 induced the expression of the amino acid transporter SLC7A5 (Figure 5B).[43] Amino acid transporters have been described to import also several chemical compounds including drugs. Therefore, we hypothesized that SLC7A5 could provide a means of cellular entry for RDC34. To verify this, we used D-phenylalanine that was previously shown to inhibit SLC7A5-dependent import.[44] Preincubation of cancer cells with D-phenylalanine reduced the accumulation of RDC34 (Figure 5D), suggesting that SLC7A5 participates in the cellular import of RDC34.

dx.doi.org/10.1021/ic500250e | Inorg. Chem. 2014, 53, 5150−5158

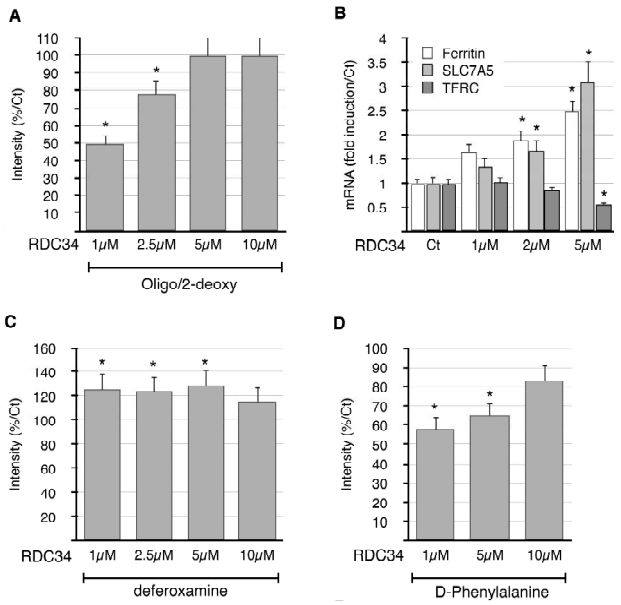


Figure 5. Importance of iron and amino acid transport in RDC intracellular import. (A) Active transport mechanisms were inhibited in A172 cells by using oligomycin (5 μM) and 2-dexoy-glucose (50 mM) preincubated for 1 h before adding RDC34 at the indicated concentration for 2 h. Accumulation of RDC34 was measured by fluorescence intensity using confocal microscopy at the end of the incubation time. Bars indicate mean (±standard deviation) of intensity. (B) Cells were treated with RDC34 at the indicated concentrations for 24 h. RT-qPCR was performed using primers for Ferritin, SLC7A5, and the transferrin receptor (TFRC). Data are represented as mean (±standard deviation) of fold inductions relative to untreated cells (Ct) and were normalized with both 18s and TBP levels. (C, D) A172 cells were preincubated with deferoxamine (100 μM) and D-phenylalanine (1 mM) for 1 h before adding RDC34 at the indicated concentration for 2 h. Accumulation of RDC34 was measured by fluorescence intensity using confocal microscopy at the end of the incubation time. Bars indicate mean (±standard deviation) of intensity. Asterisks indicate statistically significant difference ($p < 0.01$) compared to control, as calculated by a one-way ANOVA test followed by a Tukey test.

DISCUSSION

Metal-based compounds are intensively investigated as anticancer drugs due to their physicochemical properties such as their redox potential, ligand-exchange rate, the possibility of attaching more than four ligands to them, and others. Unfortunately, up to now the persistent lack of precise biochemical and biological characterizations retard their optimization and development toward clinical practice. In this regard, the ability of a specific compound to exert its biological function is dependent on multiple factors, such as its affinity to its intracellular targets, its intrinsic biochemical properties that might affect the function of its intracellular targets, and its ability to enter and be localized in specific compartments of the cell. Previously, studies were performed on this aspect with metal-based compounds, such as the anticancer compounds Nami-A or KP1019,[45] or DNA intercalators such as dipyridophenazine (dppz) complexes of Ru(II).[40,46,47] These compounds have the specificity of presenting nitrogen−metal coordination bonds, and in the case of Nami-A and KP1019, they display relatively low toxicities on cancer cells (IC_{50} > 10 μM).[30] In this study, we investigated for the first time the subcellular localization and the import processes of organometallic ruthenium compounds (that contained ruthenium "Ru−C" bond) showing strong cytotoxic properties.

Aromatic Ligands As a Tool to Follow Metal-Based Import/Export and Interaction with Biological Macromolecule. Following the outcome of a defined biologically active compound in cells in terms of import and subcellular localization is often a difficult task, being limited by available technological tools. For instance, it remains challenging to address these questions with metal-based anticancer compounds due to the limitations of the chemical analyses to locate these compounds in living cells. It often requires the use of cellular invasive methods or important chemical modifications. One of these modifications is the addition of a fluorescent moiety to the molecule. If this addition permits following the molecule *in cello* using microscopy, it also significantly modifies the molecule structure, which might bring artifacts in term of uptake, localization, and interaction with intracellular components. An alternative is to use induced coupled plasma mass spectrometry (ICP-MS) to quantify the presence of the metal in specific location after subcellular compartment isolation. This approach has two limits; the first is that ICP-MS quantifies only the metal and does not guarantee that the molecule is intact, and the second is that cellular manipulation to isolate the subcellular compartments can also alter the distribution of the compound. In our pursuit of developing highly cytotoxic anticancer compounds based on ruthenium, we designed and characterized an organometallic ruthenium compound, called RDC34, that presents Ru(II) cyclometalated to a phenylpyridine ligand via a covalent C−Ru bond that is further stabilized by a intramolecular N−Ru coordination bond. In addition, this compound presents two phenanthrolines as chelating ligands. This compound is highly cytotoxic toward cancer cells (IC_{50} < 1 μM) and reduces *in vivo* tumor growth (Table 1 and refs 27 and 33). Interestingly, the presence of the two phenanthrolines provides a fluorescence property that is amplified when RDC34 interacts with biological macromolecules such as DNA, RNA, and proteins (Figure 1). The exact biological significance of these nonselective interactions with DNA, RNA, and BSA remains to be established, as the experiments were done in tubes with purified molecules. In this respect, a confirmation of this lack of selectivity in cells would help to explain why these compounds act on several signaling pathways (CHOP/CHAC1; H2AX; SATB2/HSP60). Although RDC34 multiple mode of action might be regarded as a reason for its low selectivity, it may help to circumvent some resistance mechanisms and provide a compound being active on a very heterogeneous population of cancer cells in the tumor. The fluorescence intensity of RDC34 increases by approximately 3-fold in the presence of DNA, RNA, and BSA. Similar observations were done with an RDC34 variant that presents a spermine tail that increases its water solubility (Figure 1). Removal of a single phenanthroline, such as in the compound RDC11,[26] abrogates the fluorescence property (data not shown). Interestingly, addition of other aromatic ligands, such as in RDC56, also provides an interesting fluorescence property (Supporting Information, data #3). Therefore, derivatives of organoruthenium compounds with aromatic ligands, like RDC34 and RDC56, represent unique anticancer metal-based compounds that can be studied to gain a better understanding of the subcellular localization and import/export mechanisms of this class of novel therapeutic drugs, providing

dx.doi.org/10.1021/ic500250e | Inorg. Chem. 2014, 53, 5150−5158

information necessary for their further development and improvement of their reactivity.

Intracellular Localization of the Ruthenium Compounds. Using dyes that present subcellular selective localization, we observed accumulation of RDC34 in the nucleus, the endoplasmic reticulum, and the mitochondria of cancer cells (Figure 2, 3). Previously, accumulation of the ruthenium-based anticancer drugs Nami-A and KP1019 was observed in the nucleus and the mitochondria.[45] Here we also see an accumulation of RDC34 in the perinuclear part of the cell that corresponds in part to the endoplasmic reticulum. It remains to be established whether it is specific to the family of compounds with a cyclometalated phenylpyridine structure like those in RDC34 and RDC11. In addition, we are showing here that the presence of RDC34 in these compartments has specific functional consequences such as the induction of compartment-specific stress-response pathways like the induction of H2AX phosphorylation and CHOP/UPR and SATB2 expression (Figures 2 and 3). These molecular mechanisms can account for the cytotoxic or cytostatic activity of RDC34 on cancer cells.

Influence of the Lipophilicity on the Import of Ruthenium Compounds. The compound RDC44 has been developed to improve the water solubility of RDC34 by adding a spermine tail, which, however, drastically reduced its cytotoxicity (Table 1).[27] Interestingly, the ability of RDC44 to interact and increase its fluorescence upon interaction with DNA, RNA, or BSA does not seem to be affected: the fluorescence is improved with RDC44 *in vitro* when it interacts with biological macromolecules, in particular with BSA (Figure 1). However, the fluorescence emitted by RDC44 in cancer cells is reduced compared to that of RDC34. This observation suggests that RDC44 tends to accumulate less in cells. Although some RDC44 accumulates in cells anyway, we did not observe cytotoxicity or significant induction of stress-response pathways, such as H2AX phosphorylation or CHOP induction. It appears therefore that the lipophilicity status of the compound might impact partly the ability of the compound to enter the cells under these conditions. Additional experiments using variants of RDC34 might be necessary to assess whether there is a strict correlation between the lipophilicity and the accumulation in cancer cells.

Mode of Import of the Ruthenium Compounds. Experiments were performed with drugs that block or reduce selected cellular import mechanisms. The results obtained suggest that several import mechanisms participate in the active or facilitated entry of RDC34 in cancer cells. More specifically, we observed a contribution of active-transport mechanisms and amino acids transporters (Figure 5). The active import of ruthenium-based compounds was previously described for dipyrido[3,2-a:2′,3′-c]phenazine (dppz) DNA intercalators.[40] In this study, we now demonstrate that it is also the case for smaller organometallic compounds, and in addition we show that the contribution of these transport mechanisms is drug- and concentration-dependent. The lower the concentration of the compound, the higher the contribution of the active-import mechanism. This suggests that the concentration gradient at high concentration enforces the passive transport. We also observed that the use of the iron chelation drug deferoxamine improved the accumulation of RDC34, suggesting that RDC34 import might involve iron transport mechanisms such as ferritin and the transferrin receptor. This feature is supported by several observations. First, the normalized accumulation curves over time present concentration dependence. The dependence proves that the import is not purely diffusive, and some active transporter might be implicated (Figure 4). Second, RDC34 induces, like iron, the expression of transferrin and amino acid transporter such as SLCA7A5 (Figure 5).[41]

Selectivity between Cancer Cells and Noncancer Cells. RDC34 shows some selectivity toward glial cancer cells versus healthy glial cells, with IC_{50} values of 0.25 μM and 1.2 μM, respectively (Table 1). We already observed such selectivity with RDC11, a ruthenium compound with the cyclometalated phenylpyridine, one phenanthroline, and two acetonitriles. However, this selectivity is not observed with RDC44 that has an additional spermine tail compared to RDC34.[26] The import studies that we performed indicated that the import kinetics differed between cancer and normal cells. The import kinetics were much higher for cancer cells compared to normal cells (neurons or glial cells) (Figure 4). Interestingly, at 10 μM RDC34 the kinetics was drastically increased in all cells but even more in normal cells. These results indicated that in terms of import, cancer cells have a higher transport potential at low concentration of the drug than the healthy cells, which might be due to a constitutive high number of receptors/channels required for importing components necessary for cancer cell growth or due to a higher adaptability (induction of these receptors/channels upon treatment). This leads to selectivity between cancer cells and healthy cells, but this selectivity tends to decrease with an increasing drug concentration. Such concentration dependence could be explained by the fact that the active-import mechanisms are more important at low concentration (see above and Figure 5).

Altogether our data suggest a model in which RDC34 at low concentration enters into cancer cells more easily than it enters into normal cells through active mechanisms that are induced by RDC34 at the transcriptional level. However, at higher concentrations, this selectivity is lost due to the concentration gradient pressure (Figure 6). The distribution of RDC34 in the cells is complex and reflects the diversity of the signaling pathways that are induced by RDC34. In particular, not only nuclear and ER stress mechanisms are activated, but also a mitochondrial stress response. Hence, our findings provide novel and critical information on the possibly induced

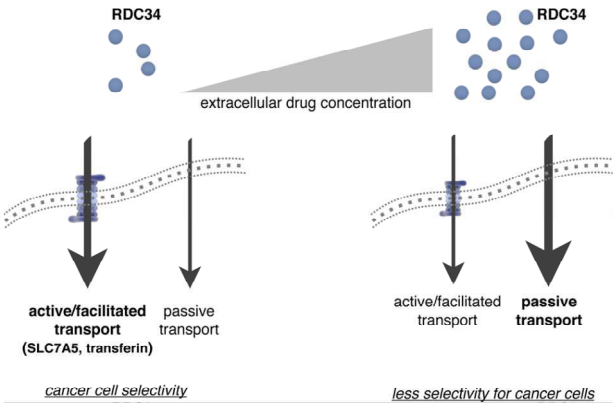


Figure 6. Scheme of the import mechanism representing proportion of active transport as a function of extracellular organoruthenium compound concentration.

dx.doi.org/10.1021/ic500250e | Inorg. Chem. 2014, 53, 5150−5158

molecular mechanisms and on the potential direct targets of organoruthenium anticancer drugs.

■ ASSOCIATED CONTENT

Supporting Information

Graph of cytotoxic response, histogram of fold inductions, table of genetic data, and RDC56 IC_{50} values. This material is available free of charge via the Internet at http://pubs.acs.org.

■ AUTHOR INFORMATION

Corresponding Authors

*E-mail: gaiddon@unistra.fr. (C.G.)
*E-mail: harlepp@ipcms.u-strasbg.fr. (S.H.)

Notes

The authors declare no competing financial interest.

■ ACKNOWLEDGMENTS

This work was supported by CNRS (C.G.), Association pour la Recherche Contre le Cancer (Grant 3288), La Ligue Contre le Cancer, Institut National du Cancer, and CONECTUS Alsace, European COST CM1105, CONACYT, the Laboratory of Excellence (LABEX) "Chemistry of Complex Systems" Univ. of Strasbourg and the FRC "synergie" (Univ. of Strasbourg). We are also thankful to P. Wlosik and L. Mathern for their technical and administrative support.

■ REFERENCES

(1) Doherty, M. M.; Michael, M. *Curr. Drug Metab.* **2003**, *4*, 131−49.
(2) Bruijnincx, P. C.; Sadler, P. J. *Curr. Opin. Chem. Biol.* **2008**, *12*, 197−206.
(3) Jakupec, M. A.; Galanski, M.; Arion, V. B.; Hartinger, C. G.; Keppler, B. K. *Dalton Trans.* **2008**, 183−94.
(4) Markman, M. *Expert Opin. Drug Saf.* **2003**, *2*, 597−607.
(5) Kelland, L. *Nat. Rev. Cancer* **2007**, *7*, 573−84.
(6) Allardyce, C. S.; Dyson, P. J. *Platinum Met. Rev.* **2001**, *45*, 62.
(7) Dyson, P. J.; Sava, G. *Dalton Trans.* **2006**, 1929−33.
(8) Giraldi, T.; Sava, G.; Bertoli, G.; Mestroni, G.; Zassinovich, G. *Cancer Res.* **1977**, *37*, 2662−6.
(9) Keppler, B. K.; Balzer, W.; Seifried, V. *Arzneim. Forsch.* **1987**, *37*, 770−1.
(10) Sava, G.; Pacor, S.; Zorzet, S.; Alessio, E.; Mestroni, G. *Pharmacol. Res.* **1989**, *21*, 617−28.
(11) Fruhauf, S.; Zeller, W. J. *Cancer Res.* **1991**, *51*, 2943−8.
(12) Morris, R. E.; Aird, R. E.; Murdoch Pdel, S.; Chen, H.; Cummings, J.; Hughes, N. D.; Parsons, S.; Parkin, A.; Boyd, G.; Jodrell, D. I.; Sadler, P. J. *J. Med. Chem.* **2001**, *44*, 3616−21.
(13) Scolaro, C.; Bergamo, A.; Brescacin, L.; Delfino, R.; Cocchietto, M.; Laurenczy, G.; Geldbach, T. J.; Sava, G.; Dyson, P. J. *J. Med. Chem.* **2005**, *48*, 4161−71.
(14) Hartinger, C. G.; Zorbas-Seifried, S.; Jakupec, M. A.; Kynast, B.; Zorbas, H.; Keppler, B. K. *J. Inorg. Biochem.* **2006**, *100*, 891−904.
(15) Rademaker-Lakhai, J. M.; van den Bongard, D.; Pluim, D.; Beijnen, J. H.; Schellens, J. H. *Clin. Cancer Res.* **2004**, *10*, 3717−27.
(16) Mei, H. Y.; Barton, J. K. *Proc. Natl. Acad. Sci. U.S.A.* **1988**, *85*, 1339−43.
(17) Brabec, V. *Prog. Nucleic Acid Res. Mol. Biol.* **2002**, *71*, 1−68.
(18) Zeglis, B. M.; Pierre, V. C.; Barton, J. K. *Chem. Commun. (Cambridge, U.K.)* **2007**, 4565−79.
(19) Gaiddon, C.; Jeannequin, P.; Bischoff, P.; Pfeffer, M.; Sirlin, C.; Loeffler, J. P. *J. Pharmacol. Exp. Ther.* **2005**, *315*, 1403−11.
(20) Hayward, R. L.; Schornagel, Q. C.; Tente, R.; Macpherson, J. S.; Aird, R. E.; Guichard, S.; Habtemariam, A.; Sadler, P.; Jodrell, D. I. *Cancer Chemother. Pharmacol.* **2005**, *55*, 577−83.
(21) Smalley, K. S.; Contractor, R.; Haass, N. K.; Kulp, A. N.; Atilla-Gokcumen, G. E.; Williams, D. S.; Bregman, H.; Flaherty, K. T.; Soengas, M. S.; Meggersqq, E.; Herlyn, M. *Cancer Res.* **2007**, *67*, 209−17.
(22) Ang, W. H.; De Luca, A.; Chapuis-Bernasconi, C.; Juillerat-Jeanneret, L.; Lo Bello, M.; Dyson, P. J. *ChemMedChem.* **2007**, *2*, 1799−1806.
(23) Dougan, S. J.; Habtemariam, A.; McHale, S. E.; Parsons, S.; Sadler, P. J. *Proc. Natl. Acad. Sci. U.S.A.* **2008**, *105*, 11628−33.
(24) Gava, B.; Zorzet, S.; Spessotto, P.; Cocchietto, M.; Sava, G. *J. Pharmacol. Exp. Ther.* **2006**, *317*, 284−91.
(25) Leyva, L.; Sirlin, C.; Rubio, L.; Franco, C.; Le Lagadec, R.; Spencer, J.; Bischoff, P.; Gaiddon, C.; Loeffler, J. P.; Pfeffer, M. *Eur. J. Inorg. Chem.* **2007**, 3055−3066.
(26) Meng, X.; Leyva, M. L.; Jenny, M.; Gross, I.; Benosman, S.; Fricker, B.; Harlepp, S.; Hebraud, P.; Boos, A.; Wlosik, P.; Bischoff, P.; Sirlin, C.; Pfeffer, M.; Loeffler, J. P.; Gaiddon, C. *Cancer Res.* **2009**, *69*, 5458−5466.
(27) Vidimar, V.; Meng, X.; Klajner, M.; Licona, C.; Fetzer, L.; Harlepp, S.; Hebraud, P.; Sidhoum, M.; Sirlin, C.; Loeffler, J. P.; Mellitzer, G.; Sava, G.; Pfeffer, M.; Gaiddon, C. *Biochem. Pharmacol.* **2012**, *84*, 1428−36.
(28) Benosman, S.; Gross, I.; Clarke, N.; Jochemsen, A. G.; Okamoto, K.; Loeffler, J. P.; Gaiddon, C. *Cell Death Differ.* **2007**, *14*, 2047−2057.
(29) Benosman, S.; Meng, X.; Von Grabowiecki, Y.; Palamiuc, L.; Hritcu, L.; Gross, I.; Mellitzer, G.; Taya, Y.; Loeffler, J. P.; Gaiddon, C. *J. Biol. Chem.* **2011**, *286*, 43013−25.
(30) Bergamo, A.; Gaiddon, C.; Schellens, J. H.; Beijnen, J. H.; Sava, G. *J. Inorg. Biochem.* **2012**, *106*, 90−9.
(31) Klajner, M.; Hebraud, P.; Sirlin, C.; Gaiddon, C.; Harlepp, S. *J. Phys. Chem. B* **2010**, *114*, 14041−7.
(32) Boff, B.; Gaiddon, C.; Pfeffer, M. *Inorg. Chem.* **2013**, *52*, 2705−15.
(33) Fetzer, L.; Boff, B.; Ali, M.; Xiangjun, M.; Collin, J. P.; Sirlin, C.; Gaiddon, C.; Pfeffer, M. *Dalton Trans.* **2011**, *40*, 8869−78.
(34) Sohm, F.; Gaiddon, C.; Antoine, M.; Boutillier, A. L.; Loeffler, J. P. *Oncogene* **1999**, *18*, 2762−9.
(35) Rene, F.; Monnier, D.; Gaiddon, C.; Felix, J. M.; Loeffler, J. P. *Neuroendocrinology* **1996**, *64*, 2−13.
(36) Gaiddon, C.; Larmet, Y.; Trinh, E.; Boutillier, A. L.; Sommer, B.; Loeffler, J. P. *J. Neurochem.* **1999**, *73*, 1467−76.
(37) Gaiddon, C.; de Tapia, M.; Loeffler, J. P. *Mol. Endocrinol.* **1999**, *13*, 742−51.
(38) Gaiddon, C.; Tian, J.; Loeffler, J. P.; Bancroft, C. *Endocrinology* **1996**, *137*, 1286−91.
(39) Broadley, S. A.; Hartl, F. U. *Trends Cell Biol.* **2008**, *18*, 1−4.
(40) Puckett, C. A.; Barton, J. K. *Biochemistry* **2008**, *47*, 11711−6.
(41) Evstatiev, R.; Gasche, C. *Gut* **2012**, *61*, 933−52.
(42) Kratz, F.; Hartmann, M.; Keppler, B.; Messori, L. *J. Biol. Chem.* **1994**, *269*, 2581−8.
(43) Fotiadis, D.; Kanai, Y.; Palacin, M. *Mol. Aspects Med.* **2013**, *34*, 139−58.
(44) Nicklin, P.; Bergman, P.; Zhang, B.; Triantafellow, E.; Wang, H.; Nyfeler, B.; Yang, H.; Hild, M.; Kung, C.; Wilson, C.; Myer, V. E.; MacKeigan, J. P.; Porter, J. A.; Wang, Y. K.; Cantley, L. C.; Finan, P. M.; Murphy, L. O. *Cell* **2009**, *136*, 521−34.
(45) Groessl, M.; Zava, O.; Dyson, P. J. *Metallomics* **2011**, *3*, 591−9.
(46) Puckett, C. A.; Ernst, R. J.; Barton, J. K. *Dalton Trans.* **2010**, *39*, 1159−70.
(47) Romero-Canelon, I.; Pizarro, A. M.; Habtemariam, A.; Sadler, P. J. *Metallomics* **2012**, *4*, 1271−9.

dx.doi.org/10.1021/ic500250e | *Inorg. Chem.* 2014, 53, 5150−5158

Results (Objective 2)

VI.C. Discovery and investigation of anticancer ruthenium-aerene Schiff-base complexes via water-promoted combinatorial three component assembley

Journal of Medicinal Chemistry

Article

pubs.acs.org/jmc

Discovery and Investigation of Anticancer Ruthenium−Arene Schiff-Base Complexes via Water-Promoted Combinatorial Three-Component Assembly

Mun Juinn Chow,[†,‡] Cynthia Licona,[§,∥] Daniel Yuan Qiang Wong,[†] Giorgia Pastorin,[‡,⊥] Christian Gaiddon,[§,∥] and Wee Han Ang*[,†,‡]

[†]Department of Chemistry, National University of Singapore, 3 Science Drive 3, 117543 Singapore

[‡]NUS Graduate School of Integrative Sciences and Engineering, Singapore

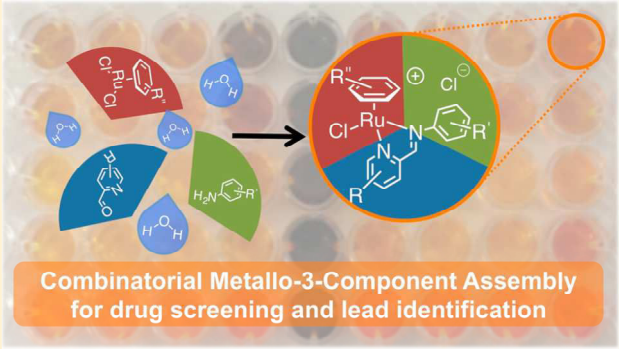
[§]U1113 INSERM, 3 Avenue Molière, Strasbourg 67200, France

[∥]Université de Strasbourg, Strasbourg, France

[⊥]Department of Pharmacy, National University of Singapore, 18 Science Drive 4, 117543 Singapore

Supporting Information

ABSTRACT: The structural diversity of metal scaffolds makes them a viable alternative to traditional organic scaffolds for drug design. Combinatorial chemistry and multicomponent reactions, coupled with high-throughput screening, are useful techniques in drug discovery, but they are rarely used in metal-based drug design. We report the optimization and validation of a new combinatorial, metal-based, three-component assembly reaction for the synthesis of a library of 442 Ru−arene Schiff-base (RAS) complexes. These RAS complexes were synthesized in a one-pot, on-a-plate format using commercially available starting materials under aqueous conditions. The library was screened for their anticancer activity, and several cytotoxic lead compounds were identified. In particular, [(η^6-1,3,5-triisopropylbenzene)RuCl(4-methoxy-*N*-(2-quinolinylmethylene)aniline)]Cl (**4**) displayed low micromolar IC_{50} values in ovarian cancers (A2780, A2780cisR), breast cancer (MCF7), and colorectal cancer (HCT116, SW480). The absence of p53 activation or changes in IC_{50} value between $p53^{+/+}$ and $p53^{-/-}$ cells suggests that **4** and possibly the other lead compounds may act independently of the p53 tumor suppressor gene frequently mutated in cancer.



INTRODUCTION

Traditionally, drug discovery research has focused on the development of organic molecules as pharmacophores. However, their limited structural diversity makes it difficult for them to access other scaffolds that span the entirety of the biologically relevant chemical space,[1−3] some of which may contain promising drug candidates. Out of the 24 million organic molecules registered under the Chemical Abstract Service (CAS) Registry, half could be classified into 143 unique motifs, a small number compared to the vast quantities of molecules being classified.[4] In addition, of the 5000 compounds in the Comprehensive Medicine Chemistry (CMC) database that were analyzed for diversity in topological shapes, half of them belong to only 32 shape classifications,[5] leaving large areas of this chemical space containing structurally and chemically unique motifs unexplored. In order to tap into this substantial and potentially valuable unexplored chemical space, scaffolds that are not accessible with organic chemistry need to be investigated.

Transition-metal scaffolds could therefore be uniquely suited for the development of potential drug candidates. They can readily accommodate higher coordination numbers and thus access different molecular geometries not possible with a purely organic framework.[6] Transition-metal complexes are also endowed with tunable properties, such as variable oxidation states that are stable under room conditions and predictable reactivity based on metal−ligand bonding interactions. Since the first successful platinum-containing drug cisplatin was discovered and approved by Food and Drug Administration (FDA) for the treatment of testicular and ovarian cancer in 1978,[7] much research has been directed at uncovering new metallodrugs that are more effective than cisplatin.[8,9] This research is beginning to bear fruit, with Ru-containing NAMI-A receiving favorable evaluations in clinical trials and KP1019 showing promising results in preclinical studies.[10,11] More recently, metal-based compounds have been designed and

Received: March 23, 2014

ACS Publications © XXXX American Chemical Society

dx.doi.org/10.1021/jm500455p | J. Med. Chem. XXXX, XXX, XXX−XXX

tested against biological therapeutic targets, which are known to regulate processes involved in the development of cancer.[12] One class of Ru compound in particular, namely, half-sandwiched Ru–arene complexes, has been garnering much interest, with a large body of evidence demonstrating their therapeutic properties against cancer[13−15] or their inhibitory activity toward enzyme targets linked to cancer.[16−19] A few examples include the antimetastatic RAPTA complexes[20] and antitumor [(η^6-biphenyl)Ru(en)Cl]$^+$ (RM175) scaffold,[21] as well as organoruthenium-based paullone complexes[22] (Figure 1). These studies pave the way for the development of Ru–arene complexes as the next generation of metal-based anticancer drugs.

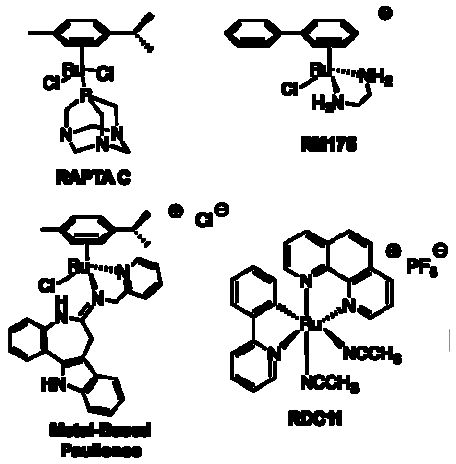


Figure 1. Examples of anticancer organoruthenium compounds.

Yet, discovery of new organoruthenium complexes with the necessary prerequisites for therapy is a laborious process involving iterative steps of synthesis, characterization, functionalization, and testing. For example, good aqueous stability and solubility are essential to ensure biocompatibility, but these attributes are not easily incorporated into the scaffolds. Combinatorial coordination chemistry and multicomponent reactions are potential tools that can generate large libraries of diverse compounds[23,24] for drug screening, but they have seldom been applied to metal-based drug discovery. One report employed a two-step combinatorial synthesis approach coupled with high-throughput screening (HTS) to identify a polypyridyl–Ru complex capable of strongly inducing apoptosis in cancer cells.[25] Another group made use of automated solid-phase combinatorial synthesis to synthesize a library of peptide-tethered Pt(II) complexes for screening and identification of cytotoxic leads.[26,27] There have also been a number of reports on one-pot multicomponent reactions for the preparation of metal complexes,[28,29] although, to the best of our knowledge, none have been used for the purpose of drug discovery.

To that end, we designed a water-promoted multicomponent reaction for the combinatorial assembly of organoruthenium–arene complexes in aqueous solutions. Using a water/DMSO system to carry out the assembly, the reaction directly "selects" for water-stable metallocomplexes of moderate solubility. We report the application of this metal-based three-component assembly (3CA) reaction methodology to prepare a library of water-soluble Ru–arene Schiff-base (RAS) complexes (Figure 2). We perform extensive functional groups variation and screen the compound library for anticancer activity. The identified lead compounds were tested against a variety of cancer cell types and their p53-dependence was also investigated.

RESULTS AND DISCUSSION

Optimization and Validation of a Novel One-Step Three-Component Assembly Reaction in Aqueous Solvents. Our approach was to design and optimize a one-pot three-component reaction that can be used to synthesize a large library of Ru–arene complexes with ease, requiring minimal purification prior to characterization and testing. The reaction comprises three components, namely, a Ru–arene complex, a picolinaldehyde, and an aniline. Imine condensation between the picolinaldehyde and aniline forms a Schiff-base ligand that is predisposed for metal chelation. Without metal chelation, such ligands are typically poorly stable in aqueous environment due to hydrolysis of the imine bond. Incorporation of the Ru–arene component yields an organoruthenium complex that is stabilized by the electrodonating Schiff-base chelate. Similar Ru–arene Schiff-base complexes have been reported, but as yet they have not been prepared in a manner suitable for library synthesis.[30] Thus, 3CA comprises Ru–arene percursor **A** with at least two accessible coordination sites (via labile ligands) that could chelate with Schiff-base ligand formed from condensation between picolinaldehyde **B** and aniline **C**, both of which are widely available from commerical sources (Figure 3a). Components **A**, **B**, and **C** with different functional

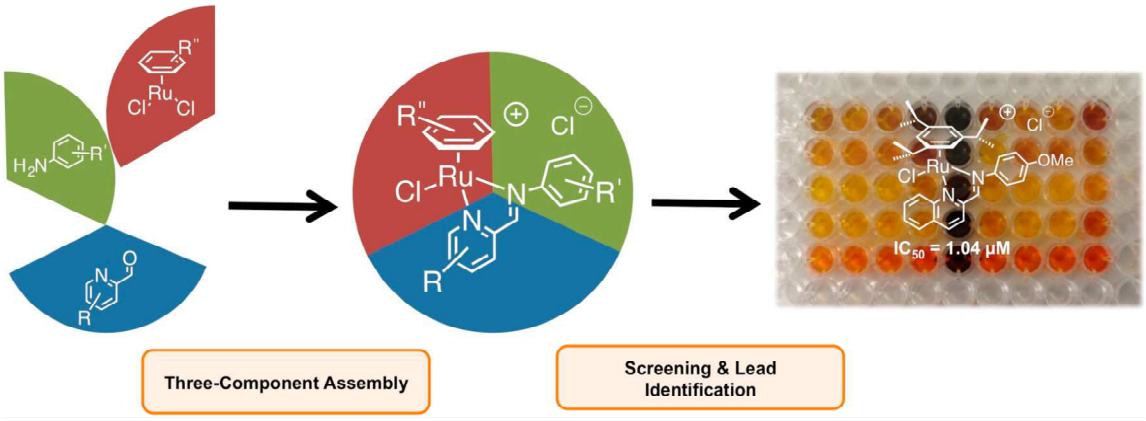


Figure 2. Concept of RAS complex library synthesis, screening, and lead identification.

dx.doi.org/10.1021/jm500455p | J. Med. Chem. XXXX, XXX, XXX–XXX

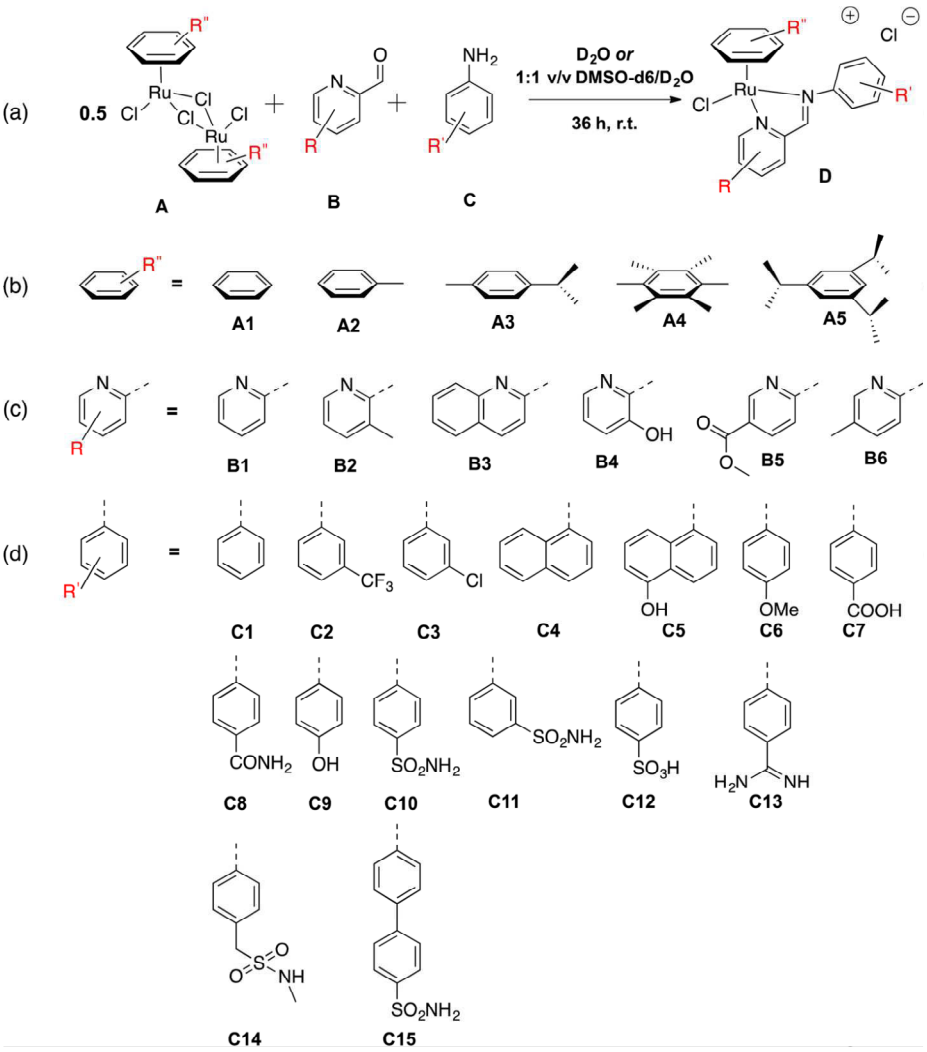


Figure 3. (a) Combinatorial, three-component assembly of RAS complexes. (b–d) The different functional groups on components **A**, **B**, and **C** used for the library synthesis.

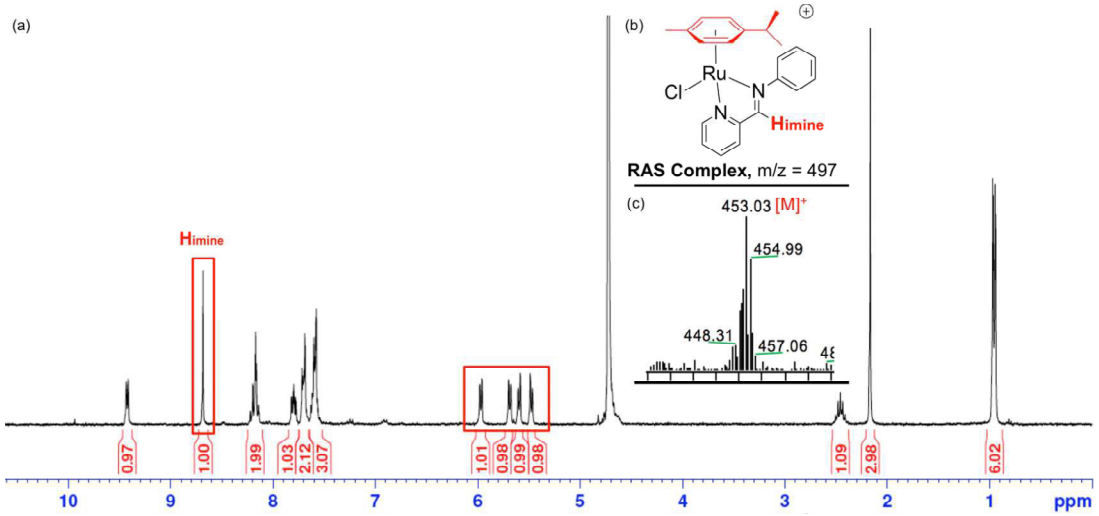


Figure 4. (a) ^{1}H NMR spectrum of crude reaction mixture in D_2O of representative RAS complex obtained using **A3**, **B1**, and **C1** (Figure 3) without any workup or purification. (b) Molecular structure and calculated molecular weight of cation. (c) Parent molecular peak observed in the ESI-MS spectrum corresponding to the expected *m*/*z*.

dx.doi.org/10.1021/jm500455p | J. Med. Chem. XXXX, XXX, XXX–XXX

groups could be mixed in a combinatorial fashion in a one-pot reaction to give a library of ruthenium−arene Schiff-base (RAS) complexes (Figure 3). Because the components were initially insoluble in water, complete dissolution provided an indication of a successful assembly. Reactions that yielded insoluble products were assumed to have failed or have led to products that were insufficiently soluble to warrant further studies and were eliminated from the library. An initial library of 48 RAS complexes were synthesized in D_2O and directly characterized with ^1H NMR and ESI-MS without prior workup or purification. Several complexes were analyzed by RP-HPLC to approximate the levels of purity achieved.

The ^1H NMR spectra typically presented resonances corresponding to the expected products with minor observable byproducts, indicating that RAS complexes were formed almost exclusively (Figure 4a). The RAS complexes exhibited two characteristic features, namely, the disappearance of the singlet peak corresponding to the aldehyde proton at ca. 10 ppm and the appearance of a singlet attributable to the imine proton at 8−9 ppm (a downfield shift from ca. 6 ppm for uncoordinated ligands). In addition, resonances of the η^6-arene protons (for **A** = toluene, cymene, and 1,3,5-triisopropylbenzene) were resolved to distinct peaks due to desymmetrization of the arene ligand upon complexation of the Schiff-base at the Ru center. ESI-MS typically revealed only one m/z peak corresponding to the molecular $[M]^+$ ions with the characteristic Ru isotopic pattern, further confirming the formation of RAS complexes in the 3CA reaction (Figure 4c). RP-HPLC analysis of seven selected RAS complexes from the initial library showed purity levels between 70 and 90% of the crude mixture, which is sufficiently pure for drug screening [see Supporting Information (SI)]. The main cause of the lower purity is the presence of excess reaction components that were added inadvertently and the formation of aquation products.

Structural information was obtained via single crystal X-ray diffraction studies of the RAS complex synthesized from **A3**, **B1**, and **C8**, with PF_6^- as the counteranion (Figure 5). The

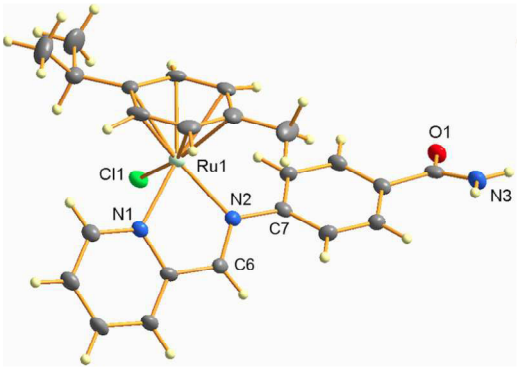


Figure 5. Molecular representation of a RAS complex formed from **A3**, **B1**, and **C8** (Figure 3). There are four cationic centers with corresponding anionic PF_6^- in each unit cell. PF_6^- anion was omitted for clarity.

complex adopted an expected pseudo-"piano stool" structure, with the cymene ligand bonded to the Ru atom as the "stool top". The Schiff-base ligand rotated slightly around N2−C7 to give a "twisted" conformation, presumably to reduce the steric interaction with the cymene ligand. Selected cystallographic and structural data are given in Tables 1 and 2.

Table 1. Selected X-ray Crystallographic Data[a]

Complex	$[RAS\text{-}A3/B1/C8]PF_6$
formula	$RuC_{23}H_{25}N_3OClPF_6$
formula weight	640.96
temp (K)	100(2)
wavelength (Å)	0.710 73
crystal size (mm^3)	0.24 × 0.12 × 0.10
crystal system	monoclinic
space group	$P2_1/n$
a (Å)	9.887(2)
b (Å)	18.473(4)
c (Å)	14.002(2)
α (deg)	90
β (deg)	104.589(3)
γ (deg)	90
V ($Å^3$)	2474.8(9)
Z	4
D_c (Mg/m^3)	1.720
μ (mm^{-1})	0.874
θ range (deg)	1.86−27.50
no. of unique data	17 246
max., min. transmn	0.9177 and 0.8176
final R indices	R1 = 0.0525
$[I > 2\sigma(I)]$	$wR2$ = 0.1214
R indices (all data)	R1 = 0.0823
	$wR2$ = 0.1308
goodness-of-fit on F^2	1.050
peak/hole (e $Å^{-3}$)	2.822 and −0.880

[a] $R = \sum||F_o| - |F_c||/\sum|F_o|$, $wR2 = [\sum[w(F_o^2 - F_c^2)^2]/\sum[w(F_o^2)^2]]^{1/2}$. Goodness-of-fit (GOF) $= [\sum[w(F_o^2 - F_c^2)^2]/(n - p)]^{1/2}$, where n is the number of data and p is the number of parameters refined.

Table 2. Selected Bond Lengths (Å) and Angles (deg)

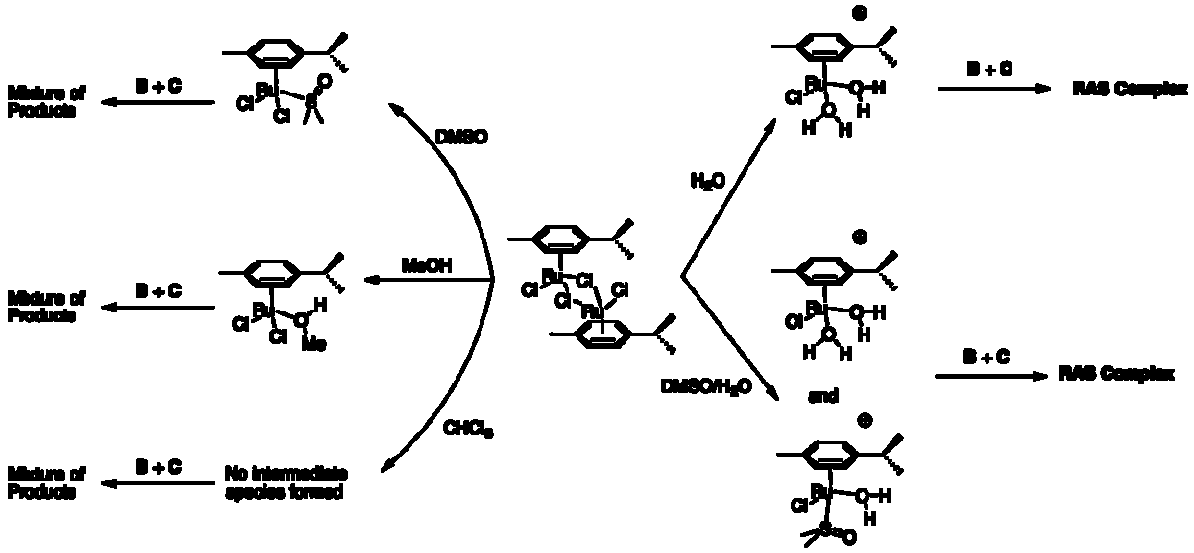
Ru(1)−N(1)	2.088(4)
Ru(1)−N(2)	2.101(4)
Ru(1)−Cl(1)	2.3976(13)
N(2)−C(6)	1.293(6)
N(2)−C(7)	1.425(6)
N(1)−Ru(1)−N(2)	76.98(15)
N(1)−Ru(1)−Cl(1)	84.50(11)
N(2)−Ru(1)−Cl(1)	86.81(11)

At this stage of the methodology development, all complexes were prepared and characterized in D_2O and thus assumed to be sufficiently water-stable for at least 72 h, which encompassed the time of experiment from the start of synthesis to the end of characterization. Upon optimization, we noted that a solvent mixture comprising 1:1 v/v DMSO-d_6/D_2O to be a more suitable solvent system for 3CA for preparation of less water-soluble RAS complexes, which were otherwise insoluble in pure D_2O.

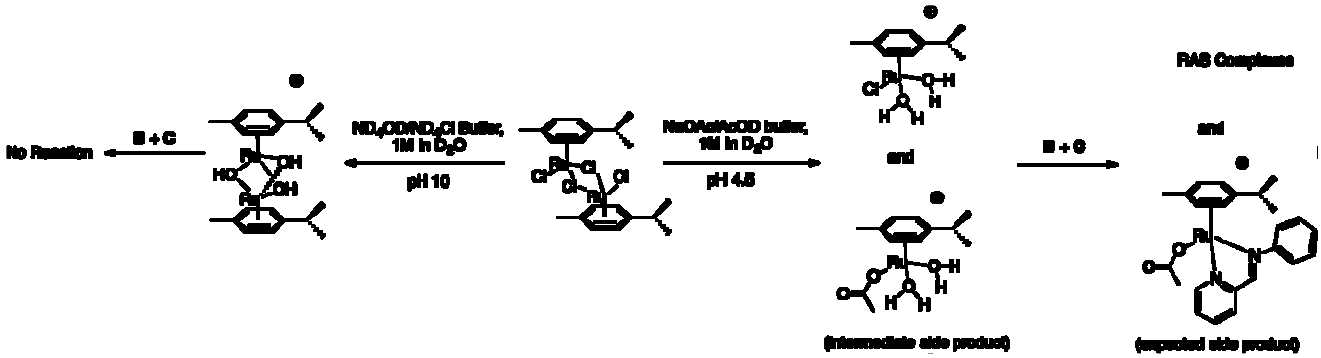
Mechanistic Investigations into Formation of RAS Complexes. We performed a mechanistic investigation of the 3CA reaction to understand the factors affecting assembly of the target complexes in order to be able to fully exploit its versatility. Several experiments were designed to probe the reaction mechanism and to understand how RAS complexes were formed. These experiments were performed in deuterated solvents to facilitate immediate ^1H NMR analysis (see SI). From the experimental results, the factors affecting the formation of RAS complexes were inferred.

dx.doi.org/10.1021/jm500455p | J. Med. Chem. XXXX, XXX, XXX−XXX

Scheme 1. Postulated Reactive Intermediates under Different Solvent Systems



Scheme 2. Putative Reactive Intermediates Formed under Different pH Conditions



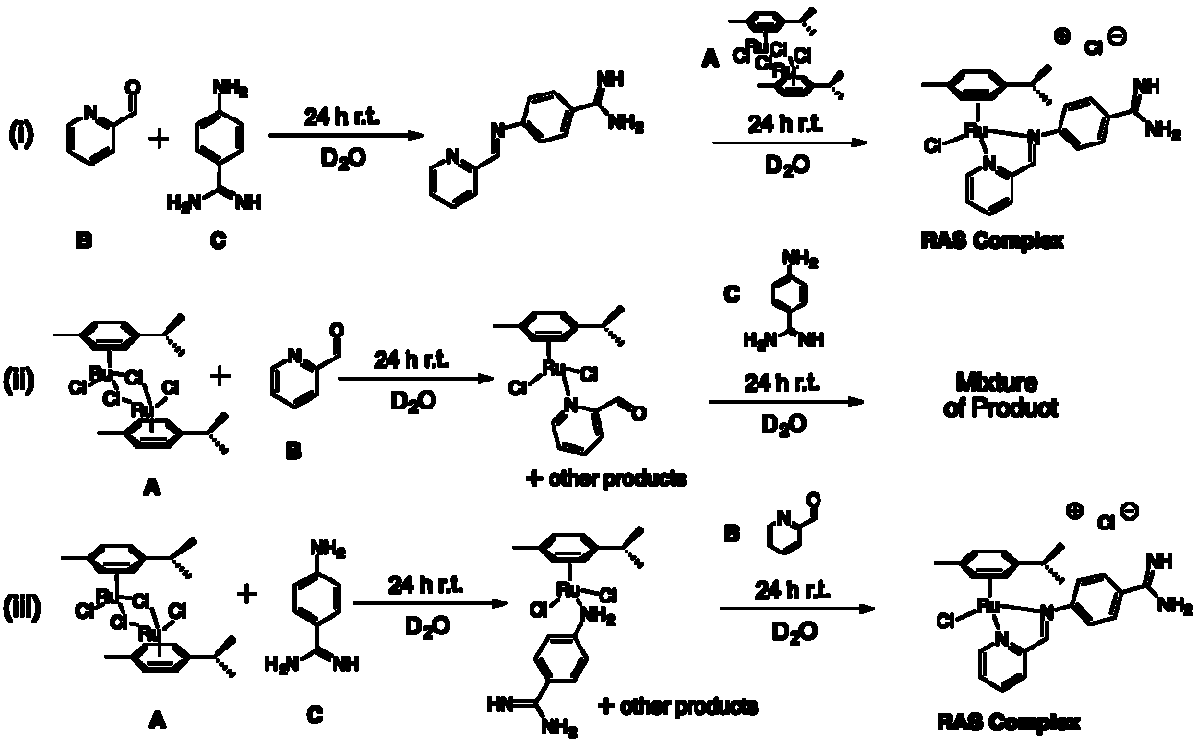
Ru precursor **A** exists as a dimer in solid state or when dissolved in noncoordinating solvents such as toluene or $CHCl_3$. However, in coordinating solvents such as DMSO, MeOH, or H_2O the dimers are cleaved to form reactive $[Ru(arene)(solvent)_{x+1}Cl_{2-x}]$ monomers.[31] We theorized that 3CA occurred via these reactive intermediates and coordinating solvents were necessary to activate **A**. Thus, 3CA was carried out in the noncoordinating solvent $CDCl_3$, as well as the coordinating solvent systems DMSO-d_6, MeOD-d_4, D_2O, 1:1 v/v DMSO-d_6/D_2O. Components that were soluble in each of the solvents were chosen so as to eliminate any possible complications arising from a difference in solubility. As expected, RAS complexes were not formed at all in $CDCl_3$. However, the 3CA reaction was also unsuccessful in the coordinating solvents DMSO-d_6 and MeOD-d_4, producing many unexpected side products. Indeed, assembly was only successful in solvent systems containing D_2O.

The unexpected observation could be explained by the difference in the reactive intermediate formed in DMSO and MeOH compared to that in H_2O (Scheme 1).[31] In DMSO and MeOH, monosolvated species $[Ru(arene)XCl_2]$ is formed as the only species (X = DMSO, MeOH). In H_2O, an additional chloride ligand is displaced from the monosolvated $[Ru(arene)(H_2O)Cl_2]$ to form the disolvated species $[Ru(arene)(H_2O)_2Cl]^+$. The presence of two labile solvent ligand in the disolvated species allowed rapid reaction with the ligand chelate, giving rise to fewer side reactions and leading to the formation of RAS complexes exclusively. The presence of water in DMSO/H_2O solvent mixture presumably replaced the second chloride to yield the reactive intermediate $[Ru(arene)(DMSO)(H_2O)Cl]^+$. This hypothesis was further validated by performing the 3CA reaction at different pH conditions (Scheme 2). We hypothesized that at acidic to neutral pH, the disolvated $[Ru(arene)(H_2O)_2Cl]^+$ would be formed primarily. At basic pH, the kinetically inert μ-OH bridged dimer $[Ru_2(arene)_2(\mu\text{-}OH)_3]^+$ would form preferentially, which would hinder 3CA.[32,33] Thus, 3CA was carried out at pH 4.5 and 10.0 using deuterated reagents in D_2O and analyzed by both ^1H NMR and ESI-MS. Indeed, the results showed that 3CA was hindered in basic pH medium.

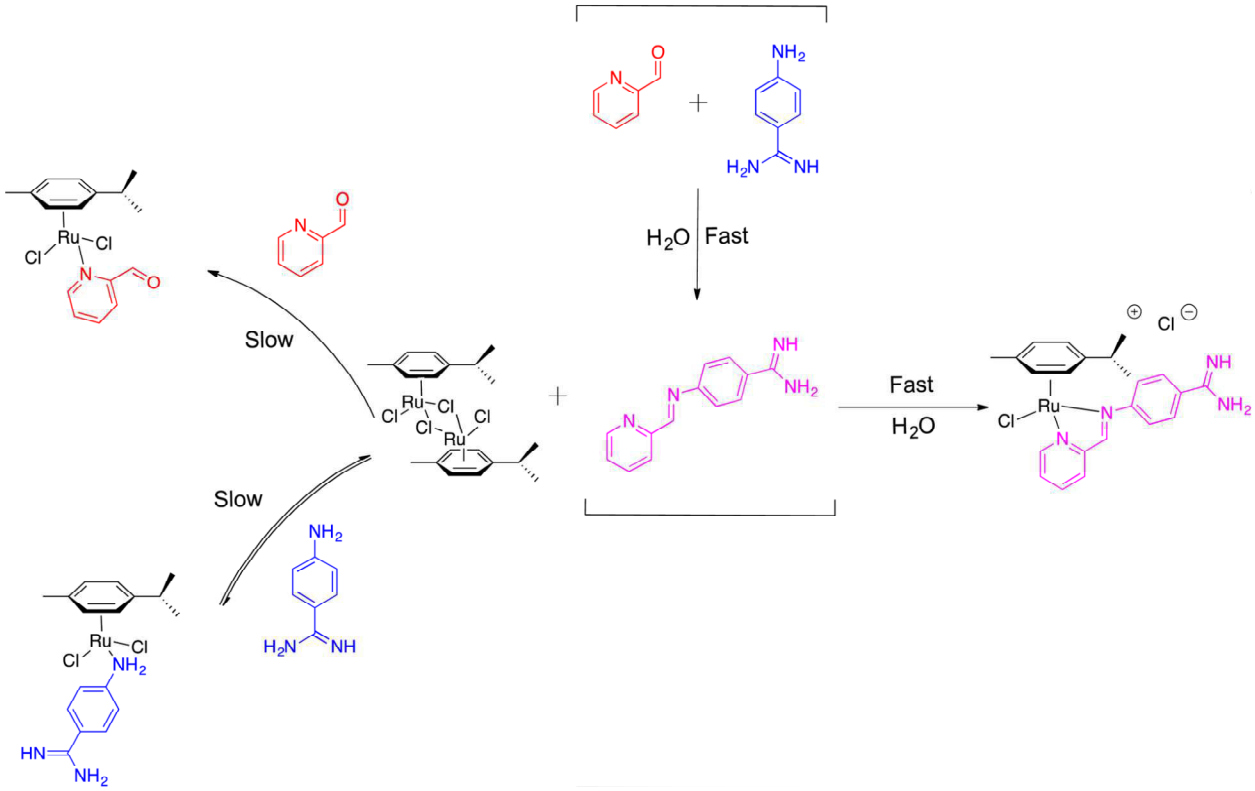
Next, we attempted to understand why little or no side products were obtained in 3CA by studying the reactivity of the individual components after they had been added sequentially (Scheme 3). We first carried out the reactions in the absence of one of the components, i.e., (i) **B** and **C**, (ii) **A** and **B**, and (iii) **A** and **C**, for 24 h and then supplemented each of the reaction mixtures with the missing component for a further 24 h. Like previous experiments, reactions i, ii, and iii were done in a deuterated solvent, D_2O, so that immediate analysis by ^1H NMR was possible. For reaction i, the expected imine product was observed after 1 h, and most of the starting material had been converted to the imine product after 24 h. Reaction ii

dx.doi.org/10.1021/jm500455p | J. Med. Chem. XXXX, XXX, XXX−XXX

Scheme 3. Influence of Reagent Addition Sequence on Product Formation



Scheme 4. Postulated Reaction Mechanism for Three-Component Assembly Reaction



yielded multiple products after 24 h. Even after **C** was added, there was further reaction. Reaction iii gave a mixture of starting materials and products after 24 h. However, after **B** was added for 24 h, the reaction mixture resolved to yield a clean ^{1}H NMR spectrum with RAS complex being the only product. This suggested that **A** reacted reversibly with **C** and subsequent addition of **B** would still drive 3CA reaction to completion. Taken together, these experiments explained why the 3CA

dx.doi.org/10.1021/jm500455p | J. Med. Chem. XXXX, XXX, XXX−XXX

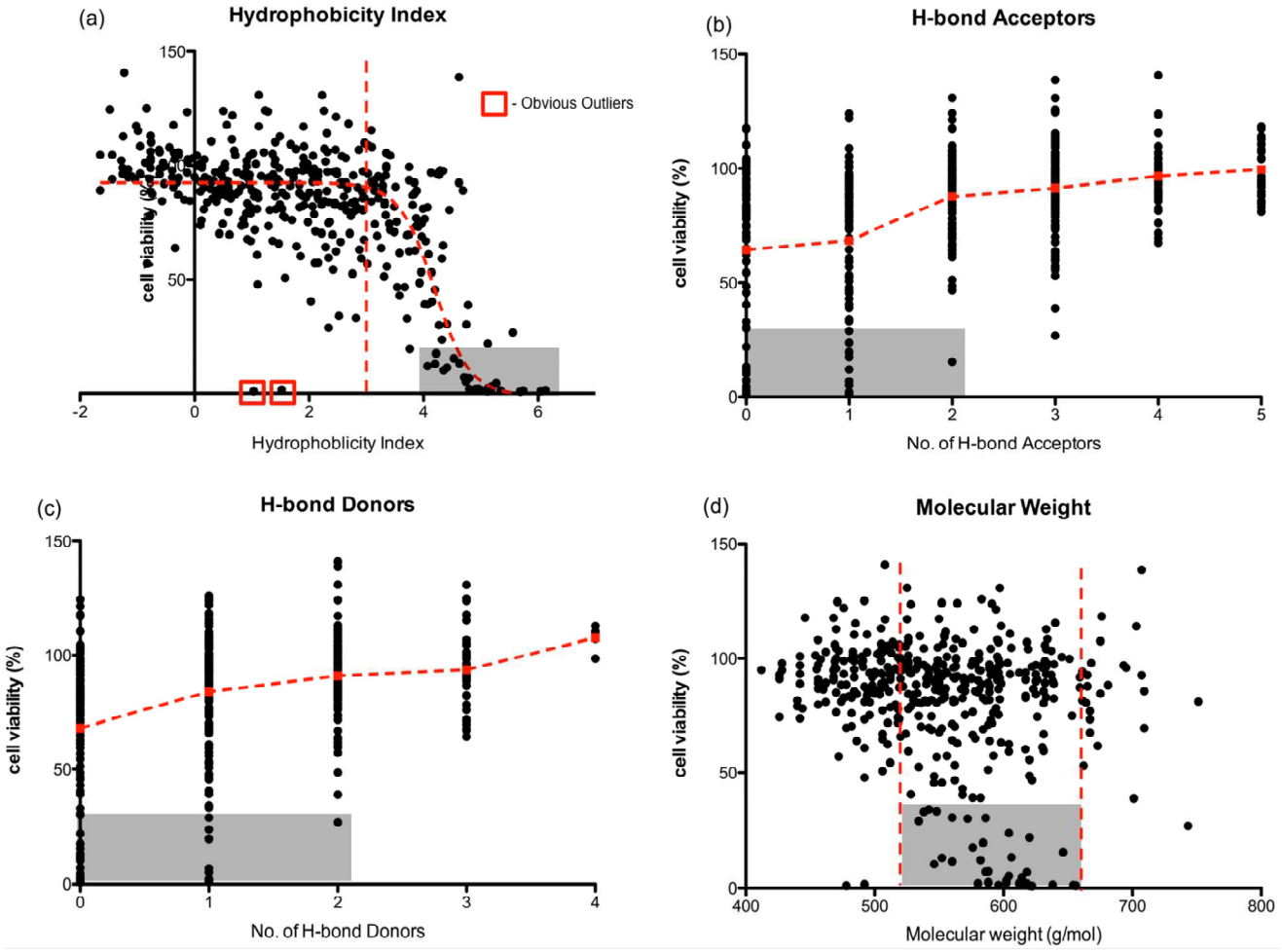


Figure 6. Analyses of cell viability data from the 442-compound library. (a) Plot of percent cell viability (CV%) against hydrophobicity index (HI). CV% decreases significantly after HI = 3, with the most cytotoxic compounds in the range 4 < HI < 6 (shaded area). (b, c) Plot of CV% against H-bond acceptor and H-bond donor, respectively. CV% increases as the number of H-bond acceptors or donors on a molecule increases, with most cytotoxic compounds having two or less H-bond acceptors or donors (shaded area). (d) Plot of CV% against molecular weight. Most cytotoxic compounds appear to have MW between 530 and 660 g/mol (shaded area).

worked despite the possibility of forming many different side products. First, RAS complexes are thermodynamically the most stable product due to the "chelate effect". Second, RAS complexes are kinetically favored. At room temperature, the reaction between $[Ru(arene)(H_2O)_2Cl]^+$ and **B** or $[Ru(arene)(H_2O)_2Cl]^+$ and **C** is slower compared to the reaction between $[Ru(arene)(H_2O)_2Cl]^+$ and the imine ligand (**B** + **C**) or the formation of the imine ligand (Scheme 4).

To validate this hypothesis, we compared 3CA using the more basic aliphatic amine, 4-aminomethylbenzenesulfonamide, in place of aniline, 4-aminobenzamidine, as component **C**. Although they are both primary amines, aniline is poorly basic by virtue of the delocalization of the N-atom lone pair into the aromatic ring. We reasoned that aniline would not undergo dative bonding with $[Ru(arene)(H_2O)_2Cl]^+$ and would not directly compete with 3CA. Indeed, ^1H NMR analysis revealed that, unlike 4-aminobenzamidine, 4-aminomethylbenzenesulfonamide reacted irreversibily with **A**, prematurely arresting 3CA. We further tested the functional group tolerance using analogues of **B** and **C** and found that functional groups that competed for direct Ru-binding, such as thiol and imidazoles, also directly interfered with 3CA. Nevertheless, a wide variety of functional groups were tolerated (Figure 3).

Plate Format Synthesis and Direct Screening of Cytotoxicity. To demonstrate the versatility of 3CA, we carried out extensive synthesis of RAS complexes using the possible combinations shown in Figure 3 on a plate format. A total of 450 compounds were prepared and characterized. Synthesis were performed on 96-well plates, in a high-throughput manner with 1:1 v/v DMSO/H_2O used as the solvent system (see SI) to maximize the solubility of the products while maintaining some degree of aqueous solubility. DMSO stock solutions of all the starting reagents were prepared and mixed in a predetermined order in wells containing an equal volume of H_2O. Each well gave a different RAS complex at 5 mM in 1:1 v/v DMSO/H_2O by the end of the reaction, and they were analyzed by ESI-MS. Successful assembly was indicated by the molecular $[M]^+$ ion as the predominant m/z peak. Out of the 450 complexes synthesized, only one was insoluble and eliminated as a candidate for screening. All complexes synthesized were used without further purification.

dx.doi.org/10.1021/jm500455p | J. Med. Chem. XXXX, XXX, XXX−XXX

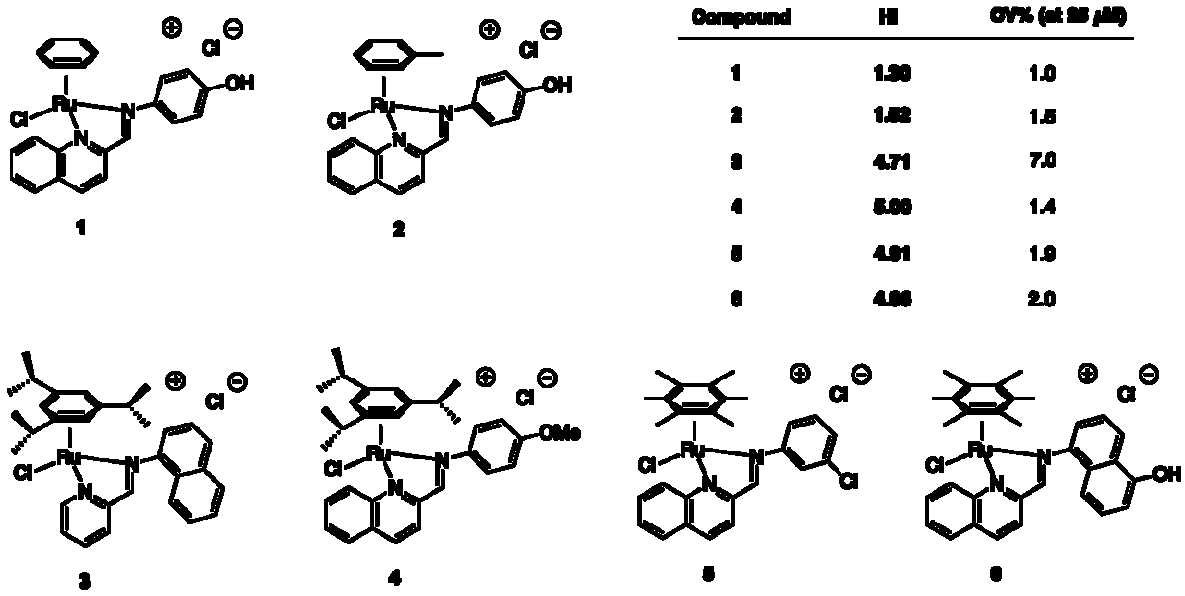
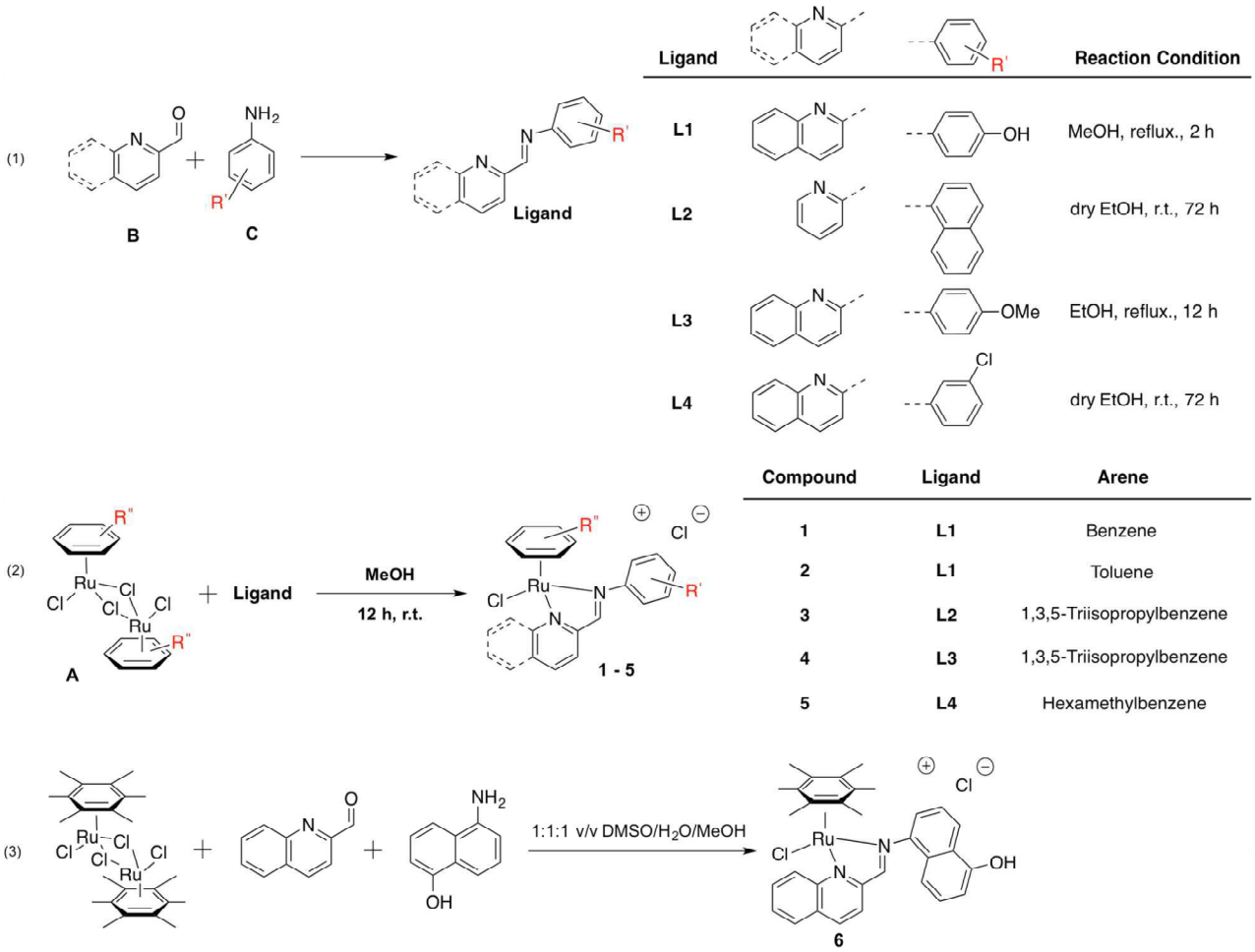


Figure 7. Lead compounds identified during the screening and their HI and CV% data.

Scheme 5. Synthetic Route for the Preparation of 1–6



For the screening of cytotoxicity, A2780 ovarian cancer cells were used because the cells are sensitive to cisplatin treatment and can be transplated to in vivo models as xenografts. Cytotoxicity of the assembled RAS complexes were tested at a single concentration by using the MTT assay.[34] The complexes were first diluted on a separate 96-well plate with RPMI 1640

dx.doi.org/10.1021/jm500455p | J. Med. Chem. XXXX, XXX, XXX–XXX

medium to give a final concentration of 25 μM in medium containing 0.5% (v/v) DMSO. Seven more compounds were insoluble under this condition and were removed from the screen. The remaining 442 RAS complexes were tested against A2780 cells in quintuplicate, and the percentage of cell viability (CV%) after treatment of each drug was then determined. Using this mass screening method, we identified 20 lead compounds with CV% below 10% at 25 μM concentration; out of these 20 lead compounds, 16 had CV% below 5%.

To determine if there was any correlation between the hydrophobicity and the cytotoxicity of the complexes, CV% could be compared with their clogP. Because there are currently no available software to calculate the clogP of these organometallic complexes, we adopted an alternative standard of measurement based on the sum of clogP values of the arene and the chelate ligand. We assumed that differences in their hydrophobicities were largely due the different R, R′, and R″ groups (Figure 3), since all 442 complexes were based on the same core structure. RAS complex [RAS-A1/B1/C1] (R = R′ = R″ = H) was assigned an arbitrary hydrophobicity index (HI) of 0 and the remaining complexes were assigned HI values relative to this, calculated from the clogP of their ligands. Similar to clogP, the more positive the HI, the greater the hydrophobicity. The CV% value of each compound was then plotted against their HI value (Figure 6a). When HI > 3, CV% decreased significantly. The most cytotoxic RAS complexes were relatively hydrophobic, having HI between 4 and 6, suggesting that cellular uptake might be via passive diffusion.[35]

We further analyzed the cell viability data against additional measures of druglikeness from "Lipinski's rule of five,"[36] such as hydrogen bond (H-bond) acceptors, H-bond donors, and molecular weight, to see if there were any additional observable trends (Figure 6b–d). In general, CV% increased with increasing number of H-bond acceptors and donors with a majority of the cytotoxic RAS complexes having less than two H-bond acceptors or donors. In addition, the most cytotoxic of these complexes tends to have a molecular weight between 530 and 660 Da.

Synthesis and Characterization of Lead Compounds. In order to validate the cytotoxic mechanisms of the lead compounds, we synthesize them on a preparative scale for detailed in vitro evaluation. This would also help us eliminate false positives, which are relatively common in high-throughput screening. We selected six out of the 20 lead compounds (Figure 7) with low CV% and resynthesized them individually according to Scheme 5, including two outliers (**1** and **2**) that did not fit into the general cytotoxicity trend. The identity and purity of compound **1**–**6** were ascertained by ^{1}H NMR, ESI-MS, and RP-HPLC or elemental analysis (EA). The ^{1}H NMR spectra of the **1**, **2**, **4**, **5**, and **6** were as expected, with the imine singlet peak appearing around 9.0–9.4 ppm and additional splitting of the arene proton peaks. However, ^{1}H NMR spectrum of **3** showed two sets of compounds instead of one (see SI). This was presumably due to the restriction of free rotation of the C–N bond caused by the steric repulsion between the bulky napthalene group and the triisopropyl groups, which resulted in the formation of pseudo-*E* and -*Z* stereoisomers (Figure 8). By increasing the temperature of NMR data acquisition to 343 K, the barrier of rotation could be overcome and the peaks coalesced, giving rise to only one set of resonances. Similar *E*/*Z* isomerism was previously reported for another class of Ru–arene Schiff-base complexes.[22] The ESI-MS spectra showed the expected molecular ion peaks for all six

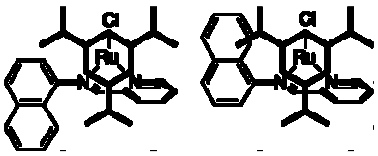


Figure 8. Steric hindrance between bulky isopropyl and naphthalene groups creates a barrier of rotation of the C–N bond, resulting in pseudo-*E*/*Z* isomerism.

compounds. All six compounds were shown to be at least 95% pure, either by EA or RP-HPLC analysis.

Determination of Aqueous Stability, Solubility and log P_{OW}. The aqueous stability, solubility, and log P_{OW} are important factors that affect a potential drug's bioavailability and cell permeability.[37] The aqueous stability of lead compounds **1**–**6** were investigated by monitoring their UV profiles over a period of 24 h at every 1 h interval. Each compound was first dissolved in DMSO to make up a 5 mM stock solution which was then diluted with water to 50 μM (1% v/v DMSO). All compounds except **6** demonstrated good stability in water with negligible variation to their UV peak profiles after 24 h. A significant change in the UV peak profile of **6** was observed with two isosbestic points at 290 and 454 nm (see SI). When the experiment was repeated for **6** in the presence of 0.6% w/v NaCl, no significant change in its UV peak profile was observed. This suggests that the chloride ligand of **6** was significantly more labile as compared to those of **1**–**5** and that aquation could be suppressed with the addition of chloride ions.

The thermodynamic solubilities of **1**–**5** were determined at saturation in ddH_2O for 24 h. After 24 h, undissolved solid was removed by centrifugation, and Ru concentration of the resulting saturated solutions was determined via ICP-OES. The lead compounds showed moderate solubilities in water, with **3** having solubility of 131.6 mg/mL, on the same order of magnitude as common inorganic salts. The solubility of **6** in 0.6% w/v NaCl was too low to warrant further analyses.

The log P_{OW} of **1**–**6** was determined using the shake-flask method.[38] **1**–**5** were partitioned between *n*-octanol and ddH_2O, and the amounts of compounds in the aqueous fractions before and after the partitioning were measured using UV–vis spectroscopy at their respective λ_{max}. The same was done for **6** using 0.6% w/v NaCl instead of ddH_2O. **1**–**5** were relatively hydrophilic, as shown by their negative log P_{OW} values. The ionic nature of the complexes endowed them with hydrophilic character, despite having hydrophobic surface groups. In general, **1**–**6** were considered "druglike" based on Lipinski's rule of five.[36] However, there was no observable correlation between the hydrophilicity (log P_{OW}) and the aqueous solubility. In fact, the more hydrophilic **1** and **2** were much less soluble compared to hydrophobic **3** and **4**. This could be due to the ability of **1** and **2** to lose a H^+ ion from the phenol functional group to form an overall charge-neutral zwitterion, which may have reduced solubility.

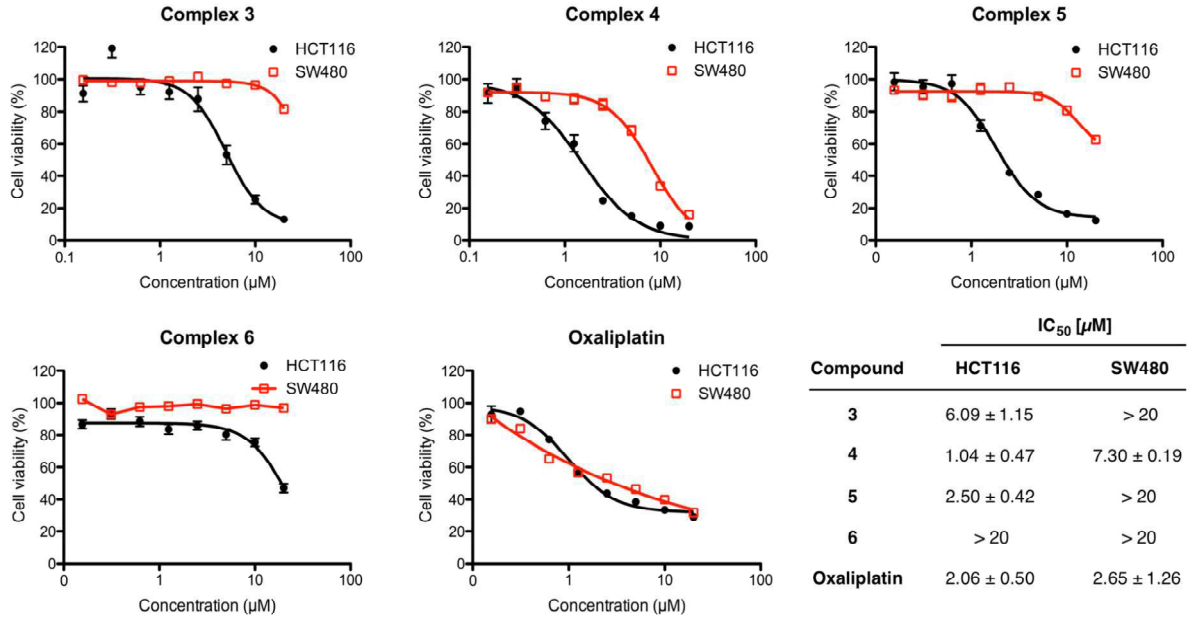
In Vitro Evaluation of Lead Compounds against Cancer Cell Lines. The efficacy values of RAS complexes **1**–**6** in the inhibition of cell viability were evaluated against a panel of human cancer cell lines (Table 3). All experiments were carried out in at least triplicates, and IC_{50} was determined from the average of three separate experiments. Ru concentrations of stock solutions were also determined using ICP-OES and the IC_{50} values were adjusted to the actual

dx.doi.org/10.1021/jm500455p | J. Med. Chem. XXXX, XXX, XXX–XXX

Table 3. Properties of Lead Compounds 1−6

complex	log P_{ow}[a]	solubility (mg/mL)[c]	IC_{50} (μM)[d] MCF7	A2780	A2780cisR	resistance factor[e]
1	−1.78 ± 0.07	2.69 ± 0.01	>50	>50	>50	NA
2	−1.92 ± 0.24	7.34 ± 0.01	>50	>50	>50	NA
3	−0.81 ± 0.01	131.6 ± 1.6	9.00 ± 0.62	9.88 ± 2.13	9.75 ± 3.47	1.0
4	−0.79 ± 0.03	35.0 ± 1.6	2.93 ± 0.21	2.76 ± 0.55	3.17 ± 0.29	1.1
5	−1.03 ± 0.01	2.16 ± 0.03	6.47 ± 0.45	7.58 ± 0.98	9.78 ± 2.14	1.3
6	0.57 ± 0.07[b]	ND	13.13 ± 1.35	11.19 ± 1.41	7.59 ± 1.24	0.7
cisplatin	−2.03 ± 0.47[51]	3.37 ± 0.05[51]	>50	9.54 ± 2.36	34.30 ± 4.01	3.6

[a]log P_{ow} values determined via the shake-flask method with 1:1 *n*-octanol:H_2O partitioning. [b]log P_{ow} for **6** was determined in 1:1 *n*-octanol: 0.6% w/v NaCl. [c]Compounds were dissolved in 0.5 mL of water to saturation at 24 h at rt and [Ru] was determined using ICP-OES. ND = not determined. [d]IC_{50} values are the concentration of Ru complexes required to inhibit 50% of cell growth with respect to control groups, measured by MTT assay after 6 h of drug exposure and 66 h of incubation. Data obtained are based on the average of at least three independent trials, and the reported errors are the corresponding standard deviations. The IC_{50} were corrected using actual [Ru] determined using ICP-OES. [e]On the basis of the ratio of IC_{50}[A2780cisR] to IC_{50}[A2780]. NA = not applicable.



Compound	IC_{50} [μM] HCT116	SW480
3	6.09 ± 1.15	> 20
4	1.04 ± 0.47	7.30 ± 0.19
5	2.50 ± 0.42	> 20
6	> 20	> 20
Oxaliplatin	2.06 ± 0.50	2.65 ± 1.26

Figure 9. Dose-dependent drug efficacy studies for **3**−**6** and oxaliplatin on colon cancer cell lines HCT116 and SW480.

concentration. Contrary to what was expected, **1** and **2** did not show significant cytotoxicity for any of the cell lines. We concluded that **1** and **2** were false positives and removed them from further testing.

RAS complexes **3**−**6** showed good killing efficacies against the cancer cell lines tested. Against A2780, the complexes exhibited efficacies comparable to or better than cisplatin, with **4** achieving IC_{50} values 3 times lower than that of cisplatin. In addition, they did not exhibit any cross-resistance toward cisplatin-resistant A2780cisR, with **6** achieving a resistance factor as low as 0.7 and **4** having IC_{50} value 10 times lower than that of cisplatin. Furthermore, **3**−**6** also demonstrated good toxicity toward MCF7, whereas cisplatin showed negligible cytotoxicity. Other classes of Ru−arene complexes have also demonstrated activity against cell lineages with reduced susceptibility to cisplatin or other platinum anticancer drugs.[39,40] In particular, the class of Ru−arene complexes (RM175) reported by Sadler et al. exhibited resistance factors between 0.7 and 1.0 in A2780cisR, similar to RAS complexes **3**−**6**.[41] This was in contrast to the cross-resistance exhibited by platinum anticancer drugs such as carboplatin or platinum(II)−oxalato complexes,[41,42] suggesting that the resistance mechanisms induced by platinum anticancer drugs do not impact the biological activity of ruthenium compounds significantly.

We further evaluated the lead compounds against colorectal carcinoma cell lines known to be resistant to treatment by cisplatin. This intrinsic resistance to cisplatin had previously been linked to overexpression of organic cation transporter (OCT) proteins in colorectal carcinoma cells. On the other hand, oxaliplatin, by virtue of its hydrophobic *R,R*-diaminocyclohexane motif (DACH), can undergo aquation to yield cationic species that were postulated to be OCT1/2 substrates.[43] As RAS complexes are persistently cationic and contained hydrophobic ligands, they could potentially be substrates of OCT1/2 and effective against colorectal carcinoma cell lines. **1**−**6** were tested against two such cell lines, HCT116 and SW480, and their activity was compared against that of oxaliplatin (Figure 9).

With the exception of **6**, RAS complexes were more cytotoxic toward HCT116 than SW480. **3** and **5** demonstrated modest toxicity toward HCT116 but displayed poor IC_{50} values above 20 μM in SW480. **4** displayed good cytotoxicity in both cell

dx.doi.org/10.1021/jm500455p | J. Med. Chem. XXXX, XXX, XXX−XXX

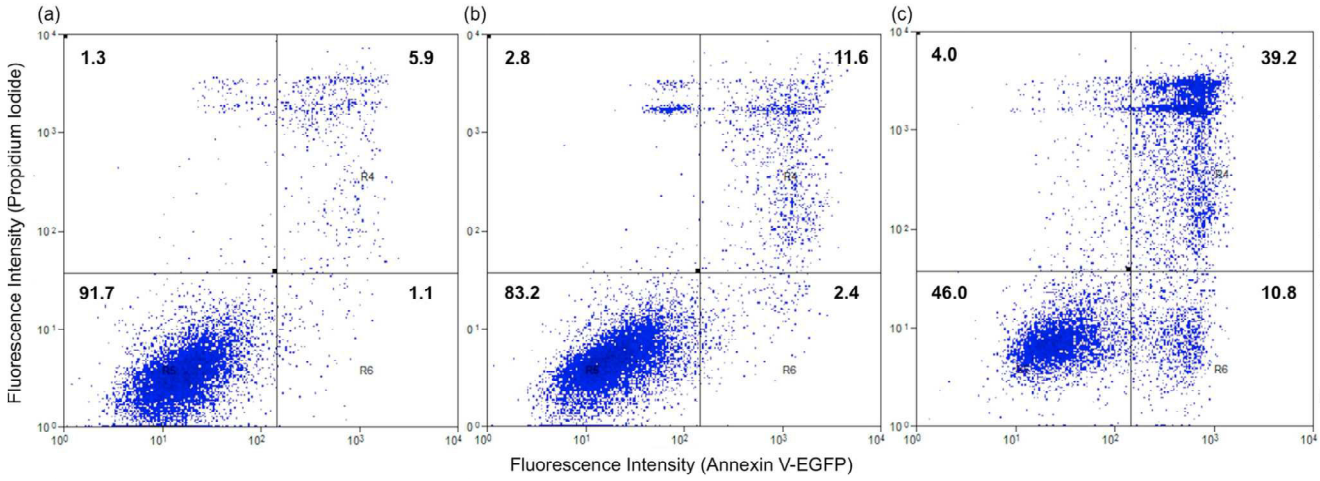


Figure 10. Dot plots of HCT116 cells after 24 h exposure to **4** at various concentrations: (a) untreated control, (b) 2.5 μM, and (c) 10 μM. Viable cells are shown in the lower left quadrant, early apoptotic cells are in the lower right quadrant, late-stage apoptotic cells are in the upper right quadrant, and necrotic cells are in the upper left quadrant. Numbers shown indicate the percentage of cells in each quadrant.

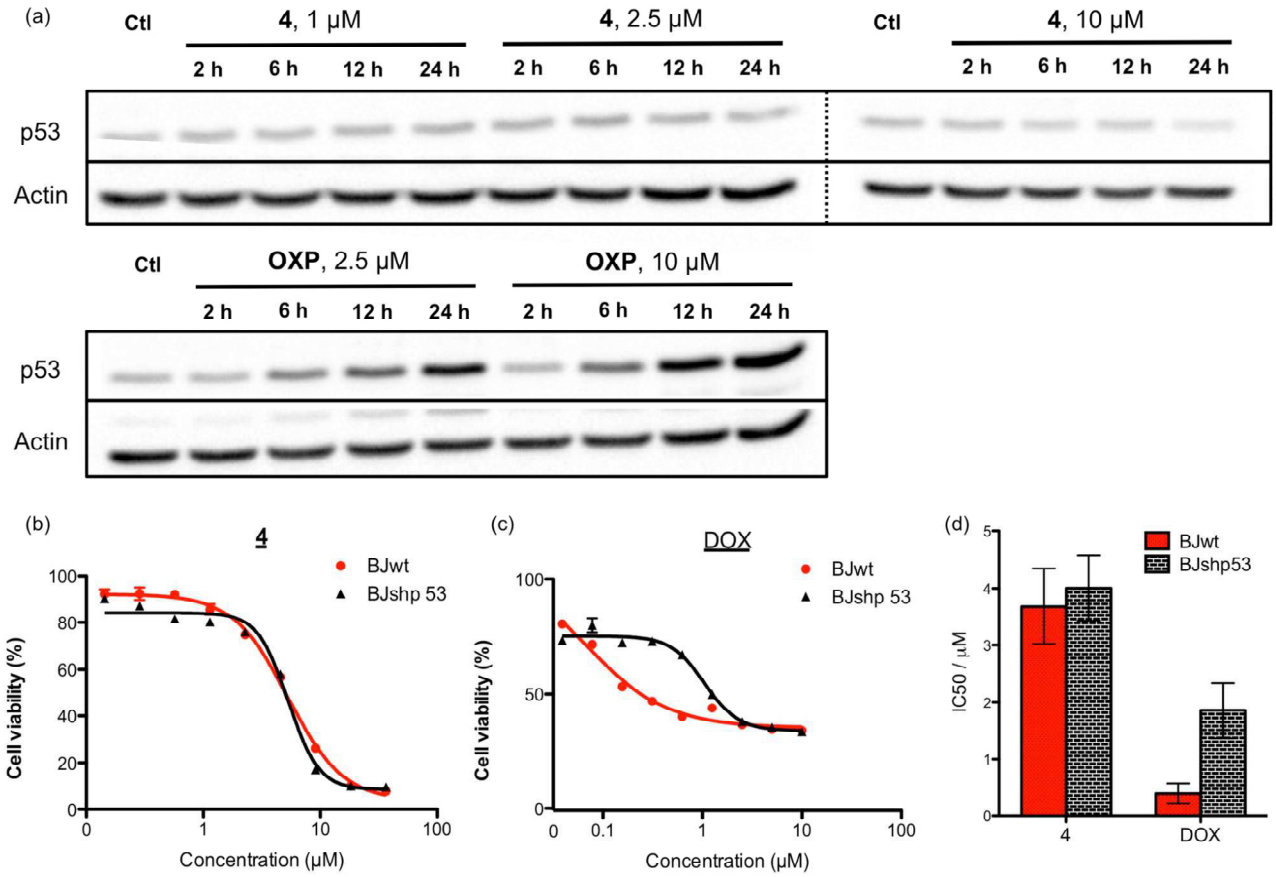


Figure 11. (a) Western blot for detection of p53 expression in HCT116 cells treated with **4** and oxaliplatin for different exposure times. Homogeneous protein loading determined with reference to actin. (b, c) Inhibition of cell viability on BJwt and BJshp53 cells treated with varying concentrations of **4** and DOX, respectively. (d) A comparison of IC_{50} values of **4** and DOX in BJwt and BJshp53 cells.

lines, achieving IC_{50} of 1.0 μM in HCT116 and 7.3 μM in SW480, compared to oxaliplatin, which was equally efficacious against both cell lines. Nevertheless, **4** demonstrated greater efficacies toward HCT116 compared to oxaliplatin.

Cell Cycle Analysis and Apoptosis Assay. The ability of **4** to cause cell cycle arrest and apoptosis was investigated. HCT116 cells were treated with **4** for 24 h at 2.5 μM and 10 μM. The cell cycle profiles of treated cells stained with propidium iodide (PI) were obtained by flow cytometry analysis and compared with that of an untreated control. Significant cell growth arrest at the G2/M phase was induced by **4** only at the higher concentration (Figure S5, SI). However, at 2.5 μM a modest G0/G1 growth arrest was observed. Flow cytometry analysis using annexin V−EGFP/PI apoptosis

dx.doi.org/10.1021/jm500455p | J. Med. Chem. XXXX, XXX, XXX−XXX

detection assay revealed that **4** induced apoptosis in a dose-dependent manner (Figure 10). The percentage of total apoptotic cells increased from 14% to 50% when concentration increased from 2.5 to 10 μM. The percentage of nercotic cells remains low at both concentrations (<5.0%).

Mechanistic Considerations: RAS Complexes Exhibit p53-Independent Cytotoxicity. p53 is a key tumor suppressor gene often mutated in human cancers and is involved in the mediation of cellular DNA repair, apoptosis induction, and cell cycle arrest.[44] p53 activation also mediates the neurotoxicity of anticancer drugs.[45] The chemoresistance of some cancer cell lines toward certain anticancer drugs such as oxaliplatin or doxorubicin (DOX) have been shown to be due to mutated p53-encoding genes or deficient p53 levels, which are less effective in inducing apoptosis even when significant DNA damage has occurred.[46,47] Anticancer agents that are p53-independent could be promising drug candidates against drug-resistant cancers. However, previous reports indicated that several ruthenium complexes of various structure, such as RAPTA-C, RM175, and RDC11 (Figure 1), induced p53 and p53 target genes at various degrees.[48−50] To investigate if lead RAS complexes inhibit cell viability via a p53-dependent or -independent mechanism, we determined the expression of p53 in HCT116 cells and AGS human adenocarcinoma cells. They were treated with varying concentration of **3**−**5** and their p53 levels were compared with that of cells treated with either oxaliplatin or cisplatin as controls. In addition, we measured the p53 expression in HCT116 cells after different exposure times (2, 6, 12, and 24 h) to **4** and oxaliplatin. We also tested the p53-dependence of **4** by measuring its cytotoxicity against wild-type human foreskin cells BJwt and the p53 knockdown BJshp53.[51] As a control, DOX was also tested against both cell lines, and the results were compared.

As expected, time- and concentration-dependent upregulation of p53 was observed in cells treated with oxaliplatin (Figure 11a). In contrast, p53 expression in HCT116 cells remained at basal levels, regardless of the duration or concentration of exposure to **4**. HCT116 cells did not show any increase in expression of p53 even at concentrations much higher than their IC_{50} values after 24 h of treatment (Figure S4, SI). These results were confirmed in the gastric cancer cell line AGS, in which cisplatin treatment induced p53 protein levels while **3**−**5** had no significant effect. Furthermore, **4** demonstrated similar efficacies in both BJwt and BJshp53, while DOX was 7 times more cytotoxic against BJwt than p53-deficient BJshp53 (Figure 11b−d). Taken together, these results suggest that **3**−**5** exert their antiproliferation activity via a p53-independent mechanism, unlike RAPTA-C, RM175, or RDC11. Recent studies by Sadler and co-workers on a class of Ru−arene complexes bearing similar structural features also demonstrated a p53-independent mechanism of action.[15] Intriguingly, they reported that the halide ligand affected p53-dependence and that p53-independent activity was only observed for iodido complexes and not for chlorido analogues. Our preliminary results were dissimilar and more extensive studies involving the several target genes of p53 are being performed to validate these findings.

Previous studies have shown that cytotoxic Ru−arene complexes that target DNA are activated by aquation[52−54] in a similar fashion to cisplatin. Hydrolysis of the chloride ligands yields a reactive aqua species that binds DNA, forming metal−DNA adducts that directly interfere with cell proliferation. An extensive study was carried out on the mechanism of aquation of RM175 and related compounds and showed that it was strongly correlated to their cytotoxicity; highly cytotoxic compounds undergo aquation, while the inactive compounds were resistant to aquation. In contrast, RAS complexes did not exhibit a similar trend, suggesting that DNA may not be the molecular target. RAS compounds **3**−**5** displayed good cytotoxicity toward the examined panel of cancer cells, even though they are resistant to aquation. On the other hand, the ability to undergo aquation did not confer improved cytotoxic efficacies to **6**. To further rule out aquation and subsequent DNA binding as the activation mechanism, we incubated lead complex **4** with DNA nucleoside dGMP and biological nucleophile GSH and monitored its UV−vis profile over a 24 h period. No change in its UV−vis profile was observed in the presence of either dGMP (2 molar equiv) or GSH (10 mM). Furthermore, no new adducts were observed in ESI-MS, indicating that **4** did not interact with the model DNA base and that the chloride ligand on **4** was stable toward nucleophilic substitution (see SI). Coupled with earlier results indicating that **4** operated via a p53-independent pathway, we hypothesized that DNA may not be a target of our RAS complexes, unlike other DNA-binding Ru agents such as RM175.

CONCLUSION

A one-pot combinatorial metal three-component reaction was validated as a methodology to prepare RAS complexes in a large-scale format. The aqueous reaction conditions for compound synthesis directly selects for complexes that exhibit water stability and solubility. Screening of these complexes against A2780 cells led to the identification of several lead compounds, most of which displaying low micromolar IC_{50} values in the inhibition of cell viability against the tested panel of cancer cell lines. Further investigations revealed RAS complex **4** to be highly efficacious and induced apoptosis via a p53-independent mechanism, suggesting that DNA was not its primary biological target. This results hold promise for treatment of cancers that are drug-resistant due to their dysfunctional p53 status.

EXPERIMENTAL SECTION

Materials. All experimental procedures were carried out without additional precautions to exclude air or moisture, unless otherwise specified. All chemicals and solvents were used as received. $RuCl_3 \cdot xH_2O$ was purchased from both Precious Metals Online. $[(\eta^6\text{-benzene})RuCl_2]_2$, $[(\eta^6\text{-toluene})RuCl_2]_2$, $[(\eta^6\text{-cymene})RuCl_2]_2$, $[(\eta^6\text{-hexamethylbenzene})RuCl_2]_2$, and $[(\eta^6\text{-1,3,5-triisopropylbenzene})RuCl_2]_2$ were synthesized according to previously reported protocols.[31,55−57] All other chemicals used were purchased from Sigma-Aldrich (Singapore). Streptomycin and thiazolyl blue tetrazolium bromide (MTT) were obtained from Sigma Chemical Co (St. Louis, MO). PBS buffer (10×, pH 7.4) was purchased from Vivantis Inc.. Hyclone RPMI 1640, DMEM medium, fetal bovine serum (FBS), and Pierce ECL Western blotting substrate were purchased from Thermo Fisher Scientific Inc. (Logan, UT). Annexin V-EGFP apoptosis detection kit (ab14153) was purchased from Abcam (Singapore). Calbiochem anti-human p53 (pAb421) was purchased from Millipore (Molsheim, France), and anti-actin was kindly provided by Dr. Aunis (Strasbourg, France). Ultrapure water used was purified by a Milli-Q UV purification system (Sartorius Stedim Biotech SA, Aubagne Cedex, France). The human ovarian carcinoma cells A2780 and A2780cisR were received with gratitude from Prof. Paul Dyson (EPFL). The human breast adenocarcinoma cells MCF7, human colorectal carcinoma cells HCT116, human colorectal adenocarcinoma cells SW480, and human gastric cancer cells AGS were acquired from

dx.doi.org/10.1021/jm500455p | J. Med. Chem. XXXX, XXX, XXX−XXX

ATCC (Manassa,VA). The wild-type human foreskin fibroblast cells BJwt and the p53-knockdown cells BJshp53 were generously provided by Prof. David Leong Tai Wei (NUS). Final compounds tested for biological activities have been shown to be >95% pure either by elemental analysis or HPLC analysis.

Instrumentation. ^{1}H NMR spectra were obtained using either a Bruker AMX 300, Avance 400, or AMX 500 spectrometer and the chemical shifts (δ) are reported in parts per million with reference to residual solvent peaks. Electrospray-ionization mass spectrometry (ESI-MS) spectra were obtained using a Thermo Finnigan MAT ESI-MS System. UV−vis spectra were obtained using the Shimadzu UV-1800 UV spectrophotometer with a TCC-240A temperate controlled cell holder. Ru concentrations were determined using the Optima ICP-OES (PerkinElmer) operated by CMMAC, NUS. Elemental analyses of selected Ru complexes were carried out using a PerkinElmer PE 2400 elemental analyzer by CMMAS, NUS. Cells were analyzed using a BD LSRFortressa cell analyzer.

HPLC Analysis of Compound Purity. Determination of the purity of a sample batch of seven RAS complexes was done using analytical HPLC on a Shimadzu Prominence system equipped with a DGU-20A$_3$ degasser, two LC-20AD liquid chromatography pumps, a SPD-20A UV/vis detector, and a Shim Pack GVP-ODS 2.0 mm 18 column (5 μM, 120 Å, 250 mm × 4.60 mm i.d.) at rt at a flow rate of 1.0 mL/min with detection at 254 nm. The gradient elution condition were as follows: 10−30% solvent B for first 10 min, followed by 30−80% over the next 20 min, where solvent A is water and solvent B is MeOH. Determination of the purity of the Ru(II) complexes **3**, **5**, and **6** was done using the same analytical HPLC system with the same column at rt at a flow rate of 1.0 mL/min with detection at both 214 and 254 nm. The gradient elution conditions were as follows: 20−80% solvent B over 30 min, where solvent A is 10 mM NH_4OAC pH 7.0 and solvent B is CH_3CN.

Solid-State Structural Determination. X-ray diffraction data were collected with a Bruker AXS SMART APEX diffractometer using Mo Kα radiation at 223(2) K with the SMART suite of programs.[58] Data were processed and corrected for Lorentz and polarization effects using SAINT software[59] and for absorption effects using the SADABS software.[60] Structural solution and refinement were then carried out using the SHELXTL suite of programs.[61] The structure was solved by direct methods. Non-hydrogen atoms were located using difference maps and were given anisotropic displacement parameters in the final refinement. All H atoms were put at calculated positions using the riding model.

General Procedure for the Synthesis of RAS Complexes. A 8.16 μmol portion of **A** (Ru−arene dimer), 16.3 μmol of **B** (picolinaldehyde analogues), and 16.3 μmol of **C** (anilines derivatives) were added in one portion and suspended in 1 mL of D_2O in a 2 mL graduated microtube with vigorous shaking at rt for 36 h. The sparingly soluble reactants dissolved at the end of the reaction, giving colored solutions. This procedure was repeated with different combinations of the three components. Not all combinations were attempted and some of the attempted combinations gave insoluble suspensions, which were excluded from the library. An initial library of 48 RAS complexes was synthesized, and they were characterized immediately by ^{1}H NMR and ESI-MS without any workup or purification steps. Distinctive signals corresponding to the expected product were observed in the ^{1}H NMR spectrum, in addition to a relatively small amount of impurities (^{1}H NMR and ESI-MS data in SI).

Studies on the Effects of Solvent on 3CA. 3CA was carried out in five different solvent systems (1 mL), namely, DMSO-d_6, MeOD-d_4, $CDCl_3$, D_2O, and 1:1 v/v DMSO-d_6/D_2O, using [(η^6-cymene)$RuCl_2$]$_2$ (10 μmol), 2-picolinaldehyde (20 μmol), and aniline (20 μmol) with vigorous shaking at rt for 24 h. Reaction mixtures were characterized immediately by ^{1}H NMR without any workup or purification steps.

Studies on the Effects of pH on 3CA. [(η^6-cymene)$RuCl_2$]$_2$ (10 μmol), 2-picolinaldehyde (20 μmol), and aniline (20 μmol) of were suspended in either NaOAc/DOAc/D_2O (1 mL, pH 4.5) or ND_4Cl/ND_4OD/D_2O buffer (1 mL, pH 10.0) with vigorous shaking at rt for 24 h. The reaction mixtures were characterized immediately by ^{1}H NMR and ESI-MS without any workup or purification steps (^{1}H NMR and ESI-MS data in SI).

Studies on the Effects of Sequential Reagent Addition on 3CA. 3CA was performed sequentially in two separate steps using [(η^6-cymene)$RuCl_2$]$_2$ (10 μmol), 2-picolinaldehyde (20 μmol), and 4-aminobenzamidine dihydrochloride (20 μmol). Briefly, two reagent components were vigorously shaken in D_2O (1 mL) at rt for 24 h, before the third component was added. The reaction mixture was analyzed by ^{1}H NMR following 24 h after addition of the third reagent component (^{1}H NMR data in SI).

General Procedure for the 450-Compound Library Synthesis on a Plate for Screening. Separate stock solutions containing **A** (10 mM), **B** (40 mM), and **C** (40 mM) were prepared in DMSO. The reactions were then carried out on a Microlon 200 96-well flat-bottom plate (Greiner Bio-One) with **A** (50 μL), **B** (25 μL), and **C** (25 μL) and ddH_2O (100 μL) added to each well in one portion, yielding RAS complexes (5 mM) in 1:1 v/v DMSO/H_2O (200 μL). Wells containing 1:1 v/v DMSO/H_2O were included as controls for subsequent experiments. The plates were sealed and incubated with shaking at rt for 48 h. This procedure was repeated until all combinations of the three components were achieved. Only one out of the 450 products was insoluble and was eliminated from later screening. The remaining 449 products were analyzed by ESI-MS.

Synthesis of 2-Quinolinylmethylene-4-aminophenol (L1). 2-Quinolinecarboxaldehyde (157 mg, 1 mmol) and 4-aminophenol (109 mg, 1 mmol) were added to MeOH (50 mL) and refluxed for 2 h. The reaction mixture was reduced to $^1/_{10}$ of its original volume and cooled in an ice bath. The resulting crystalline precipitate that formed was separated by suction filtration, washed with cold methanol (3 × 10 mL), and dried in vacuo for 1 h. Yield: 136 mg (54%). ^{1}H NMR (400 MHz, DMSO-d6): δ 9.72 (s, 1H, OH), 8.79 (s, 1H, PhN=C*H*), 8.46 (d, $^3J_{HH}$ = 9 Hz, 1H, quinolinyl), 8.27 (d, $^3J_{HH}$ = 9 Hz, 1H, quinolinyl), 8.10 (d, $^3J_{HH}$ = 8 Hz, 1H, quinolinyl), 8.05 (d, $^3J_{HH}$ = 8 Hz, 1H, quinolinyl), 7.83 (t, $^3J_{HH}$ = 8 Hz, 1H, quinolinyl), 7.67 (t, $^3J_{HH}$ = 7 Hz, 1H, quinolinyl), 7.40 (d, $^3J_{HH}$ = 9 Hz, 2H, C*H*$_4$OH), 6.86 (d, $^3J_{HH}$ = 9 Hz, 2H, C*H*$_4$OH) ppm. ESI-MS: (+ mode) m/z = 249 [M + H]$^+$, (− mode) m/z = 247 [M − H]$^-$.

Synthesis of *N*-(2-Pyridylmethylene)-1-naphthylamine (L2). 2-Picolinaldehyde (95.1 μL, 1 mmol) and 1-naphthylamine (143 mg, 1 mmol) were added to dry EtOH (15 mL) and stirred at rt over 72 h. The solvent was removed in vacuo and dried. The final product was used for the next step without any further purification. ^{1}H NMR (400 MHz, $CDCl_3$): δ 8.75 (d, $^3J_{HH}$ = 4 Hz, 1H, py), 8.71 (s, 1H, PhN=C*H*), 8.41 (d, $^3J_{HH}$ = 8 Hz, 1H, naphthyl), 8.36 (m, 1H, py), 7.88 (m, 1H, py), 7.87 (d, $^3J_{HH}$ = 7 Hz, 1H, naphthyl), 7.77 (t, $^3J_{HH}$ = 8 Hz, 1H, naphthyl), 7.53 (m, 2H, naphthyl), 7.48 (d, $^3J_{HH}$ = 8 Hz, 1H, naphthyl), 7.41 (m, 1H, py), 7.15 (d, $^3J_{HH}$ = 7 Hz, 1H, naphthyl) ppm. ESI-MS: (+ mode) m/z = 233 [M + H]$^+$, 255 [M + Na]$^+$, 487 [2M + Na]$^+$.

Synthesis of 4-Methoxy-*N*-(2-quinolinylmethylene)aniline (L3). 2-Quinolinecarboxaldehyde (157 mg, 1 mmol) and *p*-anisidine (123 mg, 1 mmol) were added to a minimal amount of dry EtOH (5 mL) and stirred at rt for 72 h. The solvent was removed in vacuo and dried. The resulting crude yellowish brown solid was used for the next step without any further purification. ^{1}H NMR (500 MHz, $CDCl_3$): δ 8.82 (s, 1H, PhN=C*H*), 8.37 (d, $^3J_{HH}$ = 8 Hz, 1H, quinolinyl), 8.24 (d, $^3J_{HH}$ = 8 Hz, 1H, quinolinyl), 8.16 (d, $^3J_{HH}$ = 9 Hz, 1H, quinolinyl), 7.87 (d, $^3J_{HH}$ = 8 Hz, 1H, quinolinyl), 7.76 (t, $^3J_{HH}$ = 7 Hz, 1H, quinolinyl), 7.60 (t, $^3J_{HH}$ = 7 Hz, 1H, quinolinyl), 7.41 (d, $^3J_{HH}$ = 9 Hz, 2H, C*H*$_4$OMe), 6.98 (d, $^3J_{HH}$ = 9 Hz, 2H, C*H*$_4$OMe) ppm.

Synthesis of [(η^6-Benzene)RuCl(L1)]Cl (1). [(η^6-Benzene)-$RuCl_2$]$_2$ (50.4 mg, 0.101 mmol) and **L1** (50.0 mg, 0.202 mmol) were added to MeOH (25 mL) and stirred at rt over 12 h. The solvent was removed in vacuo and the resulting solid was washed with ether (3 × 10 mL). The final product was dried in vacuo for 1 h to yield a orange solid. Yield: 98.0 mg (98%). ^{1}H NMR (400 MHz, MeOH): δ 8.91 (s, 1H, PhN=C*H*), 8.88 (d, $^3J_{HH}$ = 9 Hz, 1H, quinolinyl), 8.77 (d, $^3J_{HH}$ = 8 Hz, 1H, quinolinyl), 8.21 (d, $^3J_{HH}$ = 8 Hz, 2H, quinolinyl), 8.15 (t, $^3J_{HH}$ = 8 Hz, 1H, quinolinyl), 7.96 (t, $^3J_{HH}$ = 8 Hz, 1H, quinolinyl), 7.85 (d, $^3J_{HH}$ = 9 Hz, 2H, C*H*$_4$OH), 7.02 (d, $^3J_{HH}$ = 9 Hz,

dx.doi.org/10.1021/jm500455p | J. Med. Chem. XXXX, XXX, XXX−XXX

2H, CH_4OH), 5.94 (s, 6H, C_6H_6) ppm. ESI-MS: (+ mode) m/z = 463 $[M]^+$. Purity of the complex was determined to be >95% pure by elemental analysis. Anal. Calcd for $RuC_{22}H_{18}N_2Cl_2O$ (%): C 53.02, H 3.64, N 5.62. Found: C 52.81, H 3.44, N 5.62.

Synthesis of [(η^6-Toluene)RuCl(L1)]Cl (2). Complex **2** was obtained with [(η^6-toluene)$RuCl_2]_2$ (53.2 mg, 0.101 mmol) and **L1** (50.0 mg, 0.202 mmol) using the same protocol as used for **1** as a red solid. Yield: 100 mg (97%). ^{1}H NMR (400 MHz, DMSO): δ 10.42 (s, 1H, OH), 9.11 (s, 1H, PhN=C*H*), 8.87 (d, $^3J_{HH}$ = 8 Hz, 1H, quinolinyl), 8.75 (d, $^3J_{HH}$ = 9 Hz, 1H, quinolinyl), 8.29 (t, $^3J_{HH}$ = 8 Hz, 2H, quinolinyl), 8.14 (t, $^3J_{HH}$ = 7 Hz, 1H, quinolinyl), 7.98 (t, $^3J_{HH}$ = 8 Hz, 1H, quinolinyl), 7.87 (d, $^3J_{HH}$ = 9 Hz, 2H, CH_4OH), 7.03 (d, $^3J_{HH}$ = 9 Hz, 2H, CH_4OH), 6.06 (t, $^3J_{HH}$ = 6 Hz, 1H, C_6H_5), 5.98 (d, $^3J_{HH}$ = 6 Hz, 1H, C_6H_5), 5.81 (t, $^3J_{HH}$ = 6 Hz, 1H, C_6H_5), 5.72 (t, $^3J_{HH}$ = 6 Hz, 1H, C_6H_5), 5.39 (d, $^3J_{HH}$ = 8 Hz, 1H, C_6H_5), 2.16 (s, 3H, CH_3) ppm. ESI-MS: (+ mode) m/z = 477 $[M]^+$. Purity of the complex was determined to be >95% pure by elemental analysis. Anal. Calcd for $RuC_{23}H_{20}N_2Cl_2O$ (%): C 53.91, H 3.93, N 5.47. Found: C 53.57, H 4.23, N 5.27.

Synthesis of [(η^6-1,3,5-Triisopropybenzene)RuCl(L2)]Cl (3). [(η^6-1,3,5-Triisopropylbenzene)$RuCl_2]_2$ (87.1 mg, 0.108 mmol) and **L2** (50.0 mg, 0.215 mmol) were added to MeOH (15 mL) and stirred at rt over 12 h. The solvent was removed in vacuo and the resulting solid was washed with ether (3 × 10 mL). The final product was dried in vacuo for 1 h to give a yellow solid. Yield: 126 mg (96%). ^{1}H NMR (500 MHz, $CDCl_3$, 70 °C): δ 9.59 (d, $^3J_{HH}$ = 4 Hz, 1H, py), 9.02 (s, 1H, PhN=C*H*), 8.35 (m, 2H, py), 8.15 (bs, 1H, naphthyl), 8.12 (d, $^3J_{HH}$ = 8 Hz, 1H, naphthyl), 7.95 (m, 1H, py), 7.71 (bs, 5H, naphthyl), 5.85 (s, 3H, C_6H_3), 2.19 (sept, $^3J_{HH}$ = 7 Hz, 3H, $CHMe_2$), 1.06 (d, $^3J_{HH}$ = 7 Hz, 9H, $C(CH_3)_2$), 0.93 (bs, 9H, $C(CH_3)_2$) ppm. ESI-MS: (+ mode) m/z = 573 $[M]^+$. Purity (HPLC): 95.5% at 214 nm and 92.4% at 254 nm; t_R = 25.6 min. Purity of the complex was determined to be >95% pure by HPLC.

Synthesis of [(η^6-1,3,5-Triisopropybenzene)RuCl(L3)]Cl (4). [(η^6-1,3,5-Triisopropylbenzene)$RuCl_2]_2$ (244 mg, 0.324 mmol) and crude **L3** (167 mg, 0.648 mmol) were added to MeOH (40 mL) and stirred at rt over 12 h. The solvent was removed in vacuo and reconstituted in a minimum amount of MeOH (2 mL). Diethyl ether (40 mL) was than added to precipitate the product. The suspension was filtered and the resulting solid washed with ether (3 × 10 mL). The final product was then dried in vacuo for 1 h to give a reddish brown solid. Yield: 290 mg (71%). ^{1}H NMR (400 MHz, DMSO): δ 9.09 (s, 1H, PhN=C*H*), 8.96 (d, $^3J_{HH}$ = 9 Hz, 1H, quinolinyl), 8.85 (d, $^3J_{HH}$ = 8 Hz, 1H, quinolinyl), 8.25 (d, $^3J_{HH}$ = 8 Hz, 2H, quinolinyl), 8.12 (m, 1H, quinolinyl), 8.11 (d, $^3J_{HH}$ = 9 Hz, 2H, CH_4OMe), 7.97 (t, $^3J_{HH}$ = 8 Hz, 1H, quinolinyl), 7.19 (d, $^3J_{HH}$ = 9 Hz, 2H, CH_4OMe), 5.54 (s, 3H, C_6H_3), 3.90 (s, 3H, CH_3), 2.44 (sept, $^3J_{HH}$ = 7 Hz, 3H, $CHMe_2$), 1.16 (d, $^3J_{HH}$ = 7 Hz, 9H, $C(CH_3)_2$), 0.85 (d, $^3J_{HH}$ = 7 Hz, 9H, $C(CH_3)_2$) ppm. ESI-MS: (+ mode) m/z = 603 $[M]^+$. Purity of the complex was determined to be >95% pure by elemental analysis. Anal. Calcd for $RuC_{32}H_{38}N_2Cl_2O$ (%): C 60.16, H 6.00, N 4.39. Found: C 60.26, H 5.61, N 4.45.

Synthesis of [(η^6-Hexamethylbenzene)RuCl(3-chloro-*N*-(2-quinolinylmethylene)aniline)]Cl (5). 2-Quinolinecarboxaldehyde (78.6 mg, 0.5 mmol) and 3-chloroaniline (52.9 μL, 0.5 mmol) were added to dry EtOH (8 mL) and stirred at rt over 72 h. The solvent was removed in vacuo and dried. Crude 3-chloro-*N*-(2-quinolinylmethylene)aniline (135 mg) was treated with [(η^6-hexamethylbenzene)$RuCl_2]_2$ (167 mg, 0.25 mmol) in MeOH (20 mL) and stirred at rt over 12 h. The solvent was removed in vacuo and the resulting solid purified by gradient elution column chromatography (1:4 v/v EtOH/$CHCl_3$, R_f = 0.2; 1:1 v/v EtOH/$CHCl_3$, R_f = 0.6). The final product was then dried in vacuo for 1 h to give a red solid. Yield: 182 mg (61%). ^{1}H NMR (400 MHz, $CDCl_3$): δ 9.37 (s, 1H, PhN=C*H*), 8.68 (d, ^{3}J= 8 Hz, 1H, quinolinyl), 8.52 (d, $^3J_{HH}$ = 9 Hz, 1H, quinolinyl), 8.48 (d, $^3J_{HH}$ = 8 Hz, 1H, quinolinyl), 8.40 (d, $^3J_{HH}$ = 8 Hz, 1H, quinolinyl), 8.34 (s, 1H, C_6H_4), 7.99 (d, $^3J_{HH}$ = 8 Hz, 1H, C_6H_4), 7.88 (t, $^3J_{HH}$ = 7 Hz, 1H, quinolinyl), 7.79 (t, $^3J_{HH}$ = 7 Hz, 1H, quinolinyl), 7.54 (t, $^3J_{HH}$ = 8 Hz, 1H, C_6H_4), 7.44 (d, $^3J_{HH}$ = 8 Hz, 1H, C_6H_4), 1.90 (s, 18H, $C_6(CH_3)_6$) ppm. ESI-MS: (+ mode) m/z = 565 $[M]^+$. Purity (HPLC): 97.4% at 214 nm and 95.6% at 254 nm; t_R = 20.3 min. Purity of the complex was determined to be >95% pure by HPLC.

Synthesis of [(η^6-Hexamethylbenzene)RuCl(*N*-(2-quinolinylmethylene)-8-hydroxy-1-napthalenamine)]Cl (6). [(η^6-Hexamethylbenzene)$RuCl_2]_2$ (66.85 mg, 0.1 mmol), 2-quinolinecarboxaldehyde (31.4 mg, 0.1 mmol), and 8-hydroxy-1-napthalenamine (31.8 mg, 0.1 mmol) were added to 1:1 v/v DMSO/H_2O (10 mL) and stirred at rt over 48 h. MeOH was then added to the resulting suspension until a clear dark red solution was formed. The solution was left to stir at rt for 24 h. The solvent mixture was removed in vacuo and the resulting solid purified by gradient elution column chromatography (1:4 v/v EtOH/$CHCl_3$, R_f = 0.2; 1:1 v/v EtOH/$CHCl_3$, R_f = 0.6). The final product was dried in vacuo for 1 h to give a dark red solid. Yield: 86.0 mg (69%). ^{1}H NMR (300 MHz, MeOD): δ 9.11 (s, 1H, PhN=C*H*), 8.75 (d, $^3J_{HH}$ = 8 Hz, 1H), 8.53 (d, $^3J_{HH}$ = 9 Hz, 1H), 8.48 (d, $^3J_{HH}$ = 8 Hz, 1H), 8.44 (bs, 1H), 8.29 (d, $^3J_{HH}$ = 8 Hz, 1H), 8.25 (d, $^3J_{HH}$ = 8 Hz, 1H), 8.14 (m, 1H), 7.98 (t, $^3J_{HH}$ = 7 Hz, 2H), 7.62 (t, $^3J_{HH}$ = 8 Hz, 2H), 7.05 (d, $^3J_{HH}$ = 8 Hz, 1H), 1.83 (s, 18H) ppm. ESI-MS: (+ mode) m/z = 565 $[M]^+$. Purity (HPLC): 96.1% at 214 nm and 95.1% at 254 nm; t_R = 19.5 min. Purity of the complex was determined to be >95% pure by HPLC.

Tissue Culture. The human ovarian carcinoma cells A2780 and A2780cisR and gastric adenocarcinoma cells AGS were cultured in RPMI 1640 medium containing 10% fetal bovine serum (complete RPMI) and grown at 37 °C in a humidified atmosphere of 95% air and 5% CO_2. Cisplatin (1 μM) was added to A2780cisR every three passages to maintain its resistance. The human breast carcinoma cells MCF7 and colon cancer cell lines HCT116 and SW480 were cultured in DMEM medium containing 10% fetal bovine serum (complete DMEM) and grown at 37 °C in a humidified atmosphere of 95% air and 5% CO_2. The medium used for the colon cancer cell lines also contained 1% streptomycin. Experiments were performed on cells within 20 passages.

Inhibition of Cell Viability Assay (Single Concentration Screen). The antiproliferation activity of the 442 library of RAS complexes on exponentially growing cancer cells was screened using a MTT assay modified from one described previously.[34] A2780 cells were seeded at 8000 cells/100 μL per well in Cellstar 96-well plates (Greiner Bio-One) and incubated for 24 h. PBS buffer (200 μL) was added to the wells at the perimeter to prevent evaporation of the media from the enclosed wells. After that, cancer cells were exposed to the library of RAS complexes in a predetermined order, at a single concentration of 25 μM for 6 h. The complex solutions used for the exposure were made by serial dilution of the synthesized RAS complexes with RPMI 1640 medium, resulting in a final concentration of 25 μM with 0.5% (v/v) DMSO. After the 6 h, the drug-containing medium was removed, new drug-free complete RPMI was added, and the cells were incubated for additional 66 h. At 72 h after drug addition, the medium was removed and replaced with MTT solution in PBS (100 μL, 0.5 mg/mL) and incubated for an additional 4 h at 37 °C, 5% CO_2. Subsequently, the medium was aspirated, and the purple formazan crystals were dissolved in DMSO (100 μL). The absorbance due to the dissolved purple formazan was then obtained at 595 nm. A negative control (cancer cells not exposed to any RAS complexes) and a positive control (cancer cells exposed to cisplatin) were also included in the experiment. The experiments were performed in quintuplicate for each RAS complex and control, and the cell viabilities associated with each RAS complex were calculated using the measured absorbance value. The cell viability of these complexes was further analyzed using the software Prism Graphpad 5.

Aqueous Stability Studies. Stock solutions of **1**−**6** (5 mM) were each diluted with ddH_2O to a final concentration of 50 μM with 1% DMSO. The UV−vis peak profile of the sample was then monitored for 24 at 1 h intervals. The temperature was kept constant at 25 °C throughout and ddH_2O with 1% DMSO was used as the blank sample.

Determination of Thermodynamic Aqueous Solubility. Approximately 5 mg of **1**−**5** was added separately to a minimal amount of ddH_2O until a small amount of each compound was left in a saturated solution of the respective compounds. The separate

dx.doi.org/10.1021/jm500455p | J. Med. Chem. XXXX, XXX, XXX−XXX

mixtures were than left to stand with gentle agitation at rt for 24 h. The individual mixtures were than centrifuged at 10 000 rpm for 2 min, and the supernatant liquid was collected and analyzed by ICP-OES to determine the maximum solubility of each compound. The same procedure was repeated for **6** but with 0.6% w/v NaCl solution instead of ddH_2O.

Determination of log P_{OW}. log P_{OW} of **1**–**6** were determined using the shake flask method.[38] **1**–**6** were predissolved in ddH_2O that was presaturated with *n*-octanol (for 24 h and left to stand until phase separation occurs). The UV–vis spectrum for each sample was obtained, and the absorbances at the λ_{max} of each compound were determined. An equal volume of *n*-octanol was added to each sample solution, and the heterogeneous mixtures were shook for 96 h before centrifuging at 7000 rpm for 1 min to achieve phase separation. The final absorbance of the aqueous phase at the λ_{max} of each compound was determined, and their water–octanol partition coefficients were calculated. The experiment was repeated for **6** in 0.6% w/v NaCl solution instead of ddH_2O. All experiments were done in triplicate.

Inhibition of Cell Viability Assay. The antiproliferation activity of **1**–**6** on exponentially growing cancer cells was determined using MTT assay as described previously.[34] A2780 cells, A2780cisR, and MCF7 were seeded at 8000, 6000, and 4000 cells, respectively, per well (100 μL) in Cellstar 96-well plates (Greiner Bio-One) and incubated for 24 h. PBS buffer (200 μL) was added to the wells at the perimeter to prevent evaporation of the media from the enclosed wells. Thereafter, cancer cells were exposed to drugs at different concentration in RPMI medium (A2780/A2780cisR) or DMEM medium (MCF7) without FBS or antibiotics and incubated at 37 °C, 5% CO_2 for 6 h. The compounds were predissolved as DMSO stock solutions and serially diluted with DMSO to a range of concentrations. The final concentration of DMSO in medium was 1% (v/v), at which cell viability was not significantly inhibited. After the 6 h, the drug-containing medium was removed, and new drug-free complete RPMI (A2780/A2780cisR) or DMEM (MCF7) was added, and the cells were incubated for an additional 66 h. At 72 h after initial drug addition, the medium was removed and replaced with MTT solution (100 μL, 0.5 mg/mL) in PBS and incubated for an additional 4 h at 37 °C, 5% CO_2. Subsequently, the medium was aspirated, and the purple formazan crystals were dissolved in DMSO (100 μL). The absorbance due to the dissolved purple formazan was than obtained at 595 nm. The experiments were performed in six replicates for each drug concentration and were carried out at least three times independently. Inhibition to cell viability was evaluated with reference to the IC_{50} value, which is defined as the concentration needed for a 50% reduction of survival based on the survival curves. IC_{50} values were calculated from the dose–response curves (cell viability vs drug concentration) obtained in repeated experiments and adjusted to the actual Ru concentration administered, which was determined using ICP-OES. For HCT116 and SW480 cells, the protocol was applied as before except that cells were plated at 20 000 cells per well (100 μL) in Cellstar 96-well plates (Greiner Bio-One) for 24 h and exposed to varying concentration of RAS complexes continuously for 48 h in DMEM complete medium containing <0.5% v/v DMSO. Similarly for BJwt and BJshp53, cells were plated at 2000 cells per well (100 μL) in Cellstar 96-well plates (Greiner Bio-One) for 24 h and then incubated with varying concentration of **4** and DOX continuously for 48 h in medium containing <0.8% v/v DMSO. The experiments were performed in eight replicates for each drug concentration and were carried out at least three times independently.

Annexin V/Propidium Iodide Assay. The ability of **4** to induce apoptosis in HCT116 cells was investigated via the annexin V/propidium iodide assay previously described.[62] HCT116 cells were seeded at 200 000 cells per well (1 mL) in Cellstar 12-well plates (Greiner Bio-One) and incubated for 24 h. Thereafter, cancer cells were exposed to 2.5 and 10 μM of **4** in complete DMEM medium and incubated at 37 °C, 5% CO_2 for 24 h. The supernatant solution and cells detached by trypsinization were collected in separate vials and centrifuged at 100 rpm for 10 min to pellet the cells. Cells were resuspended in 500 μL of binding buffer containing annexin V–EGFP and propidium iodide and of final concentration 1 μg/mL. The fluorescence was immediately analyzed by flow cytometry. The resulting dot plots were acquired from 10 000 events and quantified by software BD FACSDiva. The experiment was performed independently twice.

Protein Extraction and Western Blot for p53. HCT116 cells were grown on Cellstar six-well plates (Greiner Bio-One) and treated with **4** at concentrations of 1 μM (IC_{50}), 2.5 μM (IC_{25}), and 10 μM and at 2.5 and 10 μM for the control drug oxaliplatin and incubated at 37 °C, 5% CO_2. Different sets of cells were treated for different durations of 2, 6, 12, and 24 h. The cells were lysed with lysis buffer [100 μL, 1% NP40, 150 mM NaCl, 50 mM Tris-HCl (pH 8.0), protease inhibitor]. The cell lysate were transferred to separate 2 mL tubes and sonicated for 10 s. The samples were then centrifuged at 13 000 rpm, 4 °C for 15 min. The supernatant liquid containing the proteins was collected and the total protein content of each sample was quantified via Bradford's assay. Thirty micrograms of proteins from each sample was reconstituted in loading buffer (5% DDT, 1× protein loading dye) and heated at 95 °C for 5 min. The protein mixtures were resolved on a 10% SDS–PAGE gel by electrophoresis and transferred to a nitrocellulose membrane. Equal loading of protein was confirmed by comparison with actin. Immunoblotting for p53 was done using anti-human p53 antibodies. The proteins bands were visualized via enhanced chemiluminescence imaging (PXi, Syngene).

■ ASSOCIATED CONTENT

Supporting Information

^{1}H NMR and UV–vis spectra for lead compounds **1**–**6**, UV–vis and ESI-MS data for **4** with dGMP and GSH, ^{1}H NMR data and ESI-MS data of 63 compounds from the initial library, HPLC chromatogram of selected RAS complexes, and X-ray crystallographic data in CIF format for [RAS-A3/B1/C8]PF_6. This material is available free of charge via the Internet at http://pubs.acs.org.

■ AUTHOR INFORMATION

Corresponding Author

*Phone: +65 6516 5131. E-mail: chmawh@nus.edu.sg.

Author Contributions

The manuscript was written through contributions of all authors. All authors have given approval to the final version of the manuscript.

Notes

The authors declare no competing financial interest.

■ ACKNOWLEDGMENTS

Financial support from Ministry of Education and the National University of Singapore (R143-000-512-112 and R143-000-572-112) and Ligue contre le Cancer, COST CM1105 is gratefully acknowledged. The authors thanks Paul J. Dyson (EPFL) and David T. W. Leong (NUS) for their gift of cell lines; Lip Lin Koh (NUS), Geok Kheng Tan (NUS), and Yimian Hong (NUS) for performing X-ray crystallographic analysis; and Ong Wei Fang Wendy for helping with flow cytometry analysis.

■ ABBREVIATIONS USED

D_2O, deuterium oxide; NMR, nuclear magnetic resonance; ESI-MS, electrospray ionization-mass spectrometry; RP-HPLC, reverse-phase high-performance liquid chromatography; DMSO-d_6, deuterated dimethyl sulfoxide; MeOH-d_4, deuterated methanol; ddH_2O, ultrapure water; ICP-OES, inductively couple-optical emission spectrometry; GSH, L-glutathione; dGMP, 2′-deoxyguanosine 5′-monophosphate sodium salt hydrate.

dx.doi.org/10.1021/jm500455p | J. Med. Chem. XXXX, XXX, XXX–XXX

REFERENCES

(1) Dobson, C. M. Chemical Space and Biology. *Nature* **2004**, *432*, 824−828.

(2) Lipinski, C.; Hopkins, A. Navigating Chemical Space for Biology and Medicine. *Nature* **2004**, *432*, 855−861.

(3) Koch, M. A.; Schuffenhauer, A.; Scheck, M.; Wetzel, S.; Casaulta, M.; Odermatt, A.; Ertl, P.; Waldmann, H. Charting Biologically Relevant Chemical Space. *Proc. Natl. Acad. Sci. U. S. A.* **2005**, *102*, 17272−17277.

(4) Lipkus, A. H.; Yuan, Q.; Lucas, K. H.; Funk, S. A.; Bartelt, W. F. I.; Schenck, R. J.; Trippe, A. J. Structural Diversity of Organic Chemistry. A Scaffold Analysis of the CAS Registry. *J. Org. Chem.* **2008**, *73*, 4443−4451.

(5) Bemis, G. W.; Murcko, M. A. The Properties of Known Drugs. 1. Molecular Frameworks. *J. Med. Chem.* **1996**, *39*, 2887−2893.

(6) Meggers, E. Targeting Proteins with Metal Complexes. *Chem. Commun.* **2009**, *9*, 1001−1010.

(7) Daniel, C. *Reputation and Power: Organizational Image and Pharmaceutical Regulation at the FDA*; Princeton Unversity Press: Princeton, NJ, 2010

(8) Kelland, L. The Resurgence of Platinum-based Cancer Chemotherapy. *Nat. Rev. Cancer* **2007**, *7*, 573−584.

(9) Clarke, M. J.; Zhu, F.; Frasca, D. R. Non-Platinum Chemotherapeutic Metallopharmaceuticals. *Chem. Rev.* **1999**, *99*, 2511−2533.

(10) Rademaker-Lakhai, J. M.; van den Bongard, D.; Pluim, D.; Beijnen, J. H.; Schellens, J. H. M. Phase I and Pharmacological Study with Imidazolium- *trans*-DMSO-imidazole-tetrachlororuthenate, a Novel Ruthenium Anticancer Agent. *Clin. Cancer Res.* **2004**, *10*, 3717−3727.

(11) Hartinger, C. G.; Jakupec, M. A.; Zorbas-Seifried, S.; Groessl, M.; Egger, A.; Berger, W.; Zorbas, H.; Dyson, P. J.; Keppler, B. K. KP1019, A New Redox-Active Anticancer Agent—Preclinical Development and Results of a Clinical Phase I Study in Tumor Patients. *Chem. Biodiversity* **2008**, *5*, 2140−2155.

(12) Hartinger, C. G.; Metzler-Nolte, N.; Dyson, P. J. Challenges and Opportunities in the Development of Organometallic Anticancer Drugs. *Organometallics* **2012**, *31*, 5677−5685.

(13) Peacock, A. F.; Sadler, P. J. Medicinal Organometallic Chemistry: Designing Metal Arene Complexes as Anticancer Agents. *Chem.-Asian J.* **2008**, *3*, 1890−1899.

(14) Nowak-Sliwinska, P.; van Beijnum, J. R.; Casini, A.; Nazarov, A. A.; Wagnieres, G.; van den Bergh, H.; Dyson, P. J.; Griffioen, A. W. Organometallic Ruthenium(II) Arene Compounds with Antiangiogenic Activity. *J. Med. Chem.* **2011**, *54*, 3895−3902.

(15) Romero-Canelon, I.; Salassa, L.; Sadler, P. J. The Contrasting Activity of Iodido Versus Chlorido Ruthenium and Osmium Arene Azo- and Imino-pyridine Anticancer Complexes: Control of Cell Selectivity, Cross-Resistance, p53 Dependence, and Apoptosis Pathway. *J. Med. Chem.* **2013**, *56*, 1291−1300.

(16) Nazarov, A. A.; Hartinger, C. G.; Dyson, P. J. Opening the Lid on Piano-Stool Complexes: An Account of Ruthenium(II)−Arene Complexes with Medicinal Applications. *J. Organomet. Chem.* **2014**, *751*, 251−260.

(17) Paira, P.; Chow, M. J.; Venkatesan, G.; Kosaraju, V. K.; Cheong, S. L.; Klotz, K.; Ang, W. H.; G, P. Organoruthenium Antagonists of Human A3 Adenosine Receptors. *Chem.-Eur. J.* **2013**, *19*, 8321−8330.

(18) Ong, J. X.; Yap, C. W.; Ang, W. H. Rational Design of Selective Organoruthenium Inhibitors of Protein Tyrosine Phosphatase 1B. *Inorg. Chem.* **2012**, *51*, 12483−12492.

(19) Blanck, S.; Cruchter, T.; Vultur, A.; Riedel, R.; Harms, K.; Herlyn, M.; Meggers, E. Organometallic Pyridylnaphthalimide Complexes as Protein Kinase Inhibitors. *Organometallics* **2011**, *30*, 4598−4606.

(20) Ang, W. H.; Casini, A.; Sava, G.; Dyson, P. J. Organometallic Ruthenium-Based Antitumor Compounds with Novel Modes of Action. *J. Organomet. Chem.* **2011**, *696*, 989−998.

(21) Bergamo, A.; Masi, A.; Peacock, A. F.; Habtemariam, A.; Sadler, P. J.; Sava, G. In Vivo Tumour and Metastasis Reduction and in Vitro Effects on Invasion Assays of the Ruthenium RM175 and Osmium AFAP51 Organometallics in the Mammary Cancer Model. *J. Inorg. Biochem.* **2010**, *104*, 79−86.

(22) Schmid, W. F.; John, R. O.; Muhlgassner, G.; Heffeter, P.; Jakupec, M. A.; Galanski, M.; Berger, W.; Arion, V. B.; Keppler, B. K. Metal-Based Paullones as Putative CDK Inhibitors for Antitumor Chemotherapy. *J. Med. Chem.* **2007**, *50*, 6343−6355.

(23) Reetz, M. T. Combinatorial and Evolution-Based Methods in the Creation of Enantioselective Catalysts. *Angew. Chem., Int. Ed.* **2001**, *40*, 284−310.

(24) Francis, M. B.; Jamison, T. F.; Jacobsen, E. N. Combinatorial Libraries of Transition-Metal Complexes, Catalysts and Materials. *Curr. Opin. Chem. Biol.* **1998**, *2*, 422−428.

(25) Mulcahy, S. P.; Grundler, K.; Frias, C.; Wagner, L.; Prokop, A.; Meggers, E. Discovery of a Strongly Apoptotic Ruthenium Complex Through Combinatorial Coordination Chemistry. *Dalton Trans.* **2010**, *39*, 8177−8182.

(26) Robillard, M. S.; Bacac, M.; van den Elst, H.; Flamigni, A.; van der Marel, G. A.; van Boom, J. H.; Reedijk, J. Automated Parallel Solid-Phase Synthesis and Anticancer Screening of a Library of Peptide-Tethered Platinum(II) Complexes. *J. Comb. Chem.* **2003**, *5*, 821−825.

(27) Robillard, M. S.; van Alphen, S.; Meeuwenoord, N. J.; Jansen, B. A. J.; van der Marel, G. A.; van Boom, J. H.; Reedijk, J. Solid-phase Synthesis of Peptide−Platinum Complexes Using Platinum-Chelating Building Blocks Derived From Amino Acids. *New J. Chem.* **2005**, *29*, 220.

(28) Patra, M.; Hess, J.; Konatschnig, S.; Spingler, B.; Gasser, G. Synthesis of Ferrocenyl and Ruthenocenyl Thioamide Derivatives Using a Single-Step Three-Component Reaction. *Organometallics* **2013**, *32*, 6098−6105.

(29) Artem'ev, A. V.; Gusarova, N. K.; Bagryanskaya, I. Y.; Doronina, E. P.; Verkhoturova, S. I.; Sidorkin, V. F.; Trofimov, B. A. Alkali Metal Thioselenophosphinates, M[SeSPR$_2$]: One-Pot Multicomponent Synthesis, DFT Study, and Synthetic Application. *Eur. J. Inorg. Chem.* **2013**, *2013*, 415−426.

(30) Filak, L. K.; Goschl, S.; Heffeter, P.; Ghannadzadeh Samper, K.; Egger, A. E.; Jakupec, M. A.; Keppler, B. K.; Berger, W.; Arion, V. B. Metal-Arene Complexes with Indolo[3,2-*c*]quinolines: Effects of Ruthenium vs Osmium and Modifications of the Lactam Unit on Intermolecular Interactions, Anticancer Activity, Cell Cycle, and Cellular Accumulation. *Organometallics* **2013**, *32*, 903−914.

(31) Zelonka, R. A.; Baird, M. C. Benzene Complexes of Ruthenium(II). *Can. J. Chem.* **1972**, *50*, 3063−3072.

(32) Kim, T. D.; McNeese, T. J.; Rheingold, A. L. Preparation and X-ray Crystal Structure Analysis of the Hydroxo-Bridged, Dinuclear (π-Arene)ruthenium(II) Cation in [Ru$_2$(η^6-C$_6$H$_6$)$_2$(μ-OH$_3$)]Cl·3H$_2$O. *Inorg. Chem.* **1988**, *27*, 2554−2555.

(33) Enyedy, É. A.; Bognár, G. M.; Kiss, T.; Hanif, M.; Hartinger, C. G. Solution Equilibrium Studies on Anticancer Ruthenium(II)−η^6-*p*-Cymene Complexes of 3-Hydroxy-2(1*H*)-pyridones. *J. Organomet. Chem.* **2013**, *734*, 38−44.

(34) Carmichael, J.; DeGraff, W. G.; Gazdar, A. F.; Minna, J. D.; Mitchell, J. B. Evaluation of a Tetrazolium-Based Semiautomated Colorimetric Assay: Assessment of Chemosensitivity Testing. *Cancer Res.* **1987**, *47*, 936−942.

(35) Di, L.; Artursson, P.; Avdeef, A.; Ecker, G. F.; Faller, B.; Fischer, H.; Houston, J. B.; Kansy, M.; Kerns, E. H.; Kramer, S. D.; Lennernas, H.; Sugano, K. Evidence-based Approach To Assess Passive Diffusion and Carrier-Mediated Drug Transport. *Drug Discovery Today* **2012**, *17*, 905−912.

(36) Lipinski, C. A.; Lombardo, F.; Dominy, B. W.; Feeney, P. J. Experimental and Computational Approaches To Estimate Solubility and Permeability in Drug Discovery and Development Settings. *Adv. Drug Delivery Rev.* **1997**, *23*, 3−25.

(37) Veber, D. F.; Johnson, S. R.; Cheng, H.; Smith, B. R.; Ward, K. W.; Kopple, K. D. Molecular Properties That Influence the Oral Bioavailability of Drug Candidates. *J. Med. Chem.* **2002**, *45*, 2625−2623.

(38) *Test No. 107: Partition Coefficient (n-octanol/water): Shake Flask Method*; OECD Publishing: Paris, 1995.

dx.doi.org/10.1021/jm500455p | *J. Med. Chem.* XXXX, XXX, XXX−XXX

(39) He, L.; Liao, S. Y.; Tan, C. P.; Ye, R. R.; Xu, Y. W.; Zhao, M.; Ji, L. N.; Mao, Z. W. Ruthenium−Arene−β-Carboline Complexes as Potent Inhibitors of Cyclin-Dependent Kinase 1: Synthesis, Characterization and Anticancer Mechanism Studies. *Chem.-Eur. J.* **2013**, *19*, 12152−12160.
(40) Busto, N.; Valladolid, J.; Martinez-Alonso, M.; Lozano, H. J.; Jalon, F. A.; Manzano, B. R.; Rodriguez, A. M.; Carrion, M. C.; Biver, T.; Leal, J. M.; Espino, G.; Garcia, B. Anticancer Activity and DNA Binding of a Bifunctional Ru(II) Arene Aqua-Complex with the 2,4-Diamino-6-(2-pyridyl)-1,3,5-triazine Ligand. *Inorg. Chem.* **2013**, *52*, 9962−9974.
(41) Aird, R. E.; Cummings, J.; Ritchie, A. A.; Muir, M.; Morris, R. E.; Chen, H.; Sadler, P. J.; Jodrell, D. I. In Vitro and in Vivo Activity and Cross Resistance Profiles of Novel Ruthenium (II) Organometallic Arene Complexes in Human Ovarian Cancer. *Br. J. Cancer* **2002**, *86*, 1652−1657.
(42) Travnicek, Z.; Starha, P.; Popa, I.; Vrzal, R.; Dvorak, Z. Roscovitine-based CDK Inhibitors Acting as N-Donor Ligands in the Platinum(II) Oxalato Complexes: Preparation, Characterization and in Vitro Cytotoxicity. *Eur. J. Med. Chem.* **2010**, *45*, 4609−4614.
(43) Zhang, S.; Lovejoy, K. S.; Shima, J. E.; Lagpacan, L. L.; Shu, Y.; Lapuk, A.; Chen, Y.; Komori, T.; Gray, J. W.; Chen, X.; Lippard, S. J.; Giacomini, K. M. Organic Cation Transporters are Determinants of Oxaliplatin Cytotoxicity. *Cancer Res.* **2006**, *66*, 8847−57.
(44) Meulmeester, E.; Jochemsen, A. G. p53—A Guide to Apoptosis. *Curr. Cancer Drug Targets* **2008**, *8*, 87−97.
(45) Benosman, S.; Gross, I.; Clarke, N.; Jochemsen, A. G.; Okamoto, K.; Loeffler, J. P.; Gaiddon, C. Multiple Neurotoxic Stresses Converge on MDMX Proteolysis to Cause Neuronal Apoptosis. *Cell Death Differ.* **2007**, *14*, 2047−2057.
(46) Boyer, J.; McLean, E. G.; Aroori, S.; Wilson, P.; McCulla, A.; Carey, P. D.; Longley, D. B.; Johnston, P. G. Characterization of p53 Wild-Type and Null Isogenic Colorectal Cancer Cell Lines Resistant to 5-Fluorouracil, Oxaliplatin, and Irinotecan. *Clin. Cancer Res.* **2004**, *10*, 2158−2167.
(47) Brantley-Finley, C.; Lyle, C. S.; Du, L.; Goodwin, M. E.; Hall, T.; Szwedo, D.; Kaushal, G. P.; Chambers, T. C. The JNK, ERK and p53 Pathways Play Distinct Roles in Apoptosis Mediated by the Antitumor Agents Vinblastine, Doxorubicin, and Etoposide. *Biochem. Pharmacol.* **2003**, *66*, 459−469.
(48) Chatterjee, S.; Kundu, S.; Bhattacharyya, A.; Hartinger, C. G.; Dyson, P. J. The Ruthenium(II)−Arene Compound RAPTA-C Induces Apoptosis in EAC Cells Through Mitochondrial and p53-JNK Pathways. *J. Biol. Inorg. Chem.* **2008**, *13*, 1149−1155.
(49) Hayward, R. L.; Schornagel, Q. C.; Tente, R.; Macpherson, J. S.; Aird, R. E.; Guichard, S.; Habtemariam, A.; Sadler, P.; Jodrell, D. I. Investigation of the Role of Bax, p21/Waf1 and p53 as Determinants of Cellular Responses in HCT116 Colorectal Cancer Cells Exposed to the Novel Cytotoxic Ruthenium(II) Organometallic Agent, RM175. *Cancer Chemother. Pharmacol.* **2005**, *55*, 577−583.
(50) Vidimar, V.; Meng, X.; Klajner, M.; Licona, C.; Fetzer, L.; Harlepp, S.; Hebraud, P.; Sidhoum, M.; Sirlin, C.; Loeffler, J. P.; Mellitzer, G.; Sava, G.; Pfeffer, M.; Gaiddon, C. Induction of Caspase 8 and Reactive Oxygen Species by Ruthenium-derived Anticancer Compounds with Improved Water Solubility and Cytotoxicity. *Biochem. Pharmacol.* **2012**, *84*, 1428−1436.
(51) Chin, C. F.; Tian, Q.; Setyawati, M. I.; Fang, W.; Tan, E. S.; Leong, D. T.; Ang, W. H. Tuning the Activity of Platinum(IV) Anticancer Complexes Through Asymmetric Acylation. *J. Med. Chem.* **2012**, *55*, 7571−7582.
(52) Wang, F.; Habtemariam, A.; van der Geer, E. P.; Fernandez, R.; Melchart, M.; Deeth, R. J.; Aird, R.; Guichard, S.; Fabbiani, F. P.; Lozano-Casal, P.; Oswald, I. D.; Jodrell, D. I.; Parsons, S.; Sadler, P. J. Controlling Ligand Substitution Reactions of Organometallic Complexes: Tuning Cancer Cell Cytotoxicity. *Proc. Natl. Acad. Sci. U. S. A.* **2005**, *102*, 18269−18274.
(53) Allardyce, C. S.; Dyson, P. J.; Ellis, D. J.; Heath, S. L. [Ru(η^6-*p*-cymene)Cl_2(pta)] (pta = 1,3,5-triaza-7-phosphatricyclo[3.3.1.1]-decane): A Water Soluble Compound that Exhibits pH Dependent DNA Binding Providing Selectivity for Diseased Cells. *Chem. Commun.* **2001**, *15*, 1396−1397.
(54) Aliende, C.; Perez-Manrique, M.; Jalon, F. A.; Manzano, B. R.; Rodriguez, A. M.; Cuevas, J. V.; Espino, G.; Martinez, M. A.; Massaguer, A.; Gonzalez-Bartulos, M.; de Llorens, R.; Moreno, V. Preparation of New Half Sandwich Ruthenium Arene Complexes with Aminophosphines as Potential Chemotherapeutics. *J. Inorg. Biochem.* **2012**, *117*, 171−188.
(55) Hull, J. W. J.; Gladfelter, W. L. η^4-Bonding in (Arene)ruthenium Complexes of Octamethylnapthalene. *Organometallics* **1982**, *3*, 605−613.
(56) Bennett, M. A.; Huang, T. N.; Matheson, T. W.; Smith, A. K.; Ittel, S.; Nickerson, W. η^6-Hexamethylbenzene)Ruthenium Complexes. *Inorg. Synth.* **1982**, *21*, 74−78.
(57) Bennett, M. A.; Smith, A. K. Arene Ruthenium(II) Complexes Formed by Dehydrogenation of Cyclo-hexadienes with Ruthenium-(III) Trichloride. *J. Chem. Soc., Dalton Trans.* **1974**, 223−241.
(58) *SMART*, version 5.628; Bruker AXS Inc.: Madison, WI, 2001.
(59) *SAINT+*, version 6.22a; Bruker AXS Inc.: Madison, WI, 2001.
(60) Sheldrick, G. W. *SADABS*, University of Gottingen: Gottingen, Germany, 2001.
(61) *SHELXTL*, version 6.14; Bruker AXS Inc.: Madison, WI, 2000.
(62) Quinn, P. J. Plasma Membrane Phospholipid Asymmetry. *Subcell. Biochem.* **2002**, *36*, 1−25.

dx.doi.org/10.1021/jm500455p | *J. Med. Chem.* XXXX, XXX, XXX−XXX

Results (Objective 2)

VI.D. Exchange of ruthenium to osmium in organometallic compound tunes redox potential and cancer cell selectivity via ROS and oxydo-reductase enzymes regulation.

Exchange of ruthenium to osmium in organometallic compounds tunes redox potential and cancer cell selectivity via ROS and oxydo-reductase enzyme regulation

Cynthia Licona,[†] Jean-Baptiste Delhorme,[†] Vania Vidimar,[†] Bastien Boff,[‡] Hugo Rico Bautista[#], Ricardo Cerón Camacho[#], Ronan Le Lagadec,[#] Jean-Noel Freund,[†] Isabelle Gross,[†] Georg Mellitzer,[†] Michel Pfeffer,[‡] and Christian Gaiddon[†*]

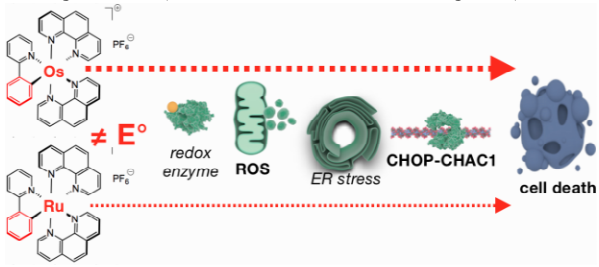
[†]INSERM 1113, Université de Strasbourg, FMTS, 3 av. Molière, 67200, Strasbourg, France

[‡]Institut de Chimie, UMR7177, Laboratoire de Synthèses Métallo-Induites, 4 rue Blaise Pascal, 67000, France

[#]Instituto de Química, UNAM, Circuito Exterior s/n, Ciudad Universitaria, México D. F. 04510, Mexico

KEYWORDS : Ruthenium; Osmium; anticancer drug; redox enzyme, p53, endoplasmic reticulum stress; NRF2; reactive oxygen species.

ABSTRACT: The exact physico-chemical determinants that account for the biological activity of metal-based anticancer drugs has yet to be clearly understood. We investigated the contribution of the metal and its redox-potential by comparing ruthenium and osmium-based compounds with the same structure. Switching from ruthenium to osmium atom while keeping identical ligands (N^C = 2-phenylpyridinato; N^N = 1,10-phenanthroline) does not change the spatial structure or the lipophilicity of organometallic compounds, but tunes the redox potential. The change in the redox potential of osmium-based compounds enhances its ability to modify redox enzyme activity and its cytotoxicity on multiple cell lines of various origins. This increased cytotoxicity does not correlate with increased affinity to DNA or activation of p53 signaling. However, it correlates with higher production of reactive oxygen species (ROS), Nrf2 activation and induction of endoplasmic reticulum stress pathway. Interestingly, ROS production and the activation of eif2α are not required for the cytotoxicity of the compounds, whereas the silencing of a specific member of CHOP, a marker of the ER stress pathway, diminishes it. This study represents a unique comprehensive physico-chemical and biological analysis highlighting the importance of the redox potential for the anticancer activity of cyclometalated compounds.



INTRODUCTION

Ruthenium- and osmium-based compounds are being intensively investigated as potential anticancer drugs encouraged by the long lasting successes of platinum-based drugs and the intrinsic physico-chemical properties of transition metals [1 2 3]. Although being the most advanced into the clinical trial process, the development of ruthenium-based compounds towards patients is handicapped by the diverse and controversial hypotheses on the physico-chemical determinant(s) relevant for their biological activity [4]. Indeed, multiple ruthenium- and osmium-based compounds have been designed with different ligands, such as half-sandwich "piano-stool" structures, and different types of bonds between the metal and the ligands (-O, -N, -C, -Cl…) [3 5]. This variety leads to a wide range of spatial structures, lipophilicities, metal charges (II to IV) and redox potentials. Such variety of physico-chemical properties may explain also the diversity of possible direct biological targets (DNA, Kinase, redox proteins) and induced signaling pathways (p53, ER stress - endoplasmic reticulum stress) [6-17]. However, the relative contribution of a specific physico-chemical property to a given effect on a direct target or signaling pathway remains often enigmatic. In particular, it is often difficult to estimate the exact contribution of the redox potential, the lipophilicity, the presence of bonds or special structures as by changing as given ligand, several of these characteristics are being modified. In an attempt to address this issue, we present here a comprehensive physico-chemical, cellular and *in vivo* biological analyses on a series of 4 cyclo-organometallic compounds with bidentate ligands that we selected to identify the relative contribution of the redox potential and the lipophilicity in their biological activity. We report that a switch from ruthenium to osmium modifies the redox potential evoking a strong increase in cytotoxicity and change in cancer cell selectivity via ROS and ER stress induction.

RESULTS AND DISCUSSION

Replacement of ruthenium by osmium alters redox potential and cell growth inhibition

Figure 1a shows the complexes depicted in this study. RDC11 and RDC34 synthesis and cytotoxicity have been in part previously

described [12,13,18,19]. The compounds are stable a RT-temperature over 24 hours (Figure S1a). In contrary to the addition of a second phenanthroline, the replacement of ruthenium by osmium does not significantly affect the spatial structure established by crystallography (Figures S1b) or the lipophilicity measured by phase separation assay (Log(Po/w), (Figure 1b). However, introduction of osmium causes a significant drop in the redox potential (E°1/2 M(III/II) value) (Figure 1b, S2a). The measures of oxygen consumption *via* a Clarke electrode show that the redox potential of the compound modifies its ability to alter *in vitro* the activity of the purified redox enzymes, glucose oxidase and peroxidase (Figure 1b). The addition of a second phenanthroline in RDC34 and ODC3 does not change the redox potential but improves the lipophilicity and changes the spatial structure, which also impact on the ability to alter redox enzyme function.

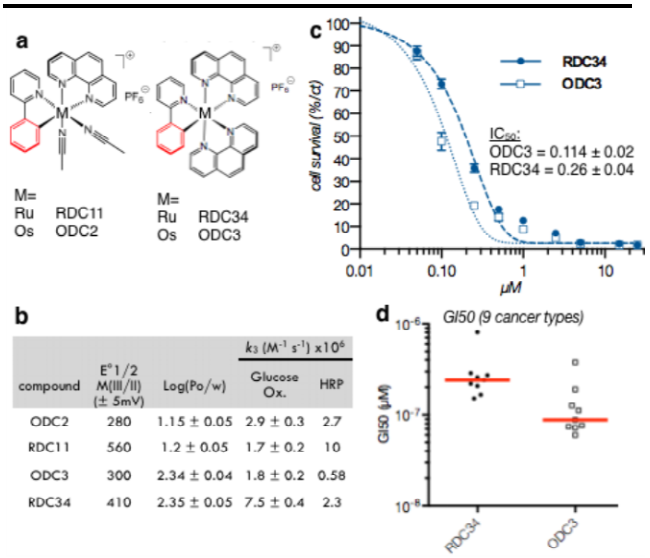


Figure 1. Structure (a) and physico-chemical properties (redox potential, lipophilicity, redox enzyme activities) (b) of the tested compounds. Cytotoxicity on HCT116 cells (MTT test; c) and on the NCI panel of 60 cancer cell lines (median of growth inhibition 50%, GI_{50}) grouped by organ origin (d).

The cytotoxicity of the drugs was tested in a panel of human cancer cell lines. The replacement of ruthenium by osmium decreases the IC_{50} values (concentrations reducing viability by 50%) of ODC2 and ODC3 in HCT116 cells measured by the MTT [3-(4,5-dimethylthiazol-2-yl)-2,5-diphenyltetrazolium bromide] assay (Figure 1b, S2b). The increase in activity was confirmed on the NCI panel of cancer cell lines, both on the GI_{50} (50% of growth inhibition, Figure 1d, S3a, b) and the LC_{50} (dose inducing 50% of lethality, Figure S3c, d). Importantly, ODC3 displayed a strong anti-proliferative activity in the nanomolar range. Furthermore, osmium-based drugs showed changes in selectivity since their activity improve mostly on colon, central nervous system and ovarian cell lines. Within cell lines of identical origin, change in selectivity was also observed since few cell lines were inversely sensitive toward ruthenium or -osmium drugs (Figure 2a).

Interestingly, osmium-based compounds are not significantly sensitive to selected drug exclusion processes (MXR1, MRP1) since there is no induction of their mRNA levels and an inhibitor of these processes does not favor significantly the activity of the drug (Figure S4a, b, c).

More detailed analyses showed that cyclo-organosmium compounds induce cell growth arrest and apoptosis as indicated by FACS analysis (Figure 2b) and confirmed by induction of the cell cycle arrest gene *p21* and the pro-apoptotic gene *noxa* (Figure S5a), and cleavage of caspase 3 and PARP (Figure S5b).

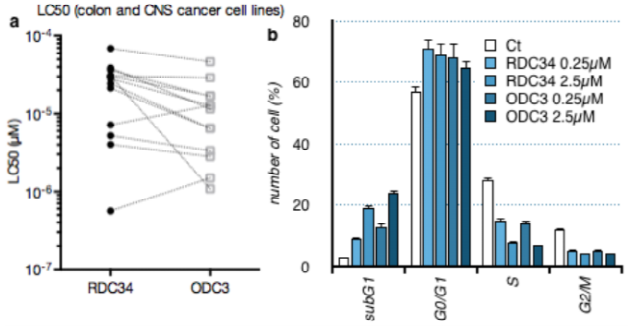


Figure 2. Activity of RDC34 and ODC3 on cell growth and cell death. Lethal concentration 50 (LC50) in cancer cell lines of colon and central nervous system origin of the NCI panel (a). Distribution of HCT116 cells in cell cycle phases after 48h of treatment (b).

Phenanthroline cyclometalated osmium compounds do not induce the p53 pathway

Previous studies using osmium compounds with one phenanthroline reported interaction with DNA and induction of cell death via p53 [14]. As previously observed with other phenanthroline-containing metallic drugs, ODC2 and ODC3 interact with a double-stranded plasmid DNA inducing a clear increase in the amount of nicked circular DNA when tested in gel electrophoresis (Figure 3a, S6a). Phosphorylation of H2Ax at serine 139 suggests the possibility that ODC compounds interact with DNA in cells (Figure S6b). However, ODC2 and ODC3 do not induce significantly p53 compared to oxaliplatin in HCT116 cells (Figure 3b). Furthermore, the average and mean of GI_{50} of ODC3 in mutated p53-expressing cells decreases compared to wild-type p53-expressing cells (Figure 3c, S6c), suggesting that ODC3 activity is independent from p53. In contrary and as expected, the GI_{50} of cisplatin increases (Figure 3d).

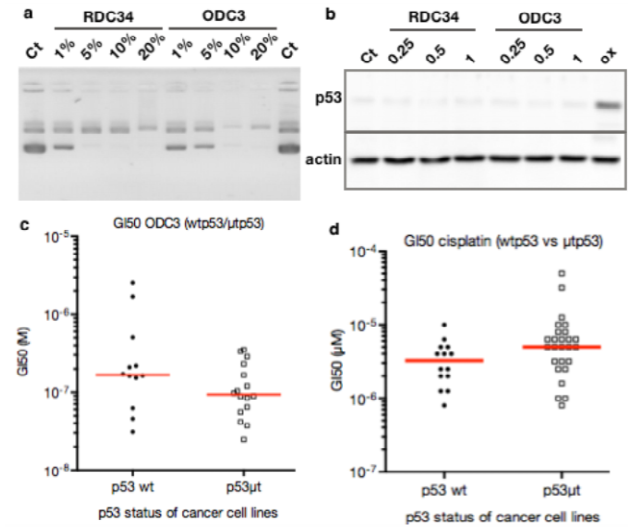


Figure 3. DNA interaction and p53 level induced by RDC34 and ODC3. Gel electrophoresis of plasmid DNA incubated with increasing

concentration of the compounds (a). p53 protein level induced by RDC34, ODC3 and cisplatin in HCT116 cells treated for 24h at the indicated concentration (μM). GI_{50} in mutated and wild type-expressing cancer cells from the NCI panel treated with ODC3 (c) or cisplatin (d).

Osmium compound ODC3 induces higher ROS level

As p53 seems not involved in ODC3 activity, we investigated alternate pathways. Based on the possibility that ODC3 alters the activity of redox enzymes (Figure 1b) that ultimately control the production of reactive oxygen species (ROS), we assessed whether the cytotoxicity of ODC3 might be dependent on ROS production. We measured ROS production using the fluorescent probe H2DFFDA in HCT116 cells after various times of treatment. As expected, after 16 hours of treatment, the compounds induce high levels of ROS (Figure S8a, b). Such late high levels of ROS are known to be part of the apoptotic process [20]. Even more interesting, cyclometalated compounds with phenanthroline induce a rapid production of ROS starting already one hour after treatment (Figure 4a). The levels are similar to the levels of ROS reached with the treatment of cells by a known superoxide inducer (menadione). Importantly, the rapid induction of ROS inversely correlates with the redox potential of the compounds since ODC3 is more active than RDC34.

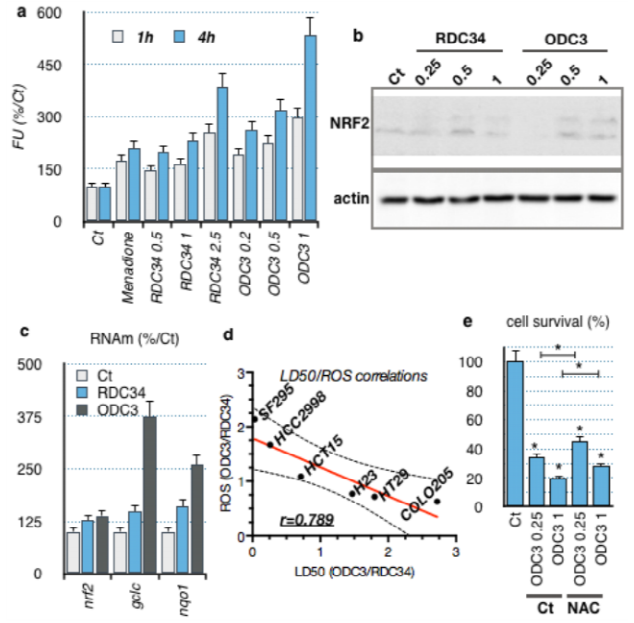


Figure 4. Correlation between radical oxygen species production and cytotoxicity of cyclo-organosmium compounds. Detection of ROS production by H2DFFDA fluorescent probe (a). Protein expression of NRF2 (b). mRNA expression of NRF2 target genes (c). Effect of ROS anti-oxidant N-acetyl cysteine (NAC) on ODC3 induced cytotoxicity (d). Correlation between the relative ROS production induced by RDC34 and ODC3 after 1 hour and their relative cytotoxicity in cancer cell lines (e).

To further establish the possible relationship between the rapid production of ROS and the biological activity of ODC compounds, the ROS-response pathway Nrf2, including *nrf2* and two of its target genes (*gclc* and *nqo1*), was investigated [21]. Western blot analyses and RT-qPCR showed that ODC3 induced Nrf2 (Figure 4b). In addition, Nrf2 target genes (*gclc* and *nqo1*) were also more strongly induced by ODC3 compared to RDC34 (Figure 4c). ROS were measured in several cancer cell lines that presented some selectivity either for RDC34 or for ODC3 (Figure 4d). To estimate the contribution of ROS production after one hour of treatment in the cytotoxicity of RDC34 or ODC3, we calculated the ratio of ROS production between ODC3 and RDC34 (ROS(ODC3)/ROS(RDC34)) and correlated it with the ratio of GI_{50} for ODC3 and RDC34 for each cell line. This analysis clearly showed that the sensitivity on a given cell line to RDC34 or ODC3 correlates well with the relative ability of ODC3 and RDC34 to induce ROS production after one hour of treatment. Hence, if a given cell line, such as COLO205, is more sensitive to RDC34 than ODC3, RDC34 induces in this cell line more ROS after one hour of treatment compared to ODC3. Inversely, a cell line more sensitive to ODC3, such as SF295, produces more ROS after one hour of treatment with ODC3 than with RDC34. To further establish the importance of the rapid production of ROS by ODC, we used the anti-oxidant NAC (N-acetyl cysteine). Cells were treated with ODC3 for 3 hours, in absence (Ct) or in presence of NAC. Interestingly, the inhibition of the early ROS production by NAC protected only partially cells from death (Figure 4e).

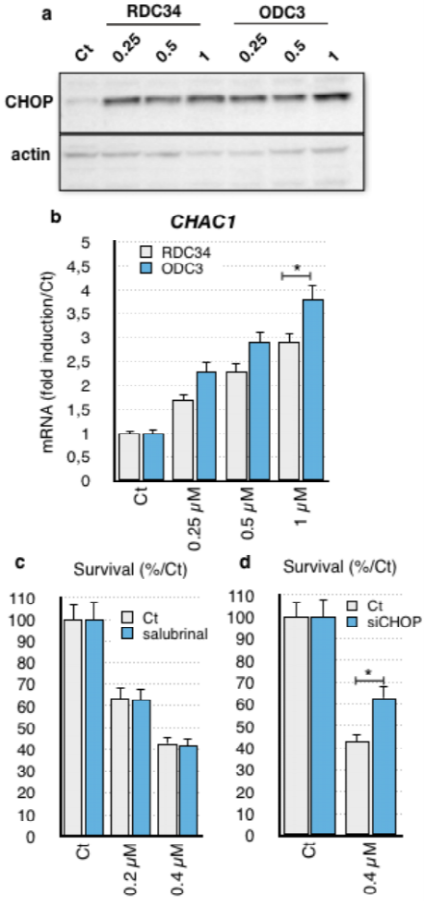


Figure 5. Role of the endoplasmic reticulum stress pathway in ODC cytotoxicity. CHOP protein expression detected by Western blot (a). RT-qPCR of CHOP target gene *chac1* (b). Effect of eif2a inhibition by salubrinal (c) or CHOP silencing by siRNA (d) on ODC3 cytotoxicity.

Phenanthroline cyclometalated osmium induced ER stress

We previously showed that cyclometalated RDC11 and RDC34 that contain phenanthroline induce the endoplasmic reticulum stress pathway (ER) [12 13]. Interestingly, a recent report shows that an osmium compound only coordinated to phenanthroline is unable to induce ER stress [14]. Therefore, we evaluated the expression of ER stress markers in cells treated with osmacycles ODC2 and ODC3 that we compared to RDC11 and RDC34. All compounds induced the pro-apoptotic ER stress transcription factor CHOP (Figure 5a, S7a, c) and its target gene, CHAC1 (Figure 5b, S7b, d). Interestingly, ODC3 displayed a stronger ability to induce CHOP and CHAC1 suggesting that the redox potential plays a role in the process. It also shows that a compound with phenanthroline can induce ER stress and that addition of a second phenanthroline favors it. To further understand the role of the ER stress in the biological activity of ODC3, we inhibited two effectors of the ER stress pathway, eif2a and CHOP. Inhibition of eif2a by salubrinal did not reduce the biological activity of ODC3 (Figure 5c). In contrast, the silencing of CHOP expression diminished the cytotoxicity induced by ODC3 (Figure 5d). These results suggest that ODC3 does not require the perk1-Eif2a component of the ER stress pathway, but does need for its activity the expression of the downstream effector CHOP. However, it is possible that the ODC3-regulated expression of CHOP might involve one of the two other components of the ER stress pathway, ATF6 or XBP1s [22].

In vivo biological properties of the compounds were investigated using mouse and syngeneic tumor models. Maximal tolerated dose (MTD, dose that induces no more than 20% of weight loss) and lethal dose 50 (LD_{50}, dose that induces death in 50% animals) were measured using Swiss mice. The replacement of ruthenium by osmium increases the toxicity of the compounds with one phenanthroline (ODC2), but decreases it in the context of two phenanthrolines (Figure S6). The anticancer properties of the compounds were tested on a syngeneic model that is subcutaneous injection of mouse lung cancer cells (3LL) into 7 weeks old female Swiss mice. IC50 of the compounds were established for 3LL cells *in vitro*. ODC3 is the most active on this cell line, followed by RDC34, ODC2 and then RDC11 (Figure S6). All compounds were injected intraperitonealy twice a week starting when tumors reached 100 mm^3 and over three weeks. All compounds were able to reduced tumor growth (Figure S6). Replacement of ruthenium by osmium induced a slight increase in the anticancer activity. Surprisingly, the increase of *in vitro* activity caused by the addition of a second phenanthroline does not correlate with a significantly improved *in vivo* activity. Hence, *in vivo* analyses indicated that the contribution of the redox and lipophilicity to the anticancer activity in animals does not correlate with the *in vitro* activity. Likely, additional variables are in play, such as the stability in the blood stream or the ability of the compounds to pass various biological barriers (cellular membrane, extracellular matrix...).

CONCLUSION

The exact contribution of the redox potential, the lipophilicity or the spatial architecture in the activity of the osmium compounds is yet debated due to the diversity of the compounds and their *in vivo* biological activity is not always documented. Here, we provide the first comprehensive description of the contribution of the redox potential into the improvement of the cytotoxic activity of cyclo-organosmium complexes and establish the importance of an early production of ROS and the induction of ER stress into this process. In addition, and to the best of our knowledge, it is the first report demonstrating that cyclometalated osmium complexes inducing ER stress display *in vivo* anticancer activity. Furthermore, the insight gained into the role of the redox potential in the biological activity of these compounds constitute a significant step toward the design of more efficient and less expensive small molecules that could target cancers cells more efficiently.

ASSOCIATED CONTENT

Supporting Information. Additional description of structure, stability and biological properties of the compounds are presented in supplementary figures S1 to S10. Complete experimental procedures are also provided. This material is available free of charge via the Internet at http://pubs.acs.org.

AUTHOR INFORMATION

Corresponding Author

* Christian Gaiddon, gaiddon@unistra.fr

Author Contributions

All authors have given approval to the final version of the manuscript.

Notes

The authors declare non-competing financial interest.

ACKNOWLEDGMENT

This work is supported by CNRS, Ligue contre le cancer, ARC, COST CM1105, DGAPA-UNAM (PAPIIT Project IN204812) and CONACyT (Project 153151 and scholarship to HRB). We are thanking E. Martin for all her help with her tissue culture expertise and support. We also acknowledge L. Mathern for her administrative support.

ABBREVIATIONS

ER: endoplamic reticulum; RDC: ruthenium-derived compound; ODC: osmium-derived compound; ROS: reactive oxygen species; NCI: National Cancer Institute;

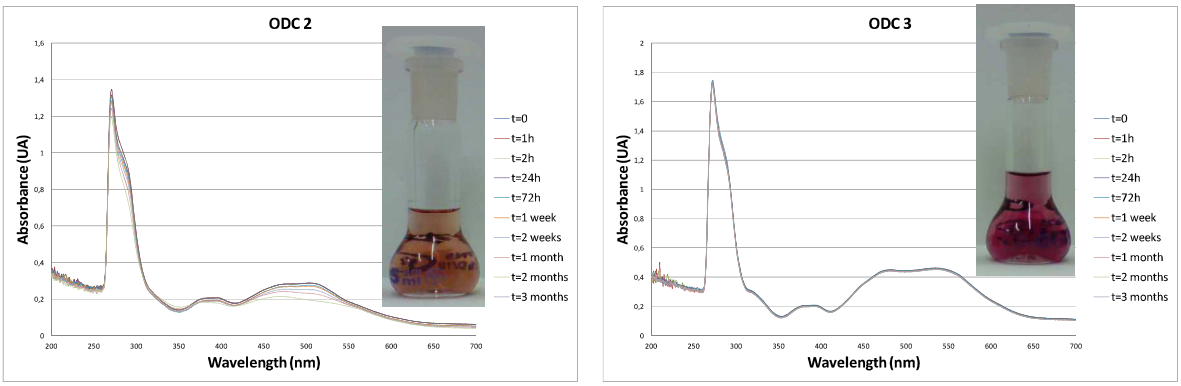
REFERENCES

(1) Jakupec, M. A.; Galanski, M.; Arion, V. B.; Hartinger, C. G.; Keppler, B. K. *Dalton Trans* **2008**, 183.
(2) Kelland, L. *Nat Rev Cancer* **2007**, *7*, 573.
(3) Gasser, G.; Ott, I.; Metzler-Nolte, N. *Journal of medicinal chemistry* **2011**, *54*, 3.
(4) Bergamo, A.; Gaiddon, C.; Schellens, J. H.; Beijnen, J. H.; Sava, G. *J Inorg Biochem* **2012**, *106*, 90.
(5) Hanif, M.; Babak, M. V.; Hartinger, C. G. *Drug Discov Today* **2014**.
(6) Mei, H. Y.; Barton, J. K. *Proc Natl Acad Sci U S A* **1988**, *85*, 1339.
(7) Brabec, V. *Prog Nucleic Acid Res Mol Biol* **2002**, *71*, 1.
(8) Zeglis, B. M.; Pierre, V. C.; Barton, J. K. *Chem Commun (Camb)* **2007**, 4565.
(9) Gaiddon, C.; Jeannequin, P.; Bischoff, P.; Pfeffer, M.; Sirlin, C.; Loeffler, J. P. *J Pharmacol Exp Ther* **2005**, *315*, 1403.
(10) Hayward, R. L.; Schornagel, Q. C.; Tente, R.; Macpherson, J. S.; Aird, R. E.; Guichard, S.; Habtemariam, A.; Sadler, P.; Jodrell, D. I. *Cancer Chemother Pharmacol* **2005**, *55*, 577.
(11) Smalley, K. S.; Contractor, R.; Haass, N. K.; Kulp, A. N.; Atilla-Gokcumen, G. E.; Williams, D. S.; Bregman, H.; Flaherty, K. T.; Soengas, M. S.; Meggers, E.; Herlyn, M. *Cancer Res* **2007**, *67*, 209.
(12) Meng, X.; Leyva, M. L.; Jenny, M.; Gross, I.; Benosman, S.; Fricker, B.; Harlepp, S.; Hebraud, P.; Boos, A.; Wlosik, P.; Bischoff, P.; Sirlin, C.; Pfeffer, M.; Loeffler, J. P.; Gaiddon, C. *Cancer Res* **2009**.
(13) Vidimar, V.; Meng, X.; Klajner, M.; Licona, C.; Fetzer, L.; Harlepp, S.; Hebraud, P.; Sidhoum, M.; Sirlin, C.; Loeffler, J. P.; Mellitzer, G.; Sava, G.; Pfeffer, M.; Gaiddon, C. *Biochem Pharmacol* **2012**, *84*, 1428.
(14) Suntharalingam, K.; Johnstone, T. C.; Bruno, P. M.; Lin, W.; Hemann, M. T.; Lippard, S. J. *J Am Chem Soc* **2013**, *135*, 14060.
(15) Ang, W. H.; De Luca, A.; Chapuis-Bernasconi, C.; Juillerat-Jeanneret, L.; Lo Bello, M.; Dyson, P. J. *ChemMedChem* **2007**.

(16) Dougan, S. J.; Habtemariam, A.; McHale, S. E.; Parsons, S.; Sadler, P. J. *Proc Natl Acad Sci U S A* **2008**, *105*, 11628.
(17) Gava, B.; Zorzet, S.; Spessotto, P.; Cocchietto, M.; Sava, G. *J Pharmacol Exp Ther* **2006**, *317*, 284.
(18) Klajner, M.; Hebraud, P.; Sirlin, C.; Gaiddon, C.; Harlepp, S. *J Phys Chem B* **2010**, *114*, 14041.
(19) Klajner, M.; Licona, C.; Fetzer, L.; Hebraud, P.; Mellitzer, G.; Pfeffer, M.; Harlepp, S.; Gaiddon, C. *Inorganic chemistry* **2014**, *53*, 5150.
(20) Simon, H. U.; Haj-Yehia, A.; Levi-Schaffer, F. *Apoptosis : an international journal on programmed cell death* **2000**, *5*, 415.
(21) Kaspar, J. W.; Niture, S. K.; Jaiswal, A. K. *Free Radic Biol Med* **2009**, *47*, 1304.
(22) Nagelkerke, A.; Bussink, J.; Sweep, F. C.; Span, P. N. *Biochim Biophys Acta* **2014**, *1846*, 277.

Figure S1

a



b

Cristal structure data

[Os(o-C_6H_4py-κC,N)(phen)$(NCMe)_2$]PF_6 **(ODC 2)**

The [Os(o-C_6H_4py-κC,N)(phen)$(NCMe)_2$]PF_6 was synthesised according to reference 25.

Anal. calcd. for $C_{27}H_{22}F_6N_5OsP \cdot 0.5\ CH_2Cl_2$:
C, 41.59; H, 2.92; N, 8.82. Found: C, 41.69; H, 2.91; N, 8.64
MS (ES, m/z): Calcd. for $C_{27}H_{22}N_5{}^{192}Os$: 608.1490 (M); Found: 608.149
IR (cm^{-1}): 2265 (medium, νN≡C), 841 (strong, νPF), 560 (medium, νPF)
^{1}H NMR (300 MHz, CD_3CN, 300K): 9.57 (dd, 1H, $^3J_{HH}$=5.2, $^4J_{HH}$=1.1, H_o), 8.48 (dd, 1H, $^3J_{HH}$=8.1, $^4J_{HH}$=1.1, H_p), 8.21 (dd, 1H, $^3J_{HH}$=7.5, $^4J_{HH}$=1.1, H_{12}), 8.17 (d, 1H, $^3J_{HH}$=9.0, H_{phen}), 8.09-8.15 (m, 1H, H_m), 8.07 (d, 1H, $^3J_{HH}$=9.0, H_{phen}), 7.99-8.05 (m, 2H, H_o +H_m ou H_p), 7.83-7.89 (m, 2H, H_5 et H_9), 7.30-7.39 (m, 2H, H_6 + H_m ou H_p), 7.25 (td, 1H, $^3J_{HH}$=7.2, $^4J_{HH}$=1.3, H_{11}), 7.19 (d, 1H, $^3J_{HH}$=6.2, H_8), 6.98 (t, 1H, $^3J_{HH}$=7.5, H_{10}), 6.51 (td, 1H, $^3J_{HH}$=6.2, $^4J_{HH}$=1.3, H_7), 2.64 (s, 3H, $NCCH_3$), 2.32 (s, 3H, $NCCH_3$)
^{13}C {^{1}H} NMR (78 MHz, CD_3CN, 300K) : 191.7, 155.2, 151.1, 150.1, 145.9, 138.1, 135.6, 135.5, 134.1, 130.1, 128.3, 127.5, 127.4, 125.9, 124.2, 123.8, 121.0, 120.5

[Os(*o*-C_6H_4py-κC,N)$(phen)_2$]PF_6 **(ODC 3)**

The [Os(*o*-C_6H_4py-κC,N)$(phen)_2$]PF_6 was synthesised according to reference 25.

Anal. calcd. for $C_{35}H_{24}F_6N_5OsP \cdot CH_2Cl_2$:
C, 46.26; H, 2.80; N, 7.49. Found: C, 46.36; H, 3.22; N, 7.69
MS (ES, m/z): Calcd. for $C_{35}H_{24}N_5{}^{192}Os$: 706.1647 (M); Found: 706.165
IR (cm^{-1}): 843 (strong, νPF), 565 (medium, νPF)
^{1}H NMR (300 MHz, CD_3CN, 300K): 8.41 (dd, 1H, $^3J_{HH}$ =5.5, $^4J_{HH}$=1.2, H_o), 8.34 (dd, 1H, $^3J_{HH}$=5.5, $^4J_{HH}$=1.2, H_o), 8.24 (dd, 1H, $^3J_{HH}$=8.1, $^4J_{HH}$=1.2, H_p), 8.1-7.99 (m, 8H), 7.95-7.88 (m, 2H), 7.81 (d, 1H, $^3J_{HH}$=8.1, $^4J_{HH}$=1.2, H_p), 7.55 (dd, 1H, $^3J_{HH}$=8.1, $^3J_{HH}$=5.5, H_m), 7.48 (m, 3H), 7.38 (d, 1H, $^3J_{HH}$=5.5), 7.25 (dd, 1H, $^3J_{HH}$=8.1, $^3J_{HH}$=5.5, H_m), 7.80-7.72 (m, 2H), 6,65 (td, 1H, $^3J_{HH}$=7.4, $^4J_{HH}$=1.3), 6.08 (dd, 1H, $^3J_{HH}$=7.4, $^4J_{HH}$=0.9)
^{13}C {^{1}H} NMR (78 MHz, CD_3CN, 300K): 155.2, 150.4, 150.2, 150.1, 149.7, 136.0, 135.1, 134.2, 133.6, 132.4, 132.3, 129.3, 128.0, 127.8, 127.7, 126.1, 125.8, 125.7, 124.5, 122.7, 120.9, 118.7

Figure S1: Stability and structure data of ODC2 and ODC3
a, Evolution of ODC2 and ODC3 stability over the time as measured by spectrometry

b, Cristal structure data for ODC2 and ODC3

Figure S2

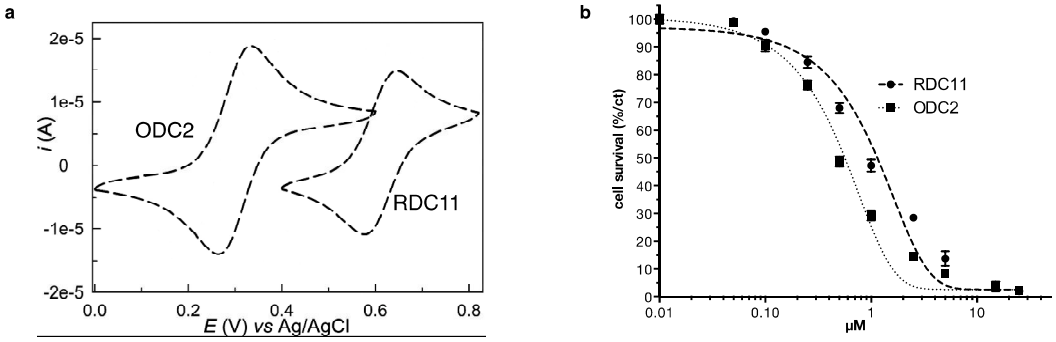


Figure S2: Redox potential and cytotoxicity of ODC2 and RDC11
a, Diagram representing the redox potential of ODC2 and RDC11
b, Cytotoxicity of RDC11 and ODC2 tested in HCT116 cells by MTT assays (n=8).

Figure S3

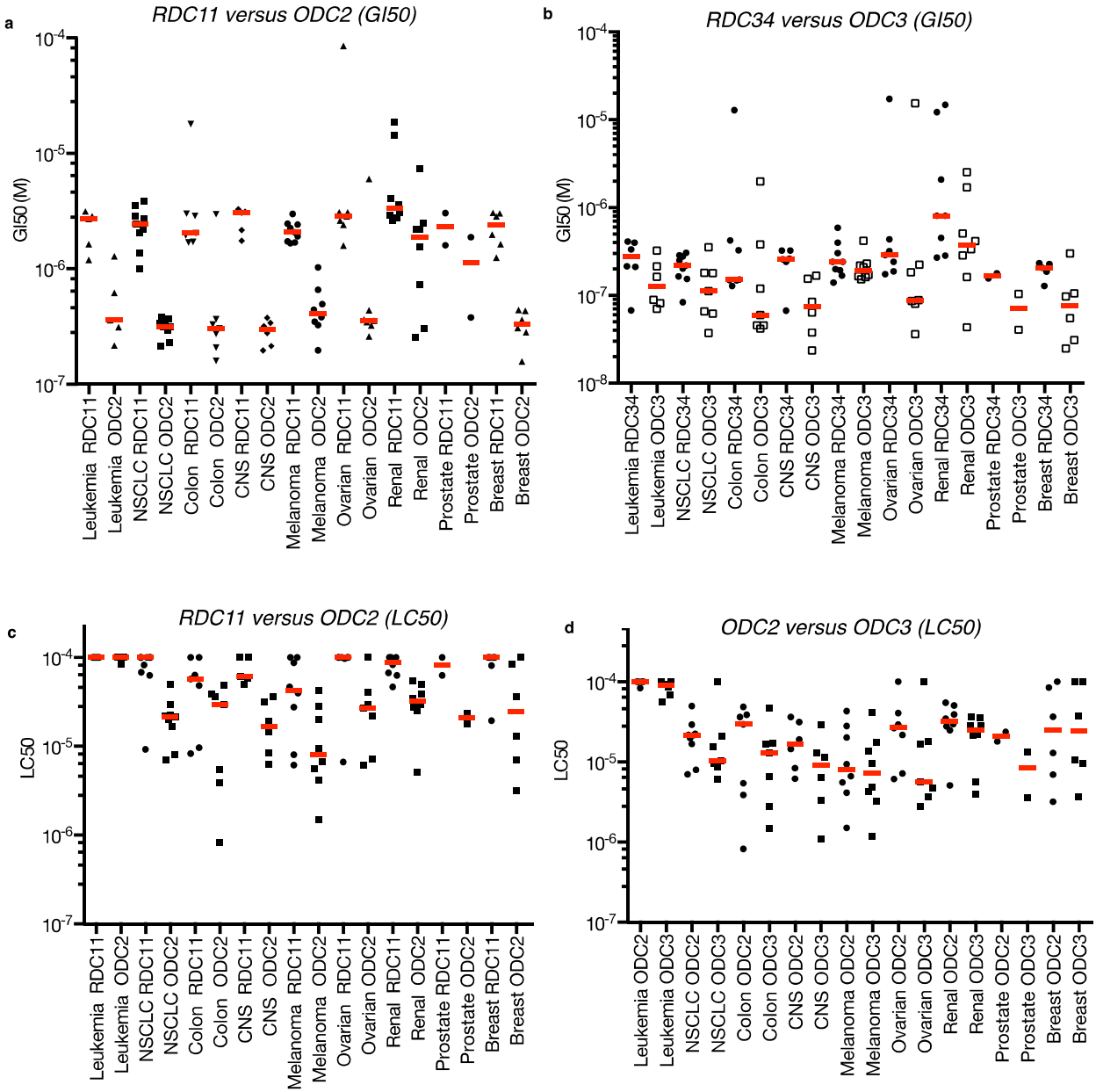


Figure S3: Cell growth and cytotoxicity of ODC2 and ODC3 compared to RDC11 and RDC34, respectively, on the 60 cancer cell lines of the National Cancer Institute

a, **b**, Diagrams representing the concentration for 50% of cell growth inhibition (GI_{50}). NCI cancer cell lines were grouped by cancer origins. Each point indicate a cell line. Red line indicate the median.

c, d, Diagrams representing the concentration for 50% of cell lethality (LC_{50}). NCI cancer cell lines were grouped by cancer origins. Each point indicate a cell line. Red line indicate the median.

Figure S4

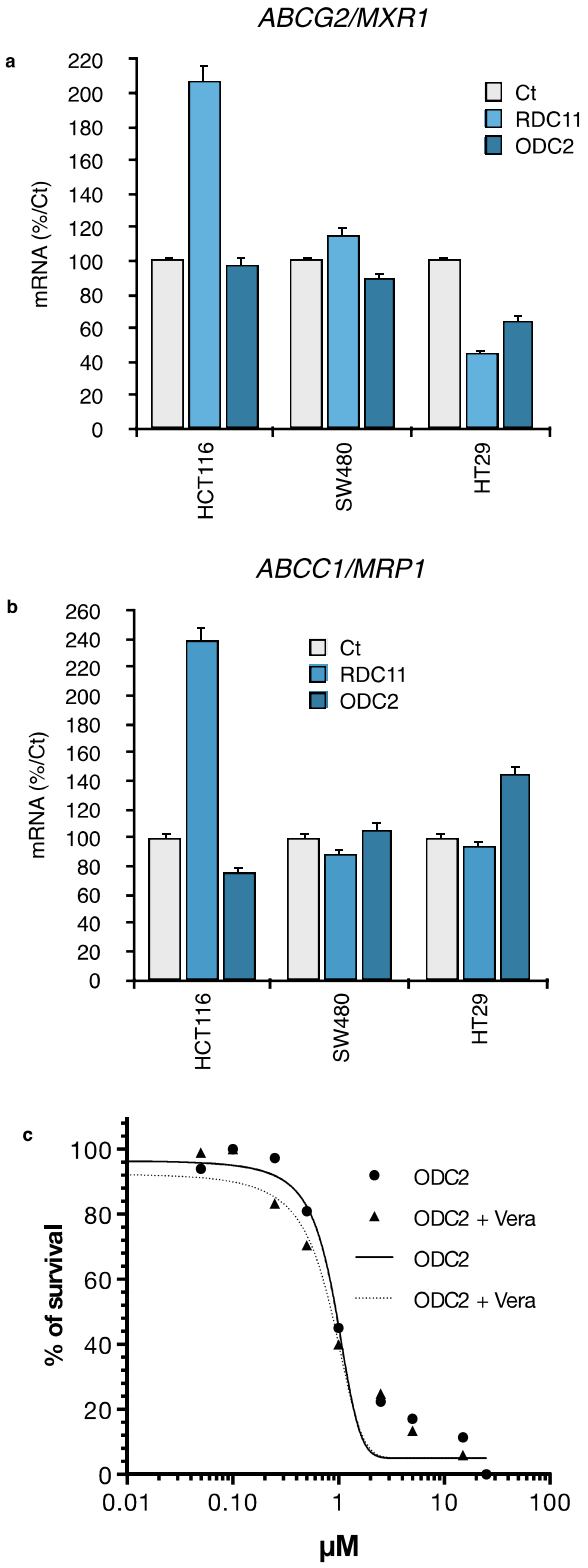


Figure S4: Gene expression of export proteins (ABCG2, ABCC1) and effect of export inhibiteur verapamil on ODC2 activity activity.
a, **b**, mRNA levels of two known drug export proteins (ABCG2 and ABCC1) in the indicated colon cancer cell lines treated with ODC2 or RDC11 at their IC_{50}. mRNA levels were assessed by RT-qPCR.
c, Effect of Verapamil on ODC2 cytotoxicity in HCT116.

Figure S5

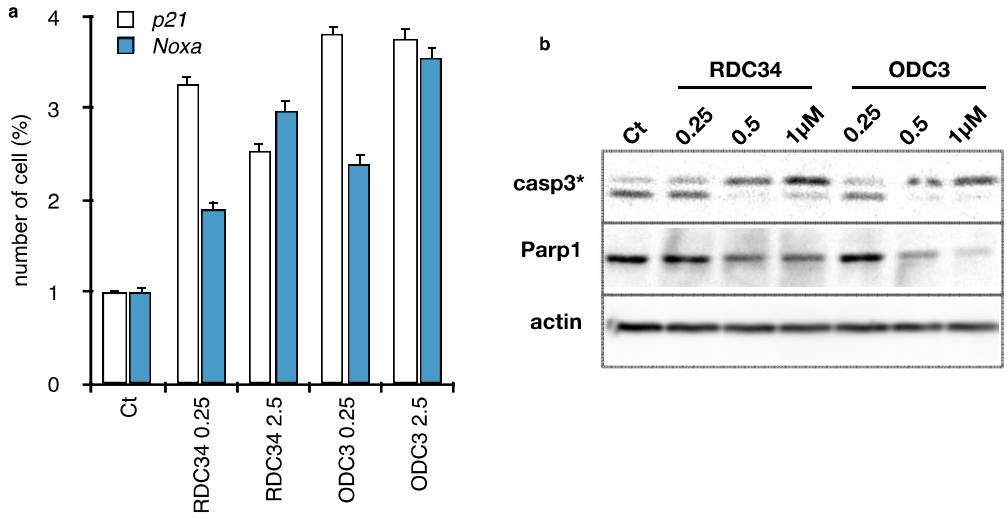
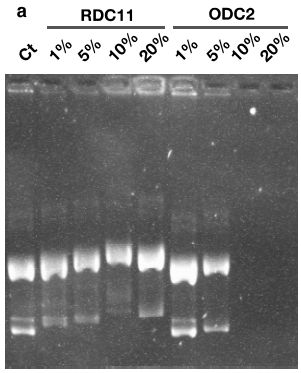
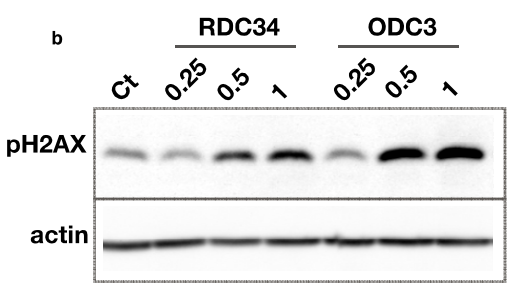


Figure S5: Expression of apoptosis markers.
a, mRNA levels of two known p53 target genes (*p21* and *noxa*) in the indicated colon cancer cell lines treated with RDC34 or ODC3 at the indicated concentrations. mRNA levels were assessed by RT-qPCR.
c, Clivage of caspase 3 (casp3*) and Parp1 detected by western blot in HCT116 cells treated with RDC34 or ODC3 at the indicated concentrations.

Figure S6





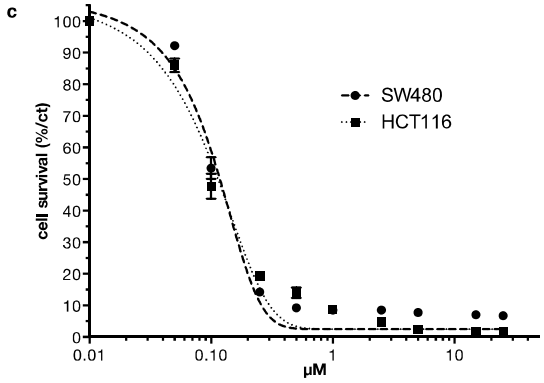


Figure S6: Interaction of RDC and ODC with DNA and role of p53
a, Migration of plasmidic DNA on an 1% agarose gel after incubation of the DNA with increasing quantity of RDC11 or ODC2 for 20 hours. Quantity is indicated as number of RDC or ODC for 100 base pairs (%).
b, Detection of H2AX phosphorylation by Western blot from protein extract of HCT116 treated with RDC34 or ODC3 at the indicated concentration.
c, Cytotoxicity of ODC3 in HCT116 cells (wild type for p53) and SW480 (mutated and inactivated p53). Cell viability was assessed by MTT assay.

Figure S7

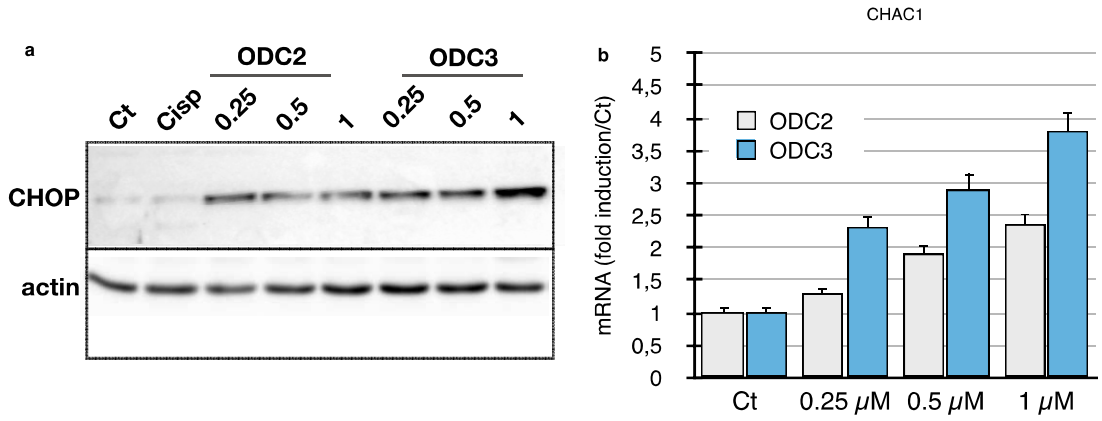


Figure S7: Expression of markers for the ER stress in ODC2 and ODC3 treated cells.
a, Protein expression of CHOP in cells treated with ODC2 or ODC3 and detected by Western blot. Actin was use as loading control.
b, mRNA levels of CHAC1 in cells treated with ODC2 or ODC3 at the indicated concentrations. mRNA levels were assessed by RT-qPCR.

Figure S8

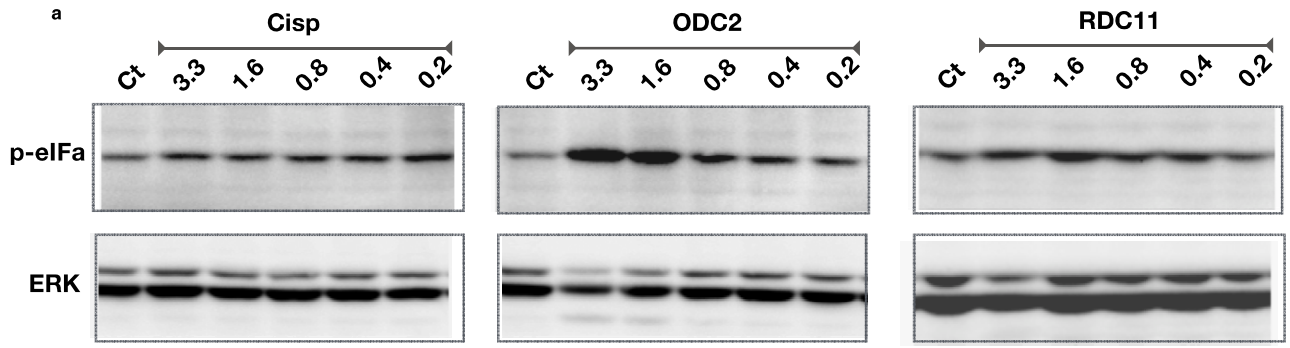


Figure S8: Phosphorylation of eif2a upon treatment with cisplatin, ODC2 and RDC11.
a, Phosphorylation of eif2a (p-eif2a) was detected by Western blot in protein extract of cells treated with cisplatin, ODC2 or RDC11 at the indicated concentration (μM). ERK was use as loading control.

Figure S9

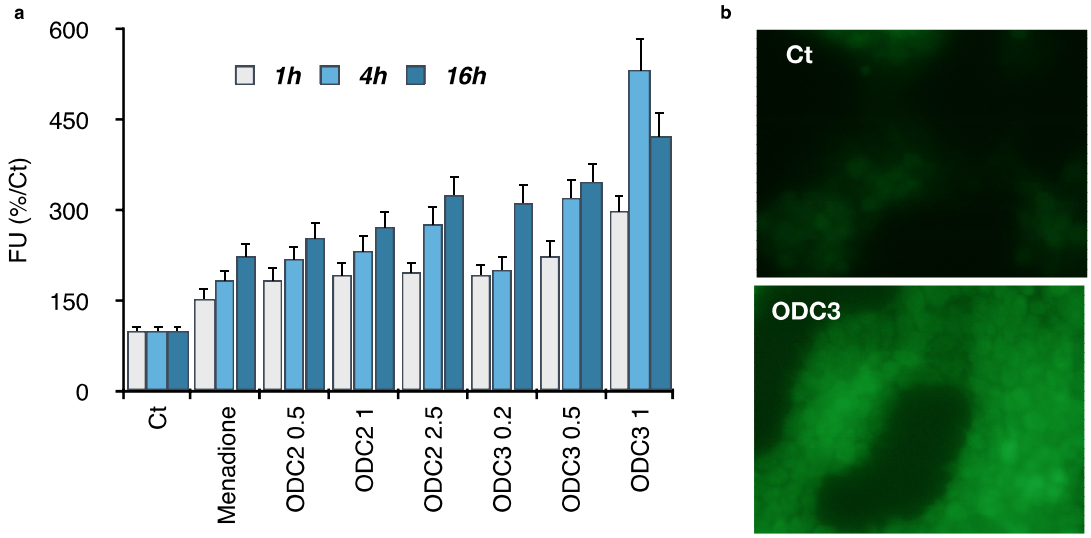
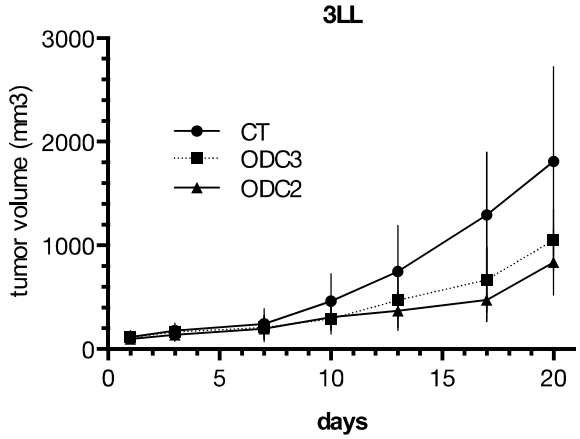


Figure S9: Production of reactive oxygen species induced by ODC2 and ODC3.
a, Levels of ROS detected by the carboxy-H2DCFDA ROS probe after treatment with the indicated concentration (µM) and time.
b, Fluorescence image of cells incubated with the ROS probe at 24h and 0.3µM of ODC3.

Figure S10

a



b

compound	IC50 (µM)	MTD *(µmole/Kg)*	LD50 *(µmole/Kg)*	3LL Tumor growth (T/C)
ODC2	0.84 ± 0.15	7,5	15	55 ± 8
ODC3	0.15 ± 0.2	5	10	60 ± 7
RDC11	1.5 ± 0.3	26	54	58 ± 5
RDC34	0.25 ± 0.2	2,5	7.5	62 ± 6

Figure S10: In vivo properties of ODC2 and ODC3.
a, Growth curve of 3LL syngeneic tumors implanted in 8 weeks old black 6 mice. Mice were treated with ODC2 or ODC3 when tumors reached 100mm^3. Drugs were injected twice a week at the MTD/
b, Table indicating the in vivo biological activity of ODC2,ODC3, RDC11 and RDC34. MTD (maximal tolerated dose, dose that induces less than 20% of weight loss), LD50 (Lethal dose 50%, dose that induces the death of 50% of the animals), Tumor growth (T/C; ratio of volume tumor between the treated and control mice.

Supplementary material and methods

Chemicals

Salubrinal and NAC were purchased from SIGMA. RDC11 [1], RDC34 [2], ODC2 and ODC3 [3] were synthesized according to published procedures. All complexes were purified over chromatography columns carried out on Merk aluminum oxide 90 standardized. Complexes were used with a purity >98%, as demonstrated by several protocols [2,3]. ES-MS spectra and elemental analyses were carried out by the corresponding facilities at the Institut de chimie, Universite´ de Strasbourg and at the Service Central d'Analyse du CNRS, Vernaison.

Cell cultures

HCT116 and SW480 cells were obtained from ATCC. Cells were manipulated and cultured in DMEM with 10% FCS (Dominique Dutcher™) and 1% Penicillin + Streptomycin (Sigma) at 37°C with 5% CO_2 atmosphere as previously described [4].

Cell survival and flow cytometer analysis

2000 cells were seeded per well in 96-well microplates (Falcon Multiwell), 48 h prior to any treatment. Cisplatin and menadione (Sigma) were applied for 48 h in fresh medium. MTT assay was performed as previously described by replacing the medium with fresh medium supplemented with 5 mg/L MTT (Sigma) for 1h [5]. Cells were lysed in isopropanol with 0.04 N HCl. Measurements were performed at 550 nm.

For DNA content analysis and distribution in the cell cycle, the fluorescence of 10,000 cells was analyzed using a FACScan flow cytometer and CellQuest software (Becton Dickinson, San Jose´, CA). Cells were labeled with propidium ionide as previously described [6].

Quantitative PCR

Cultured cells were lysed with 1ml of TRIzol per 10 cm^2. Mice were sacrificed by cervical dislocation, hindlimb gastrocnemius muscles were sampled, immediately frozen in liquid nitrogen and stored at -80°C for later use. 1 ml TRIzol (Invitrogen) per 150 mg of muscle was used to extract RNA according to manufacturer's instructions. RNA samples were ethanol-precipitated twice and 1 µg was used for reverse transcription (High-Capacity cDNA Reverse Transcription Kit, Applied Biosystems). qPCR was performed using 2 ng/µl cDNA (RNA equivalent) according to manufacturer's instructions (SYBR Green PCR Master Mix, Applied Biosystems) and with 400 µM of each primer (Supplemental data, table 1). Expression levels were normalized using average of 18S and TBP expression.

Statistical analysis

Statistical analyses were realized using a one-way ANOVA test followed by a Tukey post-test allowing a comparison between all the conditions. * Indicate statistical differences in graphs. Statistical Analyses were performed using Prism (GraphPad software).

Western blot

Cells were lysed as previously described with a lysis buffer (125 mM Tris-HCl pH 6.7, NaCl 150 mM, NP40 0.5%, 10% Glycerol) [7]. Proteins were denatured and deposed (75 µg of proteins) on 10% SDS-PAGE gel. Western blots were performed using antibodies raised against CHOP (1/1000 dilution, Santa Cruz, CA), H2AX (S139) (1/2000,

Millipore, France), p53 (FL393, 1/1000, Santacruz), NRF2 (1/500, Santacruz) and incubated with the blots overnight. Secondary antibodies (anti-rabbit, anti-mouse: Sigma, MA) were incubated at 1:1000 for 2 hours. Equal loading of the samples was controlled visualizing actin expression (rabbit anti- β-actin, Sigma, 1:4000).

Glucose oxidase activity measure

The measurements were made using a homemade Clark electrode with a mylar surface (YSI Yellow springs) equipped with a probe YSI 5331 in a 1.5 mL cell, the temperature of which was controlled at 25 °C. The calibration was performed as follows. The glass cell was filled with distilled water at 25 °C with stirring and a voltage was recorded. Then the cell was cleaned and filled with the previously deoxygenated water (in vacuum and bubbled with argon) and a lower voltage was recorded. A drop in 0.06 V was referred to 1.21×10^{-3} M of O_2 ($[O_2]$ in water at 25 °C). The buffer was first added into the cell followed by a ruthenium complex solution and GO. The solution was stirred and the recording device was turned on. The reaction was initiated by the addition of a solution of *D*-glucose after 20 s and the cell was immediately sealed. Time intervals between readings were in the range of from 3 to 10 min depending on the concentration of *D*-glucose, which was varied in the range of from 0.0025 M to 0.1 M. The concentrations of ruthenium complexes used are indicated in legends to Figures. Each measurement was made at least in duplicate.

Intracellular reactive oxygen species (ROS) measurement

5-(and-6)-carboxy-2',7'-dichlorodihydrofluorescein diacetate (carboxy-H2DCFDA) (Molecular Probes) was used to detect intracellular ROS levels according to the manufacturer's instructions and as previously described [8]. For ROS quantification, cells were seeded in 96-well black plates (Greiner Bio-One) and treated with RDCs at the indicated concentrations and times. Afterwards, cells were washed with PBS and incubated with 10μM carboxy-H2DCFDA in DPBS for 1h. Cells were then washed with PBS and fluorescence was measured by a plate reader (Perkin Elmer) with an excitation wavelength of 485 nm and an emission wavelength of 535 nm.

siRNA silencing

CHOP siRNAs against human CHOP were purchased form Dharmacon (DDIT smart pool siRNA). SiRNAs were transfected in cells using Lipofectamine 2000 (Invitrogen) as described previously

Primers

All primers were designed in regions flanking introns to exclude data alteration by possible DNA contamination.
18S: forward 5'-CGT CTG CCC TAT CAA CTT TCG-3'; reverse 5'-TTC CTT GGA TGT GGT AGC CG-3'.
TBP: forward 5'-CCA ATG ACT CCT ATG ACC CCT A-3'; reverse 5'-CAG CCA AGA TTC ACG GTA GAT-3'.
CHAC1: forward 5'- CCT GCT ACC CTG CTC TTA CCT-3' ; reverse 5'- GAG CTT GGC TCC TCA GGT C-3'

References

(1) Ryabov, A. D.; Kurova, V. S.; Ivanova, E. V.; Le Lagadec, R.; Alexandrova, L. *Anal Chem* **2005**, *77*, 1132.
(2) Fetzer, L.; Boff, B.; Ali, M.; Xiangjun, M.; Collin, J. P.; Sirlin, C.; Gaiddon, C.; Pfeffer, M. *Dalton Trans* **2011**, *40*, 8869.
(3) Boff, B.; Gaiddon, C.; Pfeffer, M. *Inorganic chemistry* **2013**, *52*, 2705.
(4) Sohm, F.; Gaiddon, C.; Antoine, M.; Boutillier, A. L.; Loeffler, J. P. *Oncogene* **1999**, *18*, 2762.
(5) Gaiddon, C.; de Tapia, M.; Loeffler, J. P. *Mol Endocrinol* **1999**, *13*, 742.
(6) Vidimar, V.; Meng, X.; Klajner, M.; Licona, C.; Fetzer, L.; Harlepp, S.; Hebraud, P.; Sidhoum, M.; Sirlin, C.; Loeffler, J. P.; Mellitzer, G.; Sava, G.; Pfeffer, M.; Gaiddon, C. *Biochem Pharmacol* **2012**, *84*, 1428.
(7) Gaiddon, C.; Tian, J.; Loeffler, J. P.; Bancroft, C. *Endocrinology* **1996**, *137*, 1286.

(8) Gaiddon, C., Mercken, L, Bancroft, C, and Loeffler, JP *Endocrinology* **1995**, *136*, 4331.

VII. Results (Objective 3)

VII.A. Design of porphyrin-dota-like scaffolds as all in one multimodal heterometallic complex for medical imaging.

EurJOC European Journal of Organic Chemistry

FULL PAPER

DOI: 10.1002/ejoc.201300678

Design of Porphyrin-dota-Like Scaffolds as All-in-One Multimodal Heterometallic Complexes for Medical Imaging

Antoine Eggenspiller,[a] Clément Michelin,[a] Nicolas Desbois,[a] Philippe Richard,[a] Jean-Michel Barbe,[a] Franck Denat,[a] Cynthia Licona,[b] Christian Gaiddon,*[b] Amira Sayeh,[c] Philippe Choquet,[c,d] and Claude P. Gros*[a]

Keywords: Imaging agents / Porphyrinoids / Gadolinium / Copper / Cytotoxicity

A series of four multimodal ligands incorporating one porphyrin moiety and one or more dota-like macrocycles all-in-one in the same molecular architecture have been synthesized and full characterized. The corresponding gadolinium(III) complexes were also synthesized and heterometallic complexes incorporating both gadolinium(III) and copper(II) ions were prepared as potential MRI/PET multimodal contrast agents. One ligand (**L4**) includes an amine moiety that can be activated for easy conversion into an isothiocyanate group for further anchoring to a biological vector. Preliminary relaxivity, cytotoxicity, and MRI studies showed that the complexes developed in this work are very promising medical-imaging agents for the enhancement of contrast in bimodal MRI techniques.

Introduction

Nowadays, noninvasive imaging modalities are commonly used tools for diagnostic and treatment efficiency evaluations for several diseases. Since its discovery in the 1970s, magnetic resonance imaging (MRI) has become one of the most powerful imaging tools. Indeed, the MRI technique does not employ any ionizing radiation, provides very good spatial resolution (by producing 3D images), and allows good contrast for soft tissues in comparison with computed tomography (CT). In almost 30% of MRI analyses, contrast enhancement is needed and is mainly based on gadolinium(III) complexes acting as contrast agents (CAs).[1] Clinically used MRI CAs reduce the relaxation time (Gd is used for T_1-weighted imaging and iron oxide is often used for T_2-weighted imaging) of water protons inducing a brighter signal in the final image. However, the major drawback of MRI is its poor sensitivity and the non-specificity of CAs.[2] Other nuclear imaging techniques, such as positron emission tomography (PET), single photon emission computed tomography (SPECT), optical imaging, and fluorescence-mediated tomography, are very specific and sensitive methods, but suffer low anatomical resolution.[3] These imaging modalities require a fluorescent dye for optical imaging or a radiotracer for nuclear imaging, which requires a radioactive element to operate. In the last decade, the concept of coupling different imaging modalities to overcome the main drawbacks and maintain or enhance the key advantages of each technique has emerged.[4] MRI multimodal imaging needs specific CAs to guarantee the same biodistribution of the specific tracers. To achieve this identical biodistribution, all-in-one molecular structures incorporating different specific CAs have been designed for use, for example, in noninvasive imaging, molecular diagnosis, and in the photothermal treatment of diseases such as cancer.[5] The ability to use the same multimodal CA for multiple imaging techniques is very advantageous owing to the reduced amount of foreign material required (and injected into the patient), the time saved (only one examination), and the increased amount of information made available at the same time.

In our case, we were particularly interested in the all-in-one incorporation of different metallic centers of medical imaging interest into the same molecular structure. The bimodal contrast agents should strongly coordinate the metallic species to avoid any toxicity effect caused by *trans* chelation or *trans* metalation under biological conditions. To easily create a heterobimetallic complex, we employed two specific ligands within the same molecular structure. A

[a] Université de Bourgogne, ICMUB (UMR CNRS 6302), 9, Avenue Alain Savary, BP 47870, 21078 Dijon Cedex, France
E-mail: Claude.Gros@u-bourgogne.fr
Homepage: www.icmub.fr
[b] Université de Strasbourg, INSERM U1113, 3, Avenue Molière, 67200 Strasbourg, France
E-mail: gaiddon@unistra.fr
Homepage: http://u1113-inserm.u-strasbg.fr/
[c] UF 6237 Imagerie Préclinique, Pôle d'imagerie, CHU Hautepierre, Hôpitaux Universitaires de Strasbourg, 1, Avenue Molière, 67098 Strasbourg Cedex, France
[d] ICube, Fédération de Médecine Translationnelle de Strasbourg (FMTS), Université de Strasbourg, 67412 Illkirch Cedex, France

Supporting information for this article is available on the WWW under http://dx.doi.org/10.1002/ejoc.201300678.

 © 2013 Wiley-VCH Verlag GmbH & Co. KGaA, Weinheim

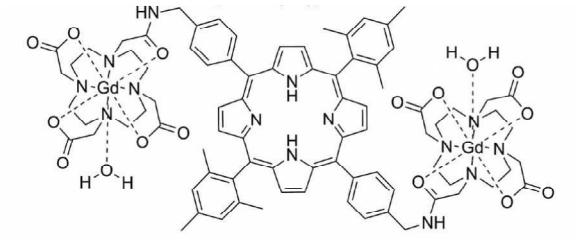
porphyrin derivative was chosen on the one hand (porphyrins display interesting properties in terms of fluorescence and metal-center complexation) and, on the other hand, dota-like (dota = 1,4,7,10-tetraazacyclododecane-1,4,7,10-tetraacetic acid) derivatives based on the cyclen macrocycle and widely used as CAs especially in magnetic resonance imaging (MRI).[6] Our group previously reported the synthesis of a heterobimetallic complex built upon a porphyrin scaffold.[7] Up to now, only a few examples of molecular structures incorporating both porphyrins and tetraazacycloalkanes have been described in the literature, mainly for biomimetic studies and use as CAs.[8]

We report herein the synthesis of four multimodal ligands incorporating one porphyrin moiety and one or several dota-like macrocycles all in the same molecular architecture. The corresponding gadolinium(III) complexes (Scheme 1) were synthesized and two heterometallic complexes incorporating both gadolinium(III) and copper(II) ions were also prepared as potential MRI/PET multimodal CAs. The metal complexes based on ligand **L4** are particularly promising because the ligand structure includes an amine moiety that can be activated for easy conversion into an isothiocyanate group for further anchoring to a biological vector (Figure 1).

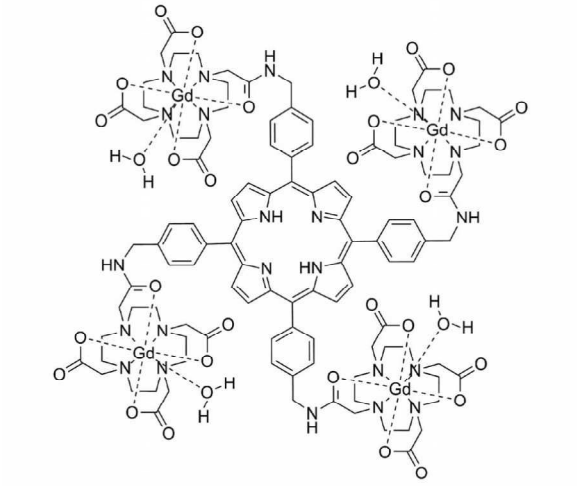
Results and Discussion

Syntheses of Ligands L1, L2, L3, and L4

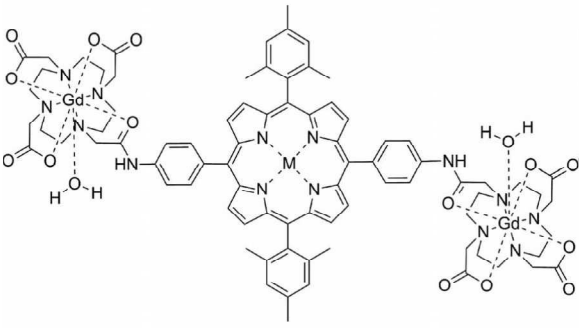
The structures of the DO3AAM-porphyrin ligands and their corresponding metal complexes, in which an amide bond connects the porphyrin and dota macrocycles, are presented in Scheme 1. The biocompatibility and stability of the amide bond is well known and numerous reaction conditions for its generation can be found in the literature.[9] dota derivatives bearing three carboxylic acid groups have been designed to chelate metal centers of potential interest in medical imaging. For reasons of solubility, the tertiary butyl ester form was used during the coupling reaction. The commercially available *t*Bu-protected cyclen derivatives (shown in Scheme SI1 in the Supporting Information) are easy to handle in classical organic solvents and can be purified by chromatography over silica gel. The *t*Bu protecting group can also be easily removed by treatment with trifluoroacetic acid to release the carboxylic acid functions. Note that despite the presence of the porphyrin moiety, which is hydrophobic due to the presence of mesityl substituents, the carboxylic acid arms of the cyclen derivatives are sufficiently hydrophilic to induce ligand solubility in water. The mesityl substituents at the *meso* positions of the porphyrin were used for synthetic reasons. Indeed, for the synthesis of *trans*-A_2B_2 porphyrins, sterically hindered substituents like mesityl are usually required to 1) avoid scrambling reactions, 2) improve the yields, and 3) facilitate the purification procedure. The dota-tris(*t*Bu)-*N*-hydroxysuccinimide activated ester form (**A**, Scheme 2) was chosen to react with an amino-substituted porphyrin for the synthesis



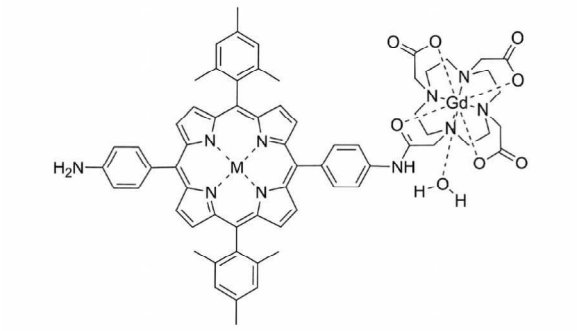
18: [Gd_2(L1)]



19: [Gd_4(L2)]



20: [Gd_2(L3)] M = 2H
22: [$CuGd_2$(L3)] M = Cu



21: [Gd(L4)] M = 2H
23: [CuGd(L4)] M = Cu

Scheme 1. Structures of the gadolinium complexes based on porphyrin and dota-like structures.

© 2013 Wiley-VCH Verlag GmbH & Co. KGaA, Weinheim

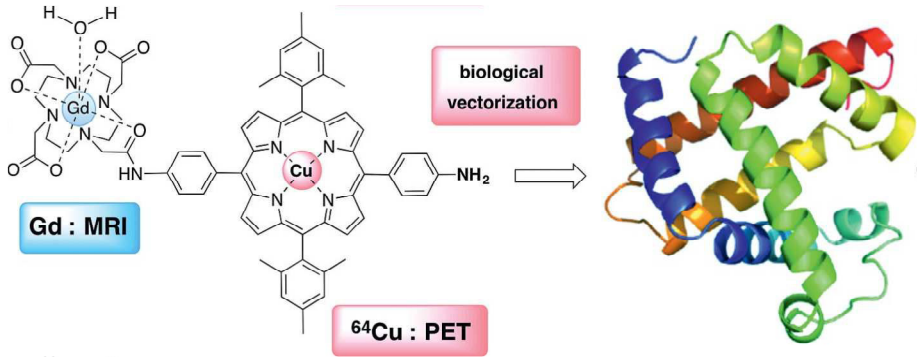
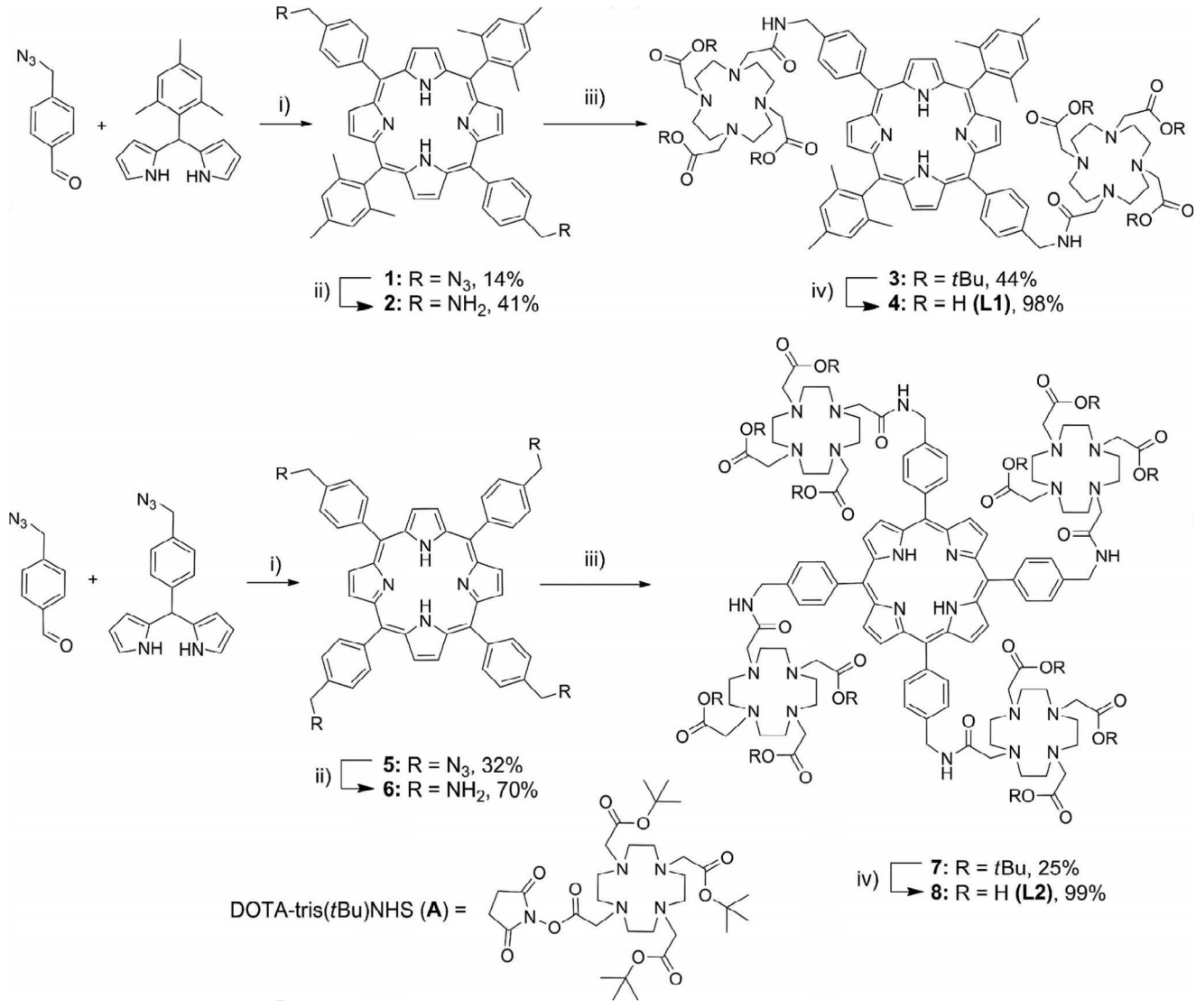


Figure 1. Example of an all-in-one multimodal Cu/Gd complex.



Scheme 2. Reagents and conditions: i) $BF_3{\cdot}OEt_2$, $CHCl_3$, room temp., N_2, 2 h, then *p*-chloranil; ii) $LiAlH_4$, dry THF, room temp., 2 h, then H_2O; iii) dota-tris(*t*Bu)NHS (**A**), $CHCl_3$, MeOH, room temp., 3 h; iv) TFA in CH_2Cl_2, room temp., 24 h.

of ligands **L1** and **L2**. To reduce the deactivating effect of the porphyrin moiety towards the arylamine, a benzylamine-substituted porphyrin was prepared. An azide function was used as a protecting group on the amine. This azide moiety was easily obtained by nucleophilic substitution of a bromide atom and was used without any further purifi-

 © 2013 Wiley-VCH Verlag GmbH & Co. KGaA, Weinheim

cation. The *p*-(azidomethyl)benzaldehyde precursor was synthesized in 80% yield starting from the commercially available *p*-(bromomethyl)benzonitrile, as recently described by our group.[10] The mesityldipyrromethane was prepared by the classical reaction of the corresponding aldehyde with an excess of pyrrole in the presence of trifluoroacetic acid.[11] The azido-substituted porphyrin was formed by a [2+2] MacDonald condensation catalyzed by boron trifluoride–diethyl ether as Lewis acid. After classical oxidation by *p*-chloranil and purification by column chromatography, porphyrin **1** was isolated in 14% yield (Scheme 2). The bis-amino-substituted porphyrin **2** was obtained by reduction of the azide group to amine in the presence of an excess of lithium aluminium hydride. The reduction of the azide moiety was confirmed by ^{1}H NMR analysis through the upfield shift of the methylene signal from 4.70 ppm for ArCH_2N_3 to 4.14 ppm for ArCH_2NH_2 (see the Supporting Information). The key step of the synthesis (Scheme 2) was the amide bond formation obtained by reaction of the benzylamine-substituted porphyrin with the nonprotected carboxylic acid group of the dota precursor. Classical approaches to amides usually require benzotriazole derivatives and carbodiimide as in situ coupling agents. However, the major drawback of these methods is the presence of stoichiometric amounts of coupling agents, which are usually quite difficult to separate from the desired compound.

To solve this problem, the pre-activated *N*-hydroxysuccinimide form of dota-tris(*t*Bu) (structure A in Scheme 2) was used. This succinimide was treated with amino-substituted porphyrins with the release of only *N*-hydroxysuccinimide as a byproduct, which can be easily extracted from the organic solvent by acidic washing. The *t*Bu-protected porphyrin-dota-like compound **3** was obtained in reasonable yield after purification (Scheme 2). After treatment with trifluoroacetic acid in dichloromethane, the solvent and volatiles were removed under vacuum. This procedure was repeated four times to remove the *tert*-butyl alcohol and trifluoroacetic acid. The formation of the porphyrin bearing two DO3AAM moieties (**L1**) was confirmed by high-resolution mass spectrometry (ESI); the mass spectrum exhibits the bis-charged cation $[M + 2H]^{2+}$ at 765.3812 Da (calcd. 765.3844) for $C_{84}H_{102}N_{14}O_{14}$ (see the Supporting Information). At room temperature, the ^{1}H NMR spectrum shows broad and unresolved signals in the aliphatic proton region due to the presence of conformers in slow exchange in solution. Therefore the temperature was increased to 400 K to obtain a better resolution of the methylene proton resonances of the tetraazamacrocyclic moiety. However, at 400 K, the signal from the amide protons are superimposed on the signals of the protons at the β positions of the porphyrin macrocycle (see the Supporting Information) whereas this signal appears at δ = 9.26 ppm at 300 K in DMSO.

Having in hand the bis-dota-porphyrin, we then synthesized the tetrakis-dota-substituted porphyrin (Scheme 2). We used the tetrakis(*p*-aminomethylphenyl)porphyrin **6** as the starting material. The synthesis of this porphyrin precursor was described in 1993 by Pina and co-workers[12] in 10% overall yield, the amine function being protected by a phthalimide group, which was quite difficult to remove. As described in Scheme 2, we report herein an improved synthetic route proceeding in 26% yield, which has allowed us to easily obtain, on the gram scale, the A_4 (aminomethylphenyl)porphyrin **6**.

We explored different pathways for the synthesis of the precursor A_4 azido-porphyrin **5**. We report here only the optimized procedure. This compound has previously been obtained in 12% yield[13] by condensation of *p*-(azidomethyl)benzaldehyde and pyrrole in dichloromethane catalyzed by boron trifluoride–diethyl ether. The classical method for the formation of A_4-substituted porphyrins, by the condensation of aldehyde with pyrrole in propionic acid, was tested and gave a yield of 24%. Another possible approach is to condense a dipyrromethane with an aldehyde by the MacDonald [2+2] condensation reaction. The *p*-(azidomethyl)dipyrromethane was obtained in 82% yield by the condensation of the corresponding aldehyde with pyrrole as both solvent and reagent in the presence of trifluoroacetic acid.[14] The A_4 azido-porphyrin **5** was then obtained in 32% yield by condensation of *p*-(azidomethyl)dipyrromethane with *p*-(azidomethyl)benzaldehyde catalyzed by the boron trifluoride–diethyl ether Lewis acid, followed by classical oxidation with *p*-chloranil.

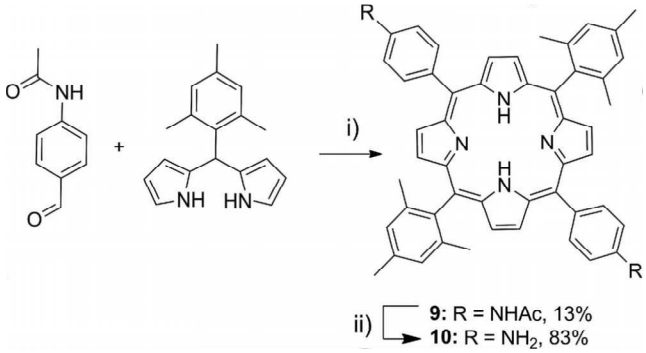
This pathway was preferred because of the easier purification step (column chromatography and recrystallization in CH_2Cl_2/MeOH). The four azide moieties were further reduced with an excess of lithium aluminium hydride in dry THF. The A_4 (aminomethylphenyl)porphyrin **6** was isolated in 70% yield and characterized by MALDI-TOF mass spectrometry; the mass spectrum exhibits the $[M + H]^+$ cation at 731.492 Da. Ligand **L2**, a porphyrin with four DO3AAM moieties, was prepared following the same procedure as described for the synthesis of bis-dota porphyrin **L1**.

Our next goal was to go one step further by designing an all-in-one ligand (based on porphyrin and cyclen derivatives) bearing, in addition, a chemical function that could be easily activated to form a covalent bond with biological vectors. Examples of the grafting of molecules on to biological materials and acting as a vector to tag proteins or antibodies have been described in the literature.[15] In this case, the amine group was chosen as the functionality to be activated. Indeed, primary amines can be easily transformed into isocyanates or isothiocyanates and form urea and thiourea bonds (e.g., reaction of amines from the lysine residues of a protein).[16] Activation of the aniline group of a porphyrin to isothiocyanates and subsequent condensation led to the ready formation of thiourea bonds.[17]

Our idea was to obtain this all-in-one ligand, integrating a dota derivative, a porphyrin macrocycle, and a primary amine, in only a few steps and, if possible, in reasonable yields. In the synthetic pathway that we developed, the porphyrin acts as a central platform and at the same time as both a strong coordinating ligand and a potential linker for biological vectorization. The targeted porphyrin should therefore bear at least two different chemical functions.

 © 2013 Wiley-VCH Verlag GmbH & Co. KGaA, Weinheim

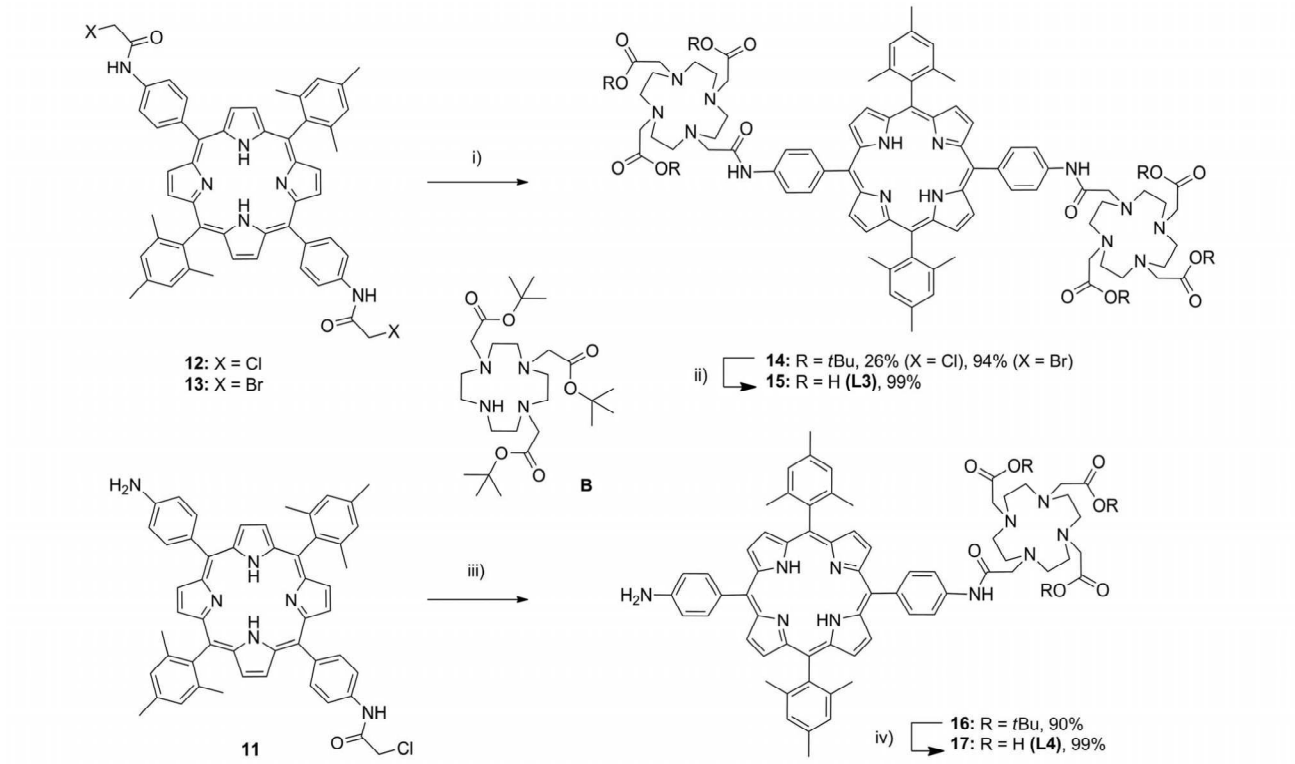
The first step of this synthetic pathway, shown in Scheme 3, is the classical [2+2] MacDonald condensation of the commercially available *p*-(acetamido)benzaldehyde with *p*-mesityldipyrromethane in the presence of the boron trifluoride–diethyl ether Lewis acid catalyst, followed by oxidation with *p*-chloranil leading to the A_2B_2 (acetamidophenyl)porphyrin **9**, as described in the literature.[18] The acetamido group was then removed by acidic treatment in EtOH. Lee et al.[18] previously recommended heating the solution at reflux in the presence of a large amount of concentrated HCl (160 mL for 500 mg of starting material) for 48 h. We employed better conditions, namely 4.4 equiv. of *p*-toluenesulfonic acid (PTSA) in EtOH for 24 h. In this way, the A_2B_2 (aminophenyl)porphyrin **10** was obtained in high yield (83%). The key step of the overall synthesis was the formation of porphyrin **11** (shown in Scheme 4), obtained by the condensation of chloroacetyl chloride and porphyrin **10** in the presence of *N*,*N*-diisopropylethylamine (DIPEA) in CH_2Cl_2. This reaction occurs in a statistical way. The mono-(chloro)porphyrin **11** and the bis(chloro)-porphyrin **12** are formed concomitantly during the reaction.



Scheme 3. Reagents and conditions: i) $BF_3{\cdot}OEt_2$, $CHCl_3$, room temp., N_2, 2 h, then *p*-chloranil; ii) 4.4 equiv. PTSA in EtOH, reflux, 24 h.

Different conditions were tested to optimize the reaction and increase the yield of compound **11** and prevent as much as possible the formation of compound **12**. Even if this statistical method implies purification, it is worth noting that A_2BC-*meso*-substituted porphyrin **11** was obtained in only one step in 33% yield, without any protection/deprotection step. In addition, the reaction was fast and the compound easily isolated by one chromatographic separation. The starting material was also isolated after the reaction and could be reused in a subsequent reaction.

The synthetic route to the dota-porphyrin compounds (Scheme 4) implies the *N*-alkylation of the commercially available DO3A*t*Bu by halogenated porphyrins. To optimize this step, we attempted to synthesize the brominated analogues of the chlorinated compounds **11** and **12**. Unfortunately, and despite different reaction conditions, only the bis(bromo)porphyrin **13** (Scheme 4) could be obtained. Substitution of DO3A*t*Bu on the halogenated porphyrin usually takes place in polar and aprotic solvents, for example, acetonitrile, in the presence of potassium carbonate. As the porphyrin derivatives are not soluble in acetonitrile, dimethylformamide was used as solvent. The *t*Bu-protected



Scheme 4. Reagents and conditions: i) DO3A*t*Bu (**B**), K_2CO_3, DMF, room temp., 1 h starting from **13**, or 70 °C, 12 h starting from **12**; ii) TFA, CH_2Cl_2, room temp., 24 h; iii) DO3A*t*Bu (**B**), K_2CO_3, DMF, room temp., 2 h; iv) TFA, CH_2Cl_2, room temp., 24 h.

 © 2013 Wiley-VCH Verlag GmbH & Co. KGaA, Weinheim

porphyrin-cyclen **14** was obtained in reasonable yield (26%) starting from bis(chloro)porphyrin **12**, and in very good yield (94%) starting from bis(bromo)porphyrin **13** (Scheme 4). The same reaction procedure was applied to obtain the amine bearing *t*Bu-protected porphyrin-dota **16** (Scheme 4). Ligands **15** (**L3**) and **17** (**L4**) were finally obtained by deprotection of the *t*Bu ester moieties, as described previously, in the presence of trifluoroacetic acid in CH_2Cl_2.

Figure 2 shows the ^{1}H NMR spectrum of **14** in [D_6]-DMSO at different temperatures. The formation of ligand **15** (**L3**) was confirmed by HRMS (ESI); the mass spectrum shows two cations, one for $[M + H]^+$ at 1501.7346 Da and the second for $[M + Na]^+$ at 1523.7154 Da (see the Supporting Information). The ^{1}H NMR spectrum recorded in DMSO at 400 K exhibits a singlet corresponding to the amide protons at δ = 10.35 ppm and the disappearance of the signal at 1.5 ppm corresponding to the *t*Bu protecting group (see the Supporting Information) was also observed.

The formation of ligand **L4** was also confirmed by HRMS (ESI); the mass spectrum exhibits one main ion peak corresponding to $[M + Na + K]^{2+}$ cation at 588.2427 Da (see the Supporting Information). A singlet at δ = 10.28 ppm corresponding to the amide proton and four doublets at 7.07, 7.87, 8.03, and 8.15 ppm corresponding to the protons of the *para*-substituted aromatic rings also appear in the ^{1}H NMR spectrum. As already observed for **L3**, the disappearance of the signal at 1.5 ppm corresponding to the *t*Bu protecting group confirms the formation of **L4** (see the Supporting Information).

X-ray Structure of $(NaBr)_2$**14**

Compound $(NaBr)_2$**14** crystallizes in the $P2_1/c$ space group with 10 chloroform molecules. The dota-like tetraaza groups are connected through amidic bonds to two opposite *meso*-phenyl groups of the porphyrin. The molecule crystallizes around a symmetry center and hence only half of the molecule is present in the asymmetric unit. As shown in Figure 3, the tetraaza pockets are directed towards the porphyrin moiety and, in accordance with the presence of a center of symmetry, the two dota-like units are located on each side of the porphyrin plane. The grafting of these two groups does not induce any distortion of the porphyrin core as the macrocycle remains flat; the RMS deviation of the 24-atom plane is only 0.038 Å. Each dota-like moiety coordinates a sodium cation (with a bromide as counter anion), which induces no distortion of the dota core as was the case in the NaBr(*tert*-butyl ester dota).[19] Figure 4 shows the best overlay fit between our dota-like moiety and the NaBr (*tert*-butyl ester dota) complex, the RMS distance between 25 atom pairs is only 0.115 Å.

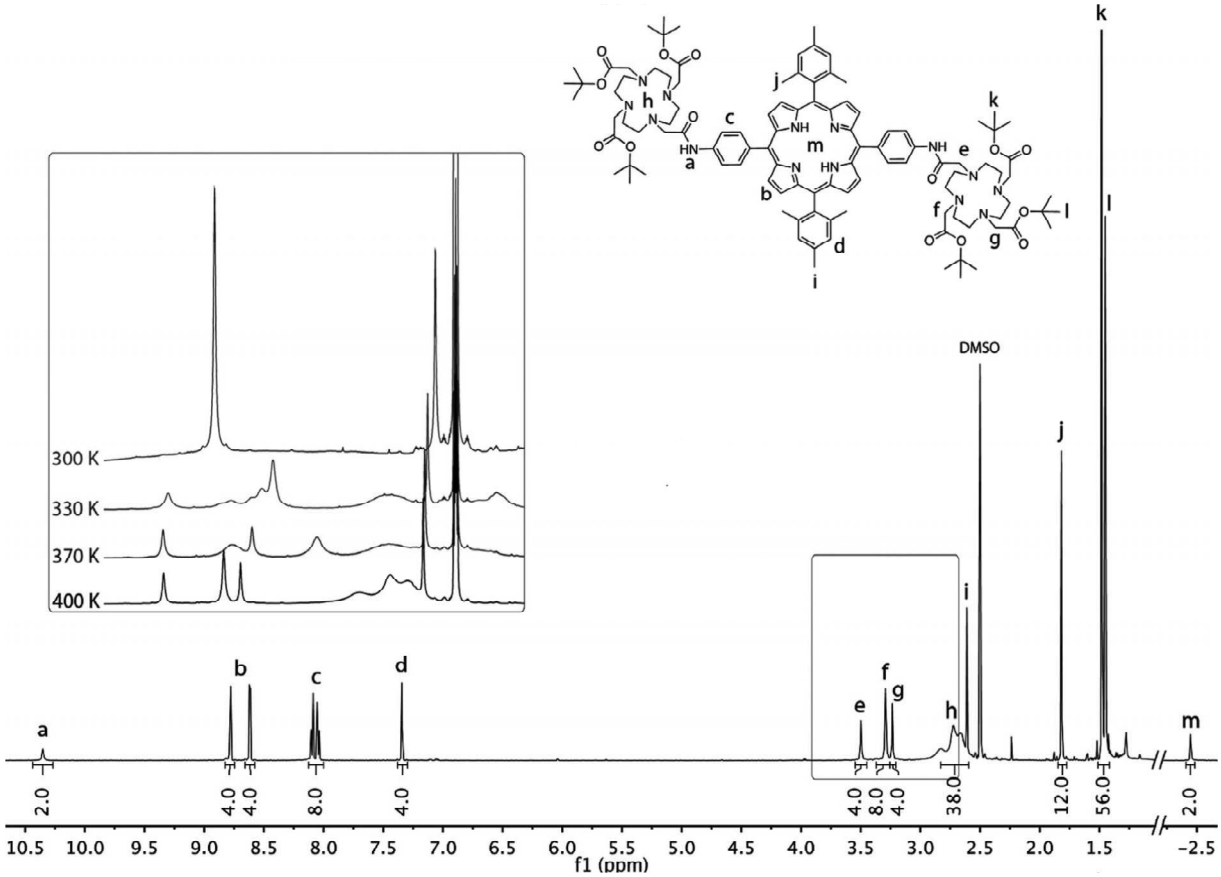


Figure 2. ^{1}H NMR spectrum of **14** in [D_6]DMSO at different temperatures.

 © 2013 Wiley-VCH Verlag GmbH & Co. KGaA, Weinheim

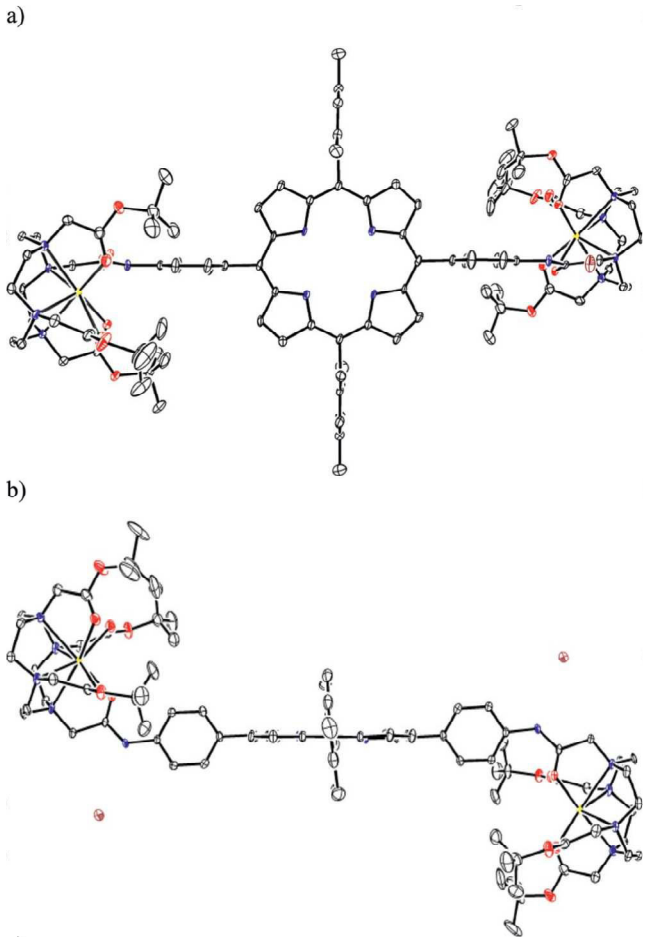


Figure 3. a) Top view and b) side view of $(NaBr)_2$**14**. Chloroform molecules have been omitted for clarity.

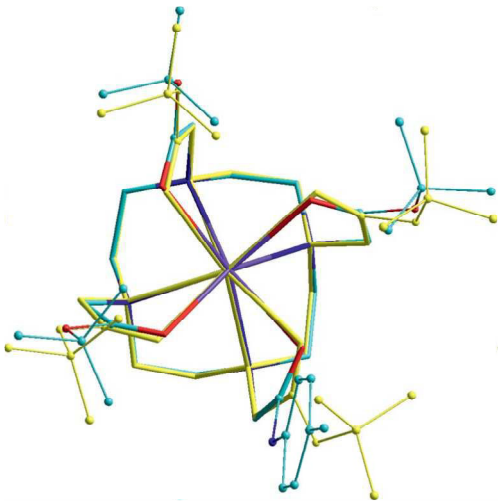


Figure 4. Overlay of the dota-like moiety of $(NaBr)_2$**14** and the NaBr(*tert*-butyl ester dota)[19] complex (yellow). The *tert*-butoxy groups were not included in the overlay fitting process.

Metalation of Ligands L1, L2, L3, and L4

The ligands **L1**, **L2**, **L3**, and **L4** were used to prepare four new gadolinium complexes (**18**–**21**), as shown in Scheme 1. All these complexes were obtained following the same procedure. The ligand was dissolved in Milli-Q water with a small amount of DMSO to prevent precipitation. The ligands were isolated in their protonated forms, and are insoluble in water (the *t*Bu deprotection step employs trifluoroacetic acid). The pH was adjusted to 8 by addition of small aliquots of NaOH solutions (1 and 0.1 M), 1.1 equiv. of gadolinium nitrate per dota-like macrocycle were added, and then the pH was adjusted to 7. After 12 h at 50 °C, the mixture was allowed to cool to room temperature and the complex precipitated from the solution. The metal complex was isolated by filtration or centrifugation and washed three times with Milli-Q water to eliminate any traces of the remaining salts. Note that the formation of gadolinium–porphyrin requires stronger reaction conditions, consequently the porphyrin ring was not metalated by this procedure. The absence of any metallic center in the porphyrin cavity was confirmed by UV/Vis analyses in which one Soret band and four Q bands characteristic of metal-free porphyrins were observed. The formation of gadolinium complexes was confirmed by HRMS (ESI) and the purity was controlled by HPLC.

In positron emission tomography (PET), the ^{64}Cu isotope is attracting increasing attention for its favorable properties [$t_{1/2}$ = 12.7 h, β+ (19%); β– (39%)], in particular, a longer half-life compared with the more commonly used ^{18}F ($t_{1/2}$ = 109.8 min) and ^{11}C ($t_{1/2}$ = 20.4 min) isotopes. The design of chelators that form high-stability complexes with copper(II) and do not suffer from *trans* chelation in vivo is of key importance. Advantageously, copper complexes of porphyrins are known to be extremely stable towards dissociation.

Two heterobimetallic complexes incorporating both gadolinium and copper atoms, [$CuGd_2$(**L3**)] (**22**) and [CuGd(**L4**)] (**23**; Scheme 1), were prepared following the same procedure. Gadolinium complexes [Gd_2(**L3**)] and [Gd(**L4**)] were dissolved in MeOH in the presence of copper nitrate and heated to 50 °C. To prevent any transmetalation of gadolinium by copper, the reaction was monitored by

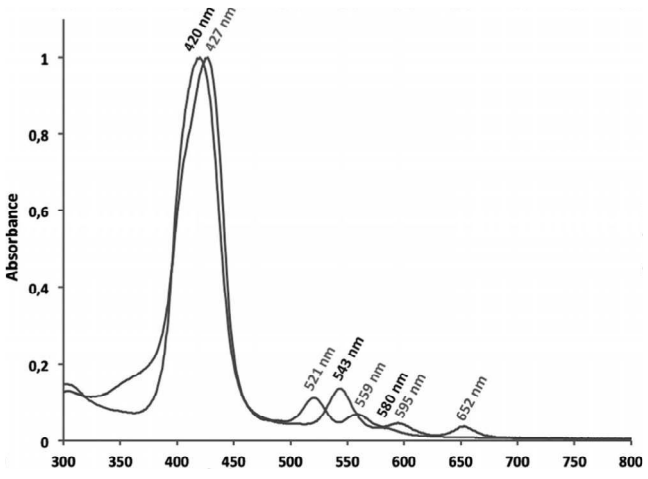


Figure 5. UV/Vis spectra of [Gd(**L4**)] (grey) and [CuGd(**L4**)] (black) in water.

 © 2013 Wiley-VCH Verlag GmbH & Co. KGaA, Weinheim

UV/Vis spectroscopy. The reaction was stopped when the UV/Vis spectrum no longer evolved and displayed in the visible region only two Q bands characteristic of copper-porphyrin (Figure 5). The formation of the heterobimetallic complexes was confirmed by HRMS (ESI) and the purity controlled by HPLC.

Relaxivity Measurements

Longitudinal relaxivity, r_1, is a characteristic property of gadolinium complexes used to evaluate the efficiency of contrast agents in MRI. r_1 is a measure of the enhancement of the relaxation rate of the water protons as a function of Gd^{III} content.[20] Longitudinal relaxivity is expressed in $mM^{-1}\,s^{-1}$ and is dependent on several macroscopic factors, for example, temperature and magnetic field, and microscopic factors, such as the number of coordinated water molecules, the rotational correlation time, and rate of exchange of water. These parameters have been incorporated into equations known as the Solomon–Bloemergen–Morgan theory.[21]

For T_1 acquisitions, gadolinium complexes (Scheme 1) were dissolved in Milli-Q water in the presence of a small amount of DMSO. As commonly admitted, the molar fraction of DMSO (x_{DMSO} = 0.01) is small enough to consider the solvation of the complex and the diffusion properties of the solution to be the same as in pure water. Therefore it is generally stated that the dynamics and relaxivity of the complexes are not affected by the presence of 1 mol-% DMSO. Three solutions of each complex at different concentrations were prepared [solutions diluted by a factor 2 and 5 were prepared for each Gd complex starting from a standard solution (10^{-4} M)] and the exact concentration of gadolinium was measured, after mineralization, by inductively coupled plasma atomic emission spectroscopy (ICP-AES).

T_1 values were determined at 300 (7 T, 25 °C, pH 7) and 20 MHz (0.5 T, 25 and 40 °C, pH 7) by a classical inversion/recovery pulse sequence with six data points and eight scans per point. The r_1 values are shown in Table 1 and were determined by linear regression of $1/T_1$ (in s^{-1}) versus Gd concentration (in mM). The transversal relaxivity r_2 values were also determined at 20 MHz under the same solutions and are available in the Supporting Information.

Table 1. Relaxivity measurements of porphyrin-dota-like complexes at different magnetic fields and temperatures.

	Relaxivity, r_1 [$mM^{-1}\,s^{-1}$]		
	20 MHz 0.5 T	20 MHz 0.5 T	300 MHz 7 T
Complex	25 °C	40 °C	25 °C
[Gd_2(**L1**)] (**18**)	7.3	9.1	4.1
[Gd_4(**L2**)] (**19**)	5.0	6.7	2.8
[Gd_2(**L3**)] (**20**)	19.8	22.2	5.4
[Gd(**L4**)] (**21**)	19.5	25.7	3.6
[CuGd_2(**L3**)] (**22**)	21.2	24.5	5.5
[CuGd(**L4**)] (**23**)	16.1	18.5	6.1

The measurements at high field (recorded at 300 MHz) give relaxivity values from 2.8 to 6.1 $mM^{-1}\,s^{-1}$, which are typical values for gadolinium complexes with one key water molecule in the first coordination sphere. For example, the relaxivity value for [Gd(dota)(H_2O)]$^-$ measured under the same conditions is in the same order of magnitude (3.6 $mM^{-1}\,s^{-1}$).[7]

The measurements at low field (recorded at 20 MHz) show two main characteristics: The complexes based on ligands **L1** (**18**) and **L2** (**19**) exhibit lower r_1 values than the others, whereas the four complexes based on ligands **L3** and **L4** have r_1 values similar to those of previously described compounds.[22]

In the cases of ligands **L3** and **L4**, it is interesting to note that the paramagnetic copper(II) does not contribute to the relaxivity value as it has no direct contact with a water molecule. Indeed, the porphyrin macrocycle usually leads to four-coordinate copper complexes (the square-planar coordination occurs through the four nitrogen atoms of the macrocyclic cavity). The relaxivities of the four complexes described here are four to five times higher than commercially available contrast agents. (r_1 = 4.2 and 4.3 $mM^{-1}\,s^{-1}$ for [Gd(dota)(H_2O)]$^-$ and [Gd(dtpa)(H_2O)]$^{2-}$, respectively).[23] The molecular weights of the complexes described herein are significantly higher than those of the commercially available dota derivatives, inducing a slower molecular tumbling, which is known to have a key role in increasing relaxivity.[24] These relaxivities are about the same order of magnitude as the values reported for compounds incorporating, in the same molecule, a gadolinium complex and a porphyrin derivative. For example, an r_1 value of 14.8 $mM^{-1}\,s^{-1}$ was measured at 20 MHz by Simonneaux and co-workers for a [Gd_2(dtpa)$_4$(H_2O)-tetrakis(*p*-aminophenyl)-porphyrin] conjugate,[22b] relaxivity values in the range 13.5–25.09 $mM^{-1}\,s^{-1}$ were measured by Pandey and co-workers at 200 MHz for different chlorin derivatives substituted by several Gd(dtpa) complexes,[22a] and Meade and co-workers reported porphyrazin derivatives substituted with Gd(dota) complexes that exhibit relaxivities of 4.2–12.8 $mM^{-1}\,s^{-1}$ at 60 MHz.[22c] Our group previously described a porphyrin derivative bearing one Gd(dota) complex, which showed relaxivities of 18.8 and 18.9 $mM^{-1}\,s^{-1}$ at 20 MHz.[7]

The paramagnetic complexes based on ligands **L1** and **L2** exhibit relaxivities of 7.3 $mM^{-1}\,s^{-1}$ for the porphyrin derivative bearing two gadolinium complexes and 5.0 $mM^{-1}\,s^{-1}$ for the porphyrin derivative bearing four gadolinium complexes, respectively. The only difference between these complexes and the complexes based on ligands **L3** and **L4** is the presence of one carbon atom on the porphyrin moiety between the amide function and the aromatic ring. This linker leads to a greater flexibility in the molecule and increases the intramolecular steric hindrance. The lower relaxivities of the complexes based on **L1** and **L2** could be due to the hydrophobic porphyrin part of the molecule hindering or preventing access of the water molecules to the gadolinium paramagnetic metal center or higher molecular tumbling.

Relaxivity corresponds to the change in the relaxation rate of solvent water protons normalized to metal ion con-

 © 2013 Wiley-VCH Verlag GmbH & Co. KGaA, Weinheim

centration (in mM) and expressed in $mM^{-1} s^{-1}$.[2,25] Many factors can affect the relaxivity: 1) The rate of water exchange in and out of the first coordination sphere, 2) the number of coordinated water molecules, and 3) the rotational correlation times.[24,26] Given that water exchange and rotational diffusion are both temperature dependent, relaxivity is also temperature dependent. However, rotation and water exchange, the two main limiting parameters of relaxivity, lead to opposite temperature behavior, that is, when rotation is the principal factor governing relaxivity, r_1 decreases with increasing temperature, whereas when the exchange of water is the limiting factor, an opposite temperature effect is observed. In the case of low-molecular-weight Gd complexes, the relaxivity is mainly limited by a short rotational correlation time, τ_R.[27] Therefore the relaxivity usually decreases with increasing temperature. For high-molecular-weight Gd complexes, the relaxivity is usually limited by the rate of water exchange ($k_{ex} = 1/\tau_m$, in which τ_m is the lifetime of the inner-sphere coordinated water molecule).[28] In our case, we hypothesize that the slightly higher relaxivity of our [Gd(L)(H_2O)] complexes observed at 40 °C (Table 1) might be explained by an increase in the rotational correlation time coupled with a favorable rate of water exchange.

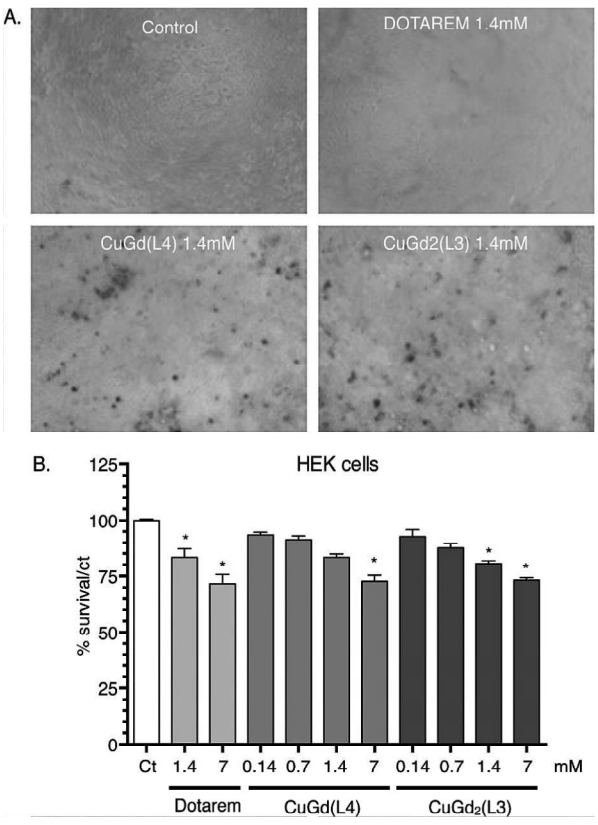


Figure 6. HEK cells were treated for 48 h at the indicated concentrations (mM) of Dotarem, [$CuGd_2$**L3**] or [CuGd**L4**]. Cell viability was observed by microscopy (A) and quantified by using the MTT test (B). Data are representative of three independent experiments. Bars are means and asterisks indicate a statistically significant difference (*: $p < 0.001$) compared with the control, as calculated by a one-way ANOVA test followed by a Tukey post-test over the three independent experiments.

Cytotoxicity

As organometallic compounds can be highly toxic against various tissues, including the kidneys and the nervous system,[29] we investigated the cytotoxicity of the CuGd molecules on cells. Increasing concentrations of [$CuGd_2$(**L3**)] (**22**) and [CuGd(**L4**)] (**23**) were applied for 48 h on human immortalized kidney cells HEK and compared with the results obtained with Dotarem. Based on the dose injected and the blood volume, we calculated that the usual concentration of Dotarem in blood during an MRI experiment is about 1.4 mM. Therefore we chose a range of concentrations between 0.14 to 7 mM to assess the potential cytotoxicity of the compounds. Cell survival was monitored by microscopy and quantified by using an MTT assay. Microscope observations did not indicate significant cell death induced by either of the compounds (Figure 6, A). However, the MTT test showed that [CuGd(**L3**)] and [$CuGd_2$(**L4**)] induced a reduction of about 20% of cell numbers relative to the control (Figure 6, B). This effect is similar to that observed with Dotarem. These results suggest that [$CuGd_2$(**L3**)] and [CuGd(**L4**)] might induce a modest cell growth arrest, similar to that of Dotarem.

MRI Experiment

A preliminary MRI experiment was carried out by using [$CuGd_2$(**L3**)] (**22**) as a contrast agent (Figure 7). A solution

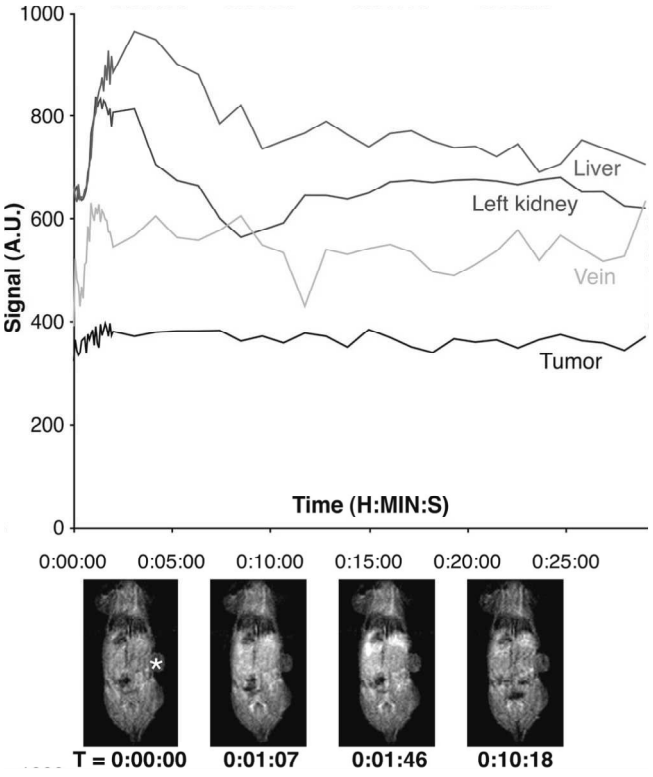


Figure 7. Time–signal (in arbitrary units) curves from regions of interest (ROI) drawn in various tissues. Typical images recorded at different times (before and following intravenous administration of the contrast agent) are shown, the white star on the first image indicating the tumor.

 © 2013 Wiley-VCH Verlag GmbH & Co. KGaA, Weinheim

(200 μL) of the contrast agent was administered intravenously through a catheter into a tail vein of mice. Images and derived curves show a quick clearance from the blood with a slight signal enhancement after a few minutes. The substrate is limited mainly by liver but also to a small extent by the kidneys. No enhancement was seen in the tumor tissue. We are currently working on the biological vectorization of these CAs to increase their tumoral tropism.

Conclusions

We have developed several new synthetic procedures leading to porphyrin-dota-like water-soluble ligands and their corresponding gadolinium complexes. We have also described a synthetic procedure that gives access in only five steps and in an acceptable yield to the key, all-in-one molecular structure (**L4**) incorporating a porphyrin, a dota derivative, and an amine function that can be activated for biological vectorization. This ligand shows very good complexation properties and we have also reported the formation of the heterobimetallic complex [CuGd(**L4**)] (**23**) incorporating both "cold" copper and gadolinium atoms, of particular interest in medical imaging. The preliminary relaxivity, cytotoxicity, and MRI studies showed that the complexes developed here are very promising medical imaging agents for enhancement of contrast using bimodal MRI techniques. We are currently working on the activation of the amine moiety within the ligand **L4** with the aim of anchoring it on a biological vector. The chelation of ^{64}Cu to the porphyrin moiety by radiochemistry needs to be developed, but the preliminary complexation step with cold copper is a fast reaction that could be performed in a last synthetic step. We have reported herein examples of heterometallic gadolinium/copper complexes, but these versatile ligands show good affinities for other metal centers of key interest in medical imaging. Indeed, porphyrins incorporating manganese have been studied as MRI contrast agents[30] and cyclen derivatives are well known to strongly chelate several metals of interest in nuclear imaging[31] and in optical imaging with fluorescent lanthanides.[32]

Experimental Section

Instrumentation: ^1H and ^{13}C NMR spectra were recorded with a Bruker 300, 500 or 600 MHz spectrometer at "Welience, Pôle chimie moléculaire". Chemical shifts are expressed in ppm relative to chloroform or DMSO. UV/Vis spectra were recorded with a Varian Cary 1 spectrophotometer. Mass spectra were recorded with a Bruker Daltonics Ultraflex II spectrometer in the MALDI-TOF reflectron mode by using dithranol or 2,5-dihydroxybenzoic acid (DHB) as the matrix or in ESI mode with a Thermo Scientific LTQ Orbitrap XL spectrometer. HPLC measurements were performed with a Dionex Ultimate 3000 system. Semipreparative and analytical HPLC were carried out by using a Nucleodur C_{18} column (100 Å, 5 μm, 250 × 10 mm and 250 × 4.6 mm, respectively, Macherey–Nagel). The samples were isolated and analyzed by using H_2O (A) and MeOH (B) as solvents without any traces of acid to prevent the eventual decomplexation of the metal centers.

Chemicals and Reagents: All chemicals and solvents were of analytical and reagent grade and used as received. Silica gel (70–120 μm) and fine silica gel (0.035–0.070 μm, 60 Å) were used for column chromatography. Analytical TLC was performed with Merck 60 F254 silica gel precoated sheets with a thickness of 0.2 mm. The reactions were monitored by TLC, UV/Vis spectroscopy, and MALDI-TOF mass spectrometry. Mesityldipyrromethane,[11] *p*-(azidomethyl)benzaldehyde,[10] and 5-[*p*-(azidomethyl)phenyl]dipyrromethane[14] were prepared as described previously.

Relaxivity Measurements: The longitudinal relaxation times T_1 were measured at 20 MHz (0.47 T) at 298 and 313 K with a Bruker Minispec "mqvar" instrument. Relaxation measurements were also performed at 300 MHz (7.07 T) with a Bruker Avance II 300 MHz NMR spectrometer. Solutions for the relaxivity measurements were prepared by dissolving the gadolinium complexes in H_2O/DMSO (95:5, pH 7, [Gd] = 0.001–0.20 mM). For each T_1 longitudinal relaxation measurement, three solutions of the complexes were prepared at different concentrations. The exact Gd^{III} ion concentration was determined by emission spectrometry with a Vista AX CCD Simultaneous ICP-AES Varian spectrophotometer. As the reported complexes are not soluble in the 2% HNO_3 solution usually used for ICP-AES analysis, they were subjected to microwave-assisted mineralization (by using HNO_3/H_2O_2, 4 mL/1 mL) before the ICP-AES measurements. Note that the absence of any free gadolinium was checked for each sample by the Xylenol Orange test.[33]

Cell Culture and MTT [3-(4,5-Dimethylthiazol-2-yl)-2,5-diphenyltetrazolium Bromide] Test: Human HEK cells were maintained at 37 °C under normoxic (20% O_2, 5% CO_2) conditions in DMEM (Dulbecco's modified Eagle's medium; Life Technology) with glucose (1 g/L) supplemented with 10% heat-inactivated fetal calf serum (Life Technology), penicillin/streptomycin (100UI/mL –100 μg/mL) and gentamycin (50 mg/mL). Cells were trypsinyzed for maintenance and experimentation plates as described previously.[34] The MTT test was performed by using 96-well culture plates (Costar) as described previously.[35]

MRI Experiment: Whole-body MR images of mice were acquired by using a 1.5 T preclinical MRI instrument (OPTImouse, RS2D, France) and a volume RF coil (RapidBiomedical, Germany) of 40 mm in diameter. The contrast agent was administered intravenously through a catheter into a tail vein of the mice, connected to an infusion pump (PHD 2000, Harvard Apparatus, USA) at a speed of 100 μL/min (total volume of 200 μL). The mice were anesthetized (Isoflurane + air) and warmed from the beginning of the injection to the end of the acquisitions in an imaging cell (Minerve, France). 2D dynamic acquisition (1 slice of 1.25 mm thickness) involved collecting 25 images every 4.8 s followed by 25 images every 64.8 s leading to a total acquisition time of 29 min. Acquisition was started about 10 s before injection of the contrast agent. Regions of interest (ROI) were drawn, encompassing part of the liver, kidney, retro-orbital vein, and the sub-cutaneous tumor. The mean values of the signal inside these ROI were computed for all images leading to time–signal curves. All animal experiments were conducted according to French regulations concerning small animal experimentation (authorization A 67-482-20).

X-ray Analysis of Compound $(NaBr)_2$14: Suitable crystals were obtained from a NMR tube containing a $CDCl_3$ solution of the compound. Intensity data were collected with a Nonius–Kappa CCD diffractometer at 110 K. The structure was solved by direct methods (SIR92)[36] and refined by full-matrix least-squares methods based on F^2 (SHELXL-97)[37] with the help of the WINGX pro-

 © 2013 Wiley-VCH Verlag GmbH & Co. KGaA, Weinheim

gram.[38] All non-hydrogen atoms were refined with anisotropic thermal parameters. Hydrogen atoms were either included in their calculated positions or found in the $\Delta\rho$ map and refined by using a riding model. The crystallographic data are reported in Table S2 in the Supporting Information.

CCDC-882546 contains the supplementary crystallographic data for this paper. These data can be obtained free of charge from The Cambridge Crystallographic Data Centre via www.ccdc.cam.ac.uk/data_request/cif.

5,15-Bis[4-(azidomethyl)phenyl]-10,20-dimesitylporphyrin (1): Mesityldipyrromethane (2.50 g, 9.46 mmol) and *p*-(azidomethyl)-benzaldehyde (1.52 g, 9.43 mmol) were dissolved in $CHCl_3$ (300 mL). Shielded from light, N_2 was bubbled through the solution and stirred at room temperature for 20 min. Boron trifluoride–diethyl ether (48%, 370 μL, 1.14 mmol) was added dropwise and the mixture was vigorously stirred for 2 h. *p*-Chloranil (1.16 g, 4.72 mmol) was then added to the reaction mixture, which was stirred for 1 h. The solvent was evaporated under reduced pressure and the crude material was purified by column chromatography over silica with CH_2Cl_2 as eluent. After recrystallization in CH_2Cl_2/MeOH, compound **1** was isolated as a purple microcrystalline solid in 14% yield (526 mg, 650 μmol). UV/Vis (CH_2Cl_2): λ_{max} (ε) = 417 (422), 514 (18), 547 (6), 590 (4), 646 nm (310^{-3} L mol^{-1} cm^{-1}). ^{1}H NMR (300 MHz, $CDCl_3$): δ = –2.62 (s, 2 H, NH), 1.83 (s, 12 H, CH_3), 2.62 (s, 6 H, CH_3), 4.70 (s, 4 H, CH_2), 7.27 (s, 4 H, H_{Mes}), 7.67 (d, J = 8.1 Hz, 4 H, H_{Ar}), 8.23 (d, J = 8.1 Hz, 4 H, H_{Ar}), 8.69 (d, J = 4.8 Hz, 4 H, H_β), 8.76 (d, J = 4.8 Hz, 4 H, H_β) ppm. MS (MALDI-TOF): calcd. for $C_{52}H_{47}N_6$ [M – $2N_2$ + 3H]$^+$ 755.386; found 755.203.

5,15-Bis[4-(aminomethyl)phenyl]-10,20-dimesitylporphyrin (2): A solution (40 mL) of bis(4-azidomethyl)phenylporphyrin (**1**; 440 mg, 581 μmol) in distilled THF was added dropwise to a suspension of $LiAlH_4$ (95%; 104 mg, 2.74 mmol) in distilled THF (20 mL) under N_2 at –80 °C, shielded from light. The mixture was allowed to warm to room temperature and vigorously stirred for 2 h. The reaction mixture was again cooled at –80 °C and the excess of $LiAlH_4$ was neutralized by the dropwise addition of water (7 mL). The product was extracted by the addition of $CHCl_3$ and the organic layer was then washed three times with a saturated $NaHCO_3$ solution, dried with $MgSO_4$, and then evaporated under reduced pressure. The crude product was purified by chromatography over silica with $CHCl_3$/MeOH (100:10) as eluent. The purple fraction was collected and evaporated under reduced pressure. Compound **2** was isolated as a purple microcrystalline solid in 41% yield (184 mg, 243 μmol). UV/Vis (CH_2Cl_2): λ_{max} (nm) ($\varepsilon \times 10^{-3}$ L mol^{-1} cm^{-1}) = 419 (426), 515 (18), 550 (8), 591 (5.5), 648 (4×10^{-3} L mol^{-1} cm^{-1}). ^{1}H NMR (300 MHz, $CDCl_3$): δ = –2.62 (s, 2 H, NH), 1.62 (s, 12 H, CH_3), 2.61 (s, 6 H, CH_3), 4.14 (s 4 H, CH_2), 7.26 (s, 4 H, H_{Mes}), 7.63 (d, J = 7.7 Hz, 4 H, H_{Ar}), 8.16 (d, J = 7.7 Hz, 4 H, H_{Ar}), 8.66 (d, J = 4.8 Hz, 4 H, H_β), 8.82 (d, J = 4.8 Hz, 4 H, H_β) ppm. ^{13}C NMR (125 MHz, $CDCl_3$): δ = 21.7, 21.8, 46.4, 118.5, 119.3, 125.6, 126.6, 126.9, 127.9, 130.3, 131.4, 134.9, 135.2, 137.9, 138.7, 139.6, 140.8 ppm. MS (MALDI-TOF): calcd. for $C_{52}H_{49}N_6$ 757.402 [M + H]$^+$; found 757.400.

5,15-Bis{[4-(DO3A*t*BuAM)*N*-methyl]phenyl}-10,20-dimesitylporphyrin (3): Bis[4-(aminomethyl)phenyl]porphyrin **2** (97 mg, 128 μmol) was dissolved in $CHCl_3$ (12 mL). Commercially available dota-tris(*t*Bu)ester NHS ester (201 mg, 246 μmol) was added and the reaction mixture was stirred at room temperature and shielded from light for 3 h. The organic layer was washed successively with a citric acid solution (pH 5) and a saturated $NaHCO_3$ solution, dried with $MgSO_4$, and then evaporated under reduced pressure. The crude product was purified by chromatography over silica with $CHCl_3$/MeOH (100:5) mixture as eluent. The purple fraction was collected and evaporated under reduced pressure. Compound **3** was isolated as a purple microcrystalline solid in 44% yield (104 mg, 56 μmol). UV/Vis (CH_2Cl_2): λ_{max} = 418 (340), 516 (12), 548 (5), 591 (3), 646 nm (2×10^{-3} L mol^{-1} cm^{-1}). ^{1}H NMR (400 K, 500 MHz, [D$_6$]DMSO): δ = –2.46 (s, 2 H, NH), 1.43 (m, 54 H, *t*Bu), 1.82 (s, 12 H, CH_3), 2.61 (s, 6 H, CH_3), 2.50–2.70 (br., 32 H, N-CH_2-CH_2-N), 3.22 (br., 12 H, N-CH_2-COO*t*Bu), 3.31 (s, 4 H, N-CH_2-CONH), 4.73 (d, J = 5.7 Hz, 4 H, Ph-CH_2-CONH), 7.34 (s, 4 H, H_{Mes}), 7.73 (d, J = 7.9 Hz, 4 H, H_{Ar}), 8.14 (d, J = 7.9 Hz, 4 H, H_{Ar}), 8.61 (br., 2 H, CONH), 8.61 (d, J = 4.7 Hz, 4 H, H_β), 8.76 (d, J = 4.7 Hz, 4 H, H_β) ppm. HRMS (ESI): calcd. for $C_{108}H_{148}N_{14}O_{14}Na_2$ 955.5542 [M + 2Na]$^{2+}$; found 955.5543.

5,15-Bis{[4-(DO3AAM)*N*-methyl]phenyl}-10,20-dimesitylporphyrin (4): Bis{[(DO3A*t*BuAM)*N*-methyl]phenyl}porphyrin **3** (50 mg, 27 μmol) was dissolved in CH_2Cl_2 (5 mL) in the presence of trifluoroacetic acid (1 mL). The solution turned from purple to green. The reaction mixture was stirred at room temperature for 24 h, shielded from light. It was then evaporated under vacuum, the residues were dissolved in CH_2Cl_2, and the volatiles were removed under reduced pressure. This procedure was repeated four times to remove the TFA and *t*BuOH. The compound was then dissolved in Milli-Q water and freeze-dried. Compound **4** was isolated as a brown powder in 98% yield (39 mg, 25.4 μmol). UV/Vis (H_2O): λ_{max} = 429 (140), 519 (10), 553 (5), 592 (4), 648 nm (3×10^{-3} L mol^{-1} cm^{-1}). ^{1}H NMR (400 K, 500 MHz, [D$_6$]DMSO): δ = 1.82 (s, 12 H, CH_3), 2.62 (s, 6 H, CH_3), 3.00–3.25 (m, 32 H, N-CH_2-CH_2-N), 3.71 (br. s, 12 H, N-CH_2-COOH), 3.86 (s, 4 H, N-CH_2-CONH), 4.74 (d, J = 4.2 Hz, 4 H, Ph-CH_2-CONH), 7.35 (s, 4 H, H_{Mes}), 7.74 (d, J = 7.9 Hz, 4 H, H_{Ar}), 8.17 (d, J = 7.9 Hz, 4 H, H_{Ar}), 8.70 (m, 10 H, H_β, CONH) ppm. HRMS (ESI): calcd. for $C_{84}H_{102}N_{14}O_{14}$ 765.3844 [M + 2H]$^{2+}$; found 765.3812.

5,10,15,20-Tetrakis[4-(azidomethyl)phenyl]porphyrin (5): *p*-(Azidomethyl)benzaldehyde (1.32 g, 8.19 mmol) and 5-[*p*-(azidomethyl)phenyl]dipyrromethane (2.32 g, 8.36 mmol) were dissolved in $CHCl_3$ (280 mL). Shielded from light, the reaction mixture was stirred with N_2 bubbling for 15 min at room temperature. Boron trifluoride–diethyl ether (48%, 232 μL, 0.88 mmol) was added dropwise and the mixture was vigorously stirred for 2 h. *p*-Chloranil (2.02 g, 8.21 mmol) was then added to the reaction mixture, which was stirred for 2 h. The solvent was evaporated under reduced pressure and the crude material was purified by column chromatography over silica with CH_2Cl_2 as eluent. After recrystallization in CH_2Cl_2/MeOH, compound **5** was isolated as a purple microcrystalline solid in 32% yield (1.10 g, 1.32 mmol). UV/Vis (CH_2Cl_2): λ_{max} = 417 (520), 514 (20), 549 (10), 589 (6), 647 nm (5×10^{-3} L mol^{-1} cm^{-1}). ^{1}H NMR (300 MHz, $CDCl_3$): δ = –2.80 (s, 2 H, NH_{porph}), 4.71 (s, 8 H, Ph-CH_2-N_3), 7.70 (d, J = 7.8 Hz, 8 H, H_{Ar}), 8.21 (d, J = 7.8 Hz, 8 H, H_{Ar}), 8.82 (s, 8 H, H_β) ppm. ^{13}C NMR (75 MHz, $CDCl_3$): δ = 55.0, 119.8, 126.7, 135.0, 135.2, 142.2 ppm. MS (MALDI-TOF): calcd. for $C_{48}H_{35}N_{16}$ 835.323 [M + H]$^+$; found 835.290.

5,10,15,20-Tetrakis[4-(aminomethyl)phenyl]porphyrin (6): Compound **6** was isolated as a purple microcrystalline solid in 70% yield (155 mg, 212 μmol), following the procedure described for compound **2**, starting from tetrakis[4-(azidomethyl)phenyl]porphyrin **5** (70%, 250 mg, 300 μmol) in the presence of distilled THF (60 mL) and $LiAlH_4$ (95%, 130 mg, 3.5 mmol). UV/Vis (CH_2Cl_2): λ_{max} = 419 (316), 515 (12), 549 (6), 588 (4), 648 nm (3×10^{-3} L mol^{-1} cm^{-1}). ^{1}H NMR (300 MHz, $CDCl_3$): δ = –2.77 (s, 2 H, NH_{porph}), 4.22 (s, 8 H, Ph-CH_2-NH_2), 7.68 (d, J = 7.8 Hz, 8

 © 2013 Wiley-VCH Verlag GmbH & Co. KGaA, Weinheim

H, H_{Ar}), 8.16 (d, J = 7.8 Hz, 8 H, H_{Ar}), 8.82 (s, 8 H, H_β) ppm. MS (MALDI-TOF): calcd. for $C_{48}H_{43}N_8$ 731.361 $[M + H]^+$; found 731.492.

5,10,15,20-Tetrakis{[4-(DO3A*t*BuAM)*N*-methyl]phenyl}porphyrin (7): Tetrakis[4-(aminomethyl)phenyl]porphyrin **6** (28 mg, 38 μmol) was dissolved in $CHCl_3$/MeOH solution (9–1, 10 mL). Commercially available dota-tris(*t*Bu)ester NHS ester (250 mg, 306 μmol) was added and the reaction mixture was stirred at room temperature, shielded from light for 3 h. The organic layer was washed successively with citric acid solution (pH 5) and saturated $NaHCO_3$ solution, dried with $MgSO_4$, and then evaporated under reduced pressure. The crude product was purified by chromatography over silica with $CHCl_3$/MeOH (100:5) as eluent. The purple fraction was collected and evaporated under reduced pressure. Compound **7** was isolated as a purple microcrystalline solid in 25% yield (29 mg, 9.8 μmol). UV/Vis (CH_2Cl_2): λ_{max} = 417 (260), 516 (10), 551 (5), 592 (3), 644 nm (2.5×10^{-3} L mol^{-1} cm^{-1}). ^{1}H NMR (400 K, 500 MHz, [D$_6$]DMSO): δ = –2.64 (s, 2 H, NH), 1.46 (br., 108 H, *t*Bu), 2.70 (br., 64 H, N-*CH*$_2$-*CH*$_2$-N), 3.24 (br., 24 H, N-*CH*$_2$-COO*t*Bu), 3.30 (br. s, 8 H, N-*CH*$_2$-CONH), 4.76 (d, J = 5.7 Hz, 8 H, Ph-*CH*$_2$-CONH), 7.75 (d, J = 7.6 Hz, 8 H, H_{Ar}), 8.15 (d, J = 7.6 Hz, 8 H, H_{Ar}), 8.65 (br., 4 H, CONH), 8.79 (s, 8 H, H_β) ppm. HRMS (ESI): calcd. for $C_{160}H_{242}N_{24}O_{28}Na_3$ 1005.5976 $[M + 3Na]^{3+}$; found 1005.5921.

5,10,15,20-Tetrakis{[(DO3AAM)*N*-methyl]phenyl}porphyrin (8): Compound **8** was isolated as a brown powder in 99% yield (52 mg, 22.8 μmol) following the procedure described for compound **4**, starting from tetrakis{[(DO3A*t*BuAM)*N*-methyl]phenyl}porphyrin **7** (70 mg, 23 μmol) in the presence of CH_2Cl_2 (5 mL) and trifluoroacetic acid (1 mL). UV/Vis (H_2O): λ_{max} = 416 (95), 517 (7), 552 (3), 595 (1.8), 649 nm (1.6×10^{-3} L mol^{-1} cm^{-1}). ^{1}H NMR (400 K, 500 MHz, [D$_6$]DMSO): δ = 3.10–3.30 (m, 64 H, N-*CH*$_2$-*CH*$_2$-N), 3.72 (s, 16 H, N-*CH*$_2$-COOH), 3.75 (s, 8 H, N-*CH*$_2$-COOH), 3.88 (s, 8 H, N-*CH*$_2$-CONH), 4.76 (br. s, 8 H, Ph-*CH*$_2$-CONH), 7.75 (d, J = 7.6 Hz, 8 H, H_{Ar}), 8.18 (d, J = 7.6 Hz, 8 H, H_{Ar}), 8.71 (br. s, 4 H, -CONH-), 8.82 (s, 8 H, H_β) ppm.

5,15-Bis[4-(acetamido)phenyl]-10,20-dimesitylporphyrin (9): Compound **9** was isolated after purification by column chromatography with CH_2Cl_2/MeOH (100–3) as eluent over silica and recrystallization in CH_2Cl_2/heptane as a purple microcrystalline solid in 13% yield (980 mg, 1.2 mmol), following the procedure described for compound **5**, starting from mesityldipyrromethane (5.0 g, 18.9 mmol) and 4-acetamidobenzaldehyde (3.08 g, 18.9 mmol) in the presence of $CHCl_3$ (2 mL), boron trifluoride–diethyl ether (48%, 1.5 mL, 5.7 mmol), and *p*-chloranil (4.65 g, 18.9 mmol). UV/Vis (CH_2Cl_2): λ_{max} = 420 (440), 516 (18), 551 (8), 591 (5.5), 649 nm (4.7×10^{-3} L mol^{-1} cm^{-1}). ^{1}H NMR (300 MHz, $CDCl_3$): δ = –2.64 (s, 2 H, NH), 1.82 (s, 12 H, CH_3), 2.34 (s, 6 H, CO-CH_3), 2.61 (s, 6 H, CH_3), 7.26 (s, 4 H, H_{Mes}), 7.86 (d, J = 8.3 Hz, 4 H, H_{Ar}), 8.15 (d, J = 8.3 Hz, 4 H, H_{Ar}), 8.66 (d, J = 4.8 Hz, 4 H, H_β), 8.78 (d, J = 4.8 Hz, 4 H, H_β) ppm. MS (MALDI-TOF): calcd. for $C_{54}H_{49}N_6O_2$ 813.391 $[M + H]^+$; found 813.388.

5,15-Bis[4-(amino)phenyl]-10,20-dimesitylporphyrin (10): Bis(acetamido)porphyrin **9** (980 mg, 1.2 mmol) was dissolved in EtOH (100 mL) in the presence of *p*-toluenesulfonic acid (1.02 g, 5.3 mmol). The reaction mixture was heated at reflux, shielded from light for 24 h. After cooling to room temperature, $CHCl_3$ (100 mL) was added and the organic layer washed three times with saturated $NaHCO_3$, dried with $MgSO_4$, and evaporated under reduced pressure. The crude material was purified by chromatography column over silica with CH_2Cl_2/MeOH (100:3) as eluent. After recrystallization in CH_2Cl_2/heptane, compound was obtained as a purple microcrystalline solid in 83% yield (730 mg, 1.0 mmol). UV/Vis (CH_2Cl_2): λ_{max} = 422 (311), 518 (14), 555 (10), 594 (5), 652 nm (5×10^{-3} L mol^{-1} cm^{-1}). ^{1}H NMR (300 MHz, $CDCl_3$): δ = –2.60 (s, 2 H, NH_{porph}), 1.82 (s, 12 H, CH_3), 2.61 (s, 6 H, CH_3), 3.99 (s, 4 H, Ph-*NH*$_2$), 7.04 (d, J = 8.4 Hz, 4 H, H_{Ar}), 7.26 (s, 4 H, H_{Mes}), 7.97 (d, J = 8.4 Hz, 4 H, H_{Ar}), 8.64 (d, J = 4.8 Hz, 4 H, H_β), 8.85 (d, J = 4.8 Hz, 4 H, H_β) ppm. ^{13}C NMR (75 MHz, $CDCl_3$): δ = 21.7, 21.8, 113.7, 118.1, 119.8, 127.9, 132.5, 135.7, 137.8, 138.9, 139.6, 146.1 ppm. MS (MALDI-TOF): calcd. for $C_{50}H_{45}N_6$ 729.3706 $[M + H]^+$; found 729.161. HRMS (ESI): calcd. for $C_{50}H_{44}N_6Na$ 751.3520 $[M + Na]^+$; found 751.3535.

5-[4-(Amino)phenyl]-15-[4-(chloromethyl)amidophenyl]-10,20-dimesitylporphyrin (11): Bis[4-(amino)phenyl]porphyrin **10** (175 mg, 240 μmol) was dissolved in CH_2Cl_2 (50 mL) in the presence of *N*,*N*-diisopropylethylamine (DIPEA; 40 μL, 241 μmol), chloroacetyl chloride (18 μL, 230 μmol) was added, and the mixture was stirred at room temperature, shielded from light for 2 h. The solvent was removed under reduced pressure and the residue was purified by chromatography over fine silica with $CHCl_3$/heptane/EtOAc (50:30:20) as eluent. Three products were isolated in the following order of elution: bis(chloro)porphyrin **12** (67 mg, 76 μmol, 32% yield), the mono(chloro)porphyrin **11**, and finally the starting material **10** (62 mg, 85 μmol, 35% yield). After recrystallization in $CHCl_3$/heptane, compound **11** was isolated as a purple microcrystalline solid in 33% yield (64 mg, 79 μmol). UV/Vis (CH_2Cl_2): λ_{max} = 421 (345), 517 (16), 553 (10), 593 (6), 650 nm (5×10^{-3} L mol^{-1} cm^{-1}). ^{1}H NMR (300 MHz, $CDCl_3$): δ = –2.61 (s, 2 H, NH), 1.82 (s 12 H, CH_3), 2.61 (s, 6 H, CH_3), 4.00 (s, 2 H, NH_2), 4.34 (s, 2 H, CH_2), 7.04 (d, J = 8.4 Hz, 2 H, *Ph*-NH_2), 7.26 (s, 4 H, H_{Mes}), 7.92 (d, J = 8.4 Hz, 2 H, *Ph*-NHCO), 7.97 (d, J = 8.4 Hz, 2 H, *Ph*-NH_2), 8.20 (d, J = 8.4 Hz, 2 H, *Ph*-NHCO), 8.56 (s, 1 H, Ph-*NH*CO), 8.66 (m, 4 H, H_β), 8.76 (d, J = 4.7 Hz, 2 H, H_β), 8.86 (d, J = 4.7 Hz, 2 H, H_β) ppm. MS (MALDI-TOF): calcd. for $C_{52}H_{46}ClN_6O$ 805.34161 $[M + H]^+$; found 805.678. HRMS (ESI): calcd. for $C_{52}H_{46}ClN_6O$ 805.3416 $[M + H]^+$; found 805.3448. $C_{52}H_{45}ClN_6O{\cdot}0.2CH_2Cl_2{\cdot}0.8C_7H_{16}$ (902.556): C 76.92, H 6.50, N 9.31; found C 76.76, H 6.72, N 9.31.

5,15-Bis[4-(chloromethyl)amidophenyl]-10,20-dimesitylporphyrin (12): This product was obtained as a byproduct during the synthesis of mono(chloro)porphyrin **11**. Compound **12** was isolated as a purple microcrystalline solid in 32% yield (67 mg, 76 μmol). UV/Vis (CH_2Cl_2): λ_{max} = 419 (350), 515 (14), 551 (6), 592 (4), 647 nm (3×10^{-3} L mol^{-1} cm^{-1}). ^{1}H NMR (300 MHz, $CDCl_3$): δ = –2.64 (s, 2 H, NH_{porph}), 1.82 (s 12 H, CH_3), 2.61 (s, 6 H, CH_3), 4.35 (s, 4 H, CH_2), 7.27 (s, 4 H, H_{Mes}), 7.94 (d, J = 8.5 Hz, 4 H, H_{Ar}), 8.20 (d, J = 8.5 Hz, 4 H, H_{Ar}), 8.57 (s, 2 H, CONH), 8.68 (d, J = 4.7 Hz, 4 H, H_β), 8.78 (d, J = 4.7 Hz, 4 H, H_β) ppm. MS (MALDI-TOF): calcd. for $C_{54}H_{46}Cl_2N_6O_2$ 880.306 $[M]^+$; found 880.261. HRMS (ESI): calcd. for $C_{54}H_{46}Cl_2NaN_6O_2$ 903.2952 $[M + Na]^+$; found 903.2991.

5,15-Bis[4-(bromomethyl)amidophenyl]-10,20-dimesitylporphyrin (13): Bis[4-(amino)phenyl]porphyrin **10** (560 mg, 767 μmol) was dissolved in CH_2Cl_2 (70 mL) in the presence of diisopropylethylamine (125 μL, 756 μmol), bromoacetyl bromide (98%; 67 μL, 766 μmol) was added, and the mixture was stirred at 0 °C, shielded from light for 1 h. The solvent was removed under reduced pressure and the residue was purified by chromatography over fine silica using $CHCl_3$/heptane/EtOAc (50:30:20) as eluent. Compound **13** was isolated as a purple microcrystalline solid in 65% yield (241 mg, 248 μmol). UV/Vis (CH_2Cl_2): λ_{max} = 419 (417), 515 (17), 551 (8), 595 (5), 649 nm (4×10^{-3} L mol^{-1} cm^{-1}). ^{1}H NMR (300 MHz, $CDCl_3$): δ = –2.64 (s, 2 H, NH), 1.82 (s, 12 H, CH_3),

© 2013 Wiley-VCH Verlag GmbH & Co. KGaA, Weinheim

2.61 (s, 6 H, CH_3), 4.34 (s, 4 H, CH_2), 7.26 (s, 4 H, H_{Mes}), 7.91 (d, J = 8.7 Hz, 4 H, H_{Ar}), 8.20 (d, J = 8.7 Hz, 4 H, H_{Ar}), 8.56 (s, 2 H, CONH), 8.66 (d, J = 4.7 Hz, 4 H, H_β), 8.77 (d, J = 4.7 Hz, 4 H, H_β) ppm. ^{13}C NMR (125 MHz, $CDCl_3$): δ = 21.7, 21.8, 29.8, 118.4, 118.7, 128.0, 135.3, 136.9, 138.0, 138.6, 139.1, 139.6, 163.8 ppm. MS (MALDI-TOF): calcd. for $C_{54}H_{47}Br_2N_6O_2$ 970.220 $[M + H]^+$; found 969.097. HRMS (ESI): calcd. for $C_{54}H_{47}Br_2N_6O_2$ 969.2122 $[M + H]^+$; found 969.2146.

5,15-Bis[(DO3A*t*BuAM)*N*-phenyl]-10,20-dimesityl-porphyrin (14): Compound **14** was synthesized by two different protocols (A and B) starting from compounds **12** and **13**, respectively. **Procedure A:** Porphyrin **12** (100 mg, 113 μmol) was dissolved in DMF (10 mL) in the presence of K_2CO_3 (156 mg, 1.13 mmol) and DO3A*t*Bu (117 mg, 227 μmol). The reaction was stirred at 70 °C, shielded from light, and monitored by TLC and MALDI-TOF MS. After 12 h, K_2CO_3 was removed by filtration and the solvent removed under vacuum. The crude material was purified by column chromatography over silica with CH_2Cl_2/MeOH (100:10) as eluent. Compound **14** was isolated as a purple microcrystalline solid in 26% yield (55 mg, 30 μmol).

Procedure B: Bis(bromo)porphyrin **13** (20 mg, 20.6 μmol) was dissolved in DMF (3 mL) in the presence of K_2CO_3 (13 mg, 94 μmol) and DO3A*t*Bu (23 mg, 44.7 μmol). The reaction mixture was stirred at room temperature and monitored by TLC and MALDI-TOF MS. After 1 h, K_2CO_3 was removed by filtration and the solvent removed under vacuum. The crude material was purified by chromatography column over silica with CH_2Cl_2/MeOH (100:10) as eluent. Compound **14** was isolated as a purple microcrystalline solid in 94% yield (35.8 mg, 19.4 μmol). UV/Vis (CH_2Cl_2): λ_{max} = 420 (318), 516 (12.5), 552 (6), 594 (3.8), 646 nm (3×10^{-3} L mol^{-1} cm^{-1}). ^1H NMR (400 K, 500 MHz, [D$_6$]DMSO): δ = –2.44 (s, 2 H, NH_{porph}), 1.45 (s, 18 H, *t*Bu), 1.47 (s, 36 H, *t*Bu), 1.82 (s 12 H, CH_3), 2.61 (s, 6 H, CH_3), 2.63–2.91 (br. s, 32 H, N-CH_2-CH_2-N), 3.23 (s, 4 H, N-CH_2-COO*t*Bu), 3.29 (s, 8 H, N-CH_2-COO*t*Bu), 3.50 (s, 4 H, N-CH_2-CONH), 7.34 (s, 4 H, H_{Mes}), 8.04 (d, J = 8.7 Hz, 4 H, H_{Ar}), 8.09 (d, J = 8.7 Hz, 4 H, H_{Ar}), 8.61 (d, J = 4.7 Hz, 4 H, H_β), 8.7 (d, J = 4.8 Hz, 4 H, H_β), 10.35 (s, 2 H, CONH) ppm. MS (MALDI-TOF): calcd. for $C_{106}H_{144}N_{14}O_{14}Na$ 1860.08 $[M + Na]^+$; found 1859.96. HRMS (ESI): calcd. for $C_{106}H_{144}N_{14}O_{14}Na_2$ 941.5385 $[M + 2Na]^{2+}$; found 941.5350.

5,15-Bis[(DO3AAM)*N*-phenyl]-10,20-dimesitylporphyrin (15): Compound **15** was isolated as a brown powder in 99% yield (81 mg, 54 μmol), following the procedure described for compound **4**, starting from bis(DO3A*t*BuAMphenyl)porphyrin **14** (100 mg, 54 μmol) in the presence of CH_2Cl_2 (5 mL) and trifluoroacetic acid (1 mL). UV/Vis (H_2O): λ_{max} = 416 (120), 517 (6), 555 (4), 588 (3), 640 nm (2×10^{-3} L mol^{-1} cm^{-1}). ^1H NMR (400 K, 500 MHz, [D$_6$]DMSO): δ = 1.82 (s 12 H, CH_3), 2.61 (s, 6 H, CH_3), 3.15–3.33 (br., 32 H, N-CH_2-CH_2-N), 3.76 (s, 4 H, N-CH_2-COOH), 3.79 (s, 8 H, N-CH_2-COOH), 3.97 (s, 4 H, N-CH_2-CONH), 7.34 (s, 4 H, H_{Mes}), 8.05 (d, J = 8.3 Hz, 4 H, H_{Ar}), 8.15 (d, J = 8.3 Hz, 4 H, H_{Ar}), 8.63 (d, J = 4.7 Hz, 4 H, H_β), 8.80 (d, J = 4.7 Hz, 4 H, H_β), 10.35 (s, 2 H, CONH) ppm. MS (MALDI-TOF): calcd. for $C_{82}H_{97}N_{14}O_{14}$ 1501.730 $[M + H]^+$; found 1501.624; calcd. for $C_{82}H_{96}N_{14}O_{14}Na$ 1523.712 $[M + Na]^+$; found 1523.607. HRMS (ESI): calcd. for $C_{82}H_{97}N_{14}O_{14}$ 1501.7303 $[M + H]^+$; found 1501.7346; calcd. for $C_{82}H_{96}N_{14}O_{14}Na$ 1523.7122 $[M + Na]^+$; found 1523.7153.

5-[4-(Amino)phenyl]-15-[(DO3A*t*BuAM)*N*-phenyl]-10,20-dimesitylporphyrin (16): Mono(chloro)porphyrin **11** (144 mg, 180 μmol) was dissolved in DMF (20 mL) in the presence of K_2CO_3 (80 mg, 580 μmol) and DO3A*t*Bu (92 mg, 180 μmol). The reaction mixture was stirred at room temperature, shielded from light, and monitored by TLC and MALDI-TOF MS. After 2 h, K_2CO_3 was removed by filtration and the solvent removed under vacuum. The crude materials were purified by column chromatography over silica with CH_2Cl_2/EtOAc/MeOH (80:10:10) as eluent. Compound **16** was isolated as a purple microcrystalline solid in 90% yield (208 mg, 162 μmol). UV/Vis (CH_2Cl_2): λ_{max} = 421 (290), 518 (13), 555 (7), 593 (4), 651 nm (3.5×10^{-3} L mol^{-1} cm^{-1}). ^1H NMR (400 K, 500 MHz, [D$_6$]DMSO): δ = –2.40 (s, 2 H, NH), 1.41 (s, 9 H, *t*Bu), 1.47 (s, 18 H, *t*Bu), 1.82 (s 12 H, CH_3), 2.61 (s, 6 H, CH_3), 2.78 (m, 16 H, N-CH_2-CH_2-N), 3.27 (s, 2 H, N-CH_2-CO-O*t*Bu), 3.31 (s, 4 H, N-CH_2-COO*t*Bu), 3.42 (s, 2 H, N-CH_2-CONH), 5.14 (s, 2 H, Ph-NH_2), 7.04 (d, J = 8.3 Hz, 2 H, *Ph*-NH_2), 7.33 (s, 4 H, H_{Mes}), 7.85 (d, J = 8.3 Hz, 2 H, *Ph*-NH_2), 8.04 (d, J = 8.5 Hz, 2 H, *Ph*-CONH), 8.15 (d, J = 8.5 Hz, 2 H, *Ph*-CONH), 8.59 (d, J = 4.8 Hz, 4 H, H_β), 8.77 (d, J = 4.8 Hz, 2 H, H_β), 8.88 (d, J = 4.8 Hz, 2 H, H_β), 10.24 (s, 1 H, -Ph-CONH-) ppm. ^{13}C NMR (300 K, 125 MHz, $CDCl_3$): δ = 21.7, 21.8, 28.2, 28.3, 28.4, 29.9, 55.9, 56.0, 57.2, 82.2, 82.4, 113.7, 118.1, 118.9, 127.9, 129.9, 132.5, 134.7, 135.1, 135.8, 136.7, 137.8, 138.9, 139.3, 139.6, 146.1, 169.9, 171.8, 172.4 ppm. MS (MALDI-TOF): calcd. for $C_{78}H_{94}N_{10}O_7Na$ 1305.72 $[M + Na]^+$; found 1305.62. HRMS (ESI): calcd. for $C_{78}H_{94}N_{10}O_7Na$ 1305.7199 $[M + Na]^+$; found 1305.7181. $C_{78}H_{94}N_{10}O_7\cdot1.5CH_2Cl_2$ (1411.043): C 67.67, H 6.93, N 9.93; found C 67.36, H 7.19, N 9.65.

5-[4-(Amino)phenyl]-15-[(DO3AAM)*N*-phenyl]-10,20-dimesitylporphyrin (17): Compound **17** was isolated as a brown powder in 99% yield (86 mg, 77 μmol), following the procedure described for compound **4**, starting from porphyrin **16** (100 mg, 78 μmol) in the presence of CH_2Cl_2 (5 mL) and trifluoroacetic acid (1 mL). UV/Vis (H_2O): λ_{max} = 482 (60), 523 (6), 560 (4), 592 (2.5), 653 nm (2.2×10^{-3} L mol^{-1} cm^{-1}). ^1H NMR (400 K, 600 MHz, [D$_6$]-DMSO): δ = 1.82 (s, 12 H, CH_3), 2.61 (s, 6 H, CH_3), 3.11–3.30 (m, 16 H, N-CH_2-CH_2-N), 3.80 (s, 6 H, N-CH_2-COOH), 4.00 (s, 2 H, N-CH_2-CONH), 7.13 (d, J = 8.3 Hz, 2 H, *Ph*-NH_2), 7.34 (s, 4 H, H_{Mes}), 7.90 (d, J = 8.3 Hz, 2 H, *Ph*-NH_2), 8.03 (d, J = 8.4 Hz, 2 H, *Ph*-CONH), 8.15 (d, J = 8.4 Hz, 2 H, *Ph*-CONH), 8.61 (d, J = 4.7 Hz, 4 H, H_β), 8.77 (d, J = 4.7 Hz, 2 H, H_β), 8.87 (d, J = 4.7 Hz, 2 H, H_β), 10.34 (s, 1 H, Ph-CO*NH*) ppm. MS (MALDI-TOF): calcd. for $C_{66}H_{71}N_{10}O_7$ 1115.55 $[M + H]^+$; found 1115.50; calcd. for $C_{66}H_{70}N_{10}O_7Na$ 1137.53 $[M + Na]^+$; found 1137.49. HRMS (ESI): calcd. for $C_{66}H_{70}N_{10}O_7KNa$ 588.2476 $[M + K + Na]^{2+}$; found 588.2427.

10,15-Bis{[gadolinium(DO3AAM)]*N*-methylphenyl}-10,20-dimesitylporphyrin (18): Porphyrin **4** (26 mg, 17 μmol) was dissolved in Milli-Q water in the presence of DMSO (10% v/v) and the pH was adjusted to 8 by the addition of NaOH solution (1 M). $Gd(NO_3)_3\cdot5H_2O$ (16.3 mg, 37.6 μmol) was added, the pH was adjusted to 7 by the addition of NaOH (0.1 M), and the reaction mixture was stirred at 50 °C, shielded from light for 12 h. After cooling to room temperature, the desired compound precipitated in solution. The solid was filtered, washed three times with Milli-Q water, and dried under reduced pressure to afford compound **18** as a purple powder in 54% yield (17 mg, 9.2 μmol). UV/Vis (H_2O): λ_{max} = 433 (90), 518 (14), 552 (9), 591 (6,5), 649 nm (5×10^{-3} L mol^{-1} cm^{-1}). HRMS (ESI): calcd. for $C_{84}H_{94}Gd_2N_{14}O_{14}Na_2$ 942.2684 $[M + 2Na]^{2+}$; found 942.2645.

5,10,15,20-Tetrakis{[gadolinium(DO3AAM)]*N*-methylphenyl}-porphyrin (19): Compound **19** was isolated as a purple powder in 62% yield (20 mg, 7 μmol), following the procedure described for compound **18**, starting from porphyrin **8** (25 mg, 11 μmol) in Milli-Q water/DMSO (10:1, 10 mL) and with $Gd(NO_3)_3\cdot5H_2O$ (24 mg, 55 μmol). UV/Vis (H_2O): λ_{max} = 431 (84), 520 (16), 557 (13), 592

 © 2013 Wiley-VCH Verlag GmbH & Co. KGaA, Weinheim

(10), 650 nm (10×10^{-3} L mol^{-1} cm^{-1}). HRMS (ESI): calcd. for $C_{112}H_{135}Gd_4N_{24}O_{28}Na_3$ 987.8830 [M + 3Na]$^{3+}$; found 987.8862.

5,15-Bis[gadolinium(DO3AAM)*N*-phenyl]-10,20-dimesitylporphyrin (20): Compound **20** was isolated as a purple powder in 54% yield (40 mg, 21.5 μmol), following the procedure described for compound **18**, starting from porphyrin **15** (60 mg, 40 μmol) in Milli-Q water/DMSO (10:1, 10 mL) and with $Gd(NO_3)_3 \cdot 5H_2O$ (38 mg, 88 μmol). After cooling to room temperature, the desired compound precipitated in solution. The solution was centrifuged and the supernatant was removed and replaced by Milli-Q water. This procedure was repeated three times to remove the salts and DMSO. The product was then freeze-dried to afford the desired compound. HPLC: t_r = (83%, λ = 430 nm, conditions: A/B 25:75 to A/B 0:100 in 10 min, then A/B 0:100 for 20 min). UV/Vis (H_2O): λ_{max} = 430 (153), 519 (16), 555 (8), 592 (5.6), 648 nm (4×10^{-3} L mol^{-1} cm^{-1}). HRMS (ESI): calcd. for $C_{82}H_{90}Gd_2N_{14}O_{14}Na_2$ 928.2513 [M + 2Na]$^{2+}$; found 928.2545.

5-[4-(Amino)phenyl]-15-[gadolinium(DO3AAM)*N*-phenyl]-10,20-dimesitylporphyrin (21): Compound **21** was isolated after purification by semi-preparative HPLC as a purple powder in 70% yield (20 mg, 15.7 μmol), following the procedure described for compound **20**, starting from bis(DO3AAM)porphyrin **17** (26 mg, 23.3 μmol) in Milli-Q water/DMSO (10:1, 5 mL) with $Gd(NO_3)_3 \cdot 5H_2O$ (11.1 mg, 25.6 μmol). HPLC: t_r = 5.925 (100%, λ = 428 nm, conditions: A/B 10:90 to A/B 0:100 in 5 min, then A/B 0:100 for 15 min). UV/Vis (H_2O): λ_{max} = 427 (75), 521 (8.5), 559 (5.4), 595 (3.4), 652 nm (2.8×10^{-3} L mol^{-1} cm^{-1}). MS (MALDI-TOF): calcd. for $C_{66}H_{68}GdN_{10}O_7$ 1270.451 [M + H]$^+$; found 1270.403. HRMS (ESI): calcd. for $C_{66}H_{66}GdN_{10}O_7$ 1268.4361 [M – H]$^-$; found 1268.4374.

Copper(II) 5,15-Bis[gadolinium(DO3AAM)*N*-phenyl]-10,20-dimesitylporphyrin (22): The gadolinium complex **20** (20 mg, 11 μmol) was dissolved in MeOH (5 mL) in the presence of a $Cu(NO_3)_2$ solution (0.0396 M, 11 μmol, 270 μL). The reaction mixture was stirred at 50 °C, shielded from light, and monitored by UV/Vis spectroscopy. After 3 h, the solvent was removed under reduced pressure. The solid was washed three times with Milli-Q water by centrifugation to remove the salts. The product was then freeze-dried to afford the desired compound **22** as a red powder in 45% yield. HPLC: t_r = 6.563 (80%, λ = 428 nm, conditions: A/B 25:75 to A/B 0:100 in 10 min, then A/B 0:100 for 10 min). UV/Vis (H_2O): λ_{max} = 428 (140), 541 (19), 579 nm (5.6×10^{-3} L mol^{-1} cm^{-1}). HRMS (ESI): calcd. for $C_{82}H_{88}CuGd_2N_{14}Na_2O_{14}$ 958.7092 [M + 2Na]$^{2+}$; found 958.7103.

Copper(II) 5-[4-(Amino)phenyl]-15-[gadolinium(DO3AAM)*N*-phenyl]-10,20-dimesitylporphyrin (23): Compound **23** was isolated as a purple powder in 40% yield (4 mg, 3.0 μmol), following the procedure described for compound **22**, starting from gadolinium complex **21** (10 mg, 7.8 μmol) in MeOH (5 mL) in the presence of $Cu(NO_3)_2$ (198 μL, 0.0396 M, 7.8 μmol). HPLC: t_r = 7.370 (80%, λ = 420 nm, conditions: A/B 10:90 to A/B 0:100in 5 min, then A/B 0:100 for 15 min). UV/Vis (H_2O): λ_{max} = 420 (83), 543 (11), 580 nm (3×10^{-3} L mol^{-1} cm^{-1}). MS (MALDI-TOF): calcd. for $C_{66}H_{66}CuGdN_{10}O_7$ 1331.365 [M + H]$^+$; found 1331.334. HRMS (ESI): calcd. for $C_{66}H_{66}CuGdN_{10}O_7$ 1331.3653 [M + H]$^+$; found 1331.3713; calcd. for $C_{66}H_{65}CuGdN_{10}NaO_7$ 1353.3473 [M + Na]$^+$; found 1353.3521.

Supporting Information (see footnote on the first page of this article): ^{1}H NMR spectra of compounds **1**–**17**, mass spectra (MALDI/TOF or HRMS-ESI) of the different compounds, HPLC chromatograms of compounds **20**–**22**, transversal relaxivity r_2 measurements of complexes at different temperatures, crystal data and structure refinement for $(NaBr)_2$ **14**.

Acknowledgments

Financial support was provided by the Centre National de la Recherche Scientifique (CNRS) (UMR 6302), the Université de Bourgogne and the Conseil Régional de Bourgogne through the 3MIM integrated project ("Marquage de Molécules par les Métaux pour l'Imagerie Médicale"). The authors are very thankful to Dr Frédéric Boschetti and CheMatech Company for providing the dota-tris(*t*Bu)ester and DO3AtBu precursors. The French Ministry of Research is acknowledged for a Ph. D. scholarship (to A. E.). The authors are also thankful to Dr. Jean-Luc Beltramo and Dr. Myriam Laly (Welience, Pôle Chimie Analytique) for the ICP-AES measurements and to Marie-José Penouilh (Welience, Pôle Chimie Moléculaire) for the T_1 measurements (300 MHz). Consejo Nacional de Ciencia y Tecnología (CONACYT), Mexico is acknowledged for a Ph. D. scholarship (to C. L.). COST action CM105 and Ligue contre le cancer also supported this study.

[1] J. L. Major, T. J. Meade, *Acc. Chem. Res.* **2009**, *42*, 893–903.
[2] W. Krause, *Contrast agents I: Magnetic Resonance Imaging*, Springer, Berlin, **2002**.
[3] a) R. Weissleder, M. J. Pittet, *Nature* **2008**, *452*, 580–589; b) B. J. Pichler, H. F. Wehrl, M. S. Judenhofer, *J. Nucl. Med.* **2008**, *49*, 5s–23s.
[4] L. Marti-Bonmati, R. Sopena, P. Bartumeus, P. Sopena, *Contrast Media Mol. Imaging* **2010**, *5*, 180–189.
[5] H. Kobayashi, M. R. Longmire, M. Ogawa, P. L. Choyke, *Chem. Soc. Rev.* **2011**, *40*, 4626–4648.
[6] a) C. S. Bonnet, E. Toth, *C. R. Chim.* **2010**, *13*, 700–714; b) P. Caravan, J. J. Ellison, T. J. McMurry, R. B. Lauffer, *Chem. Rev.* **1999**, *99*, 2293–2352; c) L. Frullano, T. J. Meade, *J. Biol. Inorg. Chem.* **2007**, *12*, 939–949; d) L. Lattuada, A. Barge, G. Cravotto, G. B. Giovenzana, L. Tei, *Chem. Soc. Rev.* **2011**, *40*, 3019–3049.
[7] C. P. Gros, A. Eggenspiller, A. Nonat, J.-M. Barbe, F. Denat, *MedChemComm* **2011**, *2*, 119–125.
[8] a) B. Andrioletti, D. Ricard, B. Boitrel, *New J. Chem.* **1999**, *23*, 1143–1150; b) A. Beeby, R. S. Dickins, S. FitzGerald, L. J. Govenlock, C. L. Maupin, D. Parker, J. P. Riehl, G. Siligardi, J. A. G. Williams, *Chem. Commun.* **2000**, *13*, 1183–1184; c) S. Murugesan, S. J. Shetty, T. S. Srivastava, O. P. D. Noronha, A. M. Samuel, *Appl. Radiat. Isot.* **2001**, *55*, 641–646; d) E. Rose, A. Kossanyi, M. Quelquejeu, M. Soleilhavoup, F. Duwavran, N. Bernard, A. Lecas, *J. Am. Chem. Soc.* **1996**, *118*, 1567–1568.
[9] E. Valeur, M. Bradley, *Chem. Soc. Rev.* **2009**, *38*, 606–631.
[10] A. Takai, M. Chkounda, A. Eggenspiller, C. P. Gros, M. Lachkar, J.-M. Barbe, S. Fukuzumi, *J. Am. Chem. Soc.* **2010**, *132*, 4477–4489.
[11] B. J. Littler, M. A. Miller, C. H. Hung, R. W. Wagner, D. F. O'Shea, P. D. Boyle, J. S. Lindsey, *J. Org. Chem.* **1999**, *64*, 1391–1396.
[12] D. K. Lavallee, Z. J. Xu, R. Pina, *J. Org. Chem.* **1993**, *58*, 6000–6008.
[13] L. Le Pleux, Y. Pellegrin, E. Blart, F. Odobel, A. Harriman, *J. Phys. Chem. A* **2011**, *115*, 5069–5080.
[14] F. Brégier, S. M. Aly, C. P. Gros, J.-M. Barbe, Y. Rousselin, P. D. Harvey, *Chem. Eur. J.* **2011**, *17*, 14643–14662.
[15] C. R. Bertozzi, E. M. Sletten, *Angew. Chem.* **2009**, *121*, 7108; *Angew. Chem. Int. Ed.* **2009**, *48*, 6974–6998.
[16] J. R. Mays, R. L. W. Roska, S. Sarfaraz, H. Mukhtar, S. R. Rajski, *ChemBioChem* **2008**, *9*, 729–747.
[17] M. Sibrian-Vazquez, T. J. Jensen, F. R. Fronczek, R. P. Hammer, M. G. H. Vicente, *Bioconjugate Chem.* **2005**, *16*, 852–863.

 © 2013 Wiley-VCH Verlag GmbH & Co. KGaA, Weinheim

[18] J. Lee, Y. Kim, S. K. Kang, I. Choi, J. Yi, *Korean J. Chem. Eng.* **2006**, *23*, 512–515.
[19] K. Kumar, C. Allen Chang, L. C. Francesconi, D. D. Dischino, M. F. Malley, J. Z. Gougoutas, M. F. Tweedle, *Inorg. Chem.* **1994**, *33*, 3567–3575.
[20] E. Terreno, D. D. Castelli, A. Viale, S. Aime, *Chem. Rev.* **2010**, *110*, 3019–3042.
[21] a) N. Bloembergen, L. O. Morgan, *J. Chem. Phys.* **1961**, *34*, 842–850; b) I. Solomon, *Phys. Rev.* **1955**, *99*, 559–565.
[22] a) L. N. Goswami, W. H. White, J. A. Spernyak, M. Ethirajan, Y. Chen, J. R. Missert, J. Morgan, R. Mazurchuk, R. K. Pandey, *Bioconjugate Chem.* **2010**, *21*, 816–827; b) F. Hindre, M. Le Plouzennec, J. D. De Certaines, M. T. Foultier, T. Patrice, G. Simonneaux, *J. Magn. Reson. Imaging* **1993**, *3*, 59–65; c) Y. Song, H. Zong, E. R. Trivedi, B. J. Vesper, E. A. Waters, A. G. M. Barrett, J. A. Radosevich, B. M. Hoffman, T. J. Meade, *Bioconjugate Chem.* **2010**, *21*, 2267–2275.
[23] P. Hermann, J. Kotek, V. Kubicek, I. Lukes, *Dalton Trans.* **2008**, *23*, 3027–3047.
[24] P. Caravan, *Chem. Soc. Rev.* **2006**, *35*, 512–523.
[25] A. S. Merbach, L. Helm, E. Toth, *The chemistry of contrast agents in medical magnetic resonance imaging*, Wiley, Chichester, UK, **2013**.
[26] a) P. Caravan, C. T. Farrar, L. Frullano, R. Uppal, *Contrast Media Mol. Imaging* **2009**, *4*, 89–100; b) S. Laurent, L. V. Elst, R. N. Muller, *Contrast Media Mol. Imaging* **2006**, *1*, 128–137.
[27] E. Balogh, M. Mato-Iglesias, C. Platas-Iglesias, E. Tóth, K. Djanashvili, J. A. Peters, A. de Blas, T. Rodríguez-Blas, *Inorg. Chem.* **2006**, *45*, 8719–8728.
[28] P. Caravan, G. Parigi, J. M. Chasse, N. J. Cloutier, J. J. Ellison, R. B. Lauffer, C. Luchinat, S. A. McDermid, M. Spiller, T. J. McMurry, *Inorg. Chem.* **2007**, *46*, 6632–6639.
[29] S. Benosman, X. Meng, Y. Von Grabowiecki, L. Palamiuc, L. Hritcu, I. Gross, G. Mellitzer, Y. Taya, J.-P. Loeffler, C. Gaiddon, *J. Biol. Chem.* **2011**, *286*, 43013–43025.
[30] a) D. P. J. Pan, A. H. Schmieder, S. A. Wickline, G. M. Lanza, *Tetrahedron* **2011**, *67*, 8431–8444; b) X. A. Zhang, K. S. Lovejoy, A. Jasanoff, S. J. Lippard, *Proc. Natl. Acad. Sci. USA* **2007**, *104*, 10780–10785.
[31] a) S. Liu, *Adv. Drug Delivery Rev.* **2008**, *60*, 1347–1370; b) T. J. Wadas, E. H. Wong, G. R. Weisman, C. J. Anderson, *Chem. Rev.* **2010**, *110*, 2858–2902.
[32] A. K. Hagan, T. Zuchner, *Anal. Bioanal. Chem.* **2011**, *400*, 2847–2864.
[33] G. Brunisholz, M. Randin, *Helv. Chim. Acta* **1959**, *42*, 1927–1938.
[34] C. Gaiddon, M. de Tapia, J.-P. Loeffler, *Mol. Endocrinol.* **1999**, *13*, 742–751.
[35] S. Benosman, I. Gross, N. Clarke, A. G. Jochemsen, K. Okamoto, J.-P. Loeffler, C. Gaiddon, *Cell Death Differ.* **2007**, *14*, 2047–2057.
[36] A. Altomare, G. Cascarano, C. Giacovazzo, A. Guagliardi, *J. Appl. Crystallogr.* **1993**, *26*, 343–350.
[37] G. M. Sheldrick, *SHELXL-97*, University of Göttingen, Germany, **1998**.
[38] L. J. Farrugia, *J. Appl. Crystallogr.* **1999**, *32*, 837–838.

Received: May 8, 2013
Published Online: August 26, 2013

 © 2013 Wiley-VCH Verlag GmbH & Co. KGaA, Weinheim

Results (Objective 3)

VII.B. Gold-phosphine-phorphyrin as potential metal-based theranostics.

J Biol Inorg Chem
DOI 10.1007/s00775-014-1220-8

ORIGINAL PAPER

Gold–phosphine–porphyrin as potential metal-based theranostics

Semra Tasan · Cynthia Licona · Pierre-Emmanuel Doulain · Clément Michelin · Claude P. Gros · Pierre Le Gendre · Pierre D. Harvey · Catherine Paul · Christian Gaiddon · Ewen Bodio

Received: 15 September 2014 / Accepted: 18 November 2014
© SBIC 2014

Abstract Two new gold-phosphine-porphyrin derivatives were synthesized and fully characterized, and their photophysical properties investigated along a water-soluble analog. The cytotoxicity of the compounds was tested on cancer cells (HCT116 and SW480), and their cell uptake was followed by fluorescence microscopy in vitro (on SW480). The proof that the water-soluble gold-phosphine-porphyrin is a biologically active compound that can be tracked in vitro was clearly established, especially concerning the water-soluble analog. Some preliminary photodynamic therapy (PDT) experiments were also performed. They highlight a dramatic increase of the cytotoxicity when the cells were illuminated for 30 min with white light.

Keywords Theranostics · Bimetallic complex · Gold complex · Optical imaging · Porphyrin

Electronic supplementary material The online version of this article (doi:10.1007/s00775-014-1220-8) contains supplementary material, which is available to authorized users.

S. Tasan · P.-E. Doulain · C. Michelin · C. P. Gros (✉) · P. Le Gendre · E. Bodio (✉)
Institut de Chimie Moléculaire de l'Université de Bourgogne, UMR 6302 CNRS, Université de Bourgogne, 9 Avenue A. Savary, BP 47870, 21078 Dijon, France
e-mail: claude.gros@u-bourgogne.fr

E. Bodio
e-mail: Ewen.Bodio@u-bourgogne.fr

C. Licona · C. Gaiddon
Unité 1113 INSERM, «Signalisation moléculaire du stress cellulaire et pathologies», Fédération de Médecine Translationelle de Strasbourg, Université de Strasbourg, Strasbourg, France

P. D. Harvey
Département de Chimie, Université de Sherbrooke, Sherbrooke JIK 2R1, QC, Canada

C. Paul
EPHE Cancer Immunotherapy Laboratory, 21000 Dijon, France

C. Paul
EA7269 EPHE-University of Burgundy, 21000 Dijon, France

C. Paul
University of Burgundy, 21000 Dijon, France

Introduction

Metal complexes are among the most currently investigated and used class of compounds in cancer chemotherapy [1–5]. Thousands of potential metallodrugs have been tested so far and have opened the way to a still increasing number of proposed targets and possible mechanisms of action [6–8]. However, these mechanisms are still poorly understood in most cases. Knowledge of the mechanism may help to suppress side effects of metal-based drugs, or at least, gives clues on how to attenuate or limit them. Nowadays, one approach is to think about some of these issues at the beginning of the study by conceiving new active compounds that can be tracked in vitro or/and in vivo. Unfortunately, adding an imaging agent to an already well-characterized drug often modifies its pharmacokinetics and sometimes it may also affect its mechanism of action. Consequently, it appears safer to start the study with a molecule already labeled. Such compounds are today considered as a kind of theranostics, even if they are not directly helpful for diagnosing a disease [9–11]. Among the promising anticancer agents, gold(I) complexes have appeared last decades as very potent cytotoxic agents [12, 13]. In particular, the study of auranofin and its derivatives is well known for their anti-arthritis and anticancer properties. Moreover,

Published online: 05 December 2014

gold compounds seem to imply innovative mechanisms of action in comparison to established anticancer drugs which should enable to overcome some resistance phenomenon issues [14–17]. In a previous study, we demonstrated the interest to couple a gold–phosphine complex to a Bodipy derivative [10]. In the present work, we have chosen porphyrin as fluorophore to have a more versatile theranostic.

Porphyrins have been pioneer agents for modern theranostics [18]. Indeed, heme derivatives have been used for cancer imaging as early as the 1920s. Porphyrin derivatives have been used to image, detect and treat different types of cancer and different forms of sick tissues including age-related macular degeneration (AMD) [19–23]. Porphyrins are known to display very rich photophysical properties: chemical and photochemical stability, high absorption coefficients and quantum yields, and emission in the therapeutical window (near-IR spectral region) which enables imaging in vivo [24]. Their versatility in cancer imaging and other pathological conditions was further demonstrated by their use as radiolabeled imaging probes and in the development of contrast enhancement agents for MRI and PET [25–27]. Recently, the roles of porphyrin molecules in imaging and PDT (and selective uptake in diseased tissue) and their utility in theranostic applications have been reviewed [14–16, 28, 29].

We now report the synthesis of gold-phosphine-porphyrin derivatives (Fig. 1). The study of these new complexes is discussed in relation to the possible applications in both imaging and therapeutic applications, and therefore, as new theranostic agents.

Experimental section

Chemicals and reagents

All reactions were carried out under an atmosphere of purified argon using Schlenk techniques. Solvents were dried and distilled under argon before use. The precursors [Au(tht)Cl] [30] and [$Au(PPh_2(CH_2)_2NH_2)Cl$] [31] and the porphyrin **6** [35] have been synthesized according to literature procedures. All other reagents were commercially available [from PorphyChem® for tetraphenylporphyrin (TPP)] and used as received. All the analyses were performed at the "Plateforme d'Analyses Chimiques et de Synthèse Moléculaire de l'Université de Bourgogne". The identity and purity (≥95 %) of the complexes were unambiguously established using high-resolution mass spectrometry and NMR.

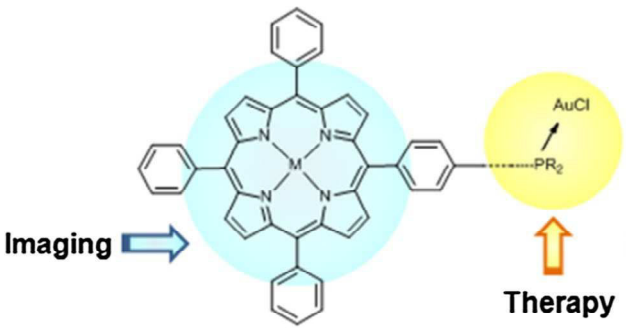


Fig. 1 General structure of targeted molecules

Instrumentation

^{1}H (300.13, 500.13, or 600.13 MHz), ^{13}C (75.5, 125.8, or 150.9 MHz), ^{31}P (121.5, 202.5, or 242.9 MHz) NMR spectra were recorded on a Bruker 300 Avance III, a Bruker 500 Avance III or on a Bruker 600 Avance II spectrometer. Chemical shifts are quoted in parts per million (δ) relative to TMS (^{1}H and ^{13}C), using the residual protonated solvent (^{1}H) or the deuterated solvent (^{13}C) as an internal standard. Alternatively, 85 % H_3PO_4 (^{31}P) was used as external standard. Coupling constants are reported in hertz and represent proton–proton coupling. Mass spectra were obtained by MALDI-TOF with a Bruker Ultraflex II spectrometer. High-resolution mass measurements were carried out using Bruker microTOF-Q ESI–MS or Thermo LTQ Orbitrap XL mass spectrometers and low-resolution mass measurements were carried out using a Bruker amaZon SL mass spectrometer. Far infrared spectra were recorded with a Bruker Vertex 70v FTIR spectrophotometer. Absorption spectra were recorded on a Varian Cary 50 spectrometer or on a JASCO V630 Bio spectrometer at the University of Burgundy and on a CARY 300 Bio at the University of Sherbrooke.

Fluorescence

The steady-state fluorescence emission and excitation spectra were obtained using a JASCO FP8560 spectrofluorometer instrument at the University of Burgundy and a double monochromator Fluorolog 2 spectrofluorometer (Spex) at the University of Sherbrooke.

Synthesis

*5-(4-Nitrophenyl)-10,15,20-triphenylporphyrin (**1a**)*

Meso-tetraphenylporphyrin (4.053 g, 6.59 mmol, 1.0 eq) was dissolved in trifluoroacetic acid (60 mL). Sodium nitrite (819 mg, 11.88 mmol, 1.8 eq) was added. The mixture was stirred exactly 3 min. The resulting solution was transferred to an erlenmeyer containing 150 mL of distilled water and 150 mL of chloroform. The trifluoroacetic

acid was neutralized with saturated aqueous $NaHCO_3$. The mixture was washed three times with water (3 × 300 mL), dried over magnesium sulfate and solvent was removed under reduced pressure. The residue was purified by silica gel column chromatography [eluent: dichloromethane/heptane (6/4)] to afford the desired pure product **1a** as a purple powder (3.278 g, 75 %).

UV–Vis (2-MeTHF): λ_{max} (nm) (ε, 10^3 M^{-1} cm^{-1}) 417 (445), 513 (17), 548 (5), 591 (1), 647 (0.4). IR: $\bar{\upsilon}$ (cm^{-1}): 1,345 (ν_{N-O}), 1,514 (ν_{N-O}), 3,313 (ν_{N-H}). ^{1}H NMR (500.13 MHz, $CDCl_3$): δ (ppm) −2.74 (br s, 2H, NH_{Porph}), 7.76 (m, 9H, H_{Ar}), 8.22 (m, 6H, H_{Ar}), 8.40 (d, 2H, $^3J = 8.7$ Hz, $C_6H_4NO_2$), 8.63 (d, 2H, $^3J = 8.7$ Hz, $C_6H_4NO_2$), 8.75 (d, 2H, $^3J = 4.8$ Hz, H_β), 8.88 (s, 4H, H_β), 8.91 (d, 2H, $^3J = 4.8$ Hz, H_β). $^{13}C\{^1H\}$ NMR (75.5 MHz, $CDCl_3$): δ (ppm) 149.4, 147.9, 142.0, 135.3, 134.7, 128.0, 127.9, 126.9, 122.0, 121.3, 120.8, 116.8. HR-MS (ESI): *m/z* calcd for $[C_{44}H_{29}N_5O_2 + Na]^+$: 682.22135 Da $[M + Na]^+$. Found: 682.21844 Da.

*Palladium 5-(4-nitrophenyl)-10,15,20-triphenylporphyrin (**1b**)*

[TPP(*p*-NO_2)] **1a** (300 mg, 0.46 mmol, 1.0 eq) and palladium dichloride (59 % Pd) (274 mg, 0.91 mmol, 2.0 eq) were dissolved in dimethylformamide (30 mL). The mixture was stirred for 16 h at reflux. The solvent was removed under reduced pressure. The solid was dissolved in dichloromethane (100 mL), washed three times with distilled water (3 × 150 mL), dried over magnesium sulfate and solvent was removed under reduced pressure. The residue was purified by silica gel column chromatography [eluent: dichloromethane/hexane (1/1)] to afford compound **1b** as a red–orange powder (347 mg, >99 %).

UV–Vis (THF): λ_{max} (nm) (ε, 10^3 M^{-1} cm^{-1}) 415 (331), 523 (27), 553 (3). IR: $\bar{\upsilon}$ (cm^{-1}) 1,347 (ν_{N-O}), 1,519 (ν_{N-O}). ^{1}H NMR (300.13 MHz, $CDCl_3$): δ (ppm) 7.75 (m, 9H, H_{Ar}), 8.17 (m, 6H, H_{Ar}), 8.31 (d, 2H, ^3J = 8.6 Hz, C_6H_4–NO_2), 8.57 (d, 2H, ^3J = 8.6 Hz, C_6H_4–NO_2), 8.69 (d, *2H*, $^3J = 5.0$ Hz, H_β), 8.85 (m, 6H, H_β). $^{13}C\{^1H\}$ NMR (75.5 MHz, $CDCl_3$): δ (ppm) 148.9, 147.9, 142.1, 142.0, 141.8, 141.6, 140.7, 134.2, 132.0, 131.9, 131.6, 131.4, 131.3, 130.1, 129.7, 129.4, 128.0, 127.9, 126.9, 124.1, 122.7, 122.4, 122.0, 118.6. HR-MS (ESI): *m/z* calcd for $[C_{44}H_{27}N_5O_2Pd + Na]^+$: 786.11074 Da $[M + Na]^+$. Found: 786.10809 Da.

*5-(4-Aminophenyl)-10,15,20-triphenylporphyrin (**2a**)*

The reaction was carried out under an argon atmosphere. [TPP(*p*-NO_2)] **1a** (316 mg, 0.48 mmol, 1.0 eq), 2-mercaptoethanol (0.34 mL, 4.79 mmol, 10.0 eq), lithium hydroxide (81 mg, 3.38 mmol, 7.0 eq) were dissolved in anhydrous dimethylformamide (20 mL). The mixture was stirred at 120 °C for 48 h. Completion of the reaction was monitored by TLC (silica gel, eluent: dichloromethane) and by MALDI-TOF spectrometer. The solution was diluted in chloroform (100 mL), washed three times with water (3 × 150 mL), dried over anhydrous calcium chloride. The solvent was removed under reduced pressure. The residue was purified by silica gel column chromatography (eluent: dichloromethane) to afford [TPP(*p*-NH_2)] **2a** (278 mg, 92 %).

UV–Vis (2-MeTHF): λ_{max} (nm) (ε, 10^3 M^{-1} cm^{-1}) 418 (400), 516 (17), 554 (9), 594 (2), 652 (1). IR: $\bar{\upsilon}$ (cm^{-1}) 1,176 (ν_{C-N}), 1,595 (δ_{NH2}), 3,313 (ν_{N-H}). ^{1}H NMR (500.13 MHz, $CDCl_3$): δ (ppm) −2.74 (br s, 2H, NH_{Porph}), 7.07 (d, 2H, $^3J = 8.7$ Hz, C_6H_4–NH_2), 7.76 (m, 9H, H_{Ar}), 8.00 (d, 2H, $^3J = 8.7$ Hz, C_6H_4–NH_2), 8.22 (m, 6H, H_{Ar}), 8.83 (m, 6H, H_β), 8.94 (d, 2H, $^3J = 4.8$ Hz, H_β). $^{13}C\{^1H\}$ NMR (75.5 MHz, $CDCl_3$): δ (ppm) 146.1, 142.5, 135.8, 134.7, 132.5, 127.8, 126.8, 121.0, 120.7, 120.2, 119.9, 113.6. HR-MS (MALDI-TOF): *m/z* calcd for $[C_{44}H_{31}N_5]^+$: 629.2574 Da $[M]^+$. Found: 629.2620 Da.

*Palladium 5-(4-aminophenyl)-10,15,20-triphenylporphyrin (**2b**)*

The reaction was carried out under an argon atmosphere. [TPP(*p*-NO_2)-Pd] **1b** (283 mg, 0.37 mmol, 1.0 eq), 2-mercaptoethanol (0.26 mL, 3.66 mmol, 9.9 eq), lithium hydroxide (62 mg, 2.59 mmol, 7.0 eq) were dissolved in anhydrous dimethylformamide (20 mL). The mixture was stirred at 120 °C for 48 h. Completion of the reaction was monitored by TLC [silica gel, eluent: dichloromethane/hexane (1/1)]. The solution was diluted in chloroform (100 mL), washed three times with water (3 × 150 mL), dried over magnesium sulfate. The solvent was removed under reduced pressure. The residue was purified by silica gel column chromatography [eluent: dichloromethane/hexane (1/1)] to afford [TPP(*p*-NH_2)-Pd] **2b** (233 mg, 86 %).

UV–Vis (2-MeTHF): λ_{max} (nm) (ε, 10^3 M^{-1} cm^{-1}) 418 (338), 526 (35), 564 (4). ^{1}H NMR (300.13 MHz, $CDCl_3$): δ (ppm) 7.16 (d, 2H, ^3J = 8.7 Hz, C_6H_4–NH_2), 7.74 (m, 9H, H_{Ar}), 7.99 (d, *2H*, ^3J = 8.4 Hz, C_6H_4–NH_2), 8.17 (m, 6H, H_{Ar}), 8.81 (m, 6H, H_β), 8.91 (d, 2H, ^3J = 5.0 Hz, H_β). $^{13}C\{^1H\}$ NMR (75.5 MHz, $CDCl_3$): δ (ppm) 146.1, 142.3, 142.0, 141.8, 141.6, 135.3, 134.3, 132.1, 131.4, 131.1, 131.0, 130.9, 127.9, 126.8, 122.5, 121.7, 121.6, 113.6. HR-MS (ESI): *m/z* calcd for $[C_{44}H_{29}N_5Pd + Na]^+$: 756.13656 Da $[M + Na]^+$. Found: 756.13922 Da.

*5-(4-Isothiocyanatophenyl)-10,15,20-triphenylporphyrin (**3a**)*

The reaction was carried out under an argon atmosphere. [TPP(*p*-NH_2)] (468 mg, 0.74 mmol, 1.0 eq) was dissolved in distilled dichloromethane (20 mL). Distilled

triethylamine (1.75 mL, 12.56 mmol, 16.9 eq) was added. The mixture was stirred for 10 min at 0 °C and under vigorous stirring, thiophosgene (0.17 mL, 2.22 mmol, 3.0 eq) was added dropwise. The resulting solution was stirred for 15 min at 0 °C and then 4 h at room temperature. The solvent was removed under reduced pressure. The residue was purified by filtration over a silica plug (eluent: dichloromethane) to afford [TPP(*p*-NCS)] **1** (351 mg, 70 %).

UV–Vis (2-MeTHF): λ_{max} (nm) (ε, 10^3 M^{-1} cm^{-1}) 417 (536), 513 (17), 548 (5), 592 (1), 647 (1). IR: $\bar{\upsilon}$ (cm^{-1}) 1,995–2,115 (ν_{NCS}), 3,317 (ν_{N-H}). ^{1}H NMR (300.13 MHz, $CDCl_3$): δ (ppm) −2.77 (br s, 2H, NH_{Porph}), 7.63 (d, 2H, ^3J = 8.3 Hz, C_6H_4-NCS), 7.78 (m, 9H, H_{Ar}), 8.22 (m, 8H, H_{Ar}), 8.79 (d, 2H, ^3J = 4.8 Hz, H_β), 8.87 (m, 6H, H_β). $^{13}C\{^1H\}$ NMR (75.5 MHz, $CDCl_3$): δ (ppm) 142.1, 141.6, 135.6, 134.7, 127.9, 126.9, 124.2, 122.1, 120.6, 116.9, 29.9. HR-MS (MALDI-TOF): *m/z* calcd for $[C_{45}H_{29}N_5S + H]^+$: 672.22164 Da $[M + H]^+$. Found: 672.22023 Da.

*Palladium 5-(4-isothiocyanatophenyl)-10,15,20-triphenylporphyrin (**3b**)*

The reaction was carried out under an argon atmosphere. Thiophosgene (0.12 mL, 1.57 mmol, 3.4 eq) was dissolved in distilled dichloromethane (4 mL). [TPP(*p*-NH_2)-Pd] (343 mg, 0.47 mmol, 3.4 eq), dissolved in distilled dichloromethane (20 mL), was added dropwise at 0 °C. Distilled triethylamine (1.11 mL, 7.96 mmol, 17.1 eq) was added. The resulting solution was stirred for 10 min at 0 °C and then 3 h at room temperature. The solvent was removed under reduced pressure. The residue was purified by filtration over a silica plug (eluent: dichloromethane) to afford [TPP(*p*-NCS)-Pd] **2** (338 mg, 93 %).

UV–Vis (2-MeTHF): λ_{max} (nm) (ε, 10^3 M^{-1} cm^{-1}) 416 (268), 523 (18), 554 (4). IR: $\bar{\upsilon}$ (cm^{-1}) 2,338–2,361 (ν_{NCS}). ^{1}H NMR (300.13 MHz, $CDCl_3$): δ (ppm) 7.59 (d, 2H, ^3J = 8.7 Hz, C_6H_4–NCS), 7.74 (m, 9H, H_{Ar}), 8.15 (m, 8H, H_{Ar}), 8.75 (d, 2H, ^3J = 5.0 Hz, H_β), 8.84 (m, 6H, H_β). $^{13}C\{^1H\}$ NMR (75.5 MHz, $CDCl_3$): δ (ppm) 141.9, 141.8, 141.3, 141.2, 135.2, 134.3, 131.5, 131.4, 131.3, 130.6, 128.0, 126.9, 124.2, 122.3, 122.1, 120.0, 29.9. HR-MS (MALDI-TOF): *m/z* calcd for $[C_{45}H_{27}N_5PdS]^+$: 775.1032 Da $[M]^+$. Found: 775.1032 Da.

*5-(4-(N-(2-(diphenylphosphino)ethyl)thiocarbamido) aminophenyl)-10,15,20-triphenylporphyrin (**4a**)*

The reaction was carried out under glove box. 2-(diphenylphosphino)ethylamine (103 mg, 0.45 mmol, 1.0 eq) and [TPP(*p*-NCS)] **1** (300 mg, 0.45 mmol, 1.0 eq) were dissolved in distilled dichloromethane (30 mL). The mixture was stirred for 4 h at room temperature. The solvent was removed under reduced pressure. The porphyrin derivative **3** was isolated as a purple powder (448 mg, >99 %).

UV–Vis (2-MeTHF): λ_{max} (nm) (ε, 10^3 M^{-1} cm^{-1}) 418 (414), 514 (19), 549 (9), 592 (5), 648 (4). IR: $\bar{\upsilon}$ (cm^{-1}) 801 ($\nu_{C=S}$), 1,348 (ν_{C-N}), 1,526 (ν_{C-N}), 1,526 (ν_{N-C-N}), 3,317 (ν_{N-H}). ^{1}H NMR (500.13 MHz, DMS0-d_6): δ (ppm) −2.87 (br s, 2H, NH_{Porph}), 2.58 (m, 2H, NH–CH_2), 3.75 (m, 2H, CH_2–PPh_2), 7.34–7.42 (m, 6H, *o*- and *p*-PPh_2), 7.52 (t, 4H, ^3J = 7.2 Hz, *m*-PPh_2), 7.56 (m, 1H, NH), 7.78–7.85 (m, 9H, H_{Ar}), 7.87 (d, 2H, ^3J = 8.4 Hz, C_6H_4–NH), 8.16 (d, 2H, ^3J = 8.4 Hz, C_6H_4 NH), 8.21 (m, 6H, H_{Ar}), 8.29 (m, 1H, NH), 8.83 (m, 6H, H_β), 8.93 (d, 2H, ^3J = 4.5 Hz, H_β). $^{13}C\{^1H\}$ NMR (125.8 MHz, DMSO-d_6): δ (ppm) 180.1, 141.2, 139.0, 137.9, 136.6, 134.6, 134.2, 132.4, 131.3, 128.7, 128.6, 128.0, 126.9, 121.0, 120.0, 119.9, 41.4, 26.9. $^{31}P\{^1H\}$ NMR (121.5 MHz, DMSO-d_6): δ (ppm) −21.6. HR-MS (ESI): *m/z* calcd for $[C_{59}H_{45}N_6PS + H]^+$: 901.32368 Da $[M + H]^+$. Found: 901.32380 Da.

*Palladium 5-(4-(N-(2-(diphenylphosphino) ethyl)thiocarbamido)aminophenyl)-10,15,20-triphenylporphyrin (**4b**)*

The reaction was carried out under an argon atmosphere. 2-(Diphenylphosphino)ethylamine (167 mg, 0.73 mmol, 1.3 eq) and [TPP(*p*-NCS)-Pd] **2** (430 mg, 0.55 mmol, 1.0 eq) were dissolved in distilled dichloromethane (11 mL). The mixture was stirred for 4 h at room temperature. The solvent was removed under reduced pressure. Distilled diethyl ether (10 mL) was added and the precipitate was filtered by cannula. The solid was washed three times with distilled diethyl ether to afford the porphyrin derivative **4** as a red–orange powder (551 mg, >99 %).

UV–Vis (2-MeTHF): λ_{max} (nm) (ε, 10^3 M^{-1} cm^{-1}) 416 (303), 523 (28), 554 (2). IR: $\bar{\upsilon}$ (cm^{-1}) 799 ($\nu_{C=S}$), 1,352 (ν_{C-N}), 1,530 (ν_{N-C-N}), 3,137 (ν_{N-H}). ^{1}H NMR (500.13 MHz, DMSO-d_6): δ (ppm) 2.56 (m, 2H, NH–CH_2), 3.73 (m, 2H, CH_2–PPh_2), 7.36–7.43 (m, 6H, *o*- and *p*-PPh_2), 7.52 (t, 4H, ^3J = 7.2 Hz, *m*-PPh_2), 7.79–7.90 (m, 12H, NH + H_{Ar} + C_6H_4–NH), 8.11 (d, 2H, ^3J = 8.2 Hz, C_6H_4–NH), 8.18 (d, 6H, ^3J = 6.7 Hz, H_{Ar}, 8.80 (m, 6H, H_β), 8.89 (d, 2H, ^3J = 4.8 Hz, H_β). $^{13}C\{^1H\}$ NMR (125.8 MHz, $CDCl_3$): δ (ppm) 180.8, 141.8, 141.7, 141.4, 140.9, 137.4, 136.0, 135.8, 134.2, 132.9, 132.8, 131.4, 131.3, 131.2, 130.7, 129.1, 129.0, 128.8, 128.6, 128.0, 127.9, 126.9, 123.2, 122.2, 122.1, 120.2, 42.8, 28.2. $^{31}P\{^1H\}$ NMR (202.5 MHz, DMSO-d_6): δ (ppm) −21.7. HR-MS (ESI): *m/z* calcd for $[C_{59}H_{43}N_6PPdS + Na]^+$: 1,027.19536 Da $[M + Na]^+$. Found: 1,027.19433 Da.

*[(5-(4-(N-(2-(diphenylphosphino)ethyl)thiocarbamido) aminophenyl)-10,15,20-triphenylporphyrin)-AuCl] (**5a**)*

The reaction was carried out under glove box. Porphyrin phosphine derivative **3** (100 mg, 0.11 mmol, 1.0 eq) and [Au(tht)Cl] (36 mg, 0.11 mmol, 1.0 eq) were dissolved in distilled dichloromethane (6 mL). The resulting mixture was stirred for 16 h at room temperature. Completion of the reaction was monitored by ^{31}P NMR (202.5 MHz, 300 K). The solvent was removed under reduced pressure. The gold complex **8** was isolated as a bright purple powder (126 mg, >99 %).

UV–Vis (2-MeTHF): λ_{max} (nm) (ε, 10^3 M^{-1} cm^{-1}) 418 (356), 514 (18), 549 (9), 592 (5), 651 (4). IR: $\bar{\upsilon}$ (cm^{-1}) 327 (ν_{Au-Cl}), 797 ($\nu_{C=S}$), 1,348 (ν_{C-N}), 1,537 (ν_{N-C-N}), 3,310 (ν_{N-H}). ^{1}H NMR (300.13 MHz, DMSO-d_6): δ (ppm) −2.89 (br s, 2H, NH_{Porph}), 3.26 (m, 2H, NH–CH_2), 3.97 (m, 2H, CH_2–PPh_2), 7.58–7.62 (m, 6H, *o*- and *p*-PPh_2), 7.78–7.91 (m, 16H, *m*-PPh_2 + NH + H_{Ar} + C_6H_4NH), 8.38 (br s, 1H, NH), 8.83 (m, 6H, H_β), 8.92 (d, 2H, ^3J = 4.8 Hz). ^{13}C{^{1}H} NMR (75.5 MHz, DMSO-d_6): δ (ppm) 141.1, 134.7, 134.2, 133.1, 132.1, 131.4, 129.6, 129.4, 128.1, 126.9, 120.0, 54.8, 31.0, 30.6. ^{31}P{^{1}H} NMR (121.5 MHz, DMSO-d_6): δ (ppm) 25.0. HR-MS (ESI): *m/z* calcd for $[C_{118}H_{90}N_{12}P_2S_2Au_2–2Cl_2]^{2+}$: 1,097.28295 Da [2M–2Cl]$^{2+}$. Found: 1,097.28256 Da.

*[(Palladium 5-(4-(N-(2-(diphenylphosphino) ethyl)thiocarbamido)aminophenyl)-10,15,20-triphenylporp hyrin)-AuCl] (**5b**)*

The reaction was carried out under an argon atmosphere. Porphyrin phosphine derivative **4** (101 mg, 0.10 mmol, 1.0 eq) and [Au(tht)Cl] (32 mg, 0.10 mmol, 1.0 eq) were dissolved in distilled dichloromethane (3 mL). The resulting mixture was stirred for 3 h at room temperature. Completion of the reaction was monitored by ^{31}P NMR (202.5 MHz, 300 K). The solvent was removed under reduced pressure. The gold complex **9** was isolated as a bright red powder (125 mg, >99 %).

UV–Vis (2-MeTHF): λ_{max} (nm) (ε, 10^3 M^{-1} cm^{-1}) 416 (276), 523 (26), 553 (2). IR: $\bar{\upsilon}$ (cm^{-1}) 795 ($\nu_{C=S}$), 1,352 (ν_{C-N}), 1,508 (ν_{N-C-N}), 3,049 (ν_{N-H}). ^{1}H NMR (500.13 MHz, DMSO-d_6): δ (ppm) 3.25 (m, 2H, NH–CH_2), 3.96 (m, 2H, CH_2–Ph), 7.59–7.64 (m, 6H, *o*- and *p*-PPh_2), 7.77–7.89 (m, 16H, *m*-PPh_2 + NH + C_6H_4NH + H_{Ar}), 8.12 (d, 2H, ^3J = 8.1 Hz, C_6H_4NH), 8.16 (d, 6H, ^3J = 6.9 Hz, H_{Ar}), 8.36 (br s, 1H, NH), 8.80 (m, 6H, H_β), 8.88 (d, 2H, ^3J = 4.9 Hz, H_β). ^{13}C{^{1}H} NMR (125.8 MHz, DMSO-d_6): δ (ppm) 140.9, 140.8, 140.7, 134.2, 133.7, 133.1, 132.0, 131.3, 131.2, 131.1, 129.4, 129.0, 128.1, 127.0, 121.7, 121.4, 53.6, 31.0, 30.6. ^{31}P{^{1}H} NMR (202.5 MHz, DMSO-d_6): δ (ppm) 24.9. HR-MS (ESI): *m/z* calcd for $[C_{59}H_{43}AuNPPdS–Cl]^+$: 1,201.17214 Da $[M–Cl]^+$. Found: 1,201.17254 Da.

*5,10,15-Tris(p-sulfonatophenyl)-20- (p-isothiocyanatophenyl)porphyrin (**7**)*

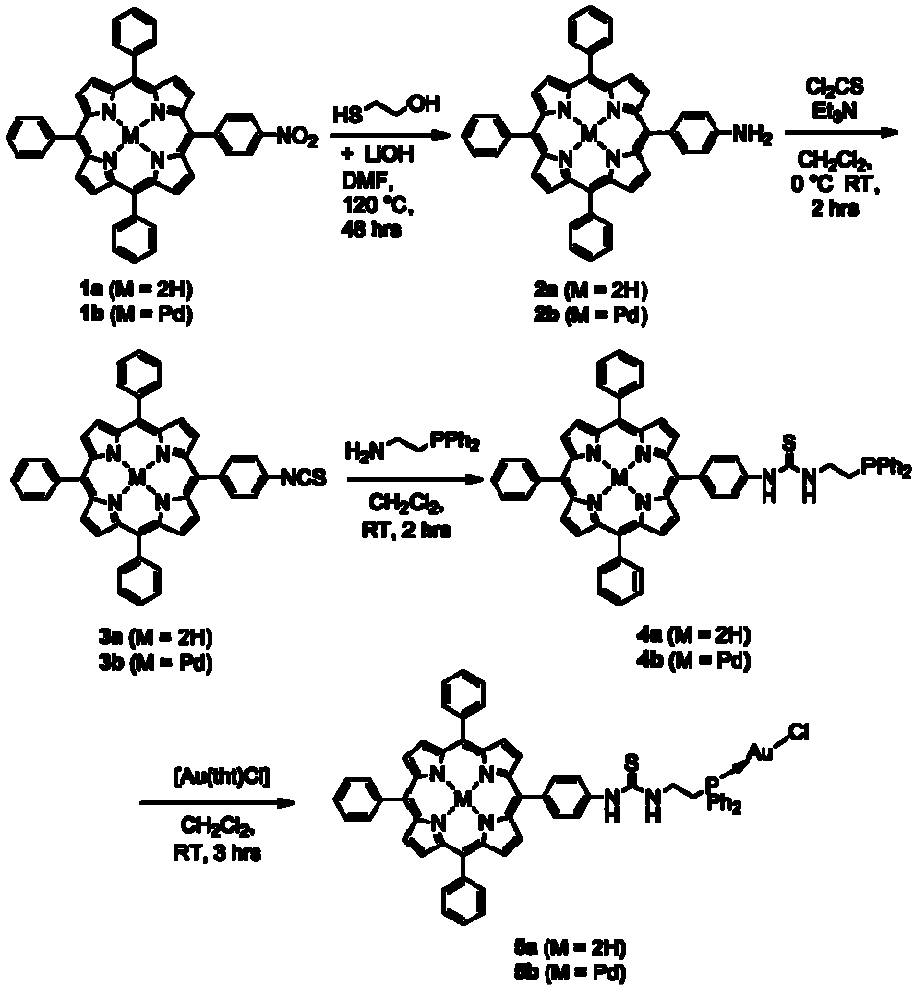
150 mg of 5,10,15-tris(*p*-sulfonatophenyl)-20-(*p*-aminophenyl)porphyrin [$TPPSO_3H$(*p*-NH_2)] (150 mg, 0.172 mmol, 1.0 eq) was added in 20 mL of water then pH was equilibrated to 7 by addition of NaOH (0.1 M). Then thiophosgene (75 µL, 0.975 mmol, ~6 eq.) in 15 mL of dichloromethane was added and the two-phase mixture was vigorously stirred at room temperature for 90 min. Aqueous phase was extracted, and then washed three times with 10 mL of dichloromethane to remove the excess of thiophosgene. The residual dichloromethane was then removed under reduce pressure and the product was isolated by lyophilization as a greenish powder (145 mg, 92 %).

UV–Vis (DMSO): λ_{max} (nm) (ε, 10^3 M^{-1} cm^{-1}) 420 (154), 518 (8), 553 (5), 593 (3), 648 (3). ^{1}H NMR (300 MHz, $CDCl_3$): δ (ppm) −2,93 (s, 2H), 7,88 (d, 2H, ^3J = 8.3 Hz), 8,05 (d, 6H, ^3J = 7.7 Hz), 8,18 (d, 6H, ^3J = 7.7 Hz), 8,31 (d, 2H, ^3J = 8.3 Hz), 8,85 (m, 8H). HR-MS (MALDI-TOF): *m/z* calcd for $[C_{45}H_{28}N_5O_9S_4]^+$: 910.0764 Da $[M]^+$. Found: 910.0777 Da.

*[5,10,15-Tris(p-sulfonatophenyl)-20-(4-(N- (2-(diphenyl phosphino)ethyl)thiocarbamido) aminophenyl-AuCl (**8**)*

The reaction was carried out under an argon atmosphere. Porphyrin isothiocyanate derivative (40 mg, 0.041 mmol, 1.0 eq) and [(2-(diphenylphosphino)ethylamine)-AuCl] (19 mg, 0.041 mmol, 1.0 eq) were dissolved in water/acetone (1:1) degassed (3 mL). The mixture was stirred for 2 h at room temperature. Completion of the reaction was monitored by ^{31}P NMR (202.5 MHz, 300 K). The solvent was removed under reduced pressure. To remove water, toluene was added four times (4 × 2 mL) and evaporated. The porphyrin derivative was isolated as a brown powder (59 mg, >99 %).

UV–Vis (DMSO): λ_{max} (nm) (ε, 10^3 M^{-1} cm^{-1}) 421 (172), 518 (8.0), 554 (4.8), 590 (2.7) 648 (2.6). ^{1}H NMR (600.13 MHz, DMSO-d_6): δ (ppm) −2.93 (br s, 2H, NH_{Porph}), 2.99–3.09 (m, 4H, NH–(CH_2)$_2$–PPh_2), 7.56–7.64 (m, 6H, *o*- and *p*-PPh_2), 7.76–7.79 (m, 4H, *m*-PPh_2), 7.88 (d, 2H, ^3J = 8.3 Hz, C_6H_4–NH), 8.05 (d, 6H, ^3J = 7.9 Hz, C_6H_4 SO_3Na), 8.18 (d, 6H, ^3J = 7.9 Hz, C_6H_4 SO_3Na + bs, 2H, 2NH), 8.30 (d, 2H, ^3J = 8.3 Hz, C_6H_4–NH), 8.79–8.89 (m, 8H, H_β). ^{31}P{^{1}H} NMR (202.5 MHz, DMSO-d_6): δ (ppm) 24.5. HR-MS (ESI): *m/z* calcd for $[C_{59}H_{42}AuClN_6Na_3O_9PS_4–Cl–3Na]^{2-}$: 667.06441 Da $[M–Cl–3Na]^{2-}$. Found: 667.06351 Da.



Scheme 1 Synthetic routes for the synthesis of phosphine-porphyrin complexes **4a,b** and **5a,b**

Cytotoxicity tests

Cell culture

HCT116 human colon cancer cells and SW480 colon cancer cells line were obtained from ATCC. Cells were manipulated and cultured in DMEM with 10 % FCS (Dominique Dutcher™) and 1 % penicillin + streptomycin (Sigma) at 37 °C with 5 % CO_2 atmosphere as previously described [32].

Cell survival

5,000 cells were seeded per well in 96-well microplates (Falcon Multiwell), 48 h prior to any treatment. RDCs were applied for 48 h in fresh medium. MTT assay was performed as previously described by replacing the medium with fresh medium supplemented with 5 mg/L MTT (Sigma) for 1 h [33]. Cells were lysed in isopropanol with 0.04 N HCl. Measurements were performed at 550 nm.

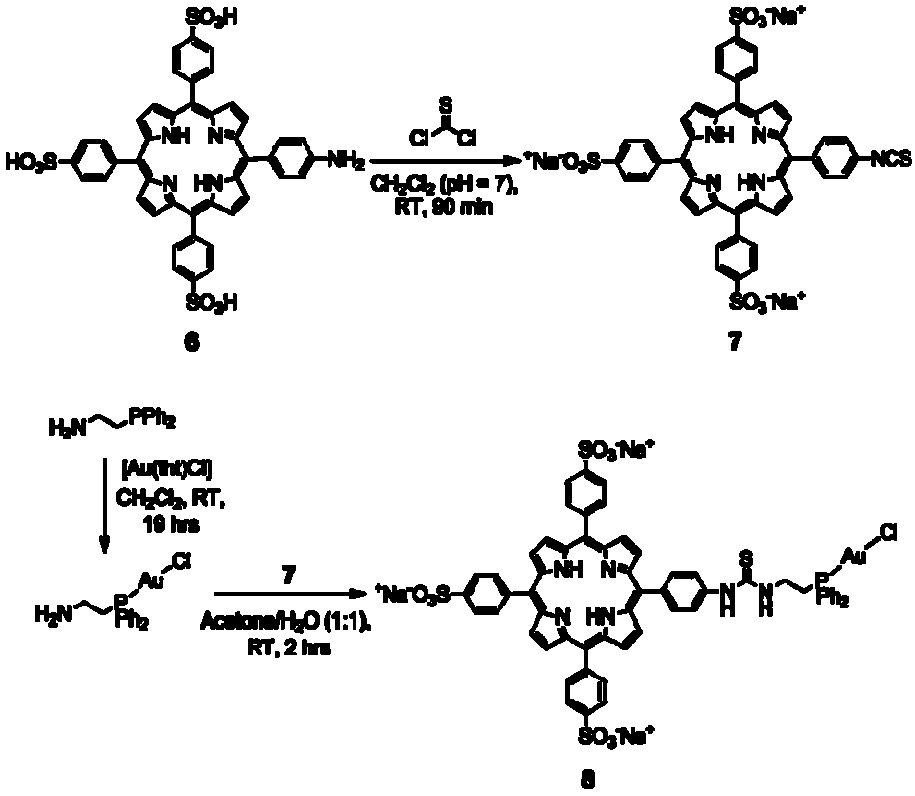
Light irradiation of the cells

HCT116 cells (2×10^4 cells/well) were grown in 96-well plates for 48 h and then treated with the compounds. 2 h after the addition of the compounds, cells were irradiated with a white light of a LED lamp (3 W, 0.75 A, white) at a 30 cm distance for 30 min. Cell survival was then tested by MTT after 48 h.

In vitro confocal microscopy experiment

SW480 cells were treated 5 min at 37 °C with different compounds (100 or 200 µM), rinsed three times with PBS before paraformaldehyde fixation. After cytospin (300 g, 10 min), cell fluorescence was visualized by confocal microscopy (Nikon Eclipse TE 2000). The transmitted light images and confocal epifluorescence images are acquired simultaneously using the same illumination beam. Excitation was provided by a 405-nm laser diode. Fluorescence emission was collected in the 688–728 nm range using the Nikon spectral imaging system. Image analysis was performed with Image J software.

Scheme 2 Synthetic route to the synthesis of water-soluble complex **8**



Results and discussion

Synthesis of the first generation of "theranostics"

There are only few reports of phosphine-porphyrin organometallic derivatives in the literature [34].[1] The previous, reported compounds were mainly dedicated to catalysis investigations or studied for their photophysical properties. We focused our attention in conceiving a simple and fast strategy which can readily furnish the desired complexes in high yield and at the gram scale.

Starting from the tetraphenylporphyrin (TPP), the phosphine-porphyrin ligand was efficiently synthesized in four steps (Scheme 1). The key step is the coupling reaction between the porphyrin isothiocyanate **3** and the aminoethyldiphenylphosphine. The TPP was monitored according to the literature method [35]. The nitro group was then reduced by mercaptoethanol [36]. This reduction was often described with $SnCl_2$ [37–39]; however, the use of a stannic derivative was not preferred because of its toxicity (we target therapeutical applications).[2] The isothiocyanate derivative was obtained by reacting **2** with thiophosgene by adapting literature procedure [40].

The coupling reaction required a particular attention to prevent the phosphine oxidation. Alkyldiphenylphosphine are well known to be quite sensitive to oxygen. Surprisingly, the free-base phosphine-porphyrin **4a** turned out to be significantly more sensitive than the metalated phosphine-porphyrin **4b** (Scheme 1). Indeed, **4a** requires synthesis and handling in a glove box whereas **4b** only requires the use of Schlenk techniques. The synthesis of metalated phosphine-porphyrin requires an additional step occurring just before the reduction of the nitro group. It consists in the metalation of the nitroporphyrin **1a**. Standard procedures were adapted to metalate the porphyrin core using palladium chloride [41]. The metalation reaction was monitored by UV–Vis spectroscopy and MALDI-TOF mass spectrometry.

After coupling **3a** and **3b** with aminoethyldiphenylphosphine, the phosphine-porphyrins **4a** and **4b** were selectively metalated on the phosphorus atom under mild conditions. The complexation reactions were monitored by ^{31}P NMR.

[1] So far to the best of our knowledge, the only publication that describes the synthesis of a phosphine-porphyrin gold derivative is from Gray's work. This molecule is totally different because the phosphine is not linked to the porphyrin.

[2] It is worth noting that mercaptoethanol is more toxic for the experimenter and for the environment than $SnCl_2$ but as it can be removed more easily by purification, it is preferred to stannic derivative for the conception of potential new drugs.

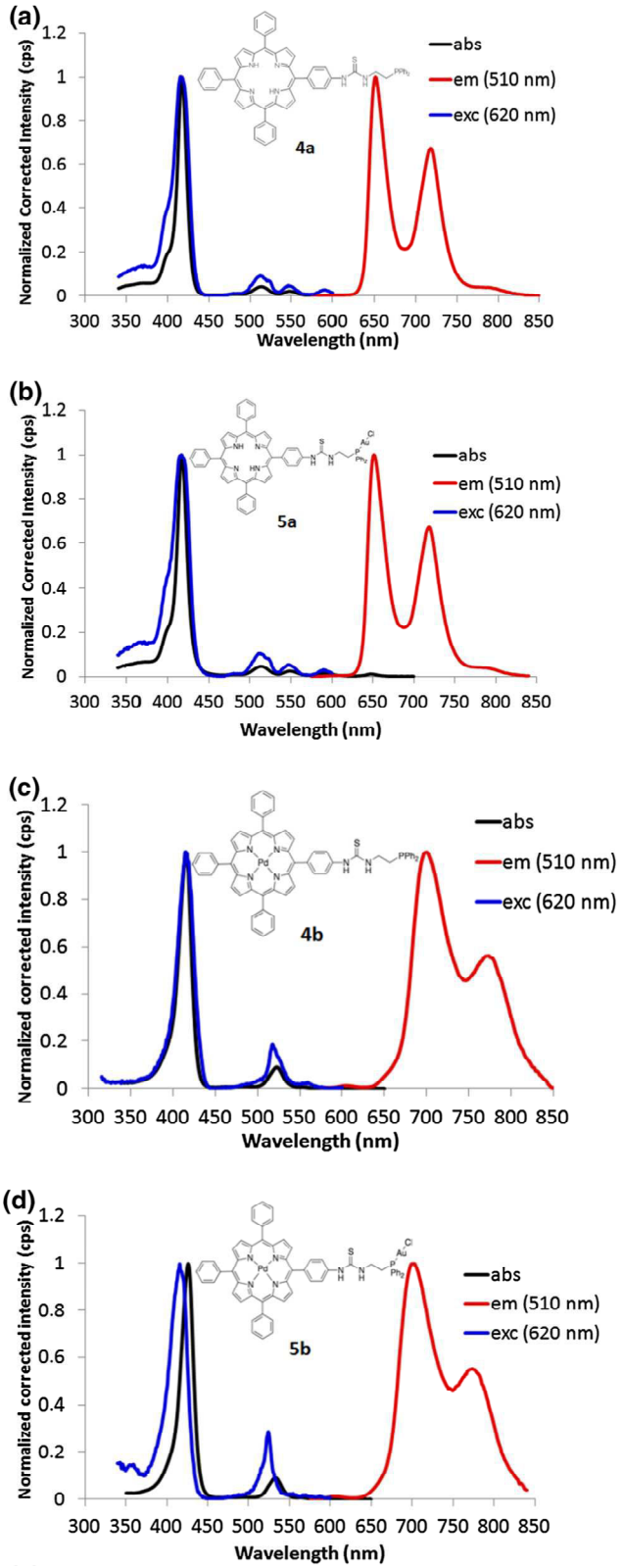


Fig. 2 Absorption (*black*), emission (*red*, λ_{exc} = 510 nm) and excitation (*blue*, λ_{em} = 620 nm) of compounds (**a**) **4a**; (**b**) **5a**; (**c**) **4b** and (**d**) **5b** in 2-MeTHF at 298 K. The 77 K spectra are placed in the ESI for convenience

Table 1 UV–Vis absorption data in 2-MeTHF at 298 K

λ_{max}, nm (ε, $\times 10^3$ M^{-1} cm^{-1})					
Dye	Soret band	Q bands			
Free-base porphyrin					
4a	418 (414.4)	514 (18.6)	549 (9.3)	592 (5.3)	648 (4.2)
5a	418 (318.4)	515 (18.6)	550 (9.9)	592 (5.5)	648 (4.4)
Pd porphyrin					
4b	416 (303.0)	523 (27.5)	554 (2.4)		
5b	416 (275.6)	523 (25.6)	553 (2.2)		

A significant shift of the resonance was observed going from the free phosphine ligands (singlet at −22 ppm) to the complexes (singlet at 25 ppm). All the steps were optimized to obtain an excellent overall yield [48 % for **5a** (5 steps)—60 % for **5b** (6 steps)] (Scheme 2).

Synthesis of the second generation of "theranostics"

The new complexes displayed poor water solubility. To address this issue, we decided to synthesize a sulfonate analog. Tris-sulfonate porphyrins are indeed known to be water soluble and they are often employed in biological studies [42, 43]. The sulfonate analog of phosphine-porphyrin **4a** was synthesized in two steps starting from the 5,10,15-tris(*p*-sulfonatophenyl)-20-(*p*-aminophenyl) porphyrin **6**. The porphyrin **6** was synthesized following the literature procedures [44]. The amino group was transformed in an isothiocyanate in good yield and this latter product **7** was directly reacted with [(2-(diphenylphosphino) ethylamine)-AuCl] to yield the desired complex **8** quantitatively [30, 31]. We chose to couple the aminophosphine already bound to the gold atom to prevent any oxidation of the phosphine. In this case, the gold atom behaved as a protecting group.

All the compounds were fully characterized by ^{1}H, ^{13}C, ^{31}P (for phosphine derivatives) NMR, and by HR-MS (see ESI). Their photophysical properties are presented below.

Photophysical properties of compounds **4a**, **4b**, **5a**, **5b**, and **8**

The absorption spectra (Fig. 2) of the free-base porphyrins (**4a** and **5a**) exhibit the expected intense Soret band (S_0–S_2 transition) at ~418 nm and four *Q* bands (S_0–$S_{1a,b}$ transitions) at ~515, 550, 592 and 648 nm at 298 K (Table 1). For the palladium(II) porphyrins (**4b** and **5b**), the typical Soret and two *Q* bands are observed at ~416 nm and ~523 and 554 nm, respectively, at 298 K (Table 1). **4a** and **5a**, and **4b** and **5b** (Fig. 2) exhibit fluorescence (~10–14 ns) and phosphorescence (~0.1–1.3 μs), respectively, as deduced by the emission lifetimes (Table 2) and the Stokes shifts (Table 3).

Table 2 Fluorescence lifetimes, τ_F, in 2-MeTHF

Dye	λ_{exc} (nm)	298 K			77 K	
		λ_{em} (nm)	τ_F (ns) (rel. int.)	Φ_e (%)	λ_{em} (nm)	τ_F (ns) (rel. int.)
Free-base porphyrin						
4a	510	651/718	10.8	12.0	644	14.5
5a	510	652/719	11.9	12.0	644	14.6
Pd porphyrins						
4b	510	700/774	101	6.9	685	1,335
5b	510	702/773	190	6.6	686	1,314

The uncertainties are ±10 % for Φ_e, ±0.1 ns for τ_F, ±50 ns for τ_e

Table 3 Stokes shifts at 298 and 77 K

Dye	298 K	77 K
	Stokes shift (cm^{-1})	
Free-base porphyrin		
4a	70	75
5a	25	100
Pd porphyrin		
4b	3,760	3,450
5b	3,840	3,440

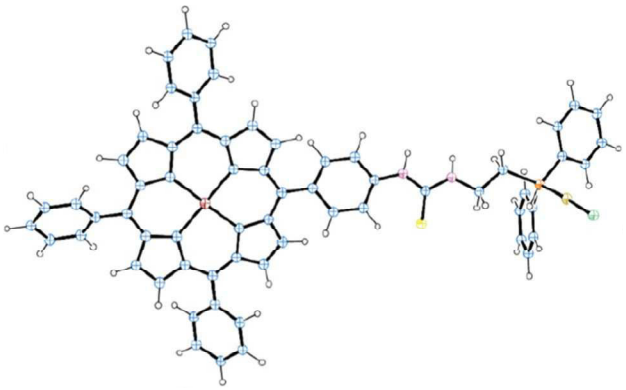


Fig. 3 Minimized structure generated image of **5b** with PCModel program (version 9.20). Center of the porphyrin···Au distance = 20.780 Å

The key feature is that the coordination of Au onto the dangling phosphorous does not change any spectral and photophysical parameters at all despite the possible heavy atom effect (the phenomenon was also observed in one of our previous study) [10]. A possible reason for this result is found in computer modeling (Fig. 3). Indeed, the lowest energy conformation shows no folding of the chain and the distance between porphyrin's centroid and gold atom is superior to 2 nm. The computed difference of energy between this conformation and that when rotations about the H_2C–CH_2 and H_2C–P bonds attempting to bring the Au atom closer to the porphyrin macrocycle is about 24.6 kJ mol^{-1} (vide infra), meaning that the folded conformation is unlikely as experimentally deduced.

The comparison of the absorption data of **5a** (Table 1) and **8** (Table 4) indicates that the absorptivity values are significantly smaller in the latter (by about a factor 2) which is most likely attributable to the different solvent conditions used for the measurements. However, their spectral positions as well as the position of the fluorescence and the Stoke shift ($\Delta\nu$) remain the same (Tables 2, 3, 4; Fig. 4). Noteworthy, the fluorescence quantum yield for **8** is 21 %, which is double that of compound **4a** (12 %). This increased quantum yield is an interesting feature for the sought applications in this work. One of such application is well illustrated below, notably in Fig. 5. Again, the objective is to design molecular devices easily optically detectable at the same time carrying a cytotoxic center.

IC50 determinations on cancer cells

The cytotoxicity of the novel metal-based compounds was tested on colon cancer cells. Colon cancer is a particularly frequent cancer with poor prognosis when diagnosed at a late stage characterized by the presence of metastasis. The sensitivity of the cancer cells toward treatment is often dependent on the status of the tumor suppressor gene p53 [46, 47]. Furthermore, a p53-mediated cytotoxicity often coincides with a possible toxicity for healthy tissues, such as the nervous system [48]. In addition, previous observation indicated that p53 might be important in porphyrin-based PDT. Therefore, we selected two cell lines with different p53 status: the HCT116 cells that express a wild-type p53 protein and the SW480 cells that express a mutated and inactivated p53 protein. The survival of the cancer cells in presence or absence of metal-based compounds was assessed by MTT assays after 48 h of treatment. The dose–response curve stopped at 200 µM (higher concentrations of **2a–5b** would imply a toxic dose of DMSO) and we calculated the IC50 when possible. Most of the compounds did not show significant toxicity (≥200

Table 4 Photophysical characterization of **8** in DMSO at 298 K

λ_{max}, nm (ε, $\times 10^3$ M^{-1} cm^{-1})					λ_{em} (nm)	Δν (cm^{-1})	Φ_e[a,b] (%)
Soret band	*Q* bands						
421 (172)	518 (8.0)	554 (4.8)	590 (2.7)	648 (2.6)	651	70	21

[a] $\lambda_{ex} = 510$ nm

[b] H_2TPP used reference, $\Phi_e = 0.11$ in 2-MeTHF, $\lambda_{ex} = 510$ nm

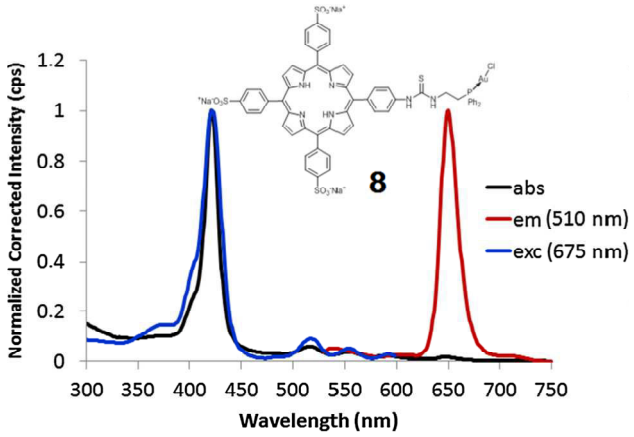


Fig. 4 Absorption (*black*), emission (*red*, $\lambda_{exc} = 510$ nm) and excitation (*blue*, $\lambda_{em} = 675$ nm) of compound **8** in DMSO at 298 K. It known that tris or tetra(*p*-sulfonatophenyl)-porphyrin can display either one or two fluorescence bands depending on the pH. For an example see: [45]

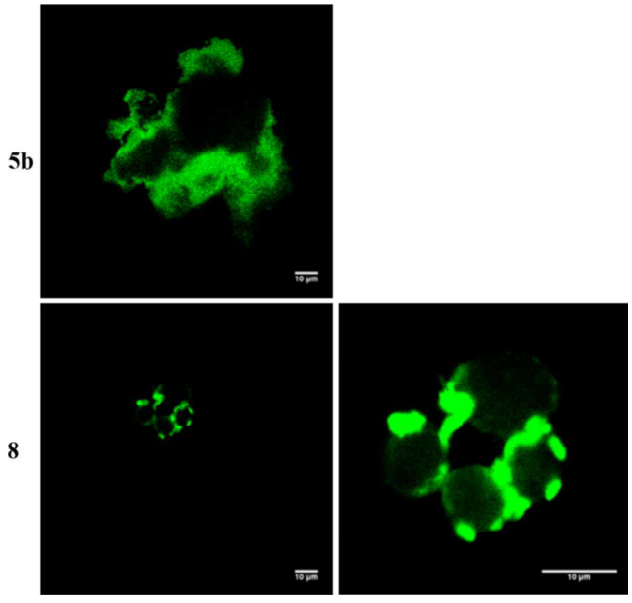


Fig. 5 Confocal microscopy images of SW480 cells incubated 5 min at 37 °C with **5b** and **8** (exc. 405 nm, filter 688–728 nm). Both the *left* pictures are at the same scale. Picture on the *right* is a zoom of *left bottom* picture

μM). Only the sulfonate complex **8** displayed an interesting cytotoxicity with an IC50 at 56 μM (±2 μM) in HCT116 and 72 μM (±2.6 μM) on SW480. These results can be explained in terms of solubility: contrary to **8**, **2a–5b** complexes are poorly soluble in water. Like **8**, compound **6** presents quite good water solubility but it displays a poor cytotoxicity with an IC50 of 197 μM (±3.2 μM) in HCT116. This result confirms that the cytotoxicity is brought mainly by the gold(I) moiety. The IC50s of these compounds were increased in SW480 expressing mutant p53 cells. It remains to establish whether this diminished sensitivity of SW480 to the compounds can be attributed to the presence of a mutated p53 and therefore a reduced p53 activity.

As mentioned in the introduction, porphyrin-based compounds are often used for PDT. Thus, we tested the possibility that our compounds might be more efficient when treated cells were illuminated. The different compounds were tested for photoactivation. In the case of complex **8**, the cytotoxicity increased dramatically, almost four times (IC50 14.8 μM) when the cells were illuminated for 30 min with white light (see "Experimental section"). The other compounds did not display significative improvement of cytotoxicity when cells were illuminated. The exact physicochemical mechanisms involved in the amelioration of compound **8** activity remain to be established.

*In vitro detection of **5b** and **8** by confocal microscopy*

The ability of the gold–phosphine-porphyrin **5b** and **8** to be detected in cells by fluorescence microscopy was also evaluated. Both compounds were incubated with SW480 cells for 5 min at 37 °C before washing and paraformaldehyde fixation. Observations were performed with a confocal fluorescence microscopy with emission fluorescence wavelengths ranging from 688 to 728 nm, thereby avoiding disturbances due to cellular autofluorescence. Interestingly, the two compounds display strong fluorescence and marked differences in terms of aggregation behavior and cellular localization, with **5b** forming large aggregate trapping cells, while **8** forms very small aggregates which localized around cells (Fig. 5). This may explain the significant difference of efficacy between **5b** and **8** compounds, especially regarding their IC50 values.

Conclusions

The efficient synthesis of new phosphine-porphyrin derivatives which can be easily and selectively metalated by two different metals, notably Pd(II) and Au(I) was reported. All the compounds displayed at least a part of their emission of luminescence in the therapeutical window (near infrared), but importantly with good emission quantum yield, where the common heavy atom effect, and intramolecular energy and electron transfers are absent. The different molecules synthesized have been tested on two cancer cell lines. We demonstrated the necessity to make a product displaying a sufficient water solubility to facilitate the evaluation of its biological properties (IC50, molecular mechanisms) and we obtained it. The activity of this water-soluble compound when attached to a phosphine–gold phosphine moiety can be significantly improved by photoactivation. The compounds water soluble or not can be easily tracked in vitro by confocal fluorescence microscopy and can be localized on cell membranes as small aggregates for the most cytotoxic complex.

Current studies are in progress to establish the physicochemical mechanisms involved during light irradiation of the cells and to optimize phosphine-porphyrin complexes (e.g., variation of the metal on the phosphorus atom to increase the cytotoxicity, and modification of the porphyrin to suppress aggregation phenomenon); this approach to theranostic agents is valuable and worth exploring.

Acknowledgments The "Centre National de la Recherche Scientifique" (ICMUB, UMR CNRS 6302) is gratefully thanked for financial support. Support was provided by the CNRS, the "Université de Bourgogne" and the "Conseil Régional de Bourgogne" through the 3MIM integrated Project ("Marquage de Molécules par les Métaux pour l'Imagerie Médicale") and PARI programs. ST thanks the French Ministry of Research for PhD grant. PDH thanks the "Agence Nationale de la Recherche (ANR)" and the Sciences and Engineering Research Council of Canada (NSERC) for financial support. CP thanks Pascale Winckler of the Dimacell imaging ressource center (Dimacell, Agrosup Dijon and University of Burgundy, Dijon, France) for technical support during confocal measurements. Dr. Fanny Picquet, Marie José Penouilh and Léo Bucher are warmly acknowledged for technical support. Dr. Jean-Michel Barbe is thanked for helpful discussions. The authors are very thankful to Dr. Benoit Habermeyer and Porphychem Company for providing the TetraPhenylPorphyrin (TPP) precursor. CG is thankful for CNRS, CONACIT, Ligue Contre le Cancer and COST CM1105 financial support.

References

1. Zhang CX, Lippard SJ (2003) Curr Opin Chem Biol 7:481–489
2. Chavain N, Biot C (2010) Curr Med Chem 17:2729–2745
3. Hernandes MZ, de S Pontes FJ, Coelho LCD, Moreira DRM, Pereira VRA, Leite ACL (2010) Curr Med Chem 17:3739–3750
4. Gasser G, Ott I, Metzler-Nolte N (2011) J Med Chem 54:3–25
5. Gaynora D, Griffith DM (2012) Dalton Trans 41:13239
6. Bergamo A, Gaiddon C, Schellens JHM, Beijnen JH, Sava G (2012) J Inorg Biochem 106:90–99
7. Casini A, Hartinger CG, Nazarov AA, Dyson PJ (2010) Top Organomet Chem 32:57–80
8. Jakupec MA, Galanski M, Arion VB, Hartinger CG, Keppler BK (2008) Dalton Trans 183–194
9. Nazarov AA, Risse J, Ang WH, Schmitt F, Zava O, Ruggi A, Groessl M, Scopelitti R, Juillerat-Jeanneret L, Hartinger CG, Dyson PJ (2012) Inorg Chem 51:3633–3639
10. Tasan S, Zava O, Bertrand B, Bernhard C, Goze C, Picquet M, Le Gendre P, Harvey PD, Denat F, Casini A, Bodio E (2013) Dalton Trans 42:6102–6109
11. Adriaenssens L, Liu Q, Chaux-Picquet F, Tasan S, Picquet M, Denat F, Le Gendre P, Marques F, Fernandes C, Mendes F, Gano L, Campello MPC, Bodio E (2014) ChemMedChem 9:1567–1573
12. Bergamo A, Masi A, Dyson PJ, Sava G (2008) Int J Oncol 33:1281–1289
13. Casini A, Gabbiani C, Sorrentino F, Rigobello MP, Bindoli A, Geldbach TJ, Marrone A, Re N, Hartinger CG, Dyson PJ, Messori L (2008) J Med Chem 51:6773–6781
14. Mjos KD, Orvig C (2014) Chem Rev 114:4540–4563
15. Nobili S, Mini E, Landini I, Gabbiani C, Casini A, Messori L (2010) Med Res Rev 30:550–580
16. Ott I (2009) Coord Chem Rev 253:1670–1681
17. Bertrand B, Casini A (2014) Dalton Trans. doi:10.1039/C3DT52524D
18. Zhang Y, Lovell JF (2012) Theranostics 2:905–915
19. Ali H, Van Lier JE (2010) Handbook of porphyrin science. In: Kadish KM, Smith KM, Guilard R (eds) World Scientific, London, pp 1–119
20. Alonso C, Boyle RW (2010) Handbook of porphyrin science. In: Kadish KM, Smith KM, Guilard R (eds) World Scientific, London, pp 121–190
21. Ethirajan M, Patel NJ, Pandey RK (2010) Handbook of porphyrin science. In: Kadish KM, Smith KM, Guilard R (eds) World Scientific, London, pp 249–323
22. Jux N, Röder B (2010) Handbook of porphyrin science. Kadish KM, Smith KM, Guilard R (eds) World Scientific, London, pp 325–401
23. Vicente MGH, Sibrian-Vazquez M (2010) Handbook of porphyrin science. Kadish KM, Smith KM, Guilard R (eds) World Scientific, London, pp 191–248
24. Osterloh J, Vicente MGH (2002) J Porphyrins Phthalocyanines 6:305–324
25. Lee T, Zhang X-A, Dhar S, Faas H, Lippard SJ, Jasanoff A (2010) Chem Biol 17:665–673
26. Eggenspiller A, Michelin C, Desbois N, Richard P, Barbe JM, Denat F, Licona C, Gaiddon C, Sayeh A, Choquet P, Gros CP (2013) Eur J Org Chem 6629–6643
27. Gros CP, Eggenspiller A, Nonat A, Barbe J-M, Denat F (2011) Med Chem Comm 2:119–125
28. Yumita N, Iwase Y, Nishi K, Komatsu H, Takeda K, Onodera K, Fukai T, Ikeda T, Umemura S-I, Okudaira K, Momose Y (2012) Theranostics 2:880–888
29. Suijkerbuijk BMJM, Klein Gebbink RJM (2008) Angew Chem Int Ed 47:7396–7421
30. Uson R, Laguna A, Laguna M, Briggs DA, Murray HH, Fackler JJP (1989) Inorg Synth 26:85–91
31. Dupré N, Brazel C, Fensterbank L, Malacria M, Thorimbert S, Hasenknopf B, Lacôte E (2012) Chem Eur J 18:12962–12965
32. Sohm F, Gaiddon C, Antoine M, Boutillier AL, Loeffler JP (1999) Oncogene 18:2762–2768
33. Gaiddon C, de Tapia M, Loeffler JP (1999) Mol Endocrinol 13:742–751

34. Partyka DV, Robilotto TJ, Zeller M, Hunter AD, Gray TG (2008) PNAS 105:14293–14297
35. Luguya R, Jaquinod L, Fronczeck FR, Vicente MGH, Smith KM (2004) Tetrahedron 60:2757–2763
36. Shao ZJ, Ou YY, Hu QI, Zeng DL, Chen ZP (2005) Wuhan University J Nat Sci 10:919–924
37. Collman JP, Gagne RR, Reed C, Halbert TR, Lang G, Robinson WT (1975) J Am Chem Soc 97:1427–1439
38. Kruper WJ, Chamberlin TA, Kochanny M (1989) J Org Chem 54:2753–2756
39. Meng GG, James BR, Skov KA (1994) Can J Chem 72:1894–1909
40. Bernhard C, Goze C, Rousselin Y, Denat F (2010) Chem Commun 46:8267–8269
41. Milot RL, Moore GF, Crabtree RH, Brudvig GW, Schmuttenmaer CA (2013) J Phys Chem C 117(117):21662–21670
42. Ogan M, Revel D, Brasch R (1987) Invest Radiol 22(822):828
43. Furmanski P, Longley C (1988) Cancer Res 48(4604):4610
44. Sansiaume E, Ricoux R, Gori D, Mahy JP (2010) Tetrahedron Asymmetry 21:1593–1600
45. Gonçalves PJ, De Boni L, Barbosa Neto NM, Rodrigues JJ Jr, Zílio SC, Borissevitch IE (2005) Chem Phys Lett 407:236–241
46. Vidimar V, Meng X, Klajner M, Licona C, Fetzer L, Harlepp S, Hebraud P, Sidhoum M, Sirlin C, Loeffler JP, Mellitzer G, Sava G, Pfeffer M, Gaiddon C (2012) Biochem Pharmacol 84:1428–1436
47. Zawacka-Pankau J, Krachulec J, Grulkowski I, Bielawski KP, Selivanova G (2008) Toxicol Appl Pharmacol 232:487–497
48. Benosman S, Gross I, Clarke N, Jochemsen AG, Okamoto K, Loeffler JP, Gaiddon C (2007) Cell Death Differ

VIII. Discussion

During my PhD, I had the chance to work on the development of new anticancer ruthenium-based drugs, and I collaborated with different groups giving me the chance to see the project from different angels. My thesis project was a symbiotic work between me as a biologist and with chemists that were producing drugs. My work consisted to elucidate the importance of the structure-activity relationship of Ruthenium organometallic compounds and to add information in terms of their mechanism of action. I think that the understanding of the chemical interactions of Ruthenium complexes with the biological environment is essential for the design of compounds with predictable properties.

VIII.A. Structure-Activity relationship.

In this interdisciplinary project, chemists synthetized new compounds for two main purposes: to have a cytotoxic activity and for theranostic.

VIII.A.1. Cytotoxic Activity.

In order to improve the cytotoxicity and perform structure-function studies, our chemist collaborators synthetized different organometallic compounds following two strategies: they change the ligands and they change the metal. My role was to test the biological activity of these compounds and try to understand what are the physico-chemical determinant parameters that confer the cytotoxic activity.

I observed that changes in the ligand, have an impact in three main physicochemical parameters; lipophylicity, structure and redox potential. Importantly, often these parameters are linked between them, as the modification of a ligand alter several parameters at once, as for example in the compounds RDC11 and RDC34. In the latter chemist added a second phénantroline in order to render the molecule more cytotoxic. This modification increased the lipophilicity, but also affected the geometry of the molecule. It is therefore difficult to ascertain if it is solely the increase in lipophylicity that improves the cytotoxicity in RDC34. Similarly, to improve the water solubility of RDC34, a spermine ligand (creating RDC44) was added, reducing significantly the cytotoxicity *in vitro*. But the addition of the spermine changed also the overall structure of the molecule. Another example was the attempt to change the redox potential of the compound. For this, a NO_2 (RDC40) or a NH_2 (RDC41) function

was introduced into the RDC34. However, these functions do not only change the redox potential, they also modified the lipophilicity and in some extend part of the geometry. Hence, the change in the cytotoxicity of RDC40 and RDC41 cannot be attributed only to modification in the redox potential.

The complexity of the identification of the chemical determinants important for cytotoxicity is also well illustrated by the work I did in collaboration with Dr. Han and Chow Mun Juinn from the University of Singapore. The compounds we tested in this collaboration have a complete different structure from our RDC. They do not have the Ru-C bound but a Ru-N bond. In addition, the ligands are more related to the RM175 compound. It was interesting to find that on over 500 compounds generated by combinatory chemistry with few ligands, only a handful of the compounds presented a cytotoxicity in the range of the µM and none in the range of our best RDC or ODC (nM range). Hence, it suggests that the Ru-C and the specific ligands used in our RDCs and ODCs might have some importance in their high cytotoxicity. In addition, if was interesting to investigate more in depth their mode of action as we observed that slight differences in the ligands strongly affected the cytotoxicity and the mode of action.

With this comparative approach, I noted that even the minimal modification of one of these physicochemical parameters (redox potential, lipophilicity, geometry…), has an impact on the biological activity of the compound. This can be traduced in several ways, for example, difficulties in the uptake of the drug, or differences in the interaction with different molecules such as DNA, enzymes, lipids or proteins and more.

After these series of my experiments, we realized that this approach was not ideal to determine the precise parameter rendering the compounds more cytotoxic because to many parameters changed at the same time. Hence we decide to turn the problem the other way around, meaning we precede with the second strategy, the change of the metal (Ru vs. Os).

I observed that changing the metal does neither change the lipophilicity nor the structure of the compound, but changes the redox potential. This was the “cleanest” way we came up with to handle the problem. As the redox potential was apparently the only parameter that changed we hypothesized that this might be a determinant physicochemical parameter. The experiments I did then let us confirm this statement and we where able to correlate the redox potential with the cytotoxicity.

The role of the redox potential in the cytotoxicity is also somehow supported by the observation by other groups that some Ruthenium compounds are capable to modulate redox enzymes like glucose oxidase and horseradish peroxidase (147). Likewise Sadler and co-workers showed that Ru could catalyze the oxidation of glutathione (119). The inconveniency of some of those experiments is that they were made in “artificial conditions”; in a test tube with purified enzymes and sometimes with enzymes that are not so relevant as target for anticancer therapy.

However and importantly, during my Ph.D. I could proof that ruthenium compounds can interact with redox enzymes in a biological microenvironment in cancerous cells. Indeed my results showed that RDC11 was capable to interact with the redox enzyme PHD2, which is responsible for the degradation of Hif-1α in normoxie conditions. Moreover, this interaction leads to a diminution of Hif-1α protein level, indicating that RDC11 might regulate the activity of PHD2. As we know Hif-1α is involved in crucial aspects of cancer biology, including angiogenesis, cell survival, glucose metabolism and invasion. Therefore, as expected by the downregulation of Hif-1α protein level, I observed that RDC11 reduced angiogenesis in tumor xenografts, showing the relevance of the RDC11-PHD2 interaction for anticancer research.

Another argument in favor of a role of the redox potential of RDCs and ODCs in their biological activity is my observation that these compounds increase the production of ROS shortly after the treatment and that they also change the ratio NAD/NADH. Altogether, these observations suggest an imbalance in the cellular redox status that is also supported by the activation of the ROS stress response pathway controlled by Nrf2 and by the regulation of the redox sensitive enzyme PHD2.

It remains to establish exactly how this redox imbalance impacts on the molecular mechanisms and signaling pathways that we have shown to play a role in RDCs and ODCs cytotoxicity, such as the reticulum endoplasmic stress pathway and the epigenetic regulations.

Finally, with the experiments I made I am able to say that the metal has an important role in the molecule, and the cytotoxicity is correlated with a specific window of redox potential. Furthermore, I think that this could be a rational way to synthetize new molecules. However, all my studies also indicate that the lipophylicity and the geometry have also to be taken into account for this rational design.

Furthermore, one should not forget that most of this structure/activity studies were done *in vitro*. Unfortunately, I also realized during my PhD that performing reliable experiments for *in vivo* activity (anticancer activity) is expensive, time consuming and subject to more variation due to the variability between animals. The few comparative experiments I performed *in vivo* indicated clearly that we could not make a perfect correlation between the *in vitro* cytotoxicity and the *in vivo* anticancer activity. For example, ODCs were not always more active *in vivo* compared to RDCs. This might be due to several parameters specific to the *in vivo* experiments, such as tissue distribution, binding to proteins of the serum, degradation by liver enzymes… Hence additional *in vivo* structure/activity studies would be necessary to have a better understanding of the physic-chemical determinants necessary for the anticancer activity.

VIII.A.2. Theranostic.

Because of the interesting features of ruthenium or other metals, I truly believe that they could be good candidates for theranostic. Although theranostic remains a niche, I also think that theranostics is an innovative approach that has several advantages, such as the possibility to follow the treatment in the patient and at the same time targeted cancer cells with a cytotoxic molecule.

During my PhD I tested some novel organometallic compounds that were designed for imagery and theranostic in collaboration with the group in Dijon of Pr. Gros. These compounds were supposed to present interesting properties for medical imagery or/and cytotoxicity. The results obtained on the properties of these compounds for biological purposes were a little disappointing. First, the structure of the compounds impact negatively on their solubility, which make some biological tests difficult or impossible. Second, the compounds that were soluble did not present enough efficiency for medical imagery or a high cytotoxicity. In addition, some of these compounds that were designed for PDT, due to the presence of a porphyrin ligand, were not strongly induced by light exposure.

The conclusion of these studies was that the chemical design of the compounds had to be improved, especially in order to increase the solubility of the compounds. I am hoping that the chemists will be able to realize that. I also believe that the difficulties

encountered pinpoint to the fact that trying to combine two active functions in one molecule could just synergize the difficulty to make it work.

VIII.B. New mechanism of action of RDC compounds.

The second objective of my project was to elucidate the mechanism of action implicated with these organometallic compounds.

VIII.B.1. DNA interaction and cytotoxicity.

It is now well established that RDC compounds are able to interact with DNA (130). Indeed the fluorescent properties of these compounds let us to observe its localization in the nucleus, however my results demonstrated that there is no good correlation between DNA interaction and cytotoxicity. One example is RDC34 and RDC40. RDC34 is notably more cytotoxic than RDC40, however RDC40 seems to have a stronger affinity to DNA than RDC34. Moreover, my results showed even if the interaction was weak there was a phosphorylation of H2AX indicating DNA damages.

Furthermore, previous experiments done in the laboratory demonstrate that the tumor suppressor gene p53 does not have a crucial role triggering cytotoxicity of RDC comounds (124). Similarly, I observed that ODC compounds are not able to induce p53. This lack of correlation demonstrates that DNA is not the principal target of RDC or ODC compounds and lead us to hypothesize that there must be other pathways responsible for their cytotoxicity.

In order to address this hypothesis, we did a transcriptome analysis that revealed precious information in terms of signaling pathways specifically regulated by RDC compounds.

VIII.B.2. Transcriptome Analysis.

This approach allowed us to highlight several signaling pathways that are targeted by RDC compounds and revealed the importance of the epigenetics.

This approach confirmed our hypothesis that DNA was not a primary target for RDC, and that mechanism involved in cellular metabolism were more implicated in RDC11 in comparison with cisplatin. For example the analysis showed the regulation of Hif1 and NRF2 in presence of RDC11, and as I said before these have an important role

in tumorigenesis. Moreover, the analysis also showed differences between cisplatin and RDC11, for example the Histone deacetylases (HDACs). It is well established that HDACs regulate the expression and activity of numerous proteins involved in both cancer initiation and cancer progression. My results showed that HDAC4 is downregulated in cells treated with cisplatin, and in the contrary upregulated with RDC11. This result suggested the implication of HDAC4 in RDC11 cytotoxicity. In order to evaluate this, we did a combinatorial treatment approach using RDC11 in combination with a HDAC inhibitor. Interestingly, the results showed that the combination RDC11 with HDAC inhibition results in an antagonist effect. This result strongly suggested that HDAC inhibitors could not be use for a combinatory therapy in order to potentiate the cytotoxicity of RDC.

However, the question to answer now is, to know whether these pathways are directly regulated by RDC or are these consequences of other primary pathways? In the same way this sort of “global” information gives us new indications for specifics pathways regulated by RDC’s. In this way we can identify and validate target genes in a more specific way. This is very important because maybe in the future drugs could target a type of cancer

IX. Perspectives

IX.A.DNA Damage or not?

One of the questions remaining unanswered is whether RDCs and ODCs do induce DNA damages and how it might participate in their biological activity. Several data point that RDCs and ODCs interact with DNA and might induce DNA damage. For example, RDCs and ODCs bind DNA *in vitro*, induce γ-H2AX phosphorylation and in some cases p53 protein level as well as a DNA damage response. But these observations are often done *in vitro* or are indirect, and there is no correlation between the cytotoxicity and the DNA binding affinity of the compounds. Therefore, it would be interesting to further investigate the effect of RDC and ODC on DNA, but in a more physiological system that we used before.

During my PhD, I started to address this using the comet assay technique. This is a method for measuring DSB in which treated cells are processed, submitted to a electric field and then observed by fluorescence to evaluate the length of the comet tail which reflects the number of DNA breaks. Using this direct technique of DNA damage visualization, my results demonstrate that RDCs and ODCs were able to induce DSB, although more weakly than cisplatin. Based on this observation, we are now interested to know what the mechanisms are by which the cell could repair this DNA damage. Preliminary results showed, that the complex Ku70/80 and 53BP1 are activated by RDC compounds, whereas RPA and BRCA1, implicated in HR mechanism, seem not to be involved consequently, and probably NHEJ could be involved in the repair of DSB.

IX.B.New Pathways to explore

The transcriptome analyses as well as the literature suggest that besides the classical apoptosis and cell cycle arrest processes, other mechanisms and signaling pathway could be induced or regulated by our family of metal-based compounds.

For example, during my Ph.D I had some key results that indicated a possible relation of RDC induced cell-death by autophagy, like the production of ROS, diminution of mTOR and the activation of the reticulum stress pathway. Autophagy has two main roles in cancer, acting as a tumor suppressor by preventing the accumulation of damaged proteins and organelles, and as a mechanism of cell

survival that can promote the growth of established tumors (148). I tested the activity of two markers of autophagy LC3, which was modulated by RDC, and p62, which was upregulated with RDC11. Of course additional experiments must be done to prove my hypothesis like fluorescent cell staining and flow cytometry.

In addition, I got interested into ferroptosis, which was described in 2012 in an article as a new form of cell death (149). Ferroptosis is an iron-dependent form of non-apoptotic cell death, implicating ROS production. Hence, as ruthenium is from the same family of iron and as our family of compounds trigger ROS production, it might be interesting to investigate whether they regulated they induce this form of cell death.

IX.C. Future direction for cancer treatment with Metal-Carbon-based compounds

Our transcriptome analysis on RDC11-treated cells pointed to several novel molecular mechanisms and signaling pathways possibly targeted by RDC11. Beside their interest at a scientific level to understand how RDCs work, these data can also be used to defined combinatory therapies. Based on that, and the regulation of HDAC expression by RDC11 and cisplatin, we tested the combination of RDC11 with an HDAC inhibitor, SAHA. Even if the experiment made was negative, I think that it is interest to continue in this same line. In my opinion RDCs should be used in combination with other drugs, in order to potentiate the cytotoxic activity, as modern chemotherapy uses also a combine different drugs, including drugs for targeted therapy such as SAHA.

For example, our preliminary experiment using inhibitors of the mTOR pathway (rapamicyne) or the glutathione synthesis pathway (BSO) show encouraging results. It is to note that this strategy was already used with success by the group of Sadler showing that Ruthenium compounds can modulate glutathione activity (119), and from the fact that RDC compounds can interact with redox enzymes. Furthermore, anticancer drugs targeting the redox systems, for example, glutathione and thioredoxin, have entered focus of interest (28).

Finally, the transcriptome analysis can also give us useful information about the identification of possible directs targets, such as PHD2. In this way we could develop and optimize our compounds in a rational way, triggering the improvement of the therapeutic activity. Nowadays, there are many approaches to improve molecules like carbon nanotubes, peptides, micelles, liposomes, receptors, antibodies and more. Of course, as my experiences showed, one has to take the necessary precautions regarding the consequence that involves the exchange of ligands and structures modifications on the cytotoxicity of the drug.

X. Conclusion

The development of new organometallic anticancer compounds is an interdisciplinary work, the interaction between chemists, biologists and doctors must be solid and dynamic in order to succeed development of a new drug. In the chemist point of view, I think each molecule has their own personality and even a minor structural or metal modification can drastically modify the physico-chemical properties of the molecule, thus modifying their activity. Thus, we have to be really attentive and maybe less ambitious when we think about changing a molecule. An in the biologist point of view I saw that the results are never black or white, results are cell dependent, and dose dependent, if we wanted to establish differences between the existed Ru compounds, and thus make general statements we should do the same experiment in the same conditions (cell type, time of exposure, technique) with all the different Ru compounds from the different labs, maybe then we could established general "rules".

In my opinion, the fact that RDC's may have these particulars and originals mechanism of action like ER stress, light activation, autophagy or ferroptose are excellent ways to overcome the principal problem of resistance-platinum compounds. RDC's are dynamics molecules that can be use in different therapeutic areas, being an excellent clinical candidate, promising a great success in clinics, moreover because of the features of ODC compounds and following the clues of the redox potential; ODC's could be even better. Thereby, the idea of the perfect drug seems a mile away, but I like to think that we getting closer little by little.

XI. Bibliography

1. Available from: http://www.cancerresearchuk.org/cancer-info/cancerstats/keyfacts/worldwide/.

2. Fact sheets by cancer; Available from: http://globocan.iarc.fr/Pages/fact_sheets_cancer.aspx. Accessed 18 February 2015.

3. Jemal A, Bray F, Center MM, Ferlay J, Ward E, Forman D. Global cancer statistics. CA Cancer J Clin 2011;61(2):69-90.

4. Fact sheets by population; Available from: http://globocan.iarc.fr/Pages/fact_sheets_population.aspx. Accessed 18 February 2015.

5. Dollinger M, Rosenbaum EH, Cable G, Dollinger MGTCT. Cancer therapy. Kansas City: Andrews and McMeel; 1994.

6. Barton-Burke M, Wilkes GM. Cancer therapies. Sudbury, Mass.: Jones and Bartlett Publishers; 2006.

7. Scaltriti M, Baselga J. The epidermal growth factor receptor pathway: A model for targeted therapy. Clinical Cancer Research 2006;12(18):5268-72.

8. Cuadros M, Villegas R. Systematic review of HER2 breast cancer testing. Applied Immunohistochemistry & Molecular Morphology 2009;17(1):1-7.

9. Bergers G, Benjamin LE. Tumorigenesis and the angiogenic switch. Nat Rev Cancer 2003, Jun;3(6):401-10.

10. Jain RK. Molecular regulation of vessel maturation. Nature Medicine 2003;9(6):685-93.

11. Cardones AR, Banez LL. VEGF inhibitors in cancer therapy. Curr Pharm Des 2006;12(3):387-94.

12. Liao D, Johnson RS. Hypoxia: A key regulator of angiogenesis in cancer. Cancer Metastasis Rev 2007, Jun;26(2):281-90.

13. Harris AL. Hypoxia--a key regulatory factor in tumour growth. Nat Rev Cancer 2002, Jan;2(1):38-47.

14. Easton JB, Houghton PJ. MTOR and cancer therapy. Oncogene 2006, Oct 16;25(48):6436-46.

15. Patel PH, Chadalavada RS, Chaganti RSK, Motzer RJ. Targeting von hippel-lindau pathway in renal cell carcinoma. Clinical Cancer Research 2006;12(24):7215-20.
16. Butler JS, Sadler PJ. Targeted delivery of platinum-based anticancer complexes. Curr Opin Chem Biol 2013, Apr;17(2):175-88.
17. Wang X, Guo Z. Targeting and delivery of platinum-based anticancer drugs. Chem Soc Rev 2013, Jan 7;42(1):202-24.
18. Vanneman M, Dranoff G. Combining immunotherapy and targeted therapies in cancer treatment. Nat Rev Cancer 2012, Apr;12(4):237-51.
19. Gerber DE. Targeted therapies: A new generation of cancer treatments. Am Fam Physician 2008, Feb 1;77(3):311-9.
20. Ethirajan M, Chen Y, Joshi P, Pandey RK. The role of porphyrin chemistry in tumor imaging and photodynamic therapy. Chem Soc Rev 2011, Jan;40(1):340-62.
21. Dolmans DE, Fukumura D, Jain RK. Photodynamic therapy for cancer. Nat Rev Cancer 2003, May;3(5):380-7.
22. Urruticoechea A, Alemany R, Balart J, Villanueva A, Viñals F, Capellá G. Recent advances in cancer therapy: An overview. Curr Pharm Des 2010, Jan;16(1):3-10.
23. Targeted cancer therapies fact sheet - national cancer institute; Available from: http://www.cancer.gov/cancertopics/factsheet/Therapy/targeted. Accessed 20 February 2015.
24. Lasley. 21st century cancer treatment. ; 2010.
25. Pelengaris Stella SKM. The molecular biology of cancer: A bridge from bench to bedside. second edition ed. ; 2013.
26. Page R, Takimoto C. Principles of chemotherapy. Cancer Management: A Multidisciplinary Approach Medical, Surgical & Radiation Oncology. Editors: R Pazdur, LR Coia, WJ Hoskins, LD Wagman. PRR, New York 2004:21-38.
27. DeVita VT, Chu E. A history of cancer chemotherapy. Cancer Res 2008, Nov 1;68(21):8643-53.
28. Jungwirth U, Kowol CR, Keppler BK, Hartinger CG, Berger W, Heffeter P. Anticancer activity of metal complexes: Involvement of redox processes. Antioxid Redox Signal 2011, Aug 15;15(4):1085-127.
29. Gasser G, Ott I, Metzler-Nolte N. Organometallic anticancer compounds. J Med Chem 2010;54(1):3-25.

30. Ott I, Gust R. Non platinum metal complexes as anti-cancer drugs. Arch Pharm (Weinheim) 2007, Mar;340(3):117-26.
31. Gianferrara T, Bratsos I, Alessio E. A categorization of metal anticancer compounds based on their mode of action. Dalton Trans 2009, Oct 7(37):7588-98.
32. Hambley TW. Developing new metal-based therapeutics: Challenges and opportunities. Dalton Trans 2007, Nov 21(43):4929-37.
33. Bruijnincx PC, Sadler PJ. New trends for metal complexes with anticancer activity. Curr Opin Chem Biol 2008, Apr;12(2):197-206.
34. Martins P, Marques M, Coito L, Pombeiro AJ, Baptista PV, Fernandes AR. Organometallic compounds in cancer therapy: Past lessons and future directions. Anticancer Agents Med Chem 2014;14(9):1199-212.
35. Dyson PJ, Sava G. Metal-based antitumour drugs in the post genomic era. Dalton Trans 2006, Apr 28(16):1929-33.
36. Nursing2013 drug handbook - google livres; Available from: https://books.google.fr/books?id=tliO2JeEZAwC&pg=PA443&lpg=PA443&dq=cisplatin+grade+3+toxicity+stop&source=bl&ots=o3Os6e0dAF&sig=iN7F2pdK7L_7dDoukI1lbmbLKao&hl=fr&sa=X&ei=JCMXVaLHFZPWar61gtAC&ved=0CC8Q6AEwAg#v=onepage&q=cisplatin%20grade%203%20toxicity%20stop&f=false. Accessed 28 March 2015.
37. Lippard SJ. New chemistry of an old molecule: Cis-[pt(NH3)2cl2]. Science 1982, Dec 10;218(4577):1075-82.
38. Muhammad N, Guo Z. Metal-based anticancer chemotherapeutic agents. Curr Opin Chem Biol 2014, Apr;19:144-53.
39. Boulikas T, Pantos A, Bellis E, Christofis P. Designing platinum compounds in cancer: Structures and mechanisms. Cancer Therapy 2007;5:537-83.
40. Dasari S, Tchounwou PB. Cisplatin in cancer therapy: Molecular mechanisms of action. Eur J Pharmacol 2014, Oct 5;740:364-78.
41. Burger H, Loos WJ, Eechoute K, Verweij J, Mathijssen RH, Wiemer EA. Drug transporters of platinum-based anticancer agents and their clinical significance. Drug Resist Updat 2011, Feb;14(1):22-34.
42. Carter SK, Canetta R, Rozencweig M. Carboplatin: Future directions. Cancer Treat Rev 1985;12:145-52.

43. Scheeff ED, Briggs JM, Howell SB. Molecular modeling of the intrastrand guanine-guanine DNA adducts produced by cisplatin and oxaliplatin. Mol Pharmacol 1999, Sep;56(3):633-43.
44. Meyerhardt JA, Mayer RJ. Systemic therapy for colorectal cancer. N Engl J Med 2005, Feb 3;352(5):476-87.
45. Luqmani YA. Mechanisms of drug resistance in cancer chemotherapy. Med Princ Pract 2005;14 Suppl 1:35-48.
46. Köberle B, Tomicic MT, Usanova S, Kaina B. Cisplatin resistance: Preclinical findings and clinical implications. Biochim Biophys Acta 2010, Dec;1806(2):172-82.
47. Cohen SM, Lippard SJ. Cisplatin: From DNA damage to cancer chemotherapy. Prog Nucleic Acid Res Mol Biol 2001;67:93-130.
48. Wiltshaw E. Cisplatin in the treatment of cancer. Platinum Metals Review 1979;23(3):90-8.
49. Siddik ZH. Cisplatin: Mode of cytotoxic action and molecular basis of resistance. Oncogene 2003, Oct 20;22(47):7265-79.
50. Crul M, van Waardenburg RCAM, Beijnen JH, Schellens JHM. DNA-based drug interactions of cisplatin. Cancer Treat Rev 2002, Dec;28(6):291-303.
51. Wozniak K, Blasiak J. Recognition and repair of dna-cisplatin adducts. Acta Biochim. Pol 2002;49:583-96.
52. Wang D, Lippard SJ. Cellular processing of platinum anticancer drugs. Nat Rev Drug Discov 2005, Apr;4(4):307-20.
53. Perez RP. Cellular and molecular determinants of cisplatin resistance. Eur J Cancer 1998, Sep;34(10):1535-42.
54. Kuo LJ, Yang L-X. Γ-H2AX-a novel biomarker for DNA double-strand breaks. In Vivo 2008;22(3):305-9.
55. Kinner A, Wu W, Staudt C, Iliakis G. Gamma-H2AX in recognition and signaling of DNA double-strand breaks in the context of chromatin. Nucleic Acids Res 2008, Oct;36(17):5678-94.
56. Shen DW, Pouliot LM, Hall MD, Gottesman MM. Cisplatin resistance: A cellular self-defense mechanism resulting from multiple epigenetic and genetic changes. Pharmacol Rev 2012, Jul;64(3):706-21.
57. Vasquez KM, Christensen J, Li L, Finch RA, Glazer PM. Human XPA and RPA DNA repair proteins participate in specific recognition of triplex-induced helical distortions. Proceedings of the National Academy of Sciences 2002;99(9):5848-53.

58. Fink D, Nebel S, Aebi S, Zheng H, Cenni B, Nehmé A, et al. The role of DNA mismatch repair in platinum drug resistance. Cancer Res 1996, Nov 1;56(21):4881-6.
59. Rosell R, Taron M, Barnadas A, Scagliotti G, Sarries C, Roig B. Nucleotide excision repair pathways involved in cisplatin resistance in non-small-cell lung cancer. Cancer Control 2003;10(4):297-305.
60. Seetharam R, Sood A, Goel S. Oxaliplatin: Pre-clinical perspectives on the mechanisms of action, response and resistance. Ecancermedicalscience 2009;3:153.
61. DNA Repair of Cancer Stem Cells. Springer; 2013.
62. Fleck O, Nielsen O. DNA repair. J Cell Sci 2004, Feb 1;117(Pt 4):515-7.
63. Zheng L, Li S, Boyer TG, Lee W-H. Lessons learned from BRCA1 and BRCA2. Oncogene 2000;19(53):6159-75.
64. Lieber MR, Ma Y, Pannicke U, Schwarz K. Mechanism and regulation of human non-homologous DNA end-joining. Nat Rev Mol Cell Biol 2003, Sep;4(9):712-20.
65. Deans AJ, West SC. DNA interstrand crosslink repair and cancer. Nat Rev Cancer 2011, Jul;11(7):467-80.
66. Johnson SW, Ferry KV, Hamilton TC. Recent insights into platinum drug resistance in cancer. Drug Resist Updat 1998;1(4):243-54.
67. Trachootham D, Alexandre J, Huang P. Targeting cancer cells by ros-mediated mechanisms: A radical therapeutic approach? Nat Rev Drug Discov 2009, Jul;8(7):579-91.
68. Cash TP, Pan Y, Simon MC. Reactive oxygen species and cellular oxygen sensing. Free Radic Biol Med 2007, Nov 1;43(9):1219-25.
69. Saad SY, Najjar TA, Alashari M. Role of non-selective adenosine receptor blockade and phosphodiesterase inhibition in cisplatin-induced nephrogonadal toxicity in rats. Clin Exp Pharmacol Physiol 2004, Dec;31(12):862-7.
70. Ishida S, Lee J, Thiele DJ, Herskowitz I. Uptake of the anticancer drug cisplatin mediated by the copper transporter ctr1 in yeast and mammals. Proc Natl Acad Sci U S A 2002, Oct 29;99(22):14298-302.
71. Howell SB, Safaei R, Larson CA, Sailor MJ. Copper transporters and the cellular pharmacology of the platinum-containing cancer drugs. Mol Pharmacol 2010, Jun;77(6):887-94.
72. Rabik CA, Maryon EB, Kasza K, Shafer JT, Bartnik CM, Dolan ME. Role of copper transporters in resistance to platinating agents. Cancer Chemother Pharmacol 2009, Jun;64(1):133-42.

73. Safaei R, Otani S, Larson BJ, Rasmussen ML, Howell SB. Transport of cisplatin by the copper efflux transporter ATP7B. Mol Pharmacol 2008, Feb;73(2):461-8.
74. Safaei R, Howell SB. Copper transporters regulate the cellular pharmacology and sensitivity to pt drugs. Crit Rev Oncol Hematol 2005, Jan;53(1):13-23.
75. Boulikas T, Pantos A, Bellis E, Christofis P. Designing platinum compounds in cancer: Structures and mechanisms. Cancer Therapy 2007;5:537-83.
76. Lai GM, Ozols RF, Young RC, Hamilton TC. Effect of glutathione on DNA repair in cisplatin-resistant human ovarian cancer cell lines. J Natl Cancer Inst 1989, Apr 5;81(7):535-9.
77. Kartalou M, Essigmann JM. Mechanisms of resistance to cisplatin. Mutat Res 2001, Jul 1;478(1-2):23-43.
78. Shen DW, Ma J, Okabe M, Zhang G, Xia D, Gottesman MM. Elevated expression of TMEM205, a hypothetical membrane protein, is associated with cisplatin resistance. J Cell Physiol 2010, Nov;225(3):822-8.
79. Liao Y, Lu X, Lu C, Li G, Jin Y, Tang H. Selection of agents for prevention of cisplatin-induced hepatotoxicity. Pharmacol Res 2008, Feb;57(2):125-31.
80. Hartmann JT, Lipp HP. Toxicity of platinum compounds. Expert Opin Pharmacother 2003, Jun;4(6):889-901.
81. Chang B, Nishikawa M, Sato E, Utsumi K, Inoue M. L-Carnitine inhibits cisplatin-induced injury of the kidney and small intestine. Arch Biochem Biophys 2002, Sep 1;405(1):55-64.
82. Al-Majed AA. Carnitine deficiency provokes cisplatin-induced hepatotoxicity in rats. Basic & Clinical Pharmacology & Toxicology 2007;100(3):145-50.
83. Argyriou AA, Polychronopoulos P, Iconomou G, Chroni E, Kalofonos HP. A review on oxaliplatin-induced peripheral nerve damage. Cancer Treat Rev 2008, Jun;34(4):368-77.
84. McWhinney SR, Goldberg RM, McLeod HL. Platinum neurotoxicity pharmacogenetics. Mol Cancer Ther 2009, Jan;8(1):10-6.
85. Sudhakar A. History of cancer, ancient and modern treatment methods. J Cancer Sci Ther 2009, Dec 1;1(2):1-4.
86. Meng X, Leyva ML, Jenny M, Gross I, Benosman S, Fricker B, et al. A ruthenium-containing organometallic compound reduces tumor growth through induction of the endoplasmic reticulum stress gene CHOP. Cancer Res 2009, Jul 1;69(13):5458-66.

87. DWYER FP, MAYHEW E, ROE EM, SHULMAN A. INHIBITION OF LANDSCHUETZ ASCITES TUMOUR GROWTH BY METAL CHELATES DERIVED FROM 3,4,7,8-TETRAMETHYL-1,10-PHENANTHROLINE. Br J Cancer 1965, Mar;19:195-9.
88. Pizarro AM, Sadler PJ. Unusual DNA binding modes for metal anticancer complexes. Biochimie 2009, Oct;91(10):1198-211.
89. Antonarakis ES, Emadi A. Ruthenium-based chemotherapeutics: Are they ready for prime time? Cancer Chemother Pharmacol 2010, May;66(1):1-9.
90. Meggers E. Exploring biologically relevant chemical space with metal complexes. Curr Opin Chem Biol 2007, Jun;11(3):287-92.
91. Bergamo A, Gaiddon C, Schellens JH, Beijnen JH, Sava G. Approaching tumour therapy beyond platinum drugs: Status of the art and perspectives of ruthenium drug candidates. J Inorg Biochem 2012, Jan;106(1):90-9.
92. Bergamo A, Sava G. Ruthenium anticancer compounds: Myths and realities of the emerging metal-based drugs. Dalton Trans 2011, Aug 21;40(31):7817-23.
93. Galanski M, Arion VB, Jakupec MA, Keppler BK. Recent developments in the field of tumor-inhibiting metal complexes. Curr Pharm Des 2003;9(25):2078-89.
94. Rademaker-Lakhai JM, van den Bongard D, Pluim D, Beijnen JH, Schellens JH. A phase I and pharmacological study with imidazolium-trans-dmso-imidazole-tetrachlororuthenate, a novel ruthenium anticancer agent. Clin Cancer Res 2004, Jun 1;10(11):3717-27.
95. Efferth. Molecular principles of cancer invasion and metastasis (review). Int J Oncol 2009, Mar 13;34(4).
96. Gava B, Zorzet S, Spessotto P, Cocchietto M, Sava G. Inhibition of B16 melanoma metastases with the ruthenium complex imidazolium trans-imidazoledimethylsulfoxide-tetrachlororuthenate and down-regulation of tumor cell invasion. J Pharmacol Exp Ther 2006, Apr;317(1):284-91.
97. Alessio E, Mestroni G, Bergamo A, Sava G. Ruthenium antimetastatic agents. Curr Top Med Chem 2004;4(15):1525-35.
98. Antonarakis ES, Emadi A. Ruthenium-based chemotherapeutics: Are they ready for prime time? Cancer Chemother Pharmacol 2010, May;66(1):1-9.
99. Vacca A, Bruno M, Boccarelli A, Coluccia M, Ribatti D, Bergamo A, et al. Inhibition of endothelial cell functions and of angiogenesis by the metastasis inhibitor NAMI-A. Br J Cancer 2002, Mar 18;86(6):993-8.

100. Sava G, Zorzet S, Turrin C, Vita F, Soranzo M, Zabucchi G, et al. Dual action of NAMI-A in inhibition of solid tumor metastasis: Selective targeting of metastatic cells and binding to collagen. Clin Cancer Res 2003, May;9(5):1898-905.
101. Bergamo A, Sava G. Ruthenium complexes can target determinants of tumour malignancy. Dalton Trans 2007, Apr 7(13):1267-72.
102. Hartinger CG, Zorbas-Seifried S, Jakupec MA, Kynast B, Zorbas H, Keppler BK. From bench to bedside--preclinical and early clinical development of the anticancer agent indazolium trans-[tetrachlorobis(1h-indazole)ruthenate(III)] (KP1019 or FFC14A). J Inorg Biochem 2006, May;100(5-6):891-904.
103. Clarke MJ. Ruthenium metallopharmaceuticals. Coordination Chemistry Reviews 2002;232(1):69-93.
104. Hentze MW, Muckenthaler MU, Andrews NC. Balancing acts: Molecular control of mammalian iron metabolism. Cell 2004, Apr 30;117(3):285-97.
105. Messori L, Kratz F, Alessio E. The interaction of the antitumor complexes na[trans-rucl(4) (DMSO)(im)] and na[trans-rucl(4)(DMSO)(ind)] with apotransferrin: A spectroscopic study. Met Based Drugs 1996;3(1):1-9.
106. Jakupec MA, Galanski M, Arion VB, Hartinger CG, Keppler BK. Antitumour metal compounds: More than theme and variations. Dalton Trans 2008, Jan 14(2):183-94.
107. Lentz F, Drescher A, Lindauer A, Henke M, Hilger RA, Hartinger CG, et al. Pharmacokinetics of a novel anticancer ruthenium complex (KP1019, FFC14A) in a phase I dose-escalation study. Anti-cancer Drugs 2009;20(2):97-103.
108. Spreckelmeyer S, Orvig C, Casini A. Cellular transport mechanisms of cytotoxic metallodrugs: An overview beyond cisplatin. Molecules 2014;19(10):15584-610.
109. Scolaro C, Bergamo A, Brescacin L, Delfino R, Cocchietto M, Laurenczy G, et al. In vitro and in vivo evaluation of ruthenium(II)-arene PTA complexes. J Med Chem 2005, Jun 16;48(12):4161-71.
110. Bergamo A, Masi A, Dyson PJ, Sava G. Modulation of the metastatic progression of breast cancer with an organometallic ruthenium compound. Int J Oncol 2008, Dec;33(6):1281-9.
111. Chatterjee S, Kundu S, Bhattacharyya A, Hartinger CG, Dyson PJ. The ruthenium(II)-arene compound RAPTA-C induces apoptosis in EAC cells through mitochondrial and p53-jnk pathways. J Biol Inorg Chem 2008, Sep;13(7):1149-55.

112. Ang WH, Parker LJ, De Luca A, Juillerat-Jeanneret L, Morton CJ, Lo Bello M, et al. Rational design of an organometallic glutathione transferase inhibitor. Angew Chem Int Ed Engl 2009;48(21):3854-7.
113. Ang WH, De Luca A, Chapuis-Bernasconi C, Juillerat-Jeanneret L, Lo Bello M, Dyson PJ. Organometallic ruthenium inhibitors of glutathione-s-transferase P1-1 as anticancer drugs. ChemMedChem 2007, Dec;2(12):1799-806.
114. Casini A, Gabbiani C, Sorrentino F, Rigobello MP, Bindoli A, Geldbach TJ, et al. Emerging protein targets for anticancer metallodrugs: Inhibition of thioredoxin reductase and cathepsin B by antitumor ruthenium(II)-arene compounds. J Med Chem 2008, Nov 13;51(21):6773-81.
115. Morris RE, Aird RE, Murdoch Pdel S, Chen H, Cummings J, Hughes ND, et al. Inhibition of cancer cell growth by ruthenium(II) arene complexes. J Med Chem 2001, Oct 25;44(22):3616-21.
116. Chen H, Parkinson JA, Parsons S, Coxall RA, Gould RO, Sadler PJ. Organometallic ruthenium(II) diamine anticancer complexes: Arene-nucleobase stacking and stereospecific hydrogen-bonding in guanine adducts. J Am Chem Soc 2002, Mar 27;124(12):3064-82.
117. Chen H, Parkinson JA, Morris RE, Sadler PJ. Highly selective binding of organometallic ruthenium ethylenediamine complexes to nucleic acids: Novel recognition mechanisms. J Am Chem Soc 2003, Jan 8;125(1):173-86.
118. Hayward RL, Schornagel QC, Tente R, Macpherson JS, Aird RE, Guichard S, et al. Investigation of the role of bax, p21/waf1 and p53 as determinants of cellular responses in HCT116 colorectal cancer cells exposed to the novel cytotoxic ruthenium(II) organometallic agent, RM175. Cancer Chemother Pharmacol 2005, Jun;55(6):577-83.
119. Wang F, Xu J, Habtemariam A, Bella J, Sadler PJ. Competition between glutathione and guanine for a ruthenium(II) arene anticancer complex: Detection of a sulfenato intermediate. J Am Chem Soc 2005, Dec 21;127(50):17734-43.
120. Aird RE, Cummings J, Ritchie AA, Muir M, Morris RE, Chen H, et al. In vitro and in vivo activity and cross resistance profiles of novel ruthenium (II) organometallic arene complexes in human ovarian cancer. Br J Cancer 2002, May 20;86(10):1652-7.
121. Smalley KS, Contractor R, Haass NK, Kulp AN, Atilla-Gokcumen GE, Williams DS, et al. An organometallic protein kinase inhibitor pharmacologically activates p53

and induces apoptosis in human melanoma cells. Cancer Res 2007, Jan 1;67(1):209-17.
122. Ryabov AD, Sukharev VS, Alexandrova L, Le Lagadec R, Pfeffer M. New synthesis and new bio-application of cyclometalated ruthenium(II) complexes for fast mediated electron transfer with peroxidase and glucose oxidase. Inorg Chem 2001, Dec;40(25):6529-32.
123. Fetzer L, Boff B, Ali M, Xiangjun M, Collin JP, Sirlin C, et al. Library of second-generation cycloruthenated compounds and evaluation of their biological properties as potential anticancer drugs: Passing the nanomolar barrier. Dalton Trans 2011, Sep 21;40(35):8869-78.
124. Gaiddon C, Jeannequin P, Bischoff P, Pfeffer M, Sirlin C, Loeffler JP. Ruthenium (II)-derived organometallic compounds induce cytostatic and cytotoxic effects on mammalian cancer cell lines through p53-dependent and p53-independent mechanisms. J Pharmacol Exp Ther 2005, Dec;315(3):1403-11.
125. Hetz C, Chevet E, Harding HP. Targeting the unfolded protein response in disease. Nat Rev Drug Discov 2013, Sep;12(9):703-19.
126. Brown MK, Naidoo N. The endoplasmic reticulum stress response in aging and age-related diseases. Front Physiol 2012;3:263.
127. Oyadomari S, Mori M. Roles of CHOP/GADD153 in endoplasmic reticulum stress. Cell Death Differ 2004, Apr;11(4):381-9.
128. Yadav RK, Chae SW, Kim HR, Chae HJ. Endoplasmic reticulum stress and cancer. J Cancer Prev 2014, Jun;19(2):75-88.
129. Dalton LE, Clarke HJ, Knight J, Lawson MH, Wason J, Lomas DA, et al. The endoplasmic reticulum stress marker CHOP predicts survival in malignant mesothelioma. Br J Cancer 2013, Apr 2;108(6):1340-7.
130. Klajner M, Hebraud P, Sirlin C, Gaiddon C, Harlepp S. DNA binding to an anticancer organo-ruthenium complex. J Phys Chem B 2010, Nov 11;114(44):14041-7.
131. Demoro B, Sarniguet C, Sánchez-Delgado R, Rossi M, Liebowitz D, Caruso F, et al. New organoruthenium complexes with bioactive thiosemicarbazones as co-ligands: Potential anti-trypanosomal agents. Dalton Trans 2012, Feb 7;41(5):1534-43.
132. Will J, Kyas A, Sheldrick WS, Wolters D. Identification of (eta6-arene)ruthenium(II) protein binding sites in E. Coli cells by combined

multidimensional liquid chromatography and ESI tandem mass spectrometry: Specific binding of [(eta6-p-cymene)rucl2 (DMSO)] to stress-regulated proteins and to helicases. J Biol Inorg Chem 2007, Aug;12(6):883-94.
133. Anilanmert B. Therapeutic organometallic compounds. INTECH Open Access Publisher; 2012.
134. Desoize B. Metals and metal compounds in cancer treatment. Anticancer Res 2004;24(3a):1529-44.
135. Nobili S, Mini E, Landini I, Gabbiani C, Casini A, Messori L. Gold compounds as anticancer agents: Chemistry, cellular pharmacology, and preclinical studies. Med Res Rev 2010, May;30(3):550-80.
136. Christodoulou CV, Ferry DR, Fyfe DW, Young A, Doran J, Sheehan TM, et al. Phase I trial of weekly scheduling and pharmacokinetics of titanocene dichloride in patients with advanced cancer. J Clin Oncol 1998, Aug;16(8):2761-9.
137. Hannon MJ. Metal-based anticancer drugs: From a past anchored in platinum chemistry to a post-genomic future of diverse chemistry and biology. Pure and Applied Chemistry 2007;79(12):2243-61.
138. Hofheinz RD, Dittrich C, Jakupec MA, Drescher A, Jaehde U, Gneist M, et al. Early results from a phase I study on orally administered tris (8-quinolinolato) gallium (III)(FFC11, KP46) in patients with solid tumors--a CESAR study (central european society for anticancer drug research--ewiv). International Journal of Clinical Pharmacology and Therapeutics 2005;43(12):590.
139. Schmid WF, John RO, Arion VB, Jakupec MA, Keppler BK. Highly antiproliferative ruthenium (II) and osmium (II) arene complexes with paullone-derived ligands. Organometallics 2007;26(26):6643-52.
140. Colangelo D, Ghiglia A, Ghezzi A, Ravera M, Rosenberg E, Spada F, Osella D. Water-soluble benzoheterocycle triosmium clusters as potential inhibitors of telomerase enzyme. J Inorg Biochem 2005, Feb;99(2):505-12.
141. Dorcier A, Ang WH, Bolano S, Gonsalvi L, Juillerat-Jeannerat L, Laurenczy G, et al. In vitro evaluation of rhodium and osmium RAPTA analogues: The case for organometallic anticancer drugs not based on ruthenium. Organometallics 2006;25(17):4090-6.
142. Cebrián-Losantos B, Krokhin AA, Stepanenko IN, Eichinger R, Jakupec MA, Arion VB, Keppler BK. Osmium NAMI-A analogues: Synthesis, structural and

spectroscopic characterization, and antiproliferative properties. Inorg Chem 2007, Jun 11;46(12):5023-33.
143. Boff B, Gaiddon C, Pfeffer M. Cancer cell cytotoxicity of cyclometalated compounds obtained with osmium(II) complexes. Inorg Chem 2013, Mar 4;52(5):2705-15.
144. Kostrhunova H, Florian J, Novakova O, Peacock AF, Sadler PJ, Brabec V. DNA interactions of monofunctional organometallic osmium(II) antitumor complexes in cell-free media. J Med Chem 2008, Jun 26;51(12):3635-43.
145. Medicinal Organometallic Chemistry. Springer; 2010.
146. Fu Y, Habtemariam A, Pizarro AM, van Rijt SH, Healey DJ, Cooper PA, et al. Organometallic osmium arene complexes with potent cancer cell cytotoxicity. J Med Chem 2010, Nov 25;53(22):8192-6.
147. Ryabov AD, Kurova VS, Ivanova EV, Le Lagadec R, Alexandrova L. Redox mediation and photomechanical oscillations involving photosensitive cyclometalated ru(II) complexes, glucose oxidase, and peroxidase. Anal Chem 2005, Feb 15;77(4):1132-9.
148. White E. Deconvoluting the context-dependent role for autophagy in cancer. Nat Rev Cancer 2012, Jun;12(6):401-10.
149. Dixon SJ, Lemberg KM, Lamprecht MR, Skouta R, Zaitsev EM, Gleason CE, et al. Ferroptosis: An iron-dependent form of nonapoptotic cell death. Cell 2012, May 25;149(5):1060-72.

Identification et caractérisation de l'activité biologique des composés organométalliques anticancéreux

Résumé de thèse en français

Cynthia Licona

I. Introduction

Le cancer est devenu la première cause de mortalité dans les pays industrialisés selon la OMS en 2012 8.2 millions des personnes ont décédé à cause du cancer, l'estimation pour 2030 est de 13,1 million des décès si la tendance continue comme aujourd'hui. Afin de traiter le cancer, plusieurs approches thérapeutiques existent parmi lesquelles les chimiothérapies sont les plus utilisées.

Des composés organométalliques tel que les sels de platine représentent une référence en clinique, comme par exemple le cisplatine et l'oxaliplatine, ces molécules comportent certaines limites qui sont des toxicités sur les tissus sains, et le développement de résistances qui rendent le traitement inefficace. Grace à l'intérêt grandissant des composés à base de platine, d'autres composés organométalliques sont en cour de développement, comme par exemple les composés à base de ruthénium et l'osmium, en général, ces composés présentent une faible toxicité, utilisent plusieurs mécanismes d'actions et il semblerait qu'ils soient insensibles aux résistances induites par le cisplatine

Plusieurs laboratoires ont développé différentes molécules à base de Ru avec différentes mécanismes d'action, les molécules les plus représentatives sont, le NAMI-A, KP1019, RAPTA-C, RM175 et le DW1/2, seul trois molécules à base de Ru sont passées en phase de développement clinique (I et II) : le NAMI-A, le KP1019 et le RAPTA-T. Cependant le mécanisme d'action de ces composés est peu caractérisé et leur stabilité et leur solubilité peuvent constituer une limite dans leur développement.

C'est pour cette raison et afin de surmonter ce problème que mon directeur de thèse, C. Gaiddon, en collaboration avec le Dr. Pfeffer (CNRS, Institut de Chimie) ont développé une chimiotèque contenant plusieurs formes de Composés à Base de Ruthénium (RDC) et à base d'Osmium (ODC). L'approche abordée consiste à mettre à profit les avantages des dérivés organométalliques à bases de ruthénium qui grâce au métal présentent: i) des potentiels rédox variables, ii) une structure spatial hexaédrique, iii) un état de charge de 0 à +3, iv) des cinétiques chimiques d'échange de ligand intéressantes, v) une toxicité moindre du à la possibilité d'élimination du

ruthénium par les voies métaboliques du fer. Les composés synthétisés par le groupe de M. Pfeffer sont caractérisés par la présence d'une liaison carbon-metal. Cette liaison confère des propriétés chimiques différentes d'une liaison de coordination classiquement présente dans les autres composés à base de métaux généralement développés. Les travaux de notre équipe ont identifié dans cette chimiotèque originale un nouveau composé, le RDC11 (Ruthénium derived compound 11), présentant une cytotoxicité forte (IC50 1-5µM), une insensibilité vis-à-vis des mécanismes de résistance au cisplatine, une toxicité réduite in vivo comparativement au cisplatine et une capacité à réduire la croissance tumorale sur plusieurs modèles. Par ailleurs, notre équipe a montré que cette molécule semblait agir en partie via des mécanismes d'action à la fois dépendant (p53) et indépendant (voie du stress du réticulum endoplasmique) de l'ADN.

II. Objectives

Bien que le RDC11 présente des propriétés intéressantes, deux aspects sont encore à améliorer. D'une part, les travaux effectués suggèrent que d'autres mécanismes d'action sont mis en jeu par le RDC11. D'autre part, l'activité anti-tumorale in vivo du RDC11 ne bloque pas complétement la croissance tumorale et doit donc être optimisé.

Ainsi, mon projet de thèse a deux objectifs complémentaires qui ont pour objectif commun d'améliorer l'activité de nos composés organométalliques anticancéreux. Ces deux objectifs sont:

1 – Identifier les mécanismes d'action régulés par le RDC11 qui nous sert d'exemple pour notre famille de composés organométalliques à liaison carbone-métal.

2 – Tester les propriétés biologiques de nouvelles générations de complexes métalliques optimisés en modifiant les ligands ou le métal.

III. Résultats

Durant la période de préparation de ma thèse avec le Dr. Christian Gaiddon j'ai participé à la réalisation de huit publications, cinq ont été déjà publiés, et trois sont en cours de publications.

III-1 Mécanismes d'action de composés organométalliques dérivés de Ruthénium (RDC)

III-1.1 Identification du transcriptome du RDC11 (Licona et al. Differential mode of action between a rutenium-based compound and cisplatin revealed by transciptomic analyses :the example fo histone-deacetylases, Publication en préparation)

Afin d'élucider les mécanismes moléculaires des RDC nous avons fait le choix d'utiliser comme première approche les puces à ADN Affimetrix®. Cette technique nous a permis de déterminer le profil d'expression de millier des gènes sans apriori. Nous avons mené cette approche en comparant le RDC11 au cisplatine chacun à l'IC50 et sur deux temps : un temps court, 6h, pour identifier des signaux précoces, et un temps long, 24h, pour les signaux plus tardifs et éventuellement causés par les signaux précoces. Ce travail représente à ce jour une première dans ce domaine. Des analyses bio-statistiques et bio-informatiques ont permis d'obtenir plusieurs niveaux d'informations.

D'une part, les analyses de regroupement (« clustering ») effectuées sur les gènes régulés par le RDC11 et le cisplatine aux deux temps nous permet d'affirmer sans aucune équivoque que les deux molécules ont des signatures transcriptionnelles différentes bien que des points communs existent (figure 1). Ceci est une indication forte que les modes d'action du cisplatine et des RDC sont différents et renforce les résultats obtenus précédemment par notre équipe. (Figure 2)

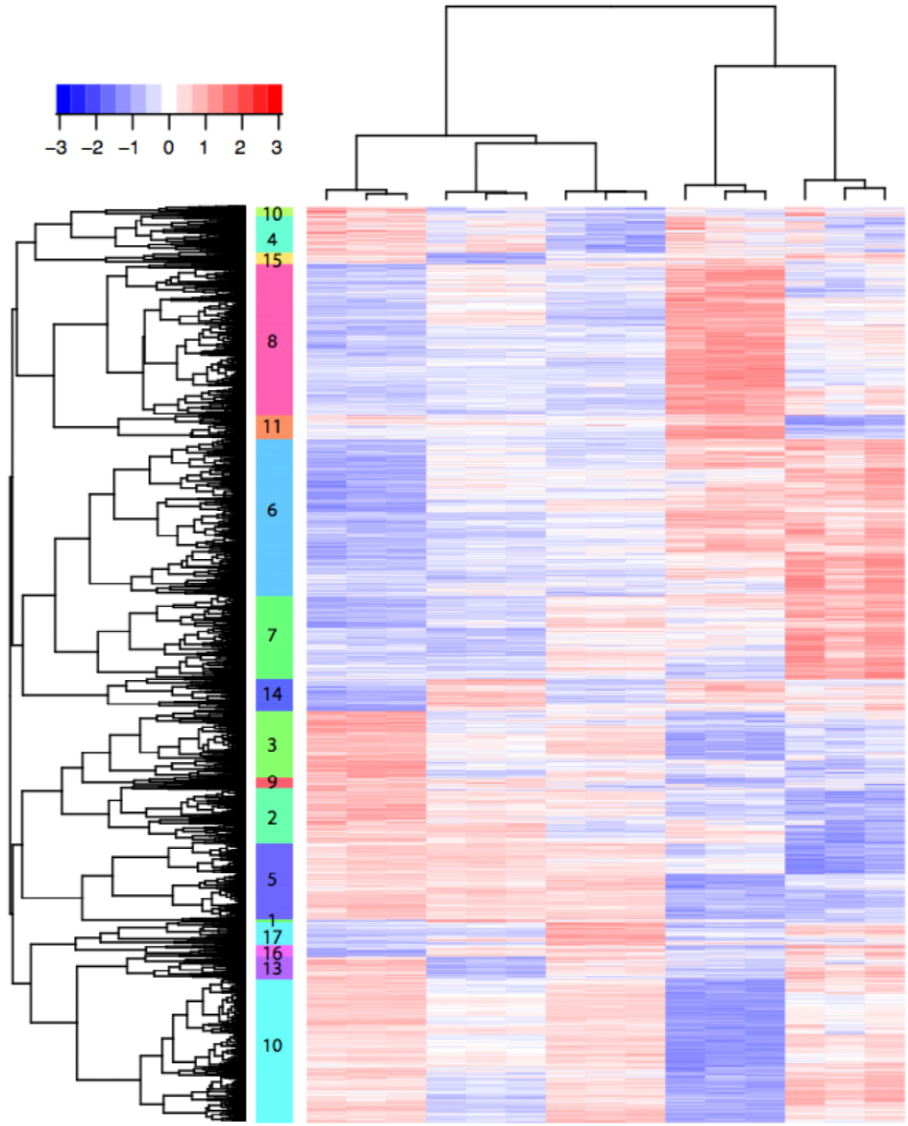


Figure 1. Clustering de l'expression de 4540 gènes. Les rangées représentent l'expression des gènes et les colonnes des échantillons biologiques. Les niveaux d'expression génique sont représentés en échelle (rangée Z-score de -3 à +3). Bleu: faible expression, Rouge: une expression élevée, blanc: modérée. 17 différents clusters ont été détectés.

D'autres part, les analyses bio-informatiques ont dégagé des signatures transcriptionnelles témoignant des signalisations cellulaires particulièrement modifiées par le RDC11 telles que:

a- La réponse aux dommages à l'ADN, y compris celle dépendante de p53.

b- Mécanismes d'import intracellulaire divers, y compris ceux des aminoacides et du fer

c- Une altération des voies métaboliques Hif1ß/Hif1a et mTOR

d- Une induction des voies de réponse au stress oxydant (NRF2 et ces gènes cibles)

e- Une modulation des ARN des complexes histones et de régulateurs épigénétiques

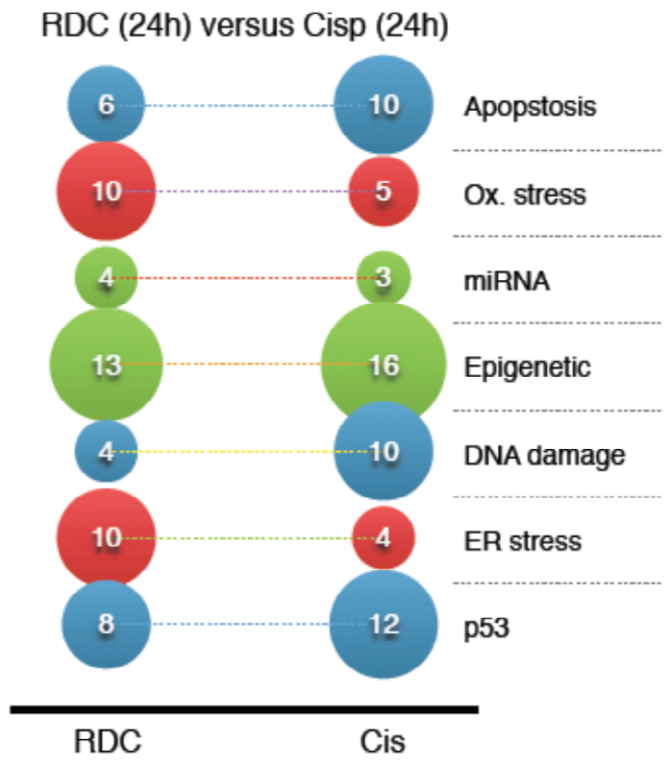


Figure 2. Voies de signalisation et mécanismes réglementés par cisplatine ou RDC11. Le graphique représente le nombre de gènes dans les voies indiquées qui sont régulés par RDC11 et cisplatine à 24 heures. Les données de puces à ADN ont été analysées utilisant les outils bioinformatiques de AltAnalysis et R afin d'identifier dans les banques de donnés tels que KEGG et Gene Ontology, les voies de signalisation et mécanismes qui corresponds à la dérégulation des gènes.

L'exploration du rôle de chacun de ces mécanismes dans l'activité biologique du RDC11 est pertinente de par leur rôle dans l'import d'une molécule bio-active (transporteurs), l'adaptation métabolique des cellules cancéreuses (Hif1, mTOR, NRF2), ou la réparation de l'ADN.

III-1.2 Modulation du Métabolisme Cellulaire (Vidimar, Licona et al. Differential regulation of the HIF-1 pathway by platinum and ruthenium anticancer organometallic drugs)

La diminution d'expression de gènes cibles (VEGF, Glu1) de Hif1a observé en microarrays a été confirmé par RT-qPCR et corrèle avec une diminution des niveaux protéiques de Hif1a dans des cellules de cancer colique (HCT116 et SW480) (Figure

3).

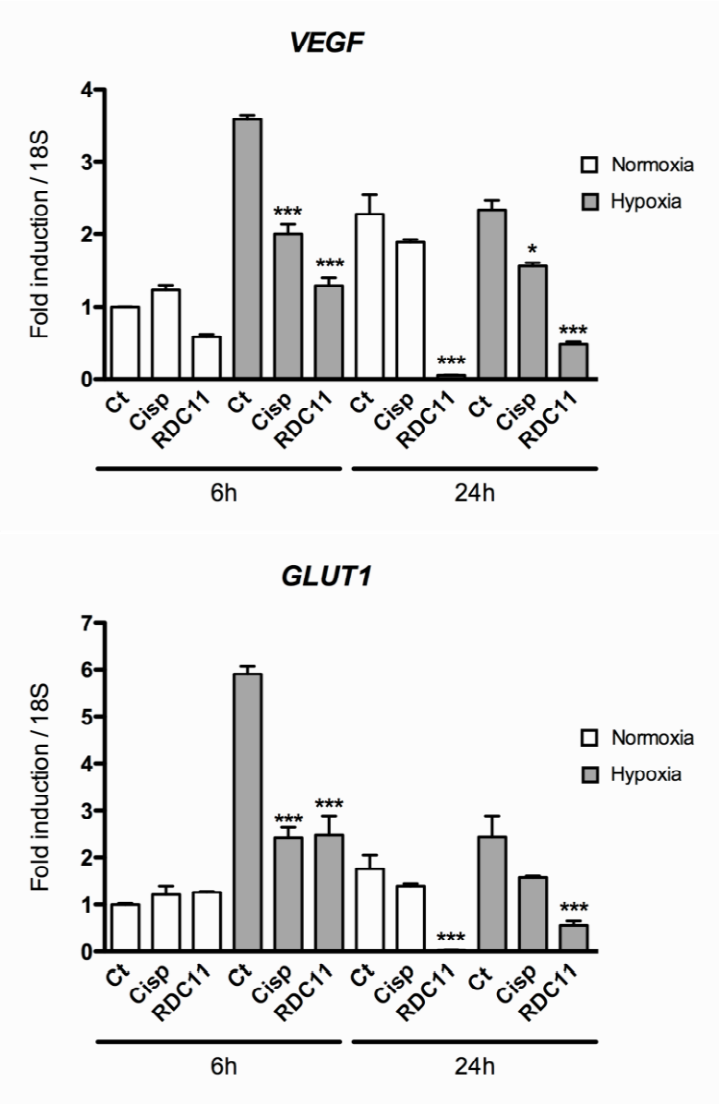


Figure 3. Diminution d'expression de deux gènes cibles de Hif-1a dans des cellules HCT116 traité par le RDC11 5µM ou cisplatine 5µM.

Cet effet est visible en hypoxie et en normoxie et s'accompagne d'une altération de la balance cellulaire redox avec une augmentation de ROS (espèces réactive d'oxygène) et du ratio NAD/NADH. J'ai confirmé ces résultats *in vivo* en montrant que l'expression de gènes cibles de Hif1a (VEGF, Glu1) sont diminués par le RDC11 dans des modèles de xénogreffes humaines primaires (Figure 4). Cette diminution d'expression du VEGF s'accompagne d'une diminution de l'angiogenèse. Nous montrons également que la perte d' Hif1a s'explique par l'action de plusieurs mécanismes : i) une augmentation d'hydroxylation d'Hif1a par l'enzyme rédox PHD2 qui interagit directement avec le RDC11 et qui dirige Hif1a vers sa dégradation, ii)

une répression de la voie mTOR diminuant ainsi la traduction de Hif1a.

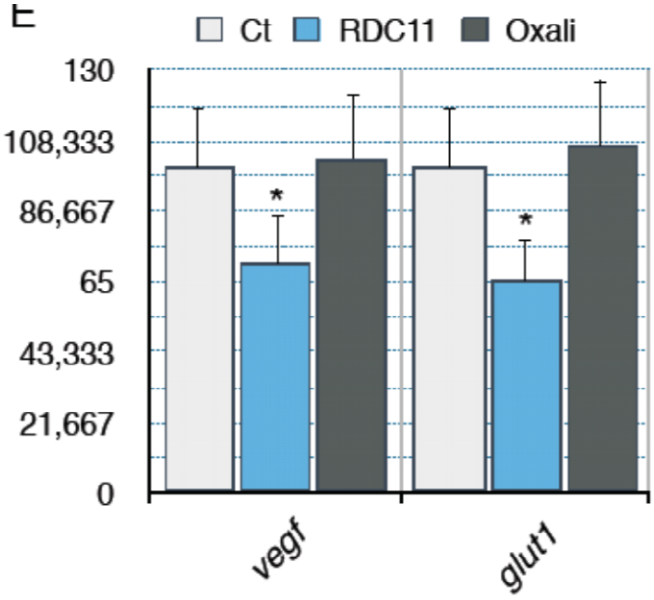


Figure 4. Tumeurs coliques de patients implantés chez la souris par voie sous-cutanée, les souris ont été traité avec oxaliplatine 10µl/Kg ou RDC11 10µmole/Kg deux fois par semaine. Le graphique montre une diminution des gènes cibles de Hif1-a par RT-qPCR.

Ce travail mis en perspective avec les propriétés d'échangeur d'électrons des RDC à permis de montrer que les RDC ont un effet anti-angiogénique vraisemblablement en affectant l'activité d'enzyme rédox, comme PHD2, participant à l'homéostasie du métabolisme cellulaire.

III-1.3 Transport cellulaire du RDC11 (Klajner, Licona et al. Subcellular localization and transport kinetics of ruthenium organometallic anticancer comounds in living cells : A dose-dependent role for amino acid and iron transporters, Inorg Chem. 2014)

Le criblage transcriptomique a permis de mettre en évidence le changement de l'expression des transporteurs d'aminoacides et de fer, suggérant leur implication dans l'import ou l'export du RDC dans les cellules. Grace à des RDC intrinsèquement fluorescents, nous avons montré qu'effectivement l'import des RDC dans les cellules mettait en jeu en partie des transporteurs d'aminoacides et du fer, ceux-là même qui sont régulés au niveau transcriptionel par le RC11. Par ailleurs l'utilisation de ces RDC fluorescentes m'a permis montrer que les RDCs ont la capacité de s'accumuler dans différentes organelles telles que : réticulum

endoplasmique (RE), mitochondrie et noyau cellulaire (Figures 5 et 6). Ceci permet d'expliquer les dommages à l'ADN que j'ai pu observer et l'activation de la voie de stress du RE.

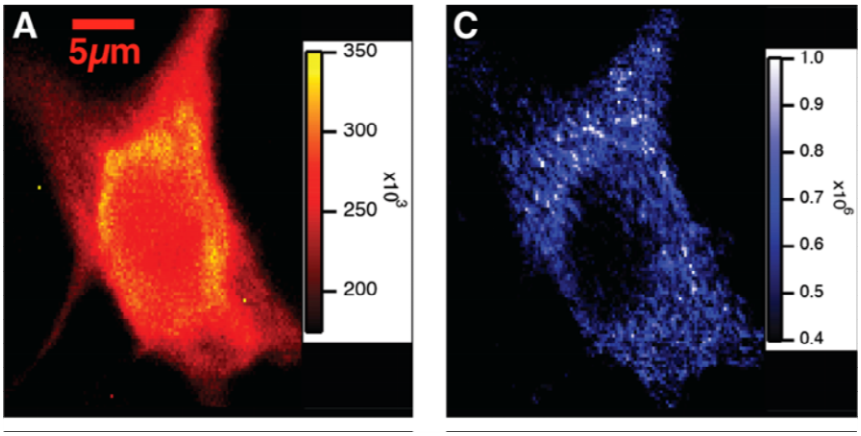


Figure 5. Accumulation du RDC34 dans le réticulum endoplasmique dans des cellules A172, traitées pendant 2h à 5µM

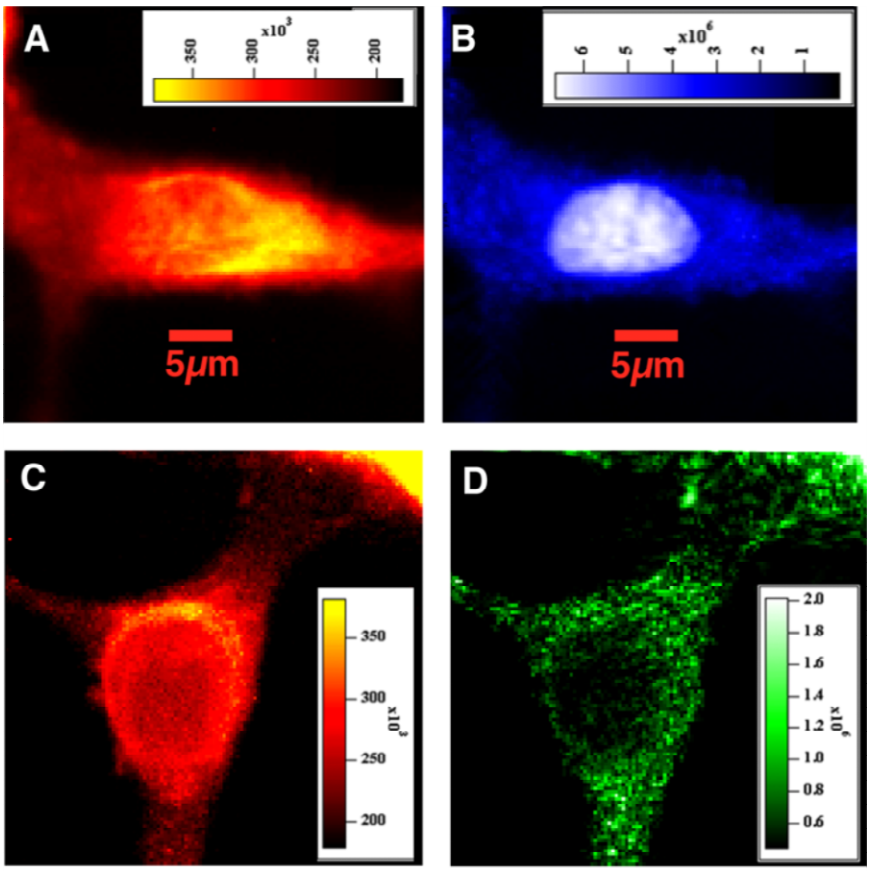


Figure 6. Accumulation du RDC au niveau du noyeu et la mitochondrie ave du propidium iodide (B) et MitoTracker Gren (D) dans des cellules A172 traitées pendant 2hr avec RDC34 à 5µM.

III-2. Nouvelle Génération des composés organométalliques.

Les résultats obtenus avec le RDC11 sont très prometteurs quant au potentiel anticancéreux. Par contre, la cytotoxicité doit être amélioré pour satisfaire le cahier des charges de l'industrie pharmaceutique. Afin de développer des nouveaux composés plus efficace *in vivo* vous avons suivi deux stratégies pour optimiser l'activité *in vitro* et/ou la solubilité aqueuse: la première stratégie est le changement de ligand et la deuxième est le changement du métal.

III-2.1 Changement de ligand (Vidimar et al. Induction of caspace 8 and reactive oxygen species by ruthenium-derived anticancer compounds with improved water solubility and cytotoxicity, Biochemical Pharmacology, 2012)

Nous avons évalué l'impact de différents changements sur les ligands autour du noyau ruthénium. Ainsi, l'ajout d'un ligand (phénantroline) augmentant la lipophilie favorise la cytotoxicité. A l'inverse, l'ajout de ligands électrodonneur NO_2, électro-attracteur NH_2, ou d'une spermine, qui augmente la solubilité aqueuse, diminue la cytotoxicité (figure 7). Par ailleurs, l'augmentation de la cytotoxicité induite par l'ajout d'une phénantroline dans le RDC34 corrèle avec une formation plus forte de ROS et de caspase 8 activée. Cependant, bien que le RDC34 soit plus cytotoxique *in vitro*, il n'est pas significativement plus efficace *in vivo* sur des modèles de xénogreffes.

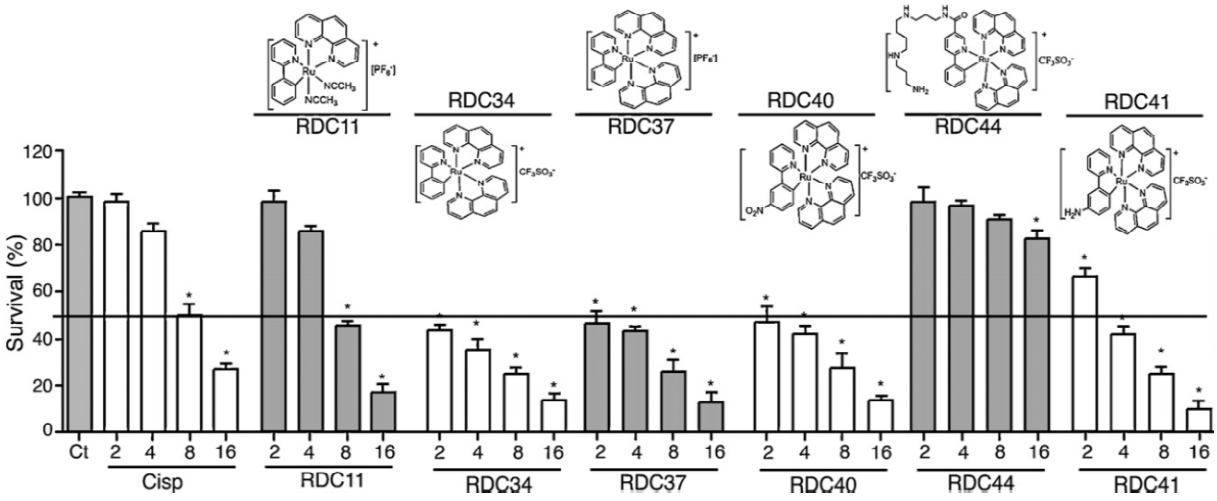


Figure 7. Nouvelle génération des composés à base de ruthénium. Les test de cytotoxicité MTT ont été réalisé dans des cellules HCT116 traité pendant 48hr.

III-2.2 Chimie combinatoire. (Chow, Licona et al. Discovery and Investigation of anticancer ruthenium-aerene schiff-base complexes via wather-promoted combinatorial three-component assembly J Med Chem. 2014)

Une des limites pour la synthèse d'une chimiotèque et la recherche des molécules actives est la capacité de synthèse d'un chimiste. En collaboration avec le groupe du Dr. Ang à Singapour, une approche de chimie combinatoire a permis de synthétiser plus de 400 composés à base de Ruthénium en peu de temps (Figure 8).

Cette capacité de synthèse permet d'envisager des approches de synthèse et de tests biologiques de type « High-throughput ». Ainsi, nous avons testé l'activité cytotoxique de ces 400 composés en plaques de 96 puits. Nous avons identifié 4 composés avec une activité cytotoxique intéressante autour du micromolaire. Les résultats ont démontré que ces composés ont une activité indépendante de p53.

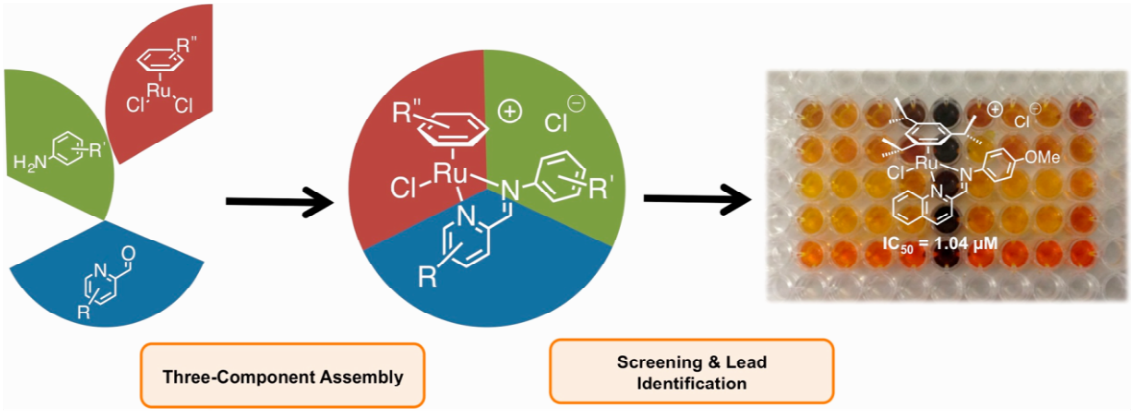


Figure 8. Illustration de la synthèse des complexes RAS, criblage et identification des cibles

III-2.3 Changement de métal (Licona et al. Exchange of ruthenium to osmium in organometallic compound tunes redox potential and cancer cell selectivity via ROS and oxydo-reductase enzymes regulaton, Pub. en cours)

Comme deuxième stratégie, nous avons substitué le Ruthénium par l'Osmium qui présente un potentiel rédox différent. Nous avons synthétisé 2 composés, l'ODC2 et l'ODC3 qui sont les équivalents structuraux du RDC11 et RDC34 respectivement à l'exception du métal (Figure 9).

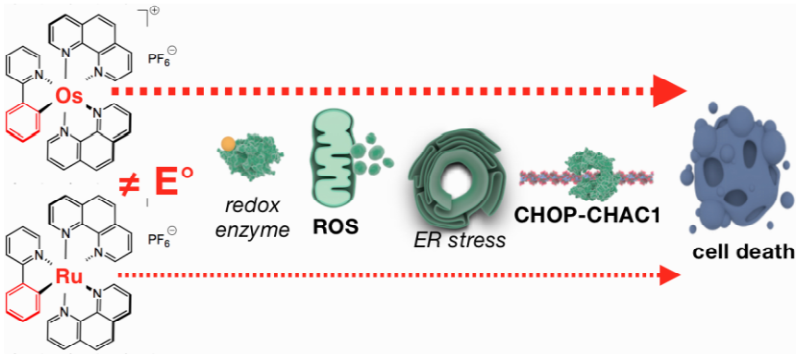
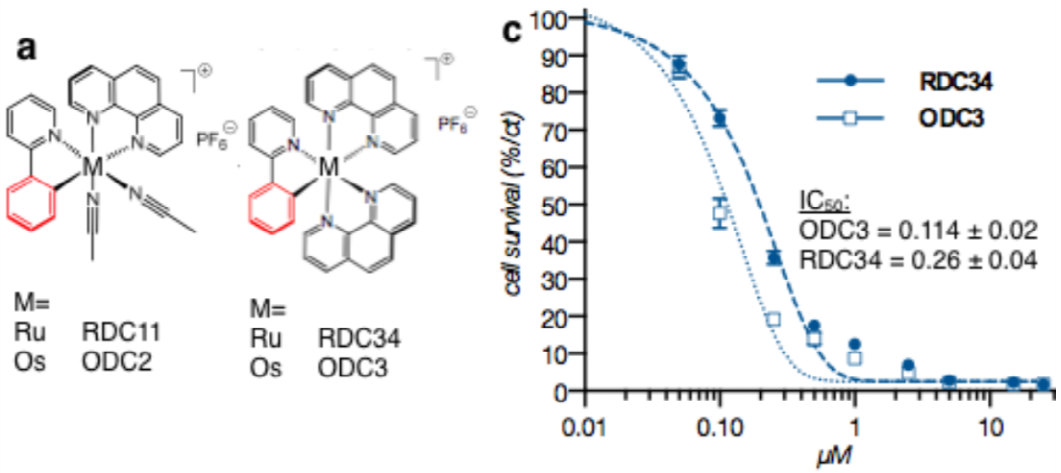


Figure 9. Schéma representative du mechanisme d'action des composés à base d'osmium et ruthéniu.

L'introduction de l'osmium ne change pas significativement la structure spatial, ni la lipophile des composés, mais modifie significativement le potentiel redox. L'analyse des 60 lignées cancéreuses humaines du NCI a mis en évidence que les composés à base d'osmium ont une activité anticancéreuse cytotoxique plus élevé, suggérant fortement que le potentiel rédox intervient dans le mode d'action. Cette augmentation ne corrèle pas avec l'affinité pour l'ADN (Figure 10 et 11).



b

compound	E°1/2 M(III/II) (± 5mV)	Log(Po/w)	k_3 (M^{-1} s^{-1}) x10^6 Glucose Ox.	k_3 (M^{-1} s^{-1}) x10^6 HRP
ODC2	280	1.15 ± 0.05	2.9 ± 0.3	2.7
RDC11	560	1.2 ± 0.05	1.7 ± 0.2	10
ODC3	300	2.34 ± 0.04	1.8 ± 0.2	0.58
RDC34	410	2.35 ± 0.05	7.5 ± 0.4	2.3

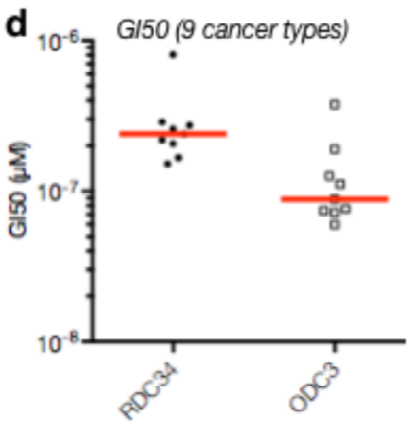


Figure 10. (a) structure chimique du composés RDC11 et RDC34 ansi que ODC2 et ODC3, (b) propriétés physico-chimiques de composés, (c) cytotoxicité des composés testés sur des cellules HCT116 (MTT test) (d) GI50 des 60 lignés cellulaires testés par le NCI.

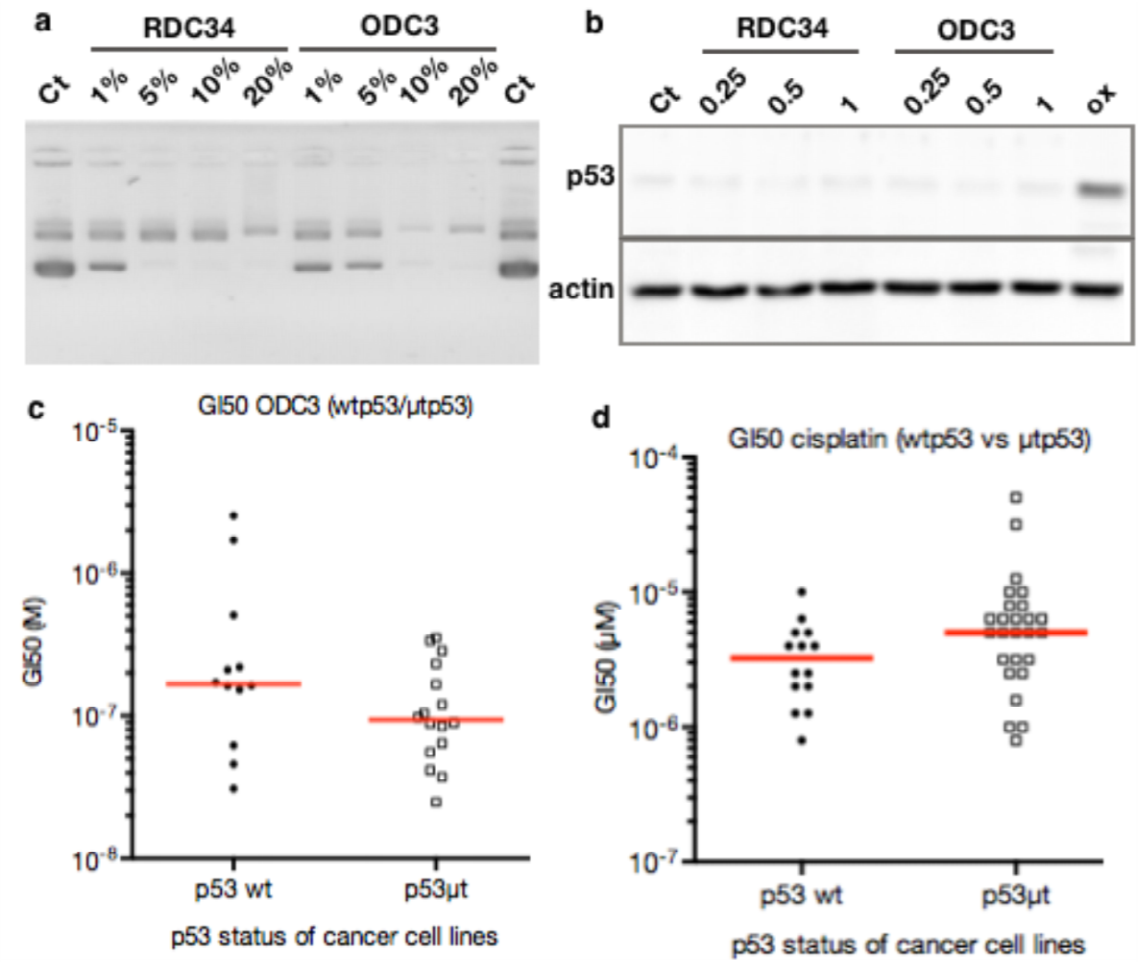


Figure 11. Interaction avec l'ADN et expression de p53 par RDC34 et ODC3. (a) Gel d'electrophorese du plasmide d'ADN incubé avec des concentrations croissantes du REDC34 et ODC3, (b) expression protéique de p53 dans des cellules HCT116 aux concentrations indiqués (µM), (c) GI50 des 60 différentes lignées cellulaires p53 sauvages et p53 mutés avec ODC3, (d) et avec cisplatine.

Par contre, nous avons observé que les composés interférent différemment avec l'activité de certaines enzymes d'oxydoréduction en fonction du métal. Ces enzymes participant à l'homéostasie rédox cellulaire, j'ai étudié les voies de signalisation sensibles aux potentiels redox, tels que la voie du stress du RE et la voie NRF2. J'ai observé qu'effectivement les ODC produisent plus de ROS et qu'ils enduisent d'avantage la voie du stress du RE (CHOP, PERK, eIF2-alfa) et induisent plus facilement la voie du NRF2 et ses gènes cibles (NQ01, GCLC) (Figure 12).

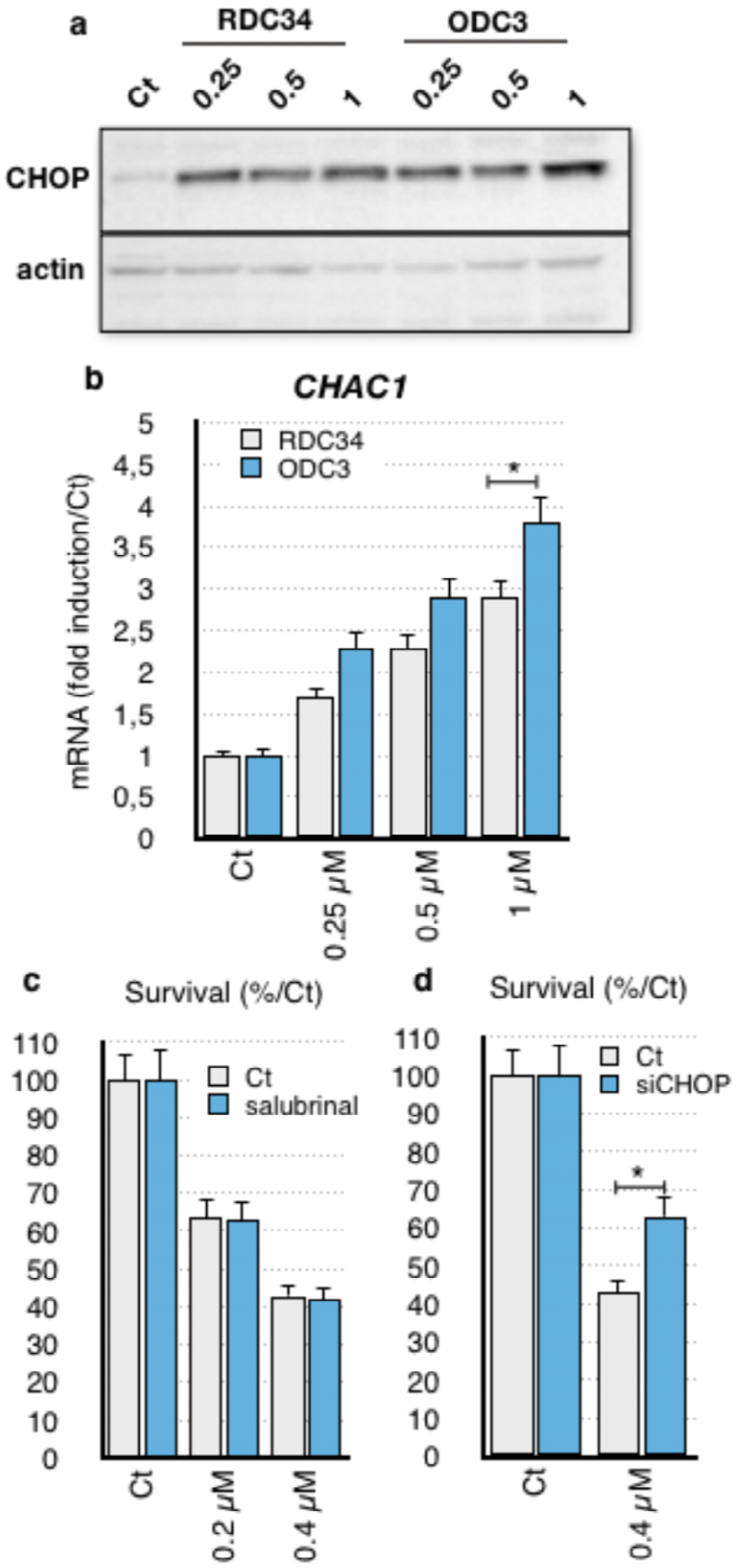
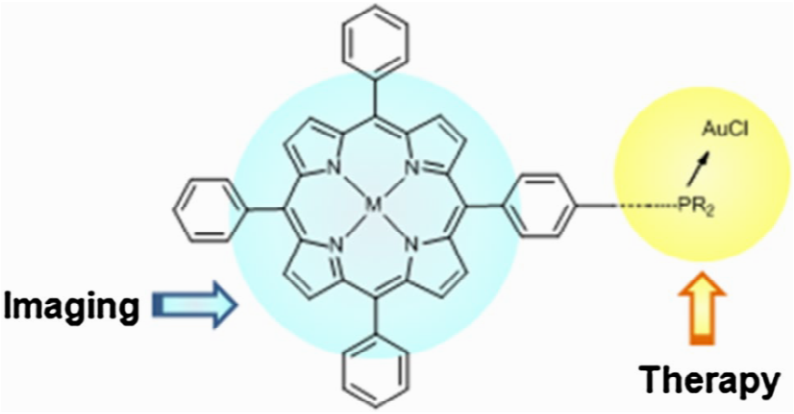


Figure 12. Stress du réticulum endoplasmique (a) expression de la protéine CHOP par Western Blot, (b) RT-qPCR pour le chac1, gène cible de CHOP, (c) inhibition de la survie cellulaire induit par le salubrinal ou (d) par le siRNA de CHOP.

III-2.4. Téranostique (Eggenspiller, et al. European J. Org. Chem ; 2013 et Tasan et al. J Biol Inorg Chem 2014)

Dans le but d'optimiser le potentiel thérapeutique de composés organométalliques, nous avons réalisé une collaboration avec le groupe du Dr. Gros, dans laquelle nous avons caractérisé des molécules organométalliques pour une application téranostique.



Il s'agit de molécules qui peuvent à la fois être actives biologiquement (activité cytotoxique) et peuvent servir en imagerie médical. Une première série des molécules a été synthétisé pour lesquelles nous avons testés l'activité cytotoxique et l'imagerie médicale en collaboration. Une deuxième série de composés a été ensuite développée dans la quelle des propriétés de photodynamique ont été mis en évidence.

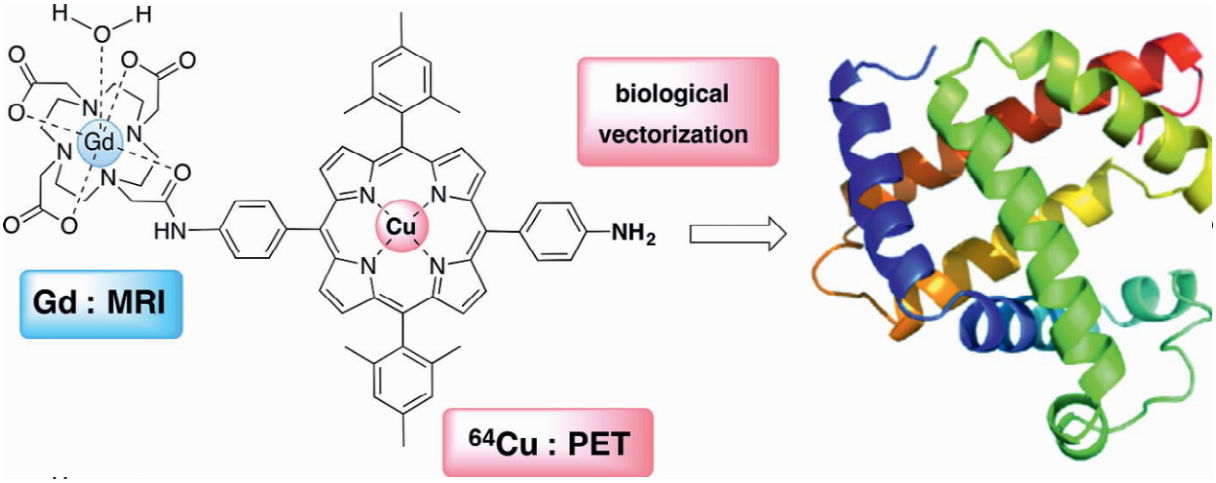


Figure 13. Molécules à base de Gd ou Cu

IV. Discussion

Les travaux réalisés pendant ma thèse ont permis d'identifier des nouveaux mécanismes d'action pour les RDC, ainsi que la réalisation d'une première étude transcriptomique qui a permis de démontrer que ces mécanismes sont différents des dérivés de platine. Ceci ouvre des nouvelles perspectives en termes de développement des ces composés et permettrait une meilleur compréhension de ces voies de signalisation. L'identification des cibles pharmacologiques pourrait ouvrir la voie à l'optimisation sélective de la drogue, et pourrait conduire à une thérapie ciblée qui est le principal défi de la chimiothérapie, et à l'identification de marqueurs permettant de sélectionner les patients les plus apte à répondre au traitement.

J'ai également pu tester des molécules de nouvelle génération qui ont permis de démontrer l'importance du métal et du potentiel d'oxydoréduction. J'ai également mis en évidence que la modification structurale, même mineure, modifient leurs propriétés physico-chimiques, leur activité cytotoxique ainsi que la sélectivité vers les différents types de tumeurs. C'est ainsi que l'osmium représente un réel intérêt dans le développement de nouveaux médicaments antitumoraux.

Enfin, j'ai pu constater que certaines molécules qui étaient particulièrement cytotoxiques *in vitro* présentaient aussi une toxicité *in vivo*, ce qui représente un frein a leur développement. A ce jour, nous sommes toujours à la recherche de la molécule idéale qui bloquerait complètement la croissance tumorale. Cependant l'ensemble des donnés indique que les composés à base de ruthénium et osmium peuvent représenter des alternatives intéressantes aux composés déjà existants.

V. Perspectives

Des études préliminaires que j'ai effectuées et qui ont été directement inspirées par mes résultats montrent de nouvelles voies de recherche. Ainsi, les propriétés rédox de nos composés donnent à ces composés une capacité d'activation par la lumière ouvrant des possibilités d'application en photothérapie. D'autre part, des altérations dans les voies régulant l'autophagie et la féroptose dans les cellules traitées au RDC laisse supposé que ces morts cellulaires pourraient être impliquées dans l'activité biologique des dérivés organométalliques d'osmium ou de ruthénium.

Cynthia LICONA

Identification et caractérisation de l'activité biologique des composés organométalliques anticancéreux

Résumé

Le cancer figure parmi les principales causes de décès dans le monde. Afin de traiter le cancer, plusieurs approches thérapeutiques existent parmi lesquelles les chimiothérapies en combinaison avec la chirurgie sont les plus utilisées. Des composés organométalliques tel que les sels de platine représentent une référence en clinique. Malgré leur succès, ils comportent des limites qui sont des toxicités sur les tissus sains et le développement de résistances.

Notre équipe collabore depuis plusieurs années avec divers chimistes afin de développer de nouvelles molécules organométalliques anticancéreuses à base de Ruthénium (RDC) et à base d'Osmium (ODC). Au cours de ma thèse, j'ai réalisé des études de type structure/fonction de nouvelles molécules afin de trouver les paramètres physicochimiques importants pour leur activité biologique et afin d'identifier leur mode d'action. Mes travaux ont démontré que le potentiel d'oxydoréduction des composés serait un facteur important pour leur cytotoxicité. De plus, j'ai identifié de nouvelles voies de signalisation régulées par ces composés, tels que les voies de signalisation d'Hif-1 et Nrf2, et les HDAC.

L'ensemble de ces résultats nous permet de mieux comprendre les propriétés biologiques des composés organométalliques ce qui à terme devrait permettre une optimisation de leur structure pour améliorer leur activité anticancéreuse.

Mots clés : composés organométalliques, ruthénium, osmium, potentiel d'oxydoréduction, cytotoxicité, Hif1, HDAC, NRF2

Sumary

Cancer is one of the leading causes of death in the world. To treat cancer, several therapeutic approaches exist. Chemotherapy in combination with surgery is one of the most used. Organometallic compounds such as platinum salts represent a reference in clinic. Despite their success, they have limitations that are toxicity to healthy tissue and the development of resistance.

Our team has been working for several years with chemists to develop new organometallic Ruthenium (RDC) and Osmium compounds (ODC). During my Ph.D. I performed structure/function studies on novel molecules in order to find the important physico-chemical parameters for their biological activity. My work demonstrated that the redox potential is a crucial factor for the cytotoxicity of the compounds. In addition, I identified novel regulatory pathways that are targeted by these compounds, such as the Hif1 and Nrf2 pathways, and the HDACs.

All together these results allow us to have a better understanding of the biological properties of the organometallic compounds, which will in time allow a optimization of their structure to favor their anticancer activity.

Keywords: organometallic compounds, ruthenium, osmium, redox potential cytotoxicity, Hif1, HDAC, NRF2